THE UNIVERSITY OF OKLAHOMA

GRADUATE COLLEGE

NETWORK MECHANISMS UNDERLYING CORE BEHAVIORAL FEATURES IN FRAGILE X SYNDROME

A DISSERTATION

SUBMITTED TO THE GRADUATE FACULTY

In partial fulfillment of the requirements for the degree of

DOCTOR OF PHILOSOPHY

By

JORDAN E. NORRIS

Norman, Oklahoma

2025

Downloaded from SHAREOK. Persistent Handle URL: https://hdl.handle.net/11244/341523

NETWORK MECHANISMS UNDERLYING CORE BEHAVIORAL FEATURES IN FRAGILE X SYNDROME

A DISSERTATION APPROVED FOR THE

DEPARTMENT OF PSYCHOLOGY

BY THE COMMITTEE CONSISTING OF

Dr. Lauren E. Ethridge, Chair

Dr. Michael J. Wenger

Dr. Michael R. Markham

Dr. Patrick D. Manapat

Dr. Andrew H. Fagg

© Copyright by JORDAN ELIZABETH NORRIS 2025

All Rights Reserved.

ACKNOWLEDGEMENTS

I am so grateful for every single person who helped me cross this finish line. I would not be where I am today without their love, support, patience, and encouragement.

First, thank you to my dissertation committee for your time, your questions, and your dedication to my growth. Every single one of you went above and beyond for me and I cannot thank you enough. To Andy, especially, who dedicated much time and effort to helping me learn new skills throughout the course of this project. Thank you for your mentorship and everything you've done to support me along the way. Your passion for students and teaching is inspirational. To both Michael Wenger and Michael Markham, you taught me so much about what it means to be a neuroscientist. The amount of gratitude I have for what you've taught me and the role you both played in my education at the undergraduate and graduate level cannot be fully expressed in an acknowledgements section but know I will carry what you taught me, always (and hopefully pass it on to my own students one day). To Patrick, thank you for agreeing to be part of my committee. You are one of the kindest, supportive, and coolest faculty members I know. I appreciate you taking the time to answer my questions and listen to me talk about all things clinical. Finally, to Lauren, there are not actual words sufficient to express how grateful I am to you. Hopefully these will be adequate: Thank you for believing in me, for holding space for me, for your patience with me (and all of my side projects and weird sense of humor), for your time and effort, and for your abundant kindness. Thank you for everything you have done to help me become an independent researcher. You extended an open invitation, and I am so glad I took you up on it.

Thank you to all of the friends I made along the way, thank you for all the laughter, the memories, and letting me part of your journeys. Catherine, I am so glad to know and be known

by you. Thank you for listening to all my complaints, sharing in my joys, helping me through the lows, and for the endless conversations about books, running, and all the other things we share. Cooper, it was a joy hitting most of our milestones together. I would not have made it through all of this without you. Thank you to Dana and Brenna for keeping me sane. To Claire and Rin for letting me be part of the spaghetti squad and for your friendship. To my cohort for sharing so much of this journey with me. And so many more. There are so many other people in this program I want to thank but will stick with acknowledging that I was deeply fortunate to work in a department filled with such amazing people. I would not have wanted to do grad school with any other group of humans.

To the friends who were there all along: To Julie, you are one of the best humans and best friends a person could ask for. Thank you for cheering me on all these years and for your love and kindness. To Elyse, I love and appreciate you. Words really cannot express how thankful I am for you and Trai's friendship.

To my family, I owe you all the biggest thank you. I have the best parents! Thank you both for always supporting me and the kindness of letting me go after my dreams, no matter what they were. Your constant support was truly why I am where I am today, and I cannot thank you enough. To my sister, I love you and I am so grateful to have a sister who is also one of my best friends. You also raised really cool humans and the joy they add to my life is exponential. Lastly, to Brad, I would not have gotten to this point without you. You are the best partner I could ask for and I am so thankful for you. Thank you for your patience, for taking care of me when things were hard, and for cheering me on the whole time.

Finally, thank you to all of the participants and their families.

Table of Contents

Table of Contents vi
List of Figures ix
List of Tables xiv
ABSTRACT xv
CHAPTER ONE: General Background 1
CHAPTER TWO 9
Abstract 10
Background 12
Methods 22
Participants 22
Clinical Measures 24
Procedure 27
Analysis 29
Frequency Band Power Analyses. 36
Statistical Routine 37
Results 39
Microstate Analysis 39
Functional Connectivity Analysis 59
Frequency Band Analysis 77
Individual Peak Alpha Frequency (PAF) Analysis 82
FMRP Analysis 84
Microstate and Functional Connectivity Correlation Analysis 84
Correlation and Clinical Variable Analysis 92
Discussion 118
Microstates 118
Functional Connectivity 124
Microstates as Functional Connectivity Proxies 128
Power and Individual Peak Alpha Frequency Differences 129
Conclusion 129
Limitations 131
Future Directions 132
CHAPTER THREE 133
Abstract 134
Background 136
Methods 140

Participants 140
Procedure 140
Analysis 143
Statistical Routine 147
Results 147
Event Related Potential (ERP) Analysis – Feedback 147
Event Related Potential (ERP) Analysis – RewP 161
Event Related Potential (ERP) Analysis – Visual 165
Microstate Analysis 168
Functional Connectivity Analysis – Whole Network Connectivity 183
Functional Connectivity Analysis: Strongest Connections 222
Triple Network Disruption Hypothesis 276
Correlation Analyses 282
Discussion 306
Feedback Event Related Potentials 306
Microstates 307
Functional Connectivity 311
Triple Network Hypothesis 321
Conclusions 322
Limitations 322
CHAPTER FOUR 326
Abstract 327
Background 329
Methods 335
Participants 335
Procedure 335
Analysis 337
Statistical Analysis 339
Results 340
Chirp Results 340
Machine Learning Results 343
Discussion 352
Limitations 357
CHAPTER FIVE 359
General Discussion 359

References 365
Appendix A. Peak Alpha Frequency by Sex and Group 401
Appendix B. ERP Difference Waves: Spatial Distribution of RewP 402
Appendix C. Model 1 EEG Composite Correlations 404
Appendix D. Model 2 EEG Composite Correlations 407

List of Figures

CHAPTER TWO

Figure 1. Fragile X Syndrome Genetics 2
Figure 2. Boxplots Depicting 4MS Solution Group Differences on GEV, Mean Duration, Complexity, and Hurst 42
Figure 3. Boxplots Depicting 4MS Solution Sex Differences on GEV, Mean Duration, Complexity, and Hurst 43
Figure 4. Boxplot for Mean GFP by Microstate and Group by Microstate Interaction for the 4MS solution 45
Figure 5. Boxplots Depicting 4MS Solution Group Differences on GEV, Mean Duration, Complexity, and Hurst 49
Figure 6. Boxplots Depicting 6MS Solution Sex Differences on GEV, Mean Duration, Complexity, and Hurst 50
Figure 7. Boxplot for Mean GFP by Microstate and Group by Microstate Interaction for the 6MS solution 52
Figure 8. Boxplots Depicting 10MS Solution Group Differences on GEV, Mean Duration, Complexity, and Hurst 56
Figure 9. Boxplots Depicting 10MS Solution Sex Differences on GEV, Mean Duration, Complexity, and Hurst 57
Figure 10. Davies-Bouldin Index for All Resting State Microstate Solutions 58
Figure 11. Default Mode Network Theta Band Functional Connectivity Circle Plots 60
Figure 12. Violin and Box Plots Depicting Default Mode Network Functional Connectivity across Different Frequency Bands 61
Figure 13. Salience Network Theta Band Functional Connectivity Circle Plots 62
Figure 14. Violin and Box Plots Depicting Salience Network Functional Connectivity across Different Frequency Bands 63
Figure 15. Control Network Theta Band Functional Connectivity Circle Plots Control Network Theta Band Functional Connectivity Circle Plots 64
Figure 16. Violin and Box Plots Depicting Control Network Functional Connectivity across Different Frequency Bands 65
Figure 17. Theta FC Top Ten Within Default Mode Network Connections 67
Figure 18. Group Differences on Default Mode Network Top Two Connections 69
Figure 19. Theta FC Top Ten Within Salience Network Connections 71
Figure 20. Group Differences on Salience Network Top Two Connections 72
Figure 21. Theta FC Top Ten Within Control Network Connections 74
Figure 22. Group Differences on Control Network Top Two Connections 75
Figure 23. Violin and Boxplots Depicting Group Differences on Functional Connectivity Summed across the Top Ten Connections for Each Network 77
Figure 24. Boxplots for Absolute Power across All Frequency Bands for the Frontal Electrode Selection 78
Figure 25. Boxplots for Relative Power across All Frequency Bands for the Frontal Electrode Selection 79
Figure 26. Boxplots for absolute power across all frequency bands for the posterior electrode selection 80

Figure 27. Boxplots for Relative Power across All Frequency Bands for the Posterior Electrode Selection..... 81
Figure 28. Relative Power Spectrum Depicting Peak Alpha Frequency Between Groups 83
Figure 29. Correlation Plot for Functional Connectivity and Individual Microstate Class Duration, Coverage, and Occurrence..... 86
Figure 30. Correlation Plot for Functional Connectivity and Individual Microstate Class GEV and GFP 87
Figure 31. Correlation Plot for Functional Connectivity and Individual Microstate Class Duration, Coverage, and Occurrence for FXS Group Only..... 88
Figure 32. Correlation Plot for Functional Connectivity and Individual Microstate Class Duration, Coverage, and Occurrence for FXS Group Only..... 89
Figure 33. Correlation Plot for Functional Connectivity and Global Microstate Variables..... 90
Figure 34. Correlation Plot for Functional Connectivity and Global Microstate Variables for FXS Only 91
Figure 35. Correlation Plot for Microstate Variables and IQ 94
Figure 36. Correlation Plot for Microstate Variables and IQ for FXS Group Only 95
Figure 37. Correlation Plot for Microstate Variables and IQ for FXS Group Only 96
Figure 38. Correlation Plot for Functional Connectivity Variables and IQ..... 98
Figure 39. Correlation Plot for Functional Connectivity Variables and IQ for FXS Group Only99
Figure 40. Correlation Plot for Microstate Variables and KiTAP for FXS Group Only..... 102
Figure 41. Correlation Plot for Functional Connectivity and KiTAP for FXS Group Only..... 103
Figure 42. Correlation Plot for Microstate Variables and Vineland-3 for FXS Group Only 105
Figure 43. Correlation Plot for Microstate Class GFP and Vineland-3 for FXS Group Only... 106
Figure 44. Correlation Plot for Functional Connectivity and Vineland-3 for FXS Group Only 107
Figure 45. Correlation Plot for Microstate Variables and ABC FXS for FXS Group Only..... 109
Figure 46. Correlation Plot for Individual Microstate Class GFP and ABC FXS for FXS Group Only..... 110
Figure 47. Correlation Plot for Functional Connectivity Variables and ABC FXS for FXS Group Only..... 111
Figure 48. Correlation Plot for Microstate Variables, Frequency Band Power, and PAF..... 113
Figure 49. Correlation Plot for Microstate Variables, Frequency Band Power, and PAF for FXS Group Only 114
Figure 50. Correlation Plot for Functional Connectivity, Frequency Band Power, and PAF ... 116
Figure 51. Correlation Plot for Functional Connectivity, Frequency Band Power, and PAF for the FXS group only..... 117

CHAPTER THREE

Figure 52. Reversal Learning Task Diagram..... 142
Figure 53. Channel Selection for ERP Measurements..... 145
Figure 54. Frontal Reversal Learning Feedback-Related ERPs 148
Figure 55. Central Reversal Learning Feedback-Related ERPs 153
Figure 56. Parietal Reversal Learning Feedback-Related ERPs..... 156
Figure 57. Scalp Topography for RewP..... 161
Figure 58. Frontocentral Difference Wave 162

Figure 59. Occipital (Visual) Reversal Learning Feedback-Related ERPs 165
Figure 60. Davies-Bouldin Indices across RLEEG Data Types for All Microstate Solutions Tested on rsEEG for FXS 169
Figure 61. Feedback 4MS Solution..... 173
Figure 62. Stimulus 4MS Solution..... 177
Figure 63. Pre-stimulus 4MS Solution..... 183
Figure 64. Box and Violine Plots Depicting Default Mode Functional Connectivity across Feedback-Related Data for the Different Frequency Bands 184
Figure 65. Feedback: Default Mode Network Theta Functional Connectivity Circle Plots..... 185
Figure 66. Feedback: Default Mode Network Alpha 2 Functional Connectivity Circle Plots .. 186
Figure 67. Box and Violine Plots Depicting Salience Network Functional Connectivity across Feedback-Related Data for the Different Frequency Bands 188
Figure 68. Feedback: Salience Network Theta Functional Connectivity Circle Plots..... 189
Figure 69. Feedback: Salience Network Alpha 2 Functional Connectivity Circle Plots 190
Figure 70. Box and Violine Plots Depicting Control Network Functional Connectivity across Feedback-Related Data for the Different Frequency Bands 192
Figure 71. Feedback: Control Network Theta Functional Connectivity Circle Plots 193
Figure 72. Feedback: Control Network Alpha 2 Functional Connectivity Circle Plots 194
Figure 73. Box and Violine Plots Depicting DMN Functional Connectivity across Stimulus-Related Data for the Different Frequency Bands..... 196
Figure 74. Stimulus Period: Default Mode Network Theta Functional Connectivity Circle Plots 197
Figure 75. Stimulus Period: Default Mode Network Alpha 2 Functional Connectivity Circle Plots..... 198
Figure 76. Box and Violine Plots Depicting SN Functional Connectivity across Stimulus-Related Data for the Different Frequency Bands..... 200
Figure 77. Stimulus Period: Salience Network Theta Functional Connectivity Circle Plots 201
Figure 78. Stimulus Period: Salience Network Alpha 2 Functional Connectivity Circle Plots. 202
Figure 79. Box and Violine Plots Depicting Control Network Functional Connectivity across Stimulus-Related Data for the Different Frequency Bands 204
Figure 80. Stimulus Period: Control Network Theta Functional Connectivity Circle Plots..... 205
Figure 81. Stimulus Period: Control Network Alpha 2 Functional Connectivity Circle Plots .. 206
Figure 82. Box and Violine Plots Depicting Default Mode Network Functional Connectivity across Pre-stimulus Data for the Different Frequency Bands..... 208
Figure 83. Pre-stimulus Period: Default Mode Network Theta Functional Connectivity Circle Plots..... 209
Figure 84. Pre-stimulus Period: Default Mode Network Alpha 2 Functional Connectivity Circle Plots..... 210
Figure 85. Box and Violine Plots Depicting Salience Network Functional Connectivity across Pre-stimulus Data for the Different Frequency Bands..... 212
Figure 86. Pre-stimulus Period: Salience Network Theta Functional Connectivity Circle Plots 213
Figure 87. Pre-stimulus Period: Salience Network Alpha 2 Functional Connectivity Circle Plots 214
Figure 88. Box and Violine Plots Depicting Control Network Functional Connectivity across Pre-stimulus Data for the Different Frequency Bands..... 216

Figure 89. Pre-stimulus Period:Control Network Theta Functional Connectivity Circle Plots. 217
Figure 90. Pre-stimulus Period: Control Network Alpha 2 Functional Connectivity Circle Plots 218
Figure 91. Violin Plot for Theta FC Across Networks by Group 220
Figure 92. Violin Plot for Alpha 2 FC Across Networks by Group 222
Figure 93. Feedback: Theta FC Top Ten Within Default Mode Network Connections 224
Figure 94. Feedback: Theta FC Top Ten Within Salience Network Connections 227
Figure 95. Feedback: Theta FC Top Ten Within Control Network Connections 230
Figure 96. Feedback: Alpha 2 FC Top Ten Within Default Mode Network Connections 233
Figure 97. Feedback: Alpha 2 FC Top Ten Within Salience Network Connections 236
Figure 98. Feedback: Alpha 2 FC Top Ten Within Control Network Connections 239
Figure 99. Stimulus: Theta FC Top Ten Within Default Mode Network Connections 242
Figure 100. Stimulus: Theta FC Top Ten Within Salience Network Connections 245
Figure 101. Stimulus: Theta FC Top Ten Within Control Network Connections 248
Figure 102. Stimulus: Alpha 2 FC Top Ten Within Default Mode Network Connections 251
Figure 103. Stimulus: Alpha 2 FC Top Ten Within Salience Network Connections 254
Figure 104. Stimulus: Alpha 2 FC Top Ten Within Control Network Connections 257
Figure 105. Pre-stimulus: Theta FC Top Ten Within Default Mode Network Connections 260
Figure 106. Pre-stimulus: Theta FC Top Ten Within Salience Network Connections 263
Figure 107. Pre-stimulus: Theta FC Top Ten Within Control Network Connections 265
Figure 108. Pre-stimulus: Alpha 2 FC Top Ten Within Default Mode Network Connections . 268
Figure 109. Pre-stimulus: Alpha 2 FC Top Ten Within Salience Network Connections 271
Figure 110. Pre-stimulus: Alpha 2 FC Top Ten Within Control Network Connections 274
Figure 111. Correlation Plot for Feedback Period Global Microstate Variables, Functional Connectivity, and IQ for FXS only 285
Figure 112. Correlation Plot for Feedback Period Individual Microstate Class Variables and Functional Connectivity for FXS only 286
Figure 113. Correlation Plot for Stimulus Period Microstates, Functional Connectivity, and IQ 288
Figure 114. Correlation Plot for Stimulus Period Individual Microstate Class Variables and Functional Connectivity 289
Figure 115. Correlation Plot for Pre-stimulus Period Microstates, Functional Connectivity, and IQ 291
Figure 116. Correlation Plot for Pre-stimulus Period Individual Microstate Class Variables and Functional Connectivity 292
Figure 117. Correlation Plot for Feedback Period Global Microstate Variables, Functional Connectivity, and ABC 294
Figure 118. Correlation Plot for Feedback Period Global Microstate Variables, Functional Connectivity, and Vineland-3 295
Figure 119. Correlation Plot for Feedback Period Global Microstate Variables, Functional Connectivity, and KiTAP 296
Figure 120. Correlation Plot for Stimulus Period Global Microstate Variables, Functional Connectivity, and ABC 299
Figure 121. Correlation Plot for Stimulus Period Global Microstate Variables, Functional Connectivity, and Vineland-3 300

Figure 122. Correlation Plot for Stimulus Period Global Microstate Variables,, Functional Connectivity, and KiTAP 301
Figure 123. Correlation Plot for Pre-stimulus Period Global Microstate Variables, Functional Connectivity, and ABC 303
Figure 124. Correlation Plot for Pre-stimulus Period Global Microstate Variables, Functional Connectivity, and Vineland-3 304
Figure 125. Correlation Plot for Pre-stimulus Period Global Microstate Variables, Functional Connectivity, and KiTAP 305

CHAPTER FOUR

Figure 126. Frontocentral channel selection used to compute chirp task values 337
Figure 127. Chirp Time-Frequency Plots Depicting Group-Level ITC and ERSP 343
Figure 128. Model 1 Fitness Progression Over All Generations 344
Figure 129. Confusion Matrix for Model 1 345
Figure 130. Model 2 Fitness Progression Over All Generations 349
Figure 131. Confusion Matrix for Model 2 350

APPENDICES

Figure A1. Relative Power Spectrum Depicting Peak Alpha Frequency Between Groups Broken Down by Sex 401

Figure B1. Frontal Difference Wave 402
Figure B2. Central Difference Wave 403

Figure C1. Correlations Between Model 1 EEG Composite and Cognitive-Related Clinical Variables 404
Figure C2. Correlations Between Model 1 EEG Composite and Vinland Subscale Scores 405
Figure C3. Correlations Between Model 1 EEG Composite and ABC Subscale Scores 406

Figure D1. Correlations Between Model 2 EEG Composite and Cognitive-Related Clinical Variables 407
Figure D2. Correlations Between Model 2 EEG Composite and Vinland Subscale Scores 408
Figure D3. Correlations Between Model 2 EEG Composite and ABC Subscale Scores 409

List of Tables

CHAPTER ONE

Table 1. Clinical Measures by Group 24
Table 2. Source Nodes Used for Each Functional Network 33
Table 3. Individual Microstate Class-Specific Variable Descriptive Statistics for the 4MS Solution 47
Table 4. Individual Microstate Class-Specific Variable Descriptive Statistics for the 4MS Solution 53
Table 5. Independent Samples Mann-Whitney U Results for Top FC Sum Scores 76
Table 6. Mann-Whitney U Test results for Frontal Absolute Power across Frequency Bands ... 78
Table 7. Mann-Whitney U Test results for Frontal Relative Power across Frequency Bands 79
Table 8. Mann-Whitney U Test results for Posterior Absolute Power across Frequency Bands 81
Table 9. Mann-Whitney U Test results for Posterior Relative Power across Frequency Bands.. 82
Table 10. Spearman's Correlations between FMRP and EEG Variables of Interest 84
Table 11. KiTAP Group Differences 101

CHAPTER TWO

Table 12. Feedback-Related Microstate Solution Mann-Whitney U Test Results for Individual Microstate Classes 172
Table 13. Stimulus-Related Microstate Solution Mann-Whitney U Test Results for Individual Microstate Classes 176
Table 14. Pre-Stimulus Microstate Solution Non-Parametric Individual Microstate Pairwise Comparisons 180
Table 15. Pre-Stimulus Microstate Solution Mann-Whitney U Test Results for Individual Microstate Classes 182

CHAPTER THREE

Table 16. Mann-Whitney U Results for Model 1 Individual Selected Features 347
Table 17. Mann-Whitney U Results for Model 2 Individual Selected Features 351

ABSTRACT

Fragile X Syndrome (FXS) is a rare, neurodevelopmental disorder stemming from a single gene mutation leading to cognitive disruptions, anxiety, sensory hypersensitivity, and other distressing clinical symptoms. Individuals with FXS have moderate-to-severe intellectual disability (ID), representing the most common single gene cause of ID, which impacts quality of life and day-to-day activities. At present, no treatment exists to target the underlying pathophysiology of FXS, and cognitive symptoms are vastly understudied relative to their impact on the patient population. The current set of studies aimed to identify targetable mechanisms contributing to functional disruptions in frontoparietal networks supporting cognitive function and other hallmark features in FXS. The use of a performance-based cognitive task to explore network connectivity disruptions is an underutilized approach in FXS research programs and the current study is the first to report on neural dynamics underlying cognitive performance. The ability to assess functional networks during a task indexing cognitive performance is novel and informs network disruptions related to clinical features that are most impactful to individuals with FXS and their families. The concept of functional time windows that vary by context as a method for reducing heterogeneity for translational target development is timely, given the most recent clinical trial failures on metabotropic glutamate receptor 5 (mGluR5) antagonists, an area in which there are a multitude of preclinical papers showing an overall effect (Berry-Kravis, 2022; Erickson et al., 2017). The application of this concept to understanding when specific network impairments are most relevant and how they vary across individuals with FXS may help elucidate treatment-target alignment that is more similar across species than current behavioral outcomes. The current study identified robust differences on both neurodynamic and more global measures of neural network function across tasks, which may serve as useful biomarkers in both

future and ongoing studies. Furthermore, findings provided critical mechanistic insight into underlying functional network disruptions in FXS, which allowed for a greater understanding of neural mechanisms contributing to cognitive disruptions in FXS. Ultimately, features from the current analyses achieved excellent to perfect diagnostic classification performance, where features and feature combinations from the current studies were more robust to heterogeneity, thus less affected by systemic sources of heterogeneity inherent to FXS. Overall, the current results provide insight into what aspects of neurophysiology are more adaptive and which are less amenable to change leading to mechanistic targets that may meaningfully translate to effective interventions for characteristic features of FXS.

CHAPTER ONE: General Background

Fragile X Syndrome (FXS) is a monogenic neurodevelopmental disorder (NDD) caused by a cytosine-guanine-guanine (CGG) trinucleotide expansion (≥ 200 CGG repeats) in the 5' untranslated region of the Fragile X messenger ribonucleoprotein 1 (*FMR1*) gene. Starting at 200 repeat counts the repeat expansion becomes unstable, leading to the attraction of methyl groups (i.e., carbon-hydrogen bonded pairs) which block the promoter region, causing partial or full silencing of the gene (Salcedo-Arellano et al., 2020; Figure 1). Methylation of *FMR1* reduces or prevents transcription of *FMR1*-related messenger RNA (mRNA) and, therefore, impacts the production of Fragile X messenger ribonucleoprotein (FMRP), which has widespread negative effects on neural function. Specifically, loss or reduction of FMRP leads to abnormal synaptic maturation, decreased protein synthesis regulation, and ultimately reduces the capacity to flexibly modulate synaptic strength to support cognition (Huebschman et al., 2020; Kao et al., 2010; Park et al., 2008). FMRP is an RNA binding protein that has a wide range of targets and performs numerous roles necessary for both the specialized properties of neurons and the eukaryotic properties. Briefly, FMRP acts at multiple levels of gene expression, functioning primarily as a translational suppressor, but also influencing RNA transport, alternative splicing, and chromatin modification by working in concert with other proteins. Additionally, FMRP can bind to various proteins to form unique protein-protein complexes that vary by cell type and allow for the diversification of FMRP function within a cell, enabling wider context-specific FMRP activity (Richter & Zhao, 2021). As a result, the loss or reduction of FMRP has a large and variable impact on the inner workings of neurons in FXS and both the corresponding functional network formation and activity. Particularly, the impacts of reduced FMRP on synaptic plasticity in hippocampal and cortical networks within frontoparietal and temporal

regions are related to impairments in social processing and general cognitive skills, including cognitive flexibility, influenced by striatal activity in FXS (Huebschman et al., 2020).

Figure 1.

Fragile X Syndrome Genetics

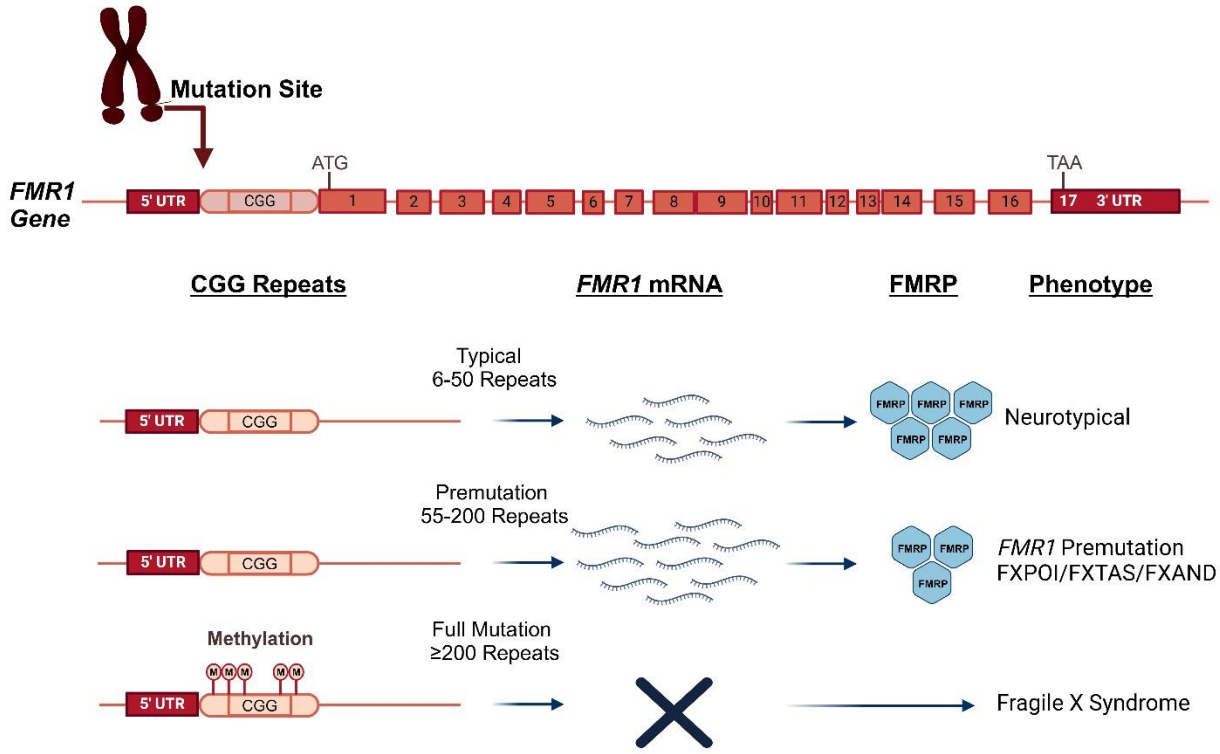

Note. Figure depicts the X chromosome with the location of *FMR1* and the mutation site on the gene (5' untranslated/promotor region). The next three rows contain phenotypes associated with CGG repeat count in the promotor region of *FMR1*: 1) Neurotypical: typical CGG repeat count (6-50), typical mRNA production, and typical FMRP; 2) *FMR1* premutation: 55-200 repeats, increased mRNA output, and reduced FMRP; 3) FXS: 200 or more CGG repeats, no mRNA, no FMRP. Created with Biorender.com.

Clinically, FXS is characterized by intellectual disability (ID), sensory hypersensitivity, executive function (EF) impairments (i.e., difficulties with alertness, attention, flexibility, and behavioral inhibition), heightened anxiety and irritability, and behavioral features of autism spectrum disorder (ASD) – resulting in a co-diagnosis in 50% of males and 20% of females

(Ciaccio et al., 2017; Salcedo-Arellano et al., 2020; Schmitt et al., 2019; 2022). Cognition impairments and anxiety are among the most distressing symptoms for patients with FXS and their families, resulting in frequent clinic visits (Abbeduto et al., 2019; Weber et al., 2019). However, whether ID/cognitive impairments and other characteristic features like anxiety, sensory hypersensitivity, and hyperactivity have similar or distinct neurobiological underpinning in FXS is widely understudied, despite recent advancements in the field demonstrating notable relationships between these features and disruptions in frontoparietal and temporal areas (Schmitt et al., 2022; Reisinger et al., 2020; Thurm et al., 2020; Ethridge et al., 2016; 2017; 2019). In particular, the functional effects of synaptic plasticity changes in frontal and temporal regions found at the cellular level have not been systematically investigated in human subjects (Huebschman et al., 2020). Further, the inability to parse co-occurring behavioral characteristics from ID/cognitive impairments makes it difficult to trace the physiological sources of these symptoms, thus impeding progress in delineating symptoms for tailored treatment development (Thurm et al., 2019).

Recent work in human stem cells showed that FMRP-deficient neurons exhibit neurite growth deficits which reduced neuronal network connectivity (Utami et al., 2020). Humans with FXS exhibit similar functional connectivity (FC) disruptions and physical neural abnormalities to those noted in animal models (e.g., atypical white matter tracks in brain areas necessary for speech and cognitive function), which are hypothesized to underlie cognitive impairments and other characteristic features of FXS (Gothelf at al., 2008; Haas et al., 2009; Huebschman et al., 2020). However, limited consensus on biological mechanisms and reduced translation to meaningful treatment options has heightened the need for researchers to seek more translational neurophysiological measures of cognition, such as those from electroencephalography (EEG), to

better understand the functional consequences of the disorder (Berry-Kravis, 2022; Ewen et al., 2019). EEG is highly scalable for clinical use in FXS where both the development and use of EEG biomarkers provide mechanistic insights into the underlying pathophysiology of FXS in a more direct way relative to behavioral measures, particularly when paired with clinical trials where the known mechanisms of drugs provide molecular insight into neurophysiology measurable with EEG (Berry-Kravis, 2022; Norris et al., 2024). While past EEG biomarkers are highly informative, most are based on averages and make use of the fast Fourier transform (FFT) method or equivalent, which assumes stationarity of the signal. Evaluating the feasibility of biomarkers that capture more dynamic neural activity and how they relate to FFT-based methods may allow for novel insight into FXS and targets for therapeutic intervention. In particular, the use of EEG for studying the dynamics of functional networks may help further bridge the gap between cellular disruptions and clinical features where the addition of a functional network framework may support a better understanding of cognitive disruptions in FXS and create novel avenues forward for translational investigation of network disruptions at the cellular level.

To date, FXS-related disruptions identified using EEG include increased theta power, reduced alpha power, increased gamma power, reduced alpha-to-gamma cross frequency coupling (CFC), increased theta-to-gamma CFC, and increased theta functional connectivity across the scalp (van der Molen et al., 2014; Wang et al., 2017; Pedapati et al., 2022). These robust resting state EEG findings indicate that FXS fail to follow the developmental shift from the predominant use of theta frequency band use to the predominant use of alpha frequency band use in mid-to-late childhood (Cellier et al., 2021). A resulting hypothesis from these findings states that increased theta power and the significant CFC relationship between theta and gamma indicate the compensatory use of theta to maintain evolutionarily necessary inhibitory dynamics

typically allocated to alpha oscillations (Wang et al., 2017). As a result, individuals with FXS may exhibit a decreased ability to functionally regulate neural networks in the low frequency bands contributing to localized hyperexcitability and reduced modulation of excitatory and inhibitory inputs (Mc Devitt et al., 2015).

Neural systems are remarkably complex and the balance of dynamics at multiple levels is required to produce optimized cognition and complex behavior (Papo & Buldu, 2024). Broadly, higher order cognition and behavior are produced by functional networks that arise from the organized and concerted efforts of anatomically distinct brain regions. As disruptions occur at multiple levels of neural function in FXS, functional network disruptions may represent a conglomeration of both consequences of FMRP loss and epigenetic modifications to compensate for protein loss (Contractor et al., 2015). As a result of aberrant excitatory/inhibitory dynamics, frontoparietal and temporal functional networks disruptions in FXS are probable. Indeed, several previous studies identified frontoparietal and temporal network connectivity issues in FXS which additionally demonstrated associations with clinical indications of reduced higher-order cognitive functions (i.e., executive dysfunction) and decreased capacity to process auditory stimuli, respectively (Gildin et al., 2022; Hall et al., 2013; Liang & Mody, 2022; Mc Devitt et al., 2015; Norris et al., 2022; Schmitt et al., 2022; van der Molen et al., 2014). As such, disruptions to functional networks may more closely relate to core, externally observable FXS clinical features over EEG variables classically computed from resting state EEG. Understanding the dynamic temporal aspects of functional disruptions in frontoparietal and temporal networks in FXS will improve the field's mechanistic understanding of neural contributions to cognitive function as distinct from other characteristic features of FXS, and thus provide enhanced targets for therapeutic interventions. Examining functional networks during active cognition may also be

more relevant or closely related to clinical concerns over typical resting state analyses, as cognitive tasks drive specific and consistent brain states beyond what resting state tasks capture.

To address whether functional network dynamics are disrupted in FXS and whether they relate to core cognitive symptoms, I conducted three studies to evaluate functional network connectivity within three robust neural networks described in the functional magnetic resonance imaging (fMRI) literature and further evaluate whether another more dynamic EEG measure captures similar functional network dynamics. Chapter two focused on these metrics using resting state EEG data, where resting state paradigms are more easily implementable in FXS clinics, as they are less invasive and more manageable for FXS participants. Chapter two also introduced the concept of using a computationally simpler measure of global brain activity, microstates – an analysis of quasi-stable brain states, as a potential proxy for functional network connectivity to enhance translational potential. Chapter three utilized a deterministic reversal learning task (i.e., cognitive task) adapted to EEG for FXS and used the same analyses from chapter two to evaluate both functional networks during active cognition, novel in FXS, and to test whether functional network dynamics were related to measures of reduced cognitive ability. Finally, for chapter four, these features were all submitted to a data-driven classification algorithm to determine the predictive capacity of cognitive features in FXS. The use of a performance-based cognitive task to explore network connectivity disruptions is an underutilized approach in FXS research programs, as the behavioral component often poses a challenge for participants (Schmitt et al., 2023). The current study also provided evidence of the feasibility of such research paradigms for FXS, which may extend to other populations with moderate-to-severe intellectual disability. The ability to assess functional networks during a task indexing cognitive performance was novel and informed network disruptions related to clinical features

that impact individuals with FXS and their families most. The concept of contextual functional time windows for pathophysiological impact as a method for reducing heterogeneity for translational target development was also novel and timely, given the most recent clinical trial failures on mGluR5 antagonists, an area in which there are a multitude of preclinical papers showing overall effect (Berry-Kravis, 2022; Erickson et al., 2017). The application of this concept to understanding when specific network impairments are most relevant and how they vary across individuals with FXS is novel and may elucidate treatment target alignment that is more similar across species than current behavioral outcomes. The use of a functional network framework is also novel, particularly the use of specific models hypothesizing disruptions to the dynamics between functional networks. Functional connectivity within these functional networks is also highly novel in FXS where comparisons between resting state and active cognition will inform the degree to which individuals with FXS are able to mobilize these networks, in addition to task-specific disruptions. Given functional network disruptions are more clinically relevant than other EEG metrics, particularly functional network dynamics during active cognition, the improved capacity to parse features of FXS and their neural underpinning provides access to new biomarkers and mechanistic targets that may meaningfully translate to effective interventions for characteristic features of FXS. Finally, the combination of variables across EEG tasks allowed for the novel investigation of which features are most predictive of the FXS phenotype. The variable combinations identified may eventually provide more insight into shared physiological disruptions between different EEG metrics leading to mechanistic insight into robust EEG outcomes in FXS.

The current set of studies reflect ongoing efforts in the field to use high density EEG in FXS to develop effective biomarkers for therapeutic applications (i.e., clinical trials and non-

invasive therapeutic interventions) and to utilize those targets transspecies to better understand the mechanisms of FXS and how interventions interact with those mechanisms. Specifically, analysis of frontoparietal and temporal networks from both resting state and a cognitive flexibility EEG task will improve our mechanistic understandings of neural contributions to cognitive function as distinct from other characteristic features of FXS, and thus provide enhanced targets for therapeutic interventions.

CHAPTER TWO

Microstates as a Proxy for Disruptions in Fragile X Resting-State Functional Neural Networks

Key Words:

Fragile X Syndrome; resting state; EEG; microstates; functional connectivity; biomarker

Abstract

Fragile X Syndrome (FXS) is a rare single gene neurodevelopmental disorder caused by a trinucleotide repeat expansion of CGG in the promoter region of the *FMR1* gene, located on the X chromosome. The repeat expansion attracts methyl groups which block the promoter and prevent transcription of the gene leading to a reduction or loss of Fragile X Messenger Ribonucleoprotein (FMRP). Clinically, FXS is characterized by sensory hypersensitivities, cognitive difficulties – including learning difficulties, and social anxiety. Additionally, FXS is the most common inherited form of intellectual disability (ID) and a monogenic cause of autism spectrum disorder (ASD). The loss of FMRP causes numerous molecular disruptions to typical neuronal function leading to wide ranging disruptions to cellular communication both exogenously and endogenously. Individuals with FXS exhibit increased functional connectivity (FC) abnormalities observed using resting electroencephalography (EEG) related to cognitive impairments and behavioral features of FXS as a consequence of FMRP reduction or loss. The ability to gauge FC disruptions and evaluate their sensitivity to treatment is of high importance to the field, as FC represents disruptions to global neural dynamics in FXS. However, FC, especially FC of source analyzed EEG data, represents a computationally intensive effort which poses challenges for clinical utility. Microstates represent a potential avenue to both explore functional network dynamics and forge a bridge between functional dynamic disruptions and known functional connectivity differences in FXS. To address these gaps, an exploratory case-control approach was used to broadly evaluate both microstates and FC in FXS. A sample of 89 adults 18-36 (41 FXS and 48 age- and sex-match typically developing controls) participated in a resting state EEG task. Data were then submitted to 1) a microstate analysis, 2) source localized and submitted to a FC analysis to evaluate theta (4-7 Hz) and alpha (8-13 Hz) FC within functional networks of interest. Results from the current

study ultimately supported previous conclusions related to the clinical significance of microstates in FXS. Specifically, both average global field power (GFP) and individual microstate class GFP were elevated in FXS and mapped onto meaningful clinical measures of cognitive performance and adaptive behavior. Next, the FC analyses identified elevated within-network theta FC in core functional networks in FXS that also correlated with IQ where increased theta FC in FXS may represent disruptions to long range information transfer. However, correlation analysis did not identify meaningful overlaps between FC and microstates. Different methodology overcoming the differences in timescales is required to accurately determine the relationship between microstates and FC, representing a future direction. The current results add support to previous microstate and FC findings in the field and further supports conclusions related to the clinical relevance of microstates and elevated theta FC in FXS while adding novel insight into theta FC by identifying disruptions within specific functional networks. As theta frequency band dynamics are important for cognition, the diffuse increases may provide insight into cognitive disruptions related to functionally-relevant long-range information transfer in FXS. In conclusion, the current study considers both microstate and FC disruptions and offers a multi-level electrophysiological profile of FXS that will support future efforts to: 1) determine whether microstate dynamics represent underlying functional network disruptions to where microstates can serve as a proxy for FC disruptions and 2) determine the translational potential of FC and microstates as biomarkers in FXS by gauging sensitivity to interventions.

Background

Fragile X Syndrome (FXS) is the most common single gene cause of intellectual disability (ID) where cognitive disruptions associated with ID represent challenges to individuals with FXS and their families (Weber et al., 2019). Chief among cognitive symptoms are disruptions to cognitive flexibility from which numerous behavior challenges arise (Schmitt et al., 2023; Weber et al., 2019). However, despite the distressing nature of cognitive disruptions and their impact to daily living, cognitive features of FXS represent an area of slower progress in the field due to the difficult nature of studying cognition in FXS populations (Hessl et al., 2019; Schmitt et al., 2023). The use of electroencephalography (EEG) as a tool to study neurophysiology in FXS is highly scalable for translational purposes allowing for the investigation of neural network activity disruptions as a function of FMRP loss; the millisecond precision of EEG also allows for dynamic evaluation of network activity and measurement of cognitive processes at the temporal level at which they occur. As such, EEG may represent a feasible tool for studying functional network activity during active cognitive tasks that rely on synaptic efficiency and flexibility. At present, EEG studies in FXS have produced a variety of measures that share relationships with clinical measures of intellectual function (Norris et al., 2025; Schmitt et al., 2022; Pedapati et al., 2022; Takarae et al., 2024). While EEG may provide more insight into the neurophysiological mechanisms contributing to cognitive symptoms – particularly cognitive flexibility, the use of cognitive tasks in FXS represents a recent advancement where the translation of these tasks to EEG remains difficult (Hessl et al., 2019; Schmitt et al., 2023; Shields et al., 2020). Further evaluating resting state EEG and applying a functional network framework which can be further tested using cognitive EEG tasks represents a reasonable approach to addressing challenges related to studying cognition in FXS. By

evaluating the resting dynamics of functional networks in FXS and finding appropriate biomarkers to reflect changes in dynamic neural network communication, the field can start exploring identified dynamics in the context of more complex tasks to better understand how disruptions to these dynamics impact task-positive processing (i.e., cognitive processes and behavior) when driving specific and consistent brain states.

Several robust resting state EEG findings in FXS point to functional network disruptions. First, increased gamma frequency band activity is well-documented in FXS across *in vivo* slice, *Fmr1*$^{-/-}$ mouse, and human studies, and may reflect network hyperexcitability and decreased regulation of individual networks by lower frequency bands (i.e., alpha) (Schmitt et al., 2022; Ethridge et al., 2017). Atypical frequency band activity in FXS is linked to disruptions in frontoparietal connectivity across multiple large-scale functional networks (e.g., "control" network, salience network, default mode network, etc.) and proposed to underlie FXS symptoms (Pedapati et al., 2022). The "control" network, the salience network, and the default mode network are of increasing interest in FXS, as recent work has either found disruptions or provided results alluding to disruptions in each network (Cohen et al., 2015; Hall et al., 2013; Pedapati et al., 2022). Further, the three comprise a network model hypothesized to underlie neural flexibility when shifting from more inward focused neural activity into patterns of activation that support cognition and active, external engagement (Menon, 2011; 2018). The "control" network, also known as the lateral frontoparietal (L-FPN) network and the central executive network (CEN), is comprised of the dorsolateral prefrontal cortex (dlPFC) and the posterior parietal cortex, which work together to accomplish higher-order cognitive functions and task-positive processing, including sustained attention and working memory (Dosenbach et al., 2006). The salience network (SN) is a large-scale neural network responsible for detecting

and directing cognitive resources toward more salient stimuli, as well as recruiting other relevant functional networks (Menon, 2018). The SN includes parts of the insular cortex, anterior cingulate cortex (ACC), the amygdala, and the temporal poles. SN activity, particularly from the anterior insula, dorsal and medial ACC, and the amygdala, contributes to social behaviors, expressive and receptive language, and integration of information across sensory, limbic, and cognitive domains (Ma et al., 2021; Schimmelpfennig et al., 2023; Seeley et al., 2007; Xu et al., 2019). Decreased alpha FC within the SN is associated with high trait anxiety and may play a role in mood dysregulation, broadly (Massullo et al., 2020). Brain regions in both SN and frontoparietal regions are involved in cognitive flexibility and response switching, both of which are disrupted in FXS (Chan et al., 2022; Dajani et al., 2015; Schmitt et al., 2022). Finally, the default mode network (DMN) is responsible for task-negative processing, internal thoughts/mentalization, and low effort cognitive processing (e.g., word reading) (Li et al., 2014; Weber et al., 2022). The DMN is made up of the posterior cingulate cortex, precuneus, and ventromedial prefrontal cortex (vmPFC) where the overlap in activation with other large-scale brain networks related to external processing highlights the complex role of DMN in cognition (Schimmelpfennig et al., 2023). Increases in gamma activity are typically associated with DMN, but the inability to regulate gamma by low frequency activity is associated with an inability to switch out of DMN effectively making it reasonable to hypothesize that flexible network shifting is disrupted in FXS based on documented disruptions to DMN and the robust observation of elevated gamma (Nair et al., 2018).

Functional network disruptions are related to cognitive symptoms in other neuropsychiatric conditions, like schizophrenia and ASD, which share global neural features with FXS (Adhikari et al., 2019; Matlis et al., 2015). A meta-analysis of functional magnetic

resonance imaging (fMRI) studies in schizophrenia found robust and consistent patterns of resting-state and cognitive functional network disruptions. Further, these disruptions were related to variations in cognitive performance on tasks primarily assessing processing speed and working memory. Of note, SN, auditory somatosensory network, and DMN exhibited the strongest relationships with measures of cognitive performance and all findings were unrelated to current medication use or symptom severity (Adhikari et al., 2019). Disruptions to the aforementioned functional networks are also detectable using EEG where reduced DMN connectivity during a passive auditory task corresponded to worse cognitive performance (e.g., worse sustained attention and working memory) and more severe negative symptoms during the first schizophrenia episode (Guha et al., 2024). Noting relationships between functional network disruptions and cognition in schizophrenia is important, as the physiological etiology of cognition impairment in schizophrenia partially stems from the excitatory/inhibitory imbalance resulting from the disruptions to both GABAergic and glutamatergic signaling, both of which are known to be disrupted in FXS (Lui et al., 2022; McCutcheon et al., 2023).

Individuals with ASD also exhibit functional network disruptions observed using source localization methods on EEG data in DMN, sensorimotor network, and the dorsal attention network (DAN) which works with the control network to accomplish external tasks requiring attention. Further, they identified disruptions in alpha related to the posterior cingulate cortex, the precuneus, and the medial frontal gyrus as part of these functional disruptions (Wantzen et al., 2022). Whether there is hyper- or hypoconnectivity in ASD is currently debated in the field where some believe the variability in connectivity patterns is due to development (i.e., age of sample). There are not strong links between FC patterns of the functional networks and cognitive symptoms in ASD, but some have noted a relationship between FC patterns in the core resting

state networks and social cognition. While functional network outcomes are more complex in ASD, likely due to the variable underlying genetic etiologies, one study using fMRI found evidence of hyperconnectivity in DMN, SN, and control network in children with ASD but only in DMN and the cerebellum in adults where all networks play some role in social cognition (Haghighat et al., 2021; Rylaarsdam & Guemex-Gamboa, 2019). However, the ASD samples in both Wantzen et al. (2022) and Haghighat et al. (2021) had typical IQ levels, which potentially suggests the link between functional network disruptions and cognitive symptoms in both FXS and schizophrenia are related to circuitry disruptions that impact cognition, broadly. A recent review of network alterations in FXS from functional neural imagining studies highlighted core disruptions to DMN, SN, and control network (Venetucci Gouveia et al., 2025).

Individuals with FXS exhibit a decreased ability to functionally regulate neural networks contributing to localized hyperexcitability and reduced modulation of excitatory and inhibitory inputs (Mc Devitt et al., 2015; van der Molen et al., 2014). The hyperexcitable phenotype stems from 3 primary functional changes including elevated numbers of excitatory synapses due to abnormal synaptic connectivity and the way synaptic connectivity changes in context dependent ways, impaired inhibitory neuron function (e.g., wide-ranging PV+ interneuron disruptions) leading to an excitatory/inhibitory imbalance, and alterations to ion channel function and expression (Juarez et al., 2024; Lui et al., 2022). FC assessments using EEG in FXS evaluated functional connectivity in frequency bands [i.e., delta (1-3 Hz), theta (4-7 Hz), alpha (8-13 Hz), beta (13-30 Hz), and gamma (31-80+ Hz)] both within and between brain regions using sensor-level data and also evaluated disruptions to FC as they pertained to cognitive and behavior features (e.g., EF; van der Molen et al., 2014; Schmitt et al., 2022). The past studies in FXS found reduced long-range FC in alpha and beta frequency bands and increased short-range FC in

the gamma band with inconsistencies in reports of theta band connectivity in FXS (van der Molen et al., 2014; Wang et al., 2017; van der Molen & van der Molen, 2013). A recent study also identified evidence of reduced FC using source analyzed data and network nodes related to disrupted thalamocortical modulation of local hyperexcitability (i.e., increased gamma power), which may drive abnormal cortical states (Pedapati et al., 2022). Pedapati et al. (2022) also investigated peak alpha frequency (PAF; i.e., the single, most utilized frequency in the alpha range, which varies by individual), which is found to track linearly with IQ (Angelakis et al., 2004). PAF at the sensor level was related to increased severity of anxiety in FXS and altered frontal connectivity (e.g., increased gamma, reduced alpha) associated with increased error rates on EF tasks (e.g., KiTAP subtests) suggesting disruptions to both gamma and alpha play a role in impaired cognitive processes in FXS and implicate both broad frontoparietal disruptions and, more specifically, control network difficulties in FXS (van der Molen et al., 2014; Pedapati et al., 2022; Schmitt et al., 2022). Alpha and gamma abnormalities are also related to sensory processing difficulties and thus could underlie salience network (SN) disruptions (Norris et al., 2022; Ethridge et al., 2016; 2017; 2019). Dynamic utilization of alpha in frontal cortices was assessed in FXS in the form of both frequency and duration of time-varying alpha "bursts", which capture brief increases in alpha power that may be functionally relevant. Efforts to evaluate alpha in a more dynamic way identified right hemisphere difficulties in dynamic alpha band utilization, specifically reduced burst frequency, related to increased sensory hypersensitivity, behavioral inflexibility, and social communication difficulties (Norris et al., 2022). Frontal right hemisphere sources for alpha dysregulation may reflect a mechanism similarly noted in ASD related to autistic symptomology and linked to frontoparietal network disruptions, suggesting cognitive flexibility could be related to alpha band utilization (Aykan et

al., 2022; Carrillo-de-la-Pena & Garcia-Larrea, 2007; Chan et al., 2022; Dawson et al., 1995; Maxwell et al., 2015; Yuk et al., 2020). Finally, these dynamic alpha bursts were evaluated in a cross-species study aiming to characterize alpha in the *Fmr1*$^{-/-}$ mouse in which alpha dynamics were successfully identified when evaluated occipitally (Kornfeld-Sylla et al., 2025). Excitingly, the cross-specific results were comparable to dynamics highlighted in Norris et al. (2022) from sensor level data for males with FXS.

Assessing individual functional networks in FXS and their link to both known atypical frequency band activity and clinical features, especially cognitive performance, is the logical next step. Again, past work in FXS only evaluated the relationship between FC computed on resting state EEG data, as opposed to during active cognition, where disruptions in FC were linked to cognitive performance using clinical measures (i.e., IQ, KiTAP; Schmitt et al., 2022). Evaluating biomarkers that index functional network performance could provide a critical understanding of disrupted neural networks and how they relate to the symptoms of FXS that are most distressing for patients and their families (i.e., cognitive impairments; Abbeduto et al., 2019; Weber et al., 2019). However, when translating these findings to clinical implementation, FC measures are computationally intensive and not scalable to everyday use, especially when computing FC on source-localized EEG data to provide more specific insights into which functional networks are driving FC results. The use of more simple EEG metrics, like quasi-stable brain state measures (i.e., microstates) that require less computational complexity may be best for clinical applicability (Pedapati et al., 2022; Hao et al., 2022). Microstates are more easily calculated from EEG data and potentially reflect similar underlying network disruptions indexed by traditional FC measures (D'Croz-Baron et al., 2019; Feng et al., 2005). There are 4 canonical microstate classes (i.e., A, B, C. and D) which represent temporally stable scalp potential fields.

Broadly, microstates A and B correspond to sensory processing networks where microstate C is thought to reflect SN and microstate D is thought to reflect DMN (Antonova et al., 2022; Milz et al., 2016). Though, a recent study evaluating microstates from EEG recording during an arithmetic task found that microstate D was associated with task-positive processing and not microstate C, as would be expected of a microstate representing SN where SN directs attention and recruits brain areas associated with task-positive processing. However, limited studies have evaluated microstates during a task, and it remains possible that microstates reflect context or task-dependent dynamics (Kim et al., 2021). Other studies also identified evidence supporting the link between DMN and the control network to C where D is more associated with the attention network or orienting processes more characteristics of SN (Custo et al., 2017; Seitzman et al., 2018; Zhao et al., 2023). Thus, the current conceptualization is that microstate C represents DMN and microstate D is more a proxy for the SN and/or task-positive processing. Interestingly, Al Zoubi et al. (2024) utilized a data-driven approach to analyze concurrent EEG-fMRI data and evaluate the relationship between the blood-oxygen-level-dependent (BOLD) signal for individual resting state networks and EEG microstates where they concluded microstates represented resting state network transitions rather than individual functional networks which may account for differences in reports on microstates as functional network proxies. Regardless of whether microstates may serve as a 1:1 comparator for functional networks, microstates still provide important spatiotemporal information about functional networks and may allow further insight into network disruptions in FXS.

Evidence suggests that intracortical alpha accounts for the emergence of EEG microstate classes with classes linked to individual global attractor states characterized by selective inhibition of intracortical regions (Milz et al., 2017). Further, a microstate analysis conducted on

local field potential (LFP) recordings from wild-type rats identified the emergence of temporal synchronization across microstates peaking in the theta/alpha range with microstate classes modulated by behavioral state. The microstates were correlated with functional connectivity between the ventral tegmental area (VTA), striatum, and the prefrontal cortex suggesting that microstates capture the interactive temporal dynamics of functional networks with power spectral dynamics predominately oscillating at lower frequencies (i.e., theta and alpha ranges) (Mishra et al., 2021).

Only one study has evaluated microstates in FXS and found significant increases in both mean global field power (GFP; i.e., averaging strength of the electric field at any given point) and the global variance explained (GEV; i.e., total variance in the EEG recording) for canonical microstates C and D compared to typically developing controls (TDC). For microstate D, both mean duration and the occurrence of microstate class D (i.e., time spent in microstate D and the frequency microstate D occurred relative to other microstate classes, respectively) were also increased relative to TDC, suggesting FXS individuals enter microstate D more often and spend more time in D than TDC. The group differences were also significantly related to relevant clinical outcomes. Increased GEV and GFP for microstate C were inversely related to nonverbal IQ scores and increased GFP of microstate D was inversely related to peak alpha. Overall, increases in microstate metrics relative to TDC corresponded to outcomes indicating worse cognitive function as a byproduct of potential network stasis (Takarae et al., 2023). Interestingly, microstate outcomes in ASD do not track with findings in FXS. Overall, microstates A, B, D, E, and F were all found to have elevated instances in ASD and were abnormal across most microstate metrics, but C was reduced compared to TDC (Das et al., 2024; D'Croz-Baron et al., 2019). Microstate E and F are less well characterized and thus interpretations are context

dependent where both classes are more data driven than the microstate classes within the canonical set (Michel & Koenig, 2018). In FXS, microstate occurrences are either elevated relative to TDC or comparable (Takarae et al., 2023). Microstate findings across FXS and ASD suggest that microstates may be specific to differences in global temporal dynamics for FXS compared to idiopathic ASD which may track with functional network differences between the disorders. Further, these differences in microstate outcomes may track with the general differences seen in functional network connectivity patterns in ASD relative to FXS.

Overall, individual microstate classes are likely to correspond to individual functional networks and more easily index specific network disruptions for individual clinical evaluation. Importantly, microstates are translational across species, as microstates also exist in rodents and have been linked to their functional network activity in a recent study (Feng et al., 2005; Megevand et al., 2008; Mishra et al., 2020; Mishra et al., 2021). Microstate measurement is more straightforward than FC in mice given the small head size and limited electrode arrays available for mouse EEG, thus providing a viable cross-species translational measure as a proxy for FC. Given the recent characterization of alpha in the *Fmr1*$^{-/-}$ mouse, microstates are a highly attractive biomarker candidate for translational evaluation (Kornfeld-Sylla et al., 2025). Although EEG has limited spatial resolution relative to fMRI, EEG remains the most cost effective, highly translatable method for biomarker development in NDDs (Megevand et al., 2008). EEG can access neural timescales typically outside of the recording capability of fMRI, allowing for more sensitive analysis of microstates during real-time cognitive processing and evaluation of context-dependent functional impairments in network dynamics. Further, the use of EEG is highly feasible in individuals with FXS across a wide range of ages and impairment levels where EEG testing is well tolerated (Berry-Kravis, 2022; Ethridge et al., 2016; 2017;

2019; Proteau-Lemieux et al., 2021; Wilkinson & Nelson, 2021). Thus, the current study focuses on evaluating neural cortical activity proposed to underlie information exchange between brain areas and how well information collected via EEG about FC disruptions in FXS can inform more computationally optimal biomarker candidates (e.g., microstates) with an emphasis on advanced EEG and data-driven methods building on recent work in the field.

The current study aims to evaluate FXS microstate dynamics in relation to functional network dynamics in order to establish microstates as a proxy for functional network FC disruptions. While the present study is highly exploratory, based on the literature, increased FC disruptions are expected in FXS and I predict those disruptions will map onto specific microstate classes/individual microstate class variables that can guide future studies testing functional network disruptions.

Methods

Participants

The current study used a case-control study design with adults under 36 years of age to minimize developmental and aging-related effects. Participants included 89 total individuals (Aged 18-36 years): 41 FXS participants (15 females) and 48 typically developing controls (TDC; 16 females) that were sex-matched and chronologically age matched with FXS. Age matching was confirmed using a Mann-Whitney U test where age was not significantly different between FXS (*M* rank = 49.57) and TDC (*M* rank = 41.91), $N = 79$, $z = 1.38$, $p = .167$, $r = 15$. All individuals were participating in two National Institute of Health (NIH) funded projects with a third supporting the current analyses under the National Institute for Child Health and Human Development (#K23 HD101416, PI: L. Schmitt; #U54 HD104461, PI: C. Erickson; #F31 HD113221-01, PI: J. Norris). All participants were recruited through Cincinnati Children's

Hospital and Medical Center (CCHMC). FXS participants were recruited through the CCHMC FXS Research and Treatment Center (RTC), directed by Dr. Craig Erickson. All study procedures and project analyses were approved by both the CCHMC Institutional Review Board (IRB) and the University of Oklahoma IRB and carried out according to the guidelines of the Declaration of Helsinki.

FXS participants were included only if they met the following criteria: 1) documented genetic testing (Southern Blot and PCR) confirming FXS diagnosis (i.e., full FMR1 mutations: > 200 CGG repeats) and 2) IQ ≤ 70 according to Stanford Binet 5 for males only (Roid, 2003). Females were allowed to vary in IQ, as that reflected real variability, where males have a mean IQ of 40 with a normal distribution where IQ ≥ 70 would be outliers. Typically developing controls were included only if they did not have FXS and were: 1) in good physical health with no history of psychiatric or neurological disorders, 2) history of typical developmental milestone achievements, 3) negative family history of psychiatric disorders (1st degree relatives), including ASD, and 4) Social Communication Questionnaire (SCQ) score ≤ 8 unless cleared via interview with a licensed clinician (Rutter et al., 2003). Any TDC who fails to meet these four criteria were excluded. Further, all participants were evaluated for and excluded if they: 1) were taking benzodiazepines or antiepileptic medications or any novel potential treatment for FXS (i.e., minocycline) known to affect EEG measures within 4 weeks of testing. Absence of all CNS-active medications was preferred at the time of testing; however, employing the CNS-active medication requirement is not typically feasible in FXS and results in a non-representative sample of the FXS population. Past resting and sensory EEG studies of individuals with FXS have not shown demonstrable effect on neural responses related to antipsychotics, antidepressants, or stimulants (Clementz et al., 2016; Norris et al., 2025).

Participation included both a standard clinical assessment battery and electroencephalography (EEG). Clinical assessment battery was selected based on precedent, as it captures the breadth of the hallmark clinical phenotype of FXS while minimizing burden on caregivers (Table 1). We set *a priori* hypotheses about how neural networks will correspond to specific clinical features derived from specific subscales of the measures listed in Table 1 (e.g., ABC Irritability & Hyperactivity, KiTAP median reaction times, Vineland subscale scores, etc.), but also examined all subscales across measures as exploratory analyses to elucidate potential unexpected relationships (Saggar & Uddin, 2019). Clinical assessments were either conducted by licensed clinicians, trained clinical research coordinators/professionals (i.e., clinician report), or collected from caregivers (i.e., caregiver report).

Clinical Measures

Table 1.

Clinical Measures by Group

Clinical Measure	**FXS**	**TDC**
Autism Diagnostic Observation Schedule – 2 (ADOS) (Gotham et al., 2007; Hus & Lord, 2014)	X	
Stanford-Binet Intelligence Scale, 5th Edition (Roid, 2003)	X	X
Repeatable Battery for Neuropsychological Status (RBANS) (Randolph, 2012)	X	
Test of Attentional Performance for Children (KiTap) (Knox et al., 2012)	X	X
NIH Cognitive Toolbox (Hessl et al., 2016; Shields et al., 2020)	X	X
Social Communication Questionnaire (SCQ) (Rutter et al., 2003)	X	X
Vineland Adaptive Behavior Scale 3rd edition (Sparrow et al., 2016)	X	X
Aberrant Behavior Checklist (ABC) (Aman et al., 1985)	X	X
Anxiety, Depression, & Mood Scale (ADAMs) (Esbensen et al., 2003)	X	X
Adolescent/Adult Sensory Profile (A/ASP) (Brown et al., 2001)	X	X

Note. The first column contains the list of clinical variables included in the standard clinical battery followed by check boxes indicating whether the measure was administered to FXS and TDC, respectively.

Autism Diagnostic Observation Schedule – 2 (ADOS). The ADOS is a clinician administered, semi-structured, and standardized evaluation used to diagnose ASD that includes 5 modules tailored to different developmental ages and varying language levels. Administering the ADOS takes approximately 90 minutes during which the clinician evaluates social interaction abilities, communication, and ability to engage in play or use objects in imaginative ways (Gotham et al., 2007; Hus & Lord, 2014).

Stanford-Binet Intelligence Scale, 5th Edition. The Stanford-Binet is a standardized IQ test which examines cognitive ability in individuals ages 2 – 85+ across 5 primary factors: fluid reasoning, quantitative reasoning, knowledge, visuospatial reasoning, and working memory in both the verbal and non-verbal domains (Roid, 2003). Deviation IQ is preferred in FXS, as typical IQ measures are often not sensitive enough to detect cognitive strengths and weaknesses (Talapatra et al., 2023). Therefore, deviation IQ scores were computed for the present study by using age-dependent raw z-score transformations to compare deviation from standardized norms. Repeatable Battery for Neuropsychological Status (RBANS). The RBANS is a brief measure of cognitive change designed to both measure cognitive decline in aging populations and act as a neuropsychological screener in younger populations. The RBANS evaluates cognition across 5 domains: immediate memory, visuospatial/constructional, language, attention, and delayed memory (Randolph, 2012)

Test of Attentional Performance for Children (KiTAP). The KiTAP is a computer-based test designed to evaluate both attention and behavioral inhibition designed for children and used as a measure of cognitive flexibility (i.e., conflict resolution). The factor structure is based on responses from children between the ages of 6 and 10 and utilizes ghosts, witches, bats, owls, and dragons to maintain engagement. Subtests include assessments of speed or alertness,

flexibility, dividing attention, reaction control (Go/No Go), and visual scanning with additional measures of distractibility, vigilance and sustained attention (Knox et al., 2012).

National Institute of Health (NIH) Toolbox Cognitive Battery (NIH – TCB). The NIH – TCB is a multi-test computer-based assessment of cognitive performance validated to evaluate cognition while minimizing floor and ceiling effects. The battery was also validated in populations with ID to ensure appropriateness for use. The NIH – TCB assesses neurological and behavioral performance in cognitive domains, specifically cognitive flexibility, inhibitory control, visual attention, receptive vocabulary, oral reading, episodic memory, processing speed, and working memory (Hessl et al., 2016; Shields et al., 2020).

Social Communication Questionnaire (SCQ). The SCQ is a screening tool for ASD filled out by caregivers (i.e., caregiver report) that includes 40 questions about behaviors related to autism likely to be observed by caregivers within the past 3 months and across the developmental history/lifetime (Rutter et al., 2003).

Vineland Adaptive Behavior Scale (VABS) 3rd edition. The VABS is an assessment of adaptive behavior used to support diagnoses of ID and developmental delay across domains of communication, daily living skills, socialization, motor skills (for those under 9 years), and maladaptive behaviors (e.g., internalization or externalization) (Sparrow et al., 2016). Measuring adaptive behavior in FXS may be more informative than other measures of cognition and an area where individuals with FXS may continue to exhibit improvements despite low IQs (Bailey et al., 1998, Kaufmann et al., 2004).

Aberrant Behavior Checklist (ABC). The ABC is a 58-item caregiver rated scale designed to evaluate behavior in individuals with ID or developmental delays across 5 domains: irritability, lethargy, stereotypic behavior, hyperactivity, and inappropriate speech (Aman et al.,

1985). The FXS-specific factor structure was identified and used to target FXS-specific behavioral features and symptoms with added specificity (Sansone et al., 2012).

Anxiety, Depression, & Mood Scale (ADAMS). The ADAMS is a 28-item informant report screening tool designed to evaluate symptoms of mood dysregulation (i.e., anxiety, depression, etc.) in individuals with developmental disorders (Esbensen et al., 2003).

Adolescent/Adult Sensory Profile (A/ASP). The A/ASP is a 60-item measure of sensory processing patterns in adolescents and adults across the primary sensory domains including taste/smell (i.e., chemosensory modalities), visual, tactile, auditory, and then also included movement and activity level. The measure further provides subscale scores for sensory processing patterns of low registration, sensation seeking, sensory sensitivity, and sensation avoiding (Brown et al., 2001). The ASP is typically a self-report measure but can be converted to caregiver report for those with intellectual disability.

Procedure

EEG Acquisition. EEG data were acquired using 128-channel MagStim/EGI HydroCel nets with a MagStim/EGI NetAmp 400 Amplifier (Magstim/EGI, Eugene, OR) in either sound-attenuated booths or a clinic space. Data were recorded continuously and sampled at 1000 Hz with saline based electrodes (impedance under ~10 KΩ). Clinical research coordinators utilized practices implemented and optimized at CCHMC to increase participant comfort for individuals with FXS or DD controls. Specifically, the use of evidence-based regulation techniques (e.g., visual schedules, social stories, and visual timers) were used to maximize EEG acquisition success while prioritizing participant comfort. Clinical research coordinators (CRCs) also engaged in co-regulation techniques to help participants reduce anxiety during recording periods.

EEG Tasks. The resting state EEG (rsEEG): Continuous data were recorded for 5 minutes total with eyes open. Participants sat quietly while watching a silent video of their choosing for both comfort and compliance, as done in previous studies (Pedapati et al., 2022; Wang et al., 2017).

EEG Preprocessing. Raw data were preprocessed prior to analysis using EEGLAB 2021.0 in MATLAB 2021b and the Cincinnati Very High Throughput Pipeline (VHTP), a GUI-based EEG cleaning tool that utilizes EEGLAB functions (version 2021b, The MathWorks Inc., Natick, MA, USA; Delorme & Makeig, 2004). Data were filtered from 0.5 Hz to 100 Hz with a 60 Hz notch filter (57 – 63 Hz with harmonics removed up to the Nyquist frequency of the original sampling rate). All EEG data were manually inspected offline for artifacts. During manual inspection, any errant channels, channels containing high amplitude artifact unrelated to physiological sources, or channels containing excessive artifact levels (e.g., high amplitude ocular artifacts or muscle tension) were interpolated (i.e., removed and replaced with an estimation from surrounding sources). No more than 5% of channels were interpolated with efforts made to not interpolate two adjacent channels, unless absolutely necessary, to limit data dependencies. Next, any segments containing high amplitude artifact not corrected with interpolation or that were pervasive throughout most channels were manually rejected (e.g., jaw related muscle tension). Data were then submitted to independent component analysis (ICA) for artifact rejection by artifact pattern type via individual component rejection. During the component removal stage, components containing ocular artifacts, cardiac artifacts, muscle tension, or line noise were removed. After preprocessing, all data were re-referenced to an average of all channels (i.e., average referenced). Files were finalized with manual inspection for remaining artifacts.

Analysis

After the preprocessing stage, data were segmented into 2000 ms epochs where any epochs containing residual artifact exceeding +/- 120 μV were rejected for the purpose of calculating power across frequency bands. Otherwise, data were kept continuous for individual peak alpha, microstate, and functional connectivity analyses.

Microstate Analysis. Microstates were calculated using a modified K-means algorithm to determine the most dominant template maps without polarity inversion in the +microstate toolbox (Tait et al., 2022). Microstates index momentary spatial distributions of the electrical field data quantified using the global field power, a measure of pattern/map strength via spatial standard deviation of electric field potential values at the scalp (Lehmann & Skrandies, 1980). Specifically, local maxima of the GFP curve are used to specify individual classes where maxima are thought to be discrete states of brain activity/EEG data (Khanna et al., 2015). Differences between groups (i.e., FXS and TDC) and sexes on microstate class: mean duration, frequency of individual microstate class occurrence per second (occurrence), and percentage of time spent within a microstate (coverage) were all evaluated to determine which microstates were meaningfully related to FXS pathophysiology. Group differences were also assessed across a series of microstate solution global measures, including: 1) global explained variance (GEV; i.e., how well a given template describes the whole dataset), 2) average global field power, 3) complexity (i.e., measure of microstate transition behavior), and 4) the Hurst exponent (i.e., time series memory measure which provides an index of long-range dependence) (D'Croz-Baron et al., 2019; Milz et al., 2017; Mishra et al., 2020; Tait & Zhang, 2022). Relationships between the microstate classes across the first 3, core microstate metrics (i.e., mean duration of each microstate class, occurrence, and coverage), as well as GEV, and FC measures were then

evaluated to establish which patterns were significantly related to FC disruptions in varying networks. The complexity measure embedded in the +microstate toolbox was Lempel Ziv complexity, which indexes the complexity of microstate transitions and represented a more novel measure of microstate transition that does not rely on stationarity or the assumption that data exhibit Markovian dynamics, unlike the traditional Markovian syntax analysis (Tait et al., 2020). The Hurst exponent is a measure of long-term memory of a time series or temporal autocorrelations with values existing between 0 and 1 (von Wegner et al., 2023). Typically, Hurst values between zero and 0.5 represent low organization and likely disrupted/disorganized brain activity and values over 0.5 represent greater signal stability. The +microstate toolbox complexity and Hurst exponents for microstate solutions were also assessed in relation to FC measures as exploratory analyses to evaluate group differences (Tait et al., 2022). The +microstate toolbox allows cluster selection, used to evaluate hypothesis-driven microstate solutions, and cluster optimization. Both a four- and a six-cluster solution were evaluated based on prior findings and field standards. The four-cluster solution was forced to approximate the four canonical microstates (i.e., field standard) and the six-cluster solution was forced to replicate the output of a recent microstate study in FXS that found the six-microstate solution fit best (Milz et al., 2027; Mishra et al., 2020 Takarae et al., 2023). The built-in optimization function in the toolbox utilized the kneedle algorithm to select an optimal cluster value for each individual and across the sample on the cohort object. Importantly, the kneedle algorithm is an elbow detection method that selects cluster solutions based on the point of diminishing returns which is appropriate for determining the appropriate number of clusters for EEG microstate analysis. The optimal solution was only fully evaluated if the optimal value was within reason (e.g., maximum of seven per field standard; D'Croz-Baron et al.,2019; Khanna et al., 2015;

Sattari et al., 2024; Sun et al., 2021). No consensus on the upper limit for microstates exists but the use of greater than seven microstate classes is rare and often selected in a hypothesis-driven manner to address specific questions (Michel et al., 2024). Ultimately, evaluating more than seven microstate classes may result in overfitting where solutions select for artifact-driven patterns (Khanna et al., 2015). Given the optimal solution exceeds seven, only global microstate measures (e.g., mean duration, GFP peaks per second, GEV, complexity, & Hurst exponent) were evaluated. Finally, the Davies-Bouldin (DB) Index was computed for each solution to put forth a recommended cluster solution from microstate exploration. The DB index provides a means for validating the cluster analysis by identifying which solution provides the greatest separability between clusters in ratio terms where the index is a ratio of the intra- vs. inter-cluster distances. The +microstate toolbox algorithm for clustering was adjusted to output the distance matrix from which both the inter- and intra-cluster distances were computed. Finally, DB indices were computed for each microstate solution according to:

$$DB= \frac{1}{k}\sum_{i=1}^{k} \max\left(\frac{\Delta(X_i)+\Delta(X_j)}{\delta(X_i,X_j)}\right),$$

where k is the total number of clusters, i is an individual cluster, j indexes all other clusters, ΔX_i represents the intra-cluster distance from the cluster centroid for cluster X_k or the spread of values for points within a specific cluster, and X_i, X_j is the intra-cluster distance between clusters X_i and X_j. Given the ratio accounts for the combined scatter of each cluster (i.e., intra-cluster distances) divided by the distance between the clusters, smaller values (i.e., values closer to 0) indicate more ideal cluster solutions because smaller values are indicative of maximal distance between clusters and minimal scatter within each cluster. It is worth noting that DB indices are conservative and biased towards smaller cluster solutions, as the cluster space is fixed.

Functional Connectivity Analysis. FC measures were calculated from high density rsEEG data to evaluate FC disruptions in the lateral frontoparietal network, also known as the "control" network, default mode (DMN), and salience (SN) networks in source space (Barzengaran & Knyazeva et al., 2017). First, source modeling was completed using a minimum-norm estimate in Brainstorm according to Pedapati et al. (2022), which utilized protocol from Tadel et al. (2011) to address the inverse problem. Source estimates were generated using minimum-norm estimate (as opposed to dipole fitting), as this approach tends to produce comparable maps across subjects. Electrode level data (128 channels) were co-registered using a Montreal Neurological Institute (MNI) averaged ICBD152 common brain template using Brainstorm and code developed for Pedapati et al. (2022). Nodes designated for the SN and DMN were then determined using the Desikan-Killiany (DK) Atlas and based on resting state network selections used in previous studies (Table 2; Desikan et al., 2006; Kabbara et al., 2017; Pedapati et al., 2022). A control network/CEN node selection for EEG data was not defined in the literature. However, previous studies selected the DMN and SN node by using the 14 networks identified in Shirer et al. (2012) and a similar approach was used to select control network nodes for analysis (Kabbara et al., 2017).

Table 2.

Source Nodes Used for Each Functional Network

DK Atlas Nodes	Network	DK Atlas Nodes	Network	DK Atlas Nodes	Network
Caudal anterior cingulate R	DMN	Caudal middle frontal L	SN	Superior frontal L	Control
Isthmus cingulate L	DMN	Caudal middle frontal R	SN	Superior frontal R	Control
Isthmus cingulate R	DMN	Insula L	SN	Rostral middle frontal L	Control
Lateral orbitofrontal L	DMN	Insula R	SN	Rostral middle frontal R	Control
Lateral orbitofrontal R	DMN	Rostral middle frontal L	SN	Caudal middle frontal L	Control
Medial orbitofrontal L	DMN	Rostral middle frontal R	SN	Caudal middle frontal R	Control
Medial orbitofrontal R	DMN	Supramarginal L	SN	Medial orbitofrontal L	Control
Para-hippocampal L	DMN	Supramarginal R	SN	Lateral orbitofrontal L	Control
Para-hippocampal R	DMN			Precuneus L	Control
Posterior cingulate L	DMN			Inferior parietal L	Control
Posterior cingulate R	DMN			Inferior parietal R	Control
Precuneus L	DMN			Superior parietal L	Control
Precuneus R	DMN			Inferior temporal L	Control
Rostral anterior cingulate R	DMN			Middle temporal L	Control
Rostral anterior cingulate L	DMN			Supramarginal R	Control

Note. DMN = Default Mode Network; SN = Salience Network; L = left hemisphere; R = right hemisphere.

Delta, theta, and alpha frequency band connectivity were assessed using debiased-weighted phase lag index (dWPLI) between network source nodes with a priority for theta and alpha connectivity. The alpha frequency band was split between alpha 1 and alpha 2 according to Pedapati et al. (2022) for reproducibility. To compute FC, dWPLI was selected based on reported robustness against volume conduction, noise, and sample-size bias and the successful use of dWPLI in recent FXS work (Bastos & Schoffelen, 2015; Cohen, 2015; Pedapati et al., 2022; Schmitt et al., 2019; Vinck et al., 2011). Previous measures of FC include the phase lag

index (PLI) which evaluated phase alignment within specific frequency bands under the assumption that increased phase alignment represents increased neural synchrony. To compute PLI, the phase alignment between two signals is calculated where $\Delta\phi$ is the phase difference of the time series t_k and k = 1,…N:

$$PLI=|\langle sign[\Delta\phi(t_k)\rangle|,$$

PLI can also be written as:

$$\Psi \equiv|E\{sgn(I\{X\})|,$$

where E is the expected value operator, X is the phase difference, and $\Im\{X\}$ is the imaginary part of the signal. While PLI is a standard coherence-based measure, PLI is sensitive to noise and volume conduction (i.e., signal smearing/electrical spread). Based on reports in the literature, PLI is biased by noise related to data length and total sample size which are largely unavoidable when working with individuals that have rare neurodevelopmental disorders (Vinck et al., 2011). Portions of the biases that impact PLI can be accounted for computationally by weighting PLI using the magnitude of the imaginary part of the signal per equation 8 in Vinck et al. (2011):

$$\Phi=\frac{|E\{I\{X\}\}|}{E\{|I\{X\}|\}} = \Phi=\frac{|E\{I\{X\}\}|sgn(I\{X\})|}{E\{|I\{X\}|\}},$$

where E is the expected value operator and $\Im X$ is the imaginary part of the signal.

which can then be debiased as follows:

$$(1)\ \Im\{X\}_{sum} = \sum(\Im\{X\}),$$

$$(2)\ \Im\{X\}_{sumW} = \sum(|\Im\{X\}|),$$

$$(3)\ Debiasing\ Factor = \sum(\Im\{X\}^2), \text{ and}$$

$$(4)\ dWPLI = \frac{\Im\{X\}_{sum}{}^2 - Debiasing\ Factor}{\Im\{X\}_{sumW}{}^2 - Debiasing\ Factor}.$$

The FC analysis provided an index of strength of phase relationships within a frequency band between network nodes. FC is typically bound between zero and one but dWPLI can provide small negative values due to the debiasing step, which are interpreted as zero/no connectivity with values approaching one representing stronger connectivity. Average within-network FC was computed by averaging across all frequency steps within the specified frequency band (e.g., FC for 1 Hz and FC for 2 Hz averaged to provide delta FC) and then across all node connections within the functional network of interest. Averaging FC across nodes within a functional network provides an index of relative strength of network FC for a given set of nodes within frequency bands of interest (i.e., quantifying total values representing full networks) (Bastos & Schoffelen, 2015; Lau et al., 2012; Vinck et al., 2011). All network connections were plotted for frequency bands where FC was significantly different between groups to visualize connectivity scaled to strength using both color and line width. Group plots were separated by color palette based on group differences where warmer colors (i.e., reds, oranges, and yellows) indicated the group with higher relative connectivity and cooler colors (i.e., blues, greens, and yellows) indicated the group with lower relative connectivity. Next, the top ten highest FC values (~10% of network connections) were further investigated to evaluate potential network drivers for frequency bands that exhibited statistically significant group differences for rsEEG. The top ~2% of connections (two connections) were statistically evaluated between groups to minimize the number of comparisons. The SN had less unique nodes both DMN and control network, but the two strongest connections were still evaluated to match DMN and control network analyses. Top connections were selected from TDC top connections, as these most likely represent typical within network function. Top connection analyses were corrected for multiple comparisons using a Bonferroni Correction. The top

connections were also plotted following the same scaling and color palette as the full network plots. An additional plot was generated for each group that normalized the top ten connections on color and line width to the full FC scale [0, 1] to ensure all connections were visible, as some of the weaker connections were less visible. Finally, top connection sum scores were generated for each group by summing across the top ten connections within group to determine whether top connection strength differed by group:

$$S_g = \sum_{i=1}^{10} F_{g,i},$$

where S_g is the connectivity sum score, i is an individual connection, F is the average FC (dWPLI) over each network, and $F_{g,i}$ is the functional connectivity of the ith connection in the top ten connections for group g.

Frequency Band Power Analyses. Both absolute and relative power were calculated across frequency bands for both frontal and posterior regions to ensure power outcomes were comparable to previous studies. Spectral power was divided into 7 frequency bands per Pedapati et al. (2022): delta (1 – 3.5 Hz), theta (3.5 – 7.5 Hz), alpha1 (8 – 10 Hz), alpha2 (10.5 – 12.5 Hz), beta (13 – 30 Hz), gamma1 (30 – 55 Hz), and gamma2 (65 – 90 Hz). Continuous absolute power (V^2/Hz) was then computed across all available data using Welch's methods. From absolute power, the relative power was computed by dividing absolute power within specific frequency bands by the total power across all frequencies (unitless).

Individual Peak Alpha Frequency. Individual PAF values were computed according to Pedapati et al. (2022) by computing the relative power spectrum density and identifying peaks between 2 and 40 Hz in 0.5 Hz steps. Frequency measurement was taken at the peak maximum.

Statistical Routine

All data were assessed for normality and for whether data met assumptions for each test. Non-parametric tests were used where data violated assumptions of normality or equality of variance. Univariate ANOVAs (one- or two-way) assessed group differences on experimental variables (i.e., microstate mean duration, GEV, GFP, complexity, and Hurst exponent). Sex effects were added as an exploratory evaluation to account for inherent sex effect in FXS related to the *FMR1* mutation. Repeated-measures ANOVAs (rmANOVAs) were used to evaluate individual microstate class variables (duration and occurrence) by group. Coverage is a percentage measure for the total amount of the whole EEG recording a specific microstate class covers where individual class variables were inherently linearly dependent. Coverage was analyzed using Friedman tests to evaluate class differences split by group with Wilcoxon sign rank tests as a post-hoc test to test pairwise comparisons for cases with significant Friedman results. Wilcoxon sign rank tests were corrected for multiple comparisons using a Bonferroni correction.

Most FC variables violated assumptions of normality. As a result, the within network FC, individual strongest connections, and sum scores were all analyzed using non-parametric tests to evaluate group differences.

Sex effects are inherent to FXS and often confounding due to systematic variability in females with FXS. Therefore, sex was used in models assessing microstates to model possible sex effects rather than using sex as a covariate. Age differences were also expected due to developmental differences from TDC. However, the limited-age adult sample and age-matching reduced these concerns. Further, age did not differ between groups ($t(88) = -1.50$, $p = .137$, $d = -.32$) and was not evaluated as a covariate, as a result. Finally, EEG data length was evaluated as a

covariate due to the increased EEG data loss resulting from artifact in NDD populations. If data length was significant covariate, it was retained.

A set of correlation analyses were conducted to understand how variables were related to 1) other experimental variables, and 2) important or core clinical features. First, a correlation analysis between microstate and FC variables was conducted to evaluate whether individual microstate variables map onto FC variables. Second, correlations between clinical variables and experimental variables were computed to evaluate whether microstate and FC variables were related to clinical variables indexing cognition or core FXS features. Correlations were not corrected for multiple comparisons, as they were regarded as exploratory and thus hypothesis generating.

All statistical tests were conducted with respect to data characteristics and statistical assumptions, with corrections for multiple comparisons using post-hoc tests, as necessary. All statistical analyses were conducted in SPSS version 29.

Statistical Power Analysis. Power analyses were based on reported EEG abnormalities in FXS noted across multiple samples with an effect size of d = 1.6 and a partial eta squared of .24 (Ethridge et al., 2016; 2017; 2019; Norris et al., 2022; Wang et al., 2017). All power calculations were computed using G*Power or R with power of .80 and alpha of .05. Univariate ANCOVAs require a minimum of 28 participants for one-way and 34 for two-way ANCOVAs. The rmANOVAs required only 8 participants to detect the target effect size.

Results

Microstate Analysis

Three separate microstate solutions were computed: a four microstate solution (4MS), a six microstate solution (6MS), and an optimal microstate solution selected by the +microstate toolbox. The 4MS and the 6MS solutions were based on hypotheses set *a priori* to capture the canonical microstate solution (4MS) and to capture the solution previously identified in a microstate study of FXS (6MS), respectively (Takarae et al., 2023). The optimization approach produced a 10-microstate solution (10MS) which was an unrealistic solution according to field standards (D'Croz-Baron et al., 2019). However, as an exploratory analysis, the solution was evaluated for differences across global microstate measures (i.e., mean duration, GEV, GFP, complexity, and Hurst exponent).

As microstates are determined by GFP, the average GFP across the whole solution and the average number of GFP peaks per second were consistent across all microstate solutions. A univariate ANOVA evaluated the group (i.e., diagnosis – FXS or TDC) by sex effects on average GFP and identified a statistically significant main effect of sex where males (M = 4.71, SD = 1.47) had higher GFP than females (M = 3.99, SD = 1.09), $F(1, 85) = 8.17$, $p = .005$, $ES = .09$. The main effect of group was not significant, suggesting FXS (M = 4.81, SD = 1.53) and TDC (M = 4.16, SD = 1.17) had similar GFP, $F(1, 85) = 2.33$, $p = .131$, $ES = .03$. However, the interaction between group and sex on GFP was significant where males with FXS exhibited elevated GFP (M = 5.42, SD = 1.54) compared to females with FXS (M = 3.77, SD = .80) and TDC males (M = 4.14, SD = 1.13) were comparable to TDC females (M = 4.19, SD = 1.30) suggesting FXS sex differences were driving the interaction and the sex effects, $F(1, 85) = 9.24$, $p = .003$, $ES = .10$. Specifically, after Bonferroni correction, the univariate test showed a robust

statistically significant difference between FXS males and females, $F(1, 85) = 16.44$, $p < .001$, $ES = .16$. GFP had non-normal residuals but the non-parametric test evaluating the main effect of group showed a similar result where the groups were not significantly different but trended towards significance without sex in the model where FXS exhibited marginally increased GFP (M rank = 50.32) compared to TDC (M rank = 40.46), $N = 89$, $z = 1.79$, $p = .073$, $r = .19$. The ANOVA evaluating GFP violated the assumption of equality of variances, but variance differences were not extreme where the ANOVA result was retained to evaluate the effect of sex in the model.

A second univariate ANOVA evaluated the group by sex effects on GFP peaks per second and identified a significant main effect of group where FXS ($M = 31.18$, $SD = 2.44$) had significantly more peaks per second compared to TDC ($M = 30.63$, $SD = 3.16$), $F(1, 85) = 4.12$, $p = .046$, $ES = .05$. There was not a main effect of sex ($F(1, 85) = 1.38$, $p = .243$, $ES = .02$, OP = .21) nor a significant interaction effect ($F(1, 85) = 2.10$, $p = .151$, $ES = .02$) suggesting that males ($M = 30.94$, $SD = 2.53$) and females ($M = 31.61$, $SD = 2.88$) have similar numbers of GFP peaks per second across both groups.

Four Microstate (4MS) Solution

Univariate ANOVAs tested group differences on GEV, mean duration, microstate complexity, and Hurst with sex as an additional variable to evaluate potential sex by group interactions (Figures 2 & 3).

For the 4MS solution GEV, there was a main effect of group with FXS exhibiting significantly higher GEV ($M = .61$, $SD = .06$) compared to TDC ($M = .57$, $SD = .06$), $F(1, 85) = 7.83$, $p = .006$, $ES = .08$. There was also a significant main effect of sex with females exhibiting higher GEV ($M = .62$, $SD = .06$) relative to males ($M = .58$, $SD = .06$), $F(1, 85) = 11.41$, $p =$

.001, *ES* = .12. However, the interaction was not significant where females exhibited higher GEV (FXS: *M* = .64, *SD* = .06; TDC: *M* = .61, *SD* = .06) than males (FXS: *M* = .60, *SD* = .07; TDC: *M* = .55, *SD* = .06) consistently between groups, *F*(1, 85) = 0.65, *p* = .423, *ES* = .01. For the interaction, the current sample contains less females than males where results may reflect reduced power to detect real sex effects. Therefore, the lack of group by sex interaction may be worth confirming in future studies better powered to detect sex effects.

For mean duration, there was not a significant main effect of group (*F*(1, 85) = 1.04, *p* = .311, *ES* = .01) or sex (*F*(1, 85) = 0.39, *p* = .635, *ES* = .00) where the mean duration of the whole 4MS microstate solution was consistent across both groups (FXS: *M* = .05, *SD* = .00; TDC: *M* = .05, *SD* = .00) and both sexes (Males: *M* = .05, *SD* = .00; Females: *M* = .05, *SD* = .00).

The analysis of complexity identified no main effect of group (*F*(1, 85) = 0.71, *p* = .402, *ES* = .00) or sex (*F*(1, 87) = .09, *p* = .769, *ES* = .00) for microstate complexity suggesting comparable microstate transition dynamics across both groups (FXS: *M* = .87, *SD* = .03; TDC: *M* = .87, *SD* = .03) and sexes (Males: *M* = .87, *SD* = .03; Females: *M* = .87, *SD* = .02).

For Hurst, there was not a significant main effect of group (*F*(1, 85) = 0.00, *p* = .986, *ES* = .00, OP = .05) or sex (*F*(1, 85) = 0.00, *p* = .980, ES = .00) with comparable Hurst values across groups (FXS: *M* = .65, *SD* = .05; TDC: *M* = .66, *SD* = .04) and sexes (Males: *M* = .66, *SD* = .04; Females: *M* = .65, *SD* = .04). Additionally, all Hurst values were above 0.5 suggesting a moderately high level of microstate solution stability or persistence.

The main effect of complexity and Hurst had non-normal residuals and were evaluated with non-parametric alternatives to determine whether the present results were comparable. Both tests of groups differences on complexity (*N* = 89, *z* = -.55, *p* = .581, *r* = -.06) and Hurst (*N* = 89, *z* = -71, *p* = .479, *r* = -.08) remained non-significant. Again, FXS (Complexity: *M* rank = 43.37;

Hurst: *M* rank = 42.90) was similar to TDC (Complexity: *M* rank = 46.40; Hurst: *M* rank = 46.79).

The effect sizes on the two main effect outcomes for mean duration, complexity, and Hurst also support a lack of meaningful group or sex difference for these three microstate variables.

Figure 2.

Boxplots Depicting 4MS Solution Group Differences on GEV, Mean Duration, Complexity, and Hurst

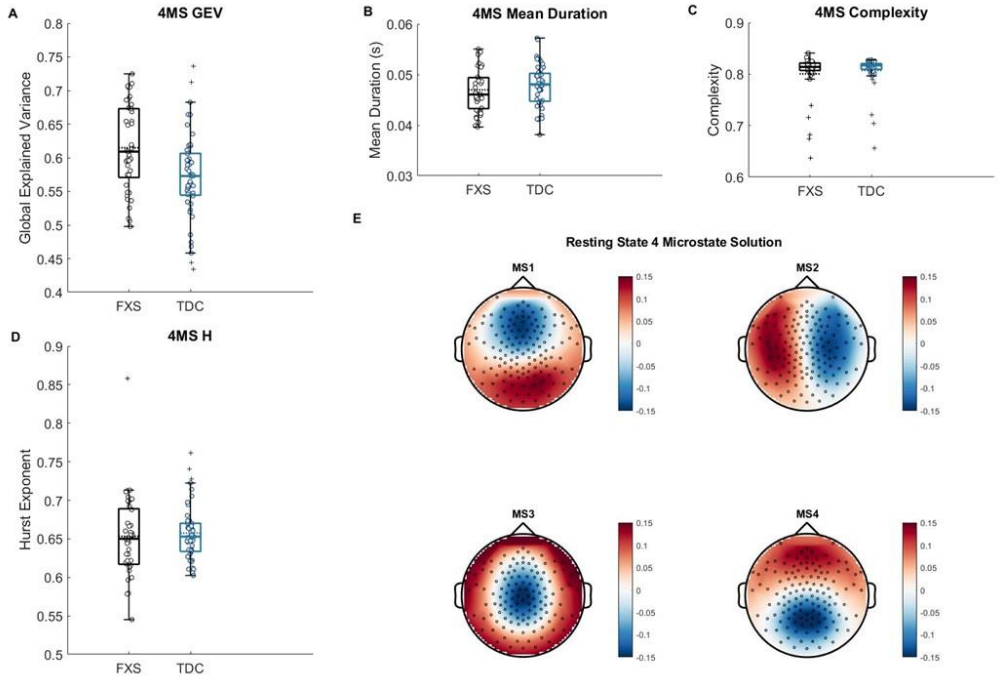

Note. Dashed lines show the mean value and solid lines show the median. **A)** 4MS solution GEV. **B)** 4MS solution mean duration. **C)** 4MS solution complexity (i.e., microstate transition dynamics) **D)** 4MS solution H. **E)** 4MS solution microstate class maps.

As the aim of evaluating the 4MS was to replicate the canonical microstate solution, it was apt to visually match the current microstate solution classes to the canonical classes. Visually, MS1 most closely approximates microstate B despite MS1 having a more frontal shift. MS2 approximates Microstate A, though, the distribution was shifted to be more activated over

the hemispheres rather than diagonal. MS3 and MS4 are most comparable to Microstate D and C, respectively.

Figure 3.

Boxplots Depicting 4MS Solution Sex Differences on GEV, Mean Duration, Complexity, and Hurst

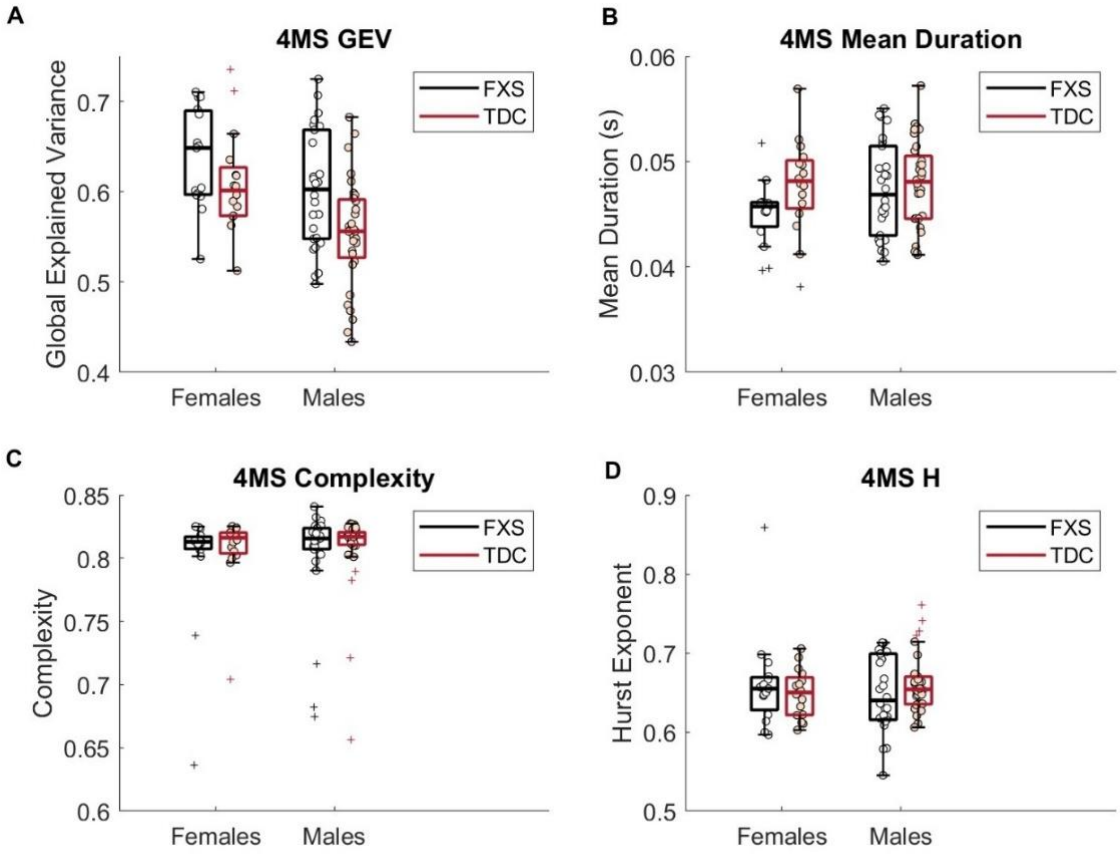

Note. **A)** group and sex differences for 4MS GEV, **B)** group and sex differences for 4MS mean duration of microstates, **C)** group and sex differences for 4MS microstate transition complexity, and **D)** group and sex differences for 4MS Hurst exponent.

Next the class-specific variables were analyzed using rmANOVAs, including microstate GEV, GFP, and mean duration for differences across the 4 microstate classes within subject by group. Additionally, individual microstate coverage and occurrence were also evaluated (see Table 3 for descriptive statistics).

For individual 4MS GEV, the rmANOVA identified an expected significant main effect of group with increased GEV for FXS (M = .65, SD = .06) compared to TDC (M = .60, SD = .06; $F(1, 85) = 9.75$, p = .002, ES = .10) but the GEV was not significantly different between microstates within subject (i.e., no main effect of individual microstate class; $F(3, 85) = 0.28$, p = .840, ES = .01) and there was no interaction between individual microstate class GEV and group ($F(3, 87) = 1.08$, p = .363, ES = .04).

While GFP is a global measure, individual microstate classes were the result of different patterns of average GFP. The average GFP of each microstate was computed and evaluated in a rmANOVA to compared across microstates and between groups. Unexpectedly, the main effect of group was significant where FXS exhibited increased GFP values (M = 4.79, SD = 1.54) compared to TDC (M = 4.14, SD = 1.17) where the mean difference was statistically significant (M difference = .65, STE = .29) after Bonferroni correction, $F(1, 87) = 5.17$, p = .025, ES = .06. Accounting for how GFP was distributed across individual microstate classes results in significant group differences on GFP where the patterns contribute to differences between groups. The main effect of individual microstate class GFP was not significant where GFP was comparable across all four microstates within-subject for the whole sample, $F(3, 85) = 0.34$, p = .795, ES = .01. Interestingly, there was a significant group by microstate class interaction for GFP but the interaction did not survive the Bonferroni correction, $F(3,85) = 3.55$, p = .018, ES = .11 (Figure 4).

Simple main effects tests (i.e., pairwise comparisons) between groups on individual microstate GFP showed that all but MS4 were significantly different between groups after applying a Bonferroni correction. Individuals with FXS had higher GFP across all microstates but exhibited the greatest difference on MS3 (M difference = .79, SE = .29, p = .008). MS1 (M

difference = .60, SE = .29, p = .039) and MS2 (M difference = .73, SE = .31, p = .021) were also significantly higher in FXS compared to TDC. Lastly, while MS4 was not significantly different between groups, it trended towards a significant difference and marginal elevation for FXS (M difference = .51, SE = .29, p = .090).

Figure 4.

Boxplot for Mean GFP by Microstate and Group by Microstate Interaction for the 4MS solution

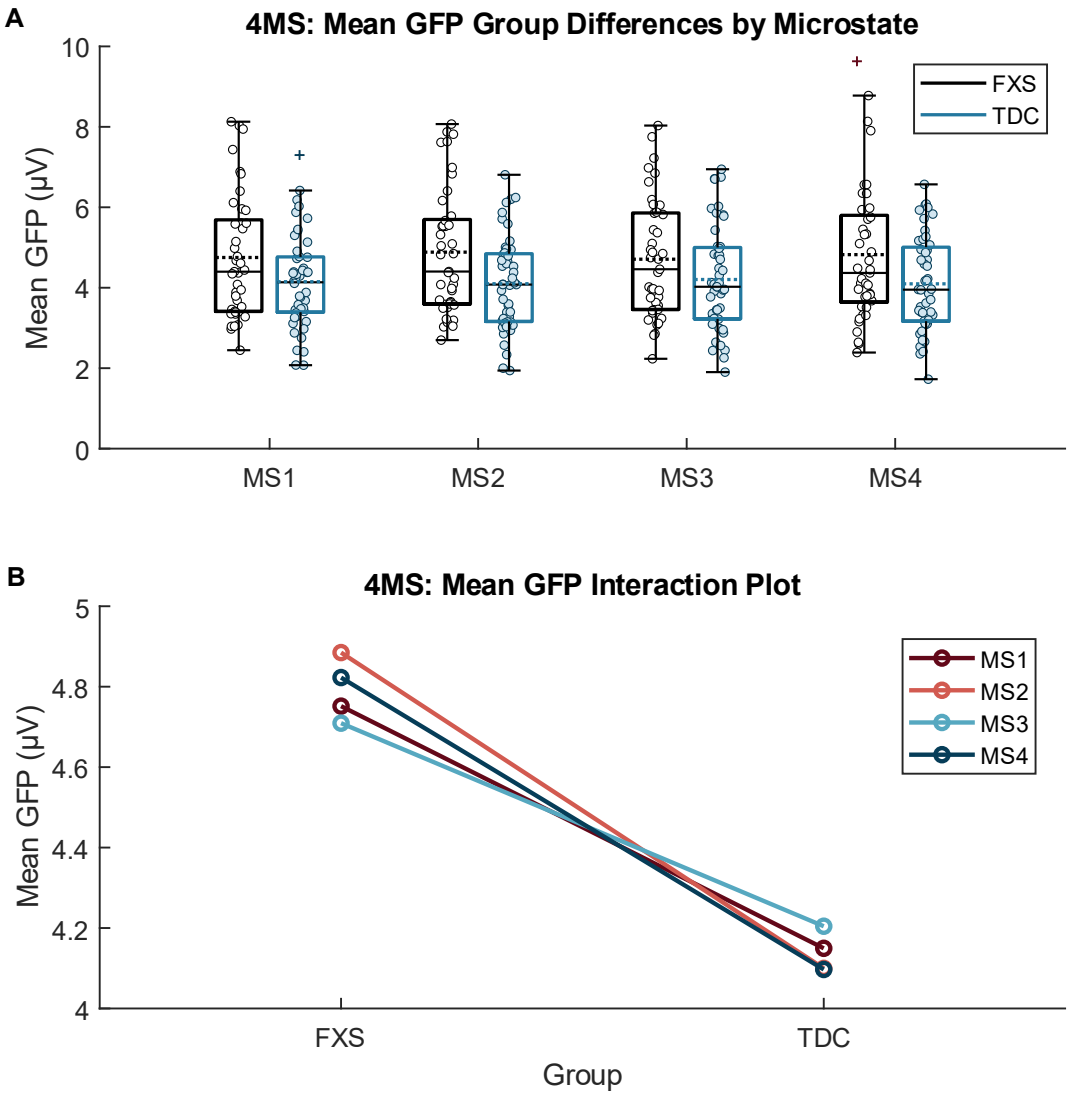

Note. **A)** boxplots depicting group differences across individual microstates. **B)** Interaction plot depicting the shift in average GFP per microstate between groups.

For mean microstate duration, there was no significant main effect of group ($F(1, 87) = 1.48$, $p = .228$, $ES = .02$) which was expected, and no significant effect of microstate class ($F(3, 85) = 1.36$, $p = .260$, $ES = .05$) where individuals spent equal amounts of time, on average, in each of the four microstate classes both within groups and between groups.

For coverage, Box's test of equality of covariance matrices was not computed suggesting an issue with the covariance matrix. As coverage is a percentage where the sum across microstates is equal to 100%, variance within each microstate may be low which impacts the ability to invert the covariance matrix. Friedman tests split by group were used to test the within subject comparison followed by Wilcoxon ranked sign test as a post-hoc test when Friedman identified significant effects for a given group. Individual microstate coverage was not significantly different between microstate class for FXS ($\chi^2(3) = .30$, $p = .960$, $W = .00$) or TDC ($\chi^2(3) = 3.06$, $p = .383$, $W = .03$).

For microstate occurrence, there was not a significant main effect of individual microstate occurrence ($F(2.64,85) = .01$, $p = .981$, ES = .00, OP = .06) nor main effect of group ($F(1, 87) = 1.18$, $p = .281$, $ES = .01$) suggesting the occurrence of each microstate per second was comparable between microstates within the 4MS solution and between groups. Individual microstate occurrence violated the assumption of sphericity, so the Greenhouse-Geisser procedure was used to estimate epsilon in order to correct the degrees of freedom.

Table 3.

Individual Microstate Class-Specific Variable Descriptive Statistics for the 4MS Solution

Microstate	MS1		MS2		MS3		MS4	
Variable	*M*	*SD*	*M*	*SD*	*M*	*SD*	*M*	*SD*
GEV								
FXS	.15	.06	.16	.06	.14	.06	.15	.07
TDC	.15	.06	.13	.05	.15	.06	.13	.05
GFP								
FXS	4.75	1.54	4.88	1.55	4.71	1.47	4.82	1.70
TDC	4.15	1.16	4.10	1.16	4.20	1.30	4.10	1.18
Mean Duration (s)								
FXS	47.91	4.06	47.06	5.98	48.90	7.16	46.40	6.36
TDC	47.77	4.43	47.02	5.71	46.03	6.19	46.73	5.96
Coverage (%)								
FXS	.26	.05	.25	.06	.25	.06	.25	.06
TDC	.26	.04	.25	.05	.25	.05	.24	.05
Occurrence								
FXS	5.50	.75	5.30	1.21	5.35	.91	5.35	1.07
TDC	5.34	.75	5.23	.79	5.25	1.00	5.22	.73

Six Microstate (6MS) Solution

Similarly to the 4MS solution, univariate ANOVAs tested the 6MS solution for group differences on GEV, mean duration, microstate complexity, and Hurst with sex as an additional variable to test for sex by group interactions (Figures 5 & 6).

The ANOVA testing group and sex differences on GEV for the 6MS solution identified a significant main effect of group where FXS (M = .65, SD = .06) exhibited increased GEV compared to TDC (M = .60, SD = .06), $F(1, 85) = 8.20$, $p = .005$, $ES = .09$. There was also a significant main effect of sex where females had higher GEV (M = .65, SD = .06) compared to males (M = .61, SD = .06), $F(1, 85) = 12.24$, $p < .001$, $ES = .13$. However, the interaction was not significant where, similarly to the 4MS, sex effects were comparable across both groups, $F(1, 85) = .89$, $p = .347$, $ES = .01$.

For mean duration, there was not a significant main effect of group ($F(1, 85) = 1.86$, $p = .177$, ES = .02, OP = .27) or sex ($F(1, 85) = .48$, $p = .490$, $ES = .01$). As with the 4MS, the average time spent in microstates accounted for by the whole 6MS solution was not different between groups (FXS: $M = .04$, $SD = .00$; TDC: $M = .04$, $SD = .00$) or sexes (Males: $M = .04$, $SD = .00$; Females: $M = .04$, $SD = .00$).

The addition of two additional microstates did not shift complexity or Hurst dynamics, as the analysis of complexity identified no main effect of group ($F(1, 85) = 0.27$, $p = .604$, $ES = .00$) or sex ($F(1, 85) = .01$, $p = .908$, $ES = .00$) where the microstate transition dynamics across both groups (FXS: $M = .87$, $SD = .03$; TDC: $M = .87$, $SD = .03$) and both sexes (Males: $M = .87$, $SD = .03$; Females: $M = .87$, $SD = .02$) were nearly equal.

The Hurst analysis also showed no main effect of group ($F(1, 85) = 0.43$, $p = .515$, $ES = .01$) or sex ($F(1, 85) = .08$, $p = .779$, $ES = .00$) where the group level (FXS: $M = .65$, $SD = .04$; TDC: $M = .66$, $SD = .04$) and sex level Hurst values (Males: $M = .66$, $SD = .04$; Females: $M = .65$, $SD = .04$) were comparable. For the 6MS solution, the Hurst values were also above 0.5 suggesting a moderately high level of microstate solution stability for the whole sample.

As with the 4MS solution, the residuals for hurst and complexity violated assumptions of normality and were evaluated using Mann-Whitney U tests to confirm group effects. Both complexity ($N = 89$, $z = -.35$, $p = .723$, $r = -.04$) and Hurst ($N = 89$, $z = -1.46$, $p = .145$, $r = -.15$) were not different between groups. Again, FXS (Complexity: M rank = 43.95; Hurst: M rank = 40.68) was similar to TDC (Complexity: M rank = 45.90; Hurst: M rank = 48.69).

Figure 5.

Boxplots Depicting 6MS Solution Group Differences on GEV, Mean Duration, Complexity, and Hurst

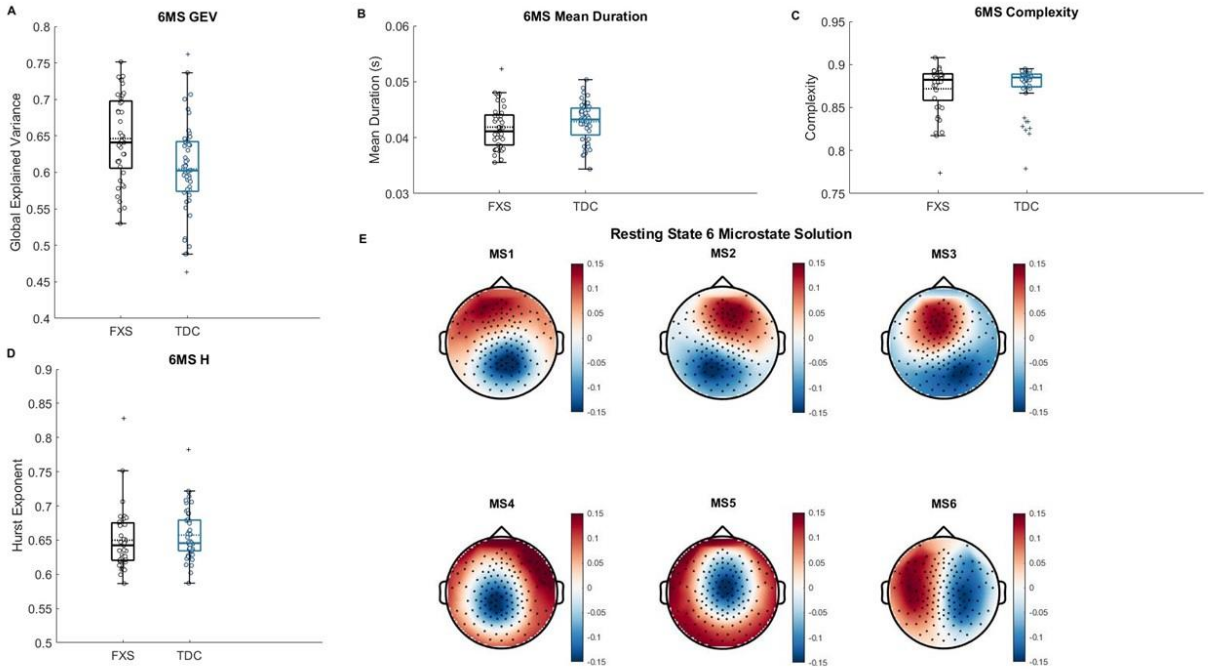

Note. **A)** Boxplot depicting group differences on 6MS solution GEV. **B)** Boxplot depicting group differences on 6MS solution mean duration. **C)** Boxplot depicting group differences on 6MS solution complexity (i.e., microstate transition dynamics) **D)** Boxplot depicting group differences on 6MS solution Hurst exponent (H). **E)** Microstate maps for the 6MS solution.

As with the 4MS solution, the 6MS solution was visually compared to the canonical maps. Unlike with the current 4MS solution, the 6MS solution more accurately captured the canonical map set where MS2 and MS3 more accurately reflected the classic microstate A and B maps, respectively. MS1 was similar to microstate C, though slightly shifted. Finally, MS5 approximates microstate D.

Figure 6.

Boxplots Depicting 6MS Solution Sex Differences on GEV, Mean Duration, Complexity, and Hurst

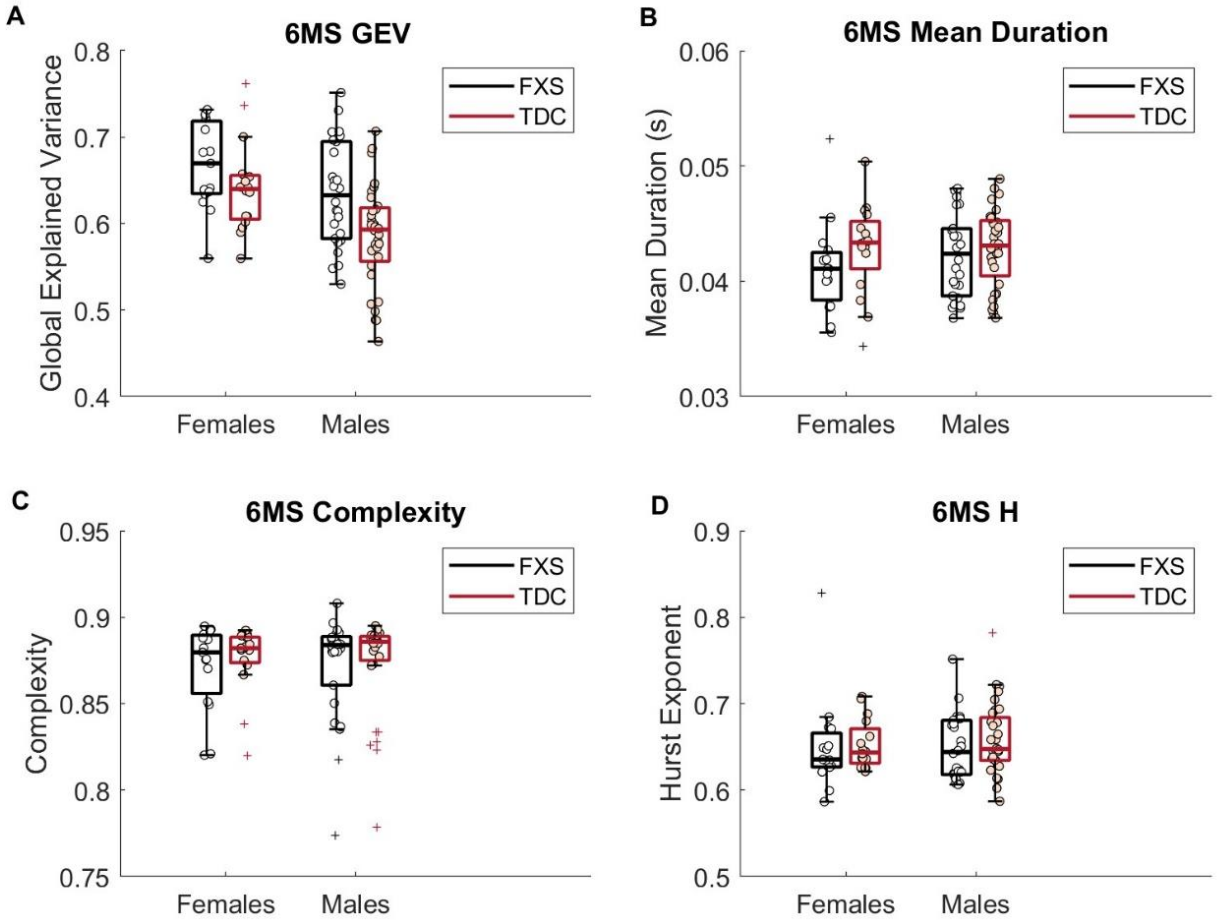

Note. **A)** group and sex differences for 6MS GEV, **B)** group and sex differences for 6MS mean duration of microstates, **C)** group and sex differences for 6MS microstate transition complexity, and **D)** group and sex differences for 6MS Hurst exponent (H).

A series of rmANOVAs were used to evaluate within subject microstate (i.e., class-specific) differences by group on GEV, GFP, mean microstate duration, microstate occurrence, and microstate coverage for the 6MS solution (see Table 4 for descriptive statistics).

For GEV, there was an expected significant main effect of group where individuals with FXS exhibited higher GEV (M = .11, SD = .01) compared to TDC (M = .10, SD = .01), F(1, 87)

= 10.33, p = .002, ES = .11. However, there was not a main effect of individual microstate class where GEV was consistent across microstate classes (F(5, 85) = .38, p = .863, ES = .02) nor was the interaction significant (F(5, 85) = 1.51, p = .196, ES = .08) where individual microstate class GEV was similar between groups.

The rmANOVA evaluating average GFP between individual microstate classes and group identified a significant main effect of group where FXS had higher GFP (M = 4.79, SD = 1.53) compared to TDC (M = 4.15, SD = 1.19), as was seen from the 4MS solution rmANOVA, F(1, 87) = 4.89, p = .030, ES = .05. Unlike with the 4MS solution, the main effect of microstate class was not statistically significant (F(5, 83) = .73, p = .602, ES = .04) nor was the interaction between individual microstate class and group (F(5, 53) = 1.25, p = .295, ES = .07; Figure 7).

Figure 7.

Boxplot for Mean GFP by Microstate and Group by Microstate Interaction for the 6MS solution

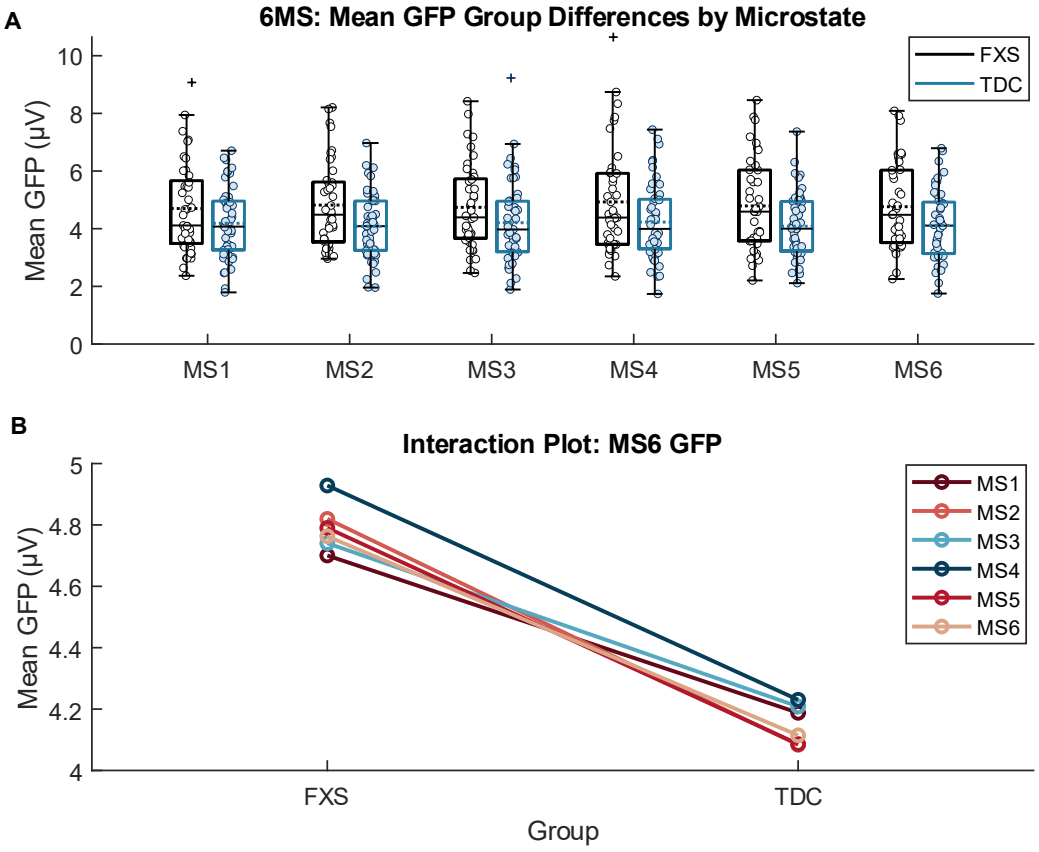

Note. **A)** boxplots depicting group differences across individual microstates. **B)** Interaction plot depicting the shift in average GFP per microstate between groups.

For the individual mean duration for the 6MS solution, the main effect of group ($F(1.76,83) = .60$, $p = .528$, $ES = .13$) and microstate class ($F(1.76,83) = 1.18$, $p = .307$, $ES = .01$) were not statistically significant suggesting equal time spent in each class across groups. Mean duration for the individual microstate classes violated assumptions of sphericity prompting the use of Greenhouse-Geisser correction.

As with the 4MS solution, Box's test of equality of covariance matrices was not computed for the rmANOVA testing coverage suggesting an issue with the covariance matrix. As coverage is a percentage where the sum across microstates is equal to 100%, variance within

each microstate may be low which impacts the ability to invert the covariance matrix. Friedman tests split by group were used to test the within subject comparison followed by Wilcoxon ranked sign test as a post-hoc test when Friedman identified significant effects for a given group. Individual microstate coverage was not significantly different between microstate class for FXS ($\chi^2(5) = 2.49$, $p = .778$, $W = .01$) or TDC ($\chi^2(5) = 8.63$, $p = .125$, $W = .04$).

From the rmANOVA testing individual microstate occurrence, the main effects of group ($F(1, 87) = 1.68$, $p = .198$, $ES = .02$) and individual microstate class ($F(5, 83) = .97$, $p = .444$, $ES = .06$) were not statistically significant. The number of times a class appears per second was different between microstates and that was consistent across both groups.

Table 4.

Individual Microstate Class-Specific Variable Descriptive Statistics for the 4MS Solution

Microstate	MS1		MS2		MS3		MS4		MS5		MS6	
Variable	*M*	*SD*	*M*	*SD*	*M*	*SD*	*M*	*SD*	*M*	*SD*	*M*	*SD*
GEV												
FXS	.10	.05	.11	.05	.11	.04	.11	.06	.11	.04	.11	.04
TDC	.11	.05	.10	.04	.09	.04	.10	.05	.10	.05	.09	.04
GFP												
FXS	4.70	1.58	4.82	1.49	4.74	1.48	4.93	1.84	4.79	1.60	4.76	1.51
TDC	4.19	1.24	4.08	1.14	4.21	1.43	4.23	1.33	4.09	1.14	4.11	1.20
Mean Duration												
FXS	41.18	5.12	42.17	5.53	41.62	4.17	41.43	5.21	42.00	5.58	41.58	4.67
TDC	43.71	5.58	42.36	4.48	43.03	7.76	45.52	18.72	42.21	3.79	42.19	4.67
Coverage												
FXS	.17	.04	.17	.05	.18	.03	.16	.04	.16	.04	.17	.03
TDC	.18	.03	.17	.03	.15	.04	.17	.04	.17	.03	.16	.04
Occurrence												
FXS	4.03	.84	3.93	1.09	4.22	.63	3.84	1.02	3.94	.86	4.09	.77
TDC	4.15	.56	4.02	.62	3.62	.97	3.87	.90	4.05	.68	3.80	.76

Toolbox Determined Optimal Microstate Solution: Ten Microstate (10MS) Solution

As the optimal microstate solution exceeded 7 microstates, only the global variables were evaluated using univariate ANOVAs to test for group and sex differences on GEV, mean duration, microstate complexity, and Hurst for the 10MS solution (Figures 8 & 9).

Optimal microstate solution GEV (10MS) exhibited a comparable pattern to the 4MS and 6MS solutions where statistically significant main effects of group ($F(1, 85) = 6.76$, $p = .011$, $ES = .07$) and sex ($F(1, 85) = 16.11$, $p < .001$, $ES = .16$) were identified. As with other microstate solutions, FXS exhibited higher GEV ($M = .68$, $SD = .05$) compared to TDC ($M = .64$, $SD = .07$) and females had higher GEV ($M = .69$, $SD = .05$) than males ($M = .64$, $SD = .06$). The interaction was not statistically significant suggesting the sex differences remain consistent across groups, $F(1, 85) = 1.22$, $p = .272$, $ES = .01$.

Mean duration for the 10MS solution was not statistically different between groups ($F(1, 85) = 1.69$, $p = .197$, $ES = .02$) nor was there a main effect of sex ($F(1, 85) = 1.27$, $p = .262$, $ES = .02$) where the mean duration of the microstate sequences was consistent between groups (FXS: $M = .04$, $SD = .00$; TDC: $M = .04$, $SD = .00$) and sexes (Males: $M = .04$, $SD = .00$; Females: $M = .04$, $SD = .00$).

Microstate complexity for the 10MS solution was not different between groups ($F(1, 85) = .02$, $p = .897$, $ES = .00$) nor was it different between sexes ($F(1, 85) = .32$, $p = .573$, $ES = .00$). The microstate transition dynamics were comparable between groups (FXS: $M = .88$, $SD = .03$; TDC: $M = .88$, $SD = .03$) and across groups between the sexes (Males: $M = .88$, $SD = .03$; Females: $M = .89$, $SD = .02$).

Microstate Hurst across the 10MS solution was not statistically different between groups ($F(1,85) = .09$, $p = .756$, $ES = .00$) and was also not statistically different between sexes ($F(1, 85)$

= .75, p = .389, ES = .01). Hurst values were still over 0.5 for the whole sample suggesting long term trends in the time series and comparable long-range correlations between both groups (FXS: M = .65, SD = .05; TDC: M = .65, SD = .04) and sexes (Males: M = .65, SD = .04; Females: M = .64, SD = .05)

Complexity and Hurst residuals violated assumptions of normality for the 10MS solution, as well. Mann-Whitney U tests confirmed that Complexity (N = 89, z = -.19, p = .850, r = -.02) and Hurst (N = 89, z = .03, p = .980, r = .00) group effects remained non-significant where FXS (Complexity: M rank = 44.44; Hurst: M rank = 45.07) and TDC (Complexity: M rank = 45.48; Hurst: M rank = 44.94) were comparable.

Figure 8.

Boxplots Depicting 10MS Solution Group Differences on GEV, Mean Duration, Complexity, and Hurst

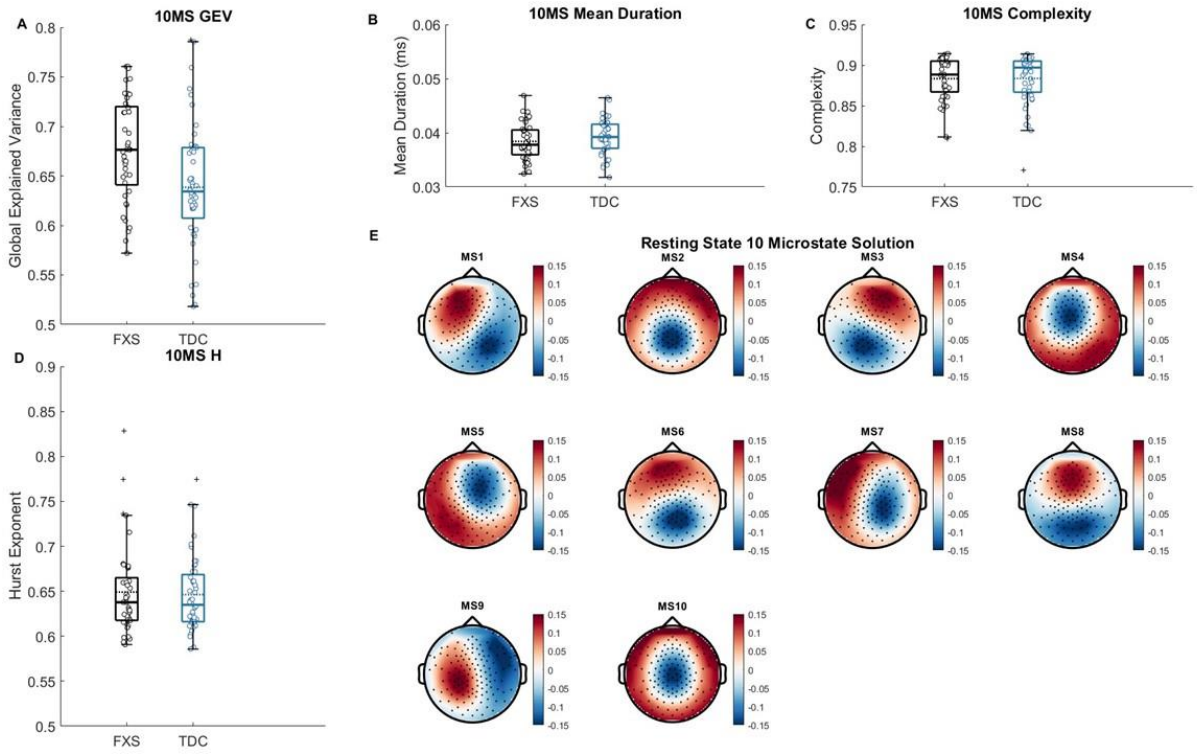

Note. **A)** Boxplot depicting group differences on 10MS solution GEV. **B)** Boxplot depicting group differences on 10 solution mean duration. **C)** Boxplot depicting group differences on 10MS solution complexity (i.e., microstate transition dynamics) **D)** Boxplot depicting group differences on 10MS solution Hurst exponent (H). **E)** Microstate maps for the 10MS solution.

Figure 9.

Boxplots Depicting 10MS Solution Sex Differences on GEV, Mean Duration, Complexity, and Hurst

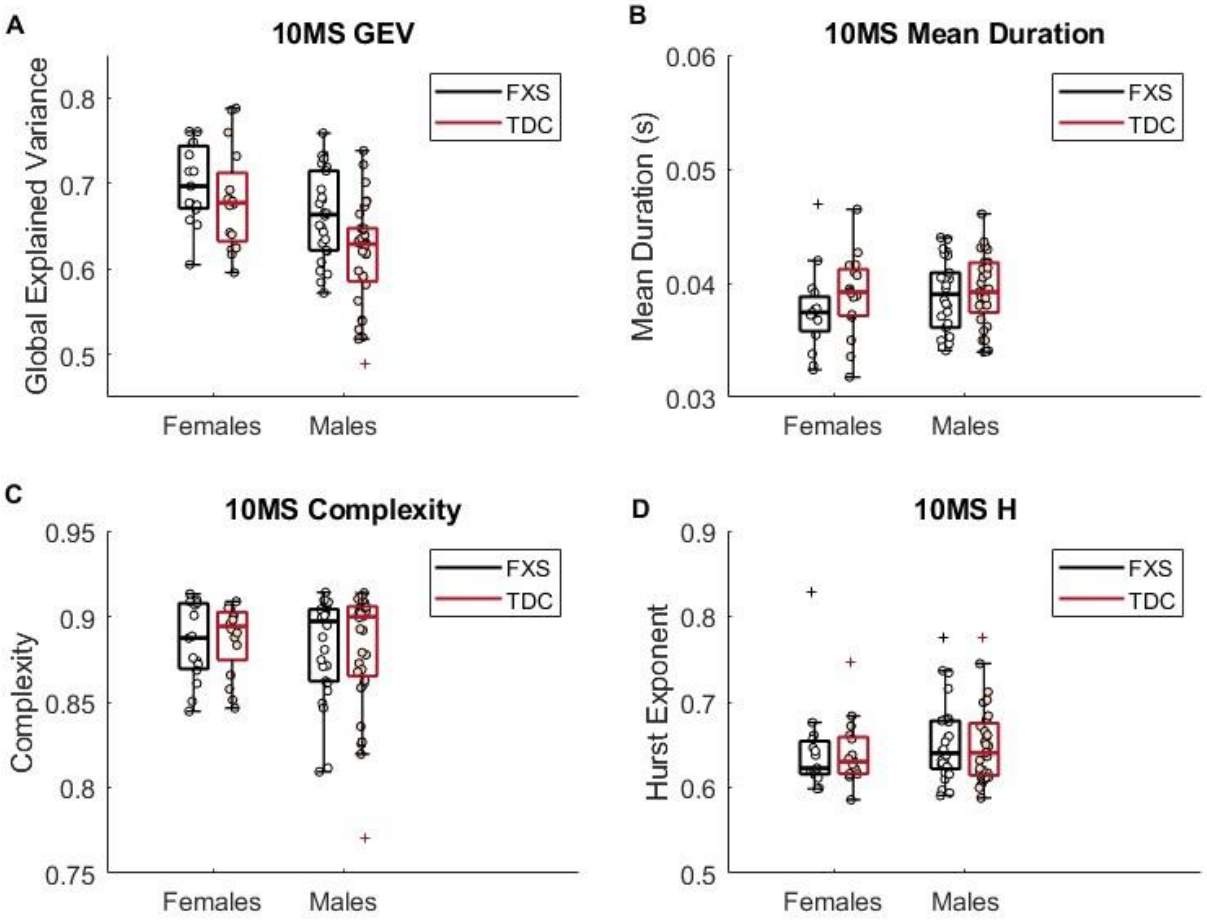

Note. **A)** group and sex differences for 10MS GEV, **B)** group and sex differences for 10MS mean duration of microstates, **C)** group and sex differences for 10MS microstate transition complexity, and **D)** group and sex differences for 10MS Hurst exponent.

Davies-Bouldin Index Cluster Solution Analysis

The DB index identified the 4MS solution as optimal, as the 4MS solution had the lowest DB index value (Figure 10). Specifically, the DB index for the 4MS solution was DB = 1.06 where the 6MS and 10MS solutions were DB = 1.50 and DB = 2.11, respectively.

Figure 10.

Davies-Bouldin Index for All Resting State Microstate Solutions

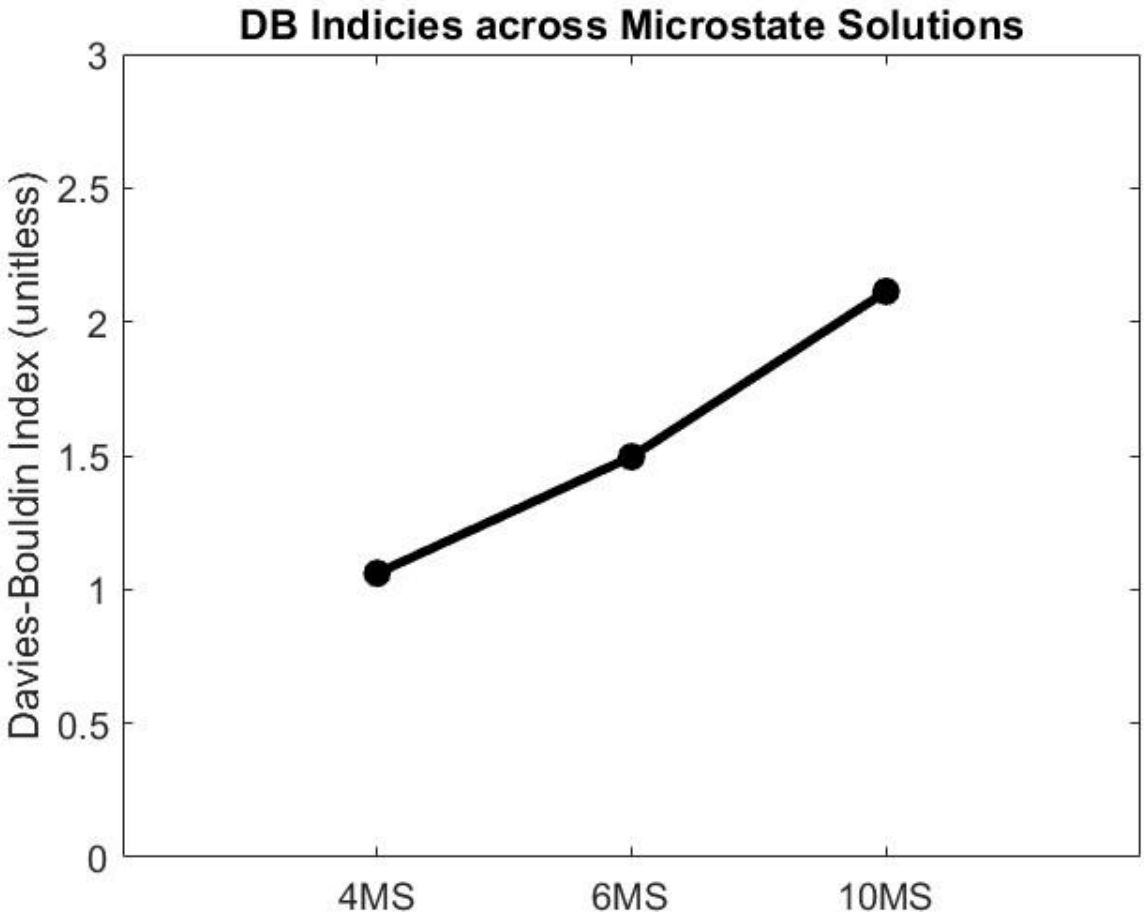

Note. Each point in the plot represents the DB index of a full model (i.e., full microstate solution).

Functional Connectivity Analysis

Non-parametric Mann-Whitney U tests evaluated FC across the rsEEG recording in the delta, theta, and both alpha1 and alpha 2 frequency bands for the within network connectivity in DMN, SN, and control network. However, the average FC values for rsEEG were substantially small indicating low FC during resting state and representing a substantial caveat to the interpretation of all group analyses. The size of the present FC values better reflect a lack of functional connectivity within the networks of interest at rest but were evaluated, as past studies found similar FC magnitude that shared relationships with clinical variables suggesting group differences in FC may be meaningful despite the small values (Schmitt et al., 2022; Wang et al., 2017).

For the DMN, only theta connectivity was significantly different between groups with elevated theta FC for individuals with FXS (*M* rank = 55.68) compared to TDC (*M* rank = 35.88), $z = 3.61$, $p < .001$, $r = .38$ (Figure 11). Delta ($z = 1.52$, $p = .128$, $r = .16$), alpha 1 ($z = 1.27$, $p = .205$, $r = .13$), and alpha 2 ($z = -.14$, $p = .889$, $r = -.01$) FC within the DMN were all comparable between FXS (delta: *M* rank = 49.51; alpha 1: *M* rank = 48.76; alpha 2: *M* rank = 44.59) and TDC (delta: *M* rank = 41.15; alpha 1: *M* rank = 41.79; alpha 2: *M* rank = 43.35; Figure 12).

Figure 11.

Default Mode Network Theta Band Functional Connectivity Circle Plots

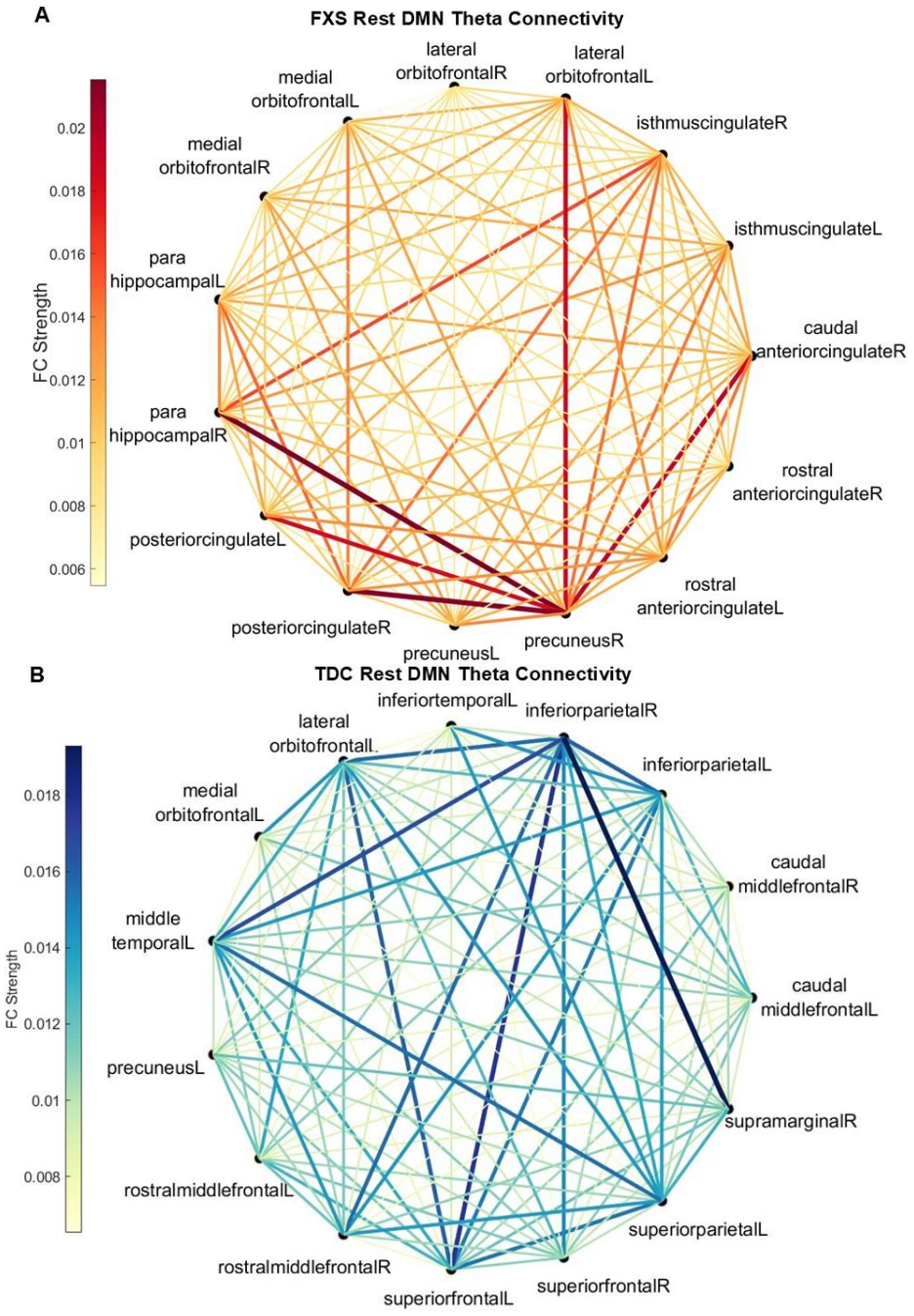

Note. Scales are different between groups. **A)** All individual connections within the DMN for FXS. **B)** All individual connections within the DMN for TDC. Colors indicate direction of group difference with warmer colors (yellow, orange, and red) indicating higher FC and cooler colors (blue, green, yellow) indicating lower FC where darker colors indicate higher FC values within each group.

Figure 12.

Violin and Box Plots Depicting Default Mode Network Functional Connectivity across Different Frequency Bands

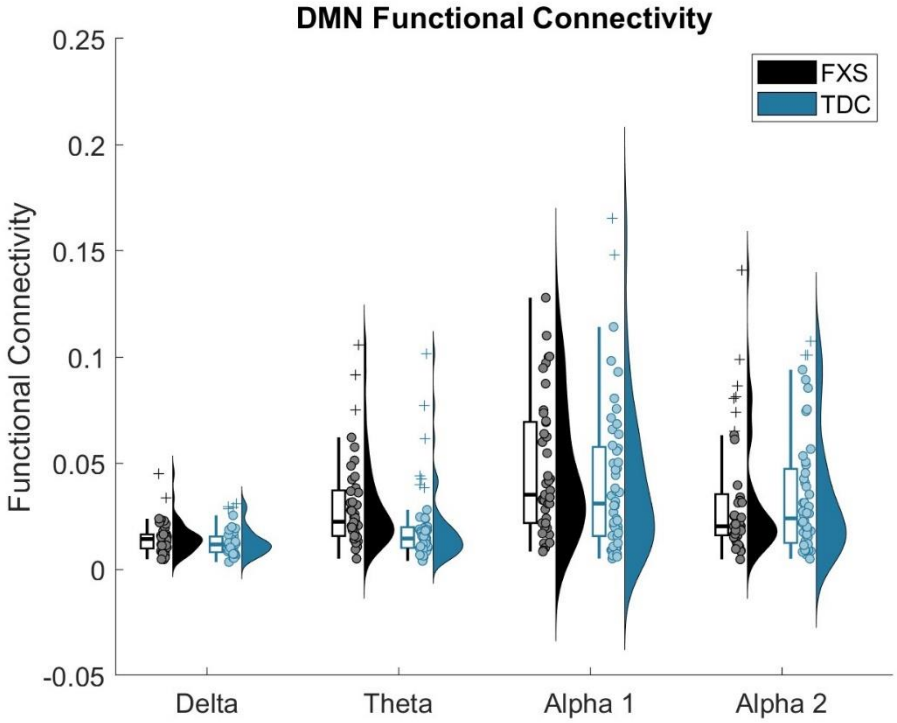

Note. Violin and boxplots depicting group differences for DMN FC across frequency bands. Dots indicate individual data points and plus signs represent outliers.

Theta connectivity was also significantly different between groups for the SN, with individuals with FXS exhibiting elevated theta connectivity (*M* rank = 53.71) relative to TDC (*M* rank = 37.56), $z = 2.94$, $p = .003$, $r = .31$ (Figure 13). Delta ($z = .81$, $p = .420$, $r = .09$), alpha 1 ($z = 1.42$, $p = .157$, $r = .15$), and alpha 2 ($z = -.08$, $p = .934$, $r = -.01$) FC within the SN were all comparable between FXS (delta: *M* rank = 47.39; alpha 1: *M* rank = 49.20; alpha 2: *M* rank = 44.76) and TDC (delta: *M* rank = 42.96; alpha 1: *M* rank = 41.42; alpha 2: *M* rank = 45.21; Figure 14).

Figure 13.

Salience Network Theta Band Functional Connectivity Circle Plots

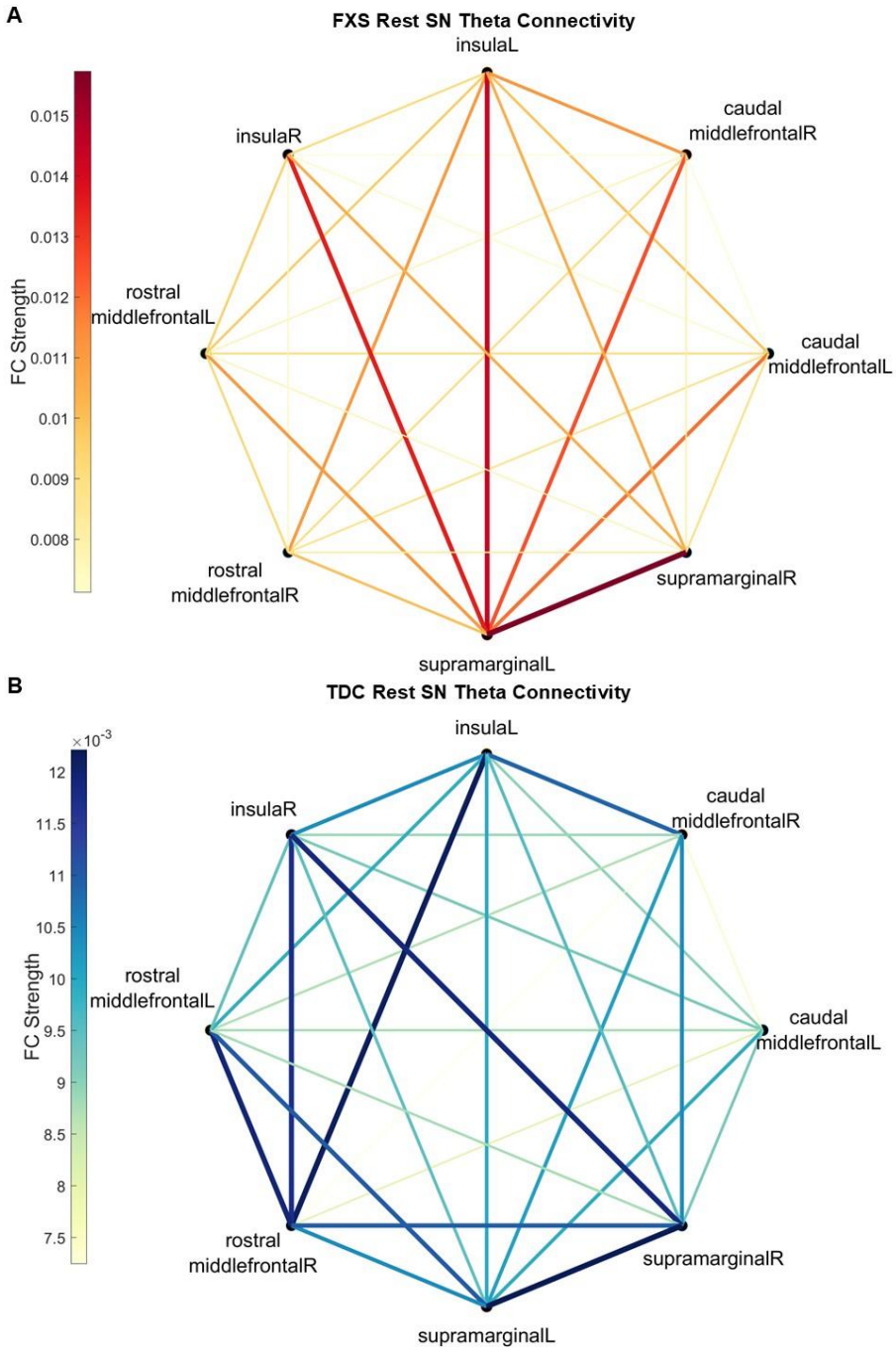

Note. Scales are different between groups. **A)** All individual connections within the SN for FXS. **B)** All individual connections within the SN for TDC. Colors indicate direction of group difference with warmer colors (yellow, orange, and red) indicating higher FC and cooler colors (blue, green, yellow) indicating lower FC where darker colors indicate higher FC values within each group.

Figure 14.

Violin and Box Plots Depicting Salience Network Functional Connectivity across Different Frequency Bands

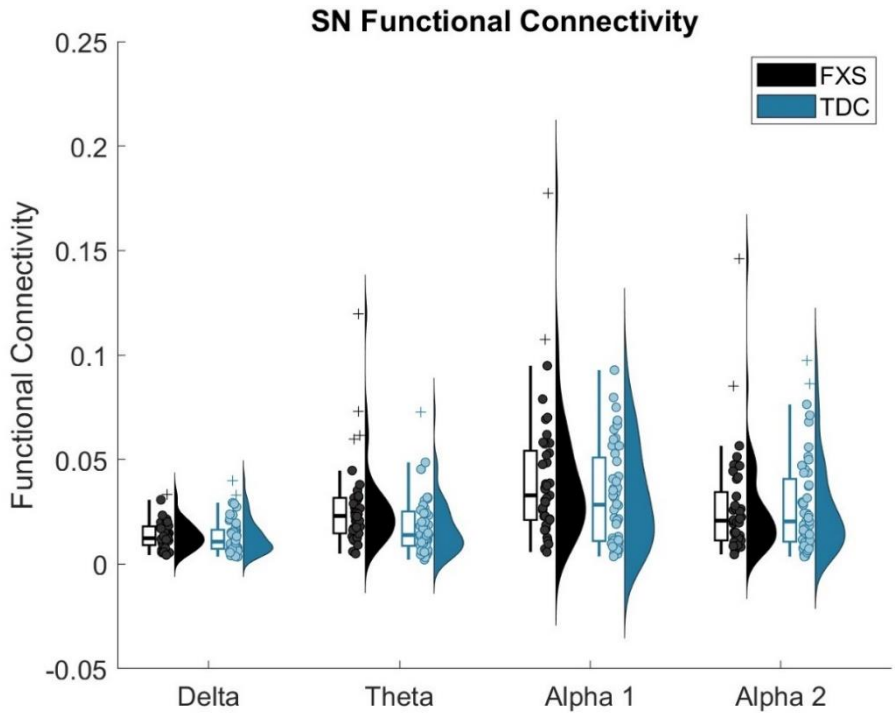

Note. Violin and boxplots depicting group differences for SN FC across frequency bands. Dots indicate individual data points and plus signs represent outliers.

Finally, similarly to both the SN and DMN, only theta FC was significantly different between groups for the control network with FXS exhibiting higher theta FC (*M* rank = 55.34) relative to TDC (*M* rank = 36.17), $z = 3.49$, $p < .001$, r = .37 (Figure 15). However, unlike with DMN and SN, control delta FC trended towards a significant difference between groups where delta FC was marginally higher in FXS (*M* rank = 50.02) compared to TDC (*M* rank = 40.71), $z = 1.70$, $p = .090$, r = .18. Both alpha 1 ($z = 1.57$, $p = .116$, r = .17) and alpha 2 ($z = -.19$ $p = .850$, r = -.02) FC were not significantly different between FXS (Alpha1: *M* rank = 49.66; Alpha 2: *M* rank = 44.44) and TDC (Alpha1: *M* rank = 41.02; Alpha 2: *M* rank = 45.48; Figure 14).

Figure 15.

Control Network Theta Band Functional Connectivity Circle Plots

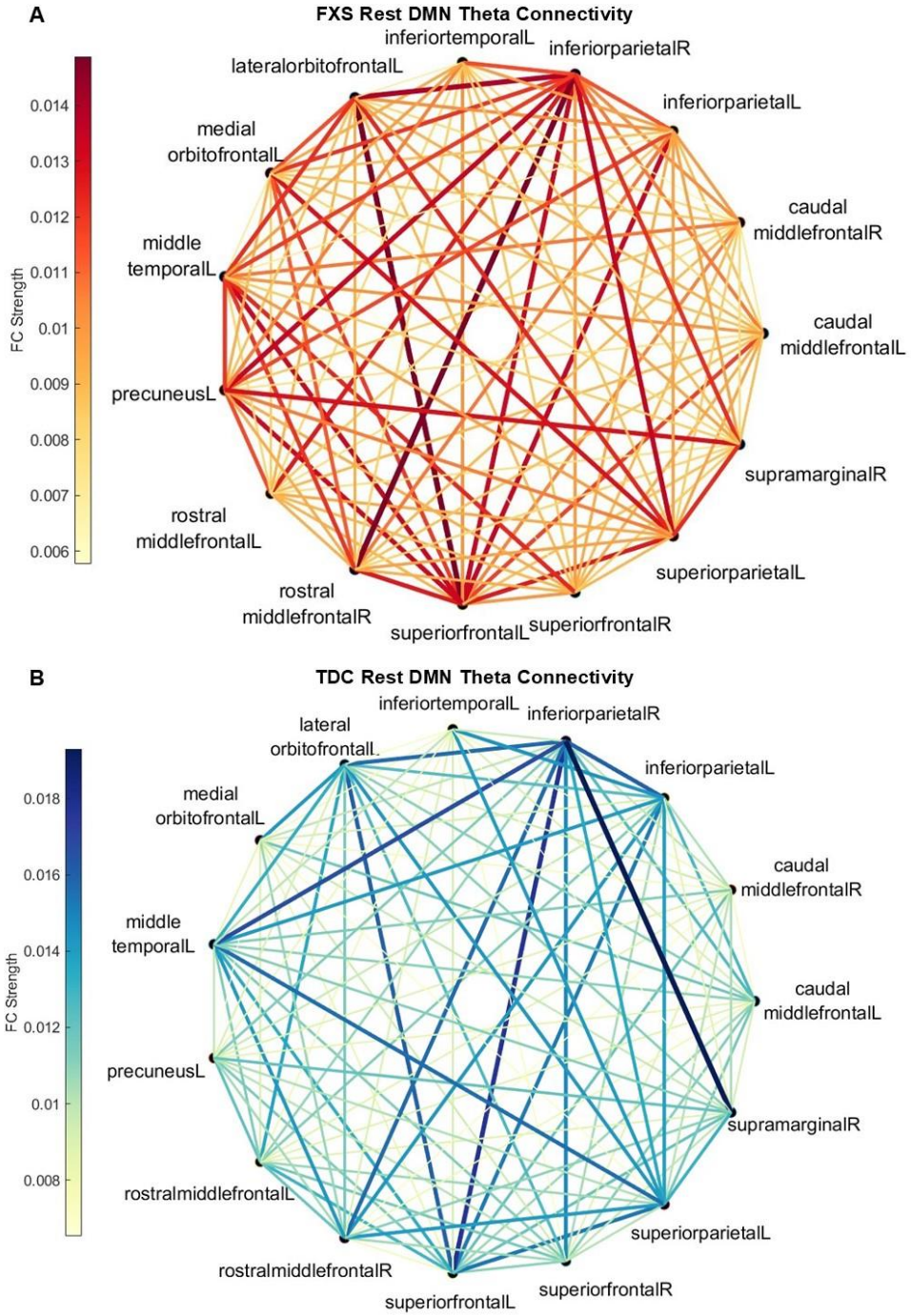

Note. Scales are different between groups. **A)** All individual connections within the control network for FXS. **B)** All individual connections within the control network for TDC. Colors indicate direction of group difference with warmer colors (yellow, orange, and red) indicating higher FC and cooler colors (blue, green, yellow) indicating lower FC where darker colors indicate higher FC values within each group.

Figure 16.

Violin and Box Plots Depicting Control Network Functional Connectivity across Different Frequency Bands

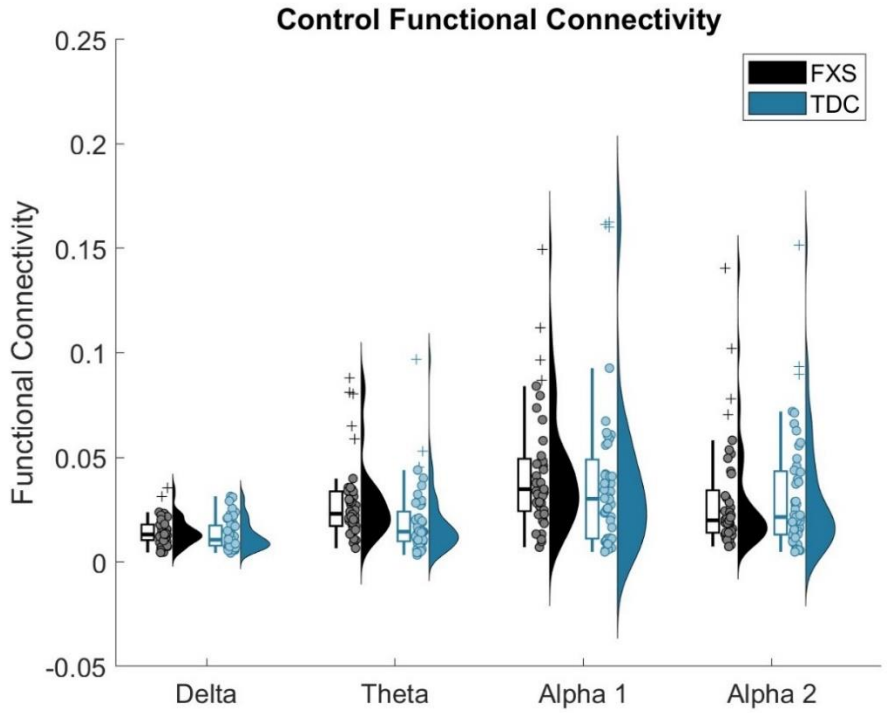

Note. Violin and boxplots depicting group differences for control network FC across frequency bands. Dots indicate individual data points and plus signs represent outliers.

Strongest Individual Functional Connectivity Connections

Next, the top ten individual connections within each network for TDC were identified to evaluate potential drivers behind group differences in theta connectivity (i.e., only frequency band with significant group differences). Only top individual theta FC connections were analyzed, as differences between groups on top connections for other frequency bands were likely less meaningful. The top theta connectivity edges (i.e., strongest connections) within each network for TDC were statistically evaluated to determine whether group-level differences across the whole network persist within the typical primary drivers of within-network connectivity.

The top ten connections for the DMN were fairly different between groups (Figure 17). The TDC top ten connections were centered on only six nodes that were all in the right hemisphere except for the left lateral orbitofrontal node where the top ten connections for FXS involve nine nodes that were more inclusive of the left hemisphere. Specifically, the left rostral anterior cingulate node, left posterior cingulate node, and the left parahippocampal node were all included in the FXS top ten but not in TDC which suggests more diffuse connectivity in FXS where diffusion was not limited to a specific hemisphere. However, the FXS top ten connections centered on the right precuneus and the strongest connections largely were to other right hemisphere nodes. While TDC top FC connections were right hemisphere dominant, the stronger connections for TDC were more distributed across nodes relative to FXS.

The strongest connection for theta connectivity within the DMN for TDC (i.e., DMN Connection 1) was the right parahippocampal node to the right isthmus cingulate node, which was a top ten connection for FXS, though one of lower strength. The next strongest connection for TDC (i.e., DMN Connection 2) was between the right parahippocampal node and the right posterior cingulate node. Connection 2 was not present in the FXS top ten connections. Overall, network connectivity for TDC was driven by connections between right parahippocampal node and other right hemisphere nodes.

The top two connections for the FXS group both involved the right precuneus where the strongest connection was between the right precuneus node to the right parahippocampal node which was still a top ten connection for TDC of moderate strength relative to other TDC connections. The second strongest connection for FXS was between the right precuneus and the right posterior cingulate node which was also a top ten connection for TDC of moderate strength. Interestingly, the top five connections for FXS all involved the right precuneus node.

Figure 17.

Theta FC Top Ten Within Default Mode Network Connections

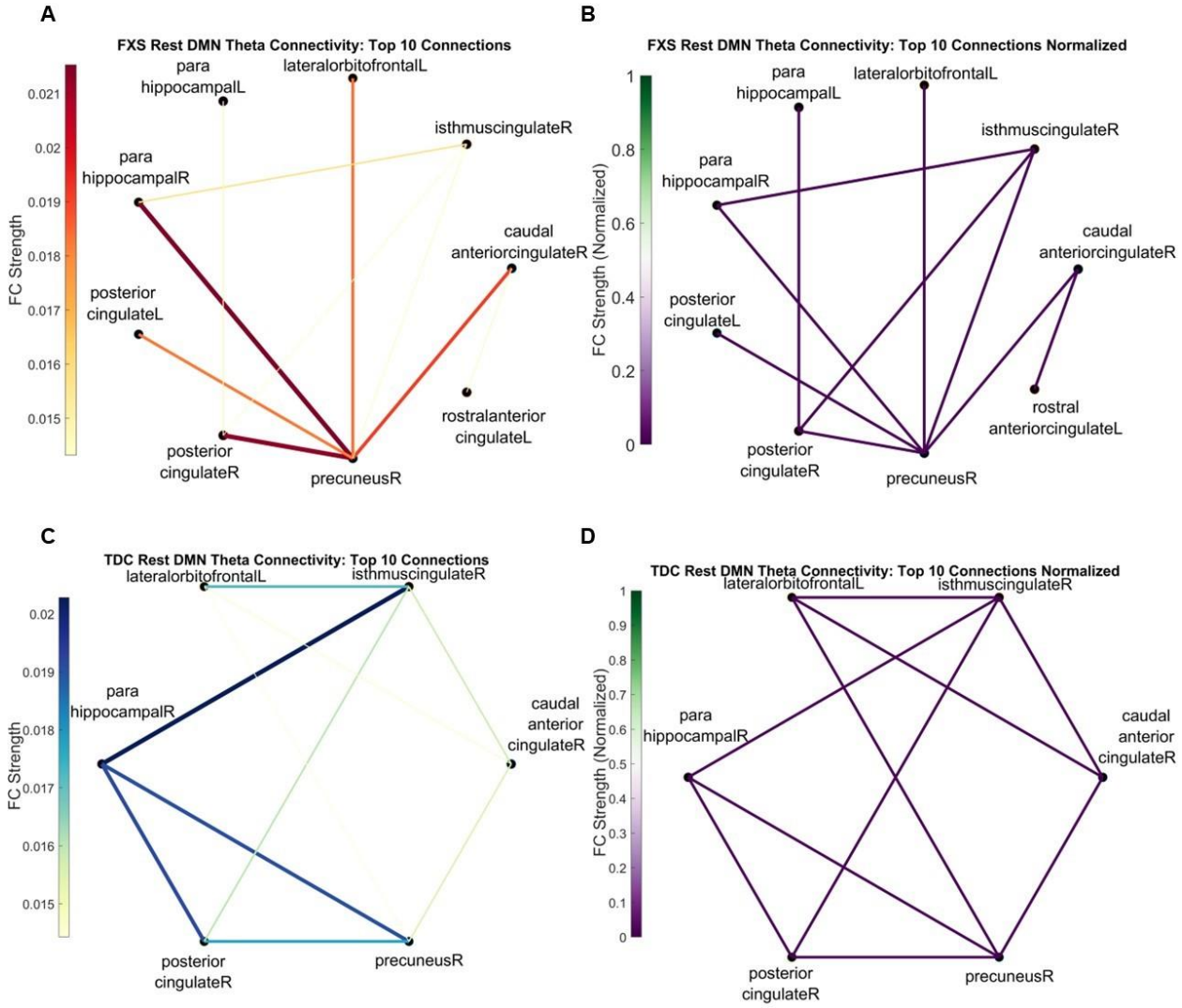

Note. Normalized plots were normalized to the full FC scale to help to visualize some of the smaller, and thus barely visible, connections in A and C. **A)** FXS top ten within network connections for the DMN (same as plot B). **B)** FXS top ten connections normalized to the full dWPLI scale. **C)** TDC top ten within network connections for the DMN (same as plot D). **D)** TDC top ten connections normalized to the full dWPLI scale.

Statistically, DMN Connection 1 was not significantly different between groups but trended towards significance after Bonferroni correction where FC was marginally higher in FXS (*M* rank = 50.85) compared to TDC (*M* rank = 40.00), $N = 89$, $z = 1.98$, $p = .096$, $r = .21$. Connection 2 was not significantly different between groups where FXS FC (*M* rank = 48.83) was comparable to TDC (*M* rank = 41.73), $N = 89$, $z = 1.29$, $p = .392$, $r = .14$ (Figure 18). The lack of significant differences in the top two connections, especially where top node connections were similar between groups, suggest that overall DMN connectivity differences are subtle and distributed across the whole network. In other words, DMN group FC differs in the overall magnitude of connectivity between groups rather than specific network mechanisms driving the difference. However, the stronger connections for FXS indirectly reconstruct the strongest TDC connections (i.e., connected through several node connections rather than a direct pathway) which may explain why top TDC connections are not statistically different from FXS. An alternative explanation could be that overall magnitude was different due to inefficient network mapping in FXS where individuals with FXS develop similar functional neural architecture but use said architecture inefficiently to accomplish neural processes.

Figure 18.

Group Differences on Default Mode Network Top Two Connections

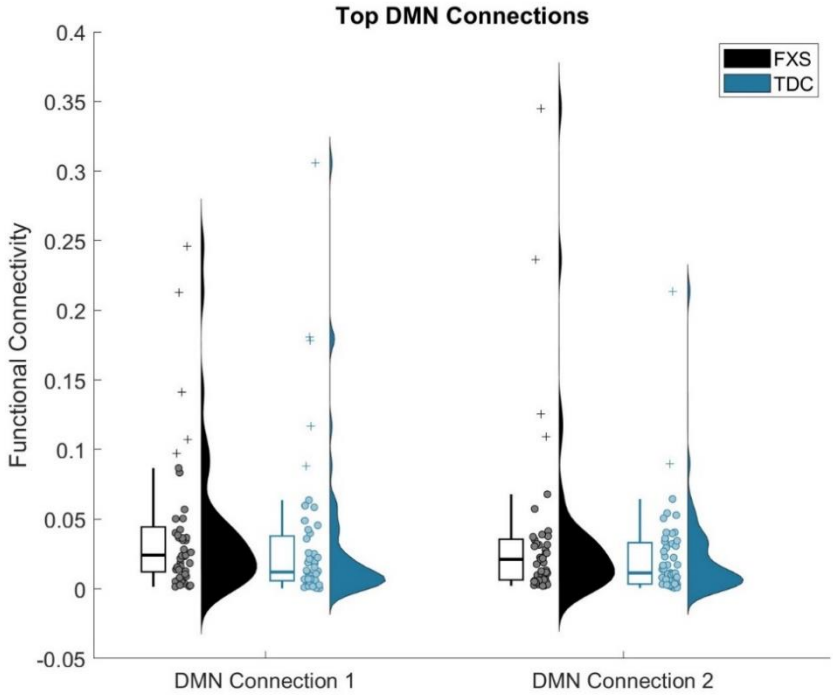

Note. Group differences for top individual connections with DMN. Connection 1 is the strongest connection for TDC (right parahippocampal node - right isthmus cingulate node) and connection 2 is the next strongest connection for TDC (right parahippocampal node - right posterior cingulate node).

Within the SN, seven nodes were present for TDC with the majority of the top ten connections sharing a connection with the right rostral middle frontal node. Eight nodes were present in the top ten connections for the FXS group with top connections involving the left supramarginal node and the left insula node. All seven nodes present for TDC were also present in the top ten connections for the FXS group except for the left caudal middle frontal node, which was the eighth node for FXS (Figure 19).

The strongest connection for TDC (i.e., SN Connection 1) was between left and right supramarginal nodes which was also the strongest connection for FXS. The second strongest connection for TDC (i.e., SN Connection 2) was between the left insula and the right rostral

middle frontal nodes, which was a top ten connection for FXS, though one of lesser strength relative to other FXS connections. For FXS, the second strongest connection was between the left insula and the left supramarginal node, which was not a top ten connection for TDC. Overall, while the top ten connections in both groups utilized similar nodes, the connectivity pattern was different between groups (Figure 19B and Figure 19C) where FXS connectivity was driven by the left supramarginal node and TDC connectivity was driven by the right rostral middle frontal node.

Figure 19.

Theta FC Top Ten Within Salience Network Connections

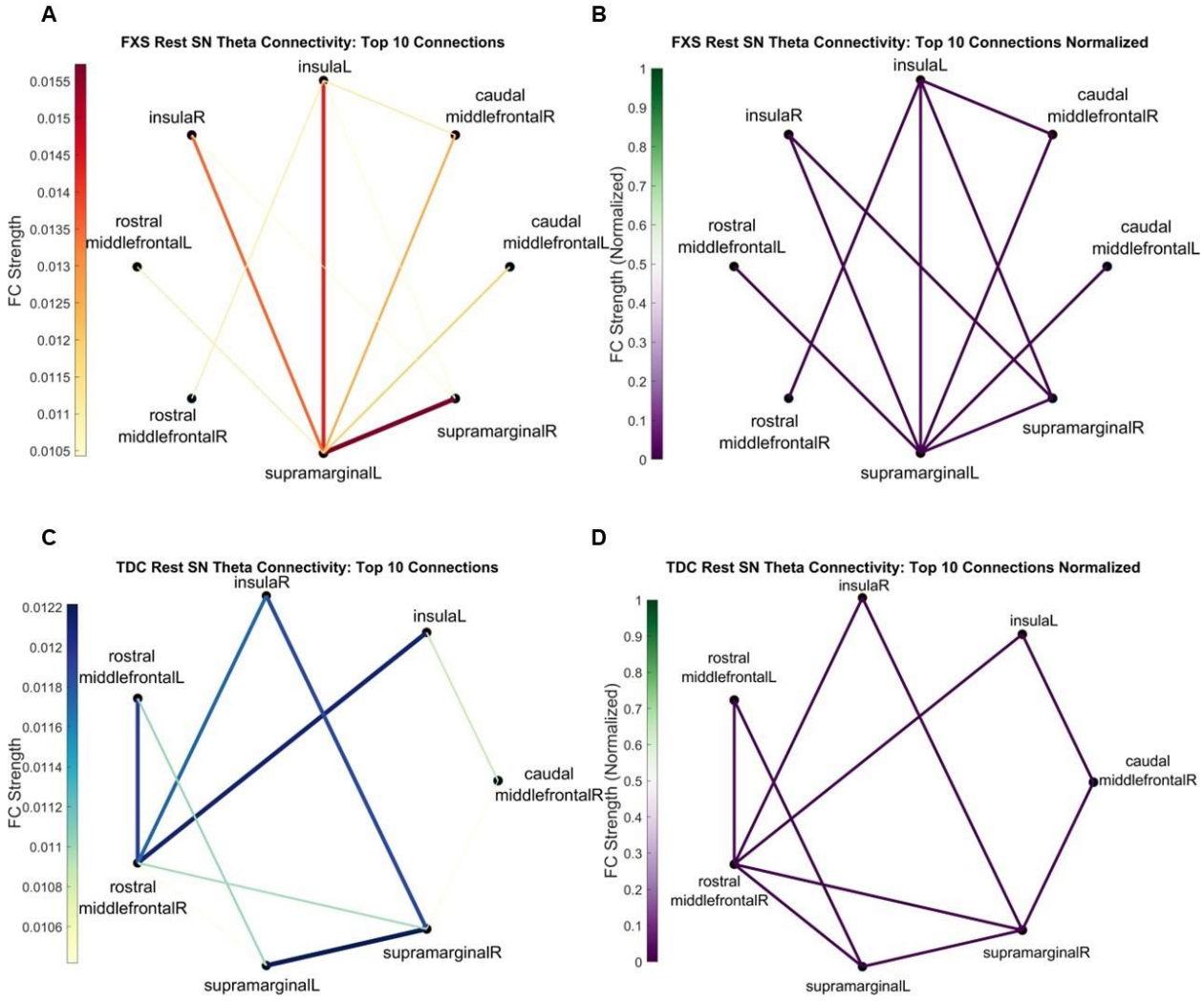

Note. Normalized plots were normalized to the full FC scale to help to visualize some of the smaller, and thus barely visible, connections in A and C. **A)** FXS top ten within network connections for the SN (same as plot B). **B)** FXS top ten connections normalized to the full dWPLI scale. **C)** TDC top ten within network connections for the SN (same as plot D). **D)** TDC top ten connections normalized to the full dWPLI scale.

Statistically, SN Connection 1 was significantly different between groups where FXS exhibited increased FC (*M* rank = 53.98) compared to TDC (*M* rank = 39.33), $N = 89$, $z = 3.03$, $p = .004$, $r = .32$. SN Connection 2 trended towards group differences after Bonferroni correction where FXS FC was marginally higher (*M* rank = 50.90) than TDC (*M* rank = 39.96), $N = 89$, $z = 1.99$, $p = .092$, $r = .21$ (Figure 20). Given the strongest connection for both groups was between the right and left supramarginal nodes, these results suggest that SN group differences primarily reflect an overall magnitude difference between FXS and TDC rather than differences in network architecture. However, the significant difference for the connection between supramarginal nodes may indicate a specific deficit in the supramarginal gyri linked to theta oscillatory activity.

Figure 20.

Group Differences on Salience Network Top Two Connections

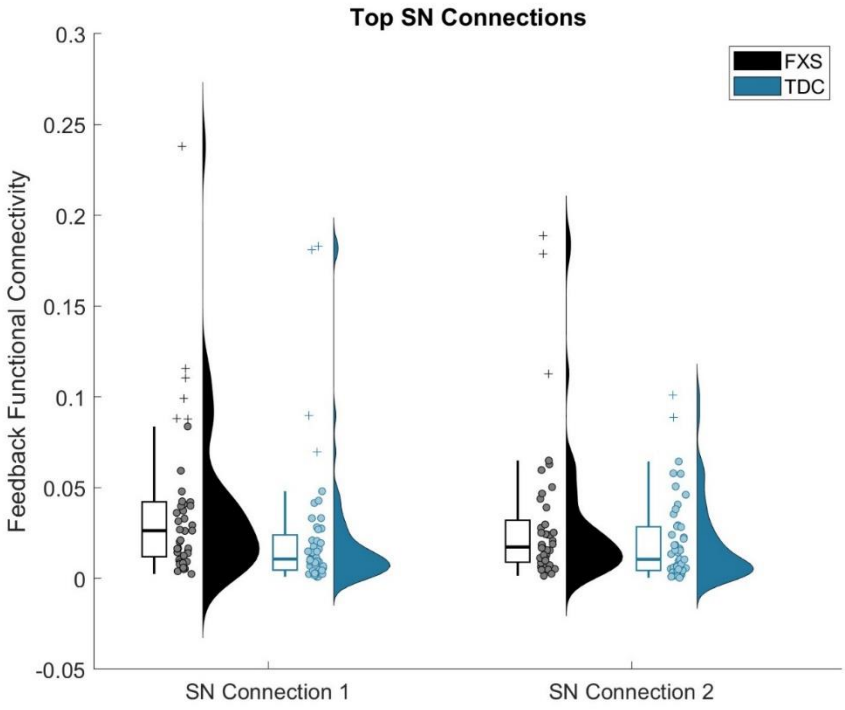

Note. Group differences for top individual connections with SN. Connection 1 is the top connection for TDC (left supramarginal node - right supramarginal node) and connection 2 is the next strongest connection for TDC (left insula - right rostral middle frontal nodes).

Similarly to both within network DMN and SN connectivity, the control network had more nodes represented in the top ten connections for FXS. The TDC top connections involved eight nodes where FXS top connections involved nine nodes. All nodes were the same between groups except for the addition of the left precuneus node in FXS.

The top/strongest control network connection for TDC (i.e., Con Connection 1) was between the right inferior parietal and right supramarginal nodes which was not a connection in the FXS top ten. The next strongest connection for TDC (i.e., Con Connection 2) was between the right inferior parietal and left superior frontal nodes which was a connection present in the FXS top ten connections but one of lesser strength relative to other FXS connections (Figure 21).

The top connection for FXS was between the right rostral middle frontal and the right inferior parietal nodes. The second strongest connection was between the left superior frontal node and the left lateral orbitofrontal node. Both of the strongest connections for FXS were present in the top ten connection for TDC but were of lesser strength relative to other TDC connections. Interestingly, the right inferior parietal node shared the greatest number of connections in both groups where the only major group difference, outside of different top connections, was the left superior frontal node shared more top ten connections in FXS than TDC.

Figure 21.

Theta FC Top Ten Within Control Network Connections

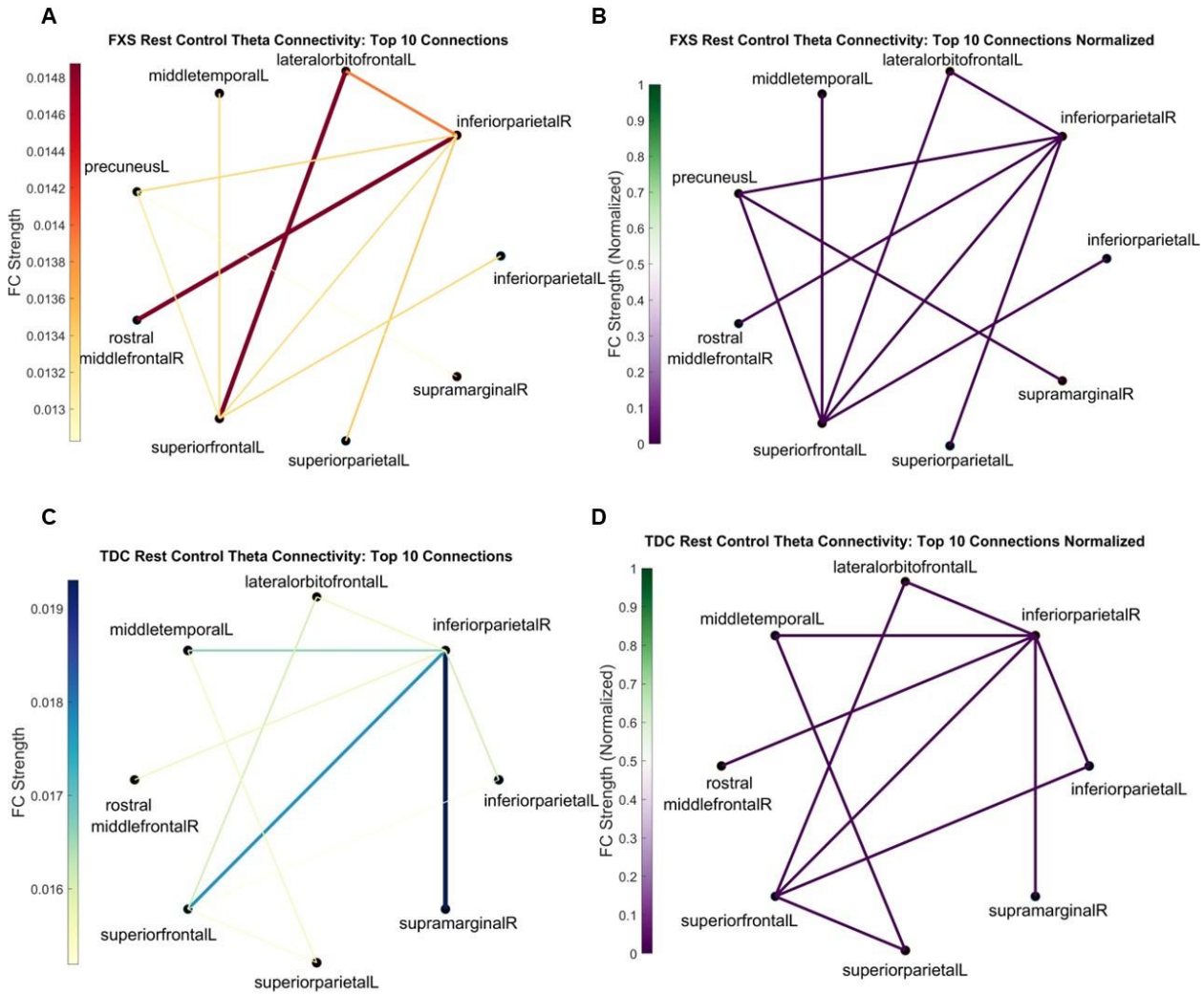

Note. Normalized plots were normalized to the full FC scale to help to visualize some of the smaller, and thus barely visible, connections in A and C. **A)** FXS top ten within network connections for the control network (same as plot B). **B)** FXS top ten connections normalized to the full dWPLI scale. **C)** TDC top ten within network connections for the control network (same as plot D). **D)** TDC top ten connections normalized to the full dWPLI scale.

Statistically, both of the strongest control network connections for TDC were not significantly different between groups (Con Connection 1: $N = 89$, $z = .35$, $p = 1.00$, $r = .04$; Con Connection 2: $N = 89$, $z = 1.20$, $p = .458$, $r = .13$; Figure 22) where FXS FC (M rank = 48.56) was largely similar to TDC (M rank = 41.96). Given the strongest connection for TDC (i.e., Con Connection 1) was not present for FXS and Con Connection 2 was of reduced strength, the lack of group differences on both nodes suggests that group differences arose from a more diffuse pattern of connectivity in FXS relative to TDC. The whole network plot suggests over connectivity in control network compared to TDC where diffusely increased FC may reflect network inefficiencies (Figure 15).

Figure 22.

Group Differences on Control Network Top Two Connections

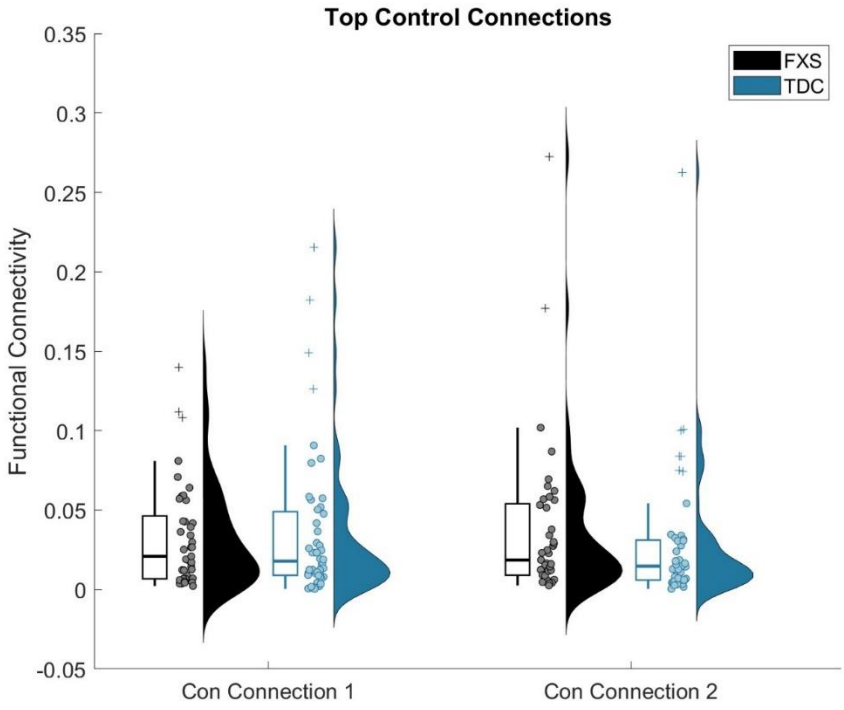

Note. Group differences for top individual connections with control network. Connection 1 is the top connection for TDC (right inferior parietal - right supramarginal nodes) and connection 2 is the next strongest connection for TDC (right inferior parietal - left superior frontal nodes).

Lastly, FC across the top ten connections was summed separately for each group to create a sum score that represents the overall strength of the individual group top ten connections. Sum scores were statistically evaluated using independent samples Mann-Whitney U tests to further explore whether the areas involved in each respective group's network FC were driving the overall group differences. Across all three networks, there were no significant group differences where FXS exhibited comparable FC over the top ten connections to TDC (Table 5; Figure 23). Overall, FC sum score results suggest that specific network mechanisms are not driving group differences. Group differences may arise from more diffuse and stronger overall connectivity across the whole network for FXS (i.e., more diffuse connectivity across moderate-to-low strength connections) where increased FC may reflect network inefficiencies.

Table 5.

Independent Samples Mann-Whitney U Results for Top FC Sum Scores

	Independent Samples Mann-Whitney U Results				
Network	FXS (*M* Rank)	TDC (*M* Rank)	*z*	*p*	*r*
DMN	44.32	45.58	-.23	.818	-.02
SN	43.93	45.92	-.36	.717	-.04
Control	43.10	47.22	.75	.454	.08

Note. Sample size was 89. Group differences on the sum of each group's top ten connections for each functional network of interest.

Figure 23.

Violin and Boxplots Depicting Group Differences on Functional Connectivity Summed across the Top Ten Connections for Each Network

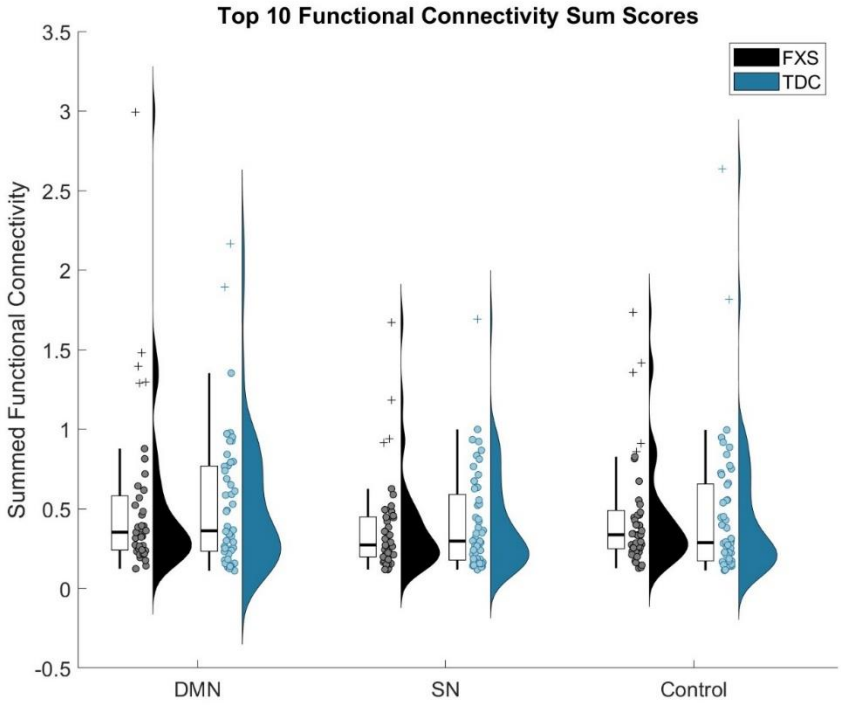

Frequency Band Analysis

Non-parametric Mann-Whitney U tests were used to evaluate group differences on both absolute and relative power across all frequency bands for both frontal and posterior regions of the head.

Absolute frontal delta, theta, and both gamma 1 and gamma 2 were significantly elevated for FXS relative to TDC (Table 6; Figure 24).

Figure 24.

Boxplots for Absolute Power across All Frequency Bands for the Frontal Electrode Selection

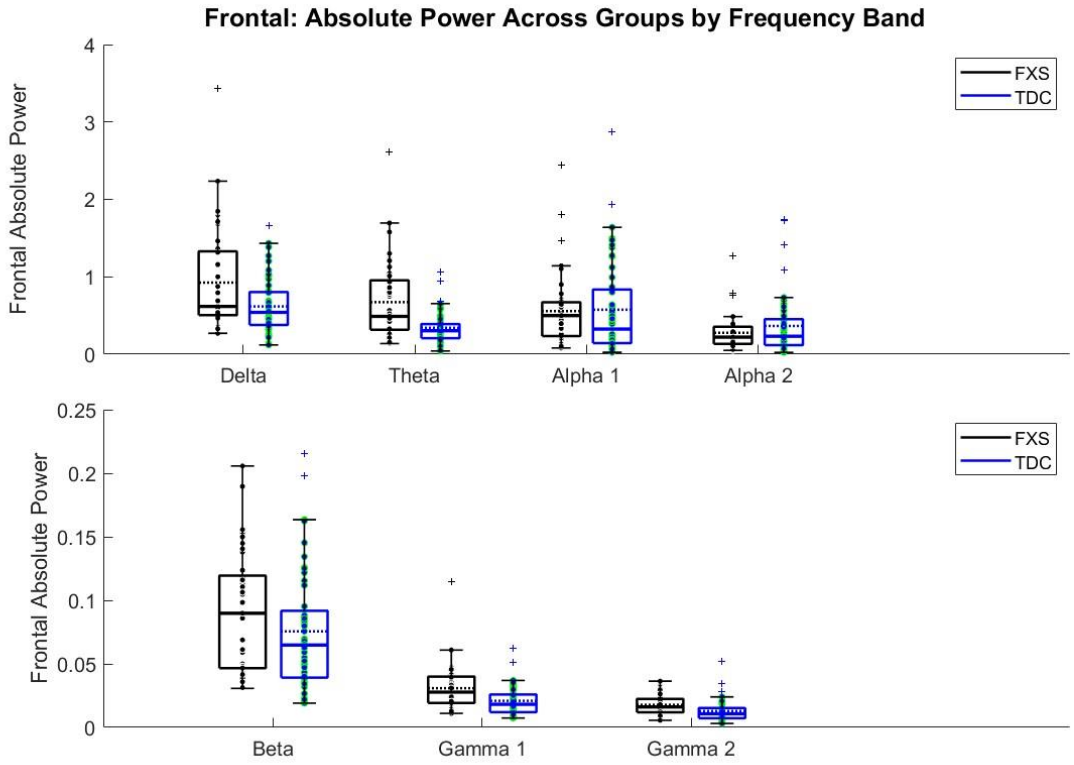

Note. Plot split due to scale differences across the different frequency bands. Plots depict the absolute power for each frequency bands between groups.

Table 6.

Mann-Whitney U Test results for Frontal Absolute Power across Frequency Bands

	Mann-Whitney U Test Results				
Frequency Band	FXS (*M* ranked)	TDC (*M* ranked)	*z*	*p*	*r*
Delta	52.00	39.02	2.36	.018	.25
Theta	55.73	35.83	3.62	< .001	.39
Alpha 1	47.95	42.48	1.00	.319	.11
Alpha 2	43.88	45.96	-.38	.705	-.04
Beta	49.39	41.25	1.48	.138	.16
Gamma 1	54.80	36.63	3.31	< .001	.35
Gamma 2	55.27	36.23	3.47	< .001	.37

Note. Sample size was $N = 89$.

For relative frontal power, only relative theta and alpha 2 were significantly different between groups where relative theta was elevated in FXS and relative alpha 2 was significantly reduced in FXS compared to TDC. Additionally, relative beta was marginally significant with FXS trending towards an elevation in power (Table 7; Figure 25).

Figure 25.

Boxplots for Relative Power across All Frequency Bands for the Frontal Electrode Selection

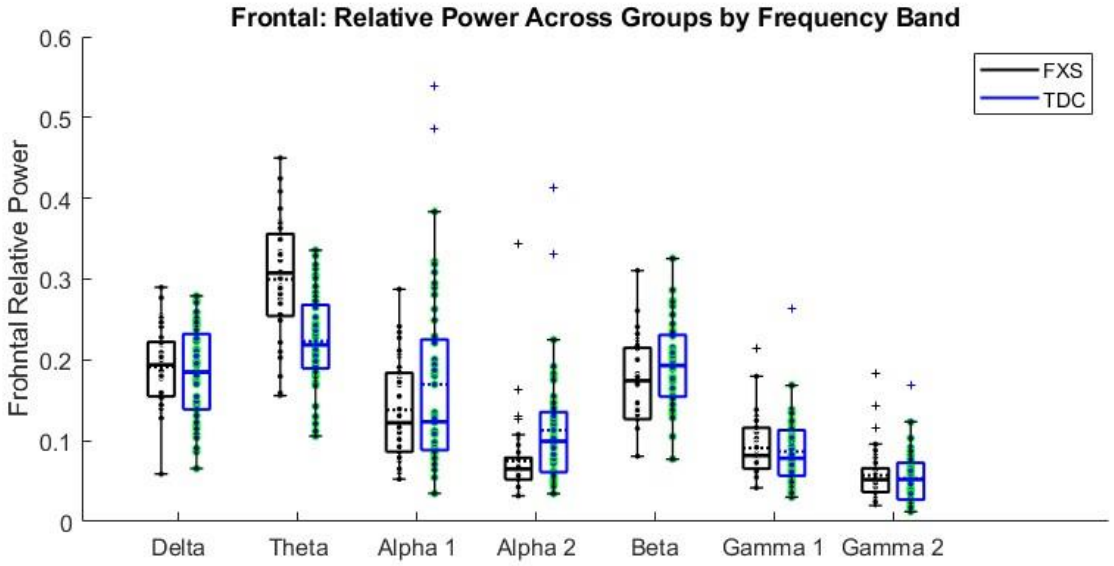

Table 7.

Mann-Whitney U Test results for Frontal Relative Power across Frequency Bands

	Mann-Whitney U Test Results				
Frequency Band	FXS (*M* ranked)	TDC (*M* ranked)	*z*	*p*	*r*
Delta	46.90	43.38	.64	.521	.07
Theta	58.63	33.35	4.60	< .001	.49
Alpha 1	42.71	46.96	-.77	.439	-.08
Alpha 2	34.54	53.94	-3.53	< .001	-.38
Beta	39.54	49.67	-1.84	.065	-.20
Gamma 1	47.39	42.96	.81	.420	.09
Gamma 2	46.39	43.81	.47	.639	.05

Note. Sample size was $N = 89$.

Absolute power for the posterior head region exhibited a similar pattern to the frontal absolute power where delta, theta, and both gamma 1 and gamma 2 were significantly different between groups with FXS exhibiting elevated power across all four frequency bands compared to TDC (Table 8; Figure 26). However, absolute beta power trended towards an elevation in FXS unlike in frontal channels.

Figure 26.

Boxplots for absolute power across all frequency bands for the posterior electrode selection

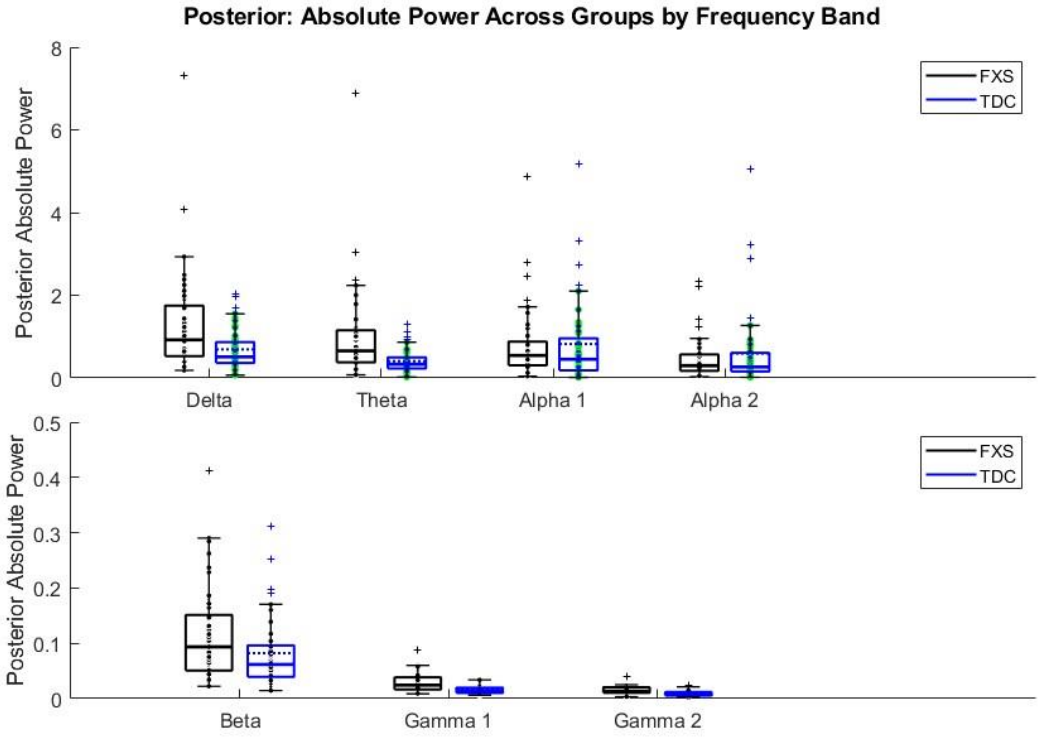

Note. Plot split due to scale differences across the different frequency bands.

Table 8.

Mann-Whitney U Test results for Posterior Absolute Power across Frequency Bands

	Mann-Whitney U Test Results				
Frequency Band	FXS (*M* ranked)	TDC (*M* ranked)	*z*	*p*	*r*
Delta	54.27	37.08	3.13	.002	.33
Theta	55.80	35.77	3.65	<.001	.39
Alpha 1	47.41	42.94	.82	.415	.09
Alpha 2	46.07	44.08	.36	.717	.04
Beta	50.34	40.44	1.80	.071	.19
Gamma 1	58.46	33.50	4.54	<.001	.48
Gamma 2	57.73	34.13	4.30	<.001	.46

Note. Sample size was $N = 89$.

Posterior relative theta and alpha 2 were significantly different between groups with FXS exhibiting elevated theta but reduced alpha 2 compared to TDC. Additionally, relative gamma 1 power trended toward a significant elevation for FXS. Absolute delta, alpha 1, and gamma 2 were not statistically significantly different between groups (Table 9; Figure 27).

Figure 27.

Boxplots for Relative Power across All Frequency Bands for the Posterior Electrode Selection

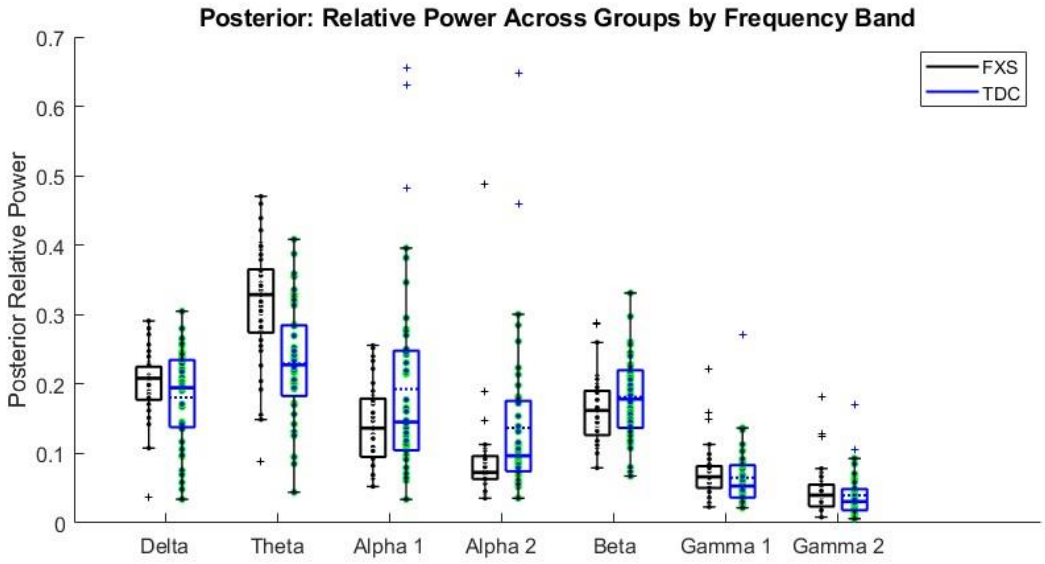

Table 9.

Mann-Whitney U Test results for Posterior Relative Power across Frequency Bands

	Mann-Whitney U Test Results				
Frequency Band	FXS (*M* ranked)	TDC (*M* ranked)	*z*	*p*	*r*
Delta	48.46	42.04	1.17	.242	.12
Theta	58.27	33.67	4.48	<.001	.48
Alpha 1	41.49	48.00	-1.19	.236	-.13
Alpha 2	35.44	53.17	-3.23	.001	-.34
Beta	40.24	49.06	-1.61	.108	-.17
Gamma 1	50.10	40.65	1.72	.085	.18
Gamma 2	48.63	41.90	1.23	.220	.13

Note. Sample size was $N = 89$.

Individual Peak Alpha Frequency (PAF) Analysis

The individual PAF values were analyzed using non-parametric Mann-Whitney U tests to evaluate PAF across frontal and posterior regions of the head, as well as globally across the whole head (i.e., all electrodes) by group. Whole head ($z = -4.30$, $p < .001$, $r = -.46$), frontal ($z = -3.51$, $p < .001$, $r = -.37$), and posterior ($z = -3.18$, $p < .001$, $r = -.34$) PAF values were all significantly different between groups with FXS exhibiting reduced values for all 3 variables (Whole head: *M* rank = 32.26, Frontal: *M* rank = 34.60, Posterior: *M* rank = 35.57) relative to TDC (Whole head: *M* rank = 55.89, Frontal: *M* rank = 53.89, Posterior: *M* rank = 53.05; Figure 28).

Figure 28.

Relative Power Spectrum Depicting Peak Alpha Frequency Between Groups

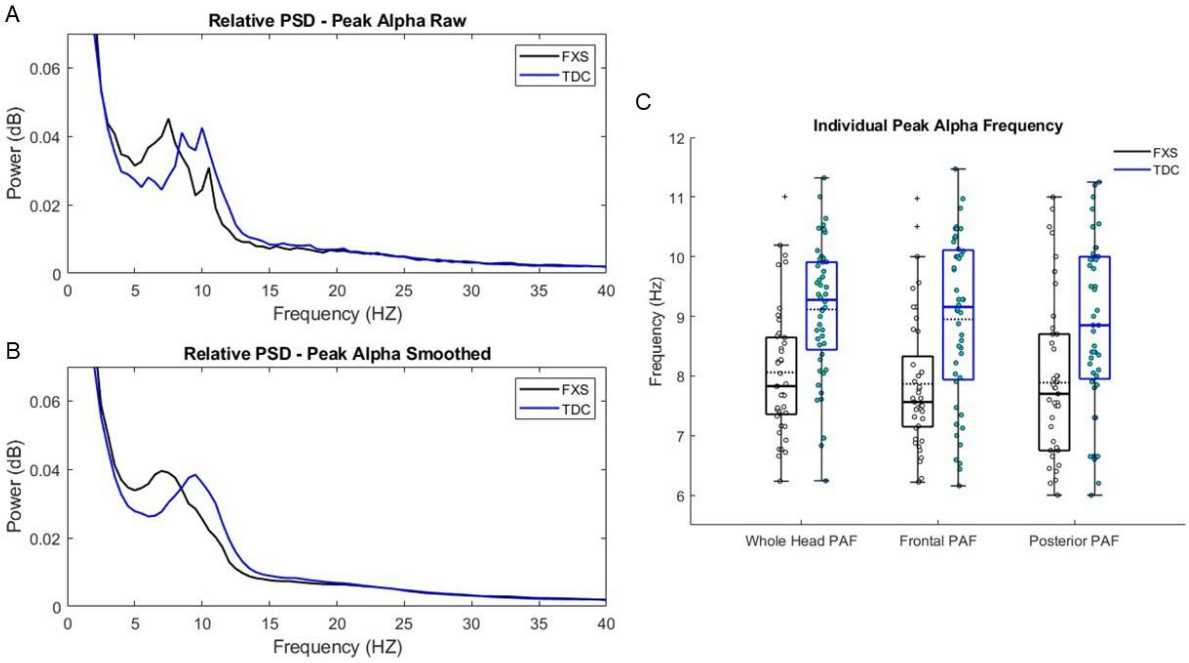

Note. **A)** Unsmoothed/raw PSD. **B)** Smoothed PSD. **C)** Boxplots for whole head, frontal, and posterior PAF.

PAF was also evaluated for potential sex effects but violated assumptions of normality and tests assessing equal variances (Appendix A). Mann-Whiney U tests were used to evaluate sex effects for FXS and TDC, separately. No statistically significant differences were identified for FXS, though all three PAF regions trended towards differences (Whole head: z = -1.87, p = .063, r = -.20; Frontal: z = -1.87, p = .063, r = -.20; Posterior z = -1.69, p = .091, r = -.18) where males had marginally reduced PAF (Whole head: *M* rank = 18.35, Frontal: 18.35, Posterior: *M* rank = 18.60) compared to females (Whole head: *M* rank = 25.60, Frontal: 25.60, Posterior: *M* rank = 25.17).

Similarly to FXS, no significant differences were identified for TDC for all three PAF regions. Though, none of the PAF regions trended towards differences (Whole head: z = .04, p =

.965, r = .00; Frontal: z = .50, p = .615, r = .05; Posterior z = .49, p = .622, r = .05) where males were comparable (Whole head: *M* rank = 24.56, Frontal: 25.22, Posterior: *M* rank = 25.20) to females (Whole head: *M* rank = 24.38, Frontal: 23.06, Posterior: *M* rank = 23.09).

FMRP Analysis

For FXS males only, correlations were evaluated for microstate and FC variables that demonstrated significant group differences where no significant relationships were identified between EEG variables and FMRP (Table 10).

Table 10.

Spearman's Correlations between FMRP and EEG Variables of Interest

Variables	*N*	Rho	p-value
Total GEV	19	.04	.863
Total GFP	19	.12	.615
MS1 GFP	19	.12	.615
MS2 GFP	19	.10	.689
MS3 GFP	19	.20	.410
MS4 GFP	19	.07	.778
DMN Theta FC	19	-.15	.542
SN Theta FC	19	.07	.778
Control Theta FC	19	.11	.663

Microstate and Functional Connectivity Correlation Analysis

One of the primary goals of the current study was to determine whether microstate variables could serve as potential proxies for FC disruptions in FXS. While unable to directly assess FC on microstate classes, a correlation analysis evaluated potential relationships for future investigation. Only the 4MS solution variables were used in correlation analyses.

First, relationships between individual microstate classes and within network FC were evaluated in correlation analyses to determine whether individual microstate measures map onto FC variables for the whole sample (Figure 29 & 30). Next, the same correlations were evaluated

for FXS only (Figure 31 & 32). Overall, only MS4 shared a pattern of relationships with FC but those patterns were not present for FXS where correlations may recapitulate group differences in one or both variables.

Next, global microstate variables (i.e. total GEV, average GFP, GFP peaks per second, mean duration, complexity, and Hurst) were evaluated in a correlation analysis with FC variables.

Across all participants, GFP peaks per second (PPS) were inversely correlated with all alpha FC variables across networks where increased GFP peaks were associated with reduced functional connectivity (Figure 30). However, this pattern does not fully hold for FXS where only the correlations between GFP PPS and SN alpha 1 FC remain significant. Instead, a pattern of inverse correlations between GFP peaks emerged for delta and theta FC for DMN and SN but not the control network (Figure 33).

GEV also exhibited a pattern of direct correlations with FC values where GEV was positively correlated with theta and alpha 1 FC where increased GEV was associated with increased FC in both theta and alpha. Given the significant group differences on theta FC, FXS correlations were of interest and showed the same pattern suggesting they were potentially driving the whole sample correlations.

Figure 29.

Correlation Plot for Functional Connectivity and Individual Microstate Class Duration, Coverage, and Occurrence

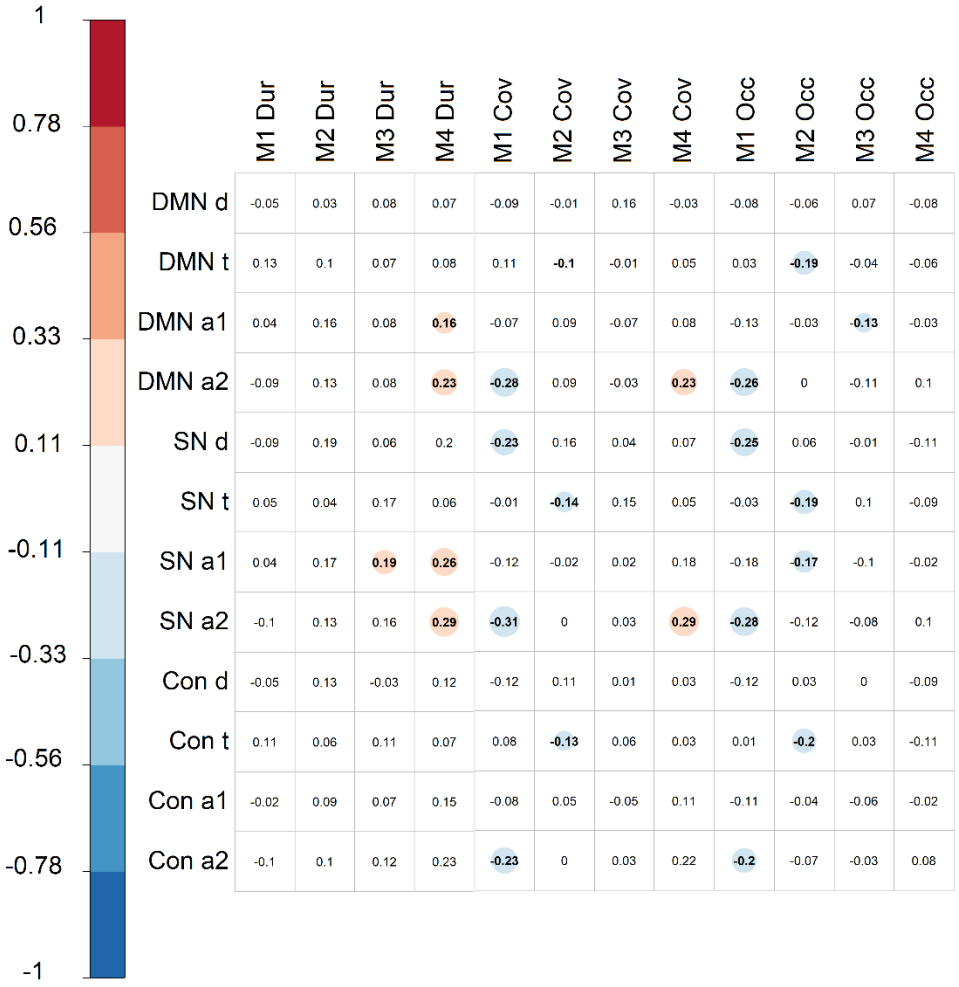

Note. $N = 89$. All statistically significant correlations are bolded and indicated by colored circles where warmer colors are direct correlations and cooler colors are inverse correlations. Dur = microstate duration; Cov = microstate coverage; Occ = microstate occurrence; DMN = default mode network; SN = salience network; Con = control network; d = delta, t = theta, a1 = alpha 1; a2 = alpha2.

Figure 30.
Correlation Plot for Functional Connectivity and Individual Microstate Class GEV and GFP

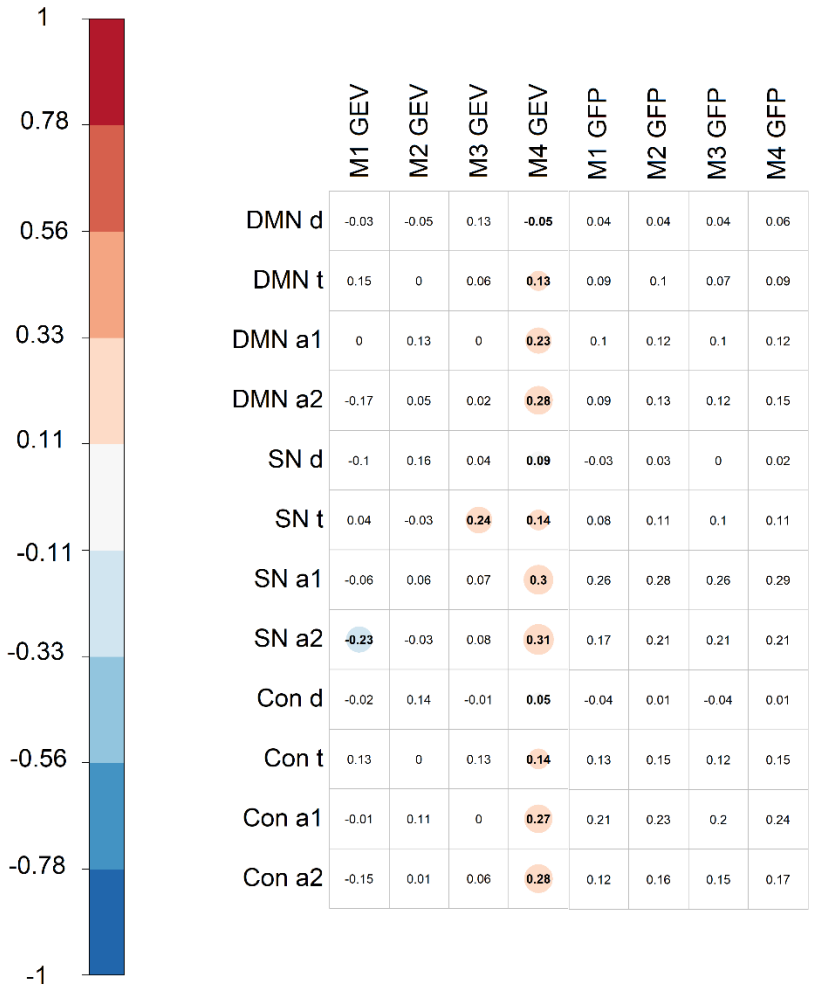

Note. $N = 89$. All statistically significant correlations are bolded and indicated by colored circles where warmer colors are direct correlations and cooler colors are inverse correlations. GEV = global explained variance; GFP = global field power; DMN = default mode network; SN = salience network; Con = control network; d = delta, t = theta, a1 = alpha 1; a2 = alpha2.

Figure 31.

Correlation Plot for Functional Connectivity and Individual Microstate Class Duration, Coverage, and Occurrence for FXS Group Only

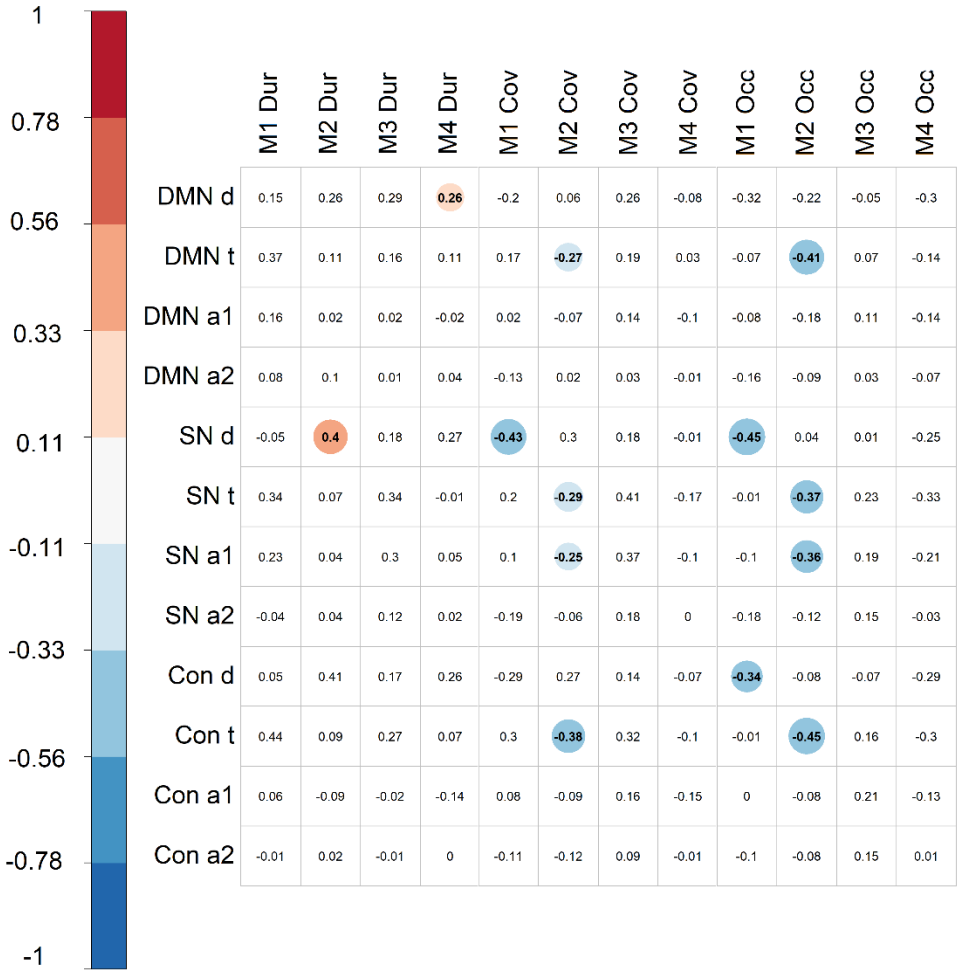

Note. $N = 41$. All statistically significant correlations are bolded and indicated by colored circles where warmer colors are direct correlations and cooler colors are inverse correlations. Dur = microstate duration; Cov = microstate coverage; Occ = microstate occurrence; DMN = default mode network; SN = salience network; Con = control network; d = delta, t = theta, a1 = alpha 1; a2 = alpha2.

Figure 32.

Correlation Plot for Functional Connectivity and Individual Microstate Class Duration, Coverage, and Occurrence for FXS Group Only

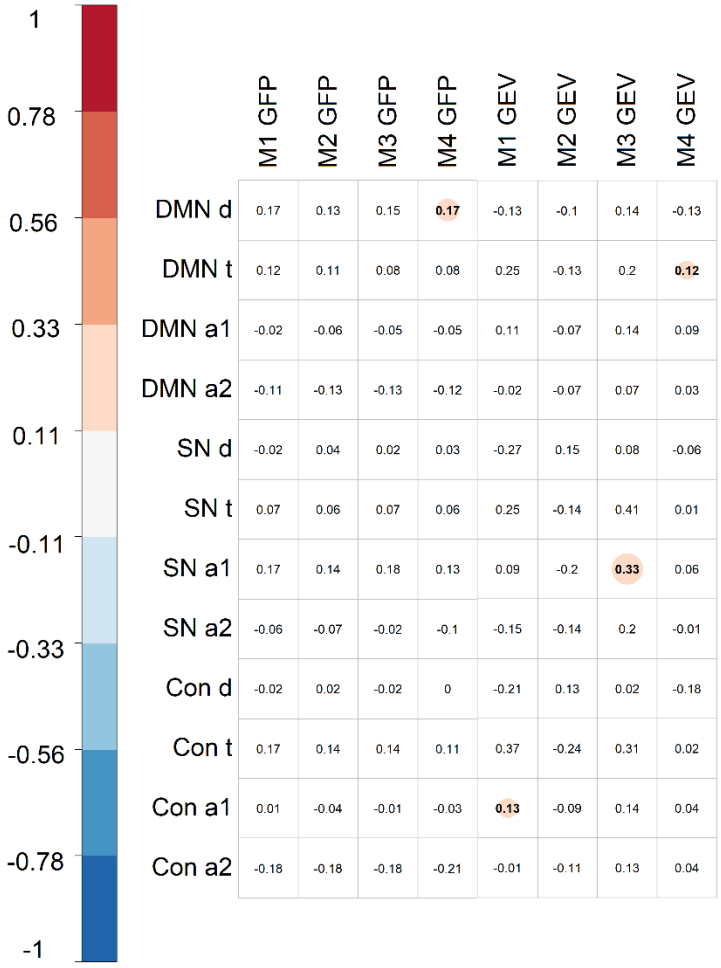

Note. N = 41. All statistically significant correlations are bolded and indicated by colored circles where warmer colors are direct correlations and cooler colors are inverse correlations. GEV = global explained variance; GFP = global field power; DMN = default mode network; SN = salience network; Con = control network; d = delta, t = theta, a1 = alpha 1; a2 = alpha2.

Figure 33.

Correlation Plot for Functional Connectivity and Global Microstate Variables

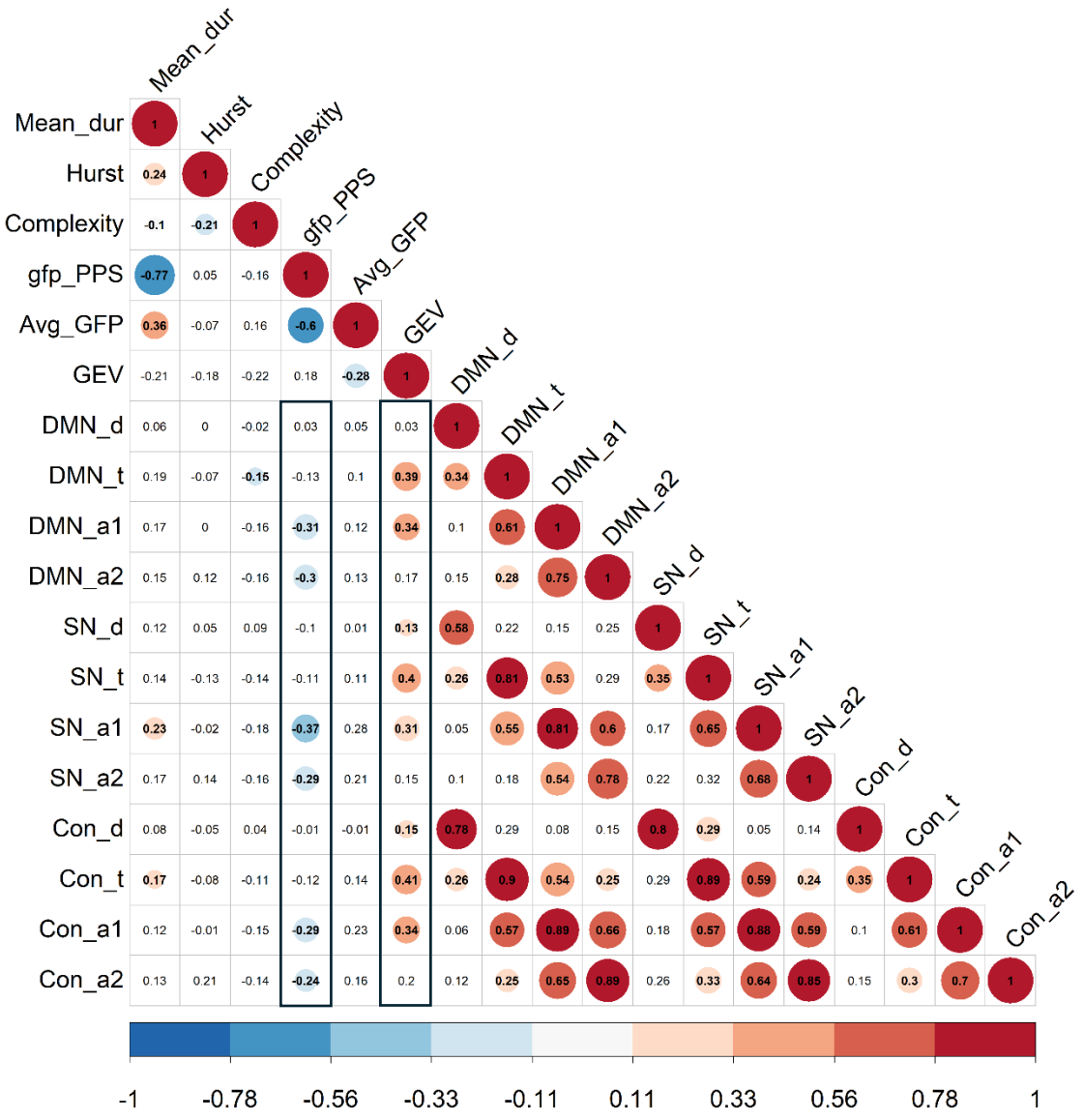

Note. N = 89. All statistically significant correlations are bolded and indicated by colored circles where warmer colors are direct correlations and cooler colors are inverse correlations. Black boxes highlight columns with correlations of interest. GFP = global field power; PPS = peaks per second; GEV = global explained variance; DMN = default mode network; SN = salience network; Con = control network; d = delta, t = theta, a1 = alpha 1; a2 = alpha2.

Figure 34.

Correlation Plot for Functional Connectivity and Global Microstate Variables for FXS Only

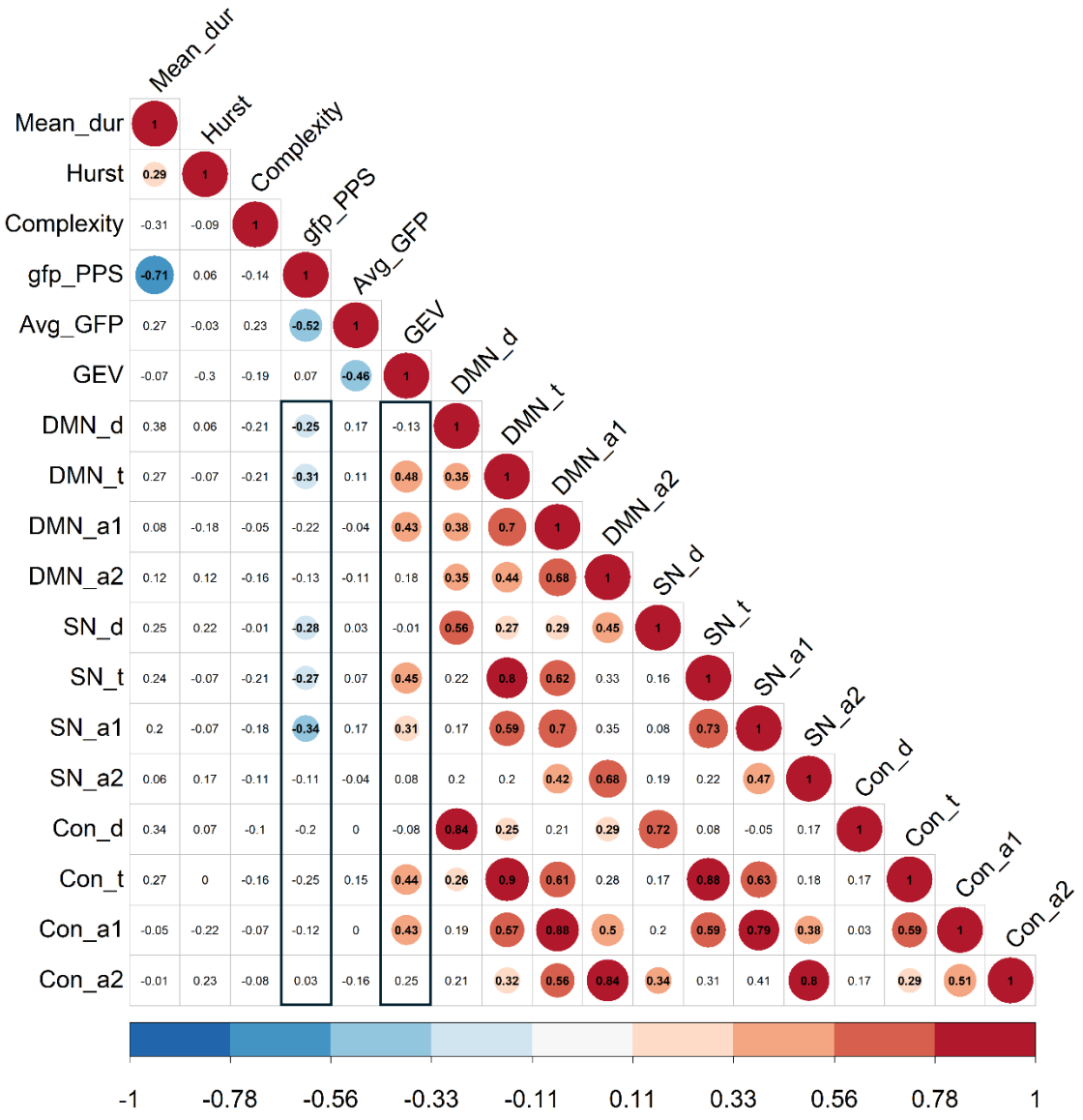

Note. $N = 41$. All statistically significant correlations are bolded and indicated by colored circles where warmer colors are direct correlations and cooler colors are inverse correlations. Black boxes highlight columns with correlations of interest. GFP = global field power; PPS = peaks per second; GEV = global explained variance; DMN = default mode network; SN = salience network; Con = control network; d = delta, t = theta, a1 = alpha 1; a2 = alpha2.

Correlation and Clinical Variable Analysis

Correlation analyses were conducted to evaluate potential relationships between EEG variables of interest (i.e., microstates and FC) and both clinical measures and other EEG variables (power and PAF).

Microstate and FC variables were evaluated in relation to IQ. A univariate ANOVA was first run to confirm the typical relationship between group and sex on the abbreviated IQ z-score, as most in the sample had the abbreviated IQ. There was a significant main effect of group where FXS (M = 41.36, SD = 30.62) had reduced IQ compared to TDC (M = 105.42, SD = 10.95), F(1, 85) = 269.30, $p < .001$, ES = .76, OP = 1.00. There was also a significant main effect of sex where females (M = 87.18, SD = 23.49) had higher IQ than males (M = 69.92, SD = 44.19), F(1, 85) = 31.55, $p < .001$, ES = .31, OP = 1.00. Finally, there was a significant interaction between group and sex where FXS males (M = 23.59, SD = 16.54) had reduced IQ relative to females with FXS (M = 72.18, SD = 24.22) and TDC males (M = 107.56, SD = 10.38) were comparable to TDC females (M = 101.13, SD = 11.12), F(1, 85) = 63.91, $p < .001$, ES = .43, OP = 1.00. Importantly, both TDC males and females were significantly different from FXS males and females at the $p < .001$ level after Bonferroni correction where males exhibited greater differences (M difference = 83.97, SE = 4.07) than females (M difference = 28.96, SE = 5.55).

The correlation analysis for IQ and microstate variables identified a significant inverse correlation between abbreviated IQ and average GFP where increased GFP was associated with reduced IQs (Figure 32). The correlations between GFP and abbreviated IQ held for FXS and was consistent with full-scale IQ and both verbal and nonverbal IQ subparts of the full-scale IQ which also exhibited similar patterns for individual microstate GFP (Figure 35 & Figure 36). Additionally, a positive correlation emerged between GEV and abbreviated IQ where increased

GEV was positively associated with IQ for FXS only (Figure 33). However, there was also a significant sex effect for GEV where females had higher GEV than males. As an exploratory step, the females were removed from the sample and the correction between GEV and abbreviated IQ was recomputed. The correlation was no longer significant (rho = .16, p = .447) which suggests females were driving the initial correlation. However, the correlations between GEV and full-scale, nonverbal, and verbal IQs all flipped sign, in addition to remaining non-significant which suggests that the resulting correlation between GEV and abbreviated IQ was not simply a result of power issues (FSIQ: rho = -.11, p = .680; NVIQ: rho = -.11, p = .663; VIQ: rho = -.15, p = .554)

Lastly, full-scale, verbal, and nonverbal IQ, but not abbreviated IQ, were positively correlated with GFP PPS in FXS only where increased peaks per second were associated with increased IQ on all but the abbreviated IQ. Given more individuals have abbreviated IQ, correlations with other IQ measures may be spurious.

Figure 35.

Correlation Plot for Microstate Variables and IQ

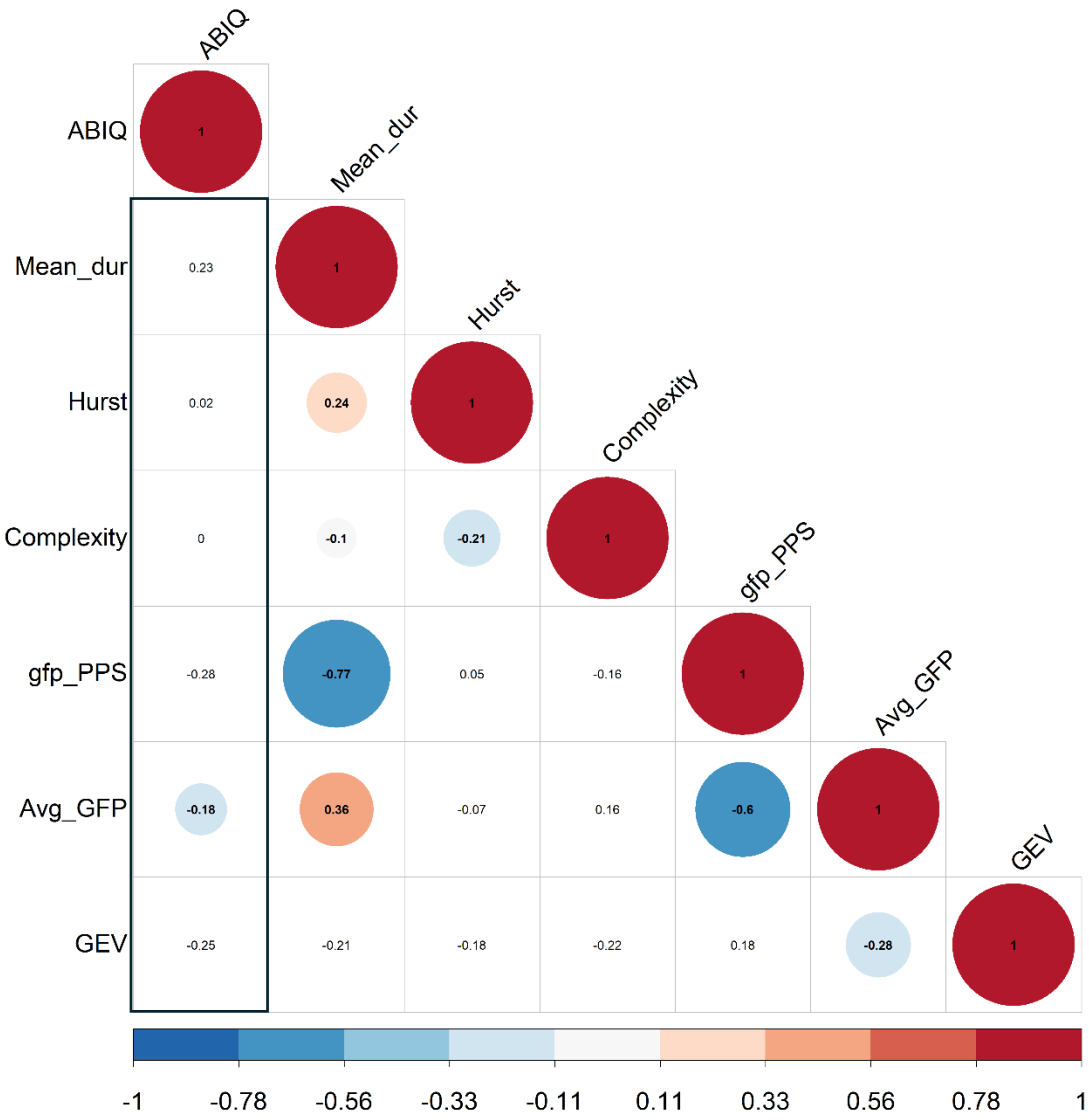

Note. $N = 88$. All statistically significant correlations are bolded and indicated by colored circles where warmer colors are direct correlations and cooler colors are inverse correlations. Black boxes highlight columns with correlations of interest. ABIQ = abbreviated IQ; Mean_dur = mean duration; GFP = global field power; PPS = peaks per second; GEV = global explained variance.

Figure 36.

Correlation Plot for Microstate Variables and IQ for FXS Group Only

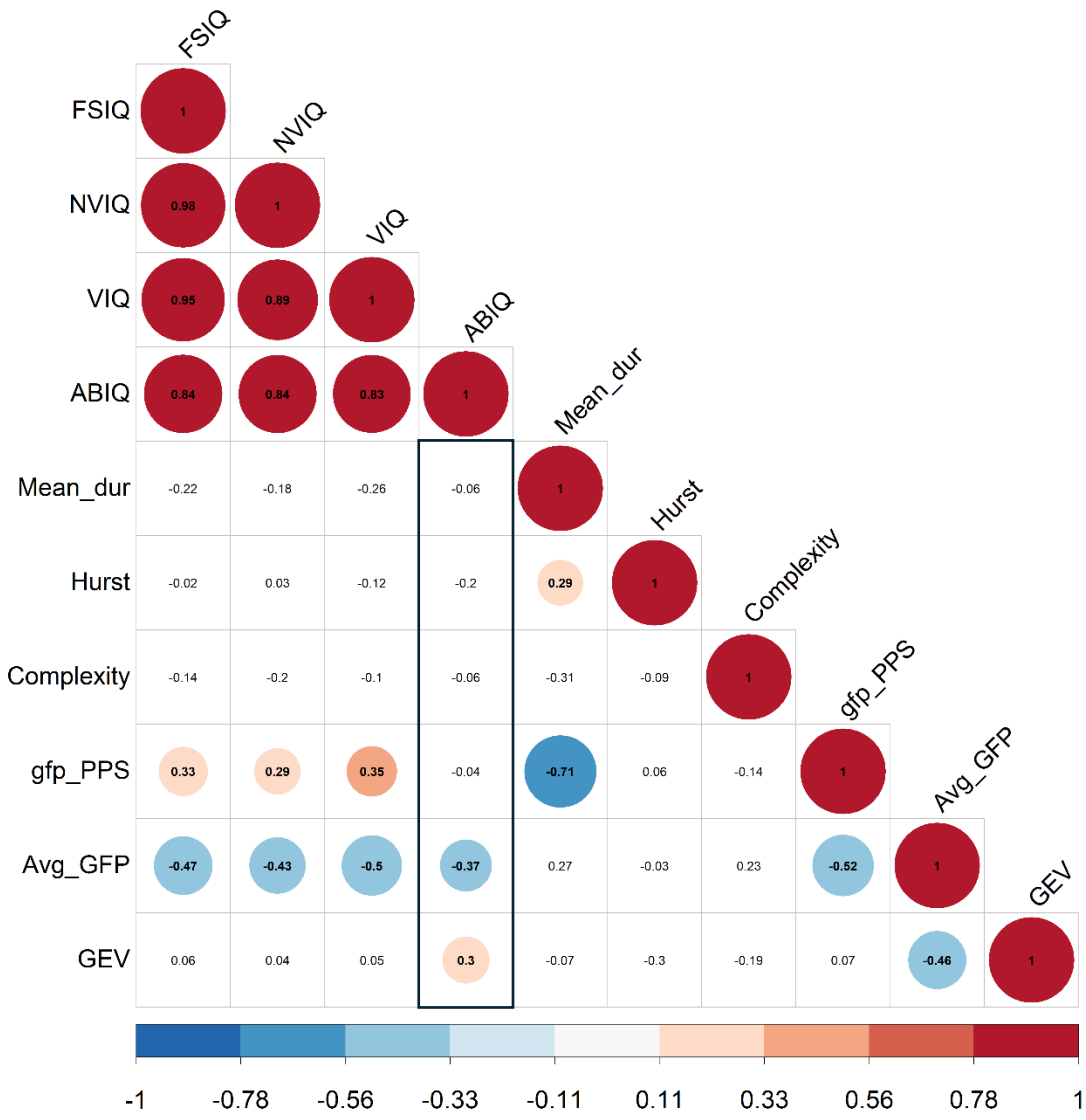

Note. $N = 40$ for ABIQ, $N = 25$ for FSIQ and VIQ, and $N = 26$ for NVIQ. All statistically significant correlations are bolded and indicated by colored circles where warmer colors are direct correlations and cooler colors are inverse correlations. Black boxes highlight columns with correlations of interest. Additional IQ variables are available for FXS that were not collected for TDC, as it was more common to give a full SB-5 to FXS than TDC. FSIQ = full-scale IQ; NVIQ = nonverbal IQ; VIQ = verbal IQ; ABIQ = abbreviated IQ; Mean_dur = mean duration; GFP = global field power; PPS = peaks per second; GEV = global explained variance.

Figure 37.

Correlation Plot for Microstate Variables and IQ for FXS Group Only

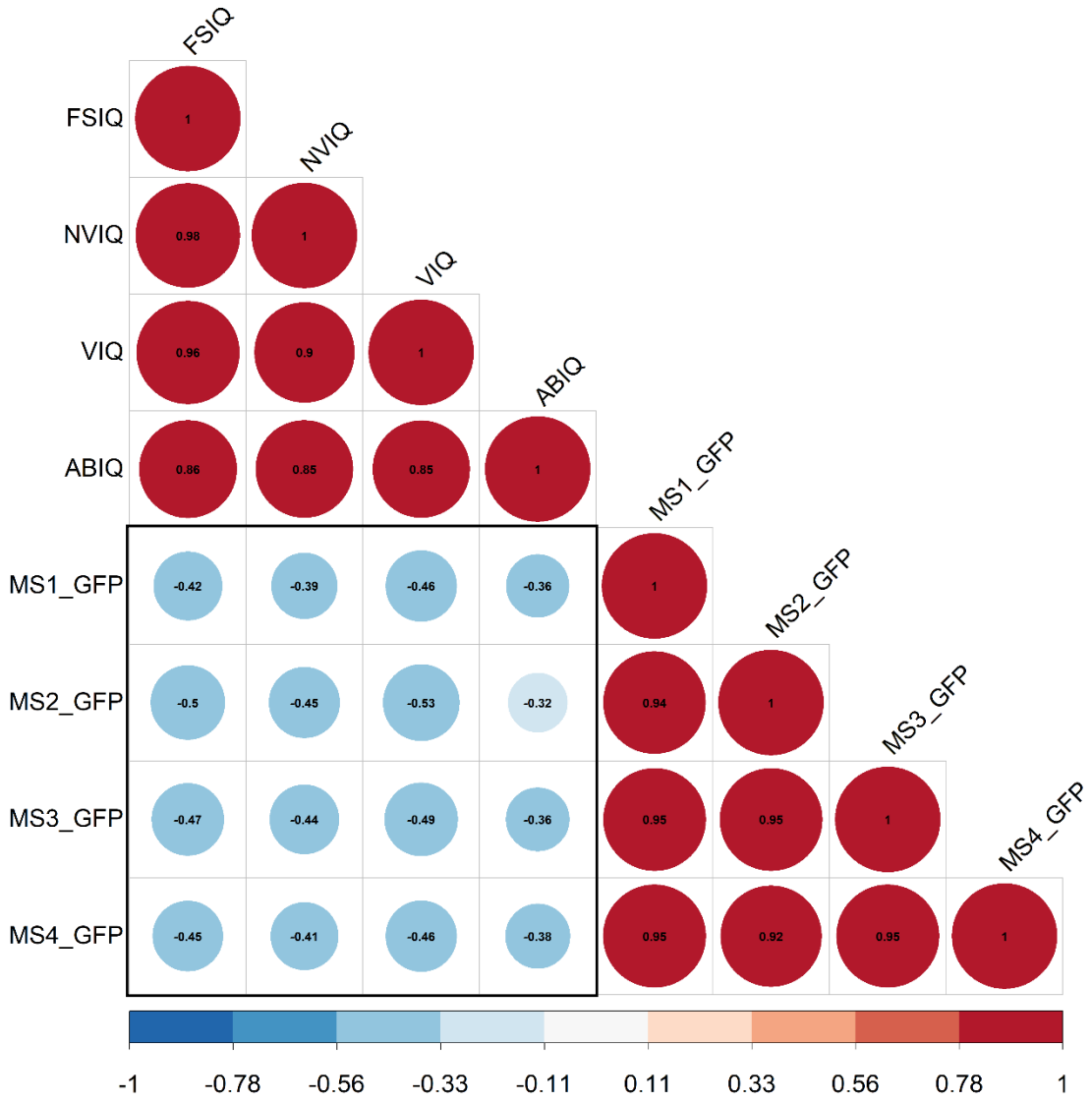

Note. $N = 40$ for ABIQ, $N = 25$ for FSIQ and VIQ, and $N = 26$ for NVIQ. All statistically significant correlations are bolded and indicated by colored circles where warmer colors are direct correlations and cooler colors are inverse correlations. Black boxes highlight columns with correlations of interest. Additional IQ variables are available for FXS that were not collected for TDC, as it was more common to give a full SB-5 to FXS than TDC. FSIQ = full-scale IQ; NVIQ = nonverbal IQ; VIQ = verbal IQ; ABIQ = abbreviated IQ; Mean_dur = mean duration; GFP = global field power; PPS = peaks per second; GEV = global explained variance.

The correlation analysis for FC and IQ across the whole sample identified three inverse correlations between abbreviated IQ and theta connectivity across all three functional networks where increased theta connectivity was associated with reduced IQ (Figure 38).

The inverse correlations did not hold for FXS with abbreviated IQ, though all rho values followed the same pattern and the correlations for the whole sample were already of small-to-moderate size where power could be a factor for the FXS correlation analyses (Figure 39). There were significant inverse correlations between full scale, verbal, and nonverbal IQ with DMN delta, DMN theta, SN delta, and control network delta FC. Additionally, control network theta was inversely correlated with nonverbal IQ only. Overall, patterns of increased connectivity in delta correlated with reduced IQ.

Figure 38.

Correlation Plot for Functional Connectivity Variables and IQ

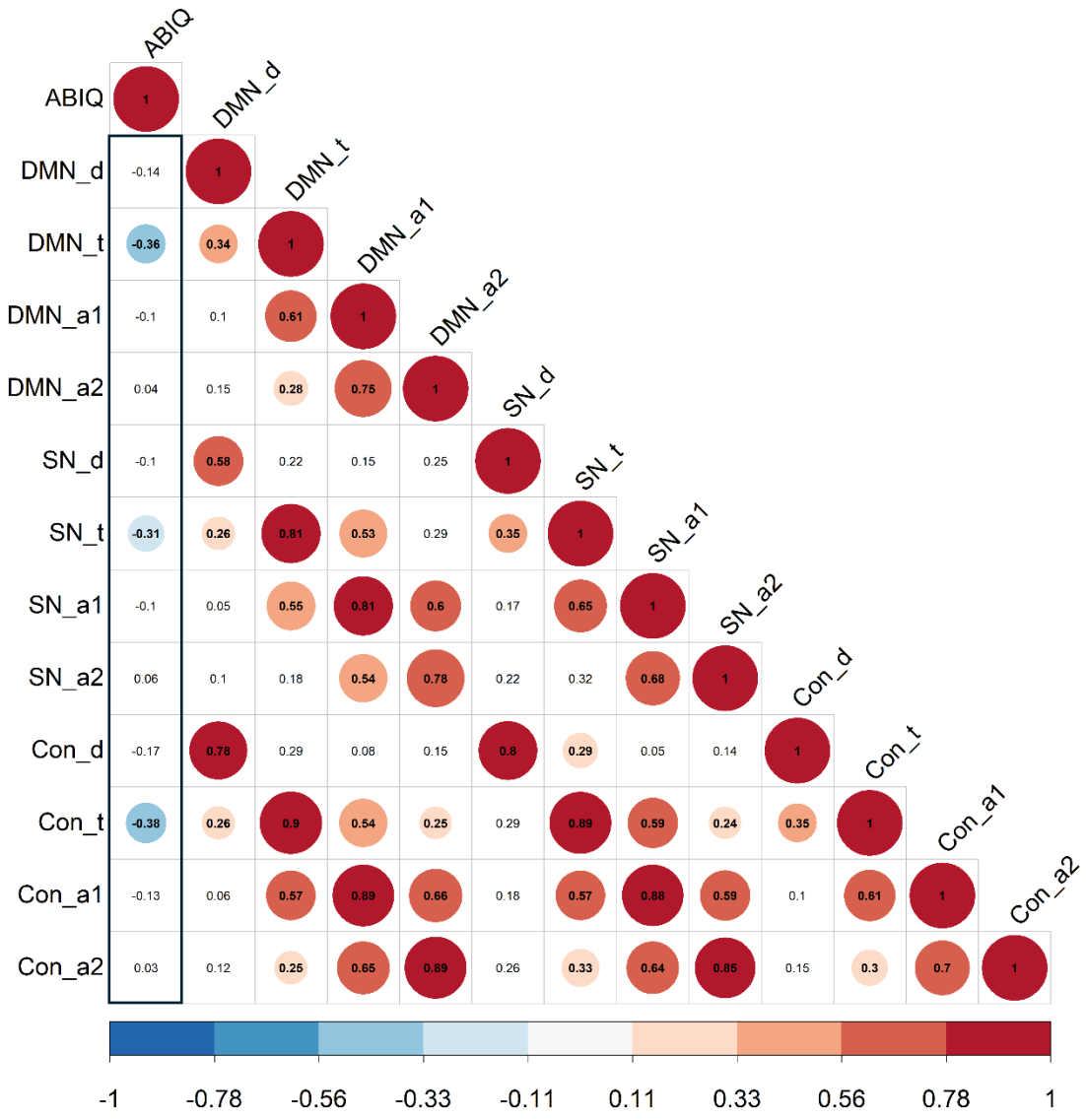

Note. $N = 88$. All statistically significant correlations are bolded and indicated by colored circles where warmer colors are direct correlations and cooler colors are inverse correlations. Black boxes highlight columns with correlations of interest. ABIQ = abbreviated IQ; DMN = default mode network; SN = salience network; Con = control network; d = delta, t = theta, a1 = alpha 1; a2 = alpha2.

Figure 39.

Correlation Plot for Functional Connectivity Variables and IQ for FXS Group Only

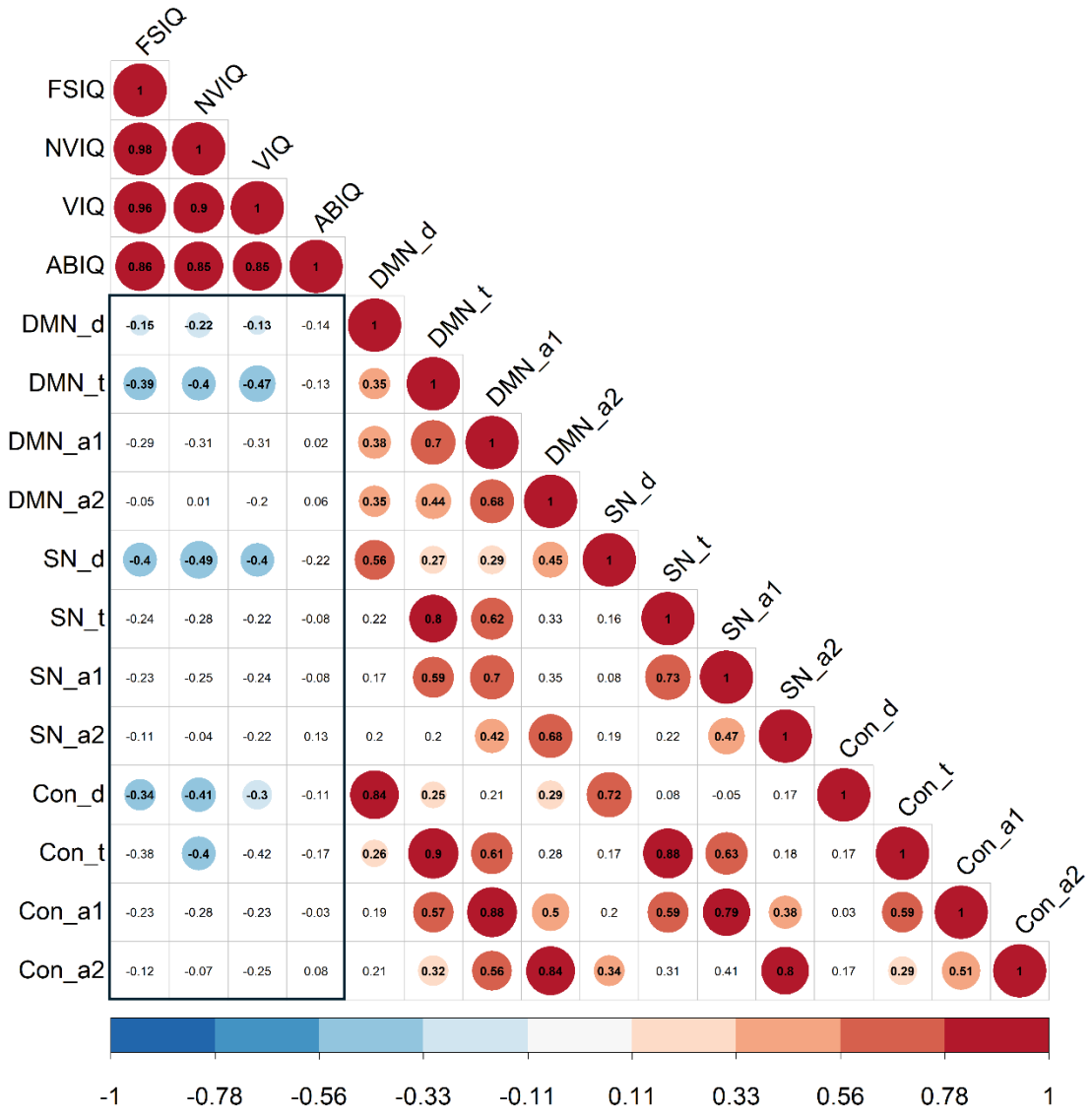

Note. $N = 40$ for ABIQ, $N = 25$ for FSIQ and VIQ, and $N = 26$ for NVIQ. All statistically significant correlations are bolded and indicated by colored circles where warmer colors are direct correlations and cooler colors are inverse correlations. Black boxes highlight columns with correlations of interest which included abbreviated IQ for ease of reference. Additional IQ variables are available for FXS that were not collected for TDC, as it was more common to give a full SB-5 to FXS than TDC. FSIQ = full-scale IQ; NVIQ = nonverbal IQ; VIQ = verbal IQ; ABIQ = abbreviated IQ; DMN = default mode network; SN = salience network; Con = control network; d = delta, t = theta, a1 = alpha 1; a2 = alpha2.

Additional correlation analyses evaluating relationships between EEG variables (MS and FC) and clinical variables indexing cognition. Analyses were conducted only for the FXS group, as clinical variables for TDC, as clinical measure delivery was more variable for TDC.

For FXS on the KiTAP, only an inverse correlation between the standard deviation of the alertness response and GEV was identified where reduced response variability was associated with increased GEV (Figure 40). For FC, several inverse correlations were identified where distractibility and Go/NoGo median response times were inversely correlated with DMN alpha 1 and alpha 2 FC where increased response times were associated with reduced FC (Figure 41). There was also an inverse correlation between DMN delta FC and Go/NoGo errors where decreased delta FC was associated with increased errors on the Go/NoGo task. However, FXS did not differ from TDC on either alpha or delta FC suggesting these relationships may reflect typical variability in FC and may not necessarily drive the reduced performance on the KiTAP (Table 11). Ultimately, the correlations between KiTAP and EEG were not particularly meaningful.

Table 11.

KiTAP Group Differences

	FXS	TDC	*Mann-Whitney U Results*			
KiTAP Variables	*M* rank	*M* rank	*N*	*z*	*p*	*r*
Alert Median	29.89	11.65	45	4.52	< .001	.67
Alert SD	29.59	12.15	45	4.32	< .001	.64
Distract Median	23.98	20.15	44	.96	.335	.14
Distract SD	27.65	14.32	44	3.41	< .001	.51
Go Median	26.96	15.41	44	2.91	.004	.44
Go Errors	26.19	16.65	44	2.51	.012	.38
Flex Median	28.59	12.82	44	3.97	< .001	.60
Flex Errors	30.50	9.79	44	5.28	< .001	.80

Note. TDC $N = 17$; FXS $N = 27$. KiTAP was designed for children thus TDC performance is at ceiling.

Figure 40.

Correlation Plot for Microstate Variables and KiTAP for FXS Group Only

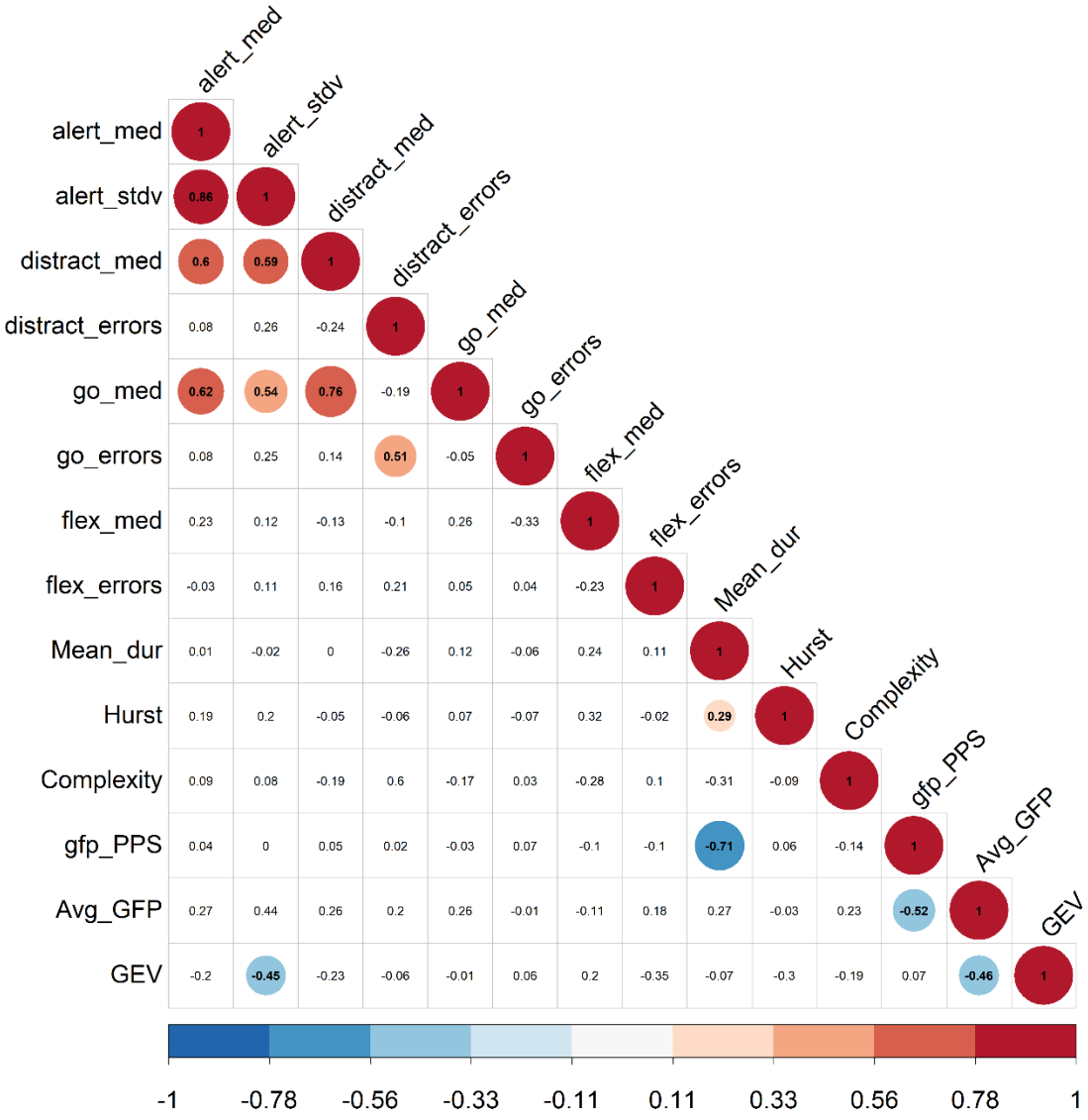

Note. All statistically significant correlations are bolded and indicated by colored circles where warmer colors are direct correlations and cooler colors are inverse correlations. Black boxes highlight correlations of note. Med = median; Alert = alertness; Distract = distractibility; Go = Go/NoGo; Flex = flexibility; Mean_dur = mean duration; GFP = global field power; PPS = peaks per second; GEV = global explained variance.

Figure 41.

Correlation Plot for Functional Connectivity and KiTAP for FXS Group Only

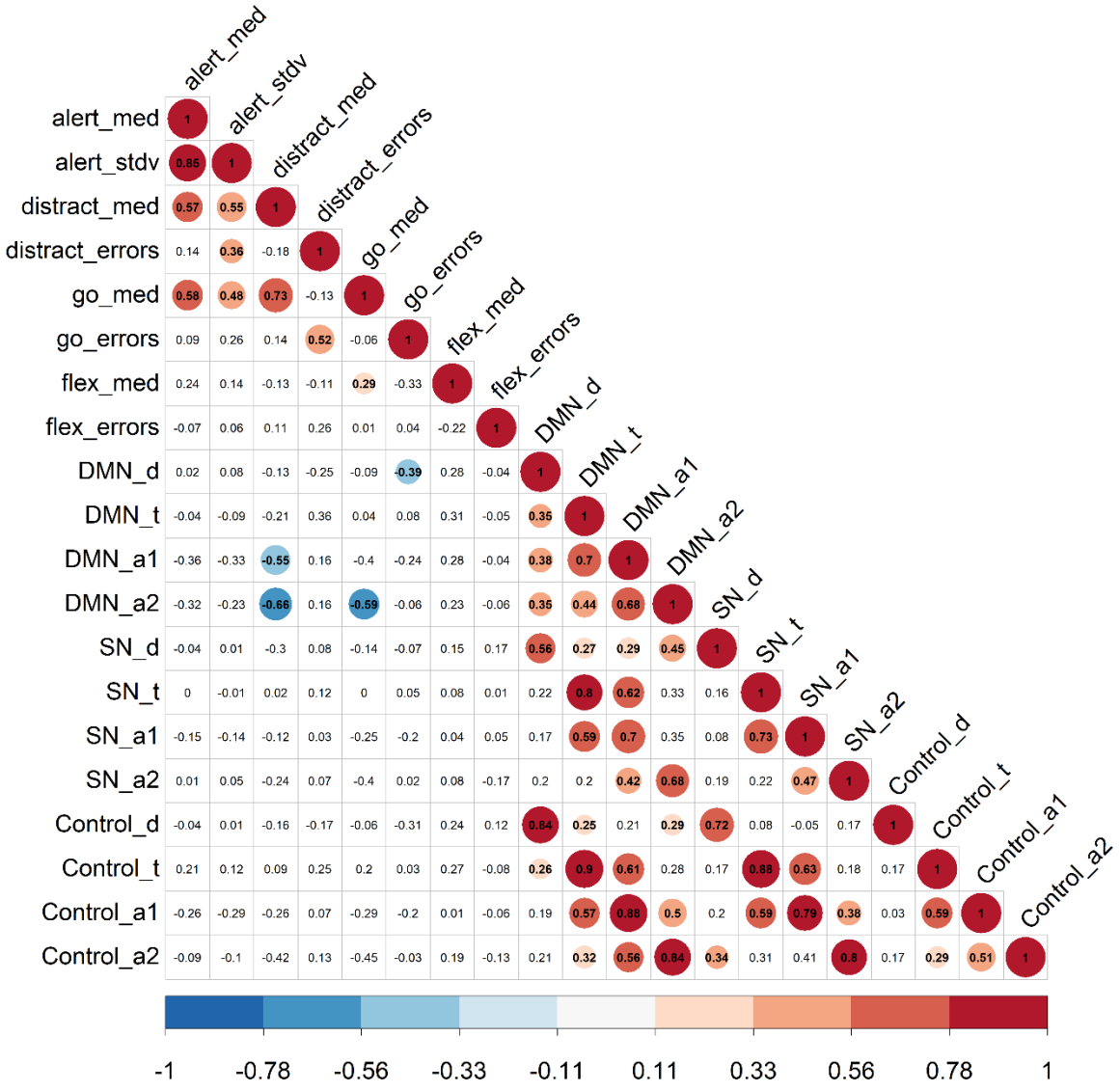

Note. $N = 27$ for alert, $N = 26$ for distract, go, and flex. All statistically significant correlations are bolded and indicated by colored circles where warmer colors are direct correlations and cooler colors are inverse correlations. Black boxes highlight the range of importance. Med = median; Alert = alertness; Distract = distractibility; Go = Go/NoGo; Flex = flexibility; DMN = default mode network; SN = salience network; Con = control network; d = delta, t = theta, a1 = alpha 1; a2 = alpha2.

For the Vineland-3, there were significant inverse correlations between several vineland subscales and microstate measures (Figure 42). First, average GFP was inversely associated with all Vineland subscales except for socialization. Reduced communication and daily living skills, in addition to an overall reduction in adaptive behavior, were associated with increased GFP in FXS which may be meaningful given group differences in GFP, albeit not on the global GFP measure. The GFP correlations prompted further analysis of individual microstate class GFP (Figure 43). Average GFP across all four microstate classes was inversely associated with all Vineland-3 subscales except for socialization. Though, MS3 GFP was inversely associated with vineland socialization. MS3 was the closest approximation for Microstate D and has been previously identified as a potential proxy for cognitive disruptions in FXS.

Mean duration was also inversely correlated with the communication subscale where increased average duration of all microstate classes was associated with reduced communication scores (Figure 38). However, there were not significant group differences on mean duration which makes the interpretation of the correlation difficult, especially without a gauge for TDC communication performance.

The vineland subscales were not correlated with any of the FC measures (Figure 44).

Figure 42.

Correlation Plot for Microstate Variables and Vineland-3 for FXS Group Only

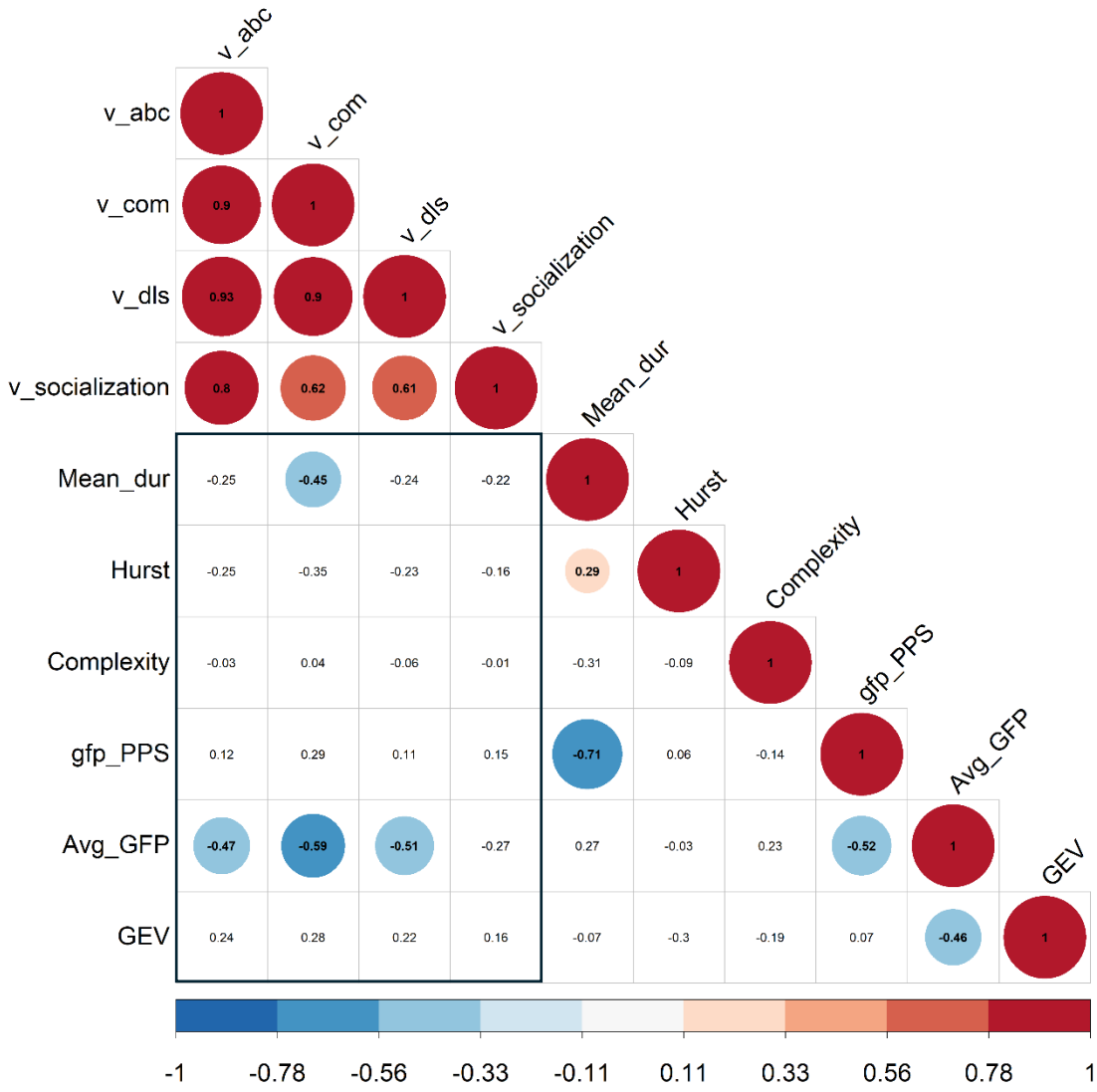

Note. All statistically significant correlations are bolded and indicated by colored circles where warmer colors are direct correlations and cooler colors are inverse correlations. Black boxes highlight correlations of note. V = vineland; abc = adaptive behavior composite; com = communication; dls = daily living skills; Mean_dur = mean duration; GFP = global field power; PPS = peaks per second; GEV = global explained variance.

Figure 43.

Correlation Plot for Microstate Class GFP and Vineland-3 for FXS Group Only

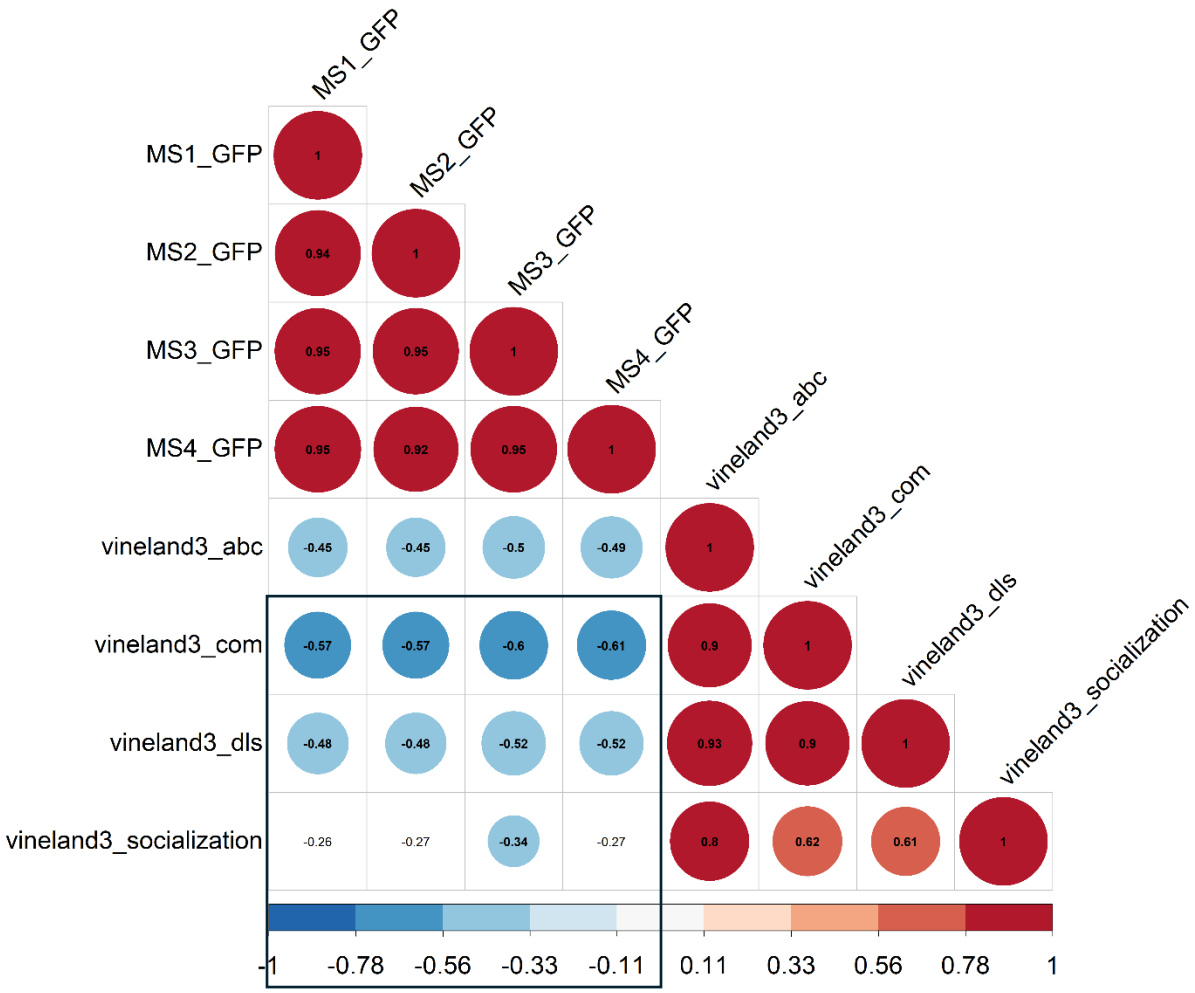

Note. All statistically significant correlations are bolded and indicated by colored circles where warmer colors are direct correlations and cooler colors are inverse correlations. Black boxes highlight correlations of note. V = vineland; abc = adaptive behavior composite; com = communication; dls = daily living skills; Mean_dur = mean duration; GFP = global field power; PPS = peaks per second; GEV = global explained variance.

Figure 44.

Correlation Plot for Functional Connectivity and Vineland-3 for FXS Group Only

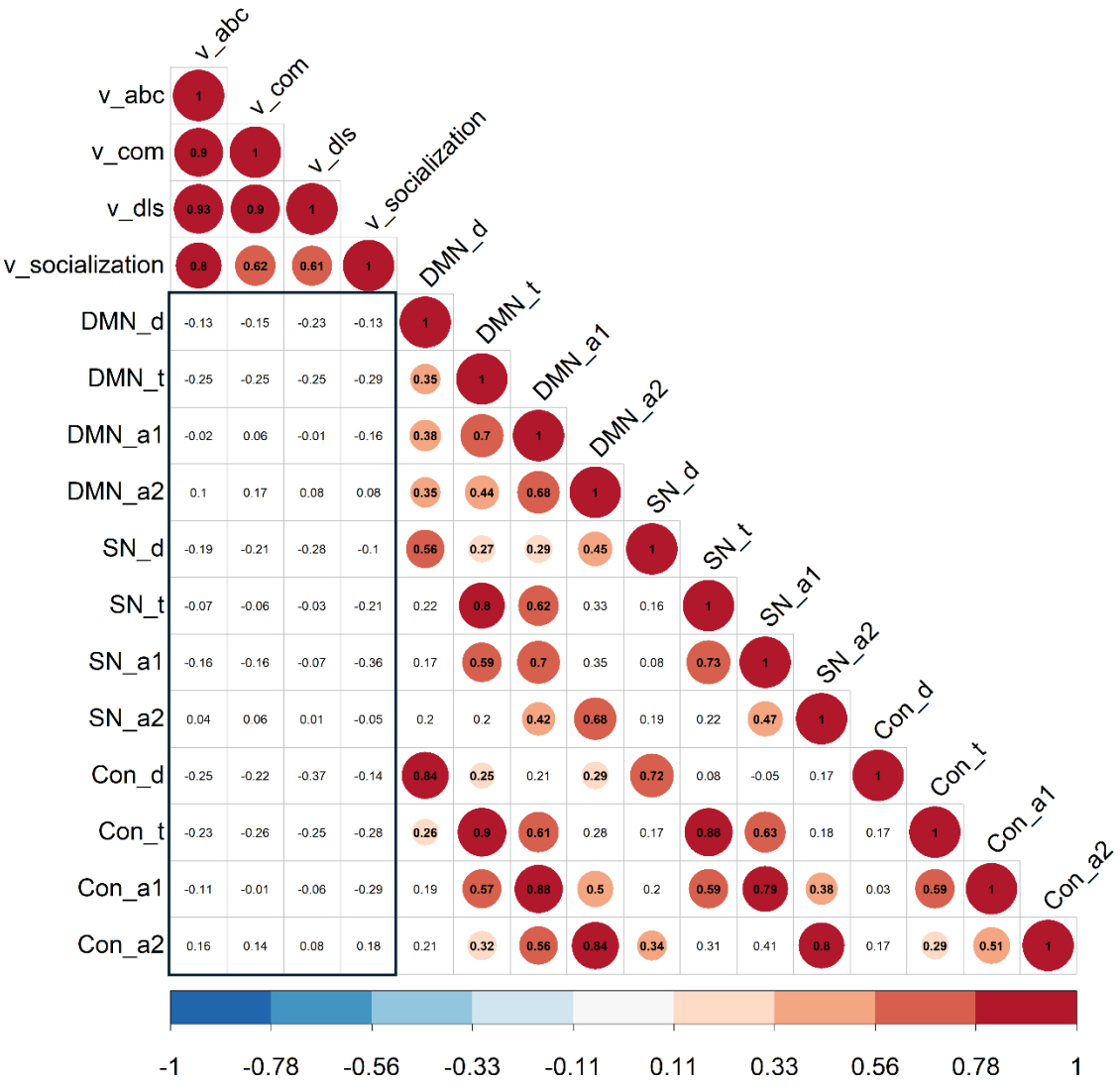

Note. All statistically significant correlations are bolded and indicated by colored circles where warmer colors are direct correlations and cooler colors are inverse correlations. Black box highlights area of interest. V = vineland; abc = adaptive behavior composite; com = communication; dls = daily living skills; DMN = default mode network; SN = salience network; Con = control network; d = delta, t = theta, a1 = alpha 1; a2 = alpha2.

For ABC FXS, which is a clinical measure that robustly indexes core FXS features, there were two direct correlations of note. Average GFP was directly associated with the stereotypy and the hyperactivity subscales (Figure 45). Stereotypy indexes stereotypic behavior unrelated to functional motor behaviors where increased scores reflect increased stereotyped behavior. The hyperactivity subscale indexes aspects of executive function where questions gauge inattention, impulsiveness, and restlessness in addition to difficulties with sustained attention and behavior inhibition. Ultimately, the hyperactivity subscale may represent behavioral manifestation of challenges with cognitive flexibility where increased GFP could serve as a proxy. Though, again, average GFP was not different between groups at the global level. Correlations with individual microstate GFP were also evaluated which identified the group-level correlations hold for essentially all individual microstates (Figure 46).

There were no meaningful patterns of correlations between ABC subscale scores and functional network FC (Figure 47).

The NIH toolbox cognitive battery was not analyzed, as few individuals with FXS had NIH TBC scores (~N = 13 for most subscale scores).

Figure 45.

Correlation Plot for Microstate Variables and ABC FXS for FXS Group Only

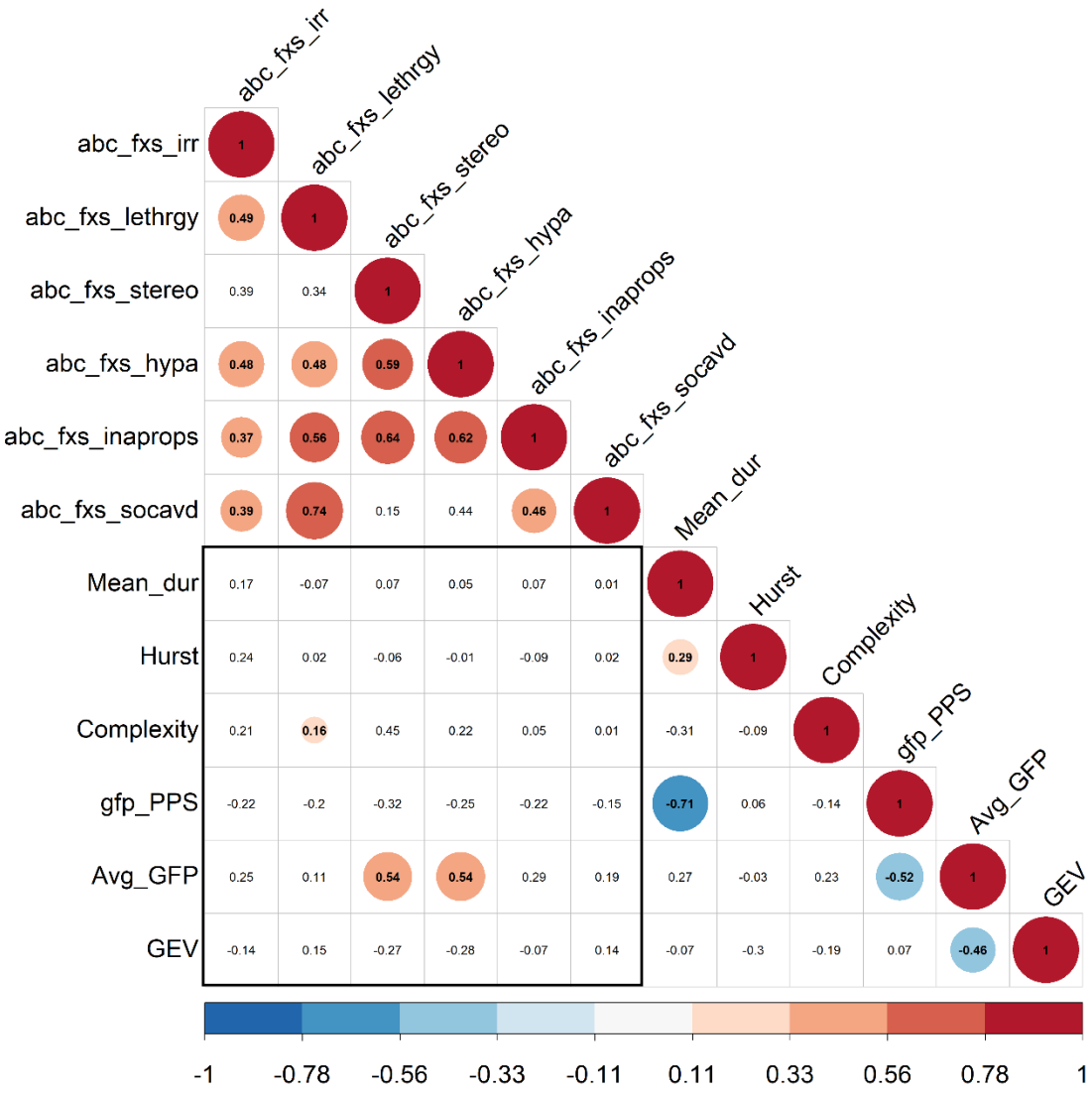

Note. All statistically significant correlations are bolded and indicated by colored circles where warmer colors are direct correlations and cooler colors are inverse correlations. Black boxes highlight correlations of note. ABC = aberrant behavior checklist; irr = irritability subscale lethrgy = lethargy subscale; stereo = stereotypy subscale; hypa = hyperactivity subscale; inaprops = inappropriate speech subscale; socavd = social avoidance subscale; Mean_dur = mean duration; GFP = global field power; PPS = peaks per second; GEV = global explained variance.

Figure 46.

Correlation Plot for Individual Microstate Class GFP and ABC FXS for FXS Group Only

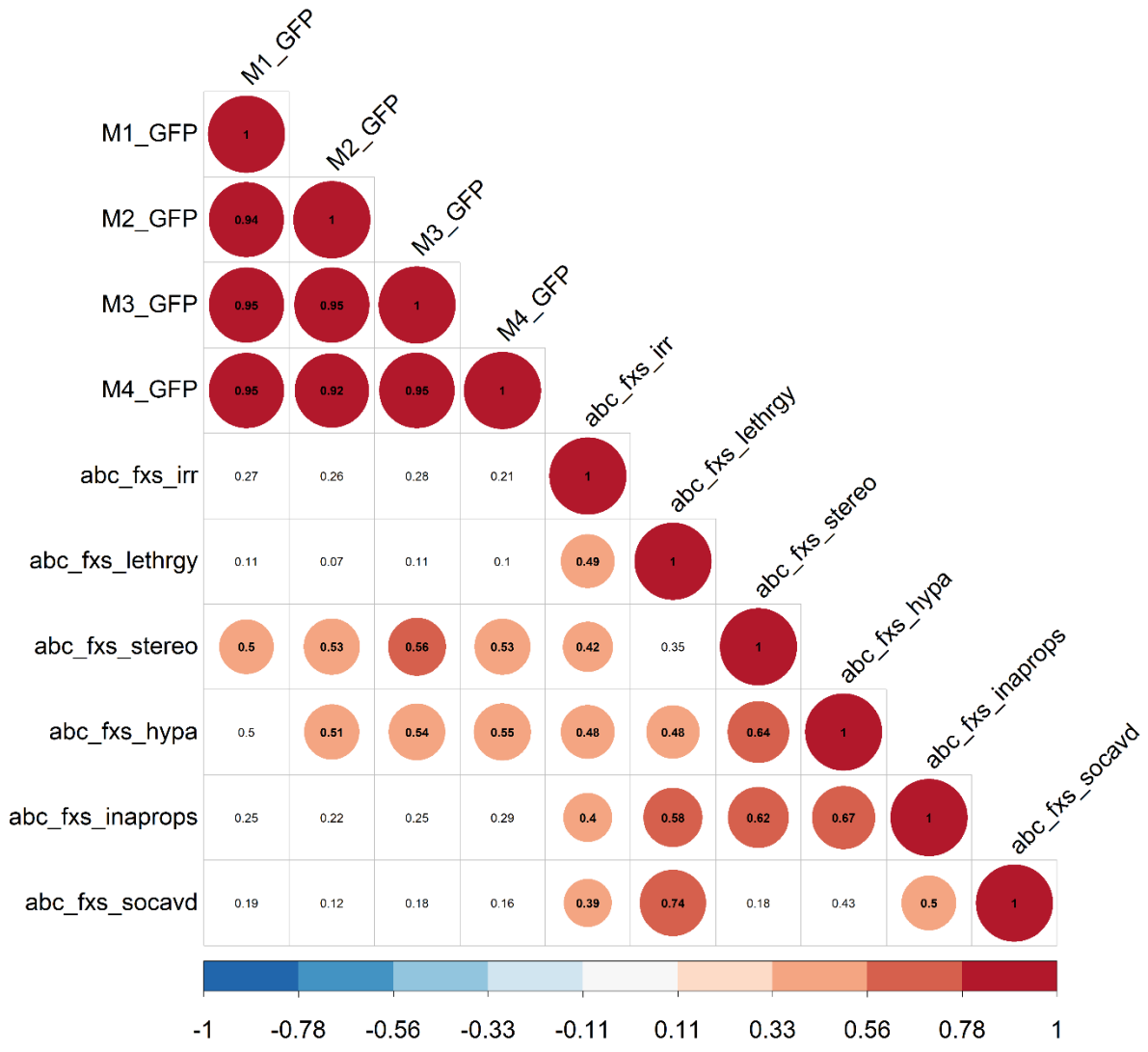

Note. All statistically significant correlations are bolded and indicated by colored circles where warmer colors are direct correlations and cooler colors are inverse correlations. Black boxes highlight correlations of note. ABC = aberrant behavior checklist; irr = irritability subscale lethrgy = lethargy subscale; stereo = stereotypy subscale; hypa = hyperactivity subscale; inaprops = inappropriate speech subscale; socavd = social avoidance subscale

Figure 47.

Correlation Plot for Functional Connectivity Variables and ABC FXS for FXS Group Only

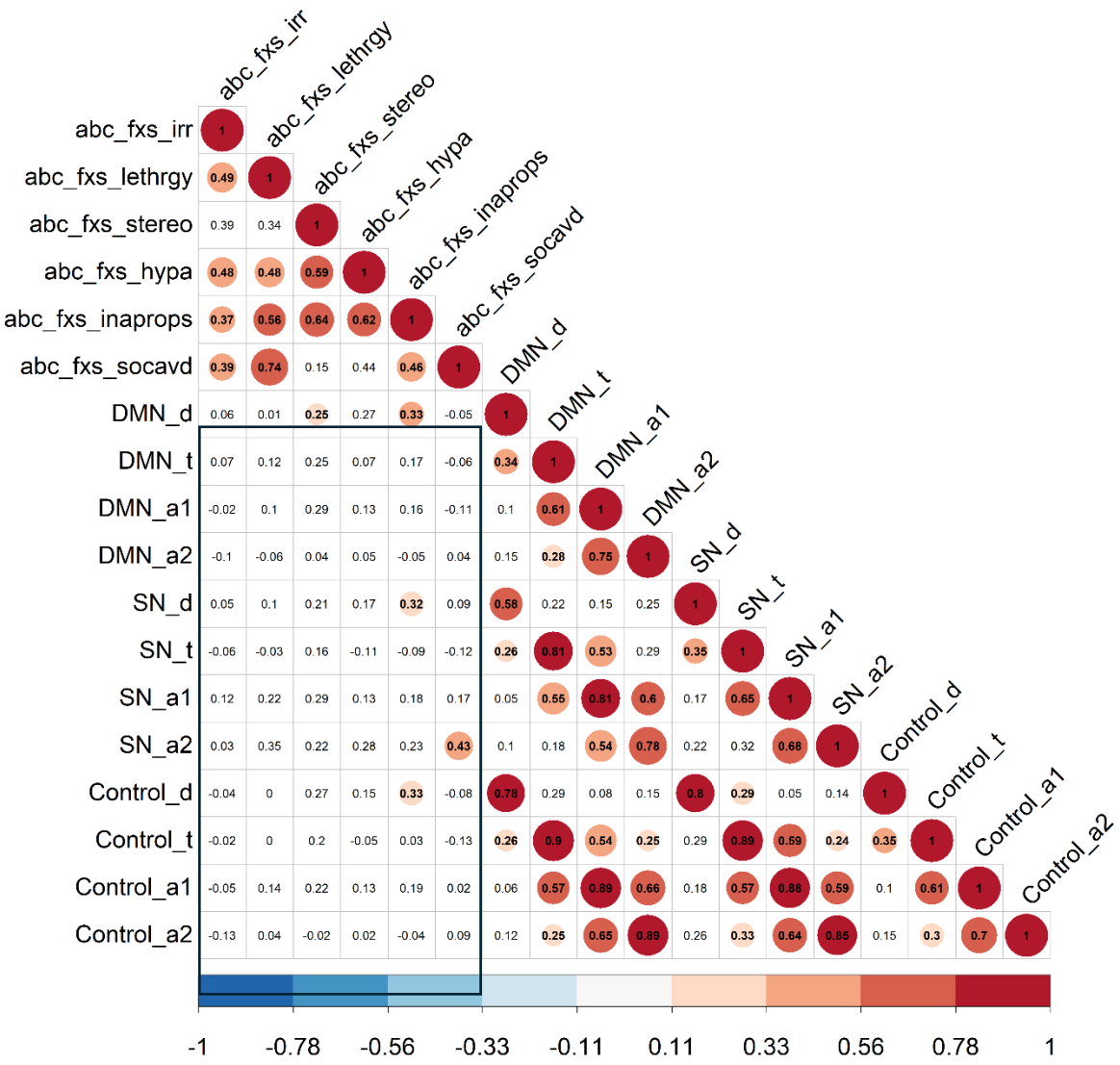

Note. All statistically significant correlations are bolded and indicated by colored circles where warmer colors are direct correlations and cooler colors are inverse correlations. Black boxes highlight correlations of note. ABC = aberrant behavior checklist; irr = irritability subscale lethrgy = lethargy subscale; stereo = stereotypy subscale; hypa = hyperactivity subscale; inaprops = inappropriate speech subscale; socavd = social avoidance subscale; DMN = default mode network; SN = salience network; Con = control network; d = delta, t = theta, a1 = alpha 1; a2 = alpha2.

Lastly, both FC and MS variables were evaluated in correlation analyses with both absolute and relative power across frequency bands, as well as all individual PAF variables (Figure 48). Interestingly, GFP peaks per second were inversely correlated with all absolute power variables except for gamma 2 and shared inverse relationships with relative theta and alpha 1 but direct relationships with relative beta, gamma 1, and gamma 2. Average GFP was positively correlated with all absolute power variables but only maintained positive correlations with relative theta and alpha 1 where correlations with alpha 2 were not significant and correlations with relative beta, gamma 1, and gamma 2 were inverse. While not different at the group level, Hurst was directly correlated with relative gamma 2 and complexity was inversely correlated with gamma 2. Lastly, GEV did not share significant relationships with power for any frequency band and no microstate variables were correlated with PAF.

For FXS only, correlations patterns were largely similar to those noted across the whole sample (Figure 49). Particularly for GFP peaks per second, the results were comparably strong for FXS suggesting FXS may drive these relationships where GFP peaks per second may map more closely onto general power disruptions in FXS. The Hurst exponent and complexity correlations also remain significant for FXS which suggest potential disruptions to microstate dynamics that may indicate network disruptions worth testing in the future.

Figure 48.

Correlation Plot for Microstate Variables, Frequency Band Power, and PAF

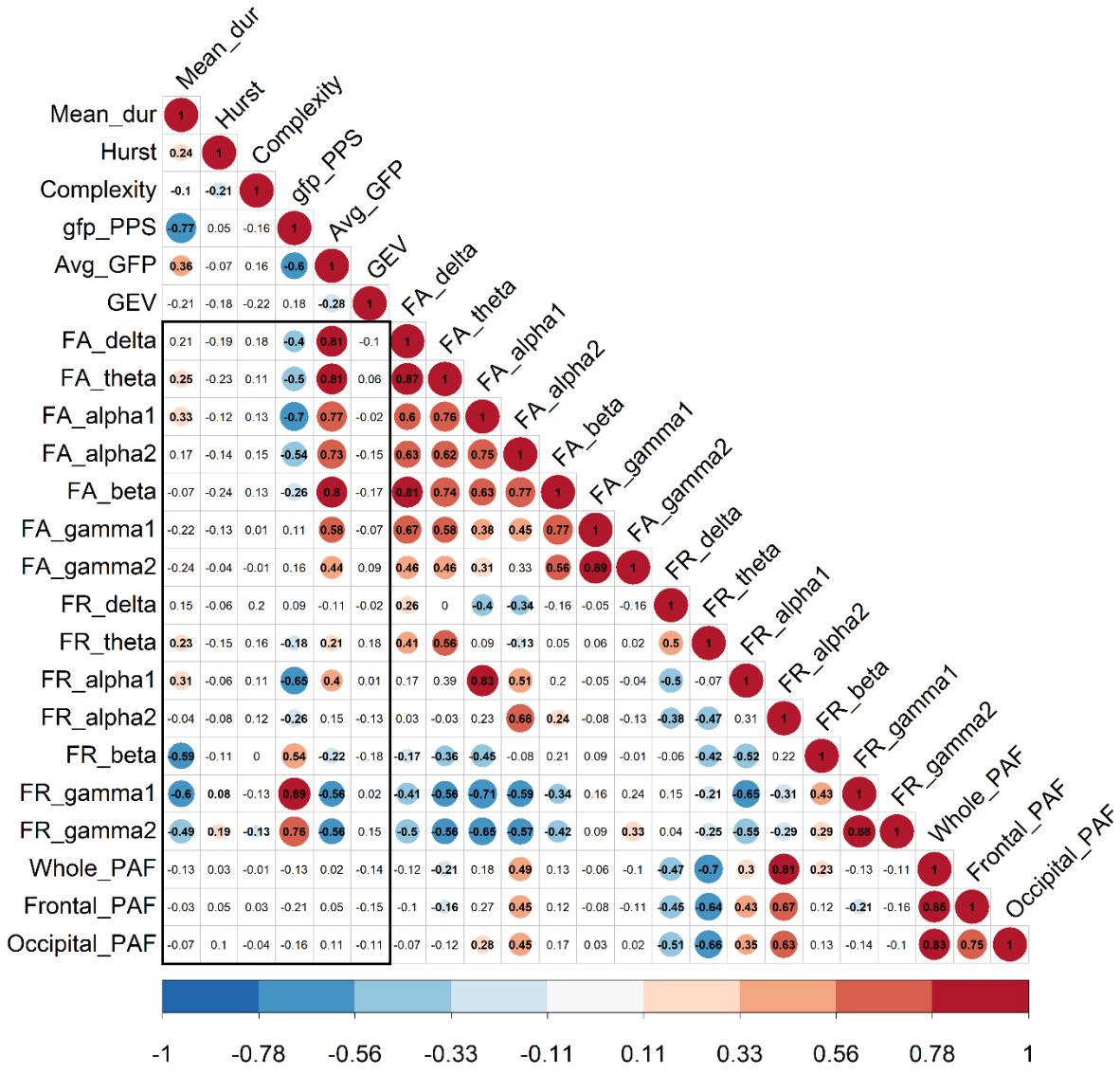

Note. All statistically significant correlations are bolded and indicated by colored circles where warmer colors are direct correlations and cooler colors are inverse correlations. Black boxes highlight correlations of note. FA = Frontal absolute power; FR = frontal relative power; PAF = peak alpha frequency; Mean_dur = mean duration; GFP = global field power; PPS = peaks per second; GEV = global explained variance.

Figure 49.

Correlation Plot for Microstate Variables, Frequency Band Power, and PAF for FXS Group Only

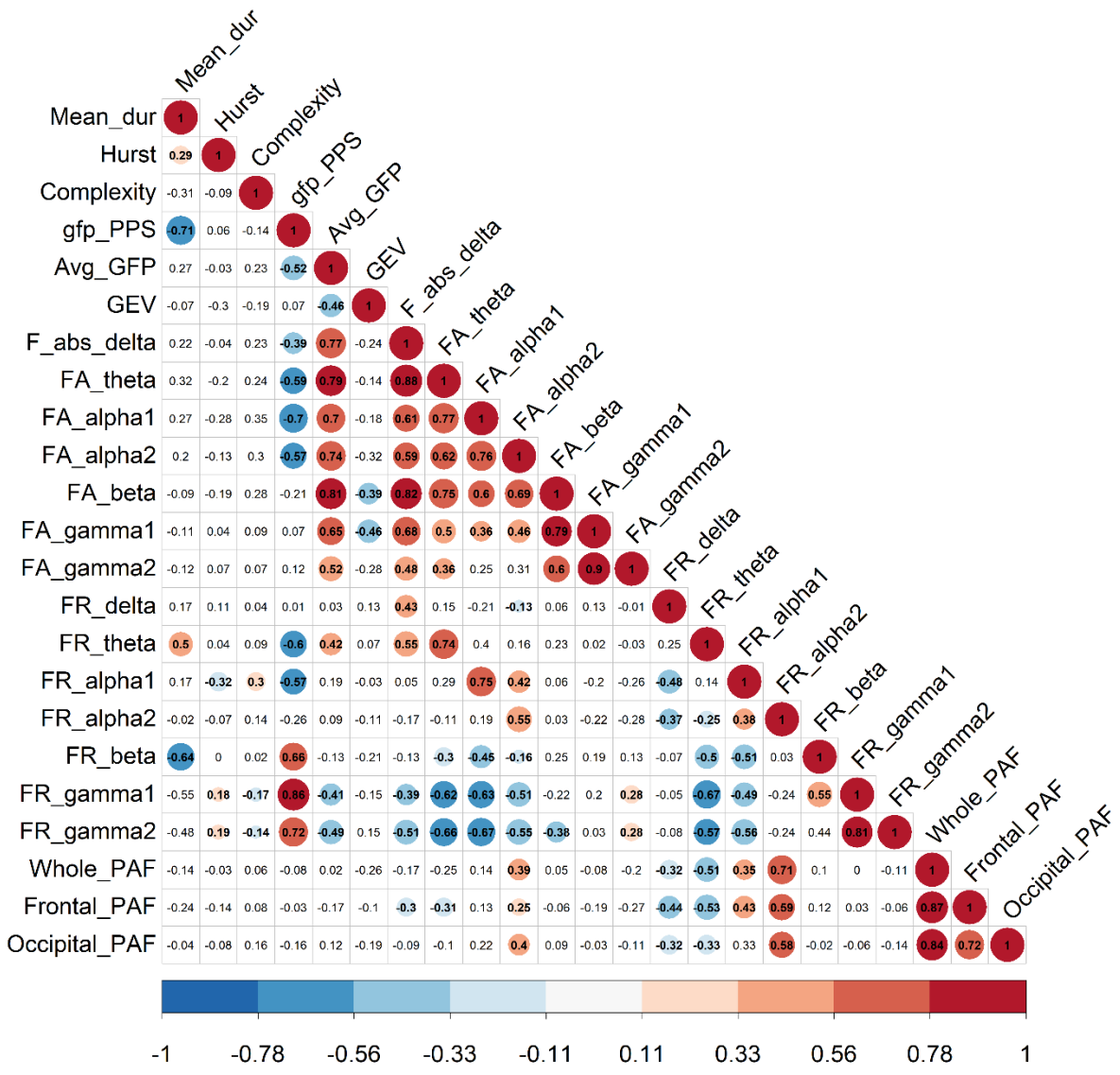

Note. All statistically significant correlations are bolded and indicated by colored circles where warmer colors are direct correlations and cooler colors are inverse correlations. Black boxes highlight correlations of note. FA = Frontal absolute power; FR = frontal relative power; PAF = peak alpha frequency; Mean_dur = mean duration; GFP = global field power; PPS = peaks per second; GEV = global explained variance.

Correlation analyses between FC and both frequency band power and PAF identified significant direct correlations between theta FC across all functional networks and both absolute and relative power. Further, theta FC across all functional networks were inversely correlated with PAF across all regions where alpha 2 FC across all networks were directly correlated with PAF across all regions (Figure 50). Of lesser interest but still of note, relative beta power was inversely correlated with theta, alpha 1 and alpha 2 FC across all functional networks. Relative gamma 1 exhibited a similar pattern of correlations, though gamma 1 power was only inversely correlated with alpha 1 and alpha 2 FC across networks.

Certain correlations were present for FXS only, though correlations were of reduced strength where present (Figure 51).

Figure 50.

Correlation Plot for Functional Connectivity, Frequency Band Power, and PAF

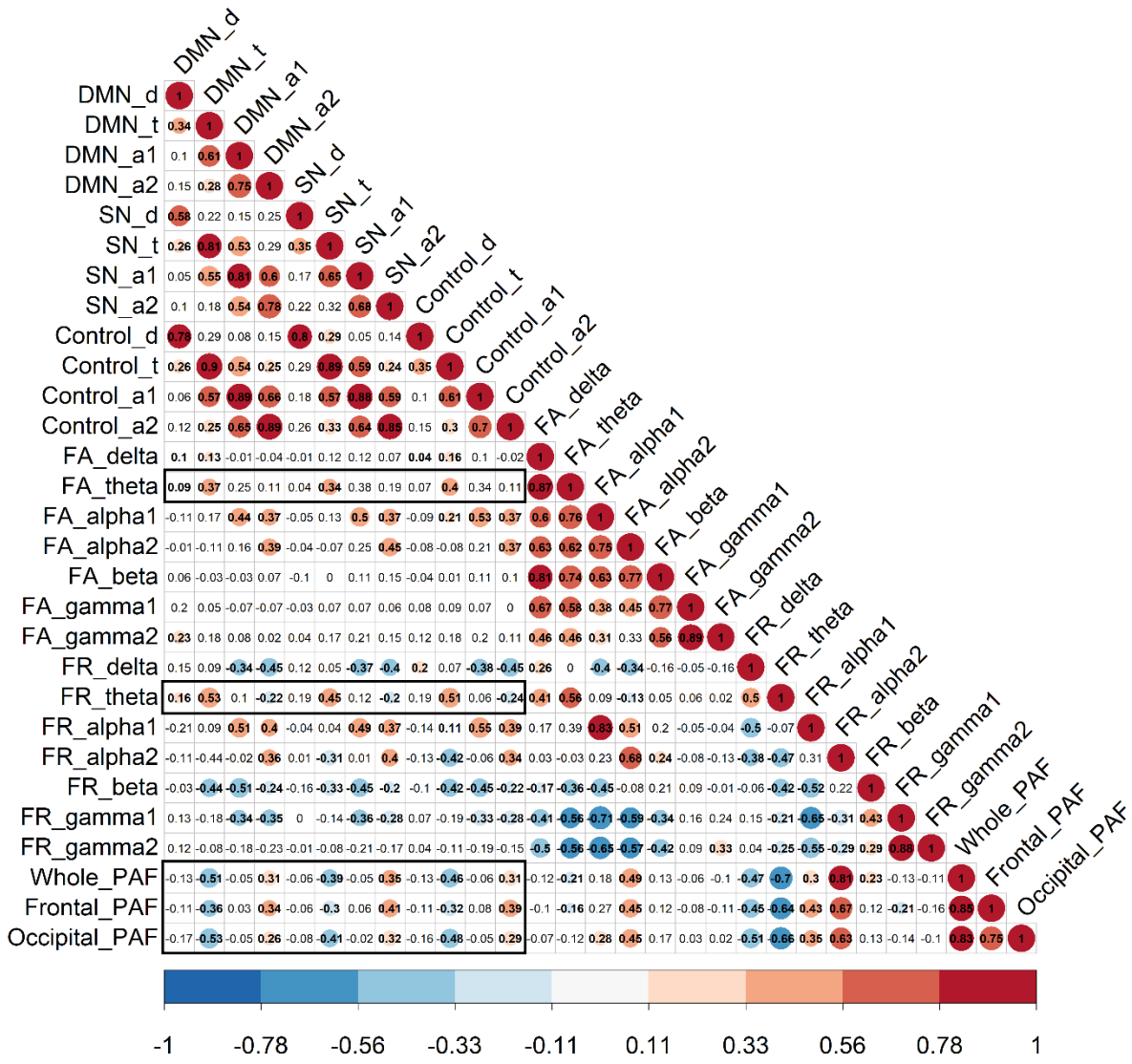

Note. All statistically significant correlations are bolded and indicated by colored circles where warmer colors are direct correlations and cooler colors are inverse correlations. Black boxes highlight correlations of note. FA = Frontal absolute power; FR = frontal relative power; PAF = peak alpha frequency; DMN = default mode network; SN = salience network; Con = control network; d = delta, t = theta, a1 = alpha 1; a2 = alpha2.

Figure 51.

Correlation Plot for Functional Connectivity, Frequency Band Power, and PAF for the FXS group only

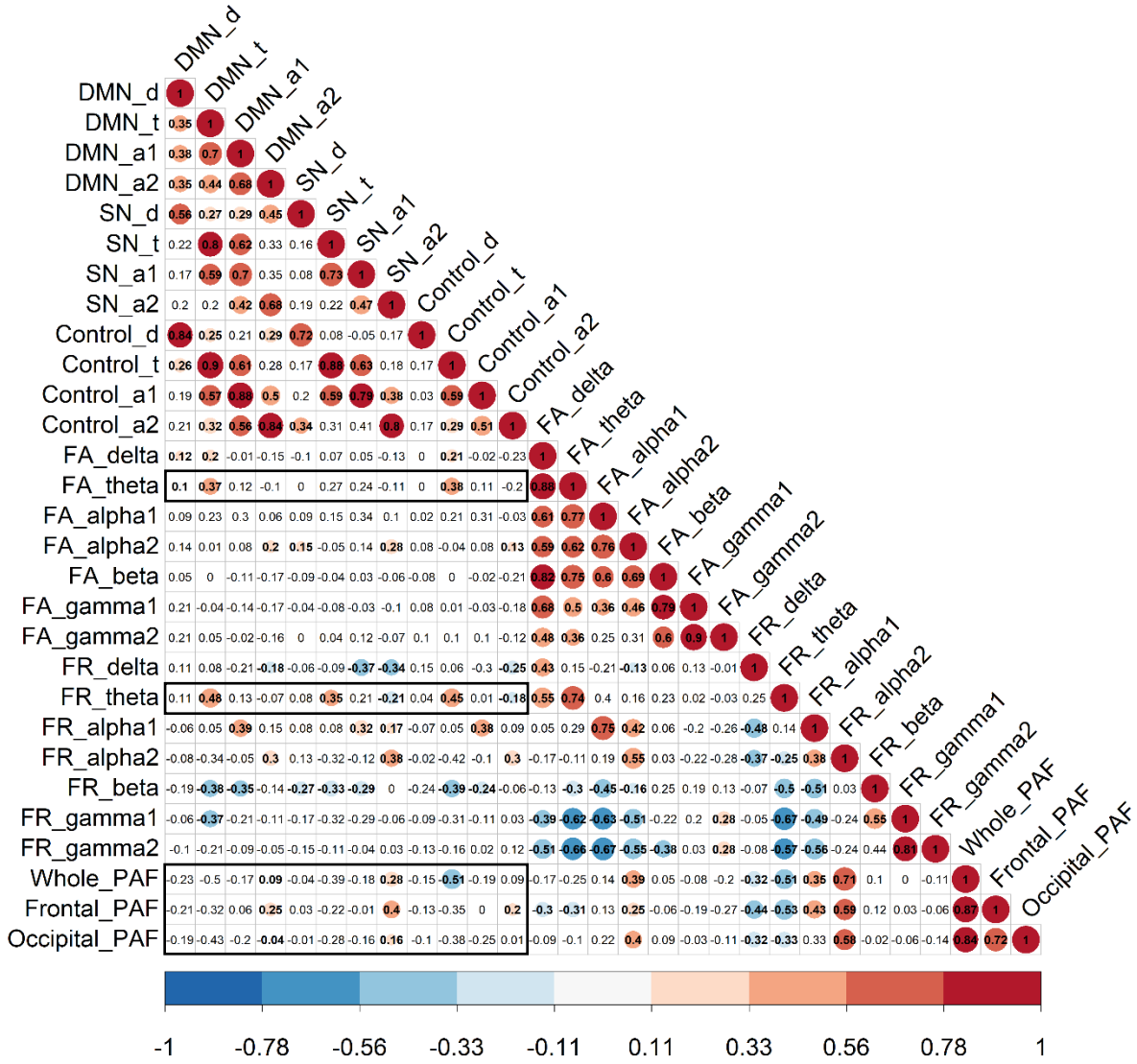

Note. All statistically significant correlations are bolded and indicated by colored circles where warmer colors are direct correlations and cooler colors are inverse correlations. Black boxes highlight correlations of note. FA = Frontal absolute power; FR = frontal relative power; PAF = peak alpha frequency; DMN = default mode network; SN = salience network; Con = control network; d = delta, t = theta, a1 = alpha 1; a2 = alpha2.

Discussion

The primary goal of the present study was to evaluate functional connectivity in specific resting state networks and determine whether microstate variables map onto functional network disruptions in FXS. The evaluation of functional connectivity within default mode, salience, and control network was a novel investigation in FXS where stablishing baseline relationships between microstates and functional network connectivity in resting state will allow for future evaluation of microstate and FC dynamics during a cognitive EEG task. As cognitive tasks drive more specific and consistent brain states, functional network dynamics and shifts related to engaging cognition may provide additional information about FXS functional pathophysiology and relationships between electroencephalography (EEG) metrics and clinical phenotypes. While evaluating cognition using EEG is a highly important goal for the field, resting state is an easier EEG measure to collect in FXS across more widely abled patients, including in young children. Additionally, the use of rsEEG in clinical trials is more ideal than measures that take increased training or instruction making biomarker comparisons between various EEG tasks an important step for both better interpretation of the present results and for future clinical interventions targeting cognitive symptoms in FXS.

Microstates

The present study identified significant group differences on GEV and GFP peaks per second. The GEV group difference between FXS and TDC indicates that the microstate classes account for more of the total EEG data in FXS than in TDC. Traditionally, the GEV of a microstate solution represents both the spatial similarity of the solution and the amplitude weighting via GFP, where GEV measures how similar each EEG sample is to the microstate map prototype (Poulson et al., 2018). Therefore, GEV is a time-independent or static measure not

influenced by the temporal dynamics or sequence of microstates (Manasova et al., 2024). GEV group differences were robust and consistent across all solutions thus microstate solutions fit FXS rsEEG data than TDC data, overall, suggesting FXS have less variable neural activity across the duration of the recording (Bagdasarov et al., 2024, Tait et al., 2022). Interestingly, GEV was positively correlated with IQ for FXS only suggesting higher GEV may represent adaptive or compensatory neural dominance. However, there was also a significant sex effect, and the correlation was not significant when looking at only males with FXS. Ultimately, higher GEV may not be directly clinically meaningful, as GEV did not exhibit any other meaningful patterns with clinical variables.

Unlike microstate GEV, GFP is inherently dynamic. Increased GFP peaks per second in FXS compared to TDC suggest rapid switching or increased GFP dynamics (i.e., represent transitions or local field strength maxima), which may correspond to greater hyper-reactivity of neural activity (Khanna et al., 2015; Michel & Koenig, 2018; Mishra et al., 2020). Increased GFP peaks per second correlated with increased relative power for both low and high gamma which are traditionally elevated in FXS, adding credence to the idea that increased GFP peaks per second correspond to neural hyperexcitability (Wang et al., 2017). While GFP peaks likely capture microstate transitions, the complexity measure (Lempel-Ziv complexity – which indexes non-stationary/non-Markovian transition properties of microstates) was not significantly different. In light of the non-significant group differences in complexity values across groups, increased GFP peaks may reflect rapid, repeated transitions into the same microstate class without transitioning into other microstate classes in between. Reactively transitioning into the same microstate may result from unstable or inefficient network function and possibly indicates a pattern of network stasis rather than sustained activation of one network.

While increased neural reactivity is one interpretation for the current results, GFP is known to change with vigilance state (Weimers et al., 2023). Hyperarousal in FXS represents a clinical concern that may be linked to neural hypervigilance where FXS have more baseline arousal and increased sensitivity to environmental input (Gara et al., 2020; Lachiewics et al., 2023). Hypervigilance may also result as a manifest of increased anxiety in FXS. Increased environmental stimulation could play a role in driving microstate differences and shifting vigilance states – as the resting task was not a true rest and participants were watching a video they selected prior to the start of the task. Increased sensory processing and attention modulation may contribute to the present results. However, complexity measures for microstates reportedly also vary across vigilance states and were not different between TDC and FXS in the current study (von Wegner et al., 2024). Again, the complexity measure used in the current study was not significantly different between groups suggesting equally stable and predictable microstate transition patterns between microstate classes relative to TDC (Tait et al., 2020). Hurst was also not different between groups where both groups were above Hurst exponent = .05, suggesting persistent long-range temporal correlations. Interesting, Hurst is often cited as a proxy for E/I imbalance in autism where group differences would suggest an imbalance in the E/I ratio. However, increased excitation/neural hyperexcitability is a core FXS phenotype and the present results indicate comparable E/I ratio between groups (Linke et al., 2024; Liu et al., 2022). Given the robust nature of neural hyperexcitability findings with congruency between cell, mouse, and human work, the present Hurst exponent result likely indicates Hurst within the context of microstates are indexing something different or more nuanced than the traditional E/I proxy interpretations (Linke et al., 2024). Both complexity and Hurst measures are known to change with vigilance and the lack of group differences lends credence to the interpretation that FXS

have increased neural reactivity based on GFP peaks per second rather than vigilance state driving microstate group differences, alone. However, increased neural reactivity does not extend to variability in either microstate transitions or signal stability during rsEEG per complexity and Hurst (von Wegner et al., 2024). Furthermore, the frequency of class occurrence per second and the duration of each occurrence were not different between groups or across the individual microstate classes suggesting comparable temporal dynamics of microstates in FXS.

While the average GFP across the whole recording was not different across groups, individual microstate class GFP was different across groups for both the 4MS and 6MS solutions. The interaction was significant for the 4MS solution only, where individual class GFP was different between groups and opposite in pattern where FXS had higher GFP in different microstate classes than TDC. Though, FXS was higher on GFP for all microstates except MS4. The microstate class that exhibited the greatest difference between groups was MS3, which most closely approximates Microstate D. Elevated GFP in microstate D was previously identified in a study that evaluated microstates in FXS where microstate D GFP was linked to clinical outcomes associated with cognition (Takarae et al., 2023). Specifically, Takarae et al. (2023) found a correlation between microstate D and non-verbal IQ. The current study identified inverse correlations between global GFP and all IQ measures, including nonverbal IQ, where the GFP of individual microstate classes was inversely correlated with IQ, including MS3. Given the significant group difference and inverse relationships with clinical measures of cognitive performance, increased GFP appears to be aberrant, particularly for a microstate class traditionally involved in task-positive processing (Custo et al., 2017; Seitzman et al., 2018; Zhao et al., 2023).

Increased GFP also inversely correlated with all Vineland-3 subscales except for socialization. Correlations were particularly strong for the communication subscale which indexes receptive, expressive, and written communication. The daily living skills subscale includes measures of personal care, domestic task engagement, and navigating the community environment (e.g., using money, understanding schedules, and navigation). Socialization indexes emotional regulation skills over communication or engagement with others. Lastly, the adaptive behavior composite score is a summary score that gauges adaptive behavior and potential support needs (Klaiman et al., 2014). Overall, correlations suggest that increased global GFP and individual microstate GFP in FXS were linked to worse language ability, reduced ability to engage with activities of daily living, and overall decreased adaptive behavior skills or need for increased real-world supports (Cordeiro et al., 2020). While Vineland-3 does not inherently measure cognitive ability, adaptive behavior is ultimately more informative of ability in FXS where better adaptive behavior is associated with better outcomes despite lower IQs, though both are positively correlated (Aishworiya et al., 2023; Cordeiro et al., 2020).

Lastly, GFP positively correlated with ABC stereotypy and hyperactivity. The stereotypy subscale indexes repetitive behaviors which are associated with rigidity and reduced adaptability, and the hyperactivity subscale indexes impulsivity, inattention, and hyperactive or disruptive behaviors (e.g., running around or excessive motor activity, intrusive behaviors, etc.) all of which result from reduced behavioral inhibition and both cognitive and behavioral inflexibility (Sansone et al., 2012; Wheeler et al., 2013). Individuals with FXS often exhibit increased hyperactivity and restrictive and repetitive behaviors which are linked to overall reduced EF (Wheeler et al., 2013). All together, these correlations are supportive of broader EF disruptions

which map onto the elevated GFP in FXS where these correlations hold for GFP across individual microstate classes.

Overall, GFP may serve as a proxy for broad cognitive disruptions which have consequences for executive processes governing behavioral inhibition and rigidity. Further, these disruptions have consequences for adaptive behavior where higher GFP maps onto worse overarching adaptive behavior driven largely by communication and behaviors of daily living.

As microstates are driven by low frequency activity, low frequency disruptions in both theta and alpha may drive the current microstate results (Milz et al., 2017). Increased reactivity of low frequency activity in FXS (i.e., increased GFP peaks) may reflect stasis in highly reactive patterns of neural activity. Recent work found that GFP peaks most commonly occur in the crest and troughs of alpha waves where a reduced ability to mobilize alpha may contribute to abnormal GFP patterns that are harder to index with discrete measures, as microstate variables tend to be (Antonova et al., 2022; Kornfeld-Sylla et al., 2025; Mishra et al., 2020; Norris et al., 2022).

Ultimately, the pattern of GFP peaks per second and GFP respective to individual microstate classes suggest FXS have more rapidly changing brain activity but not to an extent that global excitation/inhibition balance is impacted, as evidenced by increased GEV and group comparability in complexity, Hurst, and microstate variables that index temporal dynamics (e.g., duration and occurrence). Specifically, complexity and Hurst indicate no dynamic patterns of sustained hyper- or hypoactivity in rsEEG for FXS (Pretzsch & Floris, 2020). Overall, hyperactivity may not be fully detrimental to cognition but rather the patterns or ways in which FXS brain activity is hyperexcitable (e.g., rigid functional networks).

Microstate results indicate network dysfunction in FXS that are possibly relevant for cognition, as previously concluded (Takarae et al., 2023). However, insight from the current FC analysis added interpretive power to microstate analysis conclusions.

Functional Connectivity

Across all functional networks of interest, FXS within network theta FC was significantly elevated. Within network theta FC was also diffusely hyperconnected for FXS where connectivity was increased in magnitude across all functional networks of interest suggesting network inefficiencies. Further, diffuse within network hyperconnectivity suggests reduced small world network organization. Importantly, the present study adds to previous work in FXS which concluded that both long-range and short-range connectivity in theta were impaired in FXS where increased connectivity likely reflects neuronal hyperexcitability and decreased long-range information transfer (van der Molen et al., 2014). At the whole sample level, theta FC was inversely correlated with abbreviated IQ suggesting increased FC in theta was associated with reduced cognitive ability. However, for the FXS group the correlations with abbreviated IQ were not significant, suggesting this relationship either does not hold for FXS or represents a smaller effect. Though, inverse correlations were identified between DMN and control network theta FC and nonverbal IQ. In the typically developing literature, increased theta shares an inverse relationship with IQ where higher theta during development predicted lower IQ scores during adolescence (Liang & Mody, 2022). Theta oscillations and theta synchrony are important for cognition but share a complex relationship where sustained increases in theta are detrimental to cognition function, but elevated task-related theta corresponds to increased cognitive performance (Tan et al., 2024). Beyond IQ, theta FC did not share relationships with KiTAP

variables or the Vineland subscale scores suggesting increased theta FC does not map directly onto disrupted cognitive performance or adaptive behavior difficulties.

In relation to other past findings in FXS, theta FC shared a positive relationship with increased theta power in FXS indicating that increased within network phase synchronization relates to increased global activity in the theta frequency range. The pattern of elevated theta across both rsEEG and sensory tasks in FXS is robust across studies which previously concluded theta may compensate for reductions in alpha power, which is typically reduced in FXS (Wang et al., 2017; Pedapati et al., 2022; van der Molen et al., 2014). Namely, these conclusions map onto developmental shifts from the dominant use of theta to the dominant use of alpha oscillations where the individual peak frequency in the power spectral density also shifts from theta into the alpha frequency range (Campbell & Feinberg, 2009; Cellier et al., 2021; Kang et al., 2024). Individuals with FXS theoretically do not undergo the shift from theta to alpha noted in typical development, as evidenced by reduced PAF in adults with FXS where individual PAF values are often in the theta frequency band range (Cellier et al., 2021; Norris et al., 2025a; Pedapati et al., 2022; van der Molen & van der Molen, 2013). Precisely timed oscillatory activity is important for activity-dependent organization of neural functional networks and key during heightened periods of neural change, such is the case during child development (Khazipov & Luhmann, 2006; Markram et al., 2012; Peinado, 2000). The aforementioned shift from increased low frequency density into alpha-dominant utilization tracks with ongoing synaptic pruning and refinement of the neocortex where low frequency oscillations are import for the activity-dependent rewiring of neuronal networks during various stages of synaptic pruning which may be disrupted in FXS (van der Molen et al., 2014; Uhlhaas et al., 2010). Thus, heighted theta FC may reflect network inefficiencies stemming from abnormal synaptic maturation and pruning

difficulties leading to inefficient cortical networks (Contractor et al., 2015; Pfeiffer & Huber, 2009). The limited correlations with IQ suggest these inefficiencies negatively impact the ability to flexibly modulate network strength to support cognition (Huebschman et al., 2020; Kao et al., 2010; Park et al., 2008). However, this conclusion should be revisited in the context of theta FC during active cognition.

While the present study cannot shed light on whether individuals with FXS utilize theta for traditional alpha-related processes, the current results demonstrate theta-related network inefficiencies in FXS stemming from hyperconnectivity across key functional networks. Current results may additionally reflect an inability to shift out of firing in theta frequencies where theta FC is positively associated with increased absolute and relative theta power. Additionally, the present study identified significant direct correlations at the whole sample level between PAF and alpha 2 FC and significant inverse correlations at the whole sample level between PAF and theta FC. The direct correlations mostly held for FXS but not the inverse correlations, except control network theta FC and whole head PAF. Correlations may add support to the idea that increased theta, and now theta FC, correspond to down shifted alpha where theta is potentially mobilized to compensate for the reduced ability to mobilize alpha (Wang et al., 2017). As increased theta FC was loosely associated with reduced IQ, increased theta and theta FC may not be wholly compensatory for the reduced ability to mobilize alpha, though. However, both may be an issue in FXS where neither is directly causing or compensating for the other based on the results of more dynamic analyses looking at alpha in FXS (Kornfeld-Sylla et al., 2025; Norris et al., 2022).

Given GFP and theta FC inversely map onto IQ in rsEEG, the current results likely captured pathological differences between groups where networks are more inefficient and

hyperreactive in the lower frequencies. However, the GEV findings are less clearly interpretable and require further investigation to fully understand the functional and clinical relevance of elevated GEV in FXS. Though, elevated GEV may suggest FXS neural hyperreactivity is organized in increasingly predictable ways to compensate for network inefficiencies where females are more able to engage this mechanism per the significant sex effect (Contractor et al., 2015; Lui et al., 2022; van der Molen et al., 2014).

In terms of node connectivity, subtle shifts occurred in which nodes/node hubs were dominant between groups in DMN, SN, and control network. However, differences were not evident in the sum of the top ten connections for all networks nor in the individual top two connections for TDC, except for SN Connection 1 between the left and right supramarginal nodes (i.e., the strongest connection for both FXS and TDC). Overall, node results support the conclusion that increased theta FC is a widespread phenomenon resulting from a shift in magnitude of connectivity across the three core networks in FXS. The only connection-specific difference was in the magnitude of connectivity in the top TDC SN connection which was also the strongest SN connection for FXS suggesting a potential deficit in supramarginal gyri. In particular, elevated theta FC may represent increased inflexibility in areas associated with sensory integration. The anatomical coupling of SN was preserved but with elevated synchrony in FXS which may reflect either atypical sensory integration or a deficit in stimulus salience, possibly both. Overall, these findings, along with increased diffused theta FC in all three networks may reflect thalamocortical dysrhythmia where past studies in FXS made similar conclusions based on findings of elevated theta power in SN and DMN (Pedapati et al., 2022). Importantly, supramarginal gyri activation has been linked to reflect task-switching, a facet of cognitive flexibility, where parietal involvement was associated with tracking task rules (Philipp

et al., 2012). The current study adds to past findings by indicating hyperconnectivity between supramarginal nodes bilaterally, a site where thalamocortical dysrhythmia becomes most evident and may interrupt cognitive processing as a byproduct of baseline elevations in bilateral supramarginal gyrus activation. Past work supports this conclusion in FXS where reduced supramarginal gyrus activation modulation during a memory task did not shift with increasing task difficulty (1-Back vs 2-Back on an N-Back task). Further, task accuracy was associated with bilateral supramarginal gyri activation in TDC but not FXS suggesting abnormalities in supramarginal gyrus during cognitive processes. Further, activation of supramarginal gyri was significantly correlated with FMRP where the current identification of elevated supramarginal gyri connectivity may correspond to bilateral supramarginal gyri activation disruptions previously captured using fMRI where FMRP shares a known direct relationship with IQ (Schmitt et al., 2024;Kwon et al., 2001). However, of note, the previous study subjects were all female rather than inclusive of males with FXS (Kwon et al., 2001; Menon et al., 2000).

Microstates as Functional Connectivity Proxies

A core goal of the present study was to evaluate whether microstates indexed similar disruptions in FXS to where microstates could serve as a proxy for FC-related disruptions. The correlation analysis did not identify a clear pattern where microstates overlapped with FC disruptions. Though, MS3 and MS4 shared some correlations with FC variables across the whole sample which may represent shifts in underlying network activity. Given only theta FC disruptions were detectable, the correlations between MS4 and theta, alpha 1, and alpha 2 FC that were present may represent individual variable group dynamics. Conclusions were challenging to make, as microstates and FC occur on separate timescales which prevents direct

comparisons where averaging FC over the whole recording potentially reduced nuances in functional network engagement captured by microstates.

Power and Individual Peak Alpha Frequency Differences

Power and PAF were tested to determine whether robust group differences typically noted for FXS replicated. As expected, reduced individual PAF in FXS compared to TDC was observed in the present study which is consistent with the literature (van der Molen & van der Molen, 2013; Pedapati et al., 2022; Wang et al., 2017). Analysis of both absolute and relative power across various frequency bands identified similar dynamics between FXS and TDC seen in previous studies, though the increased relative gamma power was not observed (van der Molen & van der Molen, 2013; Wang et al., 2017). Overall, the current sample does not seemingly differ in baseline rsEEG measures compared to past studies.

Conclusion

At present, there is a lack of treatments specifically targeting the pathophysiology of FXS. Despite intensive efforts to develop novel treatments for FXS and high-quality research conducted alongside clinical efforts, there have been numerous failed clinical trials over the past 30 years (Erickson et al., 2017). While many factors contribute to clinical trial failure, methodological problems are chief among the issues currently faced by the FXS field (Boggs et al., 2022; Hessl et al., 2016; Verdura et al., 2021). While certain treatment avenues failed for other reasons – like the mGluR theory where associated clinical trials failed due to the quick tolerance developed by human patients that was not previously noted in the phase 1 animal studies, improvements in the way we measure FXS features may prevent trial failure in cases where treatment efficacy is present (Erickson et al., 2017; Stoppel et al., 2021).

The use of EEG is highly scalable for translational use with recent studies highlighting the ability for EEG to parse FXS from TDC and to parse intervention effects (Ethridge et al., 2024; Norris et al., 2024). EEG biomarkers identified from resting state data and auditory evoked tasks are typically robust across studies and correspond to important clinical features (Ethridge et al., 2016; 2017; 2019; Kenny et al., 2022; Pedapati et al., 2022; Proteau-Lemieux et al., 2021; 2024). In particular, resting state tasks are highly manageable for researchers/clinicians and well tolerated for patients with ID making resting state EEG measurements ideal for clinical use. However, most EEG biomarkers in FXS utilize an averaging method to provide insight into average neural activity overtime. Specifically, most are calculated using a fast Fourier transform (FFT), or something similar, to average over seconds to minutes' worth of EEG data which effectively assumes stationarity of the underlying neural dynamics. Moving into EEG metrics that do not assume stationarity of the contributing neural signal, like microstates, complements existing biomarker work in FXS while providing much needed insight into functional network dynamics which future research can build upon to improve our understanding of network mechanisms in FXS. Further, current results showing microstate outcomes in FXS will potentially allow for future cross-species evaluations which will provide more mechanistic insight into the network properties of microstates in FXS (Feng et al., 2005; Megevand et al., 2008; Mishra et al., 2020; Mishra et al., 2021).

While both microstate and FC analyses show evidence of meaningful physiological differences that map onto clinical measures of cognition and adaptive behavior, looking at the findings globally suggest that rsEEG dynamics are only minimally suggestive of network disruptions. The most important take away from the current results was the low FC values across all networks, which most surprisingly included the DMN. While there were significant

differences in theta FC across the DMN, SN, and control network, these differences were small and minimally correlated with IQ, despite being consistent with previous findings (Schmitt et al., 2022). Overarchingly, these hypotheses are worth evaluating in tasks designed to elicit specific and consistent brain states to better understand what dynamics both microstates and FC are capturing and whether those disruptions overlap. Ultimately, the evaluation of FC within DMN, SN, and control network was a novel approach and identified consistencies with prior findings in the field.

Finally, the hypothesis that microstates would map onto FC disruptions during rsEEG was not supported. There are major caveats to the interpretation of correlations between microstates and FC, as they are measured in the current study. Microstate analysis is a time-domain evaluation of neural activity where FC measures frequency synchrony between two areas across the duration of the whole EEG recording. As a result, meaningful relationships between individual microstates classes and FC disruptions were likely obscured or averaged out by taking FC at the global level. Current results likely reflect disruptions that were continuous or more ubiquitous and not specific to the dynamics of individual brain states.

Limitations

Allowing participants to watch a video during resting state EEG is a clear limitation of the current study, as DMN is a task-negative network, and they were both visually and cognitively engaged at the time of recording. Given rsEEG task settings are not truly task negative, the results likely reflect a skewed representation of FC in functional networks and microstates. The low FC values across all networks corroborates this conclusion, as the low values are suggestive of reduced or more variable network activation. Present results most likely are related to non-time locked stimulus processing where a true rest may produce different

results. Namely, increased GFP peaks per second and elevated theta FC, without clear evidence for dominance of any one functional network, may reflect sensory or attentional processes related to the video during recording. Further, gamma activity increases are generally associated with DMN where activity in lower frequencies may not fully represent overall pattern of activity within the DMN (Bartoli et al., 2024). Evaluating gamma FC may be necessary to determine whether DMN was less engaged during the rsEEG task. However, past studies found equally low values in gamma FC during rest, though not specific to DMN (Schmitt et al., 2022). The FC of faster frequency bands was not computed, as the main goal was to assess direct overlaps where the generation of microstates does not involve gamma. Overall, the relationship between microstates and gamma FC would be more difficult to interpret.

Future Directions

As the present study only presents a correlation analysis to determine potential relationships between FC and microstates, future work will prioritize methods that allow the computation of FC on microstates. Specifically, the source localized data will be submitted to the +microstate toolbox for a within-microstate FC analysis computed in order to evaluate FC within microstates for both theta and alpha frequency bands. At present, the toolbox does not support source localized EEG data preventing both source localized microstate solutions and the analysis of FC directly on individual microstate classes.

CHAPTER THREE

Functional Connectivity Underlying Neural Flexibility in Fragile X Syndrome as a Neurocognitive Biomarker

Key Words:

Fragile X Syndrome; cognition; EEG; microstates; functional connectivity; reversal learning; triple network model; salience network; default mode network; control network

Abstract

Fragile X Syndrome (FXS), being one of the most common inherited causes of intellectual disability (ID), is clinically characterized by broad difficulties with cognition including reduced language learning/communication challenges, reduced capacity to engage in behaviors of daily living, and limited ability or inability to transition to independent living. Further, there are disruptions to cognitive and behavioral flexibility leading to issues with behavioral control which underscores many of the cognitive-related symptoms noted in FXS. Cognitive symptoms are often cited as the most distressing for individuals with FXS and their families where learning difficulties are cited as chief among symptom concerns. Underlying learning difficulties and cognitive inflexibility are likely functional connectivity (FC) disruptions resulting from non-optimized neural network efficiency. From recent studies using electroencephalography (EEG), FC abnormalities in key frontal and frontocentral brain regions were identified from resting state EEG (rsEEG) where cognitive disruptions were then extrapolated based on correlations between clinical measures of cognitive ability and rsEEG variables. While rsEEG findings likely represent functional network difficulties that extend to cognitive neural processes, limited work has directly assessed FXS neural activity during a cognitive task. Importantly, from FC studies using functional magnetic resonance imaging (fMRI) a network model emerged for other neuropsychiatric conditions where salience network disruptions lead to difficulties in switching from the resting state network known as the default mode network into the task-positive processing network known as the "control" network (i.e., lateral frontoparietal network or central executive network). The current study aimed to address these gaps in the field by 1) testing the triple network hypothesis in FXS using FC during a deterministic reversal learning (RL) task with two choices and 2) evaluating the effectiveness of using microstates as a proxy for any

functional network disruptions identified from RLEEG data. A case-control study was conducted including 79 adults (35 with FXS and 44 typically developing controls [TDC]) who participated in a RLEEG task. Results included several important group differences on both microstate and FC variables which mapped onto clinically relevant symptoms of cognitive performance/ability. First, reward processing was disrupted in FXS likely stemming from neural hyperreactivity and inflexible network function during feedback-processing which resulted in rigid heighted reward processing. Next, microstate differences during feedback point to increased neural inflexibly where global field power (GFP) was significantly elevated in FXS, as noted in rsEEG. Further, both Hurst exponent and complexity were different during feedback and stimulus processing, respectively. The emergence of novel group differences on Hurst and complexity indicate network-level disruptions specific to task-processing and cognitive flexibility. Finally, FC results provided mechanistic insight into the identified neural inflexibility findings and identified support for the triple network hypothesis for theta FC. Theta FC was elevated across all networks and for all task periods indicating elevated theta FC represents a more global disruption. Given theta FC directly correlates with theta power, FC may represent a functional consequence of elevated theta power which FXS likely use to compensate for their reduced ability to utilize alpha appropriately. Across all variable types, clinical correlations suggest these indices of neural inflexibility map onto executive dysfunction and reduced cognitive ability. However, present results could not address whether microstates serve as a proxy for FC disruptions due to methodological limitations. In conclusion, the current findings add support and mechanistic insight into cognitive inflexibility in FXS within humans during active cognition which will support ongoing efforts to develop and test novel treatments for the more distressing symptoms of FXS.

Background

Fragile X Syndrome (FXS) is a rare monogenic neurodevelopmental disorder caused by a trinucleotide repeat expansion ≥ 200 CGG copies in the promoter region of the Fragile X Messenger Ribonucleoprotein 1 (*FMR1*) gene which then becomes hypermethylated, reducing or silencing transcription and thus halting the production of the protein product by the same name (i.e., Fragile X Ribonucleoprotein or FMRP) (Salcedo-Arellano et al., 2020; Hagerman & Hagerman, 2021). FXS is one of the most common inherited cause of intellectual disability (ID) – second only to Down Syndrome, with cognitive difficulties spanning from mild learning challenges to more severe intellectual disability across the whole population (Schneider et al., 2009). Specifically, individuals with FXS have a wide range of cognitive symptoms including language/communication difficulties, reduced cognitive flexibility (e.g., conflict resolution), and difficulties with attention, among others (Kaufmann et al., 2017; Schneider et al., 2009; Weber et al., 2019). Cognitive symptoms and concerns about learning, engagement in activities of daily living, and transition to independent living are some of the concerns linked to cognition in FXS that are most impactful for individuals with FXS and their families (Weber et al., 2019). Presently, no treatment or interventions exist to treat the underlying pathophysiology of FXS and there is limited consensus on existing mechanisms for treating cognitive symptoms (Erickson et al., 2017; Razak et al., 2020). Given the distressing nature and impact of cognitive symptoms on daily life, more research is needed to better understand the neural mechanisms of cognitive disruptions and how molecular features of FXS link to physiology and behavior (Erickson et al., 2017).

Interestingly, a recent study found that deviation-scored intellectual quotients (IQs) in FXS males follow a near-normal distribution where the distribution is centered around 40 and,

for males with methylation mosaicism, IQ shared a positive linear relationship where more FMRP correlated with increased IQ scores (Schmitt et al., 2024). The relationship between peripheral FMRP and IQ is a clear sign of clinical manifestation of molecular variability stemming from systematic sources of heterogeneity. Given the relationship between FMRP and IQ, as a clinical measure of cognitive performance, there may be a way to better gauge molecular variability and conduct a more thorough investigation of the link between FMRP and neural activity using more direct measures of cognition.

The use of electroencephalography (EEG) in FXS has provided valuable biomarkers for translational use and allowed further insight into molecular mechanisms underlying core symptoms specifically for EEG measures sharing relationships with measures of cognition (Norris et al., 2024; Proteau-Lemieux et al., 2024; Schmitt et al., 2024). Recent EEG studies in FXS have provided evidence of frontotemporal and temporal disruptions linked to cognition and imply these disruptions stem from network stasis (Proteau-Lemieux et al., 2024; Wang et al., 2024). EEG provides a translational method to investigate network activity disruption as a function of FMRP loss; the millisecond precision of EEG also allows for dynamic evaluation of network activity during active cognitive tasks that rely on synaptic efficiency and flexibility (Cole, 2024; Hasan et al., 2021). Understanding the dynamic temporal aspects of functional disruptions in frontoparietal and temporal networks in FXS will improve our mechanistic understanding of neural contributions to cognitive function as distinct from other characteristic features of FXS, and thus provide enhanced targets for therapeutic interventions. While cognition is a clear area of need in the field of FXS, no one has used a cognitive EEG task to study FXS cognitive neurophysiology and the relationship between cognitive neurophysiology and clinical measures of cognition. By making use of a performance-based cognitive EEG task and

evaluating functional network connectivity, we may gain insight into global network dynamics and how they support, or fail to support, behavior.

Addressing functional network activation during a cognitive task is an important next step in the field. Currently, there are known disruptions to the salience network (SN) in FXS which is responsible for directing attention toward salient stimuli in the external environment (Hall et al., 2013). The SN is theorized to facilitate switching between the "control" network or lateral frontoparietal network and default mode network (DMN), a network model known as the triple network model, which potentially underlies cognitive control disruptions and anxiety in ASD (Chen et al.,2021; Chen et al., 2022; Kronke et al., 2020; Massullo et al., 2020; Menon, 2018). Triple network findings in ASD may generalize to FXS as approximately 50% of males and 20% of females with FXS have co-occurring ASD diagnosis, and nearly all individuals with FXS have observable autistic features, even if they do not meet ASD diagnostic criteria (Kaufmann et al., 2017). Although disrupted molecular pathophysiology in FXS may impact the general function of individual functional networks (i.e., SN, DMN, and control) while they are actively engaged, the loss of FMRP impacts synaptic plasticity and may additionally decrease the efficiency of functional networks, as well, thus altering the ability to shift dynamically between networks to accomplish neural tasks resulting in core FXS cognitive and behavioral features (Menon, 2018). As the SN acts like a network switch, disruptions to the SN may impact the efficiency of cognitive processes carried out by the control and DMN linked to difficulties across domains of cognition, especially the network efficiency associated with cognitive flexibility and conflict resolution (Uddin, 2021). The neural ability to switch between networks is, in part, modulated by alpha, as intracortical alpha activity reflects lateral inhibition of higher frequencies (e.g., gamma activity) (Jensen & Mazaheri, 2010; Quax et al., 2017). Disruptions to intracortical

alpha have been linked to alterations in DMN, control, and SN function in patients with mild cognitive impairment, demonstrating the role of network flexibility in typical cognition (Gurja et al., 2022). Further, strong evidence suggests the ability to dynamically utilize alpha is linked to regulation of cortical hyperexcitability and reduced severity of clinical features, thus atypical increases in gamma activity observed in FXS may be a byproduct of poorly modulated alpha – something not yet systematically examined in FXS (Norris et al., 2022; Pedapati et al., 2022). However, research on this topic has relied entirely on resting state EEG and its correlation to behavioral or caregiver-report measures collected, separately. Evaluating alpha-band "control" and SN activity on multiple time scales during performance-based cognitive EEG will be an important step for understanding how functional disruptions directly link to cognitive and behavioral symptoms.

The current study aims to address multiple gaps in the FXS field by evaluating functional connectivity in a specific network model hypothesis using a cognitive EEG task. Reward processing will be evaluated using event-related potentials specific to feedback where I predict blunted reward-related positivity (RewP) in FXS will correspond to FC disruptions in networks that contain the anterior cingulate cortex which may represent reduced or altered dopaminergic inputs (D'Addario et al., 2024; Fish et al., 2013). Dopaminergic alterations may ultimately underscore certain facets of neural flexibility that contribute to rigidity and repetitive behaviors (D'Addario et al., 2024). I further hypothesize that microstates will be evaluated as a proxy for any observed functional network disruptions in an effort to further establish microstates as biomarkers for FXS functional network disruptions. Specifically, the FC disruptions within the SN will result in an inability to switch out of DMN and into task-positive processing (e.g., control network). Disruptions to FC between areas involved in the control network will also

predict worse clinical outcomes related to cognitive performance where SN disruptions will correspond with non-cognitive clinical features of FXS (Hessl et al., 2016; Sheilds et al., 2020). Lastly, I hypothesize overarching increases in FC disruptions in FXS compared to TDC will reflect individuals with FXS that spend more time in microstate D (i.e., SN proxy), given SN disruptions contribute to cognitive inflexibility in FXS.

Methods

Participants

Participants were 79 total individuals (Aged 18 - 36 years): 35 FXS participants (14 females; age: $M = 28.00$, $SD = 6.33$) and 44 sex-, and chronologically age matched typically developing controls (TDC; 16 females; age: $M = 25.71$, $SD = 5.03$) recruited from Cincinnati Children's Hospital and Medical Center (CCHMC). For more information on participants, see Chapter two.

Procedure

The EEG acquisition and preprocessing procedure will follow the same protocol reported in chapter two.

EEG Acquisition. EEG data were acquired using 128-channel MagStim/EGI HydroCel nets with a MagStim/EGI NetAmp 400 Amplifier (Magstim/EGI, Eugene, OR) in sound-attenuated booths or in a clinic space. Data were recorded continuously and sampled at 1000 Hz with saline based electrodes (impedance approximately under 10 KΩ). Impedances were rechecked between each task to maintain low impedances across the whole EEG recording session, as the cognitive task was comprised of two full presentations of the task. In certain instances, the system continuously recorded while impedance checks were completed. As a result, in all cases where task

files were not naturally separated when the system was paused for the impedance check, files were manually separated offline.

EEG Tasks. ***Deterministic reversal learning (RL; cognitive task).*** The RL task contained only 2-choice trials (N = 200) with stimulus and response periods lasting a maximum of 2000 ms, where participants learned to match the correct location of a box stimulus presented in one of two locations on the screen with a button press corresponding to a location on the screen, followed by a 650 ms delay, and then visual feedback. A coin was presented for correct response vs. red X for incorrect and feedback was presented for a total of 750 ms. Reversal trials, in which the reinforced/correct location on the screen changes, were presented pseudo-randomly after 3-5 consecutive correct trials for between 35-50 trials. Intertrial intervals were jittered between 750-1000 ms (Figure 52). Trials were 3400 ms maximum for a total participation time of ~ 15 minutes. The RL paradigm was previously validated for fMRI in ASD and optimized for EEG in FXS at CCHMC on trial number and allowable reaction time (D'Cruz et al., 2011). Visual stimuli during the reversal learning tasks were presented with carefully controlled luminance level for comfort and was well tolerated by participants. Given the additional demand of the RL task on individuals with ID, individuals were more closely monitored for signs of distress.

Figure 52.

Reversal Learning Task Diagram

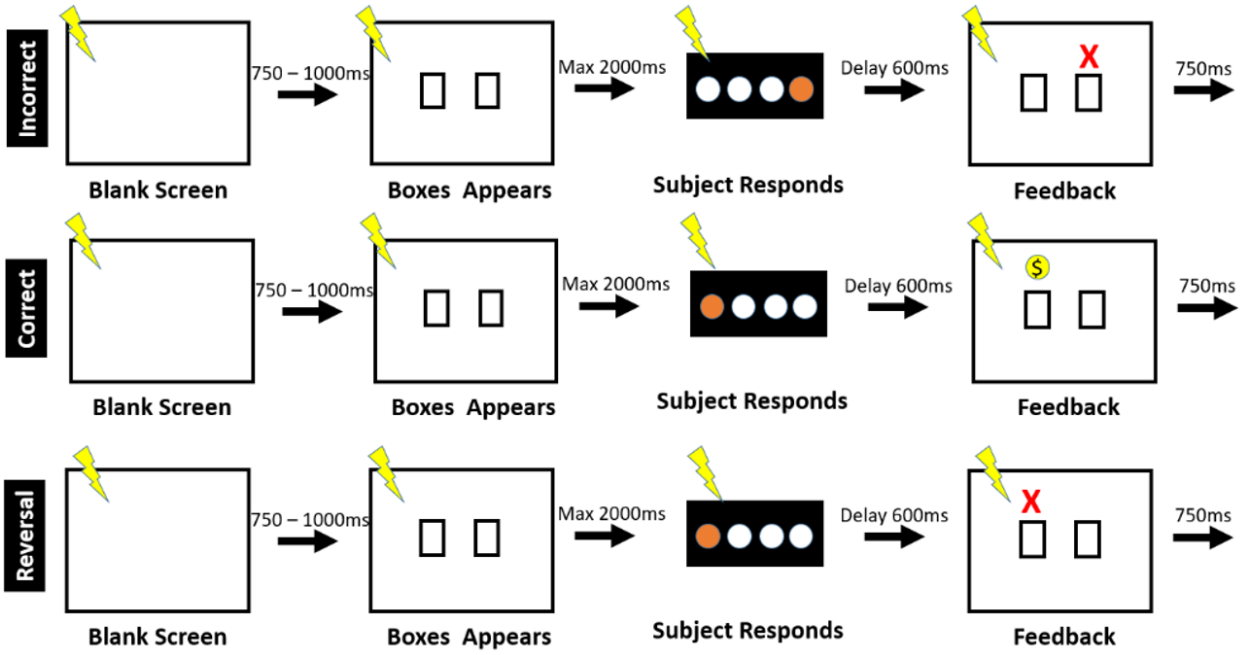

Note. RL task diagram where each row represents a different RL trial type scenario and each column represents a trial period. Trial periods included the pre-stimulus period where participants saw a blank, white screen. The stimulus period lasted a maximum of 2000 ms where participants saw two black boxes on the screen and selected one using one of two buttons on a custom button box. After box selection, the task delayed 600 ms and the feedback period began where feedback was presented over the box selected. The top row depicts a scenario where the participant selected the wrong location. The middle row depicts a scenario where participants selected the correct location. Finally, the middle row depicts the reversal trial where participants receive an error on the previously correct box location after the box location switched.

EEG Preprocessing. Raw data were preprocessed according to the detailed procedure in Chapter two. Briefly, errant channels were interpolated (no more than 5% or 7 channels total), swaths of data across both channels and time containing artifacts too extreme for the independent component analysis (ICA) algorithm were manually rejected, post-segment rejection data were submitted to ICA, and components containing predominately artifact (e.g., ocular, cardiac, or muscle artifact and components containing excessive line noise) were manually rejected. Data were re-referenced to an average of all channels. Data were then visually inspected for remaining

artifact prior to dataset finalization, which included evaluation of each file for the presence of neural signal.

FMRP. An optimized Luminex-based assay was used to detect protein levels in individuals with FXS (Boggs et al., 2022). The optimized assay allowed for the detection of trace protein levels in males with either methylation mosaicism or fully methylated males with some protein production.

Analysis

All variables were computed using MATLAB 2021b.

ERP Analysis. ERPs of interest were generated using the ERPLAB toolbox (Lopez-Calderon & Luck, 2014). Data were segmented into 1250 ms epochs (-500 ms to 750 ms). A whole sample grand average was computed to visualize ERPs topographically across all channels for channel selection. Channel selections were determined by using common channel subsets in the field and confirming signal presence in a priori channel groups using the ERP grand average topography map. Frontal, central, and parietal channel selections were used to evaluate feedback-related ERPs and an occipital channel selection was used to evaluate visual responses, as visual ERPs in FXS also represent a gap in the field. Feedback related ERPs were generated with both amplitude and latency were computed for the P1, N1, P2, and both the P3a (250 – 400 ms post feedback – central distribution) and P3b (400 – 600 ms post feedback – parietal distribution) components, where appropriate. The ERPs were used to primarily capture neural processes related to negative feedback, indicating a need for reversal in behavioral response (Kim et al., 2020). However, both the correct feedback preceding and the correct feedback following a reversal trial where they received incorrect feedback were also analyzed to evaluate correct feedback responses respective to reversal trials in order to keep trial counts similar. Both were evaluated to determine whether

responses to correct feedback showed similar patterns of group differences when preceding a reversal, and thus following a series of correct feedback inputs, or following the reversal where correct feedback follows feedback that should induce set shifting. Lastly, all correct feedback were evaluated as an exploratory analysis to increase the power on correct feedback to evaluate neural responses to reward only.

In addition, the reward-related positivity (RewP) was also analyzed by generating a difference wave where negative feedback on reversal is subtracted from positive feedback using both the correct preceding the reversal error and the correct following the reversal error. RewP was computed for both central and parietal electrode selections.

Channel selection was based on traditional electrode selections from the 10/20 system for frontal, central, parietal, and occipital regions *a priori* and then additional electrodes were added to increase area coverage for the 128 electrode net in a data-driven manner by selecting channels that maximized the ERP waveforms from a grand average topography (Figure 53). Methods used to quantify ERPs were largely selected *a priori* where fractional area and latency were preferred due to the inherent noise in FXS data. However, in certain instances (e.g., occipital-based ERPs), peak amplitude and latency were used because occipital ERPs are often well defined and proportionally distributed across the zero line or when fractional measures poorly captured ERP components on the grand average across the whole sample.

The RewP ERP component measures were computed using peak amplitude and peak latency. Frontal ERPs used numerical integration and fractional latency with rectified area to compute ERP components. Central and parietal analyses used numerical integration with positive areas for positive-going peaks and negative areas for negative-going peaks. Central used fractional area latency with rectified area and parietal used fractional latency with positive area

for latency measures. For parietal channels, the TDC N2 peak was above the zero line (i.e., fully positive) where a peak-to-peak measure was used to compute N2 amplitude. Finally, peak measures best captured ERP components for occipital ERPs, as ERP peaks were well-defined relative to the zero line which is typical. where peak amplitude and latency were used to compute component variables from occipital channels.

Figure 53.

Channel Selection for ERP Measurements

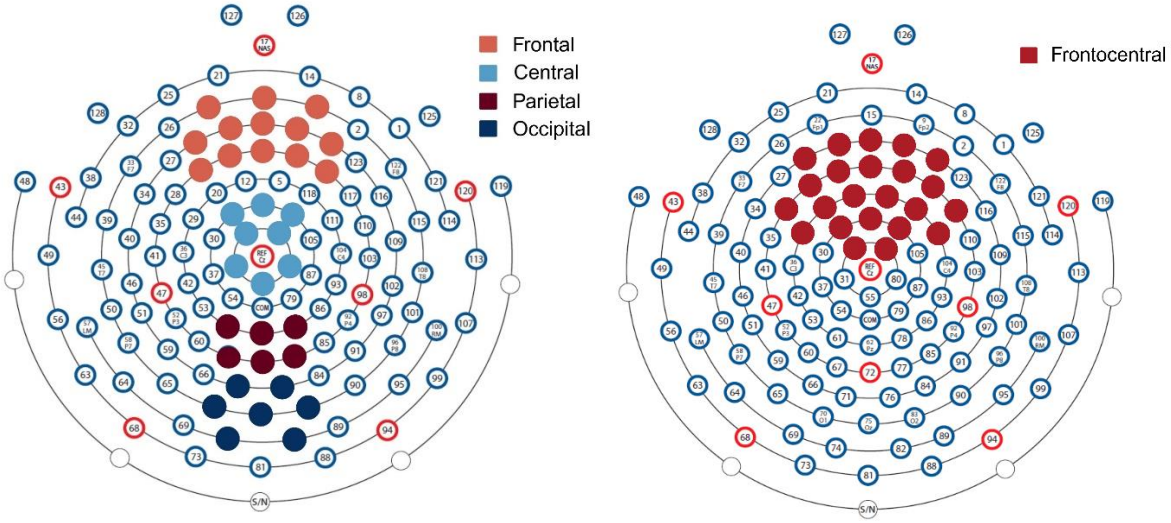

Note. Frontocentral selection range was enlarged to capture the spatial difference between groups for RewP.

Functional Connectivity Analysis. Clean data were segmented into 0-750 ms epochs and then concatenated into three separate files containing all: 1) pre-stimulus or baseline data, 2) stimulus presentation and response data, and 3) feedback data. The three file types were then treated as continuous for FC and microstate analyses. The stimulus/response window was evaluated to capture neural activity related to cognitive process of box selection, including the button press. All files were mutually exclusive, including the stimulus/response window where latency was determined by response speed which was confirmed prior to analysis.

Relationships between microstate classes across the various metrics and FC measures established in chapter two was evaluated on the RL task to see if resting state EEG (rsEEG) metrics detect similar FC dynamics captured during a cognitive task. FC measures for DMN, L-FPN, and SN were calculated from the pre-stimulus, stimulus/response, and feedback windows of the trial separately during the RL task to index neural switching between non-task related vs. task related activity. Theoretically, the pre-stimulus window should produce similar results to resting state, as there was no visual stimulation and no task-related processing outside of potential anticipation. The stimulus window and feedback window represent two distinct cognitive processes where the stimulus window captured stimulus detection, memory, and response selection (i.e., decision making which involves cognitive flexibility) and the feedback window captured reward/feedback evaluation, learning and memory updating, and emotional regulation (Izquierdo et al., 2018).

Microstate Analysis. Microstate results from chapter two were used to guide the microstate solution generated to evaluate the comparability between rsEEG microstates and task-based microstates. The four microstate, six-microstate, and optimal solutions were generated for all data types. where the optimal solution was determined using the kneedle algorithm in the +microstate toolbox. The Davies-Bouldin (DB) index was used to compare microstate solutions to select a solution for analysis. The latter is necessary, as limited work has evaluated microstates during task-positive processing. Therefore, comparability between rsEEG and task-based EEG is more of an empirical question. Microstate classes were calculated from RL pre-stimulus periods, during the task window, and during feedback separately.

Statistical Routine

All statistical analyses were conducted in SPSS version 29. Age was not significantly different between groups therefore, given the tight age range and age matching, age was not included as a covariate, $t(64.31) = -1.78$, $p = .080$, $d = -.41$.

Non-parametric Mann-Whitney U tests were used to evaluate group differences on EEG variables (i.e., ERPs, microstates, and FC variables), as residuals were largely non-normal across all variables. EEG task trial counts were added as covariates where appropriate due to the confounding effects of increased EEG data loss resulting from artifact in NDD populations.

The triple network hypothesis was tested on the RL task by assessing within-subject changes in FC from DMN in the pre-stimulus period to the control network during both the task and feedback windows using Friedman's which was split by group to determine whether FXS differs from TDC. Next, simple mediation models tested whether FC with evidence for disruptions (i.e., significant group differences) for SN in stimulus periods mediated the relationship between pre-stimulus DMN FC and stimulus control FC. The SN from the stimulus period was selected, as the SN is reactive not proactive.

Exploratory correlations evaluated relationships between experimental EEG variables, FMRP levels, and clinical variables related to cognition.

Results

Event Related Potential (ERP) Analysis – Feedback

Frontal

Frontal ERPs were evaluated to determine whether group differences were present for all feedback types, as frontal ERPs most likely reflect frontal processes related to cognitive appraisal of task feedback (Figure 54).

Figure 54.

Frontal Reversal Learning Feedback-Related ERPs

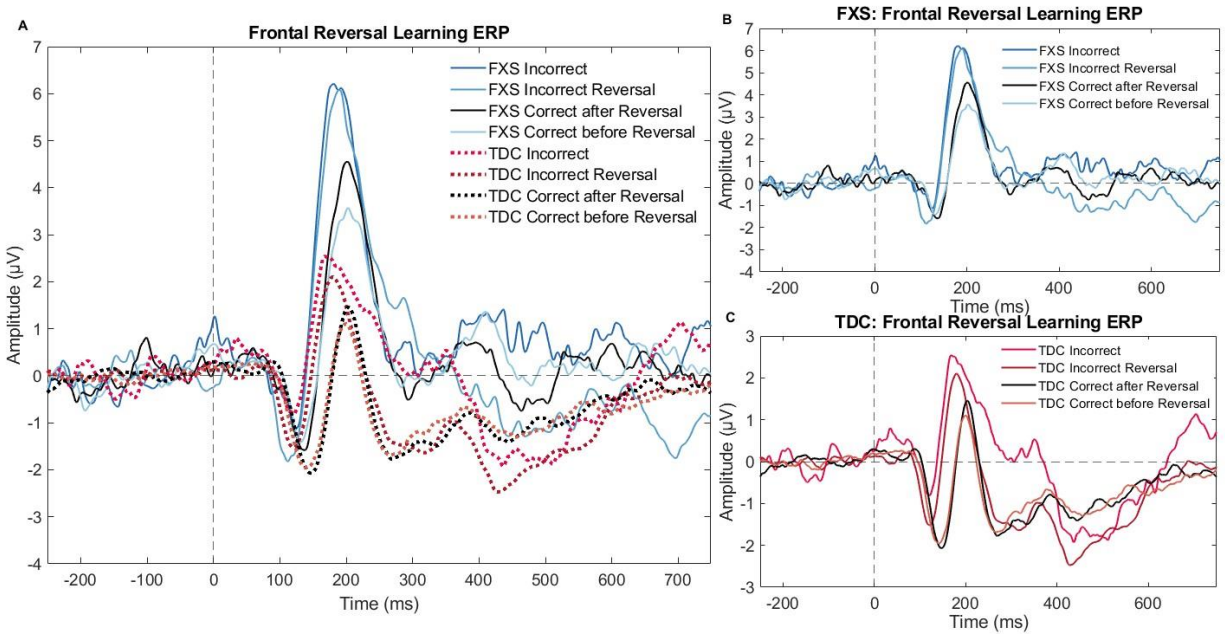

Note. **A)** All feedback-related ERPs between groups from frontal electrodes where solid lines represent FXS and dotted lines are TDC to show the magnitude of amplitude differences between groups, **B)** feedback-related frontal ERPs for FXS only for differentiation of individual feedback ERPs, and **C)** feedback-related ERPs for TDC only for differentiation of individual feedback ERPs.

Independent samples Mann-Whitney U tests were used to first evaluate group differences on both the amplitude and latencies of ERP components to incorrect/error-related (i.e., received a red X) feedback on reversal trials from the frontal electrode selection.

Analysis of frontal ERP amplitude for error-related feedback on the reversal trials identified significant group differences for the P1 component ($N = 78$; $z = 3.49$, $p < .001$, $r = .40$), the N1 component ($N = 78$; $z = 2.67$, $p = .008$, $r = .30$), and the P2 component ($N = 78$; $z = 4.64$, $p < .001$, $r = .53$). For the P1 and P2 components, individuals with FXS exhibited elevated amplitudes where for N1 amplitude they exhibited reduced amplitudes (P1: *M* rank = 49.68; N1: *M* rank = 47.29; P2: *M* rank = 53.03) compared to TDC (P1: *M* rank = 31.64; N1: *M* rank = 33.48; P2: *M* rank = 29.05). The trial count was a significant covariate for both the P1 and P2

amplitudes. The group differences remained after accounting for the significant covariate for the P2 amplitude, $F(1, 76) = 12.05$, $p = .001$. However, the P1 amplitude differences only trended towards significance when accounting for trial count, $F(1, 76) = 3.49$, $p = .066$. The reduced N1 amplitude provides some evidence to suggest reduced attention/stimulus salience in FXS where the reduction could reflect standard stimulus processing difficulties in FXS. Reduced error processing may contribute to later cognitive flexibility difficulties associated with error processing, more evident in the group differences for the P2 amplitude where FXS exhibited a large difference. Given the trending P1 amplitude differences and the N1 reduction, early stimulus processing deficits may play a later role in difficulties with appropriate task engagement.

Frontal ERP component latencies for error-related feedback on the reversal trials were not significantly different between groups but the latency of the N1 trended towards a significant difference where FXS had marginally reduced/faster N1 latencies (*M* rank = 47.29) relative to TDC (*M* rank = 33.48), $N = 78$; $z = 1.90$, $p = .057$, $r = .22$. Both the P1 component ($N = 78$; $z = .43$, $p = .671$, $r = .05$) and the P2 component ($N = 78$; $z = -1.29$, $p = .198$, $r = -.15$) latencies were comparable between FXS (P1: *M* rank = 49.68; P2: *M* rank = 35.75) and TDC (P1: *M* rank = 31.64; P2: *M* rank = 42.40). Trial count was a significant covariate for the P2 component and, interestingly, there was a significant group difference on P2 latency accounting for trial count where FXS had earlier P2 latencies compared to TDC, $F(1, 76) = 6.01$, $p = .017$. Earlier N1 peaks may represent hyper-responsivity in FXS where the early response is either a hyperactive response to sensory input or possibly a compensatory mechanism to combat increased task challenges and difficulties adjusting to task demands. The P2 latency results add support to the

idea that early processing disruptions lead to disruptions with processing later on in the stimulus processing time course.

Next, frontal ERPs to correct feedback (i.e., received coins) were tested for both the correct preceding a reversal error and the correct after the reversal error where differences on amplitude and latency were evaluated using independent samples Mann-Whitney U tests. Frontal P2 amplitudes were statistically significantly different groups for both the correct preceding the reversal ($N = 76$; $z = 4.36$, $p < .001$, $r = .50$) and the correct following the reversal ($N = 77$; $z = 4.57$, $p < .001$, $r = .52$) with FXS exhibiting higher amplitudes (Preceding: *M* rank = 51.44; Following: *M* rank = 52.45) compared to TDC (Preceding: *M* rank = 29.09; Following: *M* rank = 28.91). Trial count was a significant covariate for the P2 amplitude for the correct before the reversal where P2 amplitude was still significantly different between groups, $F(1, 77) = 9.88$, $p = .002$. Frontal P1 and N1 component amplitudes were not significantly different between groups for either the correct preceding the reversal (P1: $N = 76$; $z = 1.66$, $p = .096$, $r = .19$; N1: $N = 76$; $z = 1.64$, $p = .090$, $r = .19$) or the correct following the reversal (P1: $N = 77$; $z = 1.45$, $p = .147$, $r = .17$; N1: $N = 77$; $z = 1.46$, $p = .144$, $r = .17$). While neither reached statistical significance, the P1 and N1 for correct feedback preceding reversal trials trended towards a significant group difference where FXS had marginally higher amplitudes on P1 (*M* rank = 43.44) compared to TDC (P1: *M* rank = 34.91) and marginally reduced N1 amplitudes (*M* rank = 43.53) compared to TDC (N1: *M* rank = 34.84). However, for the correct following reversal both FXS (P1: *M* rank = 43.47; N1: *M* rank = 43.30) and TDC (P1: *M* rank = 35.80; N1: *M* rank = 35.77) were comparable. Trial count was a significant covariate for P1 amplitudes before and after the reversal where group differences no longer trended towards significance after accounting for trial count for the correct before ($F(1, 75) = .04$, $p = .838$) and the correct after ($F(1, 74) = .54$, $p =$

.466) reversal. Overall, these results suggest that FXS are more comparable to TDC in the amplitude of their early response to correct feedback but begin to differ in later components associated with cognitive processing. However, they add possible support to conclusions on reversal trials where P1 and N1 differences may reflect difficulties with specifically processing error-related feedback.

For ERP latencies to correct feedback, frontal N1 latencies differed between groups for both the correct preceding the reversal ($N = 76$; $z = -2.39$, $p = .017$, $r = -.27$) and the correct following the reversal ($N = 77$; $z = -3.28$, $p = .001$, $r = -.37$) with FXS exhibiting reduced/faster latencies (Preceding: *M* rank = 31.42; Following: *M* rank = 29.36) compared to TDC (Preceding: *M* rank = 43.65; Following: *M* rank = 46.23). The N1 differences follow the trend noted for the ERP to incorrect feedback on reversal trials where individuals with FXS exhibit/trend toward faster latencies which may reflect an overall increase in sensory/perceptual processing speed for visual feedback in FXS which may represent either sensory hyper-responsivity or a compensatory mechanism for task demands.

Both P1 and P2 component latencies were not significantly different between groups for either the correct preceding reversal (P1: $N = 76$; $z = 1.02$, $p = .306$, $r = .12$; P2: $N = 76$; $z = .59$, $p = .555$, $r = .07$) or the correct following the reversal (P1: $N = 77$; $z = .19$, $p = .848$, $r = .02$; P2: $N = 77$; $z = .71$, $p = .477$, $r = .08$). For both correct feedback types, FXS P1 (Preceding: *M* rank = 41.53; Following: *M* rank = 39.56) and P2 latencies (Preceding: *M* rank = 40.25; Following: *M* rank = 41.09) were comparable to TDC P1 (Preceding: *M* rank = 36.30; Following: *M* rank = 38.58) and P2 latencies (Preceding: *M* rank = 37.23; Following: *M* rank = 41.09).

Lastly, correct feedback unstandardized to the reversal trial count (i.e., all available correct trials) were evaluated between groups to determine whether group differences were

present on the average response to correct feedback irrespective of the reversal using independent samples Mann-Whitney U tests. Interestingly, the P1 amplitude was significantly different between groups with FXS exhibiting higher amplitudes (*M* rank = 48.14) compared to TDC (*M* rank = 33.52), $N = 79$, $z = 2.81$, $p = .005$, $r = .32$. The remaining tests followed the same pattern of group differences noted in tests evaluating correct feedback standardized to the reversal trials where the P2 amplitude was significantly different between groups ($N = 79$, $z = 4.84$, $p < .001$, $r = .54$) and the N1 amplitude was not significantly different between groups ($N = 79$, $z = .42$, $p = .671$, $r = .05$). The FXS group had significantly higher P2 amplitudes (*M* rank = 54.00) than TDC (*M* rank = 28.86) and comparable N1 amplitudes (*M* rank = 41.23) compared to TDC (*M* rank = 39.02).

ERP latencies for all correct feedback also identified similar patterns to the standardized correct feedback analyses. The N1 latency was significantly different between groups with FXS exhibiting reduced/faster latencies (*M* rank = 30.23) than TDC (*M* rank = 47.77), $N = 79$, $z = -3.40$, $p < .01$, $r = -.38$. The P1 component latency ($N = 79$, $z = .43$, $p = .666$, $r = .05$) and the P2 component latency ($N = 79$, $z = 1.24$, $p = .215$, $r = .14$) were not significantly different between groups where FXS (P1: *M* rank = 41.24; P2: *M* rank = 43.59) was comparable to TDC (P1: *M* rank = 39.01; P2: *M* rank = 37.15).

Central

Feedback ERPs from central electrode locations were next evaluated to capture the P3a component and test hypotheses related to P3a group differences to feedback (Figure 55).

Figure 55.

Central Reversal Learning Feedback-Related ERPs

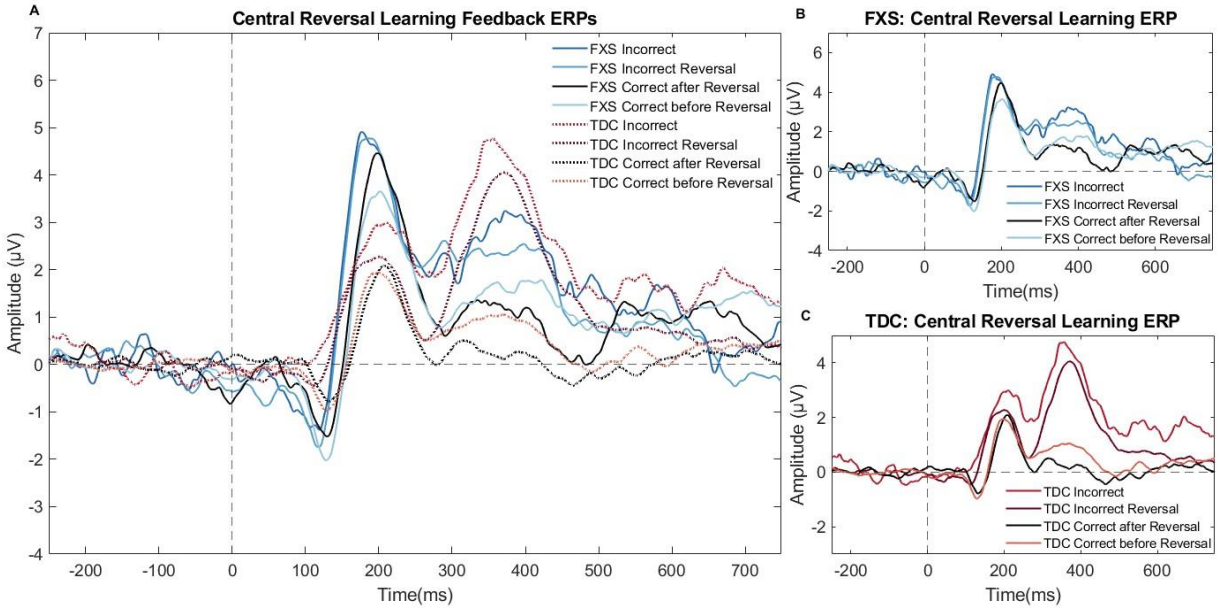

Note. **A)** All feedback-related ERPs between groups from central electrodes where solid lines represent FXS and dotted lines are TDC to show the magnitude of amplitude differences between groups, **B)** Central feedback-related ERPs for FXS only for differentiation of individual feedback ERPs, and **C)** Central feedback-related ERPs for TDC only for differentiation of individual feedback ERPs.

Central ERPs were evaluated using independent samples Mann-Whitney U tests which tested group differences on both the amplitudes and latencies of the P2 and P3a ERP components in relation to error-related feedback on reversal trials from the central electrode selection.

Analysis of central ERP amplitude for error-related feedback on the reversal trials identified significant group differences for the P2 component where individuals with FXS (*M* rank = 49.00) exhibited higher amplitudes compared to TDC (*M* rank = 29.81), $N = 75$, $z = 3.77$,

$p < .001$, $r = .44$. The P3a component amplitude was not significantly different between FXS (*M* rank = 39.47) and TDC (*M* rank = 36.16), $N = 74$, $z = .65$, $p = .516$, $r = .08$.

Central ERP latencies for error-related feedback on reversal trials for both the P2 component ($N = 78$, $z = -1.46$, $p = .143$, $r = -.17$) and P3a component ($N = 78$, $z = 1.16$, $p = .246$, $r = .13$) were not significantly different between groups where FXS (P2: *M* rank = 35.24; P3a: *M* rank = 42.88) and TDC (P2: *M* rank = 42.80; P3a: *M* rank = 36.89) were comparable.

Next ERPs to correct feedback were tested for both the correct preceding a reversal error and the correct after the reversal error for central electrodes where differences on amplitude and latency were evaluated using independent samples Mann-Whitney U tests. P2 component amplitudes for both correct preceding reversal ($N = 75$, $z = 3.80$, $p < .001$, $r = .45$) and following the reversal ($N = 75$, $z = 3.92$, $p < .001$, $r = .45$) were significantly different between groups with FXS exhibiting increased amplitudes (Preceding: *M* rank = 49.09; Following: *M* rank = 49.12) relative to TDC (Preceding: *M* rank = 29.74; Following: *M* rank = 29.26). The P3a amplitude was also significantly different between groups for the correct preceding reversal trials where FXS exhibited larger amplitudes (*M* rank = 43.13) compared to TDC (*M* rank = 32.48), $N = 73$, $z = 2.12$, $p = .034$, $r = .25$. However, the correct following the reversal only trended towards significance with marginally increased amplitudes for FXS (*M* rank = 39.27) compared to TDC (*M* rank = 30.00), $N = 68$, $z = 1.93$, $p = .053$, $r = .23$. Traditionally, the P3a results from unexpected or highly salient stimuli where P3a differences were expected for the error on reversal which was not observed. The difference between correct feedback types relative to receiving incorrect feedback on the reversal trial may be due to methodological challenges with capturing a measurement for the P3a in FXS. Alternatively, results may reflect differences in reward valuation and prediction in FXS due to either increased cognitive load or hyper-

responsivity. Specifically, differences in the P3 window for correct feedback may reflect cognitive evaluation of feedback where larger response magnitudes in FXS reflect less efficient reward processing with greater resources dedicated to processing correct feedback. The P3a amplitudes for TDC are quite small which may reflect efficient reward prediction where the increase in amplitude for the error on reversal reflects the increased salience of an unexpected error.

Latency analyses for the standardized correct feedback types identified a statistically significant group difference for the correct before the reversal where FXS exhibited increased/slower P2 latencies (*M* rank = 46.44) compared to TDC (*M* rank = 32.73), $N = 76$, $z = 2.68$, $p = .007$, $r = .31$. However, the P2 latency for the correct after the reversal was not statistically different between groups where FXS (*M* rank = 40.36) was comparable to TDC (*M* rank = 37.98), $N = 77$, $z = .46$, $p = .643$, $r = .05$. The P3a latency of both the correct preceding the reversal trial ($N = 76$, $z = .04$, $p = .971$, $r = .05$) and the correct following the reversal trial ($N = 77$, $z = .65$, $p = .51$, $r = .07$) were not significantly different between groups where FXS (*M* rank = 40.92) and TDC (*M* rank = 37.56) exhibited comparable latencies.

All correct trials were next analyzed using independent samples Mann-Whitney U tests to determine whether correct feedback responses were comparable when evaluating correct feedback irrespective of their position relative to reversal trials. Generally, analysis of all correct trials resulted in comparable outcomes to those preceding and following the reversal trials where both P2 ($N = 78$, $z = 3.35$, $p < .001$, $r = .38$) and P3a ($N = 74$, $z = 2.20$, $p = .028$, $r = .26$) amplitudes were significantly different between groups where FXS exhibited larger amplitudes (P2: *M* rank = 49.03; P3a: *M* rank = 43.47) compared to TDC (P2: *M* rank = 31.74; P3a: *M* rank = 32.43). Interestingly, the P2 latency was not significantly different where FXS (*M* rank =

43.97) and TDC (*M* rank = 36.84) exhibited comparable latencies, $N = 79$, $z = 1.37$, $p = .170$, $r = .15$. Importantly, correct response dynamics may change with increasing numbers of correct feedback inputs leading to increased sensitivity to correct feedback that is reduced back to typical response magnitudes after reversal and washed out when looking at all correct feedback irrespective of reversal trials. Finally, as noted in the analysis of correct feedback relative to reversal trials, P3a latencies were not significantly different between groups where FXS (*M* rank = 42.20) was comparable to TDC (*M* rank = 38.25), $N = 79$, $z = .76$, $p = .447$, $r = .09$.

Parietal

Lastly, feedback ERPs from parietal electrode locations were next evaluated to capture the P3b component and test hypotheses related to P3b group differences to feedback (Figure 56).

Figure 56.

Parietal Reversal Learning Feedback-Related ERPs

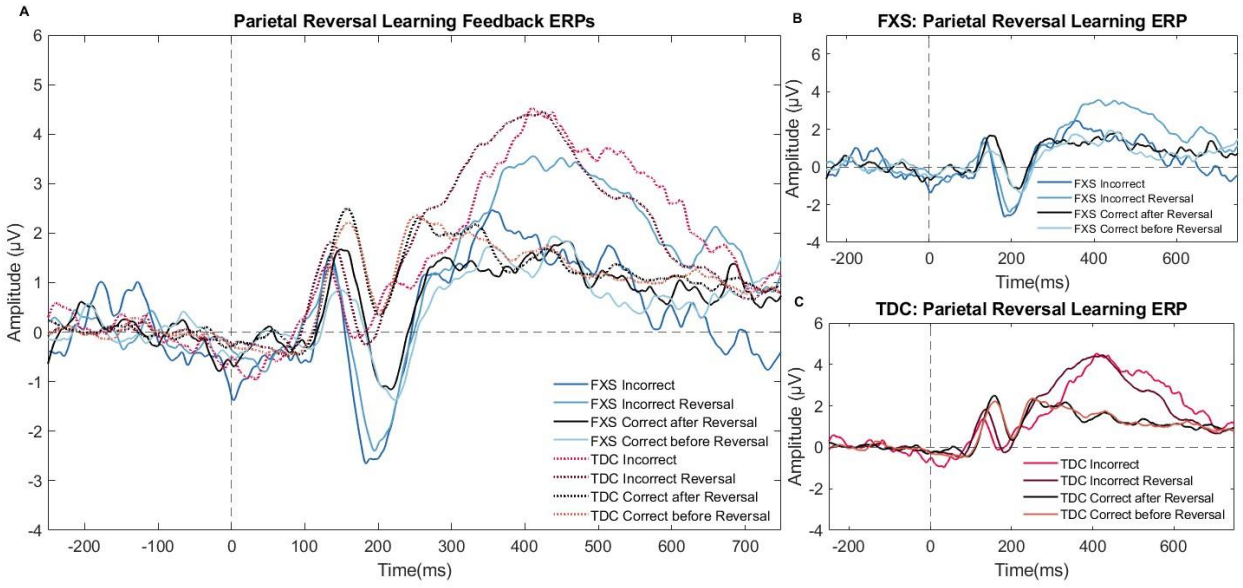

Note. **A)** All feedback-related ERPs between groups from parietal electrodes where solid lines represent FXS and dotted lines are TDC to show the magnitude of amplitude differences between groups, **B)** Parietal feedback-related ERPs for FXS only for differentiation of individual feedback ERPs, and **C)** Parietal feedback-related ERPs for TDC only for differentiation of individual feedback ERPs.

Parietal ERPs were evaluated using Mann-Whitney U tests which tested group differences on both the amplitude and latencies of the P2, N2, and P3b ERP components in relation to error-related feedback on reversal trials from the parietal electrode selection. Overall, ERP amplitudes and latencies were comparable between FXS and TDC in the parietal region.

For parietal channels, the N2 peak for TDC was above the zero line which required a peak-to-peak measure in order to appropriate index amplitude values. For the ERP to incorrect feedback on reversal, the N2 peak-to-peak amplitude was significantly different between groups with FXS exhibiting a larger N2 amplitude (*M* = rank = 29.00; N2 amplitudes are negative) compared to TDC (*M* = rank = 48.75), $N = 79$, $z = -3.80$, $p < .001$, $r = -.43$. P2 amplitude ($N = 75$, $z = -.51$, $p = .608$, $r = -.06$) and P3b amplitude ($N = 78$, $z = -.98$, $p = .328$, $r = -.11$) were not significantly different between FXS (P2: *M* rank = 36.55; P3b: *M* rank = 36.65) and TDC (P2: *M* rank = 39.14; P3b: *M* rank = 41.70).

The N2 ERP latency to error on reversal feedback was significantly different between groups where FXS exhibited larger/slower latencies (*M* rank = 46.87) compared to TDC (*M* rank = 34.53), $N = 79$, $z = 2.37$, $p = .018$, $r = .27$. The P2 component ($N = 75$, $z = .11$, $p = .915$, $r = .01$) and the P3b component ($N = 78$, $z = 1.39$, $p = .166$, $r = .16$) latencies were not significantly different where FXS (P2: *M* rank = 38.30; P3b: *M* rank = 43.54) and TDC (P2: *M* rank = 37.76; P3b: *M* rank = 36.38) exhibited similar latencies. Overall, the FXS parietal N2 component responses to error-related feedback were both greater in magnitude and slower than TDC where the P2 and more cognitive P3a were not significantly different which adds support to the idea that FXS are expending increased energetic costs to process negative feedback (Espinet et al., 2011, Xiao et al., 2019). As the more cognitive components were not different between groups,

the larger N2 may reflect a compensatory effort to recruit cognitive control-related processes that exhibit network inefficiencies.

Next, correct feedback types respective to reversal trials were evaluated. The N2 amplitude for the correct preceding reversal ($N = 79$, $z = -2.46$, $p = .014$, $r = -.28$) and the correct following reversal ($N = 79$, $z = -2.69$, $p = .007$, $r = -.30$) were both significantly different between groups where N2 amplitudes were larger for FXS (Preceding: *M* rank = 32.89; Following: *M* rank = 32.20) compared to TDC (Preceding: *M* rank = 45.66; Following: *M* rank = 46.20; N2 amplitudes are negative values). The P2 amplitude for the correct preceding reversal trended towards significance where individuals with FXS exhibited reduced amplitudes (*M* rank = 32.08) compared to TDC (*M* rank = 40.44), $N = 73$, $z = -1.66$, $p = .097$, $r = -.19$. However, the correct following the reversal was not significantly different between groups where individuals with FXS had similar amplitudes (*M* rank = 34.00) to the TDC (*M* rank = 41.95), $N = 76$, $z = -1.56$, $p = .120$, $r = -.18$. The P3b ERP amplitudes for the correct preceding ($N = 75$, $z = -.15$, $p = .880$, $r = -.02$) and the correct following ($N = 76$, $z = -.10$, $p = .921$, $r = -.01$) the reversal trial were not significantly different between groups where amplitudes to correct feedback were comparable between FXS (Preceding: *M* rank = 37.55; Following: *M* rank = 38.21) and TDC (Preceding: *M* rank = 38.32; Following: *M* rank = 38.72). The increased N2 amplitudes to correct feedback in FXS suggest abnormal salience where even non-error feedback was highly salient which may reflect reward prediction coding deficits where correct feedback was also uncertain or surprising (Mushtaq et al., 2011).

Overall, all three component latencies were not significantly different between groups. Correct feedback ERP latencies preceding and following the reversal trial were also evaluated. The N2 component latencies for the correct preceding ($N = 79$, $z = .97$, $p = .333$, $r = .11$) and

following (N = 79, z = .46, p = .643, r = .05) the reversal trial were not significantly different between the groups where FXS (Preceding: *M* rank = 42.80; Following: *M* rank = 41.34) was comparable to TDC (Preceding: *M* rank = 37.77; Following: *M* rank = 38.93). The P2 ERP latencies for the correct preceding (N = 73, z = -1.12, p = .264, r = -.13) and the correct following (N = 76, z = -1.53, p = .127, r = .) the reversal trial were also not significantly different between groups where latencies of the P2 response to correct feedback were comparable between FXS (Preceding: *M* rank = 33.68; Following: *M* rank = 34.09) and TDC (Preceding: *M* rank = 39.31; Following: *M* rank = 41.88). Finally, the P3b ERP latencies for the correct preceding (N = 75, z = -.59, p = .554, r = -.07) and the correct following (N = 76, z = .32, p = .749, r = -.18) the reversal trial were not significantly different between groups where latencies of the P3b response to correct feedback were comparable between FXS (Preceding: *M* rank = 36.23; Following: *M* rank = 39.42) and TDC (Preceding: *M* rank = 39.25; Following: *M* rank = 37.79). While the ERP amplitude of the N2 was altered, the time course of correct feedback processing was similar between FXS and TDC.

Finally, all correct stimuli were evaluated irrespective of reversal trials. Consistent with the correct feedback ERPs respective of the reversal trial, the N2 component amplitude to all correct feedback was significantly different between groups where FXS had larger N2 amplitudes (*M* rank = 29.91) compared to TDC (*M* rank = 48.02), N = 79, z = -3.48, p < .001, r = -.39. The P2 (N = 78, z = -.96, p = .337, r = -.11) and P3b (N = 78, z = .19, p = .853, r = .02) component amplitudes to all correct feedback were not significantly different between groups where FXS (P2: *M* rank = 36.77; P3b: *M* rank = 40.03) was similar to TDC (P2: *M* rank = 41.72; P3b: *M* rank = 39.07). Th

Analysis of ERP latencies to all correct feedback identified a significant group difference on the N2 latency where FXS exhibited increased/slower N2 latencies (*M* rank = 45.94) compared to TDC (*M* rank = 35.27), $N = 79$, $z = -2.05$, $p = .040$, $r = -.23$. However, similar to the latencies for correct feedback relative to error on reversal, the P2 ($N = 78$, $z = -1.25$, $p = .212$, $r = -.14$) and P3b latencies ($N = 78$, $z = -.07$, $p = .944$, $r = -.01$) were not significantly different between groups where FXS (P2: *M* rank = 35.96; P3b: *M* rank = 39.30) and TDC (P2: *M* rank = 42.38; P3b: *M* rank = 39.66) exhibited similar latencies.

Across all regions, incorrect feedback was not evaluated statistically due to low incorrect trial count for TDC, which was expected. Instead, incorrect feedback was evaluated in correlation analyses for FXS only to better understand the relationship between non-reversal-related errors and clinical manifestation of cognitive disruptions.

Event Related Potential (ERP) Analysis – RewP

A wide frontocentral range was used to capture the reward-related positivity (RewP). The spatial distribution of the RewP was different between groups where the FXS peak was more frontal and the TDC peak was more central (Figure 57; Appendix B).

Figure 57.

Scalp Topography for RewP

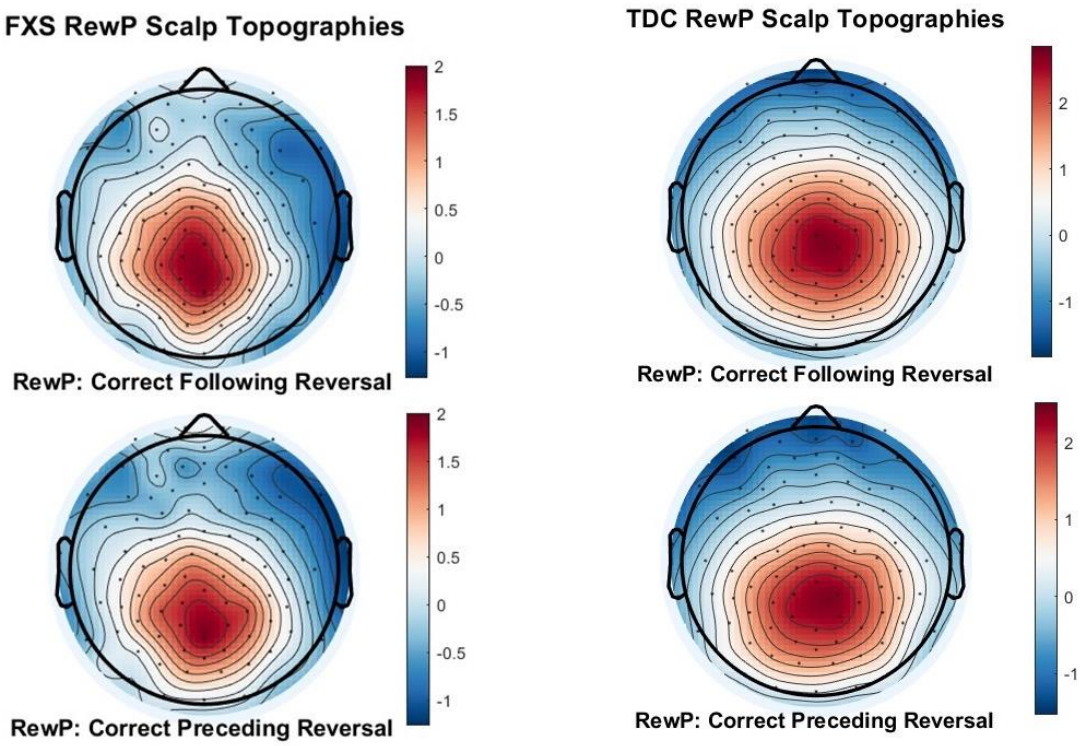

Note. Scalp plots for RewP amplitudes where colors indicate the average voltage at the scalp between 250-550 ms. Columns represent groups with FXS on the left and TDC on the right. Note scale difference between groups. Top row: RewP amplitude for the correct following the error on reversal; Bottom row: RewP amplitude for the correct preceding the error on reversal. Warm colors indicate higher voltage (positive) and color colors indicate lower (more negative) voltage.

Figure 58.

Frontocentral Difference Wave

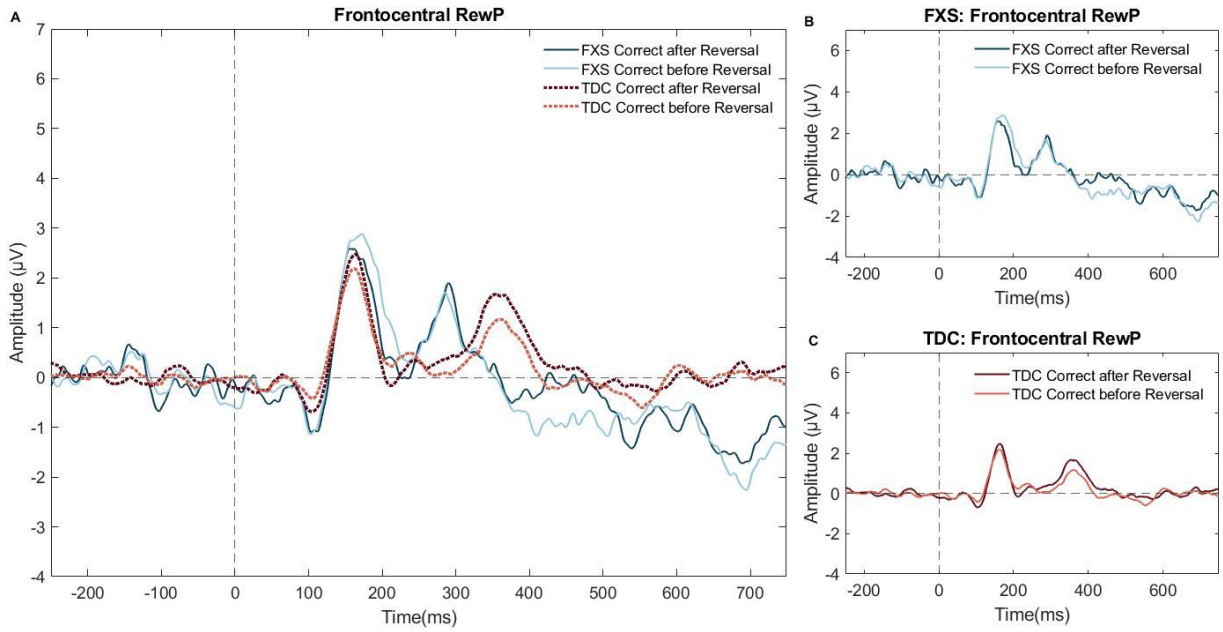

Note. A) Difference waves between groups from frontal electrodes where solid lines represent FXS and dotted lines are TDC, B) frontal difference wave for FXS only, and C) frontal difference wave for TDC only.

RewP was generated by creating a difference wave using both the correct preceding the reversal and the correct after the reversal between groups where wave subtracted the incorrect on reversal from matched correct ERPs (Figure 58). Mann-Whitney U tests evaluated group differences on ERP amplitudes and latencies for RewP. The RewP from the correct preceding was significantly different between groups where FXS exhibited increased amplitudes (*M* rank = 47.15) compared to TDC (*M* rank = 33.59), $N = 78$, $z = 2.62$, $p = .009$, $r = .30$. The RewP computed using the correct following the reversal was not significantly different between groups but did trend towards a significant difference where amplitudes were marginally elevated in FXS (*M* rank = 44.88) compared to TDC (*M* rank = 35.34), $N = 78$, $z = 1.84$, $p = .065$, $r = .21$. Increased amplitude may suggest heightened sensitivity to reward or salience of correct feedback. The lack of statistical significance for the RewP computed using correct feedback

preceding the error on reversal but not the correct following the error on reversal may reflect differences between the two RewP variables in TDC where TDC are more sensitive to reward following an error. As an exploratory test, Wilcoxon signed rank tests were used to test whether RewP amplitudes differed within subject by group. In support of the exploratory hypothesis, TDC had significantly different median amplitudes ($N = 44$, $z = -3.19$, $p = .001$, $r = -.48$) and FXS did not ($N = 34$, $z = -.22$, $p = .823$, $r = -.04$) where TDC had higher median RewP amplitudes for the correct following reversal error (med = 1.96, IQR = 2.33) compared to the RewP amplitudes for the correct preceding reversal error (med = 2.47, IQR = 1.56) and FXS were similar between the two (Preceding: med = 3.81, IQR = 4.07; Following: med = 3.75, IQR = 4.58). The inability to modulate, as TDC does, suggests heightened salience for correct feedback and less sensitivity to reward following error reflective of reduced flexibility in reward prediction updating. These results further support the conclusion that increased amplitudes in FXS are likely to reflect hyperreactivity to reward that is not an adaptability response (i.e., not using increased resources/processing to compensate).

Latencies for the RewP component computed using the correct preceding the reversal were not significantly different between groups but trended towards significance where FXS (*M* rank = 34.57) exhibited marginally reduced or faster latencies compared to TDC (*M* rank = 44.32), $N = 79$, $z = -1.88$, $p = .061$, $r = -.21$. The latency for the RewP computed using the correct following the reversal was significantly different between groups where FXS (*M* rank = 34.10) exhibited reduced or faster latencies compared to TDC (*M* rank = 44.69), $N = 79$, $z = -2.04$, $p = .042$, $r = -.23$.

Correlation analyses were run to evaluate whether early frontal ERP values for the incorrect on reversal correlated with RewP ERP variables. RewP amplitude for the correct

following error on reversal was directly correlated with P1 amplitude (rho = .39, p = .022) but not for the correct preceding reversal (rho = .21, p = .237). The P2 amplitude was also directly correlated with both RewP variables where the increased amplitudes corresponded (Preceding: rho = .37, p = .031; Following: rho = .44, p = .008). Finally, the N1 amplitude was also significantly correlated with Rewp for both the correct preceding (rho = .51, p = .003) and the correct following reversal (rho = .51, p = .002) suggesting reduced N1 amplitudes also correspond to increased RewP amplitudes. The N1 correlation is particularly interesting, as the N1 generally captures stimulus salience where the RewP amplitude correlation suggests early sensory salience or attention may contribute to altered reward processing in FXS.

A correlation analysis was conducted for FXS only to evaluate whether RewP amplitude and latencies map onto important clinical features from IQ, Vineland, and ABC. Across the whole group, the RewP amplitude preceding the reversal was inversely correlated with abbreviated IQ where increased amplitude was associated with reduced IQs (rho = -.25, p = .032) which did not hold for RewP computed from the correct after reversal but not after (rho = -.14, p = .226). The latency for RewP computed using the correct after the reversal was directly correlated with abbreviated IQ (rho = .24, p = .036) but not the RewP computed using the correct preceding reversal (rho = .20, p = .078) which only trended towards significance. These correlations between abbreviated IQ and both RewP amplitude (Preceding: rho = -.06, p = .752; After: rho = -.03, p = .890) and latency (Preceding: rho = .01, p = .978; After: rho = .02, p = .906) did not hold when computed on the FXS group, only. The whole group correlations were small where power may have been an issue but, ultimately, correlations with RewP were potentially spurious or simply indexing FXS group membership (i.e., causal third variable was

FXS diagnosis, as FXS had significantly higher amplitudes and significantly lower IQs than TDCs).

Event Related Potential (ERP) Analysis – Visual

Visual ERPs to feedback were evaluated as an exploratory analysis (Figure 59). ERPs were evaluated using Mann-Whitney U tests which tested group differences on both the amplitude and latencies of the P2, N2, and P3 ERP components in relation to feedback on reversal trials from the occipital electrode selection.

Figure 59.

Occipital (Visual) Reversal Learning Feedback-Related ERPs

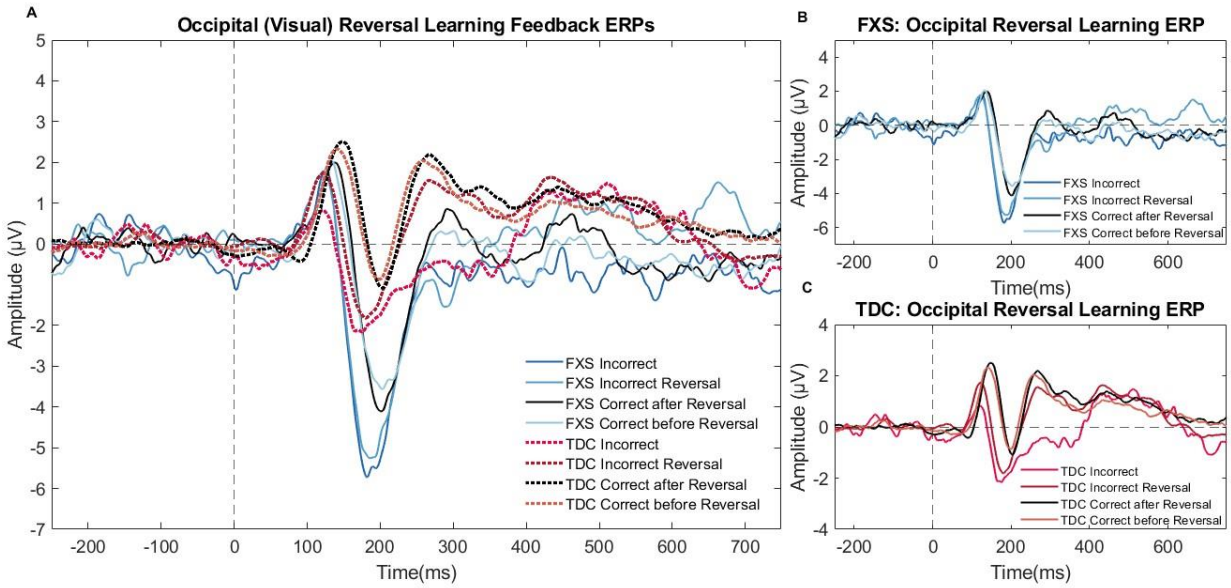

Note. **A)** All feedback-related ERPs between groups from parietal electrodes where solid lines represent FXS and dotted lines are TDC, **B)** Parietal feedback-related ERPs for FXS only, and **C)** Parietal feedback-related ERPs for TDC only.

First, ERP amplitudes to error on reversal were evaluated. The N2 amplitude was significantly different between groups where FXS had larger amplitudes (*M* rank = 24.65; more negative N2 amplitudes are larger) compared to TDC (*M* rank = 50.98), $N = 78$, $z = -5.09$, $p < .001$, $r = -.58$. The P3 amplitudes were also significantly different between groups where FXS

had reduced P3 amplitudes (*M* rank = 31.09) compared to TDC (*M* rank = 46.00), *N* = 78, *z* = -2.88, *p* = .004, *r* = -.33. The P2 amplitude was not significantly different between groups where FXS (*M* rank = 41.09) and TDC (*M* rank = 38.27) were comparable, *N* = 78, *z* = .54, *p* = .586, *r* = .06. These results suggest a hyperexcitable visual response.

Tests evaluating ERP component latencies following incorrect feedback on reversal identified a significant group difference for the N2 latency where FXS exhibited faster/reduced latencies (*M* rank = 31.09) compared to TDC (*M* rank = 46.00), *N* = 79, *z* = -2.88, *p* = .004, *r* = -.32. The P2 (*N* = 79, *z* = -.51, *p* = .611, *r* = -.06) and P3 (*N* = 79, *z* = -.69, *p* = .490, *r* = -.08) latencies were not significantly different between groups where FXS had similar latencies (P2: *M* rank = 38.53; P3: *M* rank = 38.00) to TDC (P2: *M* rank = 41.17; P3: *M* rank = 41.59).

Next, ERP amplitudes and latencies for correct feedback respective to the error on reversal were evaluated. The N2 amplitude for both the correct preceding (*N* = 76, *z* = -5.01, *p* < .001, *r* = -.57) and after (*N* = 77, *z* = -4.78, *p* < .001, *r* = -.54) the reversal were significantly different between groups where FXS had larger N2 amplitudes (Preceding: *M* rank = 23.63; Following: *M* rank = 29.94; more negative N2 amplitudes are larger) compared to TDC (Preceding: *M* rank = 49.32; Following: *M* rank = 49.55). The P3 amplitudes for both the correct preceding (*N* = 76, *z* = -2.81, *p* = .005, *r* = -.32) and after (*N* = 77, *z* = -1.98, *p* = .048, *r* = -.23) the reversal were significantly different between groups where FXS had reduced P3 amplitudes (Preceding: *M* rank = 30.16; Following: *M* rank = 33.18) compared to TDC (Preceding: *M* rank = 44.57; Following: *M* rank = 43.36). The P2 amplitude was not significantly different between groups both the correct preceding (*N* = 76, *z* = 1.14, *p* = .256, *r* = .13) and after (*N* = 77, *z* = .35, *p* = .726, *r* = .04) where FXS had comparable P2 amplitudes (Preceding: *M* rank = 41.88;

Following: *M* rank = 40.03) compared to TDC (Preceding: *M* rank = 36.05; Following: *M* rank = 38.23).

Tests evaluating ERP component latencies for correct feedback respective to the error on reversal identified a significant group difference for both the P2 and P3 components across both the correct preceding and the correct following. The P2 latency was faster/reduced for FXS (Preceding: *M* rank = 30.69; Following: *M* rank = 28.33) compared to TDC (Preceding: *M* rank = 47.41; Following: *M* rank = 49.28) on both the correct preceding ($N = 79$, $z = -3.22$, $p = .001$, $r = .36$) and following reversal ($N = 79$, $z = -4.03$, $p < .001$, $r = -.45$). The P3 latency was slower/increased for FXS (Preceding: *M* rank = 45.97; Following: *M* rank = 47.10) compared to TDC (Preceding: *M* rank = 32.25; Following: *M* rank = 34.35) on both the correct preceding ($N = 79$, $z = 2.06$, $p = .039$, $r = .23$) and following reversal ($N = 79$, $z = 2.45$, $p = .14$, $r = .28$). Lastly, the N2 latency was not significantly different between groups for either the correct preceding reversal ($N = 79$, $z = .95$, $p = .341$, $r = .11$) or the correct following reversal ($N = 79$, $z = -1.37$, $p = .170$, $r = -.15$) where FXS had comparable latencies (Preceding: *M* rank = 42.76; Following: *M* rank = 36.03) to TDC (Preceding: *M* rank = 37.81; Following: *M* rank = 43.16).

Finally, ERP amplitudes and latencies for all correct stimuli irrespective of reversal trial were evaluated which identified a similar pattern to the ERP results for correct stimuli match to the reversal trial. The N2 and P3 amplitudes were significantly different between groups but the P2 amplitude was not. The N2 amplitude was significantly increased in FXS (*M* rank = 28.86; more negative N2 amplitudes were larger) compared to TDC (*M* rank = 50.45), $N = 79$, $z = -4.54$, $p < .001$, $r = -.51$. The P3 amplitude was significantly reduced in FXS (*M* rank = 33.26) compared to TDC (*M* rank = 45.36), $N = 79$, $z = -2.33$, $p = .020$, $r = -.26$. The P2 amplitude was

comparable between FXS (*M* rank = 42.91) and TDC (*M* rank = 37.68), $N = 79$, $z = 1.01$, $p = .314$, $r = .11$.

Tests evaluating ERP component latencies for all correct feedback identified significant group differences for both P2 and P3 latencies. The P2 latency was significantly faster/reduced for FXS (*M* rank = 29.87) compared to TDC (*M* rank = 48.06), $N = 79$, $z = -3.50$, $p < .001$, $r = -.39$. The P3 latency was significantly slower/increased for FXS (*M* rank = 48.56) compared to TDC (*M* rank = 33.19), $N = 79$, $z = 2.96$, $p = .003$, $r = .33$. Trial length was a significant covariate for P2 latency but including the covariate did not dramatically alter the results and the group difference remained significant, $F(1, 77) = 6.08$, $p = .016$. Finally, the N2 latency was not significantly different between groups where N2 latencies were comparable between FXS (*M* rank = 44.71) and TDC (*M* rank = 36.25), $N = 79$, $z = 1.63$, $p = .103$, $r = .18$.

Microstate Analysis

Resting state EEG microstate analyses identified the 4MS solution as ideal determined on the solution that best minimizes the intra-cluster distance while maximizing the inter-cluster distance calculated using the DB index. From rsEEG, the 4MS solution had the lowest DB index. The DB indices for the RLEEG microstate solutions were also evaluated to determine whether this result holds for active tasks. The 4MS solution across all data types had the lowest DB index value and prioritized for analysis to reduce the number of comparisons (Figure 60).

Figure 60.

Davies-Bouldin Indices across RLEEG Data Types for All Microstate Solutions Tested on rsEEG for FXS

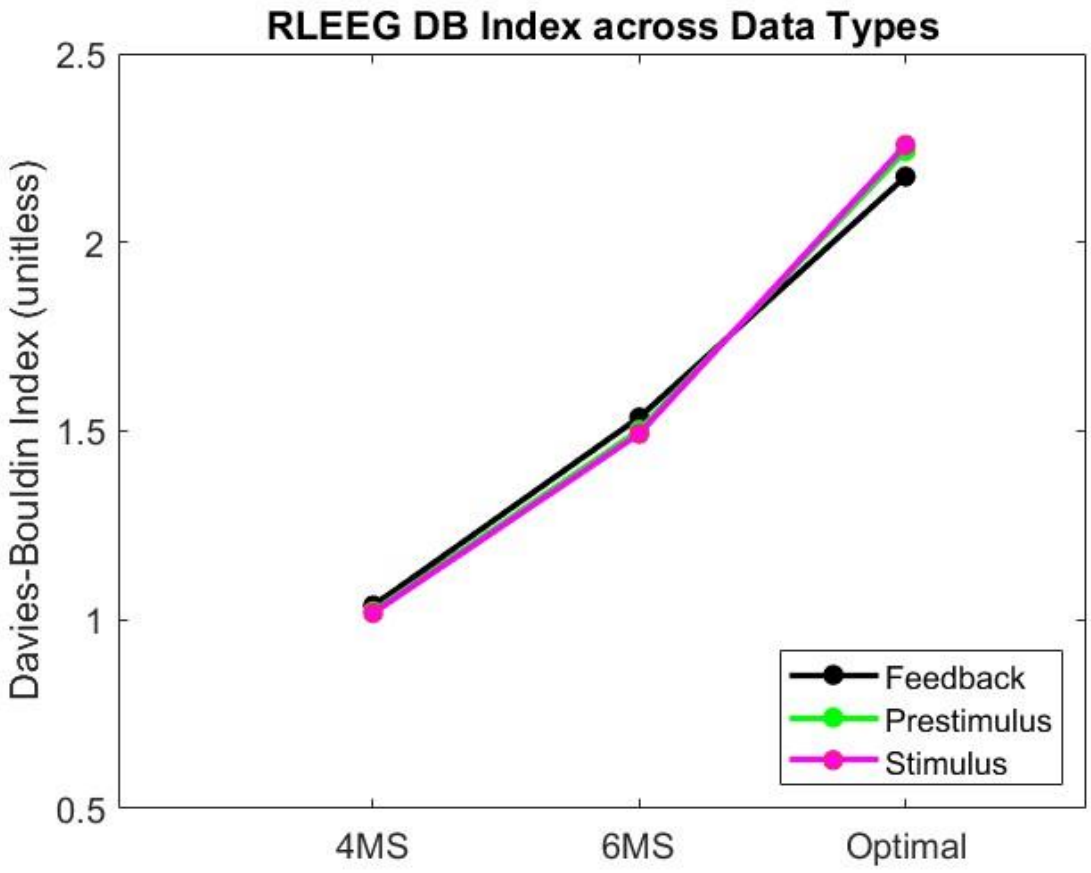

Note. Both the stimulus window and pre-stimulus period had higher DB for the "optimal" solution identified using the built-in +microstate toolbox kneedle algorithm. The DB index appears to increase with increasing K values because the optimal solution was k = 11 for both stimulus and pre-stimulus windows where k = 10 was optimal for feedback data.

Feedback Microstates (4MS)

Independent samples Mann-Whitney U tests evaluated group differences on microstate variables from the 4MS solution on feedback data due to data violating assumptions of normality. Specifically, variables analyzed included: average GFP, GFP peaks per second, GEV, mean duration, microstate complexity, and Hurst (Figure 61).

Average GFP was significantly different between groups with FXS exhibiting higher GFP (*M* rank = 49.66) compared to TDC (*M* rank = 32.32), $N = 79$, $z = 3.34$, $p < .001$, $r = .38$. There was also a significant group difference for GEV where FXS had significantly higher GEV (*M* rank = 45.86) compared to TDC (*M* rank = 35.34), $N = 79$, $z = 2.02$, $p = .043$, $r = .23$. Both increased GFP and GEV generally followed patterns noted in microstate analysis from Chapter two. Novelly, Hurst was significantly different between groups where FXS had higher Hurst (*M* rank = 46.97) compared to TDC (*M* rank = 34.45), $N = 79$, $z = 2.41$, $p = .016$, $r = .27$. There were no significant group differences for microstate mean duration ($N = 79$, $z = .71$, $p = .477$, $r = .08$), complexity ($N = 79$, $z = -1.23$, $p = .217$, $r = -.14$), and GFP peaks per second ($N = 79$, $z = .64$, $p = .521$, $r = .07$) where all three measures were comparable between FXS (Mean duration: *M* rank = 42.06; complexity: *M* rank = 36.43; GFP peaks per second: *M* rank = 41.86) and TDC (Mean duration: *M* rank = 38.36; complexity: *M* rank = 42.84; GFP peaks per second: *M* rank = 38.52).

Next, non-parametric tests were used to evaluate differences between microstates within each group individual microstate for microstate duration, coverage, occurrence, GFP, and GEV for feedback-associated data. Friedman tests were computed to evaluate within subject differences followed by Wilcoxon signed rank tests for significant cases as a post-hoc test evaluating pairwise comparisons corrected for multiple comparisons using a Bonferroni correction.

For duration, individual microstate variables did not significantly differ in duration for TDC but did trend towards significance ($\chi^2(3) = 6.63$, $p = .085$, $W = .05$). Individual microstate duration was also not significantly different for FXS, $\chi^2(3) = 4.85$, $p = .183$, $W = .05$. For individual microstate coverage, individual microstate coverage was different for TDC ($\chi^2(3) = 7.88$, $p = .049$, $W = .06$) but not FXS ($\chi^2(3) = 5.23$, $p = .156$, $W = .05$). The pairwise comparisons were not statistically significant after correction for multiple comparisons (MS2-MS1: $z = -2.33$, $p = .120$; MS3-MS1: $z = -1.70$, $p = .528$; MS4-MS1: $z = -.22$, $p = 1.00$; MS3-MS2: $z = -.09$, $p = 1.00$; MS4-MS2: $z = -1.53$, $p = .756$; MS4 – MS3: $z = -.74$, $p = 1.00$). The occurrence of individual microstates was not different for TDC ($\chi^2(3) = 7.17$, $p = .067$, $W = .05$) or FXS ($\chi^2(3) = 6.34$, $p = .096$, $W = .06$), though both trended towards significance. Finally, both individual microstate GFP and GEV were not significantly different across individual microstates for either TDC (GFP: $\chi^2(3) = .41$, $p = .938$, $W = .00$; GEV: GFP: $\chi^2(3) = .68$, $p = .877$, $W = .01$) or FXS (GFP: $\chi^2(3) = .70$, $p = .873$, $W = .01$; GEV: $\chi^2(3) = 2.35$, $p = .503$, $W = .02$).

Finally, Mann-Whitney U tests evaluated group differences to determine whether individual microstate variables were different between groups which were corrected for multiple comparisons using a Bonferroni correction by variable type.

The only variable type that had significant group differences was GFP where all four individual microstate classes were significantly different between groups. Individual microstate class GFP increased in FXS compared to TDC. All other variable types were not different between groups across individual microstate classes (Table 12).

Table 12.

Feedback-Related Microstate Solution Mann-Whitney U Test Results for Individual

	Mann-Whitney U Test Results				
Microstate Classes	FXS *M* Rank	TDC *M* Rank	Standardized Test Statistic (*z*)	p-value	Effect Size (*r*)
Duration					
MS1	38.09	41.52	-.66	1.00	-.07
MS2	44.77	36.20	1.65	.396	.19
MS3	44.09	36.75	1.41	.632	.16
MS4	38.46	41.23	-.53	1.00	-.06
Coverage					
MS1	38.71	41.02	-.44	1.00	-.05
MS2	38.51	41.18	-.51	1.00	-.06
MS3	45.29	35.80	1.83	.272	.21
MS4	36.69	42.64	-1.15	1.00	-.13
Occurrence					
MS1	38.34	41.32	-.57	1.00	-.06
MS2	36.51	42.77	-1.20	.916	-.14
MS3	42.26	38.20	.78	1.00	.09
MS4	38.83	40.93	-.41	1.00	-.05
GEV					
MS1	39.54	40.36	-.16	1.00	-.02
MS2	41.91	38.48	.66	1.00	.07
MS3	44.86	36.14	1.68	.372	.19
MS4	39.20	40.64	-.28	1.00	-.03
GFP					
MS1	49.09	32.77	3.14	.008	.35
MS2	49.26	32.64	3.20	.004	.36
MS3	49.23	32.66	3.19	.004	.36
MS4	49.17	32.70	3.17	.008	.36

Note. Group differences on individual microstate classes across various microstate variables.

Figure 61.

Feedback 4MS Solution

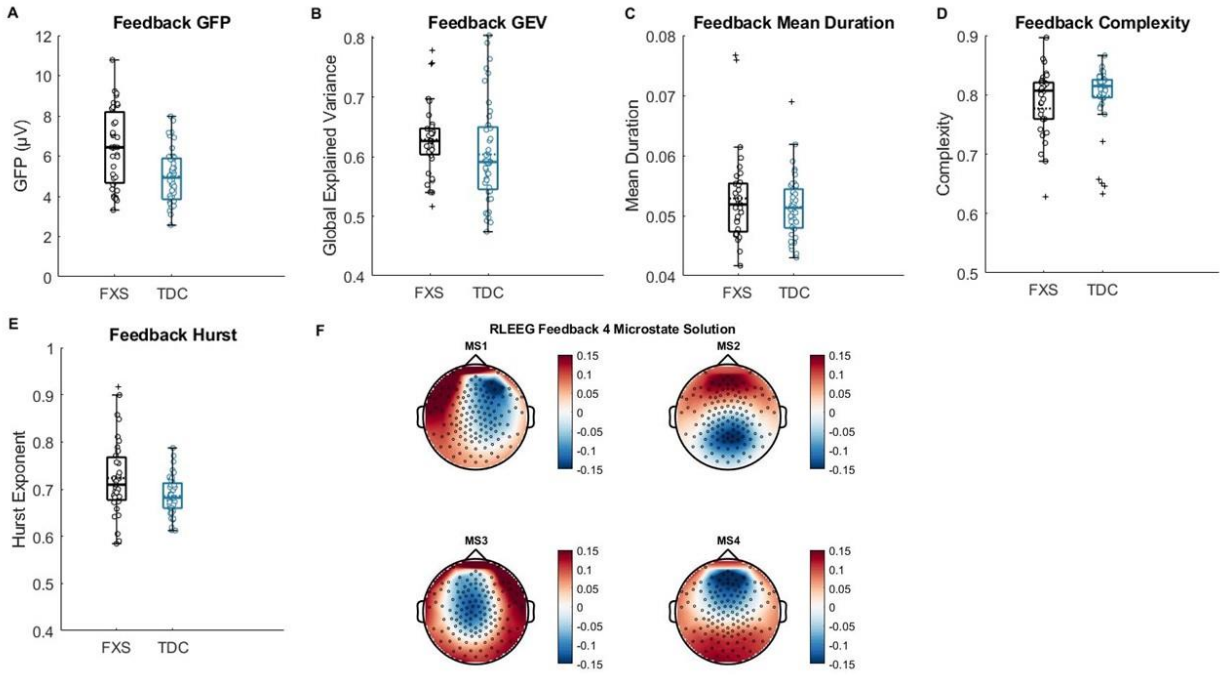

Note. Feedback-related microstate solution including boxplots for: **A)** feedback GFP, **B)** feedback GEV, **C)** feedback mean duration, **D)** feedback complexity, and **E)** feedback Hurst Exponent. **F)** the 4MS microstate solution maps where MS2 most likely represents microstate C, MS1 most likely represents microstate A, and both MS3 and MS4 do not represent canonical microstate maps.

Stimulus Period Microstates (4MS)

Independent samples Mann-Whitney U tests evaluated group differences on microstate variables from the 4MS solution on stimulus window data (i.e., box presentation and selection, including responses), as stimulus data also violated assumptions of normality. Again, average GFP, GFP peaks per second, GEV, mean duration, microstate complexity, and Hurst were evaluated (Figure 62).

Average GFP was significantly different between groups with FXS exhibiting higher GFP (*M* rank = 48.86) compared to TDC (*M* rank = 32.95), $N = 79$, $z = 3.06$, $p = .002$, $r = .34$. Interesting, complexity was significantly different between groups with FXS exhibiting reduced

complexity (*M* rank = 32.09) compared to TDC (*M* rank = 46.30), $N = 79$, $z = -2.73$, $p = .006$, $r = -.31$. Unlike the feedback microstate results, GEV was not significantly different between groups but did trend towards significance where FXS had marginally higher GEV (*M* rank = 44.86) compared to TDC (*M* rank = 36.14), $N = 79$, $z = 1.68$, $p = .093$, $r = .19$. Hurst values also trended towards a significant difference where FXS exhibited marginally increased Hurst (*M* rank = 45.11) compared to TDC (*M* rank = 35.93), $N = 79$, $z = 1.77$, $p = .077$, $r = .20$. Similarly to the feedback microstate results, there were no significant group differences for microstate mean duration ($N = 79$, $z = .67$, $p = .502$, $r = .08$) and GFP peaks per second ($N = 79$, $z = 1.31$, $p = .189$, $r = .15$) where both measures were comparable between FXS (Mean duration: *M* rank = 41.94; GFP peaks per second: *M* rank = 43.80) and TDC (Mean duration: *M* rank = 38.45; GFP peaks per second: *M* rank = 36.98).

Next, non-parametric tests were used to evaluate differences between microstates within each group individual microstate for microstate duration, coverage, occurrence, GFP, and GEV for stimulus-related data. Friedman tests were computed to evaluate within subject differences followed by Wilcoxon signed rank tests for significant cases as a post-hoc test evaluating pairwise comparisons corrected for multiple comparisons using a Bonferroni correction.

Individual microstate duration and coverage were not significantly different for either TDC (Duration: $\chi^2(3) = 3.60$, $p = .308$, $W = .03$; Coverage: $\chi^2(3) = 4.99$, $p = .172$, $W = .04$) or FXS (Duration: $\chi^2(3) = .87$, $p = .832$, $W = .01$, Coverage: $\chi^2(3) = 3.24$, $p = .356$, $W = .03$). Individual microstate occurrence was significantly different for TDC ($\chi^2(3) = 8.13$, $p = .043$, $W = .06$) but the pairwise comparisons were not statistically significant after correction for multiple comparisons (MS2-MS1: $z = -1.82$, $p = .414$; MS3-MS1: $z = -2.29$, $p = .132$; MS4-MS1: $z = -.76$, $p = .210$; MS3-MS2: $z = -.30$, $p = 1.00$; MS4-MS2: $z = -.27$, $p = 1.00$; MS4 – MS3: $z = -.74$, $p =$

1.00). Individual microstate occurrence was not significantly different for FXS ($\chi^2(3) = 3.86$, $p = .28$, $W = .04$). Finally, individual microstate class GEV and GFP were not different across classes for either TDC (GEV: $\chi^2(3) = 3.03$, $p = .387$, $W = .02$; GFP: $\chi^2(3) = .85$, $p = .839$, $W = .01$) or FXS (GEV: $\chi^2(3) = 1.73$, $p = .630$, $W = .02$; GFP: $\chi^2(3) = 5.13$, $p = .163$, $W = .05$).

Mann-Whitney U tests evaluated group differences to determine whether individual microstate variables were different between groups which were corrected for multiple comparisons using a Bonferroni correction by variable type.

Across all variable types, individual microstate GFP was significantly different between groups for all microstate classes where all microstate classes had higher GFP for FXS relative to TDC. All other variable types were not different between groups across individual microstate classes (Table 13).

Table 13.

Stimulus-Related Microstate Solution Mann-Whitney U Test Results for Individual Microstate Classes

	Mann-Whitney U Test Results				
	FXS *M* Rank	TDC *M* Rank	Standardized Test Statistic (*z*)	p-value	Effect Size (*r*)
Duration					
MS1	37.91	41.66	-.72	1.00	-0.08
MS2	41.06	39.16	.37	1.00	0.04
MS3	40.46	39.64	.16	1.00	0.02
MS4	43.26	37.41	1.13	1.00	0.13
Coverage					
MS1	37.51	41.98	-.86	1.00	-0.1
MS2	42.74	37.82	.95	1.00	0.11
MS3	37.00	42.39	-1.04	1.00	-0.12
MS4	44.94	36.07	1.71	.352	0.19
Occurrence					
MS1	36.43	42.84	-1.23	.868	-0.14
MS2	41.37	38.91	.47	1.00	0.05
MS3	36.46	42.82	-1.22	.884	-0.14
MS4	44.86	36.14	1.68	.372	0.19
GEV					
MS1	36.09	43.11	-1.35	.704	-0.15
MS2	40.09	39.93	.98	1.00	0.11
MS3	39.11	40.70	-.31	1.00	-0.03
MS4	45.80	35.39	2.00	1.00	0.23
GFP					
MS1	48.51	33.23	2.94	.018	0.33
MS2	47.89	33.73	2.72	.024	0.31
MS3	49.54	33.41	3.30	.004	0.37
MS4	49.23	32.66	3.19	.004	0.36

Figure 62.

Stimulus 4MS Solution

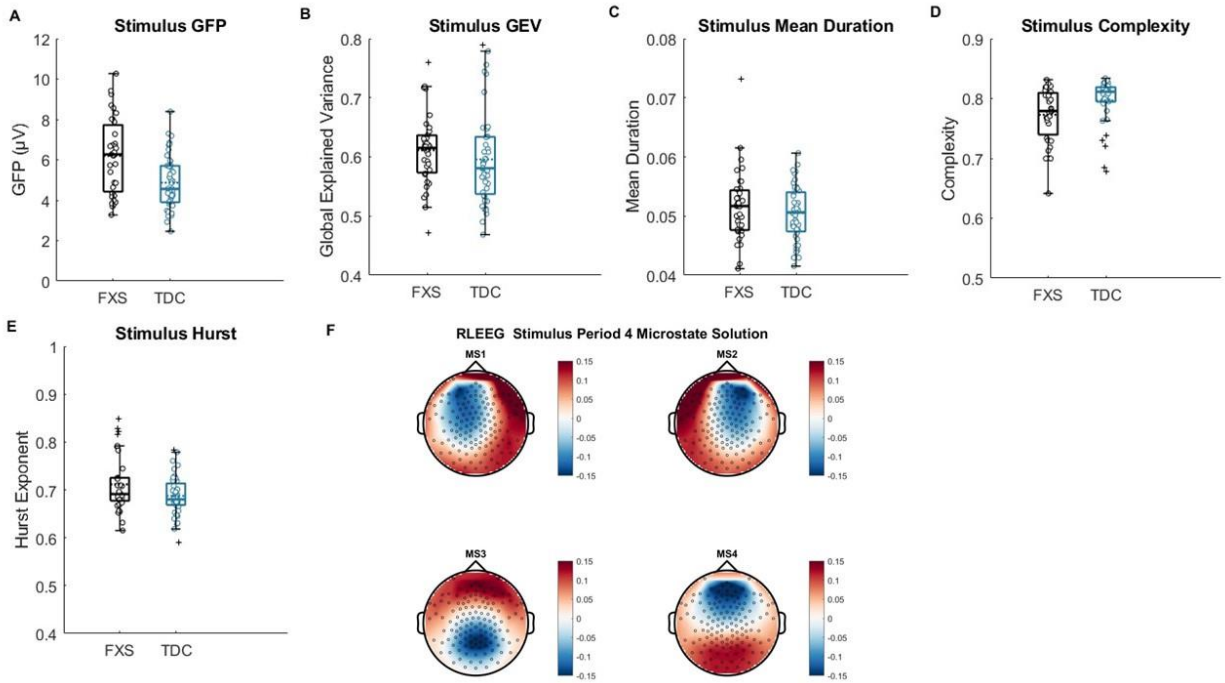

Note. Stimulus-related microstate solution including boxplots for: **A)** stimulus GFP, **B)** stimulus GEV, **C)** stimulus mean duration, **D)** stimulus complexity, and **E)** stimulus Hurst Exponent. **F)** the 4MS microstate solution maps where MS3 most likely represents microstate C, MS1 and MS2 most likely represents microstates B and A, respectively, and MS4 does not represent a canonical microstate map.

Pre-stimulus Microstates (4MS)

Lastly, Independent samples Mann-Whitney U tests evaluated group differences on microstate variables from the 4MS solution on pre-stimulus window data (i.e., no visual stimulation, blank screen), as pre-stimulus data violated assumptions of normality. Again, average GFP, GFP peaks per second, GEV, mean duration, microstate complexity, and Hurst were evaluated (Figure 63).

The only variable that was significantly different between groups was average GFP where FXS had significantly higher GFP (*M* rank = 48.69) than TDC (*M* rank = 33.09), $N = 79$, $z = 3.00$, $p = .003$, $r = .34$. Mean duration ($N = 79$, $z = 1.70$, $p = .090$, $r = .19$) and Hurst ($N = 79$, z

= 1.66, p = .097, r = .19) both trended towards significant group differences where for mean duration FXS exhibited marginally longer microstate durations on average (M rank = 44.91) compared to TDC (M rank = 36.09) and FXS had marginally higher Hurst values (M rank = 44.80) than TDC (M rank = 36.18).

GEV (N = 79, z = 1.14, p = .256, r = .13), GFP peaks per second (N = 79, z = 1.29, p = .196, r = .15), and complexity (N = 79, z = -1.46, p = .144, r = -.16) were not significantly different between groups where FXS (GEV: M rank = 43.29 ; GFP peaks per second: M rank = 43.74; Complexity: M rank = 35.77) and TDC (GEV: M rank = 37.39; GFP peaks per second: M rank = 37.02; Complexity: M rank = 43.36) were comparable on all three variables.

Pairwise comparisons were evaluated (Table 14). Individual microstate duration was significantly different for both TDC ($\chi^2(3) = 7.99$, p = .046, W = .06) and FXS ($\chi^2(3) = 9.55$, p = .023, W = .09) but pairwise comparisons for both groups did not survive Bonferroni correction. Individual microstate coverage was significantly different for TDC ($\chi^2(3) = 11.86$, p = .008, W = .09) but not FXS ($\chi^2(3) = 6.77$, p = .080, W = .06) which only trended towards significance. The only comparison that survived the Bonferroni correction was between MS1 and MS4. MS1 had significantly higher coverage (Med = .27, IQR = .06) compared to MS4 (Med = .24, IQR = .07) where MS1 had the highest coverage and MS4 had the lowest coverage. Individual microstate occurrence was significantly different for TDC ($\chi^2(3) = 10.50$, p = .015, W = .08) but not FXS ($\chi^2(3) = 4.00$, p = .262, W = .04). None of the pairwise comparisons for TDC individual microstate coverage survived Bonferroni correction. Individual microstate GEV was not significantly different for TDC ($\chi^2(3) = 7.31$, p = .063, W = .06) but trended towards significance and GEV was significantly different for FXS ($\chi^2(3) = 10.85$, p = .013, W = .10). For FXS individual microstate GEV, the only comparison that survived Bonferroni correction was

between MS1 and MS3 where MS1 had higher GEV than MS3, which had the lowest GEV value. Lastly, individual microstate GFP was not significantly different for TDC ($\chi^2(3) = 3.60$, $p = .308$, $W = .03$) or FXS ($\chi^2(3) = 6.36$, $p = .095$, $W = .06$).

Table 14.

Pre-Stimulus Microstate Solution Non-Parametric Individual Microstate Pairwise Comparisons

	Wilcoxon Signed Ranks Test Results	
TDC Duration	*z*	p-value
MS2-MS1	-2.39	.102
MS3-MS1	-2.22	.162
MS4-MS1	-2.54	.066
MS3-MS2	-.07	1.00
MS4-MS2	-.36	1.00
MS4-MS3	-.50	1.00
FXS Duration		
MS2-MS1	-1.61	.648
MS3-MS1	-2.56	.066
MS4-MS1	-2.10	.216
MS3-MS2	-1.72	.510
MS4-MS2	-.46	1.00
MS4-MS3	-.97	1.00
TDC Coverage		
MS2-MS1	-1.95	.306
MS3-MS1	-2.37	.108
MS4-MS1	-3.00	.018
MS3-MS2	-.56	1.00
MS4-MS2	-1.27	1.00
MS4-MS3	-.75	1.00
TDC Occurrence		
MS2-MS1	-1.32	1.00
MS3-MS1	-2.25	.144
MS4-MS1	-2.52	.072
MS3-MS2	-.82	1.00
MS4-MS2	-1.60	.660
MS4-MS3	-.67	1.00
FXS GEV		
MS2-MS1	-1.93	.318
MS3-MS1	-2.78	.030
MS4-MS1	-2.00	.276
MS3-MS2	-1.69	.552
MS4-MS2	-.51	1.00
MS4-MS3	-.92	1.00

Finally, Mann-Whitney U tests evaluated group differences to determine whether individual microstate variables were different between groups which were corrected for multiple comparisons using a Bonferroni correction by variable type.

Individual microstate class GFP were the only variables that were significantly different between groups where all four individual microstate classes had increased GFP for FXS relative to TDC. All other variable types were not different between groups across individual microstate classes (Table 15).

Table 15.

Pre-Stimulus Microstate Solution Mann-Whitney U Test Results for Individual Microstate Classes

	Mann-Whitney U Test Results				
	FXS *M* Rank	TDC *M* Rank	Standardized Test Statistic (*z*)	p-value	Effect Size (*r*)
Duration					
MS1	42.49	38.02	.86	1.00	.10
MS2	44.89	36.11	1.69	.364	019
MS3	40.60	39.52	.21	1.00	.02
MS4	43.31	37.36	1.15	1.00	.13
Coverage					
MS1	40.60	39.52	.21	1.00	.02
MS2	39.49	40.41	-.18	1.00	-.02
MS3	36.66	42.66	-1.16	.992	-.13
MS4	43.11	37.52	1.08	1.00	.12
Occurrence					
MS1	37.66	41.86	-.81	1.00	-.09
MS2	36.06	43.14	-1.36	.692	-.15
MS3	35.89	43.27	-1.42	.62	-.16
MS4	41.00	39.20	.35	1.00	.04
GEV					
MS1	43.03	37.59	1.05	1.00	.12
MS2	41.57	38.75	.54	1.00	.06
MS3	37.17	32.25	.33	1.00	.04
MS4	41.89	38.50	.65	1.00	.07
GFP					
MS1	48.94	32.89	3.09	.008	.35
MS2	48.94	32.89	3.09	.008	.35
MS3	48.00	33.64	2.76	.024	.31
MS4	47.31	34.18	2.53	.048	.28

Figure 63.

Pre-stimulus 4MS Solution

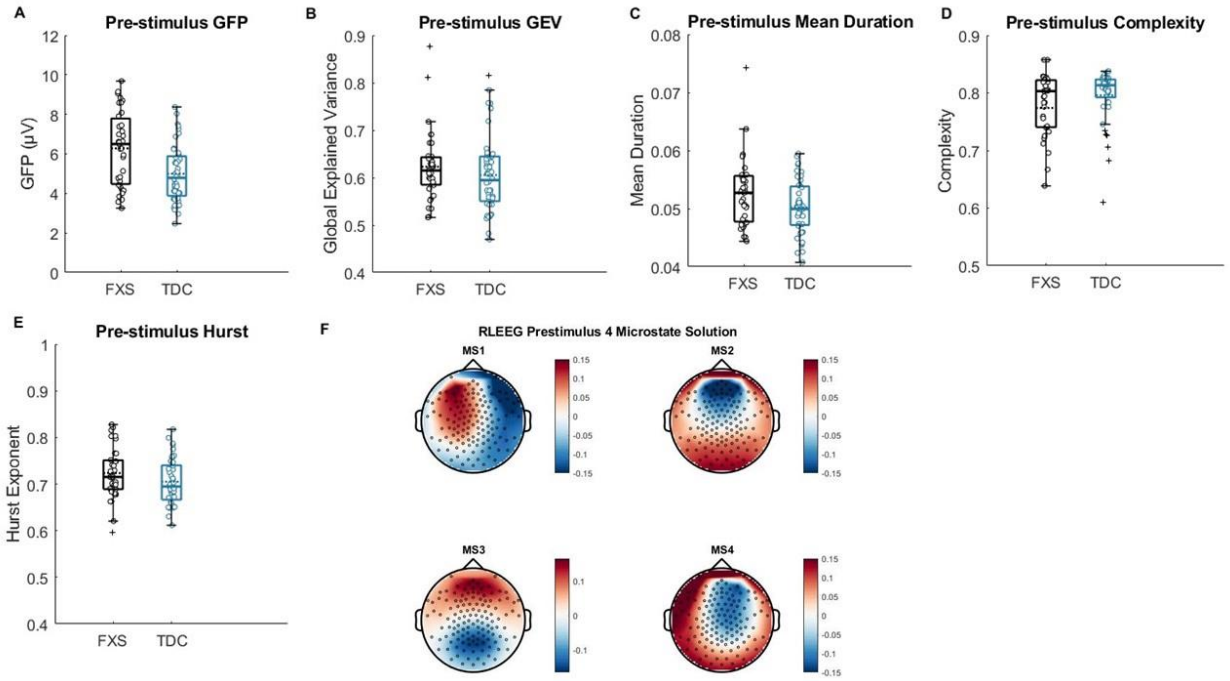

Note. Pre-stimulus-related microstate solution including boxplots for: **A)** pre-stimulus GFP, **B)** stimulus GEV, **C)** pre-stimulus mean duration, **D)** pre-stimulus complexity, and **E)** pre-stimulus Hurst Exponent. **F)** the 4MS microstate solution maps where MS3 most likely represents microstate C, MS1 most likely represents microstates B, and both MS2 and MS4 do not represent canonical microstate maps.

Functional Connectivity Analysis – Whole Network Connectivity

Feedback Functional Connectivity

Non-parametric Mann-Whitney U tests evaluated FC across all feedback periods in the delta, theta, alpha1, and alpha 2 frequency bands for the within network connectivity in DMN, SN, and control network.

For the DMN, theta FC during feedback was significantly different between groups where individuals with FXS exhibited elevated theta connectivity (*M* rank = 49.51) relative to TDC (*M* rank = 32.43), *N* = 79, z = 3.29, *p* = .001, *r* = .37 (Figure 64 & 65). Alpha 2 FC during feedback was also significantly different between groups with FXS exhibiting reduced alpha 2

FC (*M* rank = 33.06) compared to TDC (*M* rank = 45.52), *N* = 79, *z* = -2.40, *p* = .016, *r* = -.27 (Figure 66).

Both delta (*N* = 79, *z* = .15, *p* = .882, *r* = .02) and alpha 1 (*N* = 79, *z* = .23, *p* = .820, *r* = .03) FC within the DMN during feedback were comparable between FXS (delta: *M* rank = 40.43; alpha 1: *M* rank = 40.66) and TDC (delta: *M* rank = 39.66; alpha 1: *M* rank = 39.48).

Figure 64.

Box and Violine Plots Depicting Default Mode Functional Connectivity across Feedback-Related Data for the Different Frequency Bands

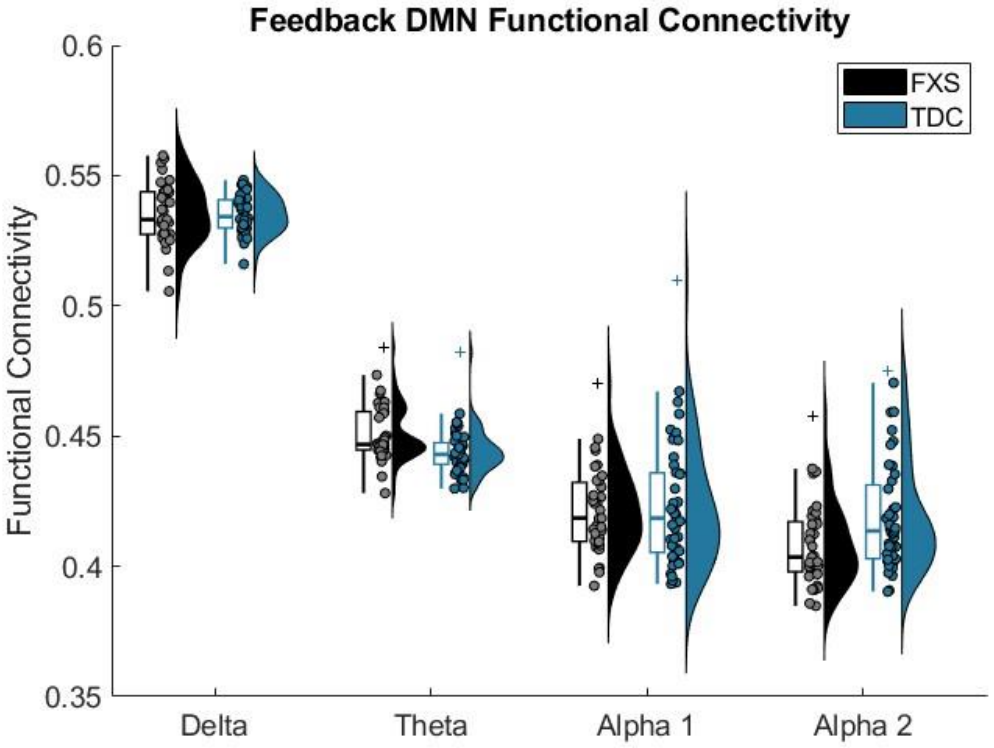

Note. Feedback-related FC analysis. Violin and boxplots depicting group differences for DMN FC across frequency bands. Dots indicate individual data points and plus signs represent outliers.

Figure 65.

Feedback: Default Mode Network Theta Functional Connectivity Circle Plots

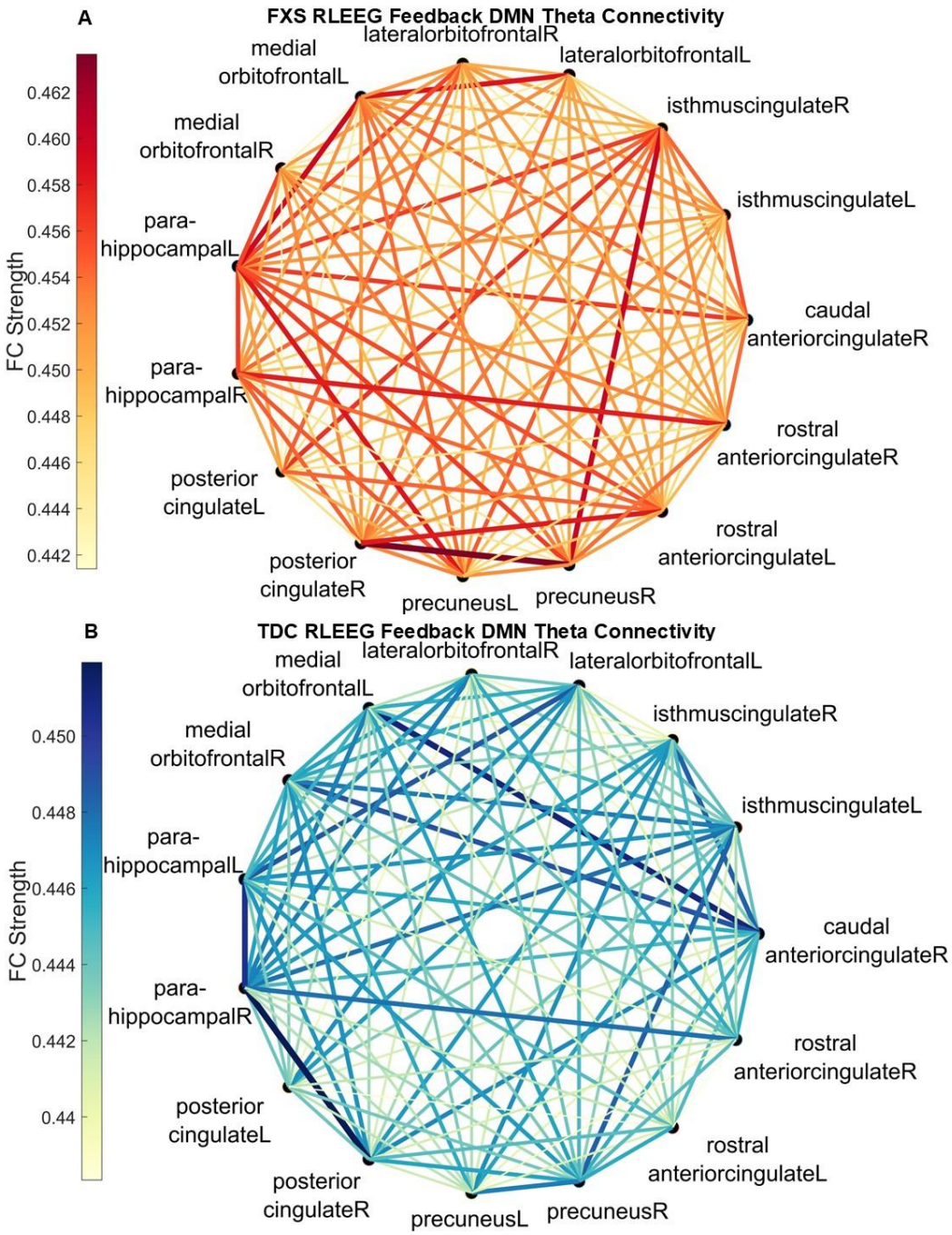

Note. Feedback data theta FC. Scales are different between groups. **A)** All individual connections within the DMN for FXS during feedback window. **B)** All individual connections within the DMN for TDC during feedback window. Colors indicate direction of group difference with warmer colors (yellow, orange, and red) indicating higher FC and cooler colors (blue, green, yellow) indicating lower FC where darker colors indicate higher FC values within each group.

Figure 66.

Feedback: Default Mode Network Alpha 2 Functional Connectivity Circle Plots

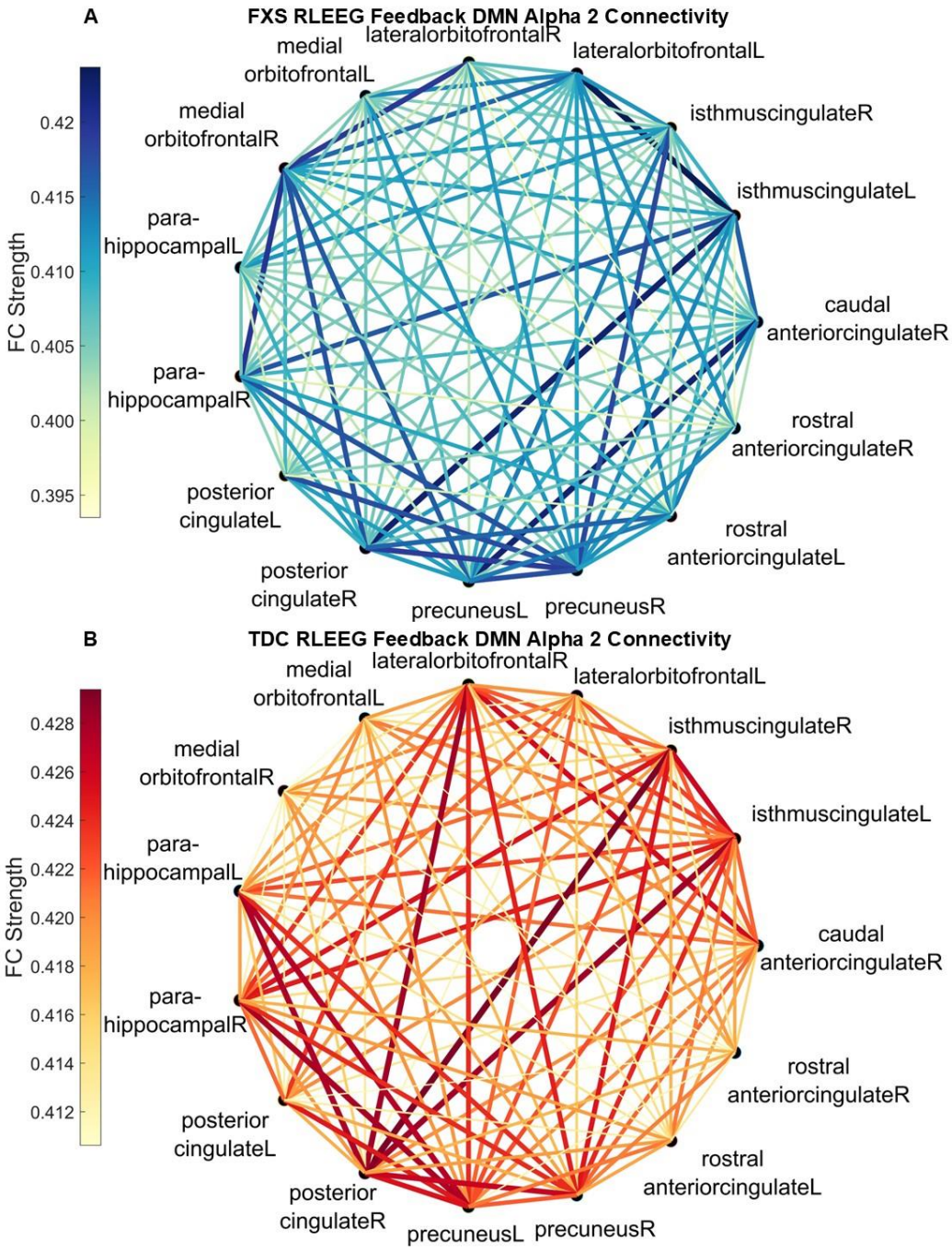

Note. Feedback data alpha 2 FC. Scales are different between groups. **A)** All individual connections within the DMN for FXS during feedback window. **B)** All individual connections within the DMN for TDC during feedback window. Colors indicate direction of group difference with warmer colors (yellow, orange, and red) indicating higher FC and cooler colors (blue, green, yellow) indicating lower FC where darker colors indicate higher FC values within each group.

For SN, theta FC during feedback was significantly different between groups where individuals with FXS exhibited elevated theta FC (*M* rank = 47.80) relative to TDC (*M* rank = 33.80), $N = 79$, $z = 2.69$, $p = .007$, $r = .30$ (Figure 67 & 68). Alpha 2 FC during feedback was also significantly different between groups where FXS exhibited reduced alpha 2 FC (*M* rank = 34.14) compared to TDC (*M* rank = 44.66), $N = 79$, $z = -2.02$, $p = .043$, $r = -.23$ (Figure 69).

Delta FC ($N = 79$, $z = -.34$, $p = .737$, $r = .$) and alpha 1 FC ($N = 79$, $z = .71$, $p = .477$, $r = .08$) were not significantly different between groups within SN during feedback where FXS (delta: *M* rank = 39.03; alpha 1: *M* rank = 42.06) was comparable to TDC (delta: *M* rank = 40.77; alpha 1: *M* rank = 38.36).

Figure 67.

Box and Violine Plots Depicting Salience Network Functional Connectivity across Feedback-Related Data for the Different Frequency Bands

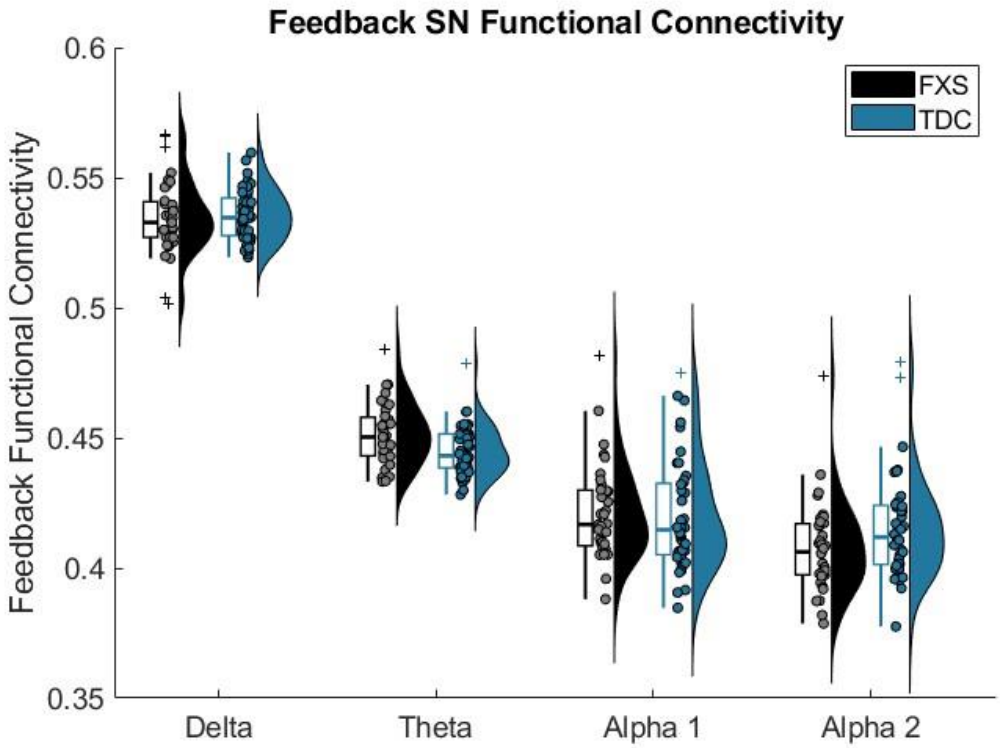

Note. Feedback-related FC analysis. Violin and boxplots depicting group differences for SN FC across frequency bands. Dots indicate individual data points and plus signs represent outliers.

Figure 68.

Feedback: Salience Network Theta Functional Connectivity Circle Plots

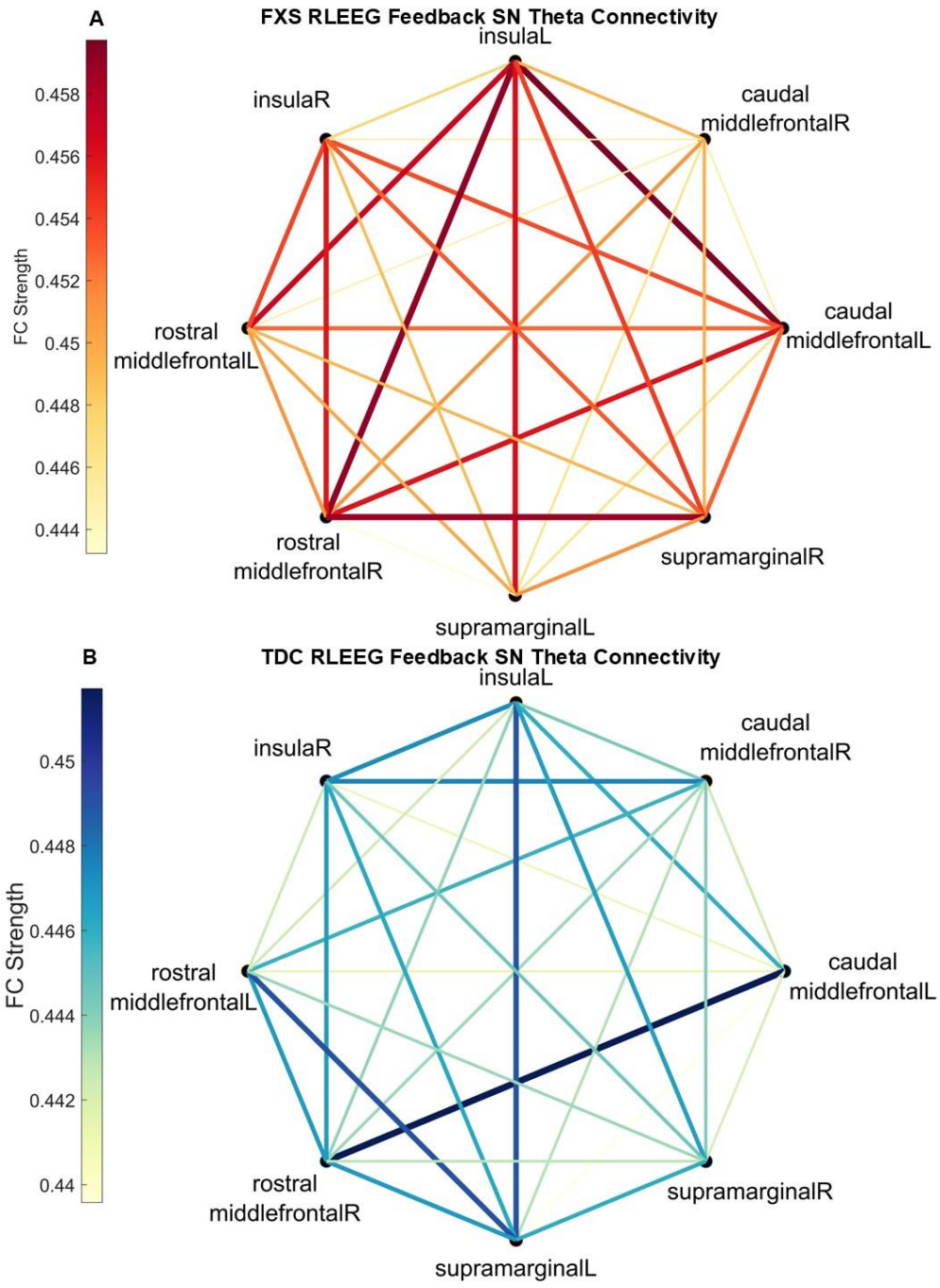

Note. Feedback data theta FC. Scales are different between groups. **A)** All individual connections within the SN for FXS during feedback window. **B)** All individual connections within the SN for TDC during feedback window. Colors indicate direction of group difference with warmer colors (yellow, orange, and red) indicating higher FC and cooler colors (blue, green, yellow) indicating lower FC where darker colors indicate higher FC values within each group.

Figure 69.

Feedback: Salience Network Alpha 2 Functional Connectivity Circle Plots

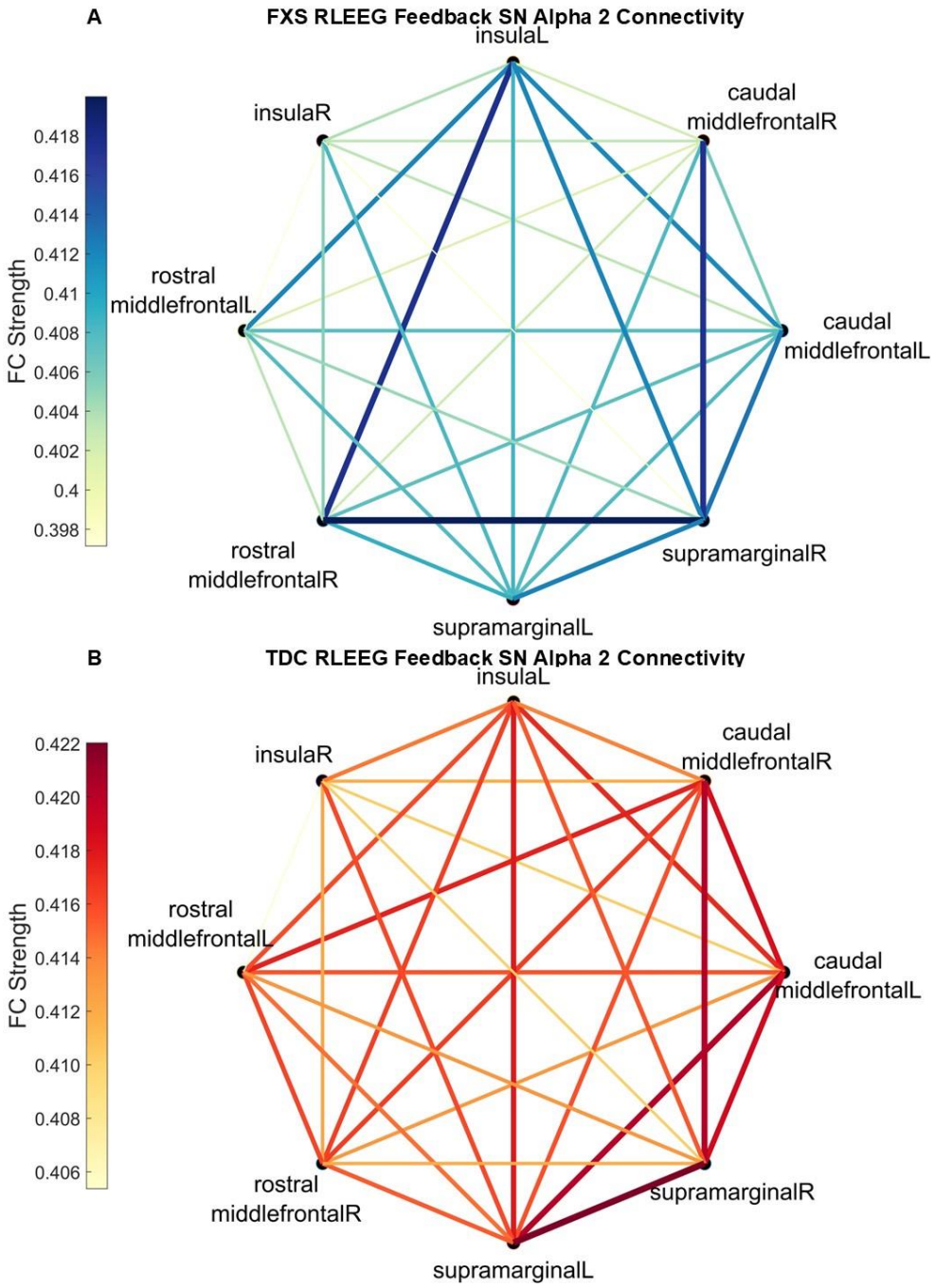

Note. Feedback data alpha 2 FC. Scales are different between groups. **A)** All individual connections within the SN for FXS during feedback window. **B)** All individual connections within the SN for TDC during feedback window. Colors indicate direction of group difference with warmer colors (yellow, orange, and red) indicating higher FC and cooler colors (blue, green, yellow) indicating lower FC where darker colors indicate higher FC values within each group.

Finally, for the control network during feedback theta FC was significantly different between groups where FXS exhibited elevated theta FC (*M* rank = 49.89) compared to TDC (*M* rank = 32.14), $N = 79$, $z = 3.42$, $p < .001$, $r = .38$ (Figure 70 & 71). However, unlike the DMN and SN, alpha 2 FC during feedback was not significantly different between groups where FXS (*M* rank = 35.46) was comparable to TDC (*M* rank = 43.61), $N = 79$, $z = -1.57$, $p = .117$, $r = -.12$ (Figure 72). Though, the FC group pattern followed the FC group patterns for DMN and SN.

Delta FC ($N = 79$, $z = -.34$, $p = .737$, $r = -.04$) and alpha 1 FC ($N = 79$, $z = .71$, $p = .477$, $r = .08$) were not significantly different between groups within the control network during feedback where FXS (delta: *M* rank = 39.03; alpha 1: *M* rank = 42.06) was comparable to TDC (delta: *M* rank = 40.77; alpha 1: *M* rank = 38.36) for both delta and alpha 1 FC. Interestingly, alpha 1 FC Mann-Whitney U results were identical between SN and control network for feedback related data.

Figure 70.

Box and Violine Plots Depicting Control Network Functional Connectivity across Feedback-Related Data for the Different Frequency Bands

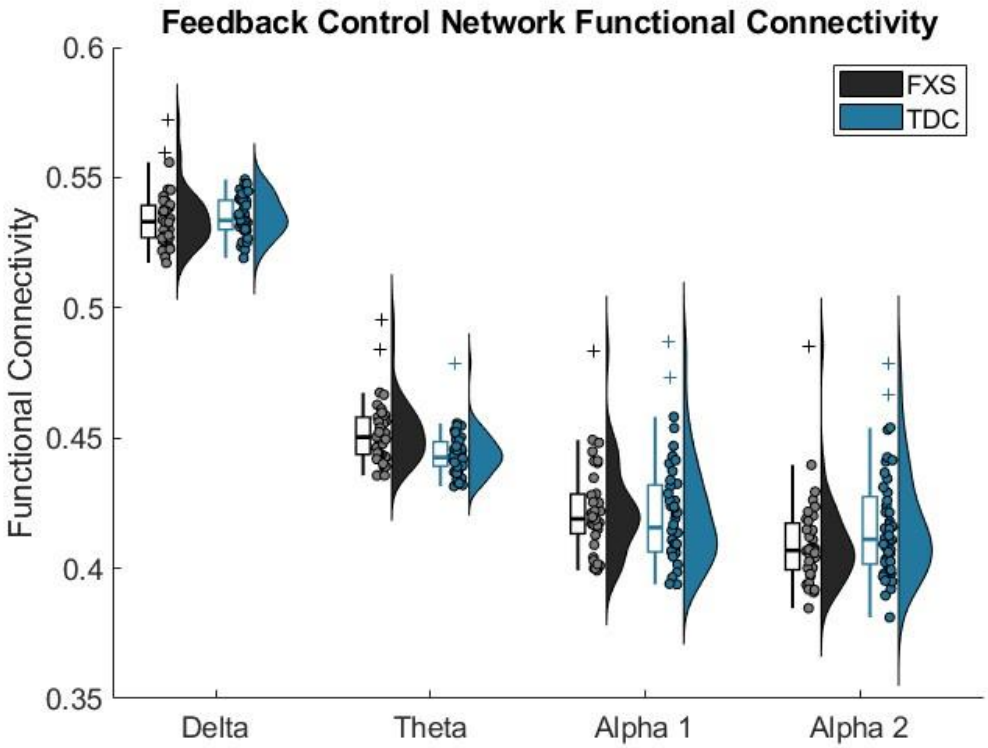

Note. Feedback-related FC analysis. Violin and boxplots depicting group differences for control network FC across frequency bands. Dots indicate individual data points and plus signs represent outliers.

Figure 71.

Feedback: Control Network Theta Functional Connectivity Circle Plots

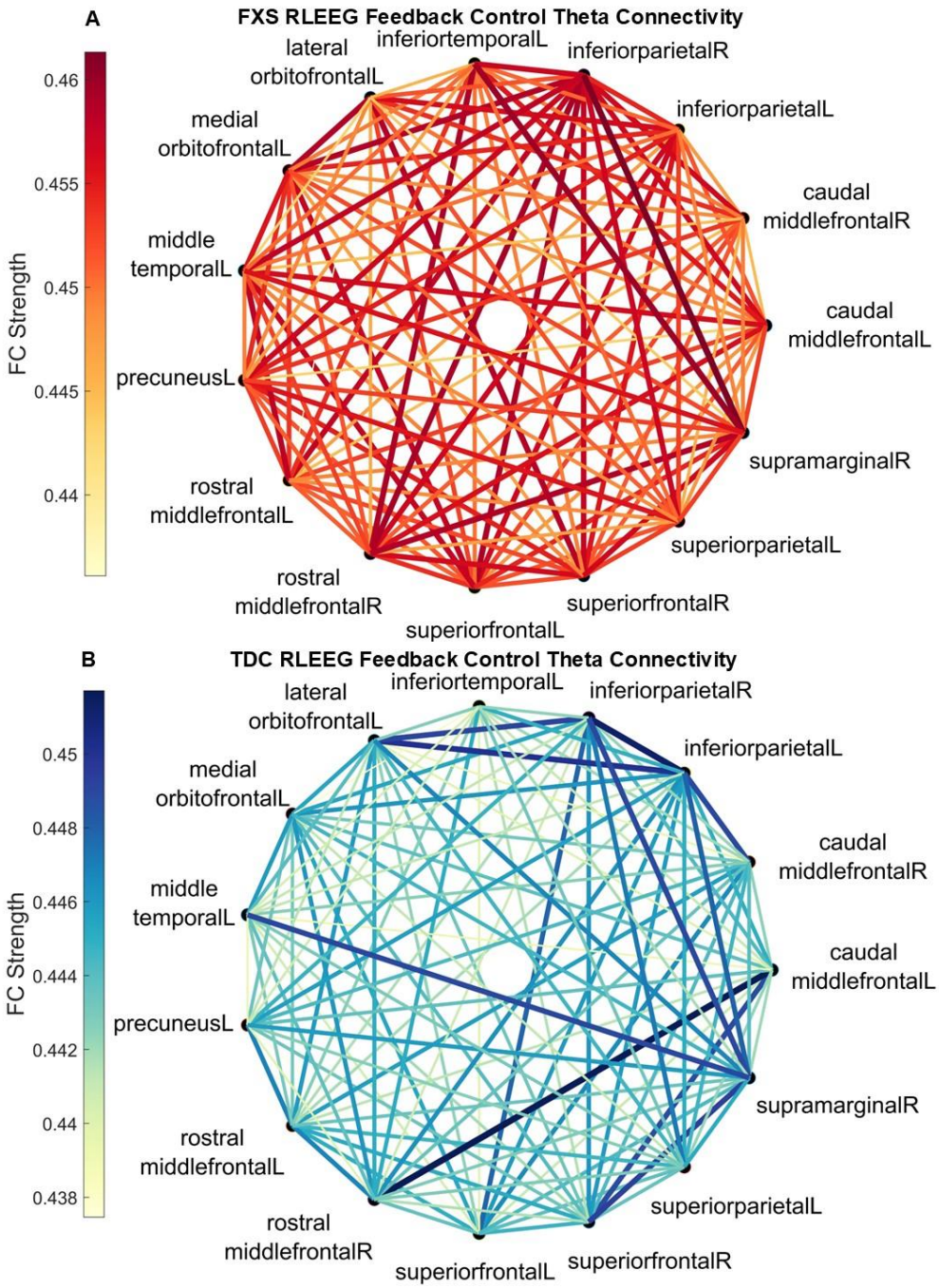

Note. Feedback data theta FC. Scales are different between groups. **A)** All individual connections within the control network for FXS during feedback window. **B)** All individual connections within the control network for TDC during feedback window. Colors indicate direction of group difference with warmer colors (yellow, orange, and red) indicating higher FC and cooler colors (blue, green, yellow) indicating lower FC where darker colors indicate higher FC values within each group.

Figure 72.

Feedback: Control Network Alpha 2 Functional Connectivity Circle Plots

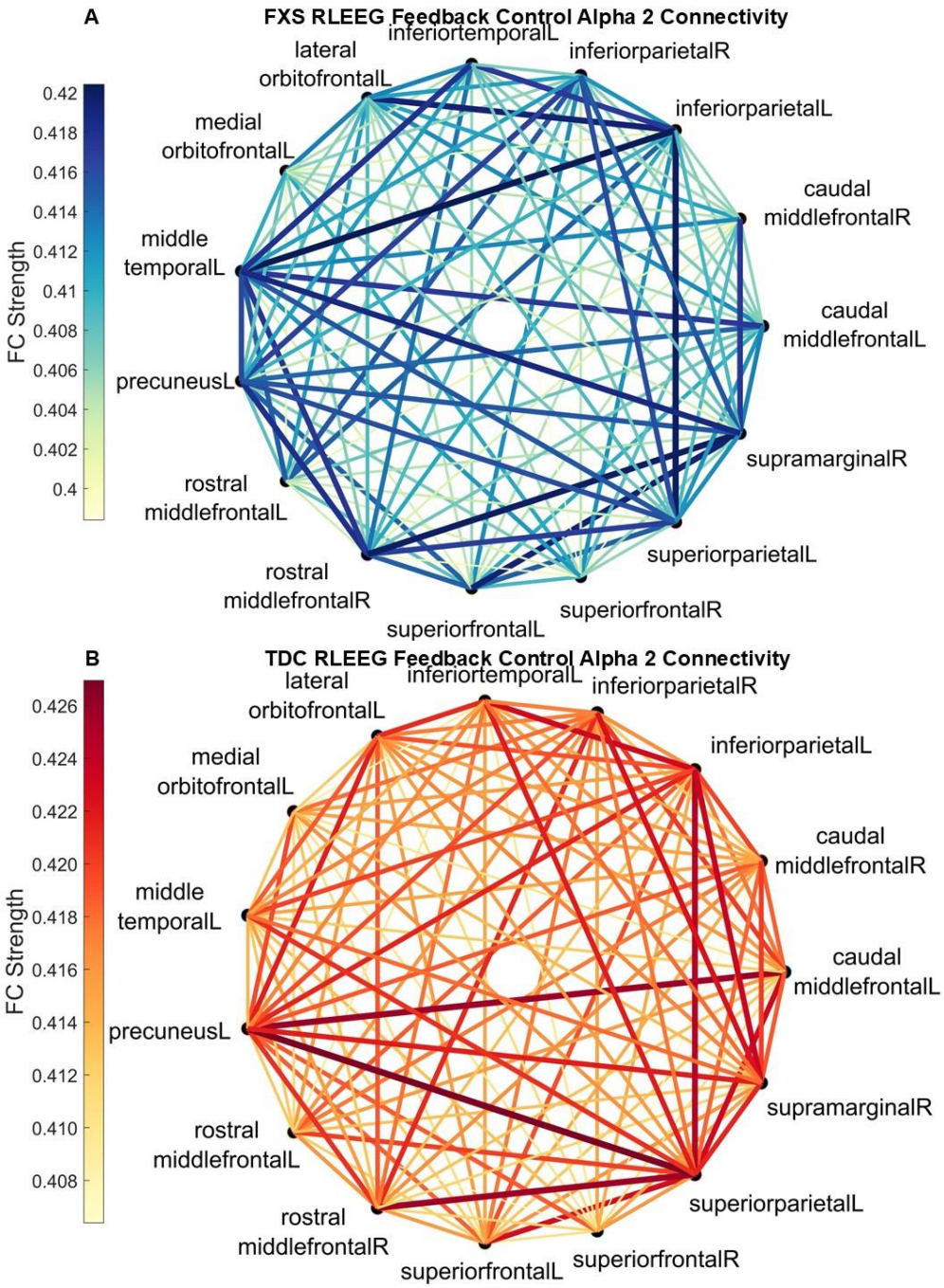

Note. Feedback data alpha 2 FC. Scales are different between groups. **A)** All individual connections within the control network for FXS during feedback window. **B)** All individual connections within the control network for TDC during feedback window. Colors indicate direction of group difference with warmer colors (yellow, orange, and red) indicating higher FC and cooler colors (blue, green, yellow) indicating lower FC where darker colors indicate higher FC values within each group.

Stimulus Period Functional Connectivity

Non-parametric Mann-Whitney U tests evaluated within network FC during stimulus-related data across all frequency bands: delta, theta, alpha1, and alpha 2.

For the DMN, theta FC during stimulus presentation was significantly different between groups where individuals with FXS exhibited elevated theta FC (*M* rank = 54.09) relative to TDC (*M* rank = 28.80), *N* = 79, z = 4.87, $p < .001$, *r* = .55 (Figure 73 & 74). Alpha 2 was also significantly different between groups with FXS exhibiting reduced alpha 2 FC (*M* rank = 32.60) compared to TDC (*M* rank = 45.89), *N* = 79, *z* = -2.56, *p* = .011, *r* = -.29 (Figure 75).

Both delta (*N* = 79, *z* = 1.62, *p* = .106, *r* = .18) and alpha 1 (*N* = 79, *z* = .47, *p* = .636, *r* = .05) FC within the DMN during stimulus presentation were comparable between FXS (delta: *M* rank = 44.69; alpha 1: *M* rank = 41.36) and TDC (delta: *M* rank = 36.27; alpha 1: *M* rank = 38.91).

Figure 73.

Box and Violine Plots Depicting DMN Functional Connectivity across Stimulus-Related Data for the Different Frequency Bands

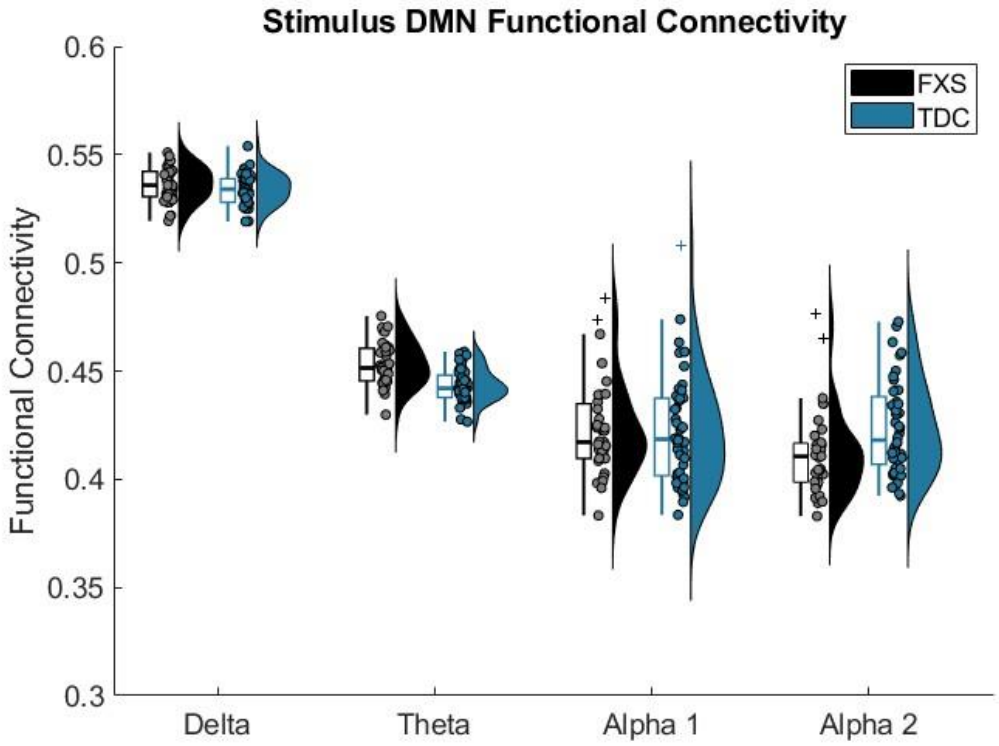

Note. Stimulus-related FC analysis. Violin and boxplots depicting group differences for DMN FC across frequency bands. Dots indicate individual data points and plus signs represent outliers.

Figure 74.

Stimulus Period: Default Mode Network Theta Functional Connectivity Circle Plots

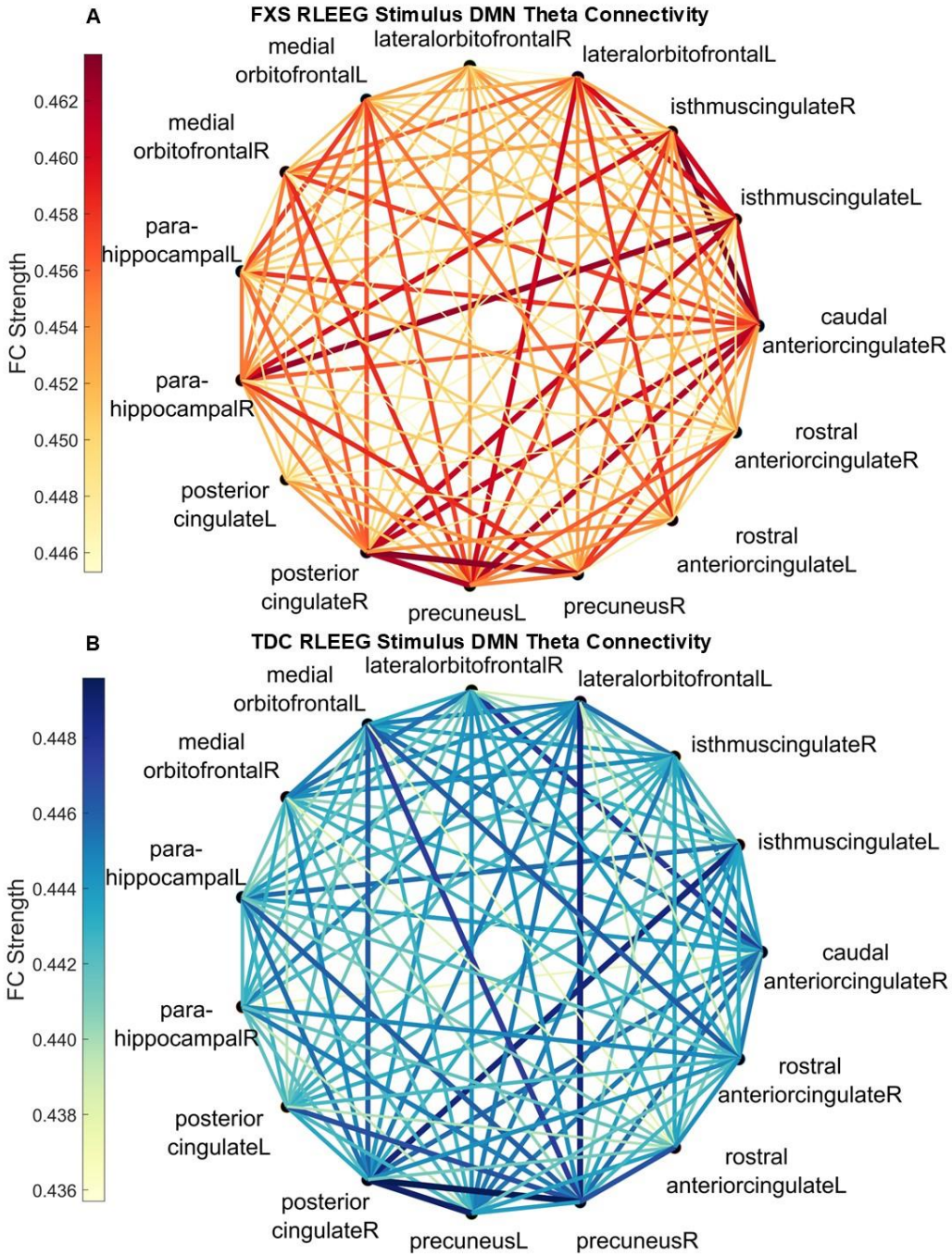

Note. Stimulus data theta FC. Scales are different between groups. **A)** All individual connections within the DMN for FXS during stimulus window. **B)** All individual connections within the DMN for TDC during stimulus window. Colors indicate direction of group difference with warmer colors (yellow, orange, and red) indicating higher FC and cooler colors (blue, green, yellow) indicating lower FC where darker colors indicate higher FC values within each group.

Figure 75.

Stimulus Period: Default Mode Network Alpha 2 Functional Connectivity Circle Plots

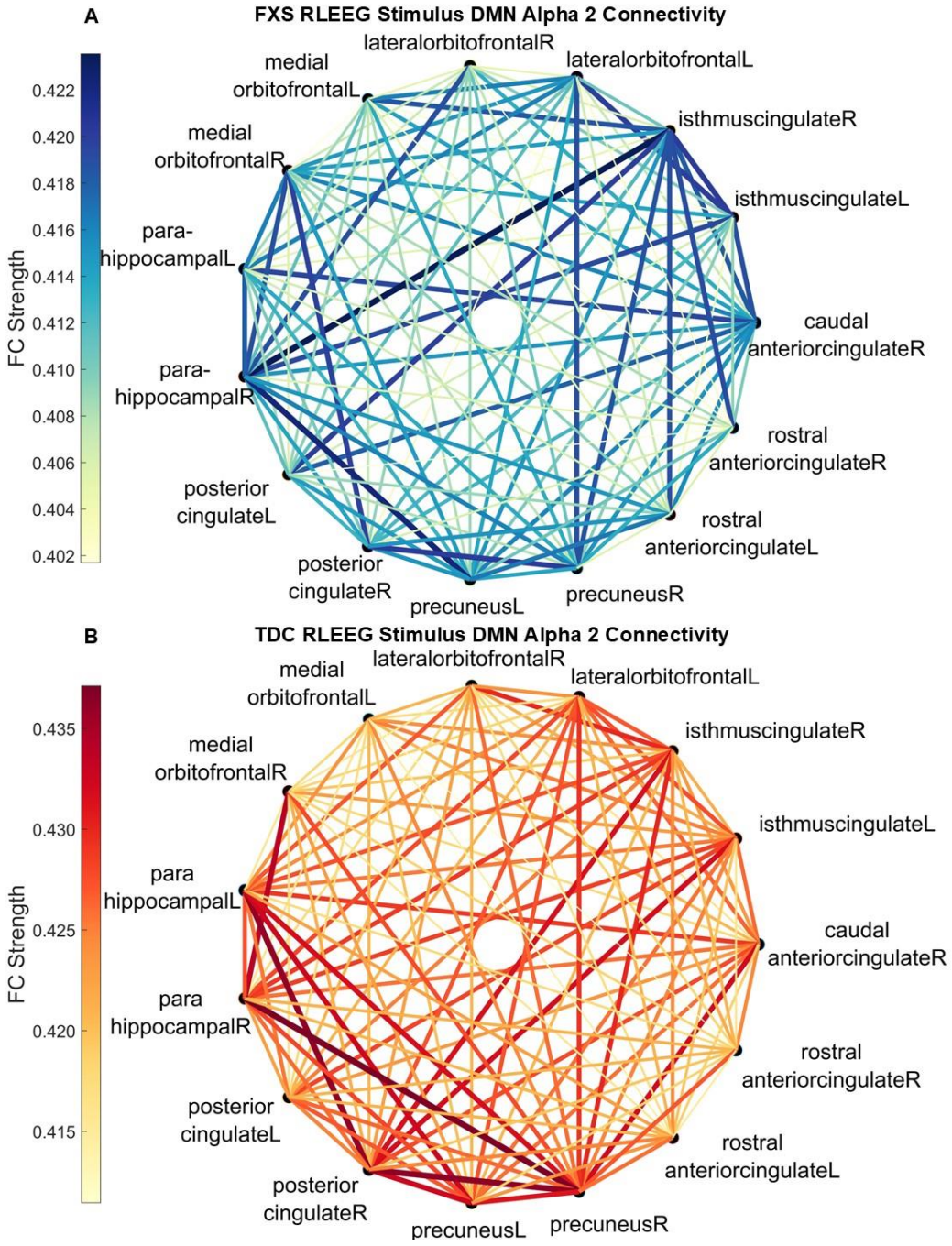

Note. Stimulus data alpha 2 FC. Scales are different between groups. **A)** All individual connections within the DMN for FXS during stimulus window. **B)** All individual connections within the DMN for TDC during stimulus window. Colors indicate direction of group difference with warmer colors (yellow, orange, and red) indicating higher FC and cooler colors (blue, green, yellow) indicating lower FC where darker colors indicate higher FC values within each group.

Within SN, theta FC during stimulus presentation was significantly different between groups with FXS exhibiting increased FC (*M* rank = 51.29) compared to TDC (*M* rank = 31.02), *N* = 79, z = 3.90, *p* < .001, *r* = .44 (Figure 76 & 77). Alpha 2 was also significantly different between groups with FXS exhibiting reduced alpha 2 FC (*M* rank = 33.29) compared to TDC (*M* rank = 45.34), *N* = 79, *z* = -2.32, *p* = .020, *r* = -.26 (Figure 78). While SN network delta FC was not significantly different between groups, delta FC during stimulus presentation did trend towards a significant difference where FC was marginally elevated in FXS (*M* rank = 45.23) compared to TDC (*M* rank = 35.84), *N* = 79, *z* = 1.81, *p* = .071, *r* = .20. Lastly, alpha 1 FC during stimulus presentation was not significantly different between groups where FXS (*M* rank = 42.51) and TDC (*M* rank = 38.00) exhibited comparable alpha 1 FC, *N* = 79, *z* = .87, *p* = .385, *r* = .10.

Figure 76.

Box and Violine Plots Depicting SN Functional Connectivity across Stimulus-Related Data for the Different Frequency Bands

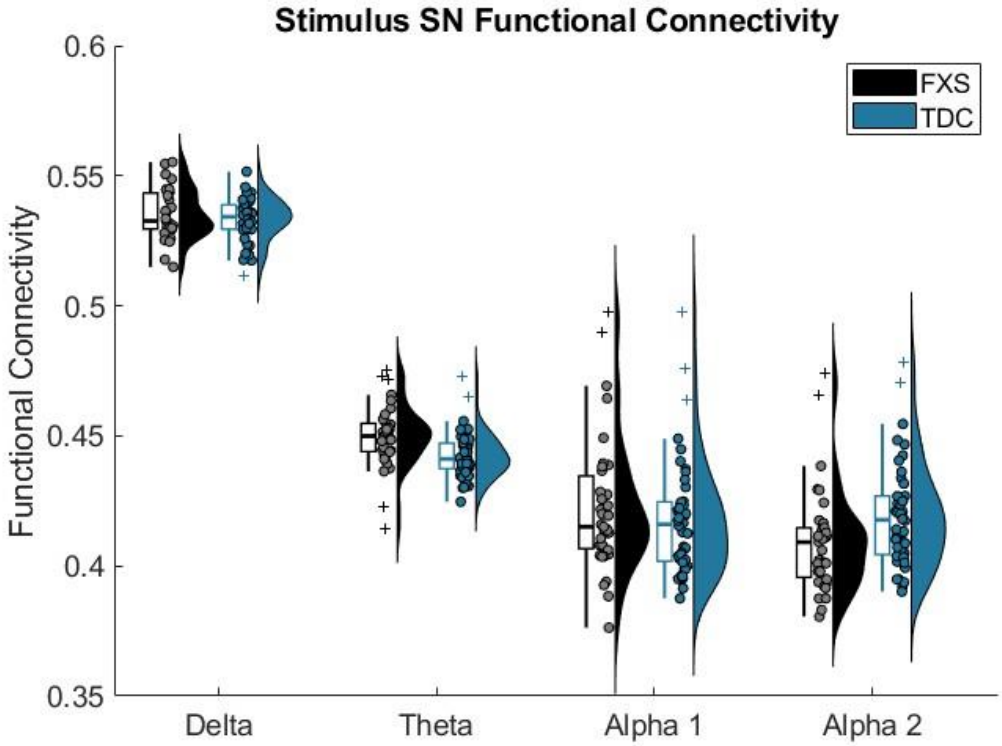

Note. Stimulus-related FC analysis. Violin and boxplots depicting group differences for SN FC across frequency bands. Dots indicate individual data points and plus signs represent outliers.

Figure 77.

Stimulus Period: Salience Network Theta Functional Connectivity Circle Plots

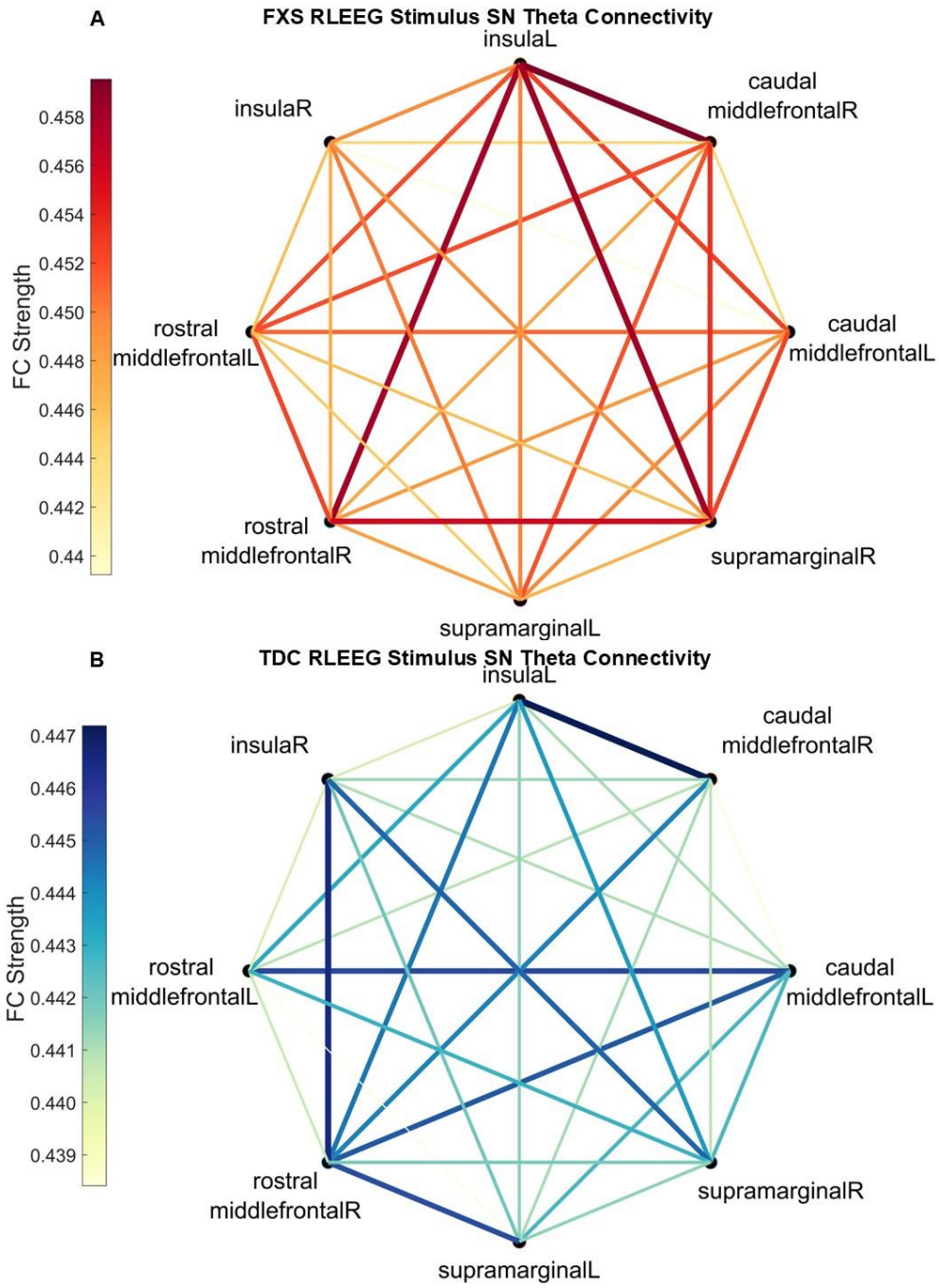

Note. Stimulus data theta FC. Scales are different between groups. **A)** All individual connections within the SN for FXS during stimulus window. **B)** All individual connections within the SN for TDC during stimulus window. Colors indicate direction of group difference with warmer colors (yellow, orange, and red) indicating higher FC and cooler colors (blue, green, yellow) indicating lower FC where darker colors indicate higher FC values within each group.

Figure 78.

Stimulus Period: Salience Network Alpha 2 Functional Connectivity Circle Plots

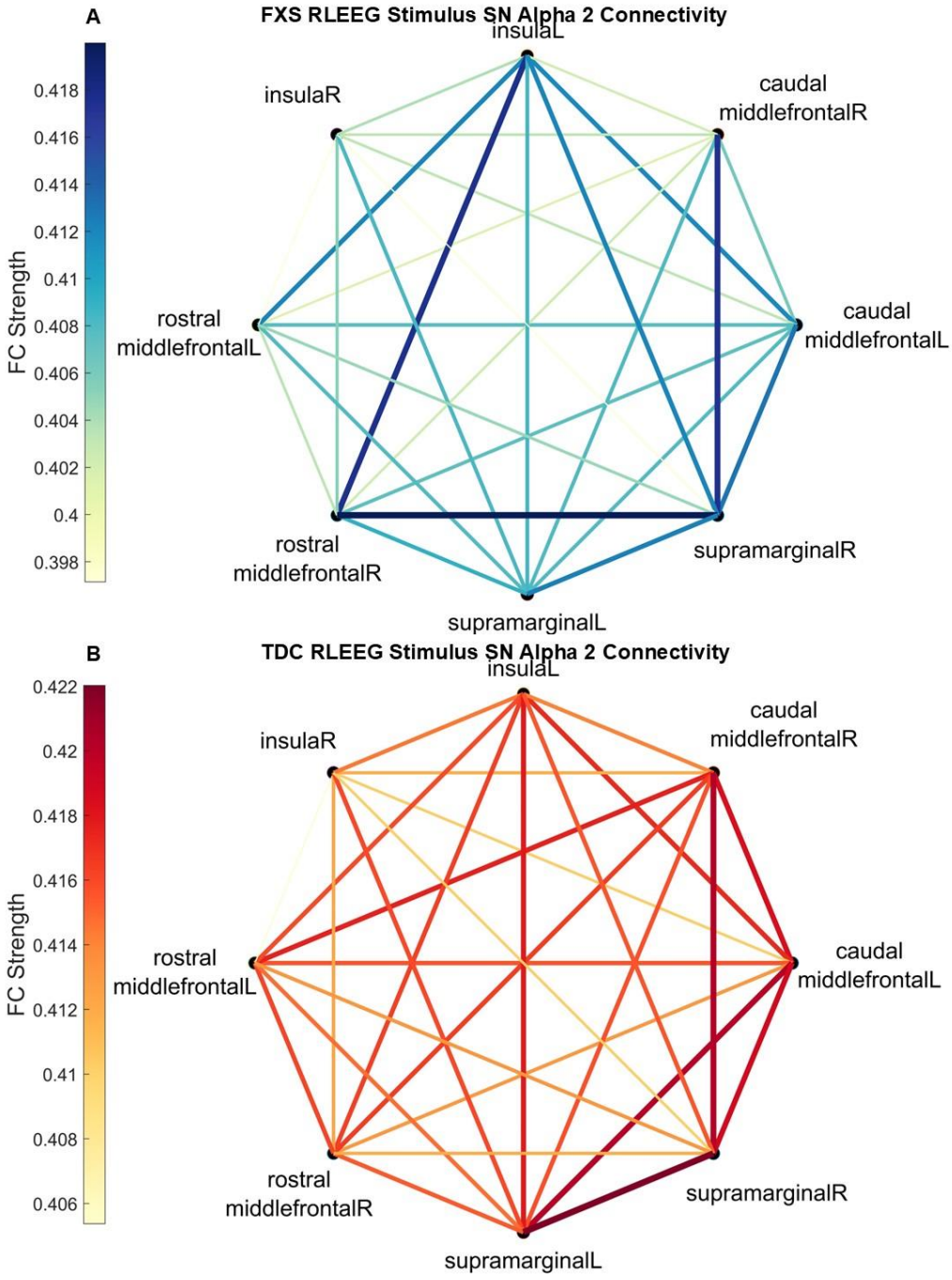

Note. Stimulus data alpha 2 FC. Scales are different between groups. **A)** All individual connections within the SN for FXS during stimulus window. **B)** All individual connections within the SN for TDC during stimulus window. Colors indicate direction of group difference with warmer colors (yellow, orange, and red) indicating higher FC and cooler colors (blue, green, yellow) indicating lower FC where darker colors indicate higher FC values within each group.

Within network FC for the control network during stimulus presentation exhibited a similar pattern to DMN where theta FC was significantly elevated in FXS (*M* rank = 54.40) relative to TDC (*M* rank = 31.02), $N = 79$, z = 4.97, $p < .001$, $r = .56$ (Figure 79 & 80). Alpha 2 was also significantly different between groups with FXS exhibiting reduced alpha 2 FC (*M* rank = 33.26) compared to TDC (*M* rank = 46.16), $N = 79$, $z = -2.68$, $p = .007$, $r = -.30$ (Figure 81).

Both delta ($N = 79$, $z = 1.60$, $p = .110$, $r = .18$) and alpha 1 ($N = 79$, $z = .99$, $p = .324$, $r = .11$) FC within the DMN during stimulus presentation were comparable between FXS (delta: *M* rank = 44.63; alpha 1: *M* rank = 42.86) and TDC (delta: *M* rank = 36.32; alpha 1: *M* rank = 37.73).

Figure 79.

Box and Violine Plots Depicting Control Network Functional Connectivity across Stimulus-Related Data for the Different Frequency Bands

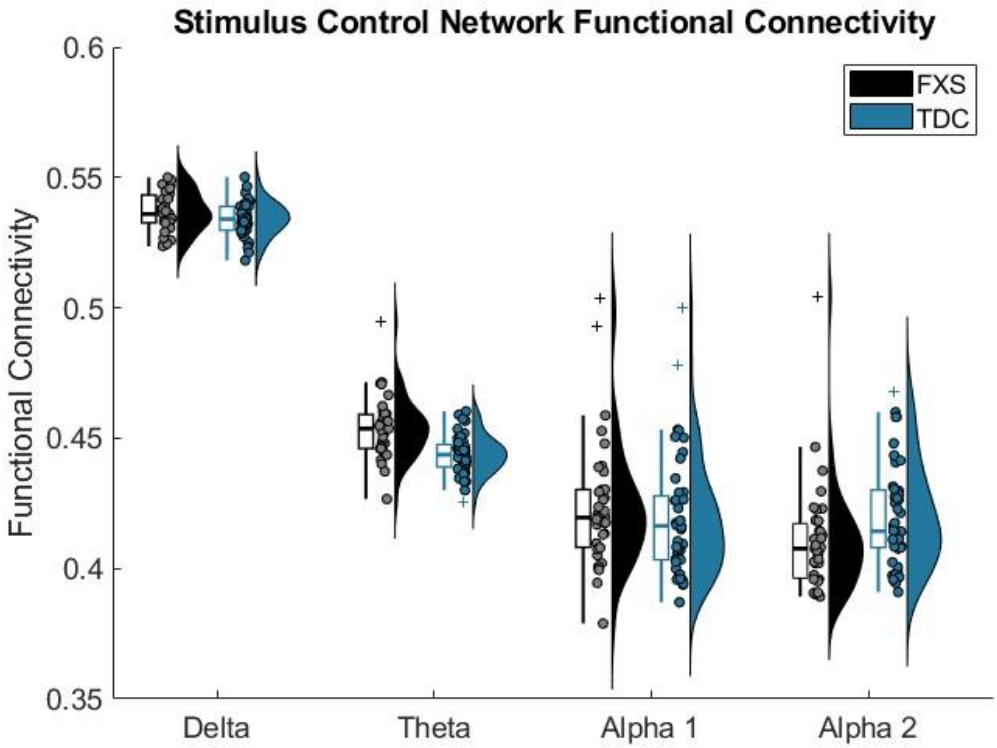

Note. Stimulus-related FC analysis. Violin and boxplots depicting group differences for control network FC across frequency bands. Dots indicate individual data points and plus signs represent outliers.

Figure 80.

Stimulus Period: Control Network Theta Functional Connectivity Circle Plots

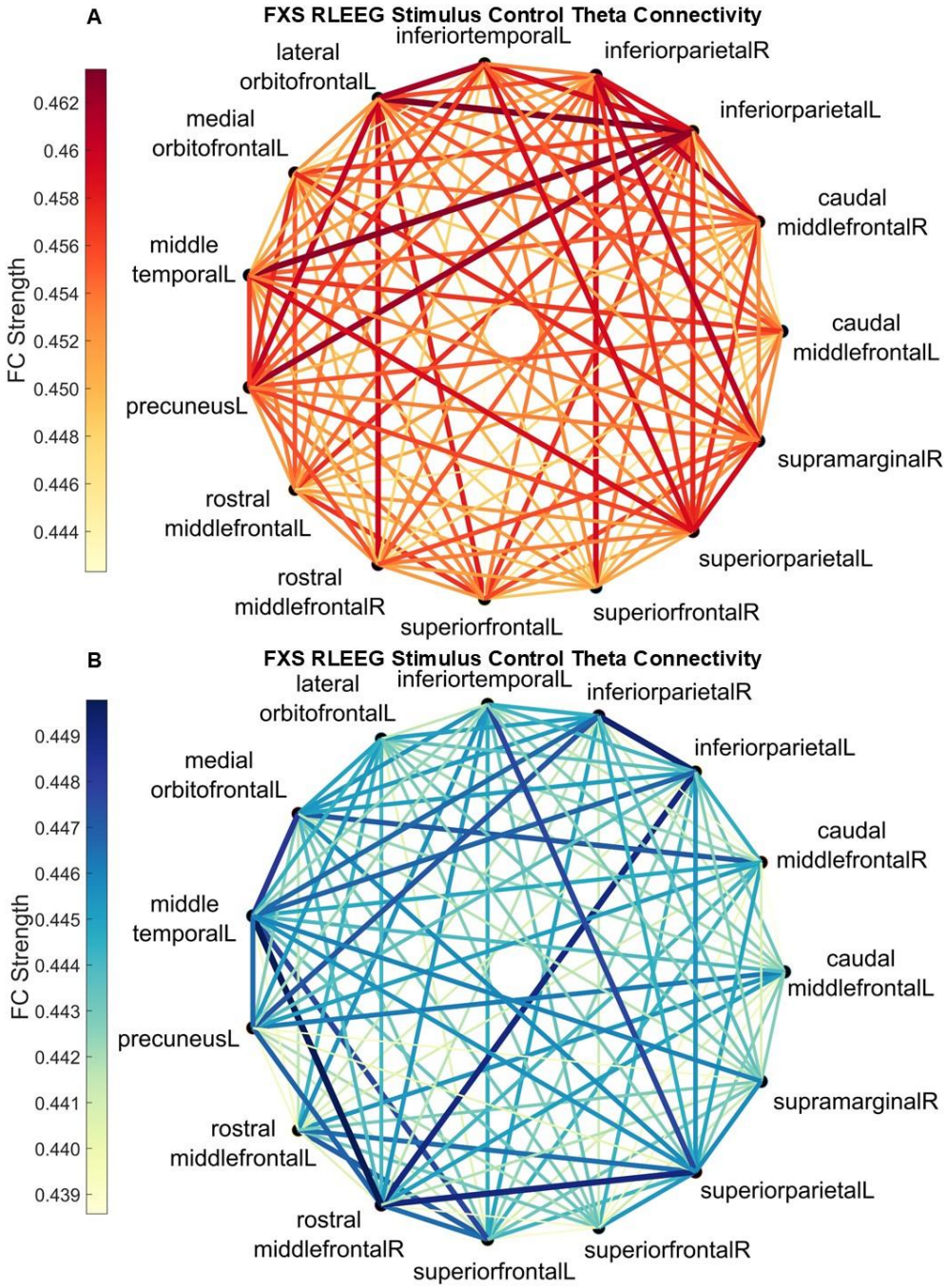

Note. Stimulus data theta FC. Scales are different between groups. **A)** All individual connections within the control network for FXS during stimulus window. **B)** All individual connections within the control network for TDC during stimulus window. Colors indicate direction of group difference with warmer colors (yellow, orange, and red) indicating higher FC and cooler colors (blue, green, yellow) indicating lower FC where darker colors indicate higher FC values within each group.

Figure 81.

Stimulus Period: Control Network Alpha 2 Functional Connectivity Circle Plots

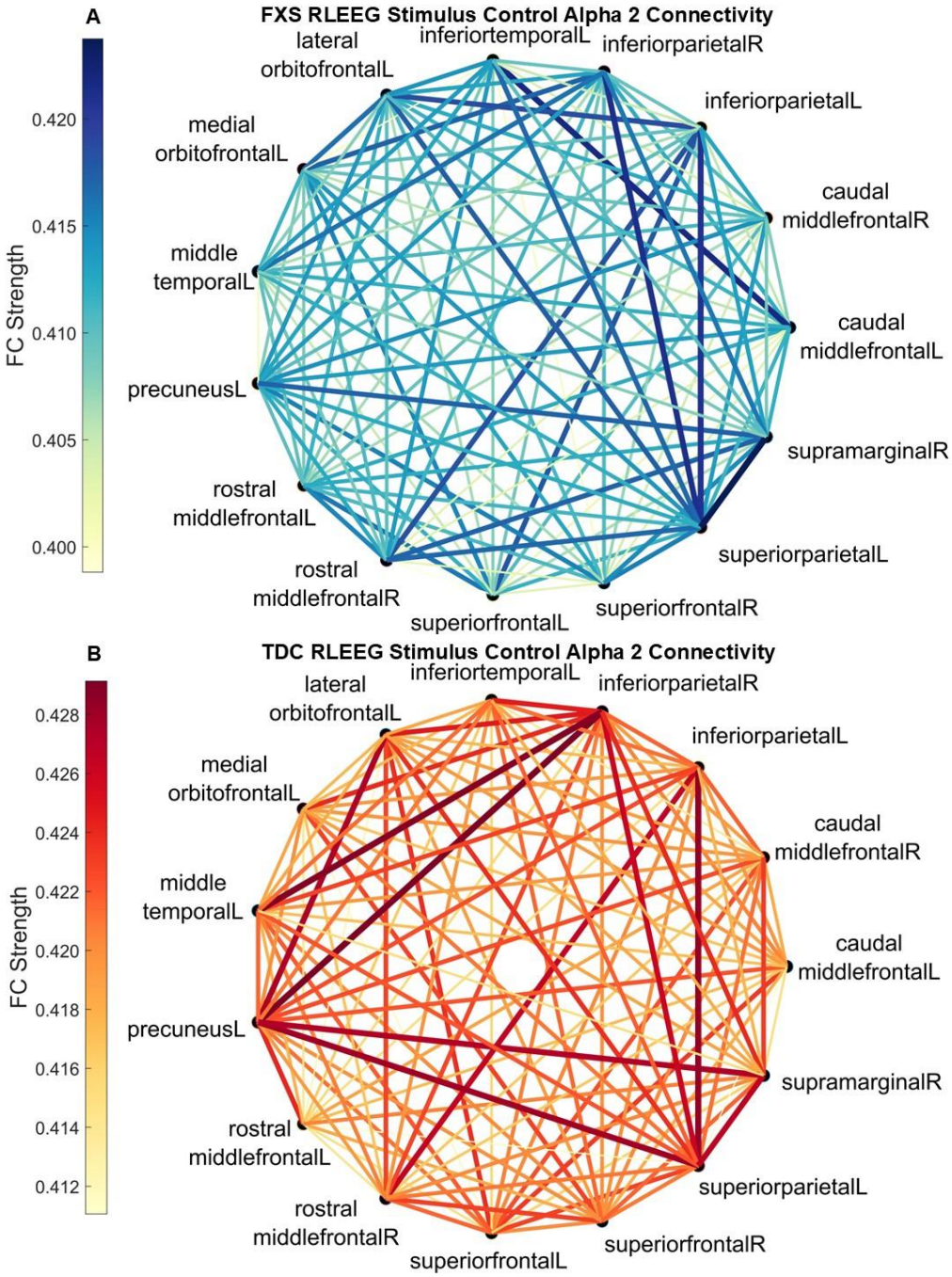

Note. Stimulus data alpha 2 FC. Scales are different between groups. **A)** All individual connections within the control network for FXS during stimulus window. **B)** All individual connections within the control network for TDC during stimulus window. Colors indicate direction of group difference with warmer colors (yellow, orange, and red) indicating higher FC and cooler colors (blue, green, yellow) indicating lower FC where darker colors indicate higher FC values within each group.

Pre-Stimulus Functional Connectivity

Non-parametric Mann-Whitney U tests also evaluated within network FC during the pre-stimulus windows in functional networks of interest (DMN, SN, and control network) across all frequency bands: delta, theta, alpha1, and alpha 2. Overall, FC group difference patterns for the pre-stimulus period were comparable to group differences on FC from the stimulus-related data.

For DMN, within network theta FC during the pre-stimulus periods was significantly elevated for FXS (*M* rank = 52.71) compared to TDC (*M* rank = 29.89), $N = 79$, $z = 4.39$, $p < .001$, $r = .49$ (Figure 82 & 83) . Alpha 2 was also significantly different between groups with FXS exhibiting reduced alpha 2 FC (*M* rank = 32.46) compared to TDC (*M* rank = 46.00), $N = 79$, $z = -2.61$, $p = .009$, $r = -.29$ (Figure 84).

Both delta ($N = 79$, $z = 1.44$, $p = .150$, $r = .16$) and alpha 1 ($N = 79$, $z = .23$, $p = .820$, $r = .03$) FC within the DMN during pre-stimulus periods were comparable between FXS (delta: *M* rank = 44.17; alpha 1: *M* rank = 40.66) and TDC (delta: *M* rank = 36.68; alpha 1: *M* rank = 39.48).

Figure 82.

Box and Violine Plots Depicting Default Mode Network Functional Connectivity across Pre-stimulus Data for the Different Frequency Bands

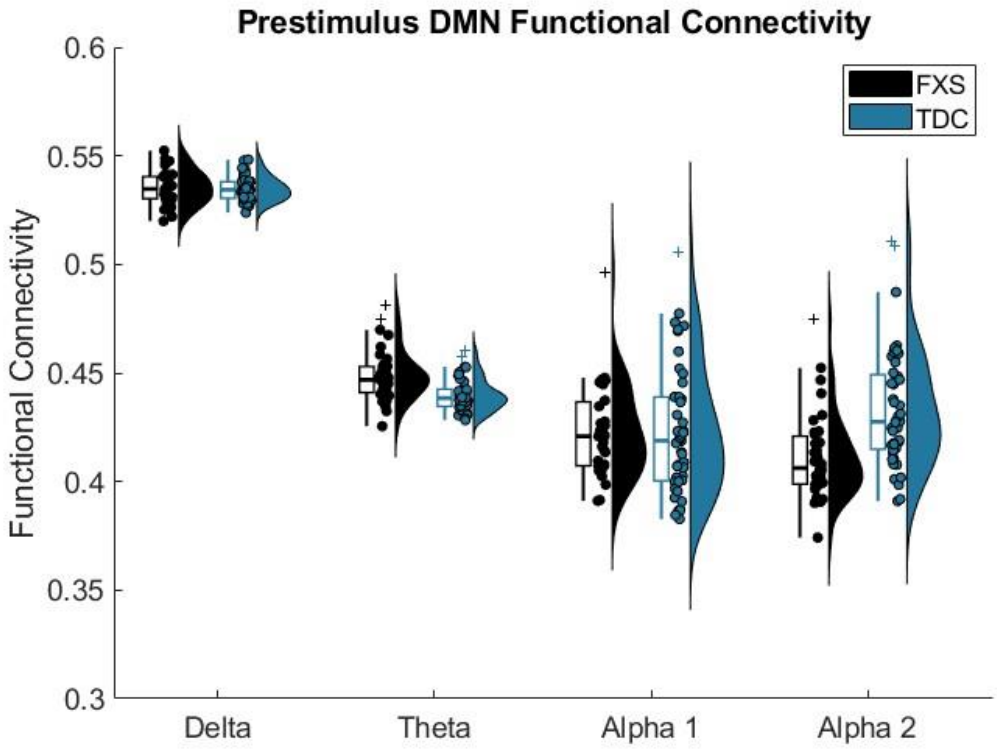

Note. Pre-stimulus-related FC analysis. Violin and boxplots depicting group differences for DMN FC across frequency bands. Dots indicate individual data points and plus signs represent outliers.

Figure 83.

Pre-stimulus Period: Default Mode Network Theta Functional Connectivity Circle Plots

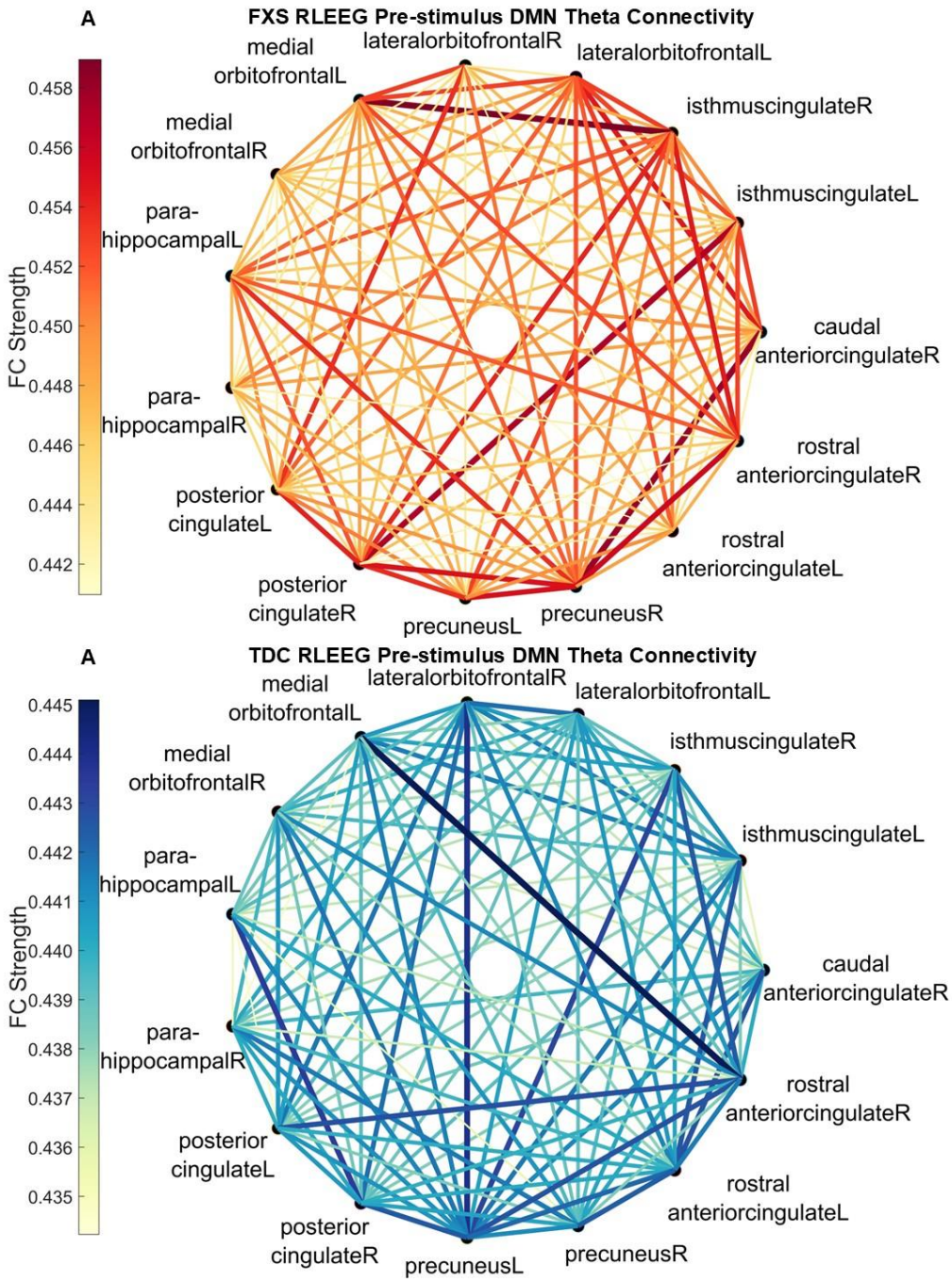

Note. Pre-stimulus data theta FC. Scales are different between groups. **A)** All individual connections within the DMN for FXS during pre-stimulus window. **B)** All individual connections within the DMN for TDC during pre-stimulus window. Colors indicate direction of group difference with warmer colors (yellow, orange, and red) indicating higher FC and cooler colors (blue, green, yellow) indicating lower FC where darker colors indicate higher FC values within each group.

Figure 84.

Pre-stimulus Period: Default Mode Network Alpha 2 Functional Connectivity Circle Plots

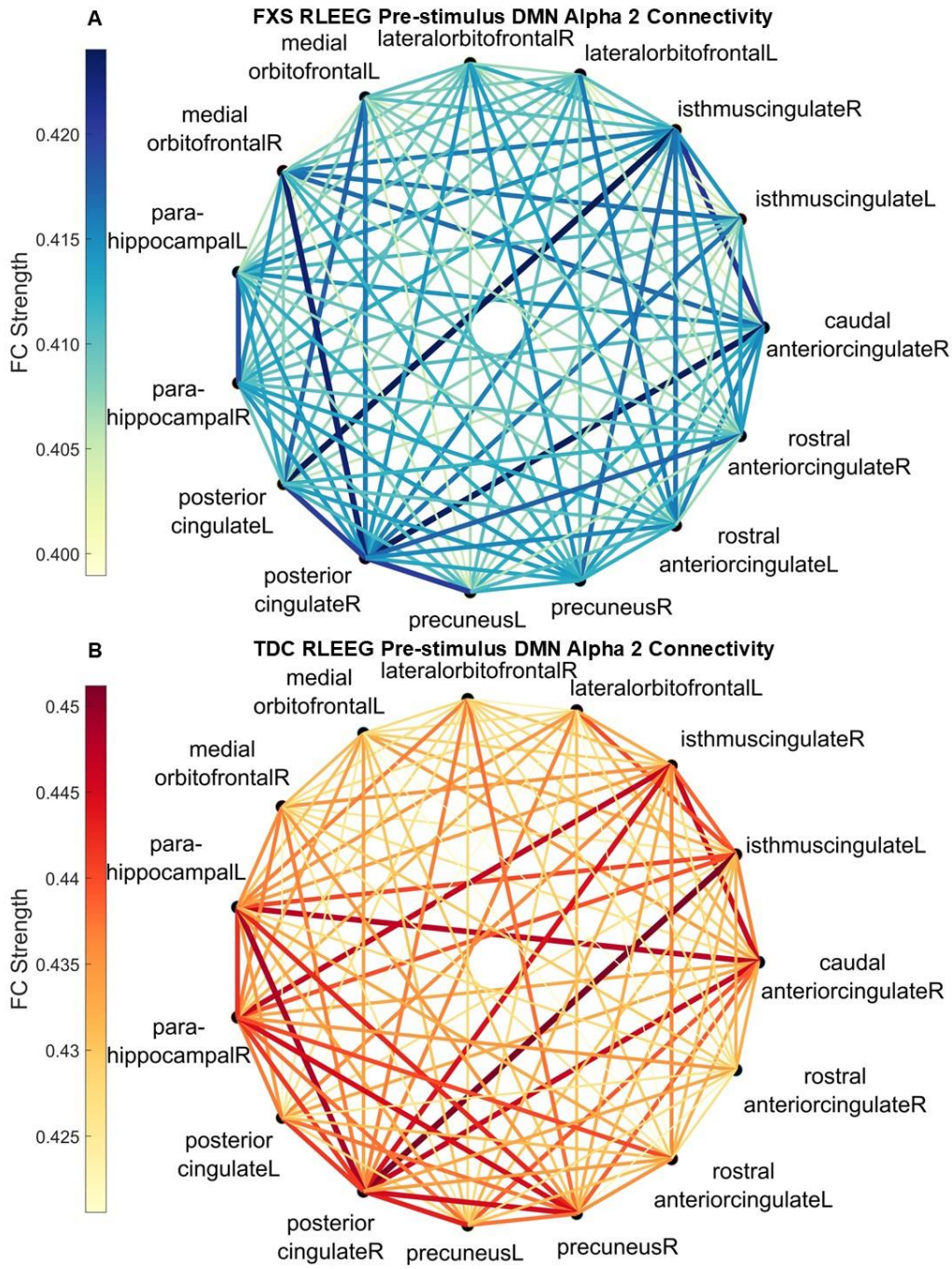

Note. Pre-stimulus data alpha 2 FC. Scales are different between groups. **A)** All individual connections within the DMN for FXS during pre-stimulus window. **B)** All individual connections within the DMN for TDC during pre-stimulus window. Colors indicate direction of group difference with warmer colors (yellow, orange, and red) indicating higher FC and cooler colors (blue, green, yellow) indicating lower FC where darker colors indicate higher FC values within each group.

For SN, within network theta FC during pre-stimulus periods was significantly different between groups with FXS exhibiting higher theta FC (*M* rank = 50.69) compared to TDC (*M* rank = 31.50), *N* = 79, z = 3.69, *p* < .001, *r* = .42 (Figure 85 & 86). Alpha 2 FC in SN was also significantly different between groups with FXS exhibiting reduced alpha 2 FC (*M* rank = 33.03) compared to TDC (*M* rank = 45.55), *N* = 79, *z* = -2.41, *p* = .016, *r* = -.27 (Figure 87).

Both delta (*N* = 79, *z* = .50, *p* = .615, *r* = .06) and alpha 1 (*N* = 79, *z* = .88, *p* = .380, *r* = .10) FC within the SN during pre-stimulus periods were comparable between FXS (delta: *M* rank = 41.46; alpha 1: *M* rank = 42.54) and TDC (delta: *M* rank = 38.84; alpha 1: *M* rank = 37.98).

Figure 85.

Box and Violine Plots Depicting Salience Network Functional Connectivity across Pre-stimulus Data for the Different Frequency Bands

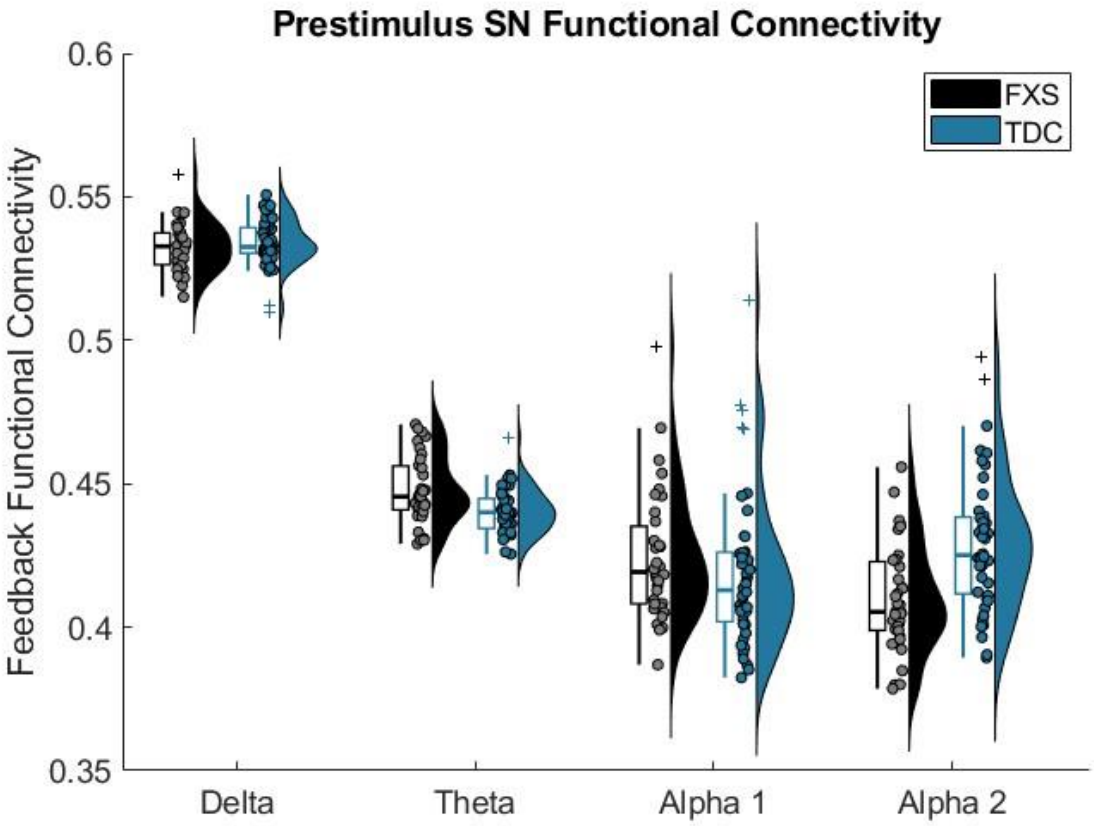

Note. Pre-stimulus-related FC analysis. Violin and boxplots depicting group differences for SN FC across frequency bands. Dots indicate individual data points and plus signs represent outliers.

Figure 86.

Pre-stimulus Period: Salience Network Theta Functional Connectivity Circle Plots

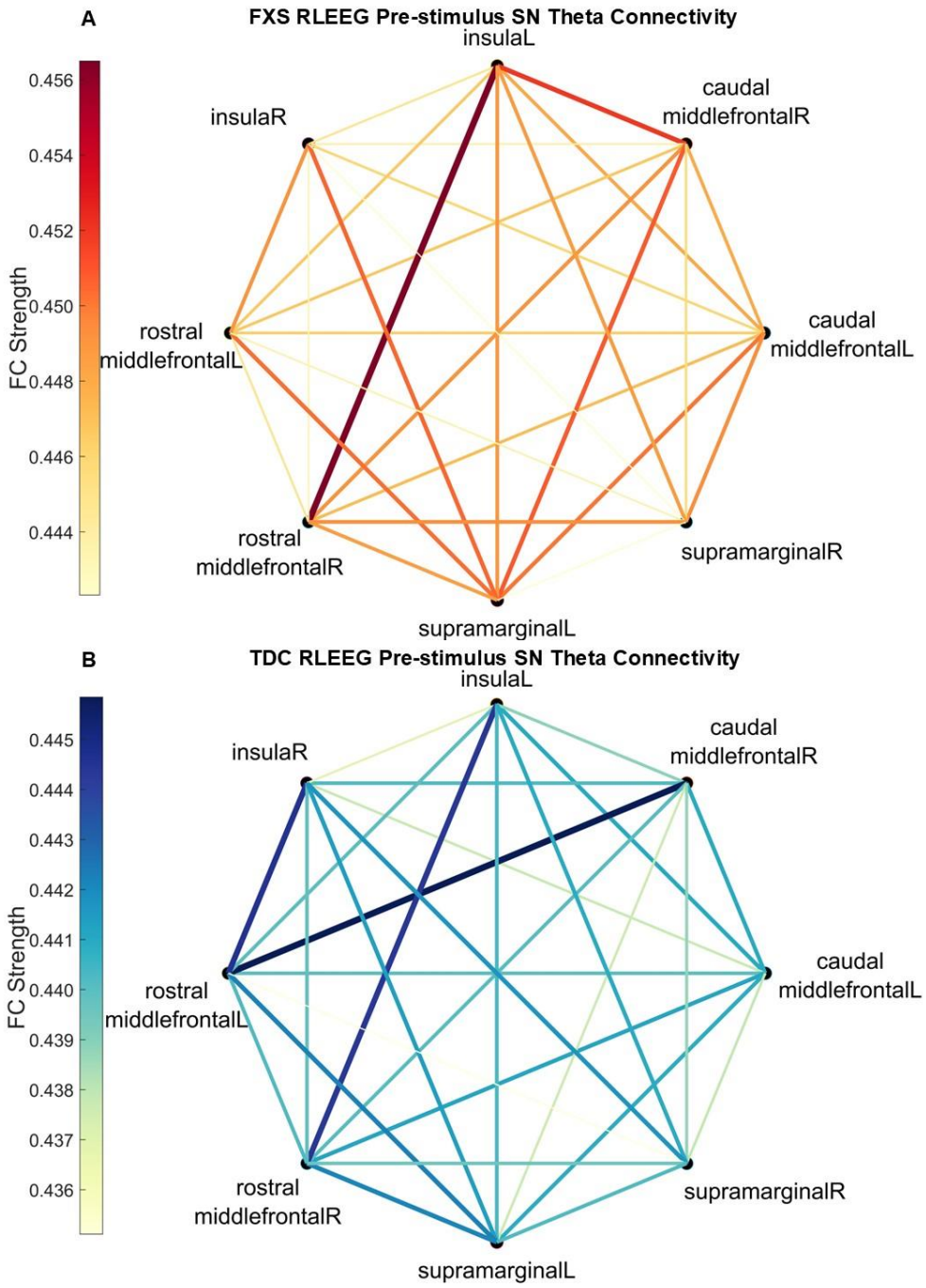

Note. Pre-stimulus data theta FC. Scales are different between groups. **A)** All individual connections within the SN for FXS during pre-stimulus window. **B)** All individual connections within the SN for TDC during pre-stimulus window. Colors indicate direction of group difference with warmer colors (yellow, orange, and red) indicating higher FC and cooler colors (blue, green, yellow) indicating lower FC where darker colors indicate higher FC values within each group.

Figure 87.

Pre-stimulus Period: Salience Network Alpha 2 Functional Connectivity Circle Plots

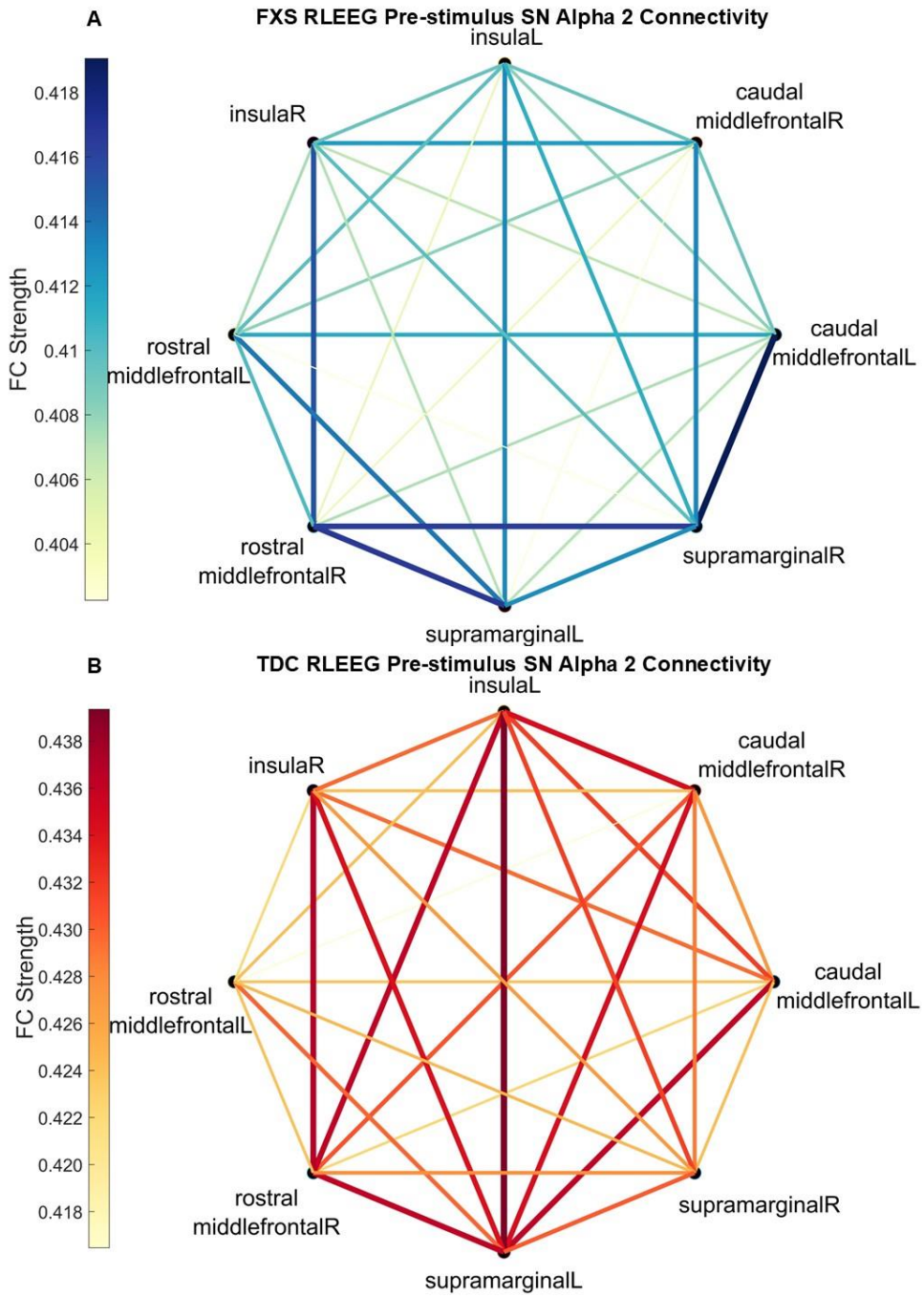

Note. Pre-stimulus data alpha 2 FC. Scales are different between groups. **A)** All individual connections within the SN for FXS during pre-stimulus window. **B)** All individual connections within the SN for TDC during pre-stimulus window. Colors indicate direction of group difference with warmer colors (yellow, orange, and red) indicating higher FC and cooler colors (blue, green, yellow) indicating lower FC where darker colors indicate higher FC values within each group.

Lastly, within network FC for control network during pre-stimulus periods was significantly different between groups where FXS exhibited significantly elevated theta FC (*M* rank = 52.11) relative to TDC (*M* rank = 30.36), $N = 79$, z = 4.19, $p < .001$, $r = .47$ (Figure 88 & 89). Alpha 2 was also significantly different between groups with FXS exhibiting reduced alpha 2 FC (*M* rank = 32.60) compared to TDC (*M* rank = 45.89), $N = 79$, $z = -2.56$, $p = .011$, $r = -.29$ (Figure 90).

Both delta ($N = 79$, $z = 1.48$, $p = .139$, $r = .17$) and alpha 1 ($N = 79$, $z = 1.09$, $p = .278$, $r = .12$) FC within the control network during pre-stimulus periods were comparable between FXS (delta: *M* rank = 44.29; alpha 1: *M* rank = 43.14) and TDC (delta: *M* rank = 36.59; alpha 1: *M* rank = 37.50).

Figure 88.

Box and Violine Plots Depicting Control Network Functional Connectivity across Pre-stimulus Data for the Different Frequency Bands

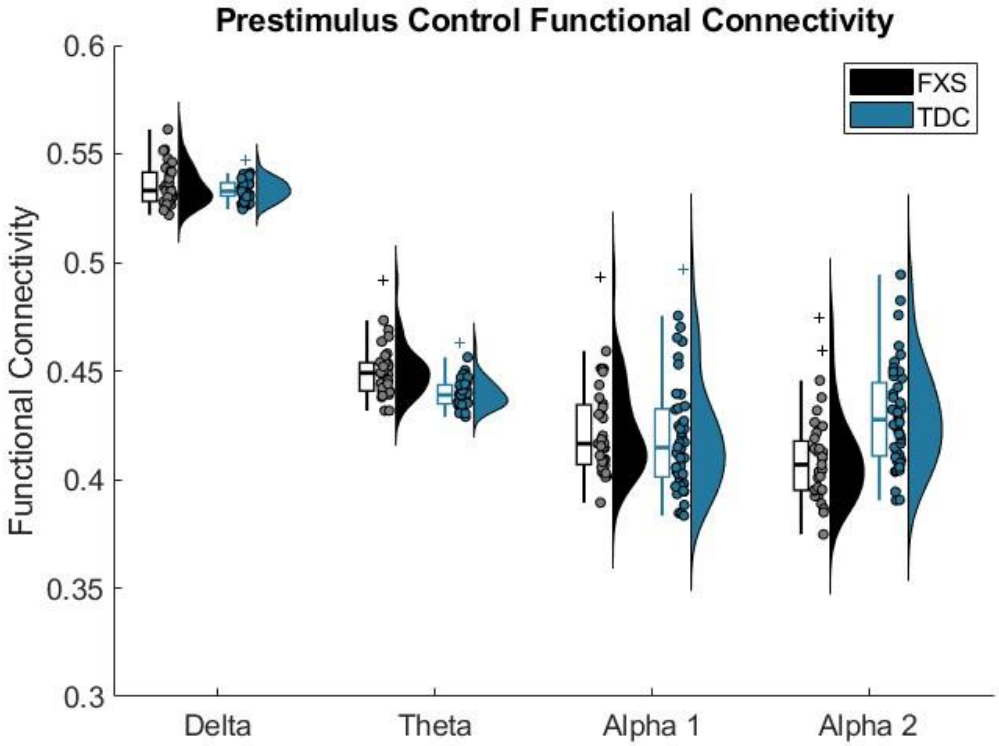

Note. Pre-stimulus-related FC analysis. Violin and boxplots depicting group differences for control network FC across frequency bands. Dots indicate individual data points and plus signs represent outliers.

Figure 89.

Pre-stimulus Period:Control Network Theta Functional Connectivity Circle Plots

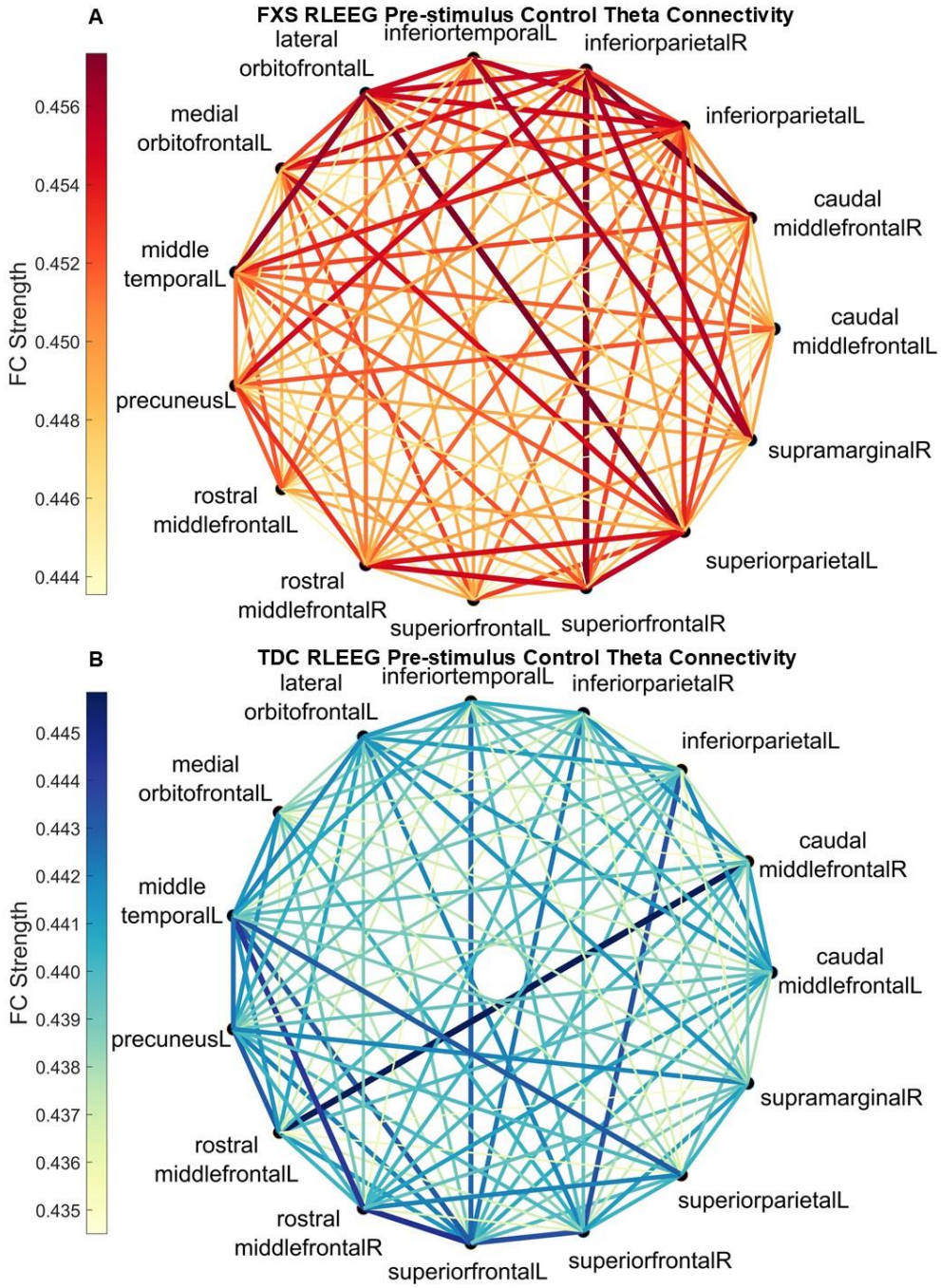

Note. Pre-stimulus data theta FC. Scales are different between groups. **A)** All individual connections within the control network for FXS during pre-stimulus window. **B)** All individual connections within the control network for TDC during pre-stimulus window. Colors indicate direction of group difference with warmer colors (yellow, orange, and red) indicating higher FC and cooler colors (blue, green, yellow) indicating lower FC where darker colors indicate higher FC values within each group.

Figure 90.

Pre-stimulus Period: Control Network Alpha 2 Functional Connectivity Circle Plots

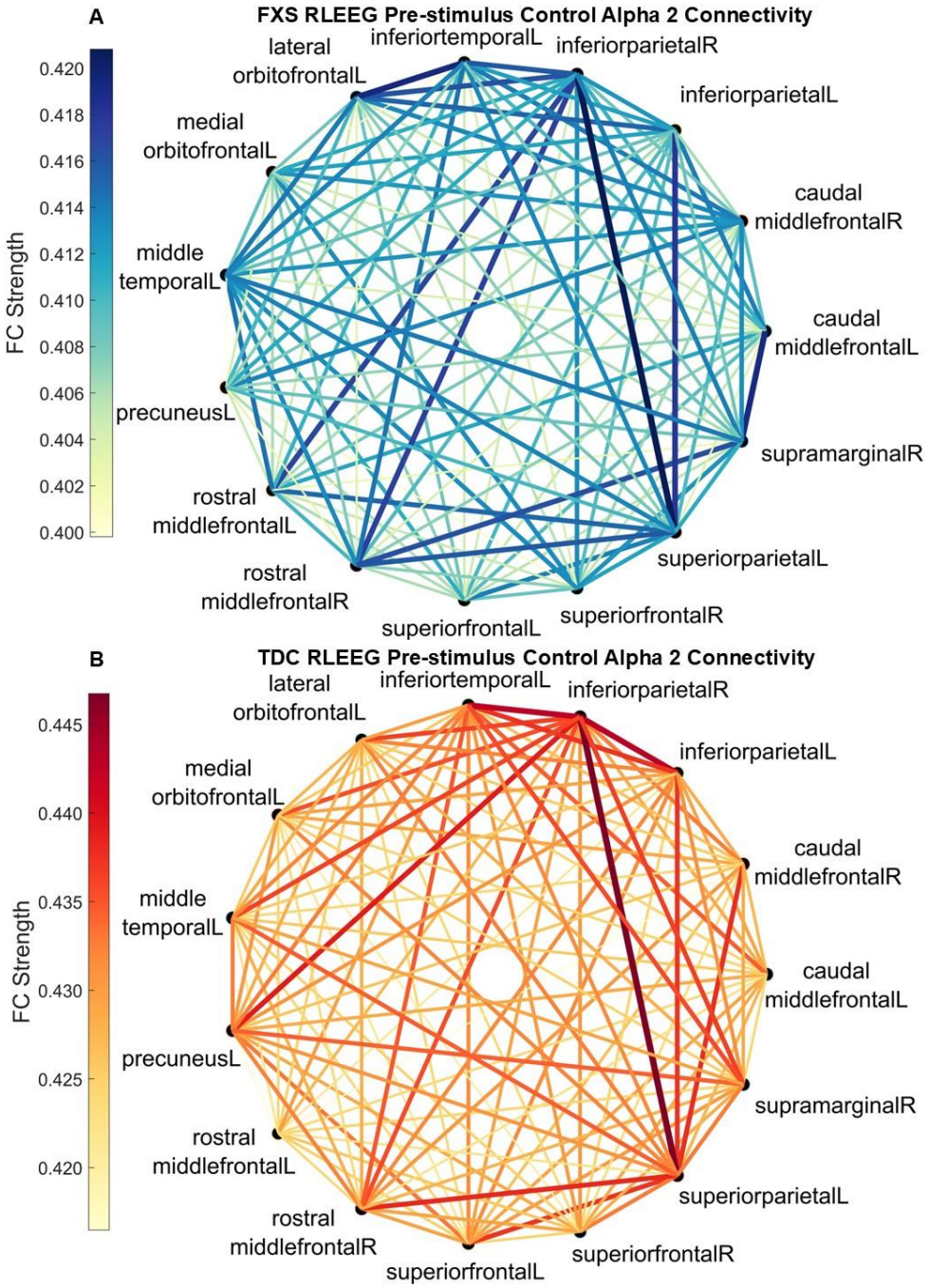

Note. Pre-stimulus data alpha 2 FC. Scales are different between groups. **A)** All individual connections within the control network for FXS during pre-stimulus window. **B)** All individual connections within the control network for TDC during pre-stimulus window. Colors indicate direction of group difference with warmer colors (yellow, orange, and red) indicating higher FC and cooler colors (blue, green, yellow) indicating lower FC where darker colors indicate higher FC values within each group.

To understand network dynamics across task windows, Friedman tests were used to evaluate within subject differences between task windows for each network. Wilcoxon sign rank tests were used when Friedman tests were significant as post-hoc tests to evaluate pairwise comparisons. Both theta FC (Figure 91) and alpha 2 FC (Figure 92) were evaluated due to significant group differences.

First, theta FC was evaluated across networks (Figure 91). Theta FC for DMN was significantly different between task windows for FXS ($\chi^2(2) = 7.60$, $p = .022$, $K = .11$) and TDC ($\chi^2(2) = 11.46$, $p = .003$, $K = .13$) where the pre-stimulus period was reduced compared to theta FC during the stimulus period for both FXS ($z = -2.67$, $p = .024$) and TDC ($z = -2.98$, $p = .009$) but the pre-stimulus was only significantly different (reduced) from the feedback window for TDC ($z = -3.03$, $p = .006$) and not FXS ($z = -1.52$, $p = .384$). For both groups, the stimulus and feedback theta FC values were similar (FXS: $z = -1.34$, $p = .537$; TDC: $z = -.77$, $p = 1.00$) suggesting comparable network engagement.

Theta FC for SN was significantly different between task windows for FXS ($\chi^2(2) = 8.23$, $p = .016$, $K = .12$) but not TDC ($\chi^2(2) = 3.68$, $p = .159$, $K = .04$) where in FXS the pairwise comparisons did not survive correction for the pre-stimulus to the stimulus period ($z = -1.74$, $p = .249$) or the pre-stimulus to the feedback period, though it trended towards significance where SN theta FC was marginally increased during the feedback period ($z = -2.23$, $p = .078$). There was no significant difference from the stimulus to the feedback period for FXS ($z = .57$, $p = .566$).

Theta FC for control network was not significantly different between task windows for FXS ($\chi^2(2) = 2.11$, $p = .347$, $K = .07$) but was for TDC ($\chi^2(2) = 23.77$, $p < .001$, $K = .17$) where theta FC during the pre-stimulus period was significantly lower than during the stimulus period ($z = -3.76$, $p < .001$) and the feedback period ($z = -3.26$, $p = .003$) where theta FC was boosted for

task engagement but the stimulus and feedback periods were similar (z = -.02, p = 1.00) suggesting similar activation levels. FXS had similarly elevated theta FC across task windows suggesting reduced modulation of theta in the control network.

Figure 91.

Violin Plot for Theta FC Across Networks by Group

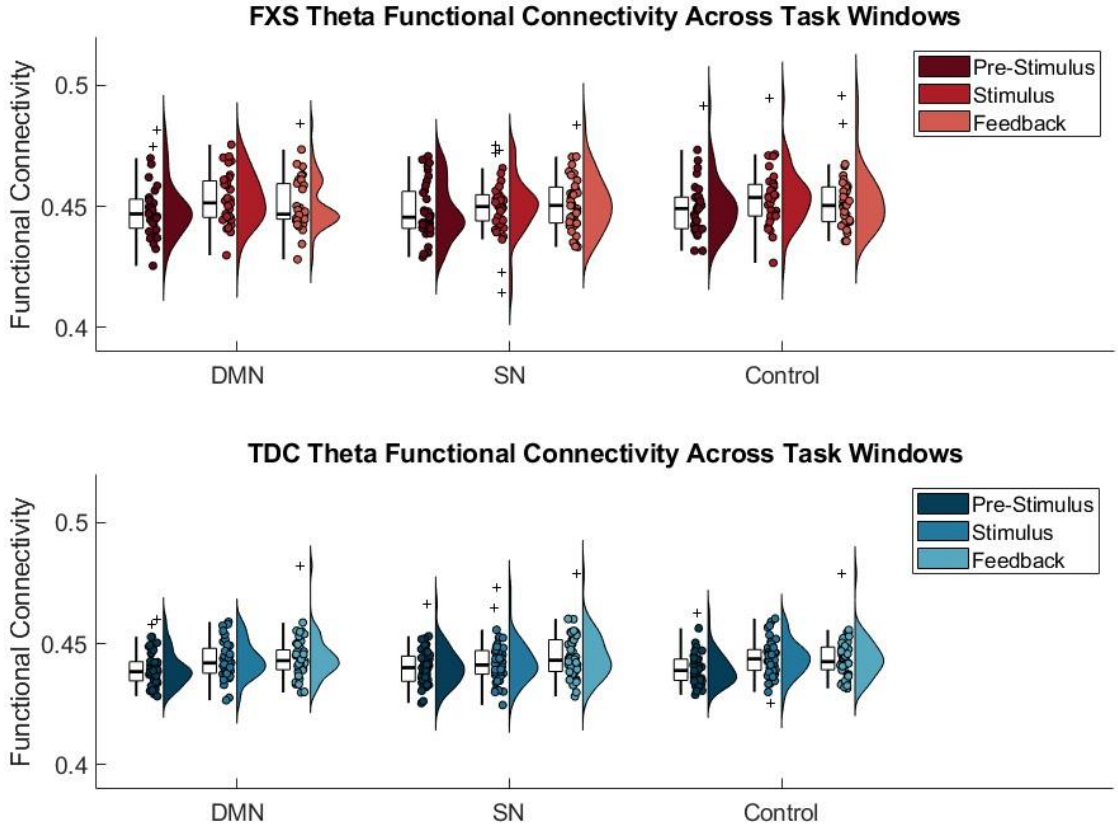

Note. Within-subject differences between task periods for each group depicted using both violin and boxplots. Dots indicate individual data points and plus signs represent outliers.

Next, alpha 2 FC was evaluated across networks (Figure 92). Alpha 2 FC for DMN was not significantly different between task windows for FXS ($\chi^2(2) = .91$, $p = .633$, $K = .01$) but was significantly different for TDC ($\chi^2(2) = 27.41$, $p < .001$, $K = .31$) where alpha 2 FC during the pre-stimulus period was significantly higher than the stimulus period (z = -3.82, $p < .001$) and the

feedback period (z = -4.81, p < .001) but the stimulus and feedback periods were similar (z = -1.91, p = .168).

Alpha 2 FC for SN was not significantly different between tasks windows for FXS ($\chi^2(2)$ = .06, p = .972, K = .00) but was significantly different for TDC ($\chi^2(2)$ = 8.23, p = .016, K = .12) where alpha 2 FC during the pre-stimulus period was higher than the stimulus period (z = -4.13, p < .001) and the feedback period (z = -4.91, p < .001) but the stimulus and feedback windows were similar (z = -1.37, p = .516).

Alpha 2 FC for control network was not significantly different between task windows for FXS but trended towards significance ($\chi^2(2)$ = 5.20, p = .074, K = .03). Alpha 2 FC for control network was significantly different between task windows for TDC ($\chi^2(2)$ = 15.05, p < .001, K = .27) where alpha 2 FC during the pre-stimulus period was significantly higher from the stimulus period (z = -3.87, p < .001) and the feedback period (z = -4.62, p < .001) but the stimulus and feedback periods were similar (z = -1.24, p = .648).

Figure 92.

Violin Plot for Alpha 2 FC Across Networks by Group

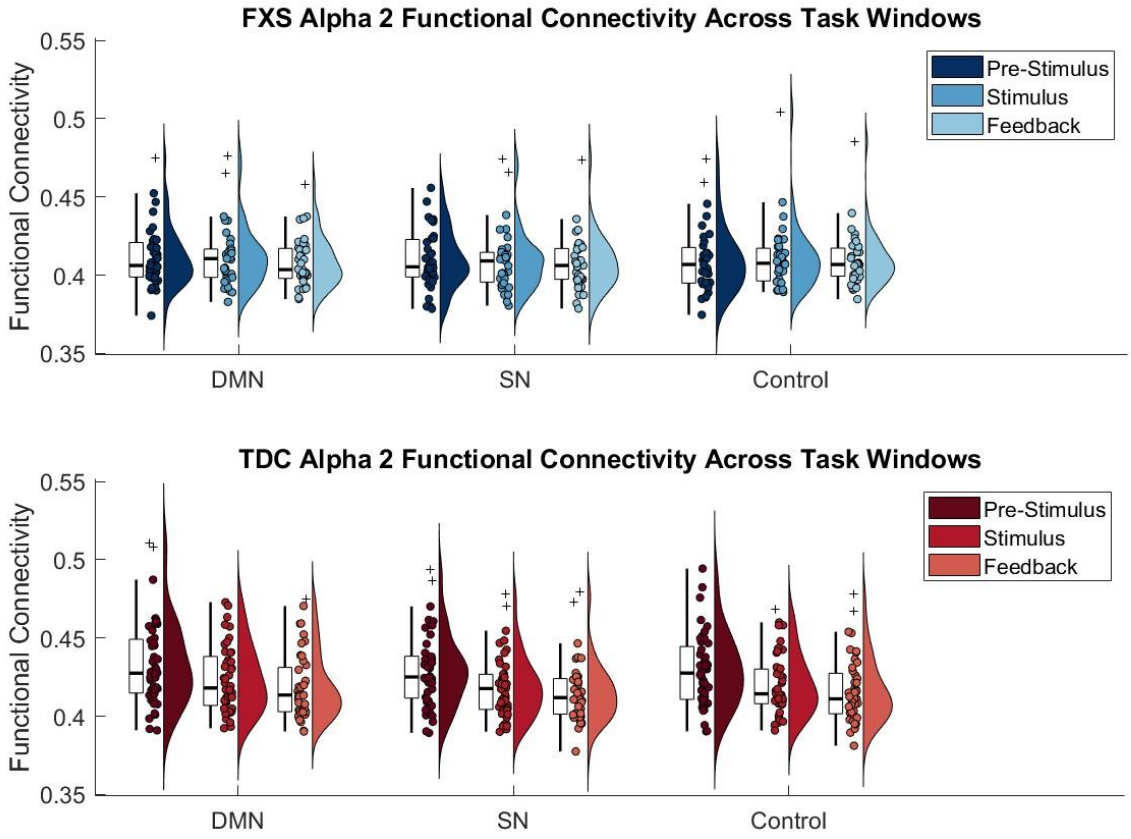

Note. Within-subject differences between task periods for each group depicted using both violin and boxplots. Dots indicate individual data points and plus signs represent outliers.

Functional Connectivity Analysis: Strongest Connections

The top ten connections from each functional network were evaluated for all frequency bands where FC was significantly different between groups to identify whether FC group differences were driven by specific node connections. Only the top two, strongest connections were evaluated and selected based on the top two TDC connections to determine whether group-level differences across the whole network persist within the typical primary drivers (i.e., top TDC connections) on overall within-network connectivity.

Feedback Strongest Individual Connections

Theta FC. Top connections for theta FC were evaluated first across networks starting with DMN. The top ten connections for the DMN during feedback were fairly different between groups where FXS had more unique nodes involved in the top ten connections (N = 12) than TDC (N = 11 nodes) (Figure 93). Further, not all nodes overlapped where FXS nodes contained the left rostral anterior cingulate node, left posterior cingulate node, and the left precuneus node which were not involved in the TDC top ten connections. All right hemisphere nodes overlapped between groups which suggests FXS DMN theta FC was more inclusive of the left hemisphere in top node connections.

The strongest DMN connection for TDC in the theta range on feedback-related data (DMN Connection 1) was between the right parahippocampal node and the right posterior cingulate node and the second strongest connection (DMN Connection 2) was between the right caudal anterior cingulate node and the left medial orbitofrontal node. The engagement of the posterior cingulate and the orbitofrontal nodes in DMN makes sense for a deterministic reversal learning task (Habiby Alaoui et al., 2021). While the current FC measures did not temporally overlap precisely with feedback delivery, these results suggest appropriate pathways are engaged during typical feedback processing (Habiby Alaoui et al., 2021; Leech et al., 2013; Alves et al., 2019). Neither of the strongest FC node connections in theta for TDC were present in the FXS top ten connections. For FXS, the strongest theta FC connections both involved the right precuneus where the strongest connection was between the right precuneus and right posterior cingulate nodes and the second strongest connection was between the right precuneus and right isthmus cingulate nodes which were both not present in the TDC top ten connections (Figure 93).

Figure 93.

Feedback: Theta FC Top Ten Within Default Mode Network Connections

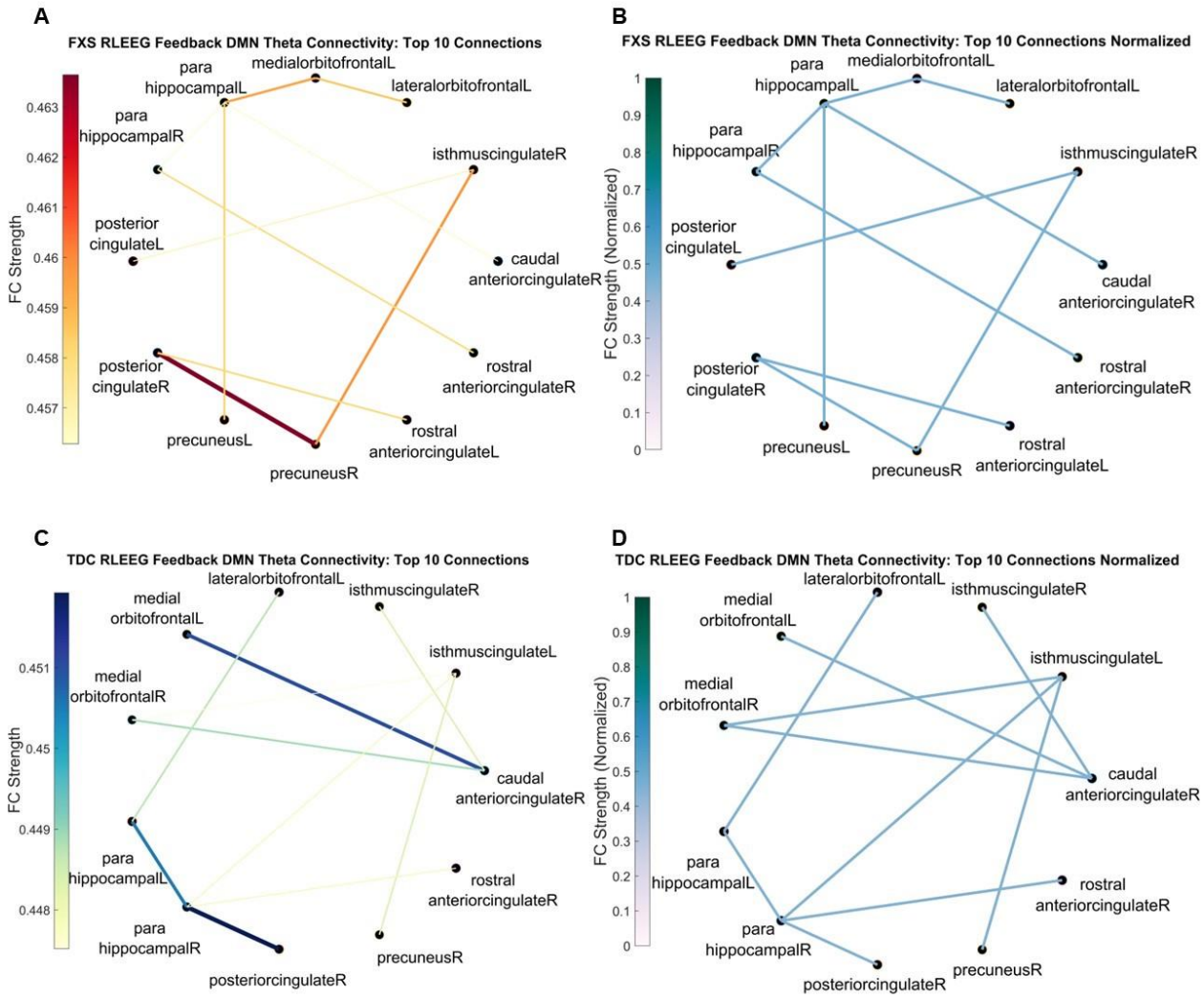

Note. Normalized plots were normalized to the full FC scale to help to visualize some of the smaller, and thus barely visible, connections in A and C. **A)** FXS top ten theta FC within network connections for feedback DMN (same as plot B). **B)** FXS top ten connections normalized to the full dWPLI scale. **C)** TDC top ten theta FC within network connections for feedback DMN (same as plot D). **D)** TDC top ten connections normalized to the full dWPLI scale.

Statistically, both theta FC DMN Connection 1 ($N = 79$, $z = .17$, $p = 1.00$, $r = .02$) and Connection 2 ($N = 79$, $z = -.42$, $p = 1.00$, $r = -.05$) were not significantly different between groups where FXS had comparable theta FC for the strongest TDC connection (DMN Connection 1: *M* rank = 40.49; DMN Connection 2: *M* rank = 38.80) compared to TDC (DMN Connection 1: *M* rank = 39.61; DMN Connection 2: *M* rank = 40.95). Given the strongest connections for TDC were not in the top ten connections for FXS, these results suggest the overall theta FC group differences were driven by more diffusely elevated theta FC across the whole DMN. However, evaluation of the sum scores for the top ten connections identified a significant difference between groups where FXS had increased theta FC across the sum of the top ten DMN connections for the FXS group (*M* rank = 56.66) compared to the sum of the top ten DMN connections for the TDC group (*M* rank = 26.75), $N = 79$, $z = 5.75$, $p < .001$, $r = .65$. Further, sum score group differences represent a large effect suggesting the top connections for FXS likely drove group differences at the whole network level. While FC on the strongest TDC connections were not different, connectivity strength for the strongest ten network connections in each group may suggest a shift in primary network architecture.

For the SN, TDC had more unique nodes ($N = 8$) in the top ten connections compared to FXS ($N = 7$). The seven nodes involved in the FXS top ten connections were shared with TDC where the only difference was the addition of the right caudal middle frontal node for TDC. The strongest connection for TDC (SN Connection 1) was between the right rostral middle frontal node and the left caudal middle frontal node which was present in the FXS top ten connections but only of moderate strength relative to other connections. The second strongest connection for TDC (SN Connection 2) was between the left rostral middle frontal node and the left supramarginal node which was not in the FXS top ten connections. For FXS, the strongest

connections both involved the left insula node where the strongest connection was between the left insula and left caudal middle frontal nodes. The second strongest connection was between the left insula and the right rostral middle frontal node. Neither of the top theta FC node connections were present in the top ten TDC connections (Figure 94).

Figure 94.

Feedback: Theta FC Top Ten Within Salience Network Connections

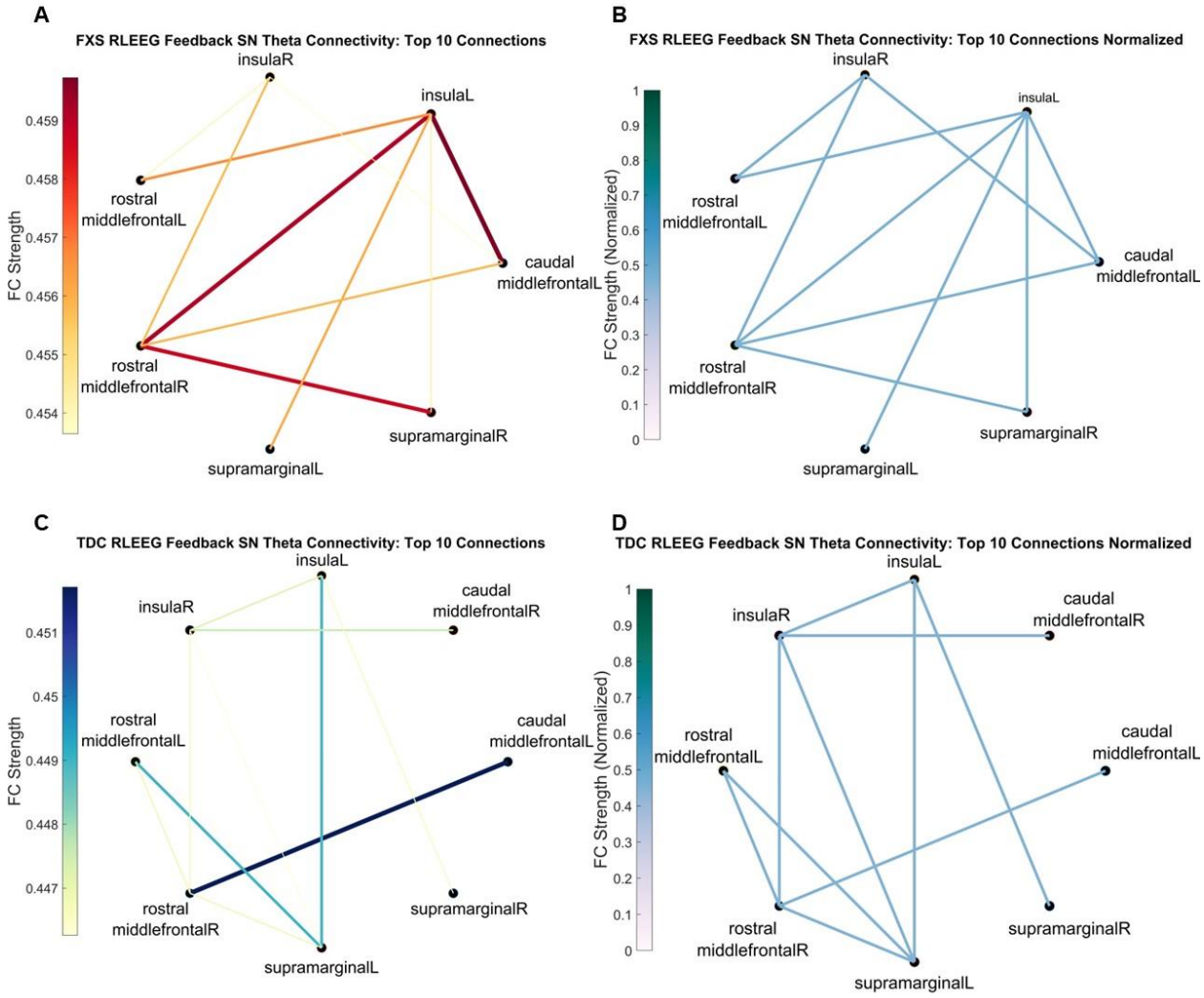

Note. Normalized plots were normalized to the full FC scale to help to visualize some of the smaller, and thus barely visible, connections in A and C. **A)** FXS top ten theta FC within network connections for feedback SN (same as plot B). **B)** FXS top ten connections normalized to the full dWPLI scale. **C)** TDC top ten theta FC within network connections for feedback SN (same as plot D). **D)** TDC top ten connections normalized to the full dWPLI scale.

Statistically, both SN Connection 1 ($N = 79$, $z = .91$, $p = .364$, $r = .10$) and Connection 2 ($N = 79$, $z = -.24$, $p = .813$, $r = -.03$) were not significantly different between groups where FXS had comparable theta FC for the strongest TDC connection (SN Connection 1: *M* rank = 42.63; SN Connection 2: *M* rank = 39.31) compared to TDC (SN Connection 1: *M* rank = 37.91; SN Connection 2: *M* rank = 40.55). These results suggest theta FC was more diffusely spread across the whole FXS SN. However, similarly to DMN, the sum score was significantly different between groups where FXS exhibited increased theta FC in the top ten SN connections for FXS (*M* rank = 48.86) compared to the top ten SN for TDC (*M* rank = 32.95), $N = 79$, $z = 3.06$, $p = .002$, $r = .34$. Also, SN Connection 2 was also in the top ten for FXS which suggests a shift in network theta FC for the top FXS connections over the typical node activity for TDC. Differences in FC exist for the top ten connections between groups suggesting differences in primary network architecture for SN activity during feedback may exist. While a significant shift in architecture use may have occurred, the overall magnitude of the top ten was higher for FXS than TDC where limited node pairs overlap.

Lastly, the strongest network connections for TDC in the control network were largely different due to limited node overlap. The number of unique nodes in the top ten connections for each group were different with FXS having one additional node ($N = 10$) compared to TDC ($N = 9$). Only six nodes overlapped between groups: right inferior parietal, left lateral orbitofrontal, left middle temporal, right rostral middle frontal, right superior frontal, and right supramarginal nodes.

The strongest connection for TDC (Con Connection 1) was between the right rostral middle frontal and the left caudal middle frontal nodes. The second strongest connection for TDC (Con Connection 2) was between the right and left inferior parietal nodes. Neither of the

strongest TDC connections were represented in the top ten connections for FXS because nodes involved were not nodes involved in the FXS top ten connections. Namely, the left caudal middle frontal and the left inferior parietal nodes. Both of the top connections for FXS involved the right supramarginal node where the strongest theta FC connection for FXS was between the right supramarginal node and the right inferior parietal node which was a top ten connection for TDC of lower strength relative to other top TDC connections. The second strongest connection for FXS was between the right supramarginal node and the left inferior temporal node which was not a top ten connection for TDC (Figure 95).

Figure 95.

Feedback: Theta FC Top Ten Within Control Network Connections

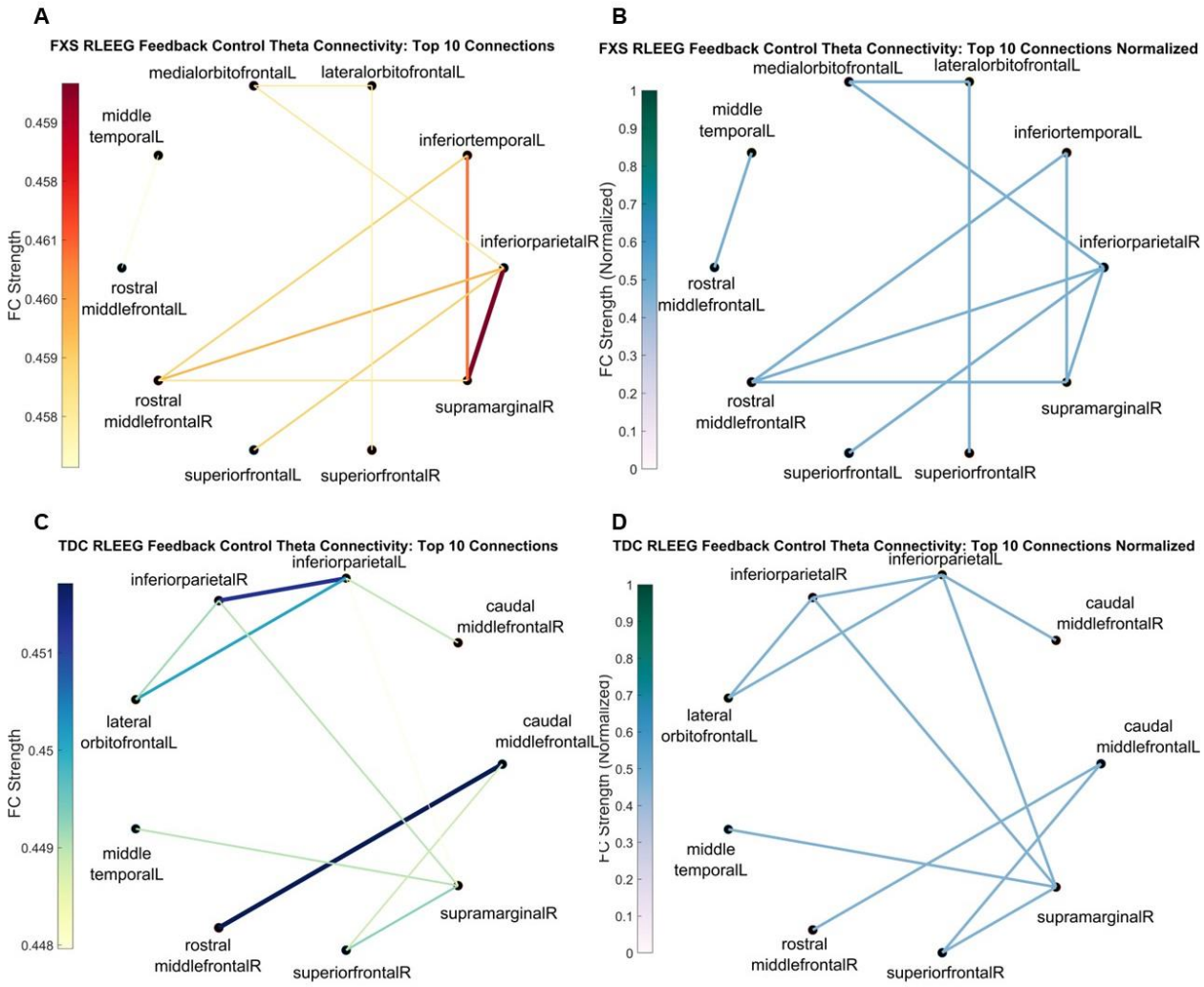

Note. Normalized plots were normalized to the full FC scale to help to visualize some of the smaller, and thus barely visible, connections in A and C. **A)** FXS top ten theta FC within network connections for feedback control network (same as plot B). **B)** FXS top ten connections normalized to the full dWPLI scale. **C)** TDC top ten theta FC within network connections for feedback control network (same as plot D). **D)** TDC top ten connections normalized to the full dWPLI scale.

Statistically, both control network Connection 1 ($N = 79$, $z = .91$, $p = .364$, $r = .02$) and Connection 2 ($N = 79$, $z = .61$, $p = .541$, $r = .07$) were not significantly different between groups where FXS had comparable theta FC for the strongest TDC connections (Con Connection 1: *M* rank = 42.63; Con Connection 2: *M* rank = 41.77) compared to TDC (Con Connection 1: *M* rank = 37.91; Con Connection 2: *M* rank = 38.59). Unlike DMN and SN, the sum score representing individual group top ten connections was not significantly different between groups but did trend towards significance where FXS had marginally higher theta FC (*M* rank = 45.06) compared to TDC (*M* rank = 35.98), $N = 79$, $z = 1.75$, $p = .081$, $r = .20$. Overall, these results suggest group differences on control network theta FC are more diffuse across the full network in FXS rather than resulting from differences in primary network drivers or neural hubs which indicates global network inefficiencies and a lack of task-specific network engagement. Visually, network connections for FXS indicate hyperconnectivity across the whole network

In the statistical evaluation of theta FC for feedback-related activity across all functional networks, the strongest theta FC connections for TDC within DMN, SN, and control network from the feedback windows were not statistically different between groups suggesting feedback-related theta FC was more diffuse across the entire network rather than driven by specific node connections. However, DMN and SN sum score differences imply network reorganization where the control network was more diffusely disrupted across the whole network.

Alpha 2 FC. Next, the individual connections for alpha 2 FC on feedback-related data were evaluated across all networks. The total number of unique nodes involved in FXS top ten connections was higher ($N = 11$) than in TDC ($N = 9$) where the difference between groups was mainly related to the increased number of unique nodes featured in the FXS top ten. The left lateral orbitofrontal, and right medial orbitofrontal were both present for FXS and not TDC. Further FXS had the left posterior cingulate node instead of the left parahippocampal node in the top ten connections. Interestingly, five of the top ten FXS connections involved the right precuneus where TDC only had one connection to the right precuneus in the top ten, though they were not the strongest connections. Four of the top ten TDC connections involved the right posterior cingulate node, three of which were the strongest connections.

The two strongest alpha 2 FC DMN connections during feedback for TDC both involved the right posterior cingulate node. The top/strongest connection (DMN Connection 1) was between the right posterior cingulate and right isthmus cingulate nodes where the second strongest connection (DMN Connection 2) was between right posterior cingulate and left isthmus cingulate nodes. The strongest connection was not in the FXS top ten, but DMN Connection 2 was also the second strongest connection for FXS. The strongest connections for FXS both involved the left isthmus cingulate node where the strongest connection was between the left isthmus cingulate node and the left lateral orbitofrontal node. The top connection for FXS was not present for TDC, as the left lateral orbitofrontal node was not a node involved in the top ten TDC DMN connections (Figure 96). Again, the second strongest alpha 2 FXS connection within DMN during feedback was also the second strongest connection TDC (right posterior cingulate node to left isthmus cingulate node).

Figure 96.

Feedback: Alpha 2 FC Top Ten Within Default Mode Network Connections

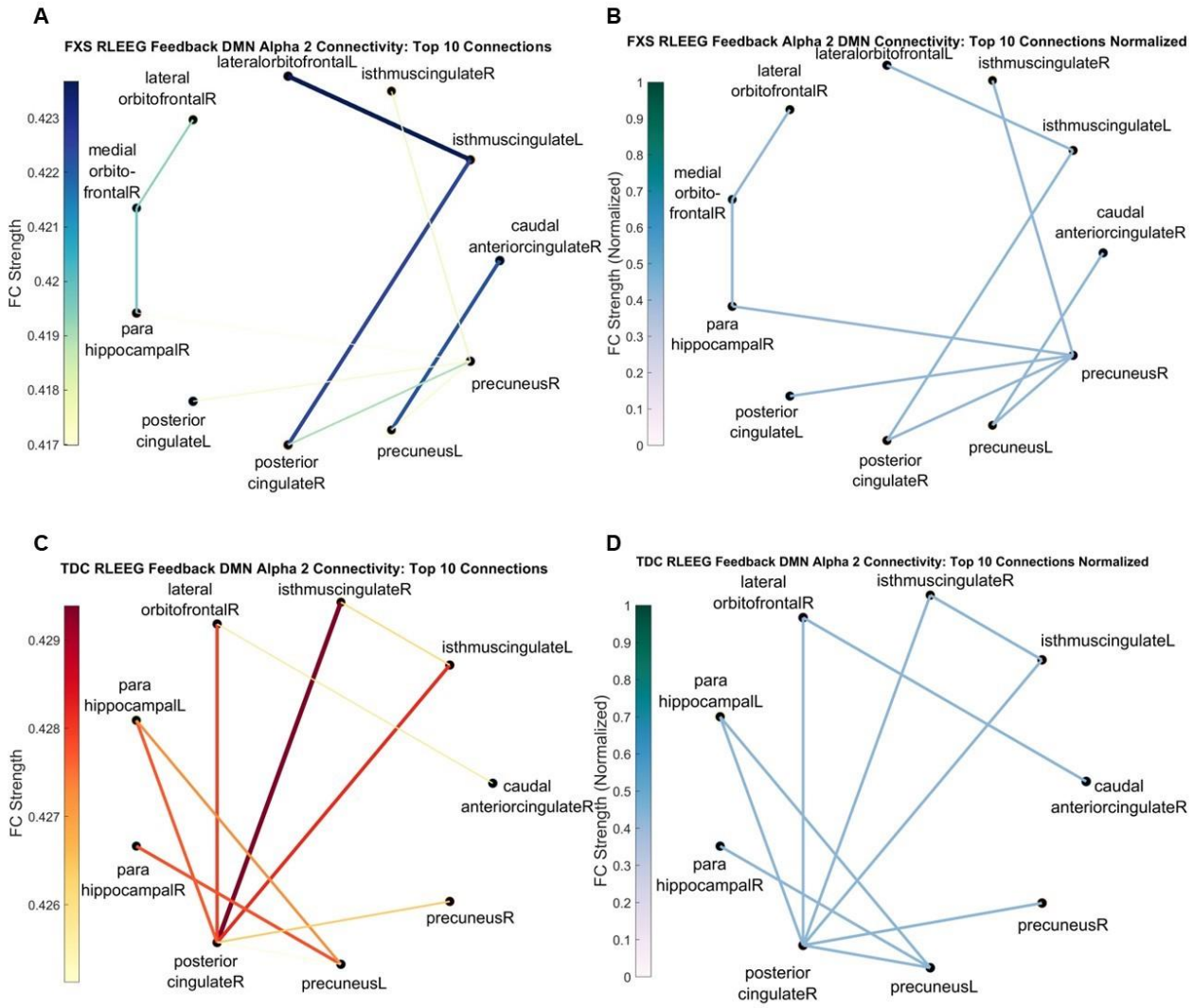

Note. Normalized plots were normalized to the full FC scale to help to visualize some of the smaller, and thus barely visible, connections in A and C. **A)** FXS top ten alpha 2 FC within network connections for feedback DMN (same as plot B). **B)** FXS top ten connections normalized to the full dWPLI scale. **C)** TDC top ten alpha 2 FC within network connections for feedback DMN (same as plot D). **D)** TDC top ten connections normalized to the full dWPLI scale.

Statistically, DMN Connection 1 was significantly different between groups where FXS exhibited reduced alpha 2 FC for the strongest TDC connection (*M* rank = 32.11) compared to TDC (*M* rank = 46.27), *N* = 79, *z* = -2.72, *p* = .012, *r* = -.31. However, DMN Connection 2 was not significantly different between groups where FXS exhibited comparable alpha 2 FC (*M* rank = 39.51) to TDC (*M* rank = 40.39), *N* = 79, *z* = -.17, *p* = 1.00, *r* = -.02. Given DMN Connection 2 was also the second strongest connection for FXS, the group difference suggests some level of FC strength modulation within FC where the most strongly functionally engaged node pairs are of typical strength in FXS. These results suggest alpha 2 FC disruptions in FXS at the network level were driven by specific hub/node disruptions and, given only the top TDC connection differs, suggests possible reduced connectivity with the right posterior cingulate cortex which appeared to serve as a typical hub for feedback-related processing in the alpha frequency range. However, the sum score representing the individual group top ten connections for each group was not significantly different between groups where FXS had similar alpha 2 FC (*M* rank = 36.40) compared to TDC (*M* rank = 42.86), *N* = 79, *z* = -1.24, *p* = .214, *r* = -.14. As the sum score was not significantly different between groups, DMN alpha 2 connectivity was likely more diffusely disrupted for FXS where some disruptions to right posterior cingulate cortex were present, or disruptions were more evidence in the lack of increased connectivity with the right posterior cingulate cortex.

For the SN, the unique nodes were identical between FXS and TDC where both had seven nodes. The majority of the FXS top ten connections (*N* = 7 connections) involved the supramarginal nodes with most centered on the right supramarginal node. Only half of the TDC connections involved the supramarginal nodes and were more distributed between left and right relative to FXS.

The strongest connections for TDC both involved the right supramarginal node where the strongest connection for TDC (SN Connection 1) was between the left and right supramarginal nodes, which was also a top ten connection in FXS of moderate strength. The second strongest connection for TDC (SN Connection 2) was between the right supramarginal node and the right caudal middle frontal node which was also a strong connection for FXS. For FXS, the strongest connections both included the right rostral middle frontal node where the strongest connection was between the right rostral middle frontal node and the right supramarginal node which was not a top ten connection for TDC. However, the second strongest connection for FXS, which was between the right rostral middle frontal node and the left insula node, was a top ten connection for TDC, though one of lower strength relative to other TDC connections (Figure 97).

Figure 97.

Feedback: Alpha 2 FC Top Ten Within Salience Network Connections

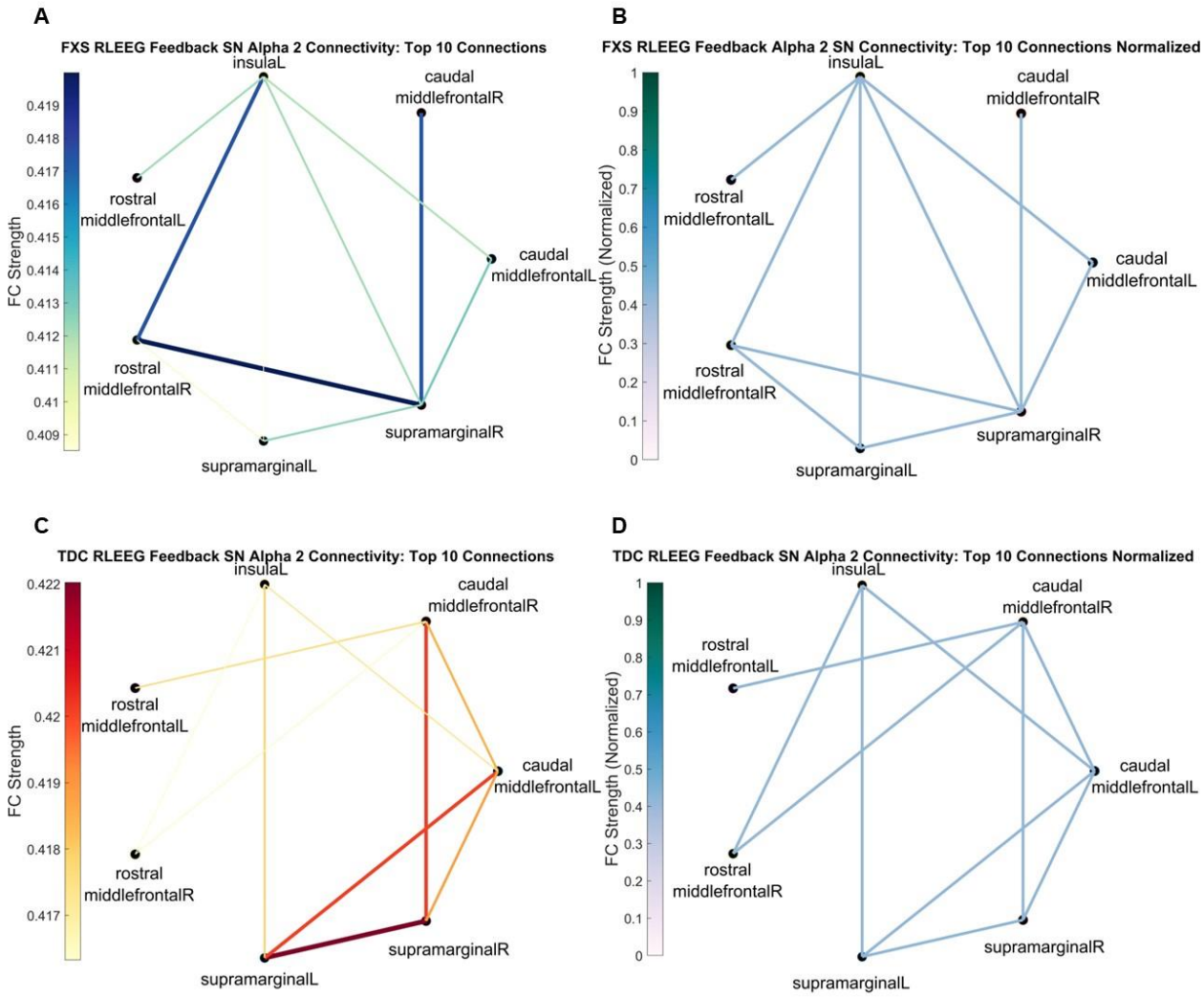

Note. Normalized plots were normalized to the full FC scale to help to visualize some of the smaller, and thus barely visible, connections in A and C. **A)** FXS top ten alpha 2 FC within network connections for feedback SN (same as plot B). **B)** FXS top ten connections normalized to the full dWPLI scale. **C)** TDC top ten alpha 2 FC within network connections for feedback SN (same as plot D). **D)** TDC top ten connections normalized to the full dWPLI scale.

Statistically, SN Connection 1 (N = 79, z = -1.04, p = .600, r = -.12) and SN Connection 2 (N = 79, z = -.22, p = 1.00, r = -.02) were not significantly different between groups where FXS had comparable alpha 2 FC for the strongest TDC connections (SN Connection 1: M rank = 37.00; SN Connection 2: M rank = 39.37) compared to TDC (SN Connection 1: M rank = 42.39; SN Connection 2: M rank = 40.50) on the top connections for TDC in the SN. The sum score representing the individual group top ten connections for each group was also not significantly different between groups where FXS exhibited similar alpha FC across the sum of the top ten FXS connections (M rank = 36.63) compared to the sum of the top ten TDC connections (M rank = 42.68), N = 79, z = -1.17, p = .244, r = -.13. Overall, these results indicate that reduced alpha 2 FC in the SN for feedback related data is more diffusely spread across the whole network rather than representative of individual node disruptions or network reorganization.

Lastly, the top connections in alpha 2 within control network were evaluated despite no group differences on whole network FC for consistency with DMN and SN and the ability to compare alpha 2 FC from feedback data to both stimulus and pre-stimulus periods.

The unique nodes differed between groups where FXS had more nodes (N = 10) compared to TDC (N = 9) where seven nodes were overlapping between groups. The left caudal middle frontal node was present for FXS where the right caudal middle frontal node was present for TDC. The right inferior parietal node was involved in the top ten connections for TDC but not FXS where FXS top ten connections involved the left lateral orbitofrontal node where TDC did not.

The strongest connections for TDC both involved the left precuneus where the strongest connection (Con Connection 1) was between the left precuneus and the left superior parietal nodes, a connection not in the top ten connections for FXS. The second strongest connection for

TDC (Con Connection 2) was between the left precuneus node and the left caudal middle frontal node which was also not in the FXS top ten connections. The top two connections for FXS both involved the left inferior parietal node where the strongest connection for FXS was between the left inferior parietal and the left middle temporal nodes which was not a connection present in the TDC top ten connections. The second strongest connection for FXS was between the left inferior parietal and the left superior parietal nodes which was a top ten connection of moderate strength for TDC (Figure 98).

Figure 98.

Feedback: Alpha 2 FC Top Ten Within Control Network Connections

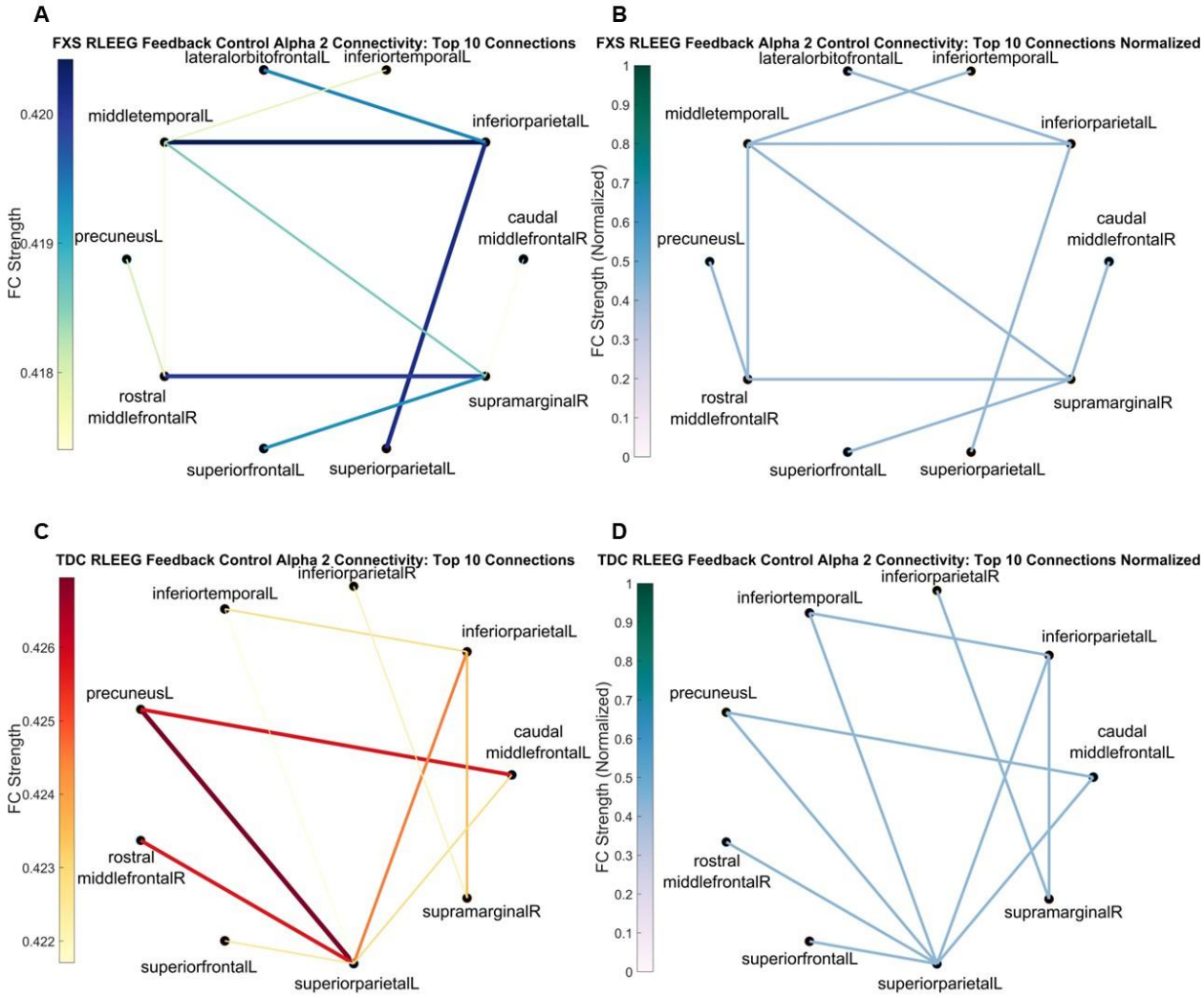

Note. Normalized plots were normalized to the full FC scale to help to visualize some of the smaller, and thus barely visible, connections in A and C. **A)** FXS top ten alpha 2 FC within network connections for feedback control network (same as plot B). **B)** FXS top ten connections normalized to the full dWPLI scale. **C)** TDC top ten alpha 2 FC within network connections for feedback control network (same as plot D). **D)** TDC top ten connections normalized to the full dWPLI scale.

Statistically, both of strongest connections for TDC were not significantly different between groups (Con Connection 1: $N = 79$, $z = -1.31$, $p = .378$, $r = -.15$; Con Connection 2: $N = 79$, $z = -1.85$, $p = .130$, $r = -.21$) where FXS had comparable alpha 2 FC for the strongest TDC connections (Con Connection 1: *M* rank = 36.20; Con Connection 2: *M* rank = 34.66) compared to TDC (Con Connection 1: *M* rank = 43.02; Con Connection 2: *M* rank = 44.25). Further, the sum score was not significantly different between groups where the sum of the top ten FXS alpha 2 FC connections was similar (*M* rank = 37.17) to the sum of the top ten TDC connections (*M* rank = 42.25), $N = 79$, $z = -.98$, $p = .329$, $r = -.11$. Alpha 2 FC was comparable between groups across the whole network (i.e., no whole network differences) where the lack of group differences may represent more typical control network engagement during feedback for FXS in the alpha band.

Stimulus Period Strongest Individual Connections

Theta FC. Top connections for theta FC were evaluated first across networks for stimulus period data starting with DMN. The number of unique nodes were different between groups where FXS had less unique nodes represented in the top ten connections ($N = 8$) compared to TDC ($N = 11$) with six nodes overlapping.

Several of the top ten TDC connections were centered on the right precuneus and the right posterior cingulate, specifically both of the strongest connections for TDC involved the right posterior cingulate node where the strongest stimulus DMN connection for TDC (DMN Connection 1) was between the right posterior cingulate node and the right precuneus node. The second strongest connection (DMN Connection 2) was between the right posterior cingulate node and the left precuneus node. Both of the top two TDC connections were in the FXS top ten connections where the top TDC connection was the second strongest connection for FXS. The

strongest DMN connections for FXS during the stimulus period also centered on the right posterior cingulate node, similarly to TDC, but centered more on the right caudal anterior cingulate than the right precuneus. For FXS, the strongest DMN theta FC connection was between the right caudal anterior cingulate node and the right isthmus cingulate node which was not a top ten connection for TDC. The second strongest connection for FXS was the strongest connection for TDC: right posterior cingulate node to right precuneus node (Figure 99). Only three of the top ten connections overlapped between groups.

Figure 99.

Stimulus: Theta FC Top Ten Within Default Mode Network Connections

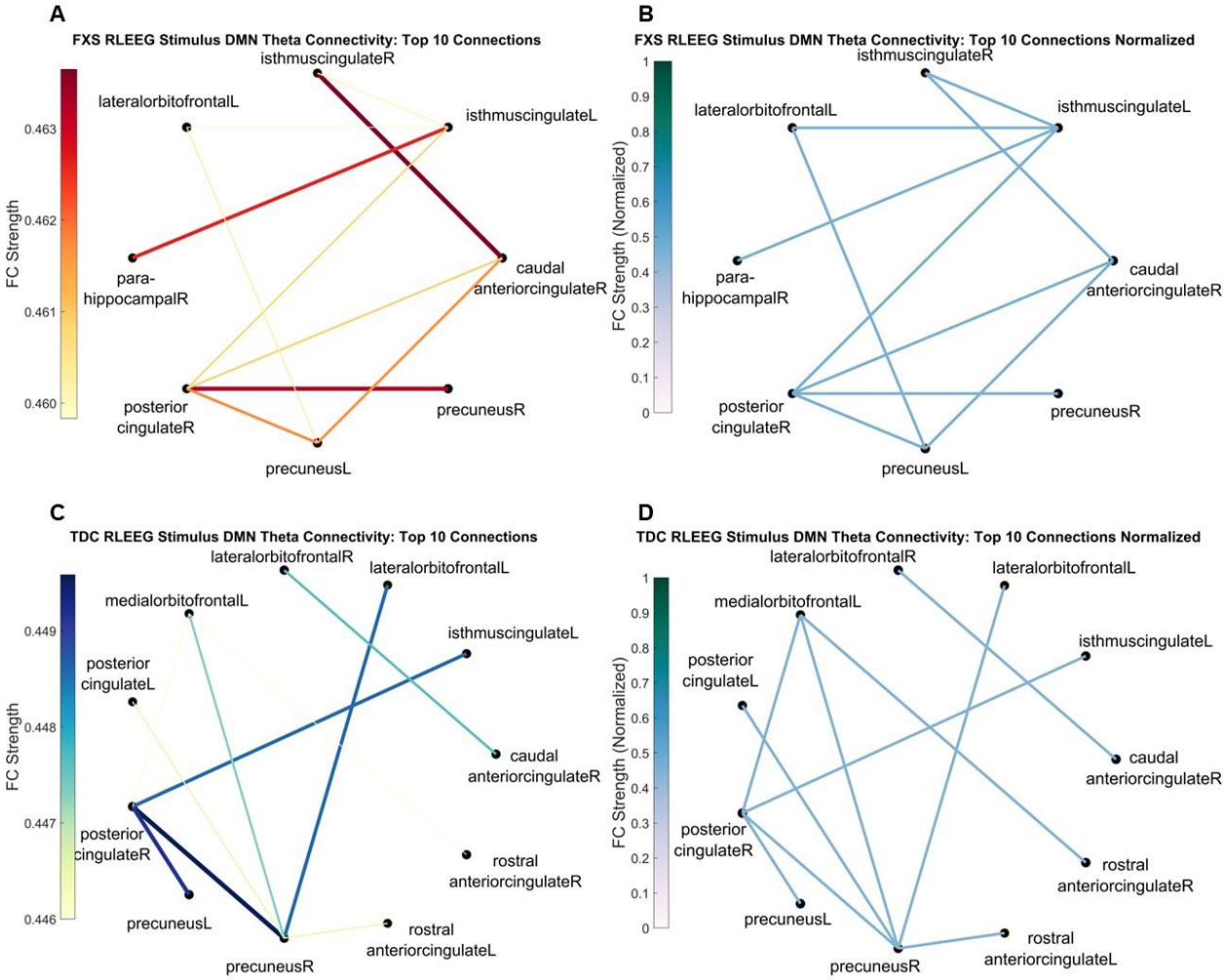

Note. Normalized plots were normalized to the full FC scale to help to visualize some of the smaller, and thus barely visible, connections in A and C. **A)** FXS top ten theta FC within network connections for stimulus DMN (same as plot B). **B)** FXS top ten connections normalized to the full dWPLI scale. **C)** TDC top ten theta FC within network connections for stimulus DMN (same as plot D). **D)** TDC top ten connections normalized to the full dWPLI scale.

Statistically, both DMN Connection 1 ($N = 79$, $z = 2.36$, $p = .036$, $r = .27$) and Connection 2 ($N = 79$, $z = 2.38$, $p = .017$, $r = .27$) were significantly different between groups where FXS had increased theta FC on the strongest two TDC connections (DMN Connection 1: *M* rank = 46.83; DMN Connection 2: *M* rank = 48.89) compared to TDC (DMN Connection 1: *M* rank = 34.57; DMN Connection 2: *M* rank = 34.52). Further, the sum score representing the individual group top ten connections for each group was significantly different between groups where FXS exhibited increased theta FC across the top ten FXS connections (*M* rank = 51.37) compared to theta FC across the top ten TDC connections (*M* rank = 30.95), $N = 79$, $z = 3.92$, $p < .001$, $r = .44$. Combined, these results suggest a shift in FC magnitude within the DMN for FXS compared to TDC. Again, the top TDC connection was the second strongest connection for FXS and DMN Connection 2 was also in the FXS top ten which indicates a possible shift in magnitude of theta FC rather than a network architecture shift. However, only three connections in the top ten overlapped between groups where the group difference on the sum of the top ten connections possibly suggests the whole network shifted to the use of a different set of hubs, or even the use of subnetworks with variable architecture, as the pattern of connectivity differences was broader but not quite diffuse across the whole network. Importantly, the shift away from the right precuneus as a dominant node in DMN and increased magnitude of FC in nodes connected to the right posterior cingulate for FXS may reflect disruptions to typical DMN function. Overall, these results point to a shift in theta FC magnitude for a specific set of network hubs rather than diffuse connectivity increases.

For stimulus SN theta FC, the unique nodes involved in the top ten connections were highly similar between groups where FXS had less nodes involved in the top ten connections ($N = 6$) compared to TDC ($N = 8$) where all six FXS nodes overlapped with TDC. Only the right

caudal middle frontal node was different between groups. In the SN, top connections were centered on the left and right insula nodes in both groups.

The top connection for TDC (SN Connection 1) was between the left insula node and the right caudal middle node which was also the top connection for FXS. The second strongest connection for TDC (SN Connection 2) was between the right insula node and the right rostral middle node which was a top connection for FXS of moderate strength relative to other FXS top connections. For FXS, both of the strongest connections involved the left insula where the strongest connection was between the left insula node and the right caudal middle frontal node, same as TDC. The second strongest connection for FXS was between the left insula node and the right supramarginal node which was a top ten connection for TDC but one of lesser strength compared to other TDC top connections. Of note, the top FXS connection was between the same brain areas as the top TDC connection but to the caudal middle frontal node in the opposite hemisphere (Figure 100).

Figure 100.

Stimulus: Theta FC Top Ten Within Salience Network Connections

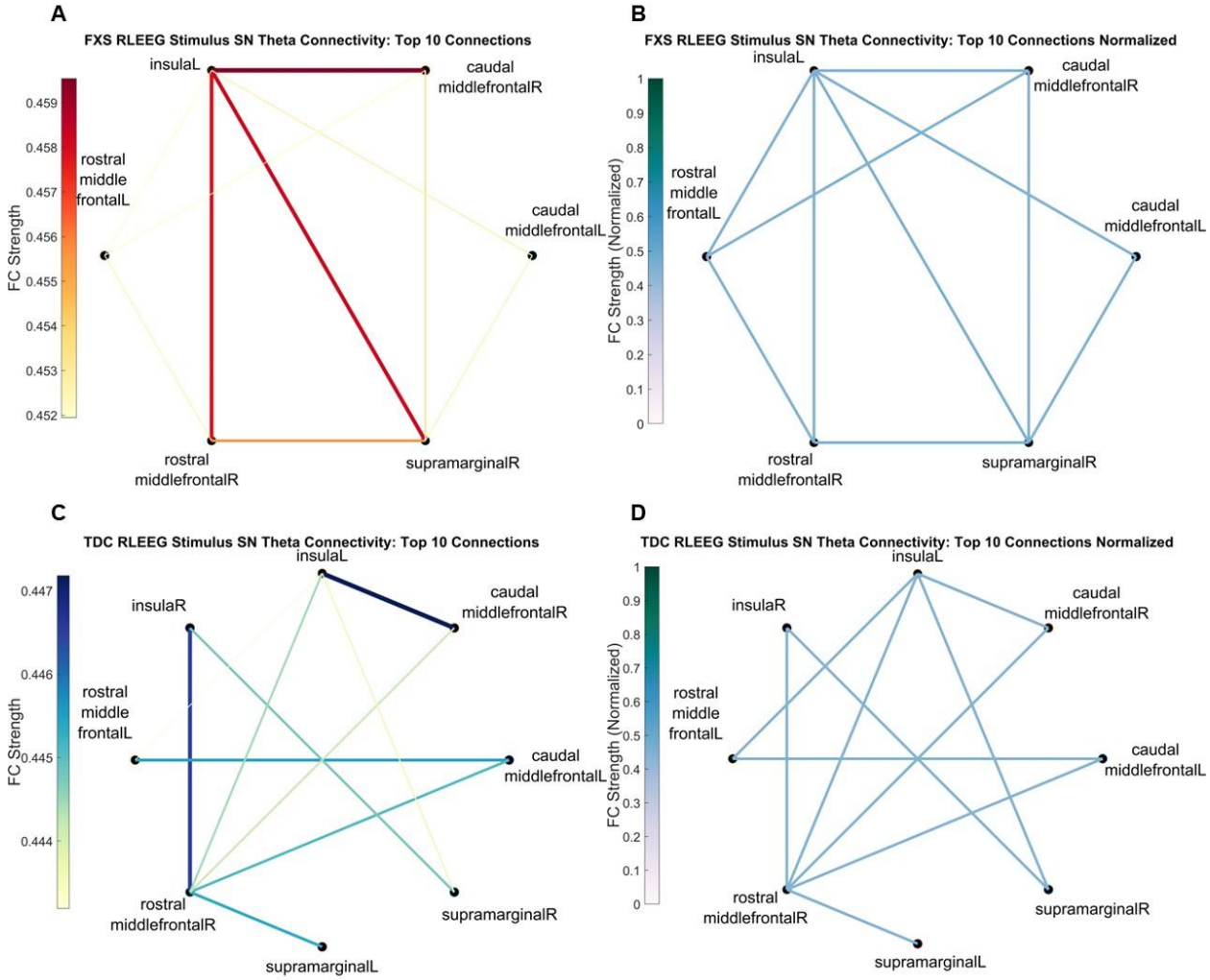

Note. Normalized plots were normalized to the full FC scale to help to visualize some of the smaller, and thus barely visible, connections in A and C. **A)** FXS top ten theta FC within network connections for stimulus SN (same as plot B). **B)** FXS top ten connections normalized to the full dWPLI scale. **C)** TDC top ten theta FC within network connections for stimulus SN (same as plot D). **D)** TDC top ten connections normalized to the full dWPLI scale.

Statistically, SN Connection 1 was significantly different between groups where FXS exhibited stronger theta FC for the strongest TDC connection (*M* rank = 46.86) compared to TDC (*M* rank = 34.55), $N = 79$, $z = 2.37$, $p = .036$, $r = .23$. The top connection for both groups was the same (left insula node to right caudal middle frontal node) where the difference suggests comparable network anatomy for stimulus processing where whole network group differences were generally representative of a magnitude shift in the strongest network connections. SN Connection 2 was not significantly different between groups where FXS exhibited comparable theta FC (*M* rank = 41.49) to TDC (*M* rank = 38.82), $N = 79$, $z = .51$, $p = 1.00$, $r = .06$. The sum score representing the individual group top ten connections for each group was significantly different between groups where FXS exhibited increased theta FC across the top ten FXS connections (*M* rank = 48.51) compared to the sum of the top ten TDC connections (*M* rank = 33.23), $N = 79$, $z = 2.94$, $p = .003$, $r = .33$. Given only four connections overlapped between groups, these results may represent potential subnetwork differences where a separate set of nodes were working together to accomplish stimulus-related neural processes in FXS compared to TDC. A difference in magnitude of the shared strongest connection paired with the top ten connection sum score differences, however, points to an overall magnitude difference between groups where the sum score likely reflects a shift in theta FC magnitude for the top connections.

Lastly, top connections for theta FC in the control network during the stimulus periods were evaluated. The number of unique control network nodes for theta FC on stimulus data differed between groups where TDC had more nodes ($N = 11$) involved in the top ten connections than FXS ($N = 10$). The top connections were also fairly similar where eight nodes overlapped between groups. However, none of the top connections overlapped between groups.

Several of the TDC top ten connections involved the right rostral middle frontal node and the left middle temporal node, including the strongest connection for TDC (Con Connection 1). The second strongest connection for TDC (Con Connection 2) was between the right inferior parietal node and the left inferior parietal node. The strongest connections for FXS both involved the left inferior parietal node where the strongest connection was between the left inferior parietal node and the left lateral orbitofrontal node. The second strongest FXS connection was between the left inferior parietal node and the left middle temporal node (Figure 101). Again, none of the top ten connections overlapped between groups indicating a shift in primary control network architecture.

Figure 101.

Stimulus: Theta FC Top Ten Within Control Network Connections

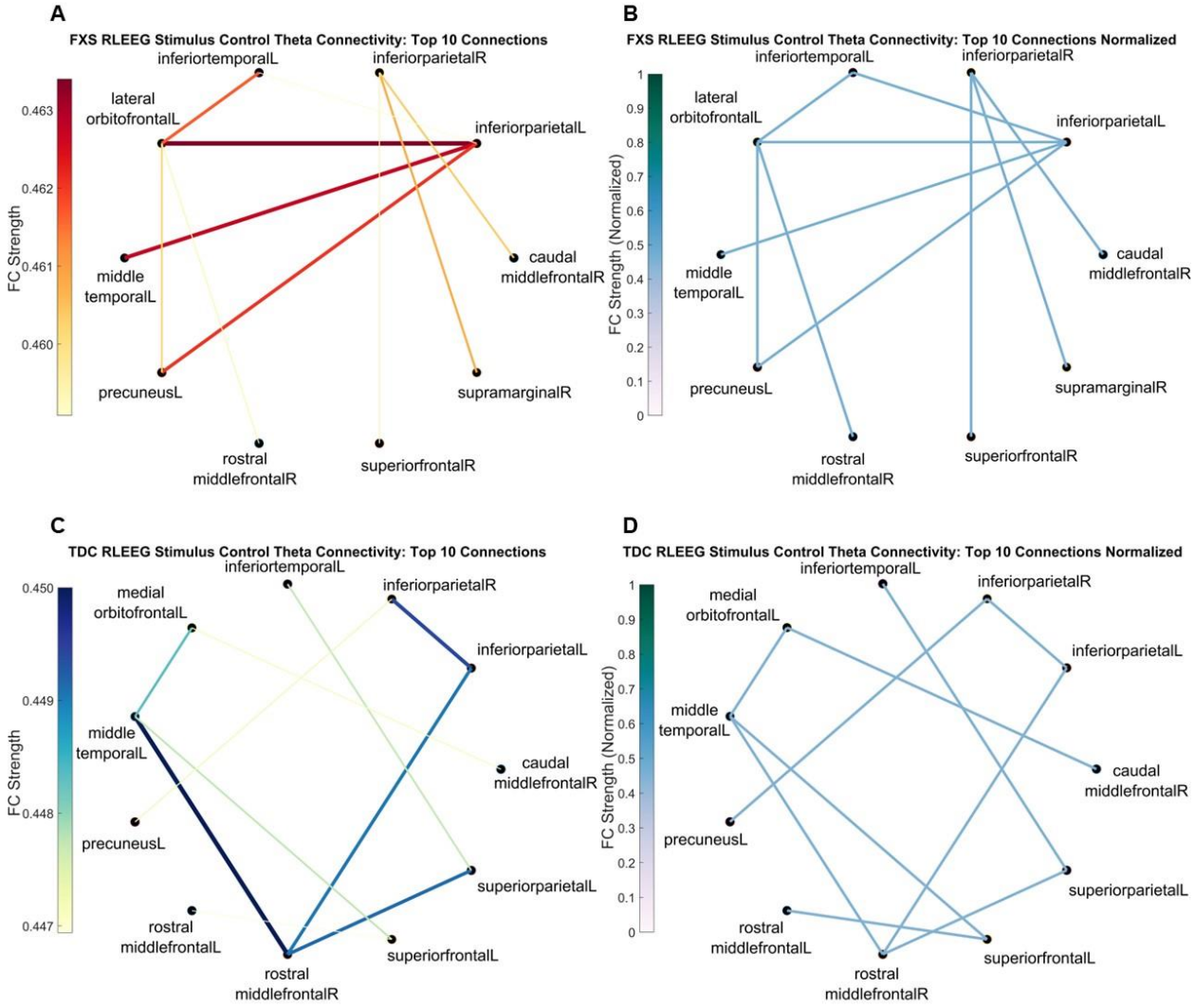

Note. Normalized plots were normalized to the full FC scale to help to visualize some of the smaller, and thus barely visible, connections in A and C. **A)** FXS top ten theta FC within network connections for stimulus control network (same as plot B). **B)** FXS top ten connections normalized to the full dWPLI scale. **C)** TDC top ten theta FC within network connections for stimulus control network (same as plot D). **D)** TDC top ten connections normalized to the full dWPLI scale.

Statistically, both Con Connection 1 ($N = 79$, $z = .10$, $p = 1.00$, $r = .01$) and Connection 2 ($N = 79$, $z = 1.80$, $p = .144$, $r = .20$) were not significantly different between groups where FXS had comparable theta FC for the strongest TDC connections (Con Connection 1: *M* rank = 40.29; Con Connection 2 : *M* rank = 45.20) compared to TDC (Con Connection 1: *M* rank = 39.77; Con Connection 2: *M* rank = 35.86). However, the sum score representing the individual group top ten connections for each group was significantly different between groups where FXS exhibited increased theta FC across the top ten FXS connections (*M* rank = 51.91) compared to the sum of the top ten TDC connections (*M* rank = 30.52), $N = 79$, $z = 4.12$, $p < .001$, $r = .46$. The lack of significant differences in the top two typical control connections suggests broader network disruptions where the significant network sum indicates possible sub-network differences and different sets of network connections were used to accomplish similar, stimulus-related neural processes. The sum score difference further supports the conclusion that the primary network architecture used during stimulus-related processing was significantly different in FXS compared to TDC where whole network group differences indicate a focal shift in primary node use.

Alpha 2 FC. Next, alpha 2 FC top connections for stimulus period data were evaluated starting with DMN. In DMN, FXS had more unique nodes involved in the top ten connections (*N* = 12) than TDC (*N* = 9) where the nodes involved in TDC top connection all overlapped with FXS nodes.

Over half of the top ten connections for TDC involve the precuneus, including both of the strongest TDC connections, which involved the right precuneus. Specifically, the strongest connection for TDC (DMN Connection 1) was between the right precuneus node and the right parahippocampal node, which was not a FXS top ten connection. The second strongest TDC connection (DMN Connection 2) was between the right precuneus and the right posterior cingulate nodes which was a top ten connection for FXS of moderate strength (third strongest connection for FXS). Only two of the top ten FXS connections involved the precuneus and instead centered on the isthmus nodes. The top two FXS connections both involved the right parahippocampal node where the strongest connection was between the right parahippocampal node and the right isthmus node. The second strongest FXS connection was between the right parahippocampal node and the left precuneus, which was a top ten connection for TDC of lower strength relative to other TDC connections. Neither of the top connections for FXS were in the TDC top ten connections (Figure 102).

Figure 102.

Stimulus: Alpha 2 FC Top Ten Within Default Mode Network Connections

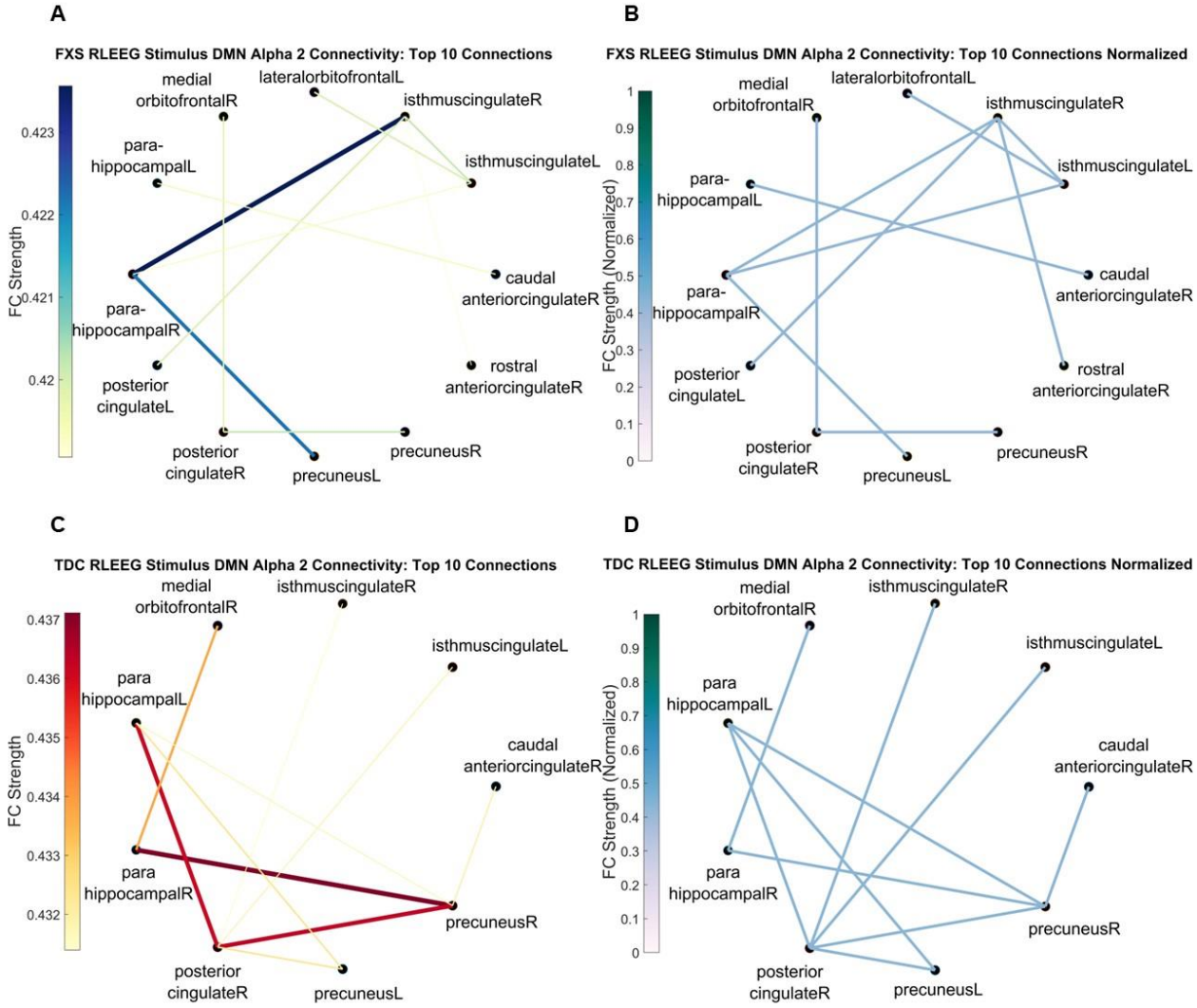

Note. Normalized plots were normalized to the full FC scale to help to visualize some of the smaller, and thus barely visible, connections in A and C. **A)** FXS top ten alpha 2 FC within network connections for stimulus DMN (same as plot B). **B)** FXS top ten connections normalized to the full dWPLI scale. **C)** TDC top ten alpha 2 FC within network connections for stimulus DMN (same as plot D). **D)** TDC top ten connections normalized to the full dWPLI scale.

Statistically, DMN connection 1 was significantly different between groups where FXS exhibited reduced alpha 2 FC for the strongest TDC connection (*M* rank = 32.51) compared to TDC (*M* rank = 45.95), *N* = 79, *z* = -2.59, *p* = .020, *r* = -.29. However, DMN Connection 2 was not significantly different between groups, as FXS exhibited comparable alpha 2 FC (*M* rank = 35.34) to TDC (*M* rank = 43.70), *N* = 79, *z* = -1.61, *p* = .216, *r* = -.18. As DMN Connection 1 was a FXS connection of lower strength and DMN Connection 2 was a FXS connection of moderate strength, these results suggest that the top connections for both groups may be similar in strength but overall, alpha 2 FC was distributed between different nodes across groups. Ultimately, alpha 2 FC group differences were not concentrated in typical or TDC-dominate connections suggesting FXS partially deviated from typical DMN architecture. The sum score representing the individual group top ten connections for each group was significantly different between groups where FXS exhibited reduced alpha 2 FC across the top ten FXS connections (*M* rank = 33.14) compared to the sum of the top ten connections for TDC (*M* rank = 45.45), *N* = 79, *z* = -2.37, *p* = .018, *r* = -.27. The sum score difference adds support to the conclusion that subnetwork architecture in DMN may differ where connectivity was more broadly disrupted in FXS but not diffusely reduced across the whole network.

For SN top alpha FC connections, the unique nodes were similar with only one node difference across groups, the left rostral middle frontal node involved in FXS top ten connection but not TDC. All other nodes (*N* = 7) overlapped.

The two strongest TDC connections both involved the left supramarginal node where the strongest TDC connection (SN Connection 1) was between the left supramarginal node and the left insula which was a top ten connection for FXS. The second strongest TDC connection (SN Connection 2) was between the left supramarginal node and the right rostral middle frontal node

which was not a top ten connection for FXS. The strongest connection for FXS was between the right caudal middle frontal node and the left supramarginal node which was a top ten connection for TDC of lower strength relative to other TDC top connections. The second strongest was between the right rostral middle frontal node and the right supramarginal node and was also not a top ten connection for TDC (Figure 103).

Figure 103.

Stimulus: Alpha 2 FC Top Ten Within Salience Network Connections

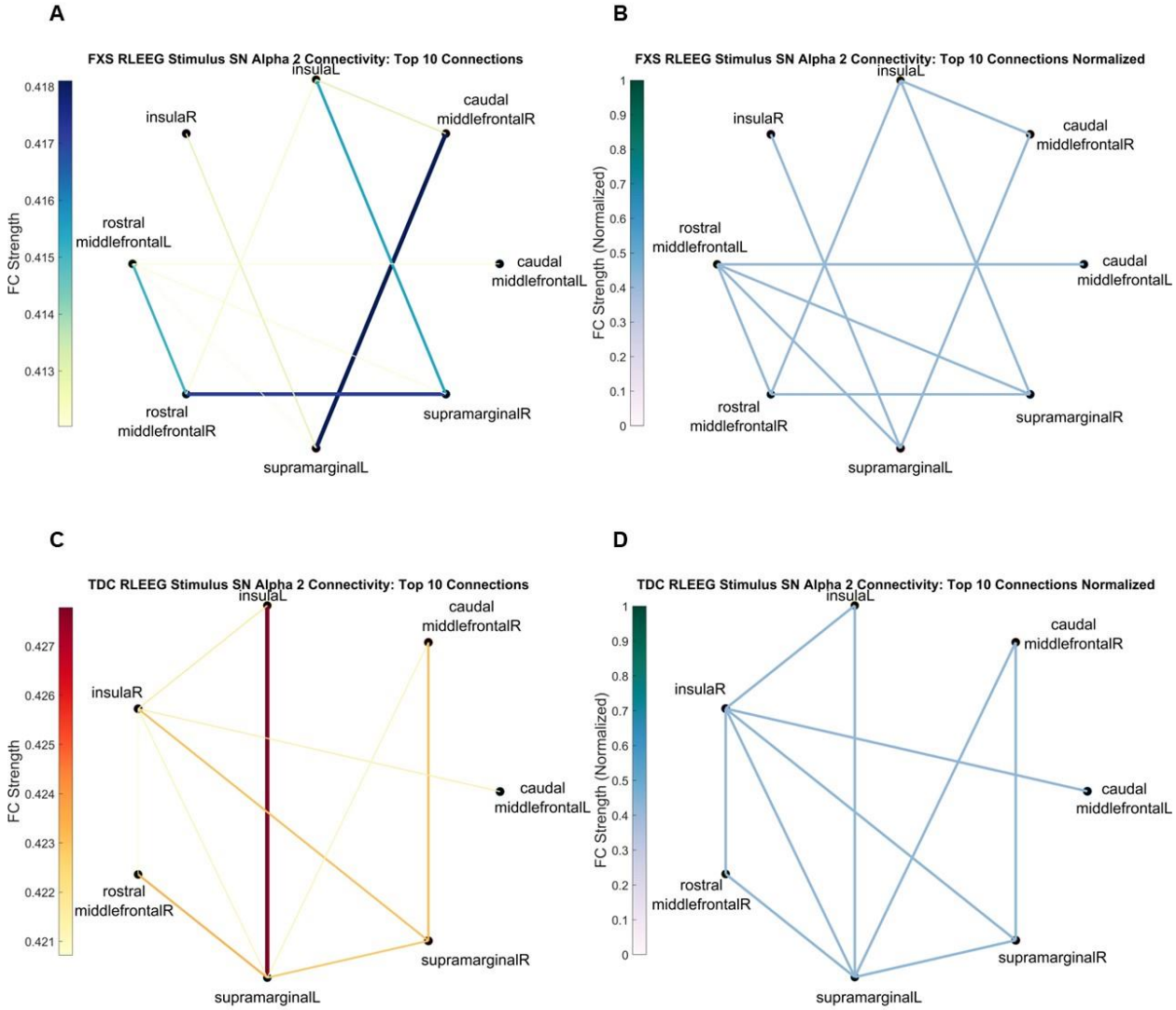

Note. Normalized plots were normalized to the full FC scale to help to visualize some of the smaller, and thus barely visible, connections in A and C. **A)** FXS top ten alpha 2 FC within network connections for stimulus SN (same as plot B). **B)** FXS top ten connections normalized to the full dWPLI scale. **C)** TDC top ten alpha 2 FC within network connections for stimulus SN (same as plot D). **D)** TDC top ten connections normalized to the full dWPLI scale.

Statistically, SN Connection 1 was statistically different between groups where FXS exhibited reduced alpha 2 FC on the top TDC connection (*M* rank = 32.77) compared to TDC (*M* rank = 45.75), *N* = 79, *z* = -2.50, *p* = .026, *r* = -.28. SN Connection 2 was not statistically different between groups after Bonferroni correction but trended towards significance where FXS exhibited marginally reduced alpha FC (*M* rank = 33.63) compared to TDC (*M* rank = 45.07), *N* = 79, *z* = -2.20, *p* = .056, *r* = -.25. These results suggest FXS partially deviated from typical SN architecture for SN-related stimulus processing. The sum score representing the individual group top ten connections for each group was also significantly different between groups where FXS exhibited reduced alpha 2 FC across the top ten FXS connections (*M* rank = 33.80) compared to the sum of the top ten connections for TDC (*M* rank = 44.93), *N* = 79, *z* = -2.01, *p* = .044, *r* = -.23. Together, these results suggest FC disruptions are driven by deviation from typical alpha 2 FC in the strongest typical pathways, as connectivity was not concentrated in TDC-dominate paths for FXS where both primary drivers and difference between the top ten connections for individual groups drive the overarching alpha 2 FC differences in SN.

Lastly, the top alpha 2 FC connections for the control network during stimulus periods were evaluated where FXS had more unique nodes represented in the top ten connection (*N* = 10) compared to TDC (*N* = 8). Out of the eight nodes for TDC, six nodes overlapped with FXS.

The top ten TDC connections centered on the left precuneus, the left superior parietal, and the right inferior parietal nodes. In fact, the two strongest connections both involved the right inferior parietal node with the strongest TDC connection (Con Connection 1) between the right inferior parietal node and the left precuneus. The second strongest connection for TDC (Con Connection 2) was between the right inferior parietal node and the left middle temporal node. Neither Con Connection 1 nor Con Connection 2 were in the FXS top ten connections. The FXS

top connections were also centered on the left superior parietal node but centered on the left inferior parietal node instead of the right, unlike TDC. The strongest connection for FXS was between the left superior parietal node and the right supramarginal node which was a top ten connection for TDC of moderate strength. The second strongest connection for FXS was between the left inferior temporal node and the left caudal middle frontal node (Figure 104).

Figure 104.

Stimulus: Alpha 2 FC Top Ten Within Control Network Connections

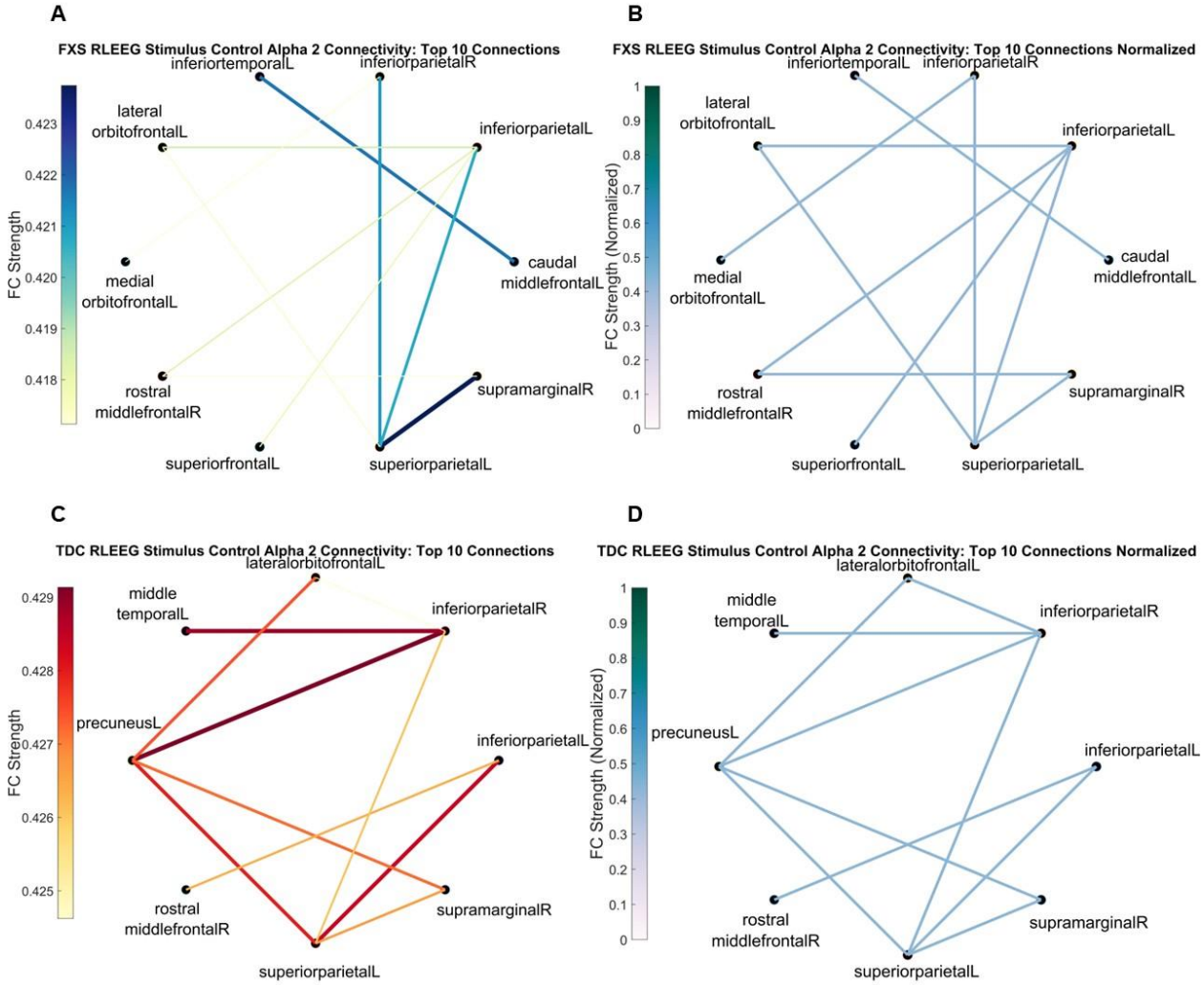

Note. Normalized plots were normalized to the full FC scale to help to visualize some of the smaller, and thus barely visible, connections in A and C. **A)** FXS top ten alpha 2 FC within network connections for stimulus control network (same as plot B). **B)** FXS top ten connections normalized to the full dWPLI scale. **C)** TDC top ten alpha 2 FC within network connections for stimulus control network (same as plot D). **D)** TDC top ten connections normalized to the full dWPLI scale.

Statistically, Con Connection 1 was not significantly different between groups after Bonferroni correction but trended toward significance where alpha 2 FC was marginally reduced for the top TDC connection in FXS (*M* rank = 35.57) compared to TDC (*M* rank = 45.91), *N* = 79, *z* = -2.18, *p* = .058, *r* = -.25. However, Con Connection 2 was not significantly different between groups where FXS (*M* rank = 36.66) and TDC (*M* rank = 42.66) had similar alpha 2 FC, *N* = 79, *z* = -1.52, *p* = .258, *r* = -.17. The sum score representing the individual top ten connections for each group was not significantly different between groups where FXS exhibited comparable alpha 2 FC across the top ten FXS connections (*M* rank = 36.03) compared to the sum of the top ten connections for TDC (*M* rank = 43.16), *N* = 79, *z* = -1.37, *p* = .170, *r* = -.15. These results suggest the alpha 2 FC group differences were driven by a diffuse disruption to alpha 2 FC in FXS control network during stimulus processing rather than specific node connection disruptions. Though, alpha 2 FC was marginally different for the connection between the right inferior parietal node and the left precuneus suggesting potential disruptions there.

Pre-stimulus Strongest Individual Connections

Theta FC. Top connections for theta FC were evaluated first across networks starting with DMN. The number of unique nodes involved in the top theta FC connections differed between groups where FXS had less nodes involved in the top ten connections (*N* = 10) compared to TDC (*N* = 11) where nine nodes overlapped.

The strongest connection for TDC (DMN Connection 1) was between the right rostral anterior cingulate node and the left medial orbitofrontal node where the second strongest connection (DMN Connection 2) was between the right lateral orbitofrontal node and the left precuneus node. Neither of the strongest TDC connections were in the FXS top ten connections. The strongest FXS connection was between the right isthmus cingulate and the left medial

orbitofrontal nodes where the second strongest connection was between the right caudal anterior cingulate and the right precuneus nodes. Similarly to TDC, both of the strongest FXS connections were not in the TDC top ten connections (Figure 105).

Figure 105.

Pre-stimulus: Theta FC Top Ten Within Default Mode Network Connections

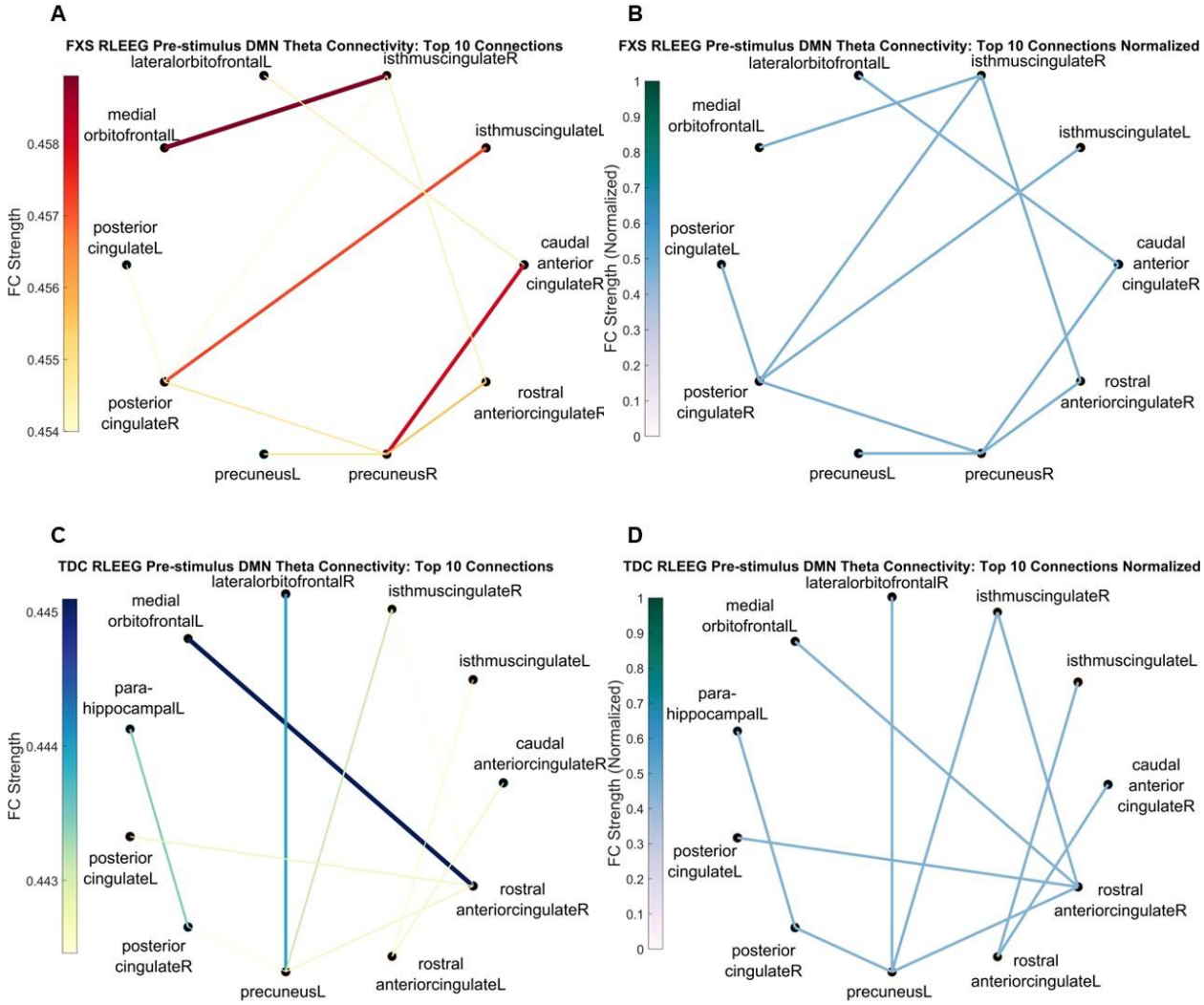

Note. Normalized plots were normalized to the full FC scale to help to visualize some of the smaller, and thus barely visible, connections in A and C. **A)** FXS top ten theta FC within network connections for pre-stimulus DMN (same as plot B). **B)** FXS top ten connections normalized to the full dWPLI scale. **C)** TDC top ten theta FC within network connections for pre-stimulus DMN (same as plot D). **D)** TDC top ten connections normalized to the full dWPLI scale.

Statistically, DMN Connection 1 ($N = 79$, $z = 1.15$, $p = .504$, $r = .13$) and DMN Connection 2 ($N = 79$, $z = -.28$, $p = 1.00$, $r = -.03$) were not significantly different between groups where FXS had comparable theta FC (DMN Connection 1: *M* rank = 43.31; DMN Connection 2: *M* rank = 39.20) to TDC (DMN Connection 1: *M* rank = 37.36; DMN Connection 2: *M* rank = 40.64). Similarity in theta FC between groups on the TDC strongest connections suggest more diffuse connectivity disruptions in DMN. However, the sum score representing the individual group top ten connections for each group was significantly different between groups where FXS exhibited increased theta FC across the top ten FXS connections (*M* rank = 50.94) compared to the sum of the top ten TDC connections (*M* rank = 31.30), $N = 79$, $z = 3.78$, $p < .001$, $r = .43$. The significant sum score difference suggests broader disruptions centered on architectural differences in SN during pre-stimulus windows rather than diffuse increases across DMN.

For theta FC in SN, the unique nodes involved in the top ten connections were identical between groups. Out of the top ten connections, six involved the supramarginal nodes for FXS, though not the strongest two connections. The TDC top connections were more distributed across the eight unique nodes compared to FXS.

The top two connections for TDC both involved the left rostral middle frontal node where the strongest connection (SN Connection 1) was between the left rostral middle frontal node and the right caudal middle frontal node, which was not a top ten connection for FXS. The second strongest connection for TDC (SN Connection 2) was between the left rostral middle frontal node and the right insula node, which was a top ten connection for FXS, though one of lower strength. For FXS, the top two connection both involved the left insula node where the strongest connection was between the left insula and the right rostral middle frontal nodes, which was also

a top ten connection for TDC of moderate strength (top three). The second strongest connection for FXS was between the left insula node and the right caudal middle frontal node which was not a top ten connection for TDC (Figure 106). Of note, in FXS, several of the weaker top ten connections centered on the left supramarginal node.

Figure 106.

Pre-stimulus: Theta FC Top Ten Within Salience Network Connections

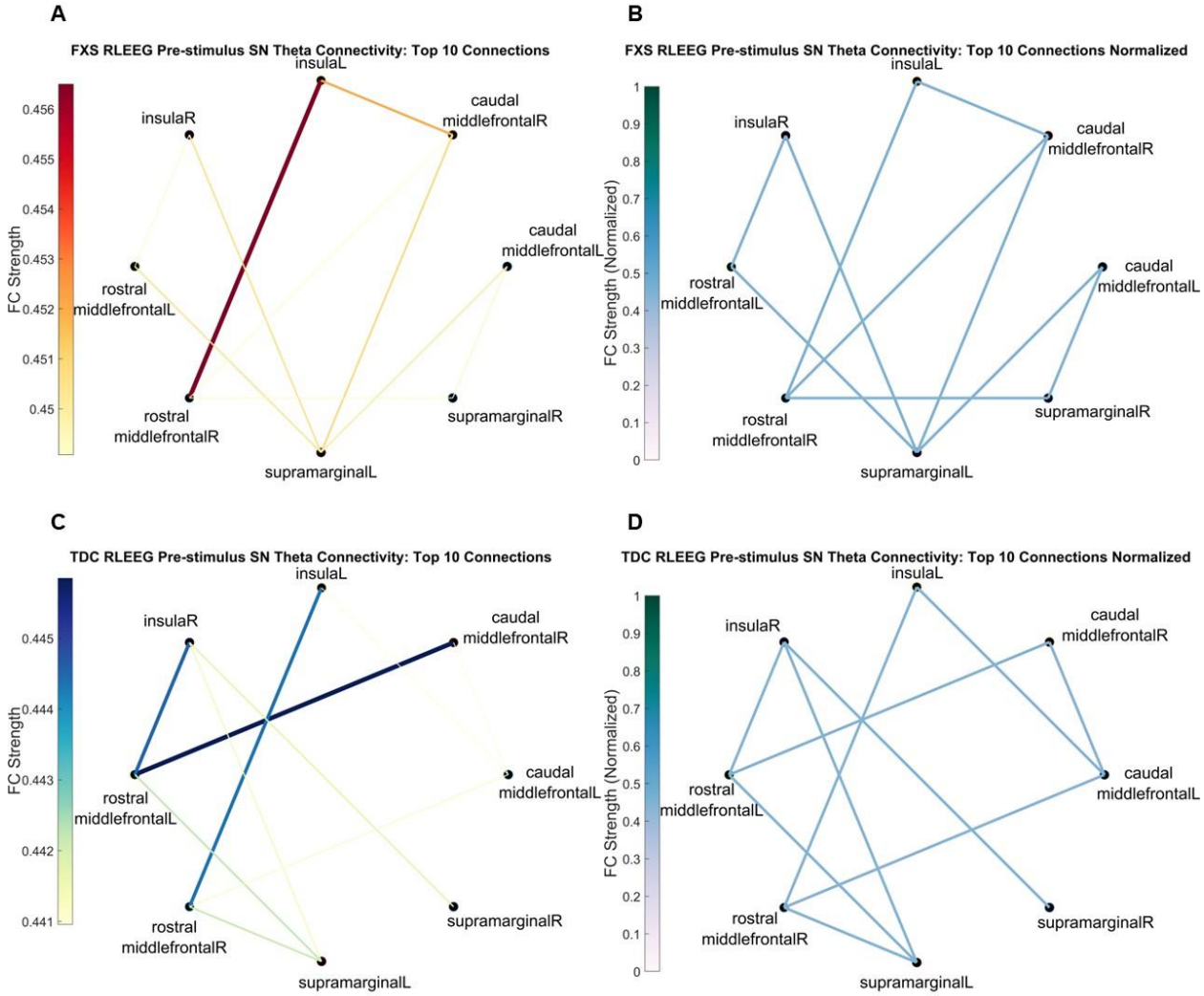

Note. Normalized plots were normalized to the full FC scale to help to visualize some of the smaller, and thus barely visible, connections in A and C. **A)** FXS top ten theta FC within network connections for pre-stimulus SN (same as plot B). **B)** FXS top ten connections normalized to the full dWPLI scale. **C)** TDC top ten theta FC within network connections for pre-stimulus SN (same as plot D). **D)** TDC top ten connections normalized to the full dWPLI scale.

Statistically, SN Connection 1 ($N = 79$, $z = .34$, $p = 1.00$, $r = .04$) and SN Connection 2 ($N = 79$, $z = .42$, $p = 1.00$, $r = .05$) were not significantly different between groups where FXS had comparable theta FC (SN Connection 1: *M* rank = 40.97; SN Connection 2: *M* rank = 41.20) compared to TDC (SN Connection 1: *M* rank = 39.23; SN Connection 2: *M* rank = 39.05) on the top SN connections for TDC. As with DMN, the lack of statistical differences between groups on the top TDC connections suggests more diffuse theta FC disruptions across SN. However, the sum score representing the individual group top ten connections for each group was significantly different between groups where FXS exhibited increased theta FC across the top ten FXS connections (*M* rank = 47.09) compared to the sum of the top ten TDC connections (*M* rank = 34.36), $N = 79$, $z = 2.45$, $p = .014$, $r = .28$. Again, the pattern sum score differences paired with no statistically significant differences on the top TDC connections suggests broader architectural differences in SN driving increased theta FC at the whole network level.

Lastly, the top ten control network connections were evaluated for theta FC. The number of unique nodes was different between groups where FXS had less nodes involved in the top ten connections ($N = 9$) compared to TDC ($N = 10$) with only six overlapping nodes.

The strongest connection for TDC (Con Connection 1) was between the left rostral middle frontal node and the right caudal middle frontal node and the second strongest connection (Con Connection 2) was between the right rostral middle frontal node and the left superior frontal node. Neither of the top TDC connections were in the FXS top ten connections. The strongest FXS connection was between the right caudal middle frontal and the right inferior parietal nodes where the second strongest connection was between the left lateral orbitofrontal and the left superior parietal nodes. As with TDC, neither of top FXS connections were in the TDC top ten (Figure 107).

Figure 107.

Pre-stimulus: Theta FC Top Ten Within Control Network Connections

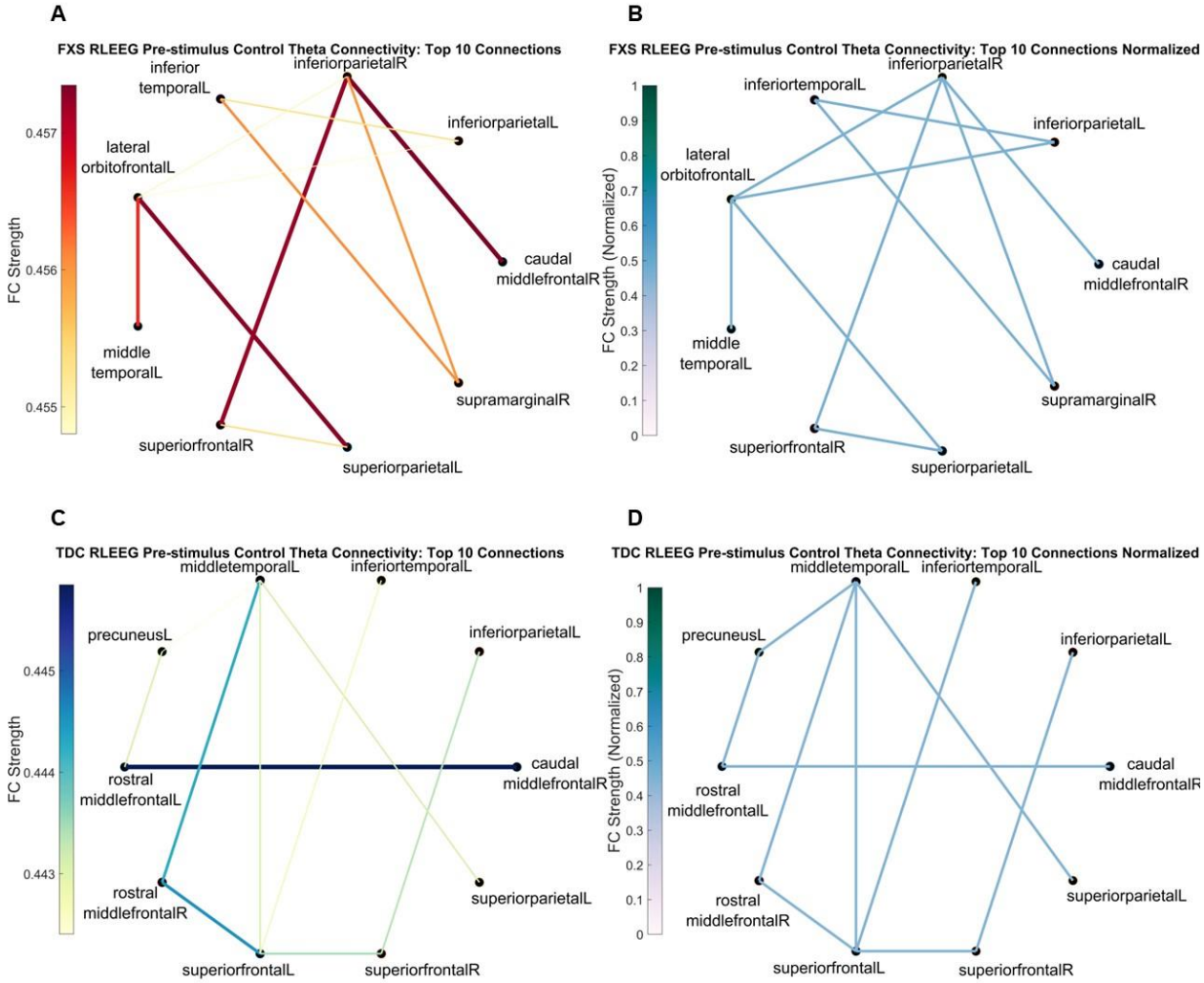

Note. Normalized plots were normalized to the full FC scale to help to visualize some of the smaller, and thus barely visible, connections in A and C. **A)** FXS top ten theta FC within network connections for pre-stimulus control network (same as plot B). **B)** FXS top ten connections normalized to the full dWPLI scale. **C)** TDC top ten theta FC within network connections for pre-stimulus control network (same as plot D). **D)** TDC top ten connections normalized to the full dWPLI scale.

Statistically, Con Connection 1 ($N = 79$, $z = .34$, $p = 1.00$, $r = .04$) and Con Connection 2 ($N = 79$, $z = 1.02$, $p = .618$, $r = .11$) were not significantly different between groups where FXS had comparable theta FC (Con Connection 1: *M* rank = 40.97; Con Connection 2: *M* rank = 42.94) to TDC (Con Connection 1: *M* rank = 39.23; Con Connection 2: *M* rank = 37.66) on the top control network connections for TDC. Similarly to both DMN and SN, the sum score representing the individual group top ten connections for each group was significantly different between groups where FXS exhibited increased theta FC across the top ten FXS connections (*M* rank = 51.66) compared to the sum of the top ten TDC connections (*M* rank = 30.73), $N = 79$, $z = 4.03$, $p < .001$, $r = .45$.

Overarchingly, during the pre-stimulus windows, theta FC was increased across all networks, but differences were driven by the overall strength of connectivity in the strongest connections for FXS which differed from TDC where FXS exhibited a distinct dominant pattern of connectivity.

Alpha 2 FC. Next, alpha 2 FC top connections for pre-stimulus period data were evaluated starting with DMN. As with alpha 2 FC in DMN from both feedback and stimulus periods, the number of unique nodes was different between groups where FXS had more nodes involved in the top ten connections ($N = 10$) compared to TDC ($N = 8$). Of the eight nodes involved in TDC top ten connections, six nodes overlapped with FXS. The top ten TDC connections were centered on the right posterior cingulate node, which was involved in six of the ten connections, including the top two. The strongest connection for TDC was between the right posterior cingulate node and the left isthmus node where the second strongest connection was between the right posterior cingulate node and the left parahippocampus. Neither of the top two connections for TDC were in the FXS top ten.

The top ten connections for FXS were also centered on the right posterior cingulate node, which was involved in five of the top ten connections, but the other connections were more distributed across the other unique nodes than in TDC. Further, only one of the top two connections included the right posterior cingulate node. The strongest connection for FXS was between the left posterior cingulate node and the right isthmus cingulate node which was not in the TDC top ten. The second strongest connection for FXS was between the right posterior cingulate node and the right caudal anterior cingulate node which was in the TDC top ten but of low-to-moderate strength (Figure 108).

Figure 108.

Pre-stimulus: Alpha 2 FC Top Ten Within Default Mode Network Connections

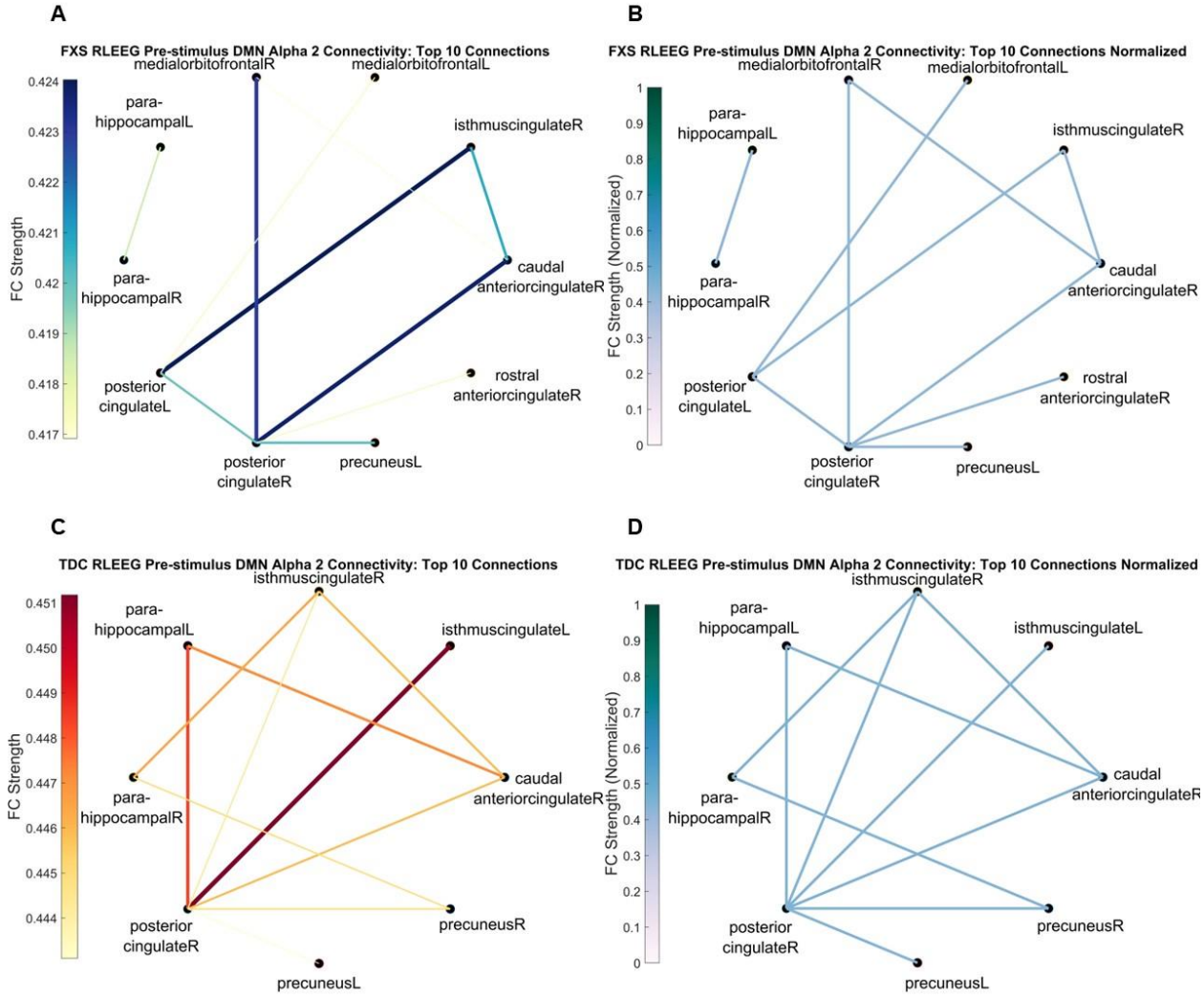

Note. Normalized plots were normalized to the full FC scale to help to visualize some of the smaller, and thus barely visible, connections in A and C. **A)** FXS top ten alpha 2 FC within network connections for pre-stimulus DMN (same as plot B). **B)** FXS top ten connections normalized to the full dWPLI scale. **C)** TDC top ten alpha 2 FC within network connections for pre-stimulus DMN (same as plot D). **D)** TDC top ten connections normalized to the full dWPLI scale.

Statistically, DMN connection 1 ($N = 79$, $z = -3.83$, $p < .001$, $r = -.43$) and DMN connection 2 ($N = 79$, $z = -3.77$, $p < .001$, $r = -.42$) from pre-stimulus period data were significantly different between groups where FXS exhibited reduced alpha 2 FC (DMN Connection 1: *M* rank = 28.91; DMN Connection 2: *M* rank = 29.09) compared to TDC (DMN Connection 1: *M* rank = 48.82; DMN Connection 2: *M* rank = 48.68) for the strongest DMN connections for TDC. Additionally, the sum score representing the individual group top ten connections for each group was significantly different between groups where FXS exhibited reduced alpha 2 FC across the top ten FXS connections (*M* rank = 30.51) compared to the sum of the top ten TDC connections (*M* rank = 47.55), $N = 79$, $z = -3.28$, $p = .001$, $r = -.37$. These results suggest both focal network disruptions where FXS exhibited reduced alpha 2 in typical DMN pathways during pre-stimulus period, as well as broader network restructuring in FXS where FXS prioritized separate DMN pathways compared to TDC.

Next, the top ten connections for alpha 2 FC in SN were compared between groups. FXS had more unique nodes involved in the top ten connections ($N = 8$) compared to TDC ($N = 7$) where the nodes all overlapped, with the exception the rostral middle frontal node which was not involved in TDC top connections. Connections in both groups were centered on the left supramarginal node and the right rostral middle frontal node, though FXS connections largely involved both the left and right supramarginal nodes.

Several connections for both groups were centered on the left supramarginal node where the strongest connection for TDC (SN Connection 1) was between the left supramarginal node and the left insula node and the second strongest connection (SN Connection 2) was between the right rostral middle frontal node and the right insula. Both were connections present in the FXS top ten and of either moderate or high strength. For FXS, the strongest connection was between

the right supramarginal node, and the left caudal middle frontal node and the second strongest connection was between the left supramarginal node and the right rostral middle frontal node. Neither of the top two connections for FXS were in the TDC top ten connections (Figure 109).

Figure 109.

Pre-stimulus: Alpha 2 FC Top Ten Within Salience Network Connections

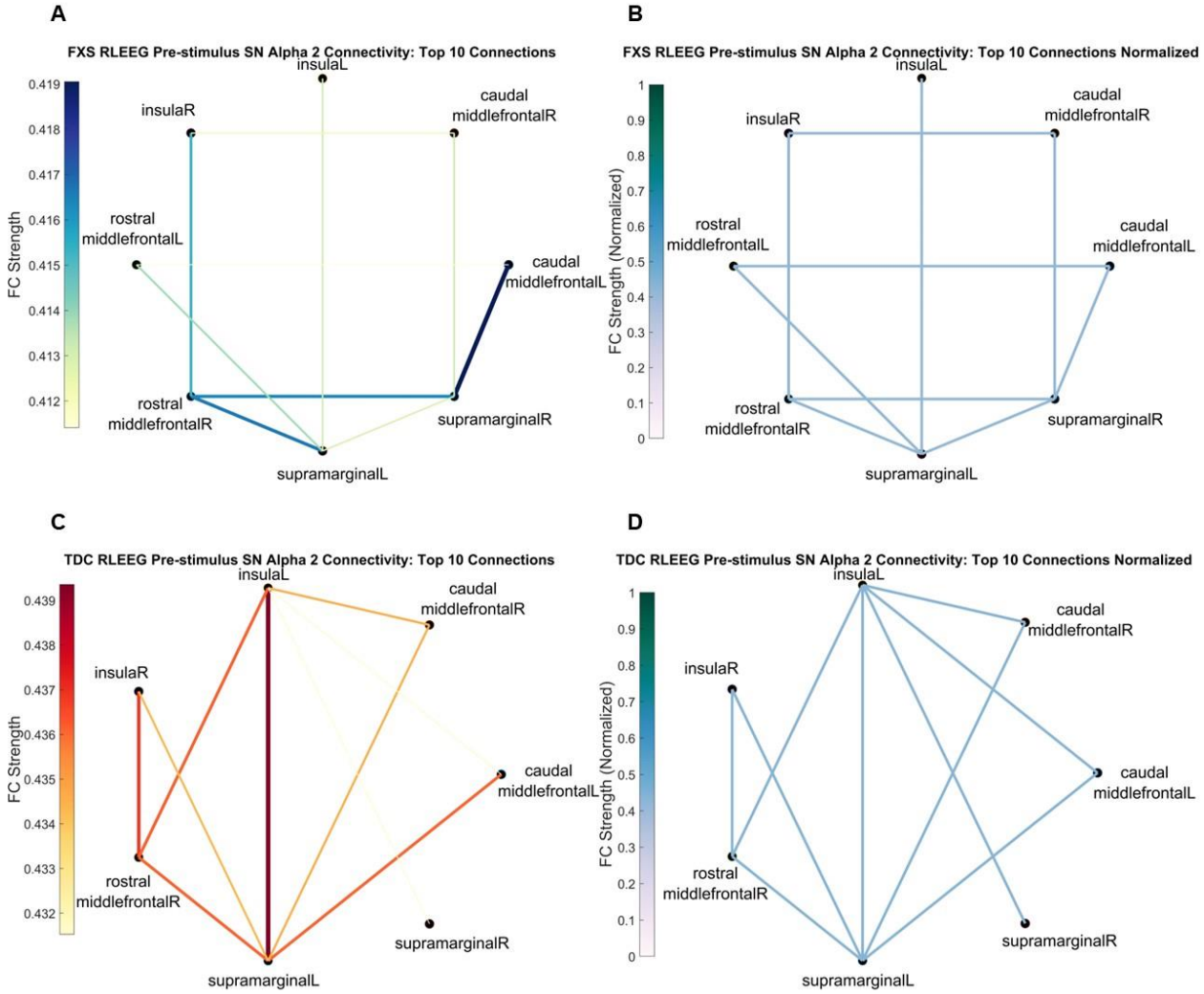

Note. Normalized plots were normalized to the full FC scale to help to visualize some of the smaller, and thus barely visible, connections in A and C. **A)** FXS top ten alpha 2 FC within network connections for pre-stimulus SN (same as plot B). **B)** FXS top ten connections normalized to the full dWPLI scale. **C)** TDC top ten alpha 2 FC within network connections for pre-stimulus SN same as plot D). **D)** TDC top ten connections normalized to the full dWPLI scale.

Statistically, SN Connection 1 ($N = 79$, $z = -3.04$, $p = .004$, $r = -.34$) and SN connection 2 ($N = 79$, $z = -2.60$, $p = .018$, $r = -.29$) from the pre-stimulus period were significantly different between groups where alpha 2 FC was reduced for FXS (SN Connection 1: *M* rank = 31.20; SN Connection 2: *M* rank = 32.49) compared to TDC (SN Connection 1: *M* rank = 47.00; SN Connection 2: *M* rank = 45.98) on the strongest SN connections for TDC. Further, the sum score representing the individual group top ten connections for each group was significantly different between groups where FXS exhibited reduced alpha 2 FC across the top ten FXS connections (*M* rank = 30.37) compared to the sum of the top ten TDC connections (*M* rank = 47.66), $N = 79$, $z = -3.33$, $p < .001$, $r = -.37$. Similarly to DMN, these results indicate whole network alpha 2 FC differences resulted from both focal and broader network restructuring of SN in FXS.

Lastly, alpha 2 FC top connections were evaluated for the control network where FXS and TDC had the same number of unique nodes involved of which six overlapped between groups. The FXS top ten connections involved the left lateral orbitofrontal, left middle temporal, and the right superior frontal nodes where TDC involved the left precuneus, right rostral middle frontal, and right rostral middle frontal nodes.

The top ten connections for TDC centered on the right inferior parietal node which was involved in the top two connections where the strongest connection for TDC (Con Connection 1) was between the right inferior parietal node and the left superior parietal node, which was the top connection for FXS, as well. The second strongest connection (Con Connection 2) was between the right and left inferior parietal nodes, which was not in the FXS top ten connections (Figure 110). The second strongest connection for FXS was between the left lateral orbitofrontal node and the left inferior temporal node which was not in the TDC top ten connections. Interestingly,

FXS appear to recapitulate the strongest connections for TDC through indirect connections in the FXS top ten connections (Figure 110).

Figure 110.

Pre-stimulus: Alpha 2 FC Top Ten Within Control Network Connections

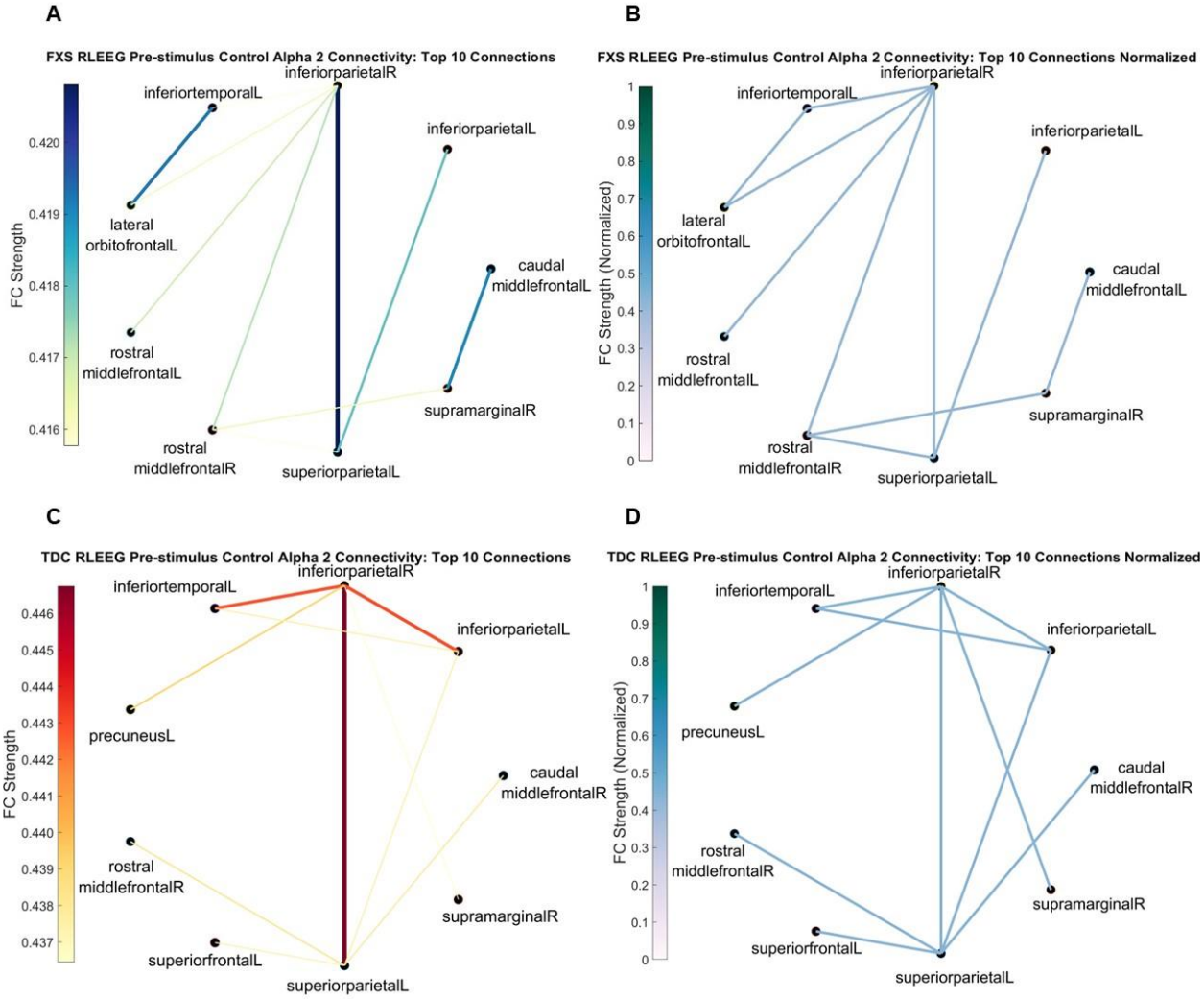

Note. Normalized plots were normalized to the full FC scale to help to visualize some of the smaller, and thus barely visible, connections in A and C. **A)** FXS top ten alpha 2 FC within network connections for pre-stimulus control network (same as plot B). **B)** FXS top ten connections normalized to the full dWPLI scale. **C)** TDC top ten alpha 2 FC within network connections for pre-stimulus control network (same as plot D). **D)** TDC top ten connections normalized to the full dWPLI scale.

Statistically, Con Connection 1 ($N = 79$, $z = -3.04$, $p = .004$, $r = -.34$) and Con Connection 2 ($N = 79$, $z = -3.90$, $p < .001$, $r = -.44$) were significantly different between groups. Similarly to DMN and SN, and in alignment with whole network FC, FXS exhibited reduced alpha 2 FC (Con Connection 1: *M* rank = 31.20; Con Connection 2: *M* rank = 28.71) compared to TDC (Con Connection 1: *M* rank = 47.00; Con Connection 2: *M* rank = 48.98) on the strongest control network connections for TDC from the pre-stimulus period data. Further, the sum score representing the individual group top ten connections for each group was significantly different between groups where FXS reduced alpha 2 FC across the top ten FXS connections (*M* rank = 29.54) compared to the sum of the top ten TDC connections (*M* rank = 48.32), $N = 79$, $z = -3.61$, $p < .001$, $r = -.41$. Overall, these results suggest wide-spread disruptions to control network function during pre-stimulus periods for FXS. Alpha 2 FC in the control network during the pre-stimulus periods was focally disrupted and broadly restructured for FXS where alpha 2 FC group differences were driven by both large FC differences in the typical control network pathways and the sum of all top ten connections for FXS.

Overall, the strongest connections during pre-stimulus periods for TDC within DMN, SN, and the control network for alpha 2 FC were all statistically different between groups suggesting differences in primary network drivers for FXS during the pre-stimulus window in the alpha 2 range.

Triple Network Disruption Hypothesis

Non-parametric Friedman tests were used to evaluate within-subject differences on network connectivity between the pre-stimulus, stimulus, and feedback windows for both theta and alpha 2 FC. Wilcoxon signed rank tests were used for significant cases as a post-hoc test evaluating pairwise comparisons corrected for multiple comparisons using a Bonferroni correction.

For theta FC, there were significant differences between the different data types for both FXS ($\chi^2(2) = 9.83$, $p = .007$, $W = .14$) and TDC ($\chi^2(2) = 9.96$, $p = .007$, $W = .11$). Pairwise comparisons for TDC identified significant differences between pre-stimulus DMN and stimulus control network theta FC where pre-stimulus DMN theta FC was significantly reduced compared to stimulus period control network theta FC, $z = -3.48$, $p = .002$. Further, for TDC, there were also significant differences between pre-stimulus DMN and feedback period control network theta FC where DMN theta FC was also significantly reduced compared to feedback-period control network theta FC, $z = -2.79$, $p = .005$. The difference between stimulus and feedback period control theta FC was not significantly different for TDC, $z = -.02$, $p = 1.00$. The FXS pairwise comparisons were similar to TDC where the difference between pre-stimulus DMN and stimulus control network theta FC was significant where pre-stimulus DMN theta FC was significantly reduced compared to stimulus period control network theta FC, $z = -3.03$, $p = .006$. However, there was not a significant difference between pre-stimulus DMN and feedback period control network theta FC where DMN theta FC was similar to feedback-period control network theta FC, $z = -2.28$, $p = .069$. The difference between stimulus and feedback period control theta FC was also not significantly different for TDC, $z = -1.05$, $p = .885$. Within subject differences

differ between groups indicating sufficient modulation of network activity over the pre-stimulus, stimulus, and feedback time windows which were similar across groups.

For alpha 2 FC, there was a significant difference between individual data types for TDC ($\chi2(2) = 31.09$, $p < .001$, $W = .35$) but not for FXS ($\chi2(2) = .40$, $p = .819$, $W = .01$) where alpha 2 FC was comparable across pre-stimulus DMN and both stimulus and feedback control network. Pairwise comparisons for TDC found significant differences between pre-stimulus DMN and stimulus control network alpha 2 FC where pre-stimulus DMN theta FC was significantly reduced compared to stimulus period control network alpha 2 FC, $z = -4.60$, $p < .001$. Further, for TDC, there were also significant differences between pre-stimulus DMN and feedback period control network alpha 2 FC where DMN alpha 2 FC was also significantly reduced compared to feedback-period control network theta FC, $z = -4.94$, $p < .001$. The difference between stimulus and feedback period control theta FC was not significantly different for TDC, $z = -1.24$, $p = .648$. Within subject differences across time windows show TDC modulate alpha FC over the course of a cognitive task between pre-stimulus (no task-related stimulation) and task-related windows that engage cognitive processes. FXS did not exhibit modulation across task windows where alpha 2 FC was consistent across the RLEEG task. Paired with reduced alpha 2 FC across networks of interest, these results may reflect less flexible network dynamics in FXS where within network connectivity does not fluctuate with changing task demands.

Mediation analyses via the Hayes PROCESS Macro were then used to evaluate whether within-network SN FC from the stimulus period mediated the relationship between pre-stimulus within-network DMN FC and stimulus within-network control FC for both theta and alpha 2 in order to test whether triple network dynamics were disrupted in FXS. Simple mediation models were used to test study hypotheses which predicted disruptions for FXS in the ability to shift

from DMN to the control network resulting from SN disruptions and run separately for each group. All mediation models utilized bootstrapping with 10,000 resamples for stability and to avoid biased from non-normality.

The mediation analysis of theta FC for FXS identified a significant path between pre-stimulus DMN to stimulus SN where within-network theta FC significantly predicted within-network connectivity of stimulus period SN (B = .40, SE = .17, t(34) = 2.37, p = .024, CI [.02, .75], β =.38) with 14.5% of the variance in stimulus SN theta FC explained by pre-stimulus DMN theta FC, R^2 = .15, F(1, 33) = 5.61, p = .024. In the full model for FXS including both DMN and SN, both DMN (B = .45, SE = .08, CI [.29, .61], β =.44, t(34) = 5.77, p < .001) and SN (B = .64, SE = .07, CI [.49, .79], β =.66, t(34) = 8.65, p < .001) were significantly predictive of within-network theta FC of control network during the stimulus window where 84.2% of the variance in control network theta FC was explained by the model, R^2 = .84, F(2, 32) = 85.43, p < .001.

Mediation analysis results showed the total effect of pre-stimulus DMN theta FC on stimulus control network theta FC was significant (B = .71, SE = .13, CI [.44 .97], t(34) p < .001, R^2 = .69, F(1, 33) = 29.71, p < .001) with a significant direct effect of pre-stimulus DMN on stimulus period control theta FC (B = .45, SE = .08, p < .001, CI [.29, .61]). However, the indirect effect of pre-stimulus DMN theta FC on stimulus control network through stimulus SN for theta FC was not significant (B = .26, bootSE = .16, β = .25, bootCI [-.06, .52]), as determined by bootstrapping with 10,000 re-samples, suggesting that within-network SN theta FC does not significantly mediate the relationship between DMN and control network theta FC for FXS.

Next the same model was evaluated for TDC only which identified a significant path between pre-stimulus DMN to stimulus SN, similarly to FXS, where within-network theta FC significantly predicted within-network connectivity of SN (B = .69, SE = .15, CI [.38, 1.00], β =.57, $t(43) = 4.51$, $p < .001$) where 32.6% of the variance in stimulus SN theta FC was explained by pre-stimulus DMN theta FC, $R^2 = .33$, $F(1, 42) = 20.37$, $p < .001$. In the overall mediation model for TDC, only stimulus within-network SN theta FC was significantly predictive of within-network theta FC of control network during the stimulus window ($R^2 = .62$, $F(2, 41) = 33.71$, $p < .001$) where 62.2% of the variance in control network theta FC was explained by the model. Again, the within-network theta FC of the SN during the stimulus window had a significant direct effect on control network theta FC (B = .52, SE = .10, CI [.32, .71], β =.63, $t(43) = 5.39$, $p < .001$) but the within-network theta FC in pre-stimulus DMN was not significantly predictive of within-network theta FC during the stimulus control window, though it trended towards significance (B = .23, SE = .12, CI [.32, .71], β =.23, $t(43) = 2.00$, $p = .052$).

Mediation analysis results showed the total effect of pre-stimulus DMN theta FC on stimulus control network theta FC for TDC was significant (b = .59, SE = .12, $t(43) = 4.79$, $p < .001$, CI [.84, .59], $R^2 = .35$, $F(1, 33) = 23.00$, $p < .001$) where the direct effect was not significant but trended towards significance (b = .23, SE = .12, $t(43) = 2.00$, $p = .052$, CI [-.002, .47]). Though, the indirect effect of pre-stimulus DMN on stimulus control network through stimulus SN for theta FC was significant (b = .36, bootSE = .14, β = .36, bootCI [.11, .66]), as determined by bootstrapping with 10,000 re-samples, suggesting that within-network SN theta FC fully mediates the relationship between pre-stimulus DMN and stimulus control network theta FC for TDC. Although FC in the current study was a measure of within-network connectivity, these results suggest that SN network integrity fully explains the relationship

between pre-stimulus DMN and stimulus period control network integrity for TDC where within-network connectivity for SN does not play a role in this relationship for FXS despite within subject differences on theta FC indicating FXS were able to modulate theta FC similarly to TDC. Ultimately, the modulation may not have been sufficient to overcome whatever difficulties were indexed in group analyses of theta FC.

While running separate models was not ideal and moderated mediation would be most appropriate for addressing the triple network hypothesis on within-network FC, these results provide limited evidence that SN integrity does facilitate the relationship between DMN and control network where SN fully mediates the shift for TDC in the theta frequency range but not in FXS which may have consequences for stimulus processing in FXS.

Next, the same models were evaluated for alpha 2 FC. For FXS, there was a significant path between pre-stimulus DMN to stimulus SN where within-network alpha 2 FC significantly predicted within-network connectivity of SN (b = .67, SE = .13, CI [.40, .94], β =.66, $t(43)$ = 5.09, $p < .001$) with 43.9% of the variance in stimulus SN alpha 2 FC explained by pre-stimulus DMN alpha 2 FC, R^2 = .44, $F(1, 33) = 25.86$, $p < .001$. In the overall mediation model for FXS, stimulus SN alpha 2 FC was predictive of within-network alpha 2 FC of control network during the stimulus window (B = .92, SE = .11, CI [.70, 1.13], β = .87, $t(34) = 8.71$, $p < .001$) but within-network pre-stimulus DMN was not (B = .05, SE = .11, CI [-.16, .27], β = .05, $t(34)$ = .51, p = .613) where 82.1% of the variance in control network alpha 2 FC was explained by the model (R^2 = .82, $F(2, 32) = 73.19$, $p < .001$).

Mediation analysis results showed the total effect of pre-stimulus DMN alpha 2 FC on stimulus control network alpha 2 FC was significant (b = .67, SE = .14, $t(33) = 4.64$, $p < .001$, CI [.38, .97], R^2 = .40, $F(1, 33) = 21.56$, $p < .001$) but the direct effect was not significant (b = .05,

SE = .11, *t*(34) = .51, *p* = .613, *CI* [-.16, .27]). However, the indirect effect of pre-stimulus DMN on stimulus control network through stimulus SN for theta FC was significant (*b* = .62, boot*SE* = .23, *β* = .58, boot*CI* [.23, 1.10]), as determined by bootstrapping with 10,000 re-samples, suggesting that within-network SN alpha 2 FC fully mediated the relationship between pre-stimulus DMN and stimulus control network alpha 2 FC for FXS.

Lastly, a mediation model was run for alpha 2 FC in TDC which identified a significant path between pre-stimulus DMN to stimulus SN where within-network alpha 2 FC significantly predicted within-network connectivity of SN (*b* = .53, *SE* = .08, *CI* [.38, .69], *β* = .72, *t*(43) = 6.81, *p* < .001) with 52.4% of the variance in stimulus SN alpha 2 FC explained by pre-stimulus DMN alpha 2 FC, R^2 = .52, *F*(1, 42) = 46.32, *p* < .001. In the overall mediation model for TDC, stimulus SN alpha 2 FC (*B* = .74, *SE* = .06, *CI* [.62, .87], *β* = .77, *t*(43) = 11.92, *p* < .001) and within-network pre-stimulus DMN (*B* = .17, *SE* = .05, *CI* [.08, .26], *β* = .24, *t*(43) = 3.70, *p* < .001) were both significantly predictive of within-network alpha 2 FC of control network during the stimulus window where 91.8% of the variance in control network alpha 2 FC was explained by the model (R^2 = .92, *F*(2, 41) = 230.86, *p* < .001).

Mediation analysis results showed the total effect of pre-stimulus DMN alpha 2 FC on stimulus control network alpha 2 FC was significant (*b* = .57, *SE* = .07, *t*(43) = 8.57, *p* < .001, *CI* [.43, .70], R^2 = .80, *F*(1, 42) = 73.37, *p* < .001) where the direct effect of pre-stimulus DMN on stimulus control network was also significant (*b* = .17, *SE* = .05, *t*(43) = 3.70, *p* < .001, *CI* [.08, .26]). Further, the indirect effect of pre-stimulus DMN on stimulus control network through stimulus SN for theta FC was significant (*b* = .39, boot*SE* = .05, *β* = .56, boot*CI* [.31, .52]), as determined by bootstrapping with 10,000 re-samples, suggesting that within-network SN alpha 2

FC partially mediated the relationship between pre-stimulus DMN and stimulus control network alpha 2 FC for TDC.

Given FXS exhibit full mediation for alpha 2 FC where TDC exhibit partial mediation suggests a possible flexible path for connectivity integration between networks for TDC where the relationship between within-network DMN and control network alpha 2 FC was only explained by increased within-network SN during the stimulus period. However, as alpha 2 FC was reduced in FXS relative to TDC, this may reflect a more global deficit where those with reduced alpha 2 FC in SN impact the ability to appropriately bring the other network online for external stimulus engagement. Additionally, FXS were not able to modulate alpha 2 FC between the pre-stimulus and stimulus period where there were not significant differences in FC between pre-stimulus DMN, stimulus SN, and stimulus control network.

Correlation Analyses

Correlation analyses were conducted to evaluate both whether FC and microstate variables overlap for RLEEG and whether RLEEG variables share meaningful relationships with clinical variables for FXS only. A hypothesis driven correlation analysis was also conducted to determine whether FC for SN and control network in theta and alpha 2 share a relationship with RewP variables in order to test whether increased the RewP amplitudes identified in FXS reflect heightened salience and disruptions to control network in FXS only ($N = 34$).

Interestingly RewP shared significant direct relationships with theta FC within the control network during feedback for both the RewP calculated using the correct preceding (rho = .35, $p = .041$) and the correct following (rho = .43, $p = .012$) but not alpha 2 FC (Preceding: rho = .19, $p = .287$; Following: rho = -.04, $p = .815$). Correlations between RewP were not significant for theta or alpha 2 FC in SN during feedback for either the RewP calculated using the correct

preceding (Theta FC: rho = .11, p = .552; Alpha 2 FC: rho = .22, p = .212) or the correct following (Theta FC: rho = .16, p = .344; Alpha 2 FC: rho = .09, p = .626). As an exploratory step, theta FC during the stimulus and pre-stimulus periods were also evaluated to determine whether the relationship between theta FC and RewP was specific to feedback or extended to cognitive disruptions more broadly throughout the task. Theta FC shared significant direct relationships with theta FC for both the RewP using the correct preceding (Pre-stimulus: : rho = .43, p = .012; Stimulus: rho = .37, p = .032) and the RewP using the correct following (Pre-stimulus: : rho = .35, p = .042; Stimulus: : rho = .36, p = .039) reversal error. These results suggest RewP differences for FXS were more linked to cognitive control process disruptions than salience detection disruptions and that disruptions across the whole task, even pre-stimulus periods, contribute to disrupted reward processing. The direct relationship also highlights the possibility that FXS dedicated increased neural resources for task engagement which continue into the pre-stimulus periods.

Next, correlations were evaluated across feedback, stimulus, and pre-stimulus periods to evaluate relationships between microstates, FC, and IQ.

First, for on feedback-related microstate and FC correlations, GEV was directly correlated with theta FC where both were increased for FXS relative to TDC. Next, several correlations were identified between microstates and FC with IQ: GFP was inversely correlated with IQ across all IQ measures, Hurst exponent was also inversely correlated with IQ, and both theta and alpha 2 FC were inversely correlated with full-scale IQ, non-verbal, and verbal IQ but not abbreviated where more individuals had abbreviated IQ (Figure 111).

Correlations between feedback related FC variables and individual microstate class variables from the feedback microstate solution were evaluated. Individual microstate class variables did not exhibit a meaningful pattern of correlations with FC variables (Figure 112).

Figure 111.

Correlation Plot for Feedback Period Global Microstate Variables, Functional Connectivity, and IQ for FXS only

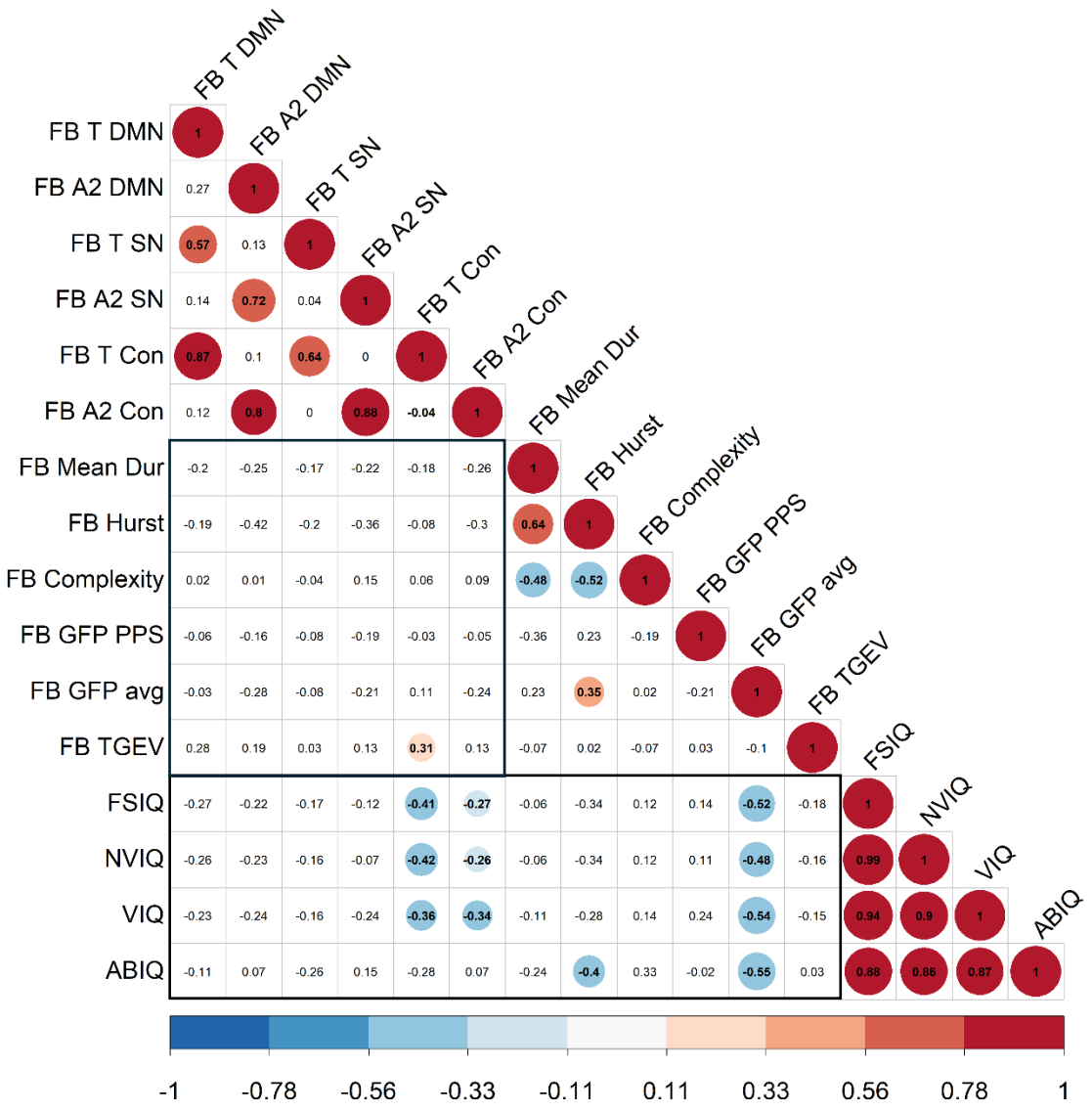

Note. All statistically significant correlations are bolded and indicated by colored circles where warmer colors are direct correlations and cooler colors are inverse correlations. Black boxes highlight columns with correlations of interest. FB = feedback; T = theta, A2 = alpha 2; DMN = default mode network; SN = salience network; Con = control network; FSIQ = full scale IQ; NVIQ = non-verbal IQ; VIQ = verbal IQ; ABIQ = abbreviated IQ; Mean Dur = mean duration; GFP = global field power; PPS = peaks per second; GEV = global explained variance.

Figure 112.

Correlation Plot for Feedback Period Individual Microstate Class Variables and Functional Connectivity for FXS only

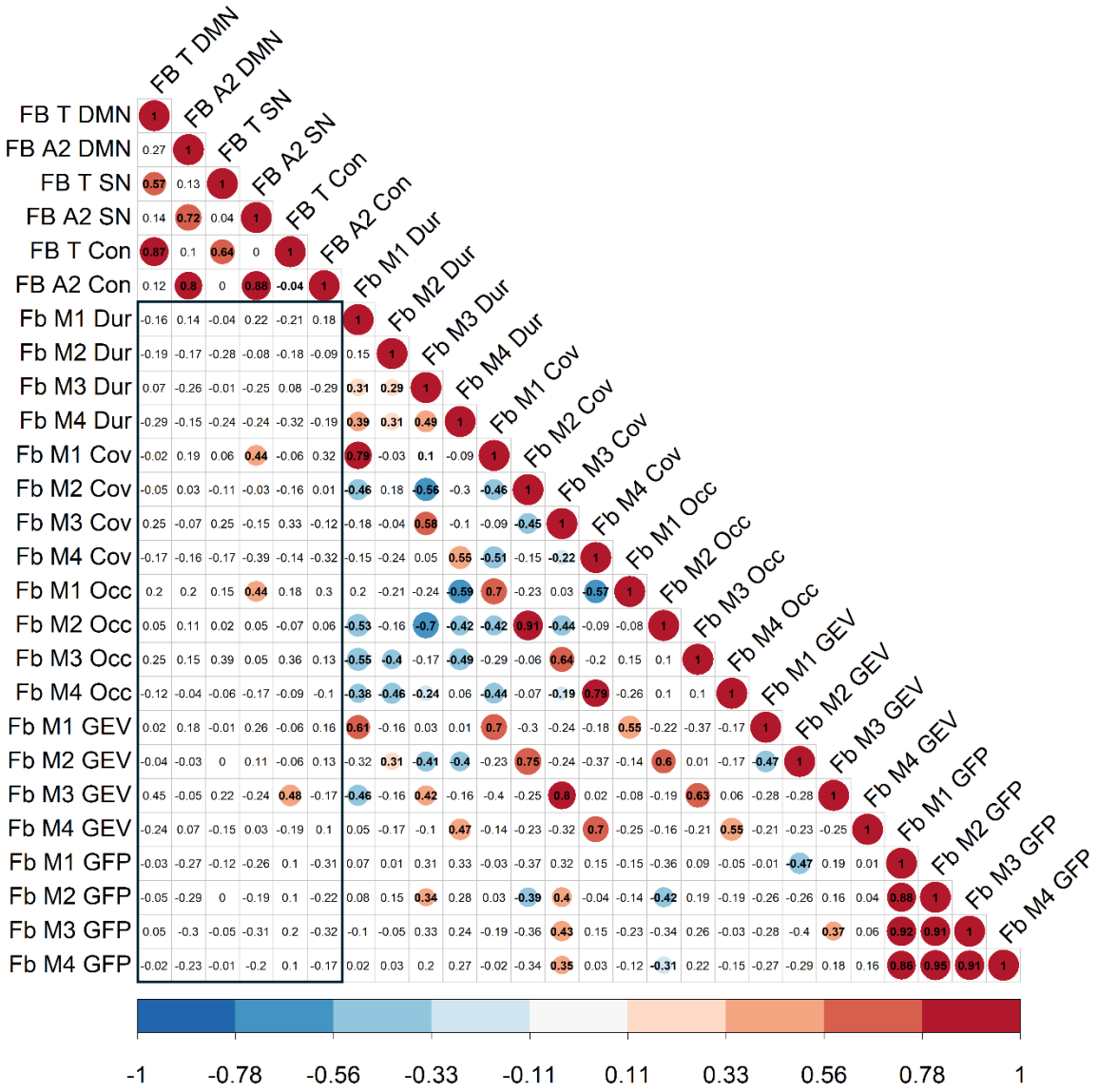

Note. All statistically significant correlations are bolded and indicated by colored circles where warmer colors are direct correlations and cooler colors are inverse correlations. Black boxes highlight columns with correlations of interest. FB = feedback; T = theta, A2 = alpha 2; DMN = default mode network; SN = salience network; Con = control network; Dur = mean duration; Cov = coverage; Occ = occurrence; GEV = global explained variance; GFP = global field power.

For stimulus-related microstate and FC correlations, GFP peaks per second shared an inverse correlation with alpha 2 FC in SN. Unlike with resting state, GFP peaks per second were not different between groups. However, the present results indicate that individuals with FXS who exhibit increased GFP peaks per second have reduced alpha 2 FC in SN which was different between groups. Next, GFP was inversely correlated with IQ across all IQ measures (Figure 113).

Correlations between feedback related FC variables and individual microstate class variables from the stimulus microstate solution were evaluated. Individual microstate class variables did not exhibit a meaningful pattern of correlations with FC variables (Figure 114).

Figure 113.

Correlation Plot for Stimulus Period Microstates, Functional Connectivity, and IQ

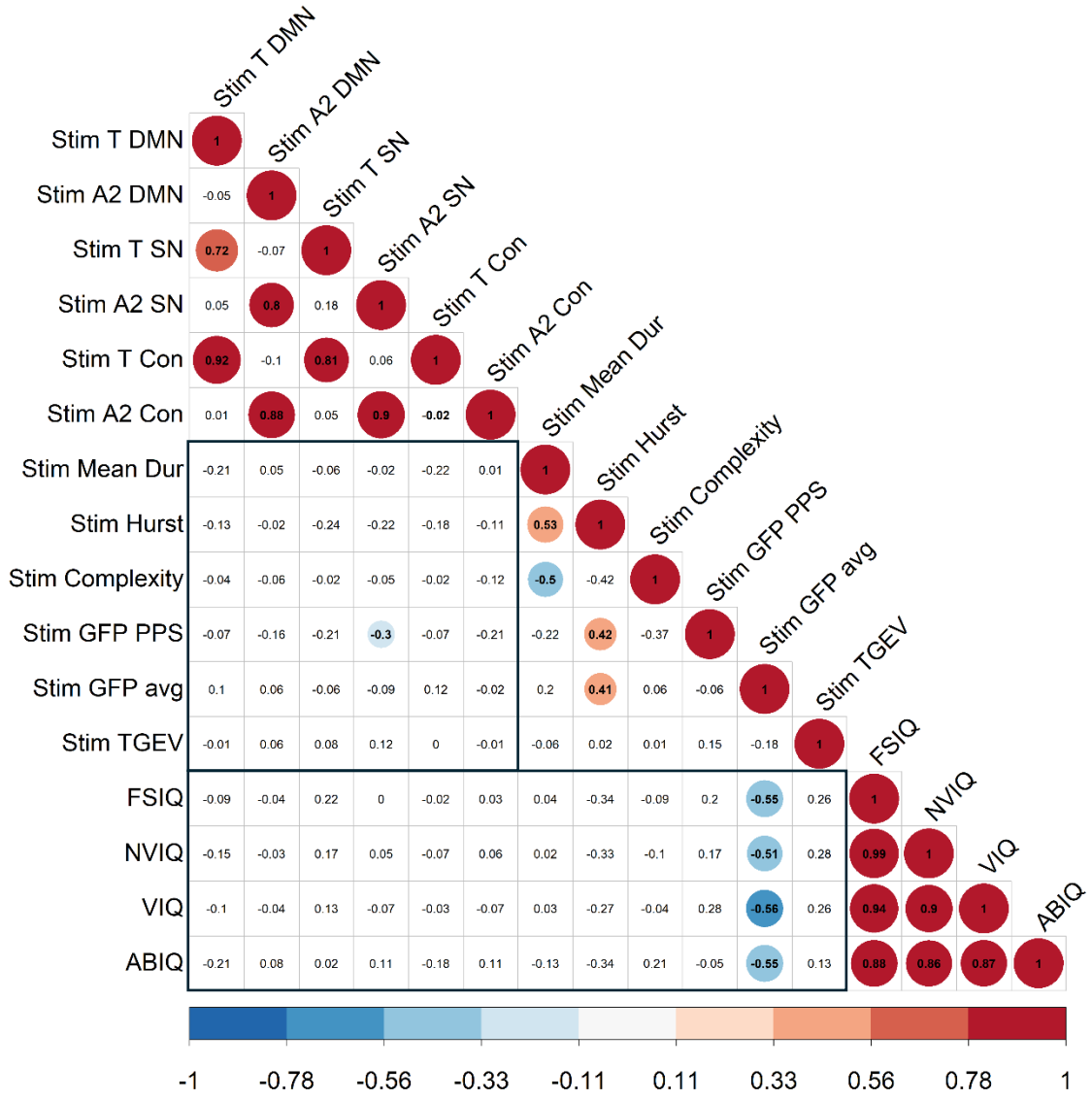

Note. All statistically significant correlations are bolded and indicated by colored circles where warmer colors are direct correlations and cooler colors are inverse correlations. Black boxes highlight columns with correlations of interest. Stim = stimulus; T = theta, A2 = alpha 2; DMN = default mode network; SN = salience network; Con = control network; FSIQ = full scale IQ; NVIQ = non-verbal IQ; VIQ = verbal IQ; ABIQ = abbreviated IQ; Mean Dur = mean duration; GFP = global field power; PPS = peaks per second; GEV = global explained variance.

Figure 114.

Correlation Plot for Stimulus Period Individual Microstate Class Variables and Functional Connectivity

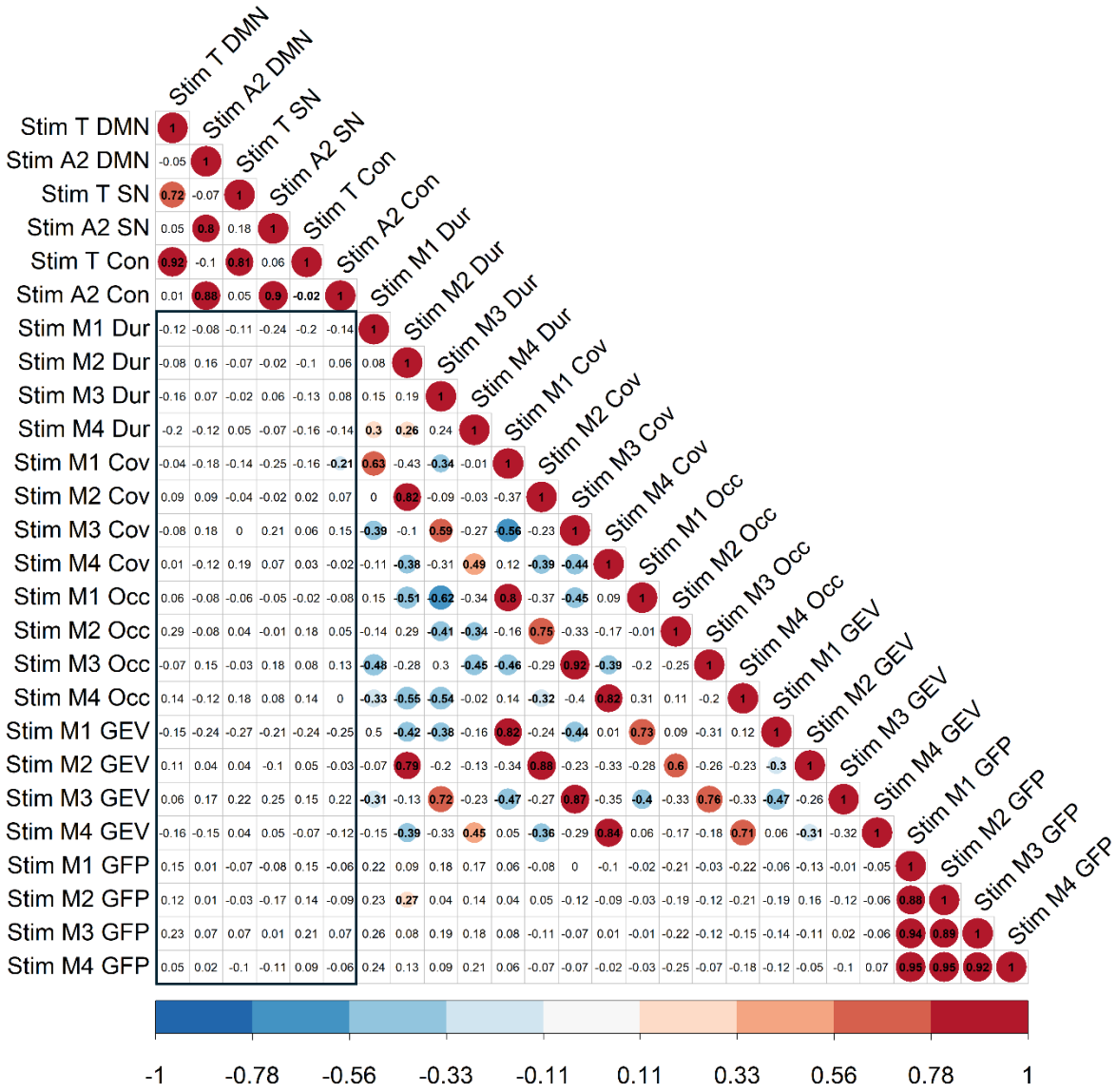

Note. All statistically significant correlations are bolded and indicated by colored circles where warmer colors are direct correlations and cooler colors are inverse correlations. Black boxes highlight columns with correlations of interest. Stim = stimulus; T = theta, A2 = alpha 2; DMN = default mode network; SN = salience network; Con = control network; Dur = mean duration; Cov = coverage; Occ = occurrence; GEV = global explained variance; GFP = global field power.

Correlations computed between pre-stimulus microstate variables and FC identified a pattern of direct correlations between theta FC across all networks and microstate GFP. Similarly to feedback and stimulus periods, GFP was inversely correlated with IQ across all IQ measures. Lastly, abbreviated IQ was inversely correlated with theta FC in SN and the control network. Other IQ variables but not abbreviated IQ were correlated with alpha 2 FC in SN and the control network but these correlations are more difficult to interpret, especially given the lack of correlation with abbreviated IQ where the rho values were very low (Figure 115).

Correlations between feedback related FC variables and individual microstate class variables from the stimulus microstate solution were evaluated. Individual microstate class variables did not exhibit a meaningful pattern of correlations with FC variables. However, the correlation between theta FC and average GFP was also largely evident for individual microstate class GFP (Figure 116).

Figure 115.

Correlation Plot for Pre-stimulus Period Microstates, Functional Connectivity, and IQ

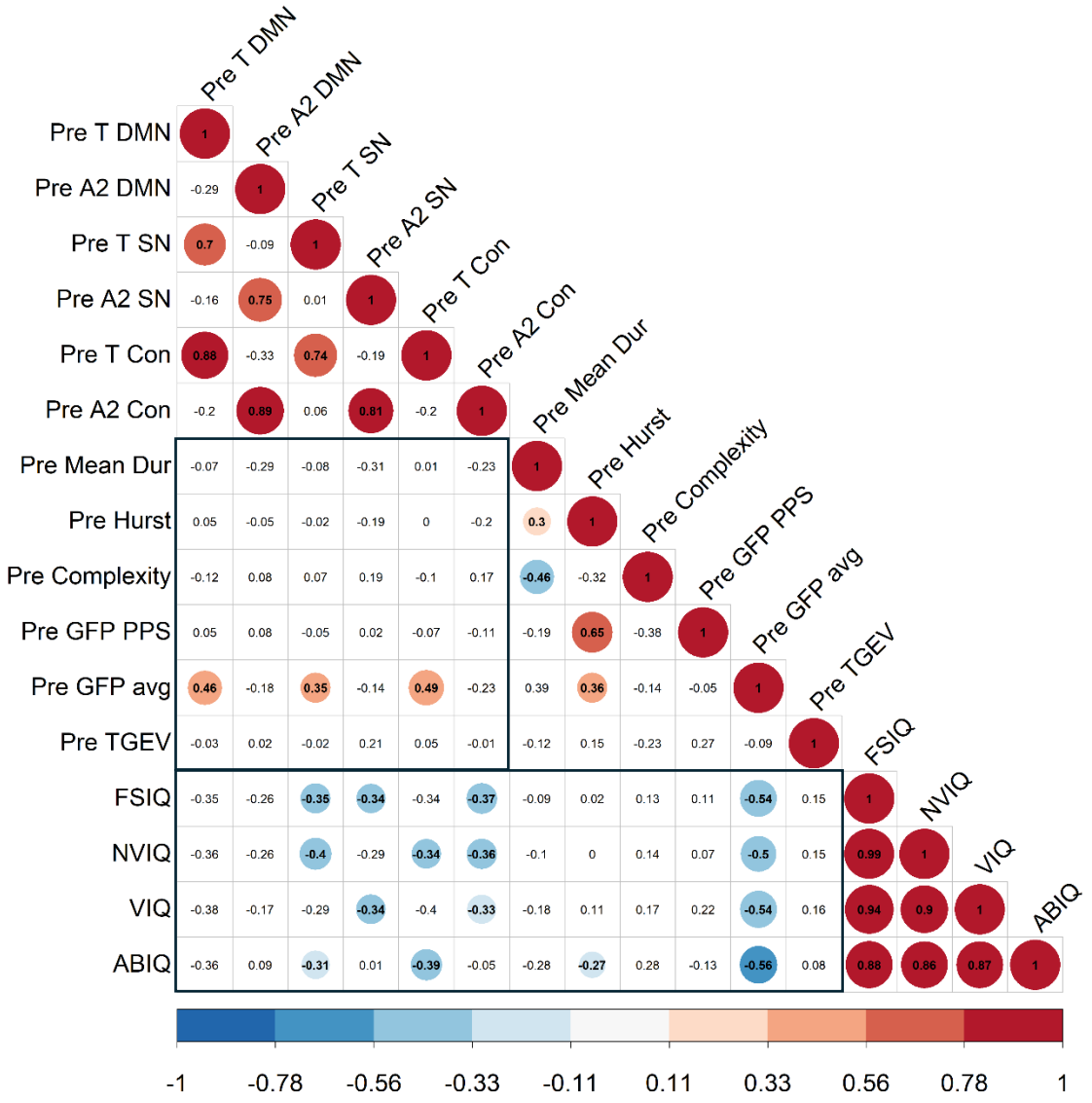

Note. All statistically significant correlations are bolded and indicated by colored circles where warmer colors are direct correlations and cooler colors are inverse correlations. Black boxes highlight columns with correlations of interest. Pre = pre-stimulus; T = theta, A2 = alpha 2; DMN = default mode network; SN = salience network; Con = control network; FSIQ = full scale IQ; NVIQ = non-verbal IQ; VIQ = verbal IQ; ABIQ = abbreviated IQ; Mean Dur = mean duration; GFP = global field power; PPS = peaks per second; GEV = global explained variance.

Figure 116.

Correlation Plot for Pre-stimulus Period Individual Microstate Class Variables and Functional Connectivity

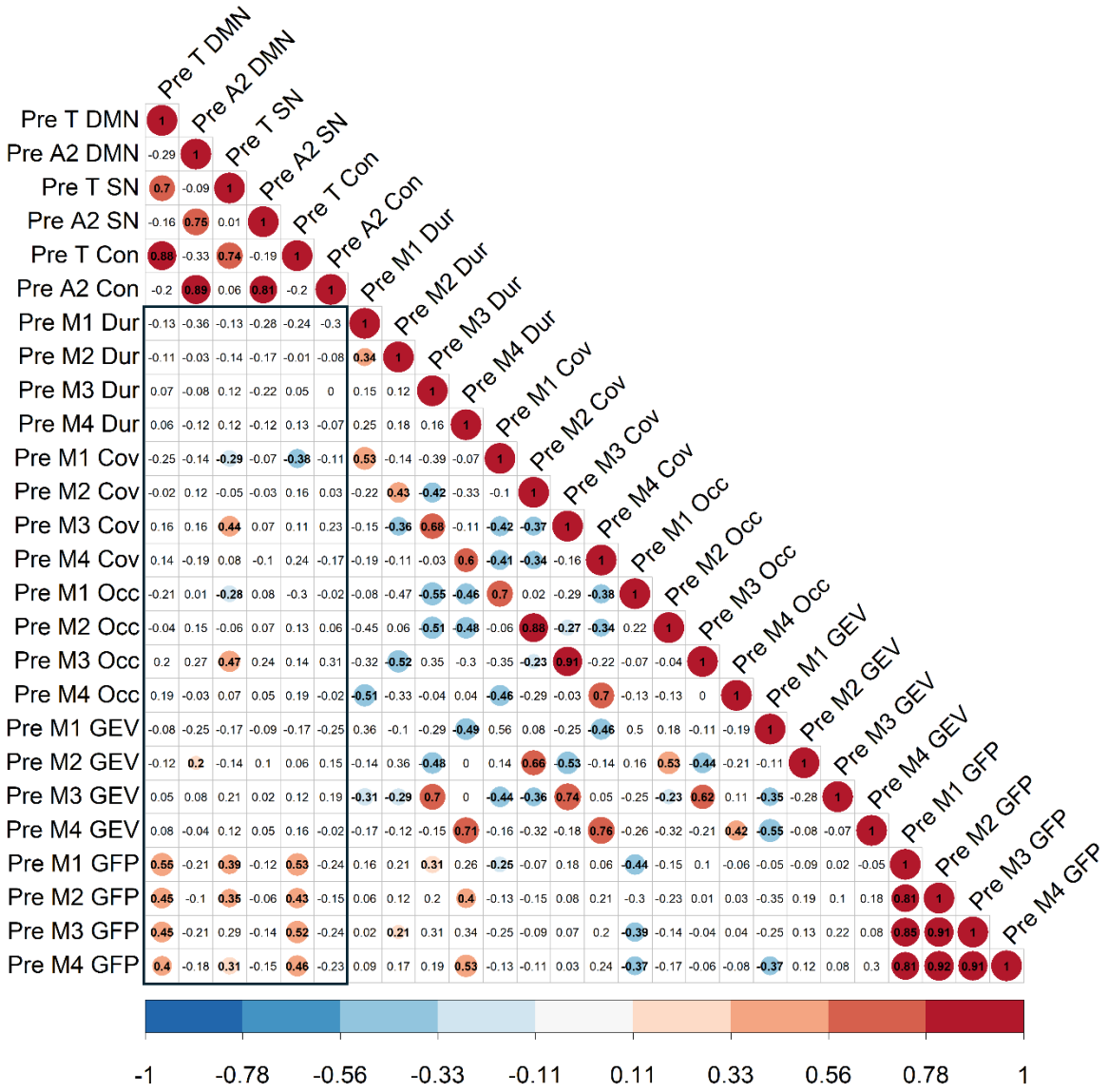

Note. All statistically significant correlations are bolded and indicated by colored circles where warmer colors are direct correlations and cooler colors are inverse correlations. Black boxes highlight columns with correlations of interest. Pre = pre-stimulus; T = theta, A2 = alpha 2; DMN = default mode network; SN = salience network; Con = control network; Dur = mean duration; Cov = coverage; Occ = occurrence; GEV = global explained variance; GFP = global field power.

Microstate and FC variables were next evaluated in correlation analyses with select clinical variables to determine the clinical relevance of the EEG variables from the RL task. Of note, feedback-related microstate GFP was directly correlated with ABC hyperactivity and stereotypy which were correlations observed in chapter two. Additionally, microstate mean duration was correlated with the ABC irritability subscale, but mean duration was not different between groups (Figure 117).

For Vineland 3, GFP was inversely correlated with all Vineland subscales where reduced adaptive behavior across all domains correlated with increased GFP during feedback processing. Hurst from microstates was also inversely correlated with the daily living skills subscale, only (Figure 118).

Correlations between EEG variables of interest from feedback data and KiTAP were limited. There were direct correlations between microstate mean duration and Hurst with Go/No Go errors and there was a direct correlation between alpha 2 FC in SN and median reaction times on the flexibility subtask where higher alpha 2 FC was associated with increased reaction times. Though the relationship was counterintuitive, higher alpha 2 FC in SN may result in higher attention to stimuli where slower reaction times were compensatory for better task performance (i.e., speed-accuracy trade-off). However, alpha 2 FC in SN was not correlated with flexibility errors suggesting higher alpha 2 FC did not impact performance during feedback processing. Lastly, there was a direct correlation between GFP and alertness subtask response standard deviations where increased GFP corresponded to increased response variability (i.e., proxy for inconsistencies in attention control) (Figure 119).

Figure 117.

Correlation Plot for Feedback Period Global Microstate Variables, Functional Connectivity, and ABC

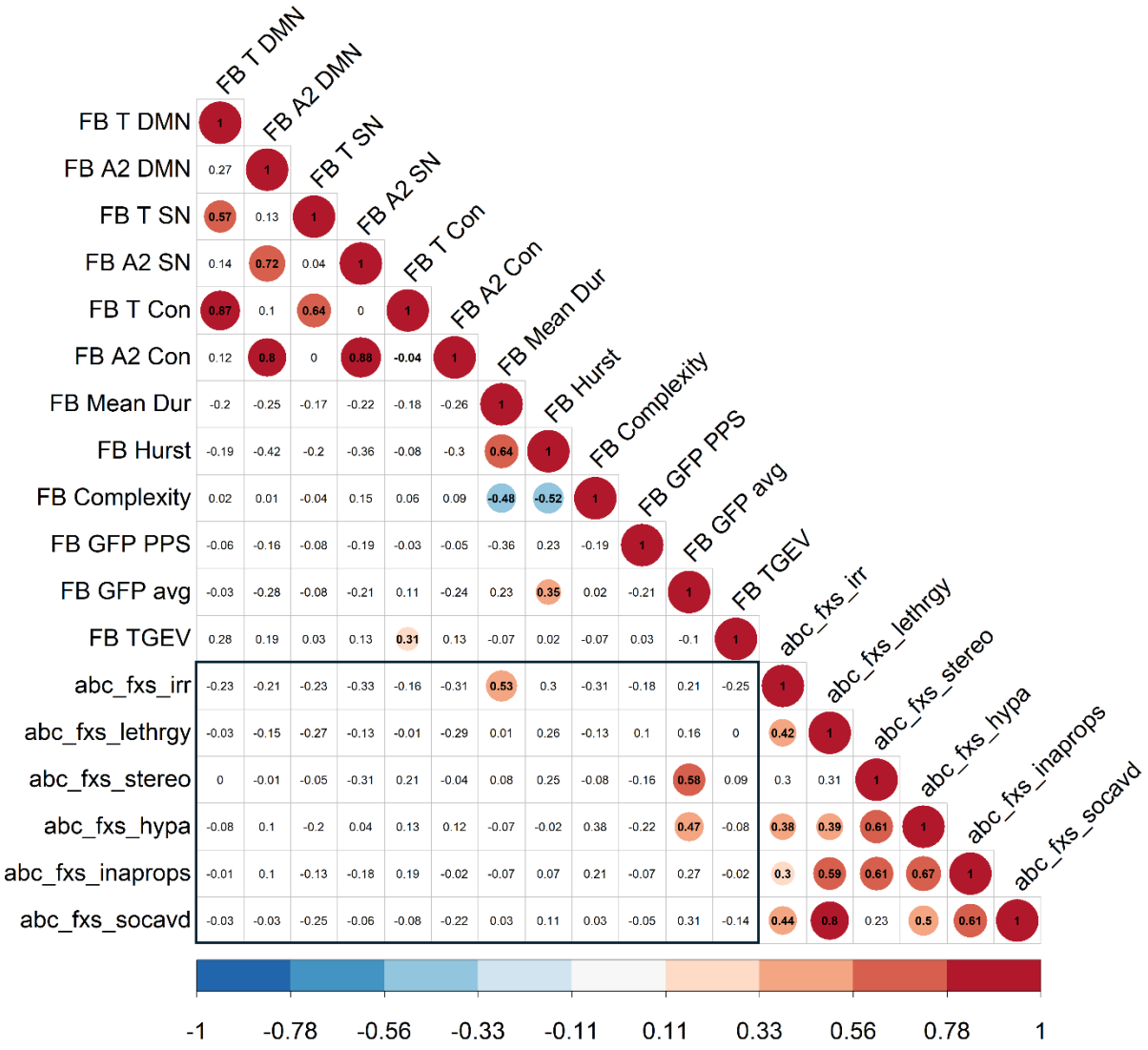

Note. All statistically significant correlations are bolded and indicated by colored circles where warmer colors are direct correlations and cooler colors are inverse correlations. Black boxes highlight columns with correlations of interest. FB = feedback; T = theta, A2 = alpha 2; DMN = default mode network; SN = salience network; Con = control network; Dur = mean duration; Cov = coverage; Occ = occurrence; GEV = global explained variance; GFP = global field power; Irr = irritability; Lethrgy = lethargy; Stereo = stereotypy; hypa = hyperactivity; inaprops = inappropriate speech; socavd = social avoidance.

Figure 118.

Correlation Plot for Feedback Period Global Microstate Variables, Functional Connectivity, and Vineland-3

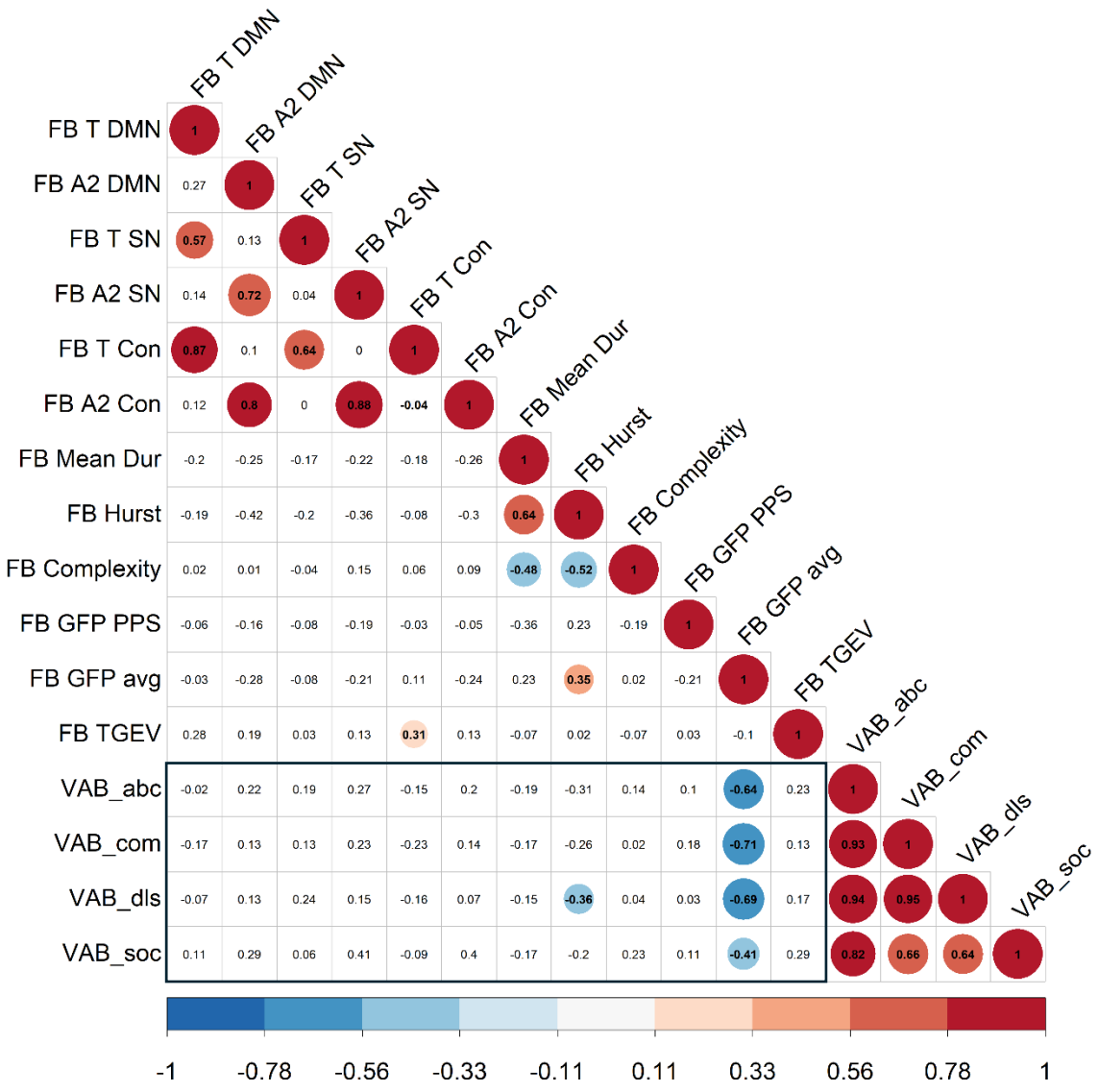

Note. All statistically significant correlations are bolded and indicated by colored circles where warmer colors are direct correlations and cooler colors are inverse correlations. Black boxes highlight columns with correlations of interest. FB = feedback; T = theta, A2 = alpha 2; DMN = default mode network; SN = salience network; Con = control network; Dur = mean duration; Cov = coverage; Occ = occurrence; GEV = global explained variance; GFP = global field power; abc = adaptive behavior composite; com = communication; dls = daily living skills; soc = socialization.

Figure 119.

Correlation Plot for Feedback Period Global Microstate Variables, Functional Connectivity, and KiTAP

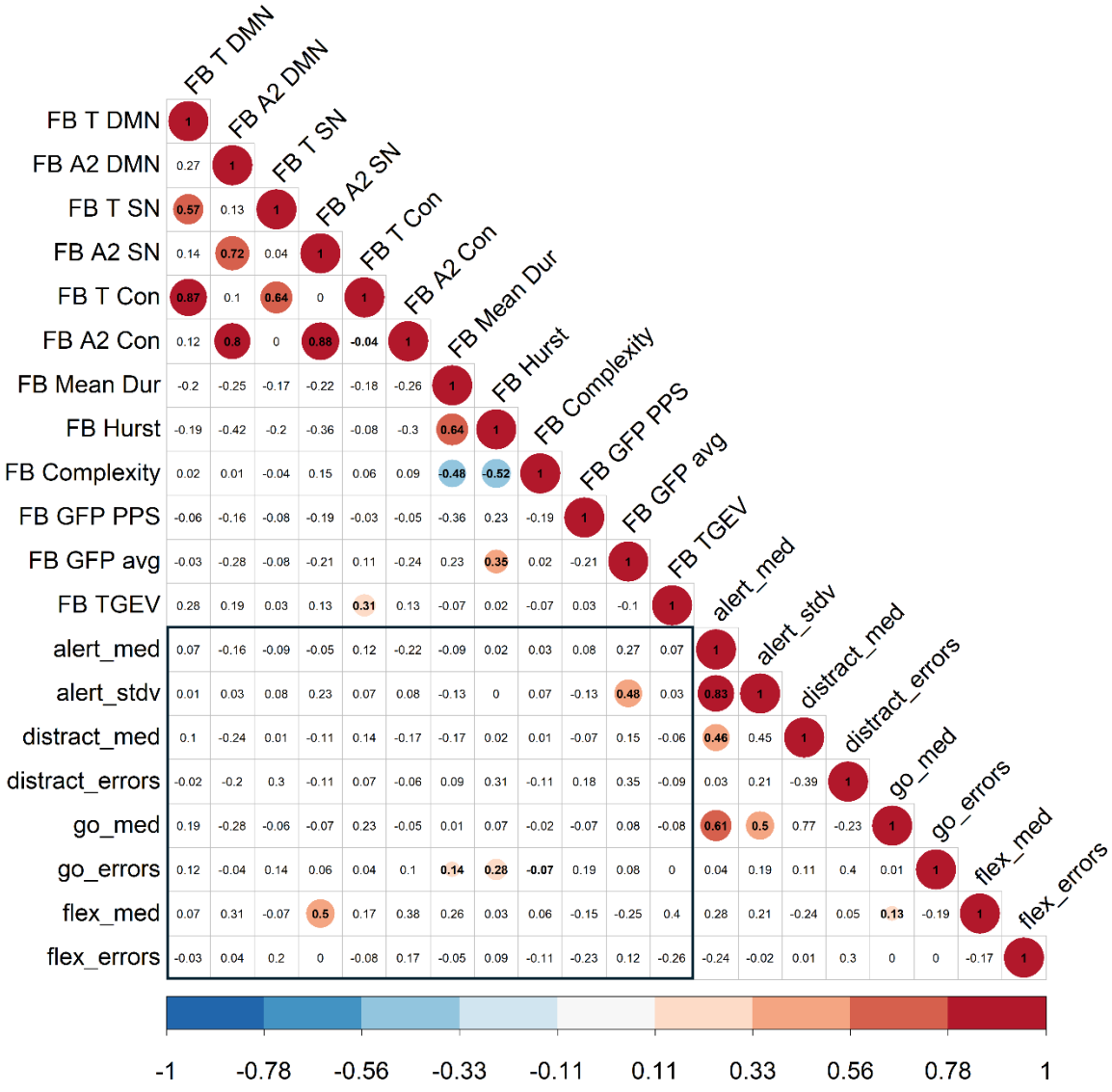

Note. All statistically significant correlations are bolded and indicated by colored circles where warmer colors are direct correlations and cooler colors are inverse correlations. Black boxes highlight columns with correlations of interest. FB = feedback; T = theta, A2 = alpha 2; DMN = default mode network; SN = salience network; Con = control network; Dur = mean duration; Cov = coverage; Occ = occurrence; GEV = global explained variance; GFP = global field power; med = median rection time; stdv = standard deviation of reaction time; alert = alertness subtask; distract = distractibility subtask; go = go/no go subtask; flex = flexibility subtask.

Correlations between select clinical variables stimulus-related microstates and FC identified several correlations with the ABC subscales. GFP was directly correlated with ABC stereotypy but not hyperactivity, as with feedback-related GFP. Microstate mean duration was directly correlated with the ABC irritability subscale, as was noted in correlations with feedback-related microstates, and complexity was directly correlated with ABC hyperactivity. Stimulus-related microstate complexity was significantly different between groups where FXS had reduced complexity indicating those with more typical microstate transition dynamics have higher hyperactive behavior. Finally, there were direct correlations between alpha 2 FC across all networks and ABC lethargy where increased alpha 2 FC (which was reduced for FXS) was associated with increased lethargy (Figure 120).

For Vineland 3 correlations with stimulus-related microstates and FC, we see the same pattern noted for feedback-related EEG variables where GFP was inversely correlated with all subscales on the Vineland indicating reduced adaptive behavior across all domains correlated with increased GFP during feedback processing. Hurst from stimulus microstates was again inversely correlated with the daily living skills subscale (Figure 121).

Correlations between EEG variables of interest from stimulus data and KiTAP were limited. There was a direct correlation between microstate GFP and standard deviation of the response times for the alertness subtask where increased GFP again related to increased response time variability or inconsistencies in response times from trial to trial. Additionally, unlike with feedback-related microstates, GEV was inversely correlated with errors on both the Go/No Go and Flexibility subtasks. However, GEV was only marginally elevated between groups which makes the inverse correlations difficult to interpret. However, results may reflect sex effects

which were not tested as GEV was higher in females in chapter two where females likely make less errors (Figure 122).

Figure 120.

Correlation Plot for Stimulus Period Global Microstate Variables, Functional Connectivity, and ABC

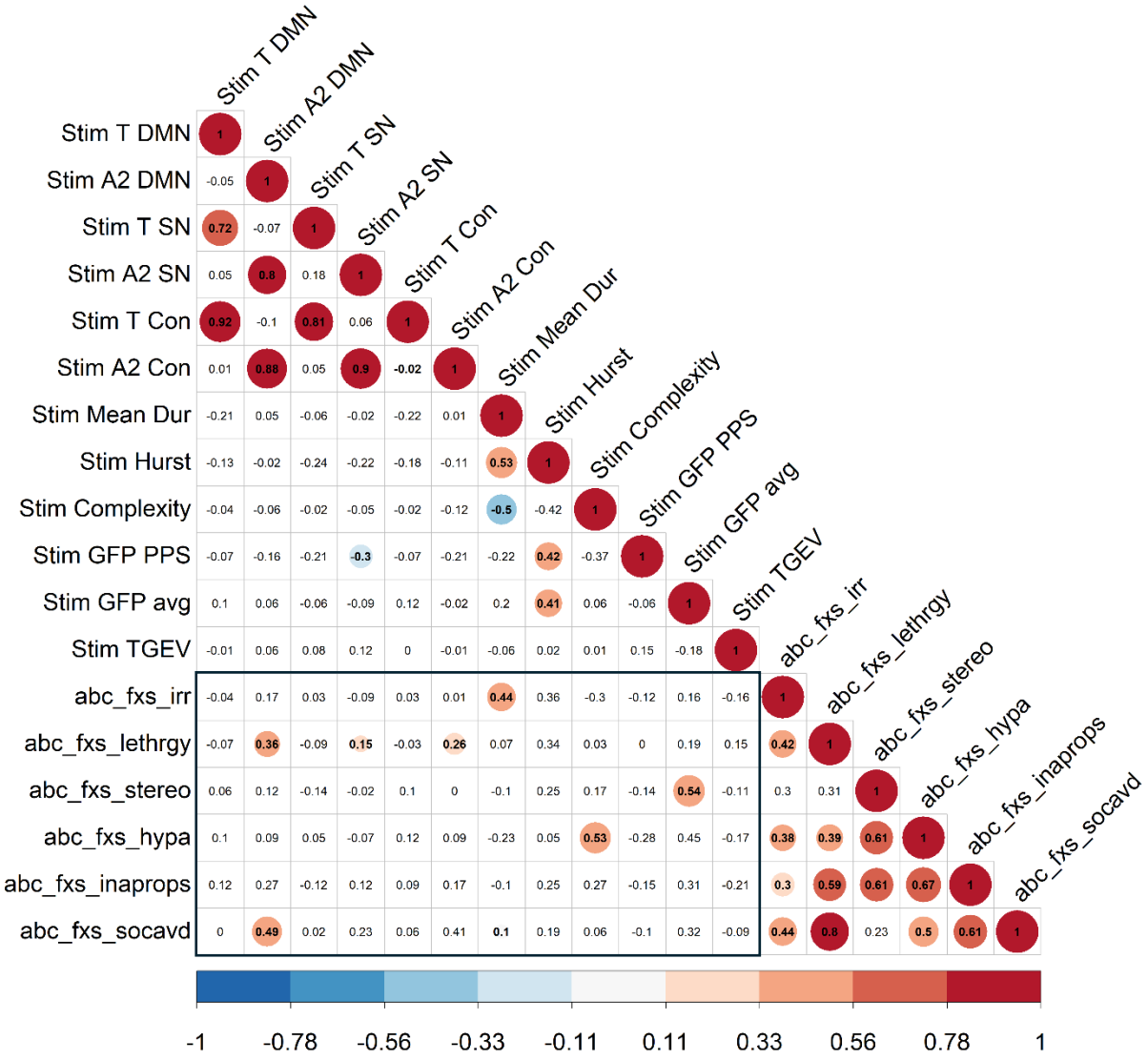

Note. All statistically significant correlations are bolded and indicated by colored circles where warmer colors are direct correlations and cooler colors are inverse correlations. Black boxes highlight columns with correlations of interest. Stim = stimulus ; T = theta, A2 = alpha 2; DMN = default mode network; SN = salience network; Con = control network; Dur = mean duration; Cov = coverage; Occ = occurrence; GEV = global explained variance; GFP = global field power; Irr = irritability; Lethrgy = lethargy; Stereo = stereotypy; hypa = hyperactivity; inaprops = inappropriate speech; socavd = social avoidance.

Figure 121.

Correlation Plot for Stimulus Period Global Microstate Variables, Functional Connectivity, and Vineland-3

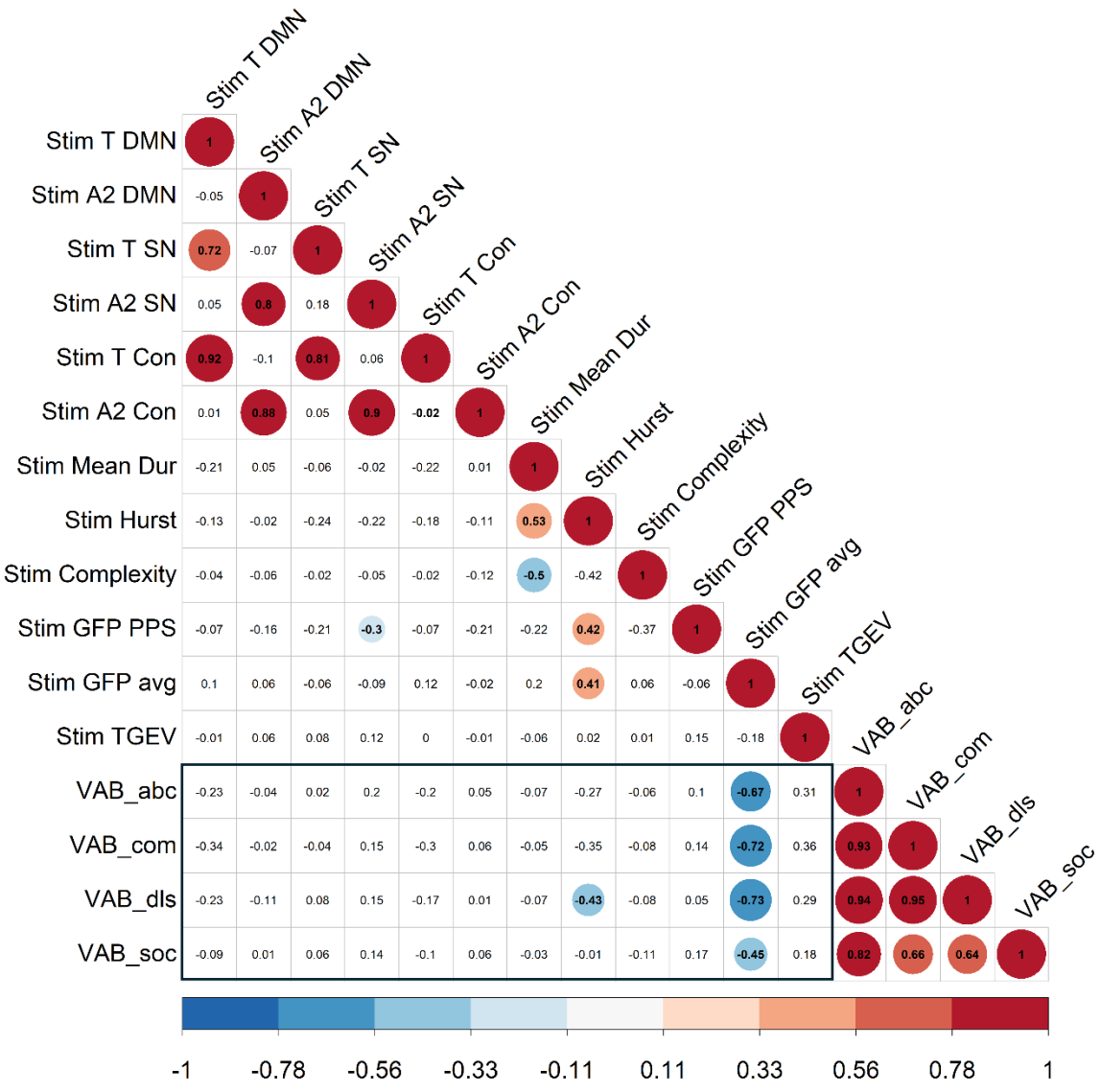

Note. All statistically significant correlations are bolded and indicated by colored circles where warmer colors are direct correlations and cooler colors are inverse correlations. Black boxes highlight columns with correlations of interest. Stim = stimulus; T = theta, A2 = alpha 2; DMN = default mode network; SN = salience network; Con = control network; Dur = mean duration; Cov = coverage; Occ = occurrence; GEV = global explained variance; GFP = global field power; abc = adaptive behavior composite; com = communication; dls = daily living skills; soc = socialization.

Figure 122.

Correlation Plot for Stimulus Period Global Microstate Variables,, Functional Connectivity, and KiTAP

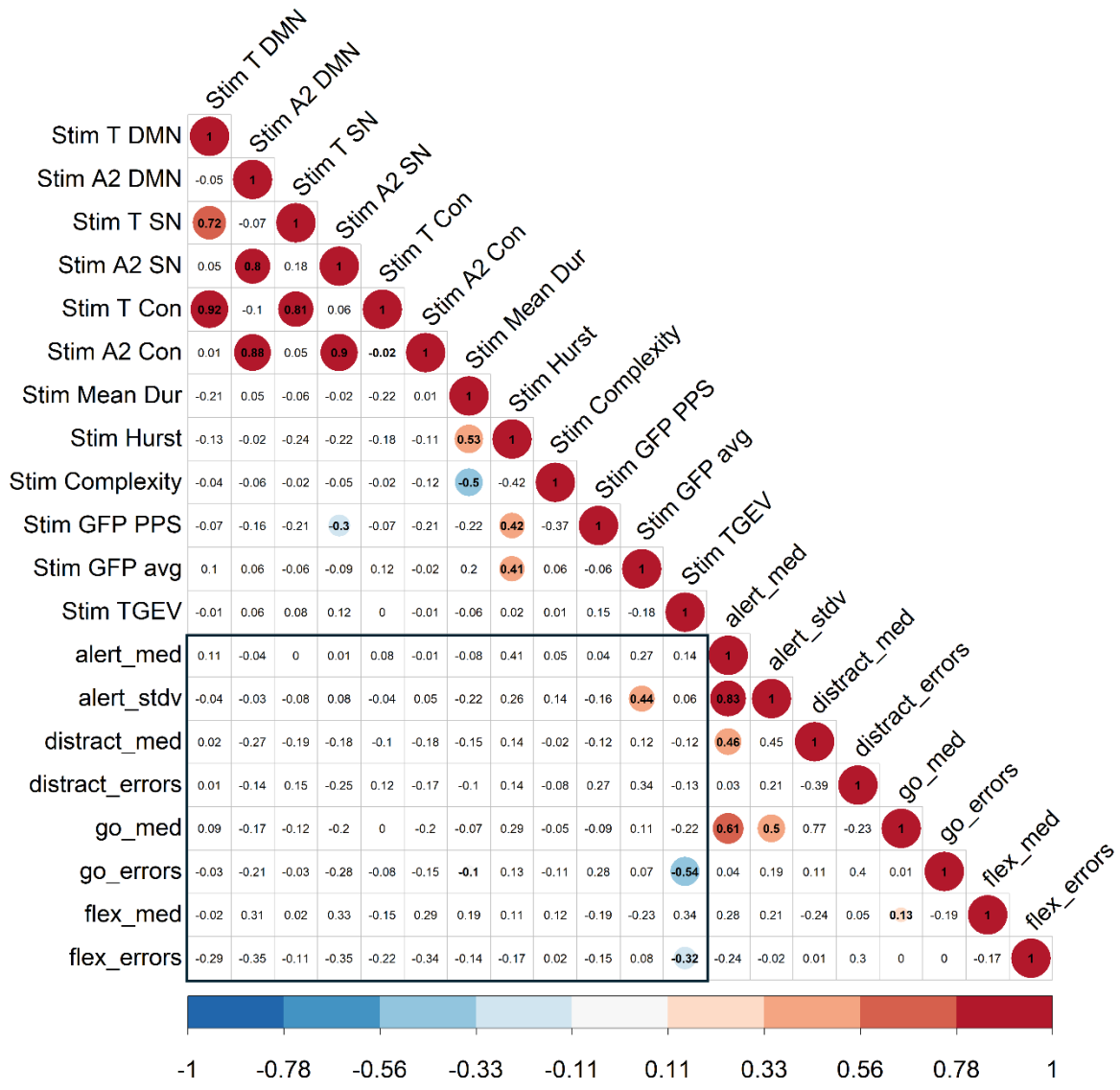

Note. All statistically significant correlations are bolded and indicated by colored circles where warmer colors are direct correlations and cooler colors are inverse correlations. Black boxes highlight columns with correlations of interest. Stim = stimulus; T = theta, A2 = alpha 2; DMN = default mode network; SN = salience network; Con = control network; Dur = mean duration; Cov = coverage; Occ = occurrence; GEV = global explained variance; GFP = global field power; med = median rection time; stdv = standard deviation of reaction time; alert = alertness subtask; distract = distractibility subtask; go = go/no go subtask; flex = flexibility subtask.

Correlations between select clinical variables and microstates and FC from pre-stimulus periods identified several correlations with the ABC subscales. GFP was directly correlated with both ABC stereotypy and hyperactivity, as with feedback-related GFP. Microstate mean duration was directly correlated with the ABC irritability subscale, as was noted in correlations with feedback-related microstates. Finally, there were direct correlations between alpha 2 FC across all networks and ABC lethargy where increased alpha 2 FC (which was reduced for FXS) was associated with increased lethargy, as were observed for stimulus-related data (Figure 123).

For Vineland 3 correlations with stimulus-related microstates and FC, we see the same pattern noted for feedback-related EEG variables where GFP was inversely correlated with all subscales on the Vineland indicating reduced adaptive behavior across all domains correlated with increased GFP during feedback processing. However, Hurst from pre-stimulus microstates was not inversely correlated with the daily living skills subscale unlike with stimulus and pre-stimulus which was an intuitive finding, given Hurst did not differ between groups in the pre-stimulus period (Figure 124).

Correlations between EEG variables of interest from pre-stimulus data and KiTAP were also limited. There was a direct correlation between microstate GFP and standard deviation of the response times for the alertness subtask where increased GFP again related to increased response time variability or inconsistencies in response times from trial to trial. Lastly, there was an inverse correlation between microstate complexity and errors on the distractibility subtask where increased errors were associated with reduced complexity. However, complexity was not significantly different between groups during the pre-stimulus period (Figure 125).

Figure 123.

Correlation Plot for Pre-stimulus Period Global Microstate Variables, Functional Connectivity, and ABC

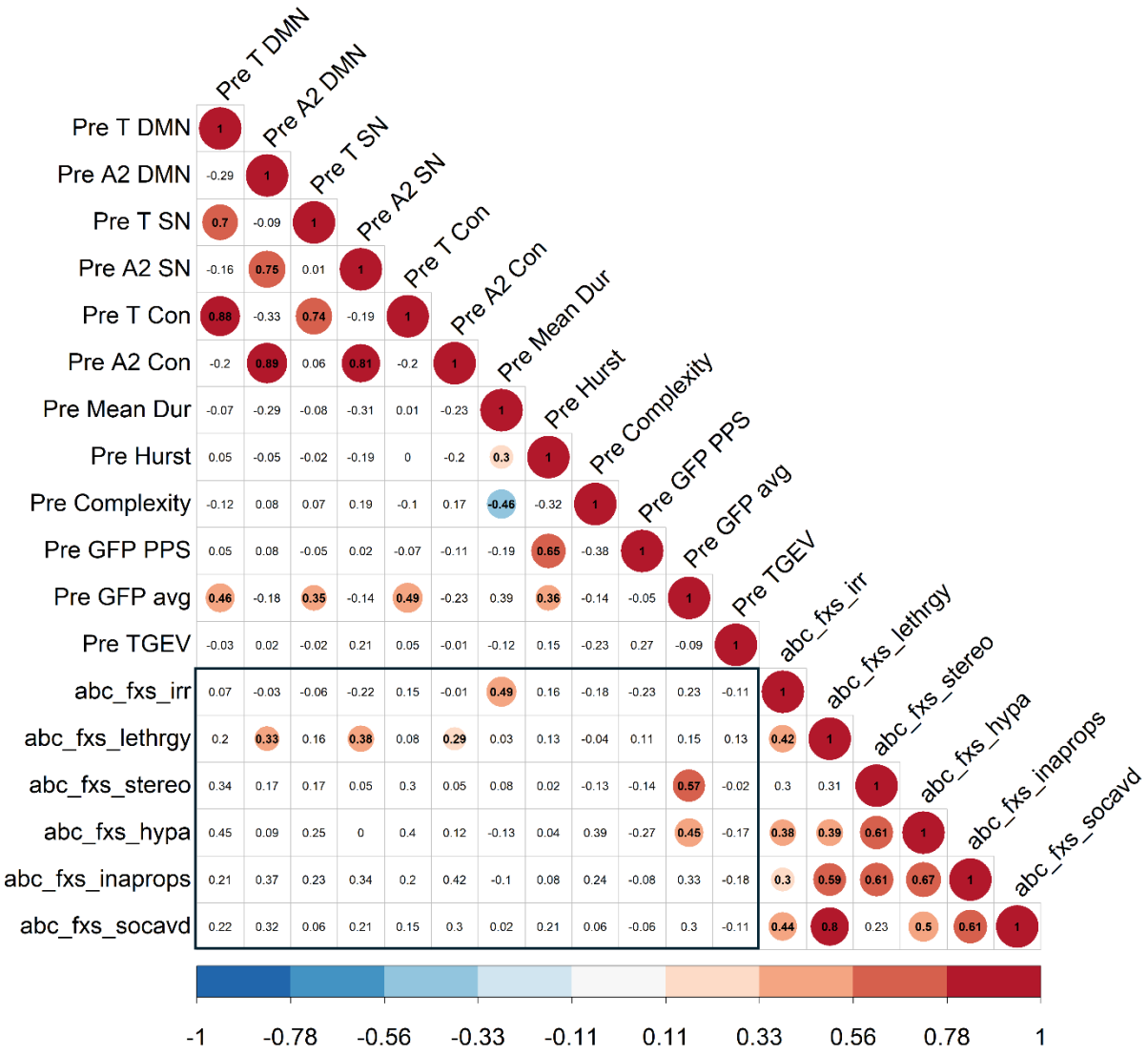

Note. All statistically significant correlations are bolded and indicated by colored circles where warmer colors are direct correlations and cooler colors are inverse correlations. Black boxes highlight columns with correlations of interest. Pre = pre-stimulus ; T = theta, A2 = alpha 2; DMN = default mode network; SN = salience network; Con = control network; Dur = mean duration; Cov = coverage; Occ = occurrence; GEV = global explained variance; GFP = global field power; Irr = irritability; Lethrgy = lethargy; Stereo = stereotypy; hypa = hyperactivity; inaprops = inappropriate speech; socavd = social avoidance.

Figure 124.

Correlation Plot for Pre-stimulus Period Global Microstate Variables, Functional Connectivity, and Vineland-3

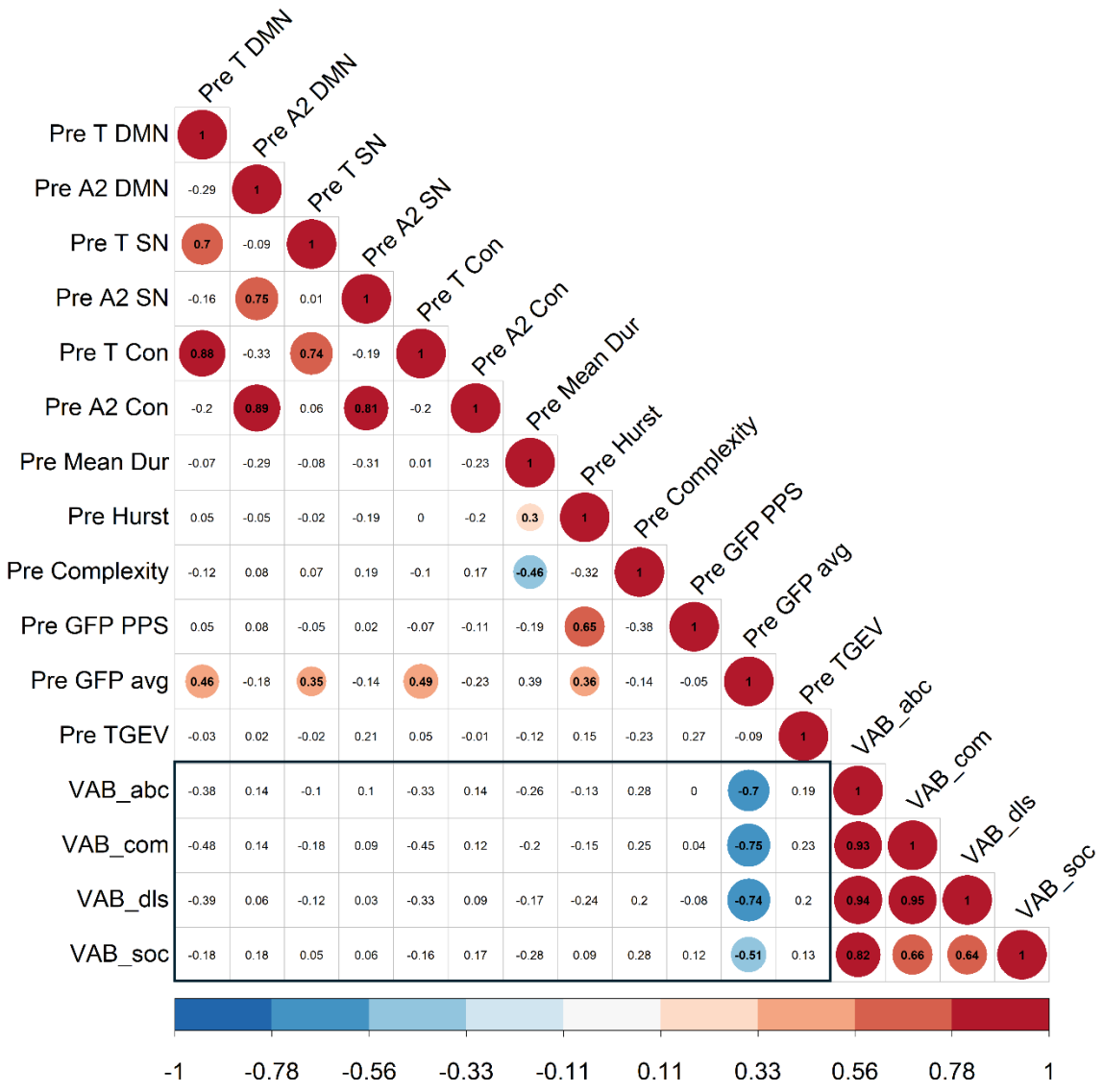

Note. All statistically significant correlations are bolded and indicated by colored circles where warmer colors are direct correlations and cooler colors are inverse correlations. Black boxes highlight columns with correlations of interest. Pre = pre-stimulus; T = theta, A2 = alpha 2; DMN = default mode network; SN = salience network; Con = control network; Dur = mean duration; Cov = coverage; Occ = occurrence; GEV = global explained variance; GFP = global field power; abc = adaptive behavior composite; com = communication; dls = daily living skills; soc = socialization.

Figure 125.

Correlation Plot for Pre-stimulus Period Global Microstate Variables, Functional Connectivity, and KiTAP

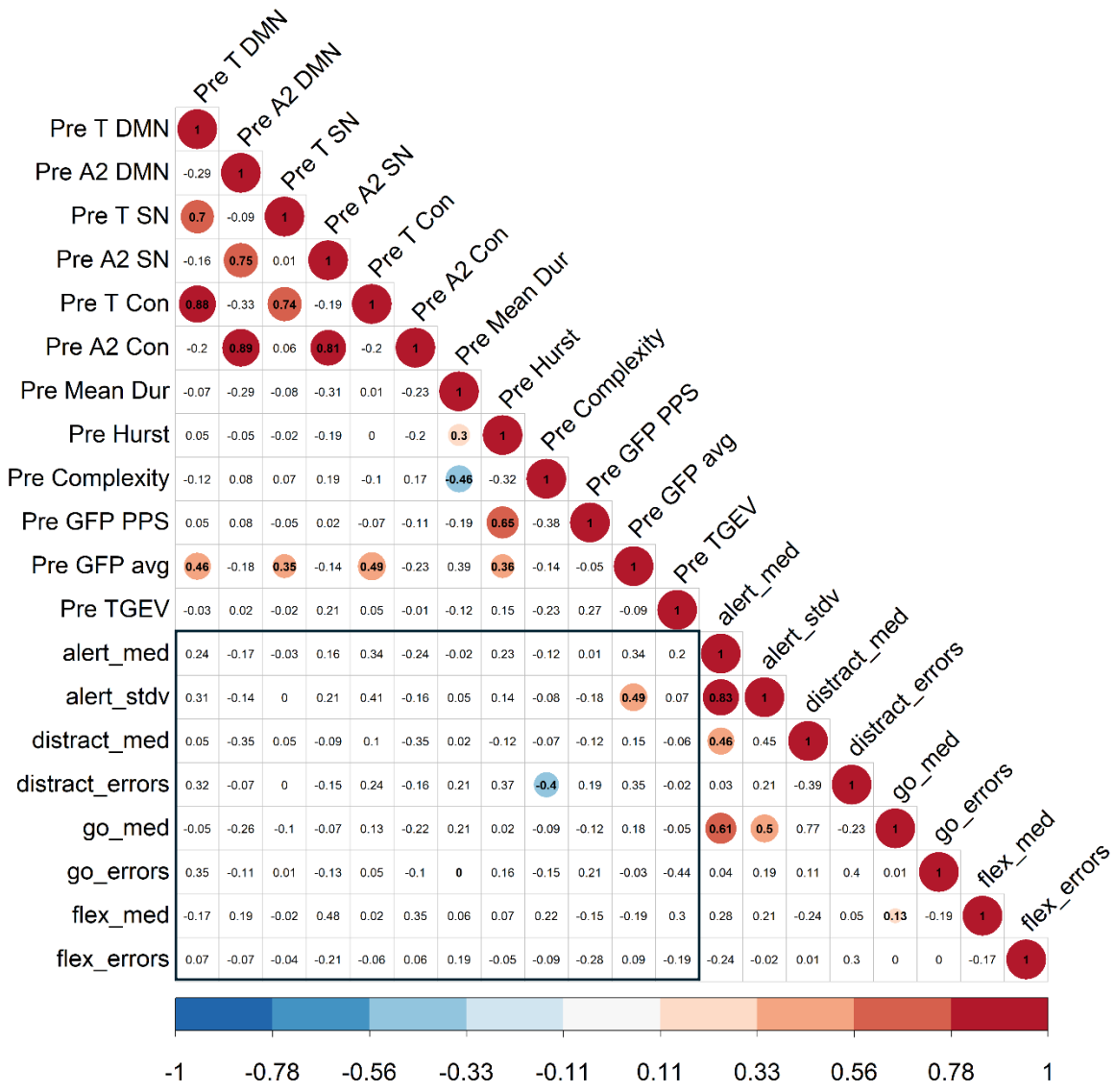

Note. All statistically significant correlations are bolded and indicated by colored circles where warmer colors are direct correlations and cooler colors are inverse correlations. Black boxes highlight columns with correlations of interest. Pre = pre-stimulus; T = theta, A2 = alpha 2; DMN = default mode network; SN = salience network; Con = control network; Dur = mean duration; Cov = coverage; Occ = occurrence; GEV = global explained variance; GFP = global field power; med = median rection time; stdv = standard deviation of reaction time; alert = alertness subtask; distract = distractibility subtask; go = go/no go subtask; flex = flexibility subtask.

Discussion

Symptoms across the cognitive domain are cited as highly disruptive and distressing for both individuals with FXS and their families (Weber et al., 2019). In an effort to direct research toward addressing patient-centered concerns, the current study employed a cognitive EEG task adapted for FXS to evaluate neural processes related to cognitive flexibility where cognitive flexibility is a core cognitive-related concern in FXS (Huddleston et al., 2014; Salcedo-Arellano et al., 2020; Schmitt et al., 2023). Recent work identified a link between frontal alpha FC and executive function disruptions in FXS from rsEEG where FC disruptions were linked with performance indicators of cognitive inflexibility (Schmitt et al., 2022). The current study employed a RLEEG task, designed to address similar hypotheses, in order to drive and measure brain states specific to cognitive flexibility by evaluating functional connectivity through a functional network lens. Additionally, the present study addressed more complex hypotheses related to functional network dynamics to begin bridging cognitive neurophysiology and behavior.

Feedback Event Related Potentials

Briefly, ERP results suggest both neural hyperreactivity to the sensory stimulation associated with feedback during the RLEEG task and reward processing disruptions. Specifically, the RewP amplitude group differences reflect increased response magnitude to reward in FXS, particularly for correct feedback received before the error on reversal trials. This response was also related to earlier sensory hyperresponsivity to feedback in FXS, suggesting an overall hyperresponsive response pattern rather than feedback-specific modulation. Group differences were driven by TDC, who had significantly different amplitudes between RewP for the correct preceding the reversal error compared to the RewP for the correct following the

reversal error, where amplitudes were not significantly different between groups, which suggests modulation of the RewP response depending on whether receiving repeated correct feedback inputs or processing correct feedback after receiving an error which indicates a need to shift behavior (Bauer et al., 2025). Elevated RewP amplitudes in FXS were consistent regardless of whether receiving repeated correct feedback or whether correct feedback followed an error, a feature of cognitive inflexibility and reduced executive control where expectance of feedback valence is altered, as in ASD (Bauer et al., 2025; Cannon et al., 2021). For TDC, the increased responses to correct after receiving an unanticipated error likely reflect several underlying processing including increased salience, increased reward value (i.e., reward of the correct after an unexpected error is worth more than a correct after a series of correct/rewarding inputs), increased resources dedicated to reinforcement of the choice made, and potential monitoring systems engaged for updating prediction coding and reward certainty (Bauer et al., 2023; Cockburn & Holroyd, 2018; Donaldson et al., 2017; Muir et al., 2021). Overall, these processes are likely disrupted in FXS where reward outcomes are likely always uncertain reflective of prediction coding disruptions (Bauer et al., 2023). Additionally, FXS exhibited heightened neural responses to feedback where increased amplitudes of early components were correlated with an increased RewP amplitude which may reflect heightened salience of reward-related stimuli and hyperreactivity to feedback throughout the neural processing stream indicative of processing rigidity. Specifically, the correlations suggest neural hyper-reactivity may contribute to cognitive disruptions (Knoth & Lippe, 2012).

Microstates

Overall, microstate findings highlight the robustness of GFP, as GFP was higher for FXS across all data types which was consistent with resting state. However, GFP was only marginally

different during resting state and was only significantly different between groups when accounting for how GFP was distributed across individual microstate classes. As such, increased GFP in FXS was more notable when engaged in task-positive processing. Microstate GFP represents the strength of the electric field where higher GFP likely reflects increased response amplitude and spatial consistency. More specifically, GFP is thought to represent the degree of neural synchrony between network activity generators, where elevations likely reflect network rigidity (Khanna et al., 2015; Takarae et al., 2023). GFP was different between groups for all task periods suggesting elevated GFP represents a more global disruption representing diffuse cortical rigidity not modulated by external task type/task engagement.

Microstate GEV was increased for FXS during feedback but not during the pre-stimulus or stimulus periods. Increased GEV represents less variability in the FXS EEG signal where FXS feedback EEG was better explained by a limited set of more dominant microstate templates than TDC. GEV differences may also reflect increased rigidity in FXS network engagement corresponding to reduced ability to modulate neural activity over the course of the task which is necessary for effective and efficient prediction coding (de-Wit et al., 2010; Hall-McMaster et al., 2019; Hauser et al., 2015). Increased GEV was also identified at rest which suggests rsEEG may capture similar disruptions captured by feedback periods where pre-stimulus and stimulus periods differ. This pattern is interesting given pre-stimulus periods were hypothesized to be more similar to resting state than stimulus and feedback periods. Pre-stimulus periods, despite the absence of external stimulation still involve attentional and anticipatory processes where heightened cognitive process engagement in FXS may drive differences from resting state differences. Specifically, differences in hyper-responsivity between FXS and TDC may be

heightened during time periods where TDC modulate more effectively than FXS, such as pre-stimulus periods, where TDC return to a state more akin to resting, where FXS do not.

Interestingly, during feedback periods, Hurst exponents were elevated for FXS and trended towards significance for stimulus and pre-stimulus periods which differed from rsEEG findings. The Hurst exponent is a measure of long-range temporal correlations, where values higher than 0.5 represent increased long-range stability. In FXS higher values relative to TDC may indicate increased rigidity in neural networks where FXS EEG is more self-similar across the feedback periods. Increased Hurst values also shared inverse correlations with abbreviated IQ where Hurst may serve as a bridge between indices of network rigidity and worse cognitive ability. As Hurst was not different between groups during rsEEG, Hurst may be sensitive to the rigidity of specific neural states related to feedback processing.

The Hurst exponent has also recently garnered interest as a proxy measure for excitation/inhibition imbalance in which reduced Hurst exponent values reflect increased excitation (Ahmad et al., 2022; Nishio et al., 2024). Further, Hurst exponents were found to map onto ex vivo parvalbumin (PV) mRNA expression in the mouse model of FXS; PV positive interneurons are hypoactive in FXS and linked to disruptions in the theta range, the mouse equivalent of alpha (Kornfeld-Sylla et al., 2025). However, Hurst exponent results should be regarded with care, as E/I dysfunction could occur at various neural system levels (e.g., neurotransmitters, individual cells, network, or globally) (Ahmad et al., 2022; Sohal & Rubenstein, 2019). In FXS, E/I imbalance may stem from disruptions at multiple levels (Cea-Del Rio et al., 2020). The increase in Hurst relative to TDC suggests increased inhibition/reduced excitation, which is counterintuitive, as FXS are reportedly hyperexcitable (Liu et al., 2022). Further, inhibitory function is notably altered in FXS where inhibitory networks are unable to

regulate excitatory flow resulting in hyperexcitability resulting in hyperexcitable phenotypes (Cea-Del Rio & Huntsman, 2014). The current Hurst findings, paired with ERP findings where there was evidence for increased neural hyperexcitability during feedback periods when engaged with valanced stimuli important for task performance, are incongruent with the conclusion that Hurst exponents represent E/I imbalance in favor of inhibition. Rather, the conclusion that Hurst exponents reflect increased neural rigidity at lower frequencies better supports the current pattern of findings where, rather than Hurst values representing less excitation, they capture persistently reduced dynamic responses. Increased Hurst exponent levels have been shown to reflect elevated cognitive load where increased Hurst in FXS may also index greater effort or resources dedicated to task engagement (Stier et al., 2023). Further, Hurst was computed as part of the microstate analysis where data were filtered at 40 Hz. As such, Hurst does not index E/I dynamics accurately/ as it typically would when computed in different contexts. As both microstates and ERPs are generated by low frequency brain dynamics, increased Hurst within microstates may reflect more complex dynamics within the lower frequencies. Ultimately, Hurst calculated as part of the microstate analysis may capture the low frequency consequences of inhibitory network dysfunction and increased neural hyperexcitability but was not a direct measure of hyperexcitability or E/I dynamics.

An important take away from microstate results was the number and size of group differences for the pre-stimulus microstate solution. Further, within subject differences for individual microstate duration, coverage, and occurrence were observed for TDC and not FXS. While pairwise comparisons did not broadly survive correction, thus representing smaller effects, the overarching difference suggested increased modulation between individual microstates in TDC but not in FXS. Coverage and occurrence were also significantly different across

microstates for TDC only from feedback and stimulus periods, respectively. Overall, these likely represent typical microstate variability where class differences on duration, coverage, and occurrence during pre-stimulus periods reflect varying neural dynamics. Modulation is likely required for typical task engagement where increased differences in TDC from pre-stimulus-to-stimulus-to-feedback periods represent modulation appropriate for task engagement and to keep pace with task demands. Importantly, pre-stimulus periods may represent the most extreme differences between groups where TDC cognitive networks were less engaged and FXS still exhibited hyperexcitability, possibly as a consequence of inefficient task processing.

Functional Connectivity

An important observation from FC computed on RLEEG data was that all FC values in the current study were higher in magnitude than FC values identified in chapter two and observed in published studies on FXS. The increased FC values indicate greater neural synchrony was achieved when driving specific and consistent brain states using external tasks (Schmitt et al., 2022; Wang et al., 2017).

Importantly, FC analyses identified increased theta FC across all data types for all functional networks of interest, similar to findings from resting state data and past resting state studies in FXS (van der Molen et al., 2014). Thus, increased theta FC in FXS relative to TDC is seemingly robust and consistent across task types. Numerous previous studies have identified increased theta power in FXS, irrespective of task type (Ethridge et al., 2017; 2019; Pedapati et al., 2022; van der Molen et al., 2013; Wang et al., 2017). While dWPLI is a phase-based measure and thus does not directly index theta power/is not sensitive to changes in power, elevated theta FC may share similar physiological mechanisms to those resulting in increased theta power in FXS. Namely, elevated theta FC may represent a functional consequence of the cross frequency

relationship between theta power and higher frequency activity where increased theta is used in FXS to regulate gamma activity instead of alpha regulating gamma activity, as noted in TDC (Wang et al., 2017; Pedapati et al., 2022). While increased theta power may represent a compensatory activity for the inability to mount a functionally relevant alpha response, the increased theta activity may prevent temporal and context specificity during stimulus processing and task engagement, potentially via a ceiling effect (Kornfeld-Sylla et al., 2025; Norris et al., 2022; Tan et al., 2024; Wang et al., 2017). Specifically, the seeming inconsistencies in correlations between theta activity and cognitive performance suggest the way theta is utilized (i.e., when and between which neural source) is more important for cognitive performance than whether theta is more or less online (i.e., higher or lower power) (Tan et al., 2024). In the literature, increased frontal midline theta during cognitive tasks is linked to working memory performance, especially with increasing cognitive load where theta may encode additional information about task difficulty (Kottlow et al., 2015). Sustained theta FC in FXS may prevent the appropriate fluctuation in the flow of information during stimulus and feedback windows as a byproduct of an inability to modulate phase-alignment within functional networks. Past studies also found evidence for rhythmic excitability in mid-frontal theta where certain signals engaged in the processes of cognitive control from mid-frontal sources may result in entrainment of anatomically distinct neural areas which may present as elevated EEG FC due to the way it is analyzed (Cavanagh & Frank, 2014). The inability to modulate theta FC across task windows was also observed where FXS exhibited heightened control network theta FC during the pre-stimulus periods where theta FC was similarly elevated across pre-stimulus, stimulus, and feedback periods. Unlike FXS, theta FC increased from the pre-stimulus to the stimulus and feedback windows for TDC indicating increased cognitive engagement during task-positive

processing where FXS engaged the control network equally across the whole task, even during periods with no sensory input or task requirements. The pre-stimulus period may represent the most extreme difference between FXS and TDC where TDC are able to successfully modulate theta for appropriate task engagement and FXS were not. In addition to a lack of modulation, heighted theta FC in the control network during the pre-stimulus window may represent ongoing cognitive processing as a consequence of inefficient network processing and/or a neural prioritization of global theta as inhibitory control, at the expense of task-specific modulation. As all networks analyzed play a role in cognitive control, the global and diffuse theta FC increases in FXS represent possible disruptions to neural specificity required for theta activity to engage networks for appropriate cognition, though these dynamics may be most disrupted within the control network (Breukelaar et al., 2020).

Theta Functional Connectivity

The present study identified important differences in how diffuse the strength of theta FC was between task windows across the three functional networks of interest when driving cognitive-specific neural processes. Resting state theta FC was diffusely increased across all networks in chapter two which was not the case for theta FC computed on RLEEG.

Feedback Theta Functional Connectivity

From individual network node analyses of feedback related data, the top connections for all networks were not significantly different between groups where theta FC was equal within the strongest DMN, SN, and control network connections for TDC. However, for DMN and SN, the sum score was significantly different which differed from resting state FC. The top two DMN connections involved different node pairs where connections in FXS did not largely overlap with TDC. Further, the sum score differed, and node pairs did not largely overlap between groups for

DMN. Together, these results suggested a shift in the primary architecture of DMN for FXS compared to TDC. Given DMN should not be active during task-related processing, the difference in primary node activation may reflect a shift towards DMN-specific nodes for feedback processing which may disrupt typical feedback engagement. For SN, the top TDC connections partially overlapped between groups (five connections), including the second strongest connection for TDC. Paired with a significant sum score difference, the group difference for SN at the whole network level likely represents a shift in magnitude for the top ten FXS connections. Finally for feedback-related control network, theta FC was diffusely increased across the network for FXS, as there were no differences in theta FC for the primary TDC connections and no sum score differences where increased theta FC at the whole network level reflects a more diffuse increase across the whole network rather than a difference in the primary network architecture used to accomplish control network processing. Specifically, comparable sum scores indicate connections outside of the top ten connections were elevated compared to TDC. The diffuse increase of theta FC in control network was further evident in the whole network plot where elevated FC seems more distributed across network node pairs compared to TDC during feedback periods.

Stimulus Theta Functional Connectivity

The analysis of the strongest connections for network activity during stimulus periods identified differences in the top connections for FXS relative to TDC rather than a diffuse network increase. The two strongest TDC connections were significantly different between groups and the sum of the top ten was also different. Though, the two strongest TDC connections were also in the top ten connections for FXS suggesting increased top ten FC magnitude for FXS drove increased theta FC whole-network group difference. However, limited node pairs

overlapped between groups where combined results indicated a shift in primary network architecture on top of a magnitude shift indicating a more focal increase in theta FC during stimulus processing (Bassett & Sporns, 2017). Interestingly, FXS had less connections centered on the right precuneus which is a central component of the DMN typically supporting self-referential components of mentalization and integrative processes during cognition. The precuneus is anatomically and functionally connected to sensory and attention areas and precuneus activity relates to external monitoring and integrative processes (Cavanna & Trimble, 2006; Fransson & Marrelec, 2008). The top ten connections for FXS additionally were centered on the right posterior cingulate node, as in TDC. Though, the significant sum score suggests elevated theta FC in those connections where FXS may shift toward increased use or reliance on the posterior cingulate cortex. The posterior cingulate cortex is a primary hub of the DMN that serves to focus attention primarily for internally directed cognition but also a key area for arousal and awareness where disruptions are linked to difficulties with sustained attention (Leech & Sharp, 2014). Together, precuneus/posterior cingulate disruptions in FXS during task engagement in the stimulus window may reflect disruptions to sustained task attention.

Theta FC within the SN during the stimulus window was elevated in FXS relative to TDC where the top TDC connection was significantly different between groups. The top TDC connection was also the top FXS connection which, paired with a significant sum score difference, indicates a focal shift in theta FC magnitude within the strongest connections for FXS. Theta FC in SN was diffusely increased at rest but the increase relative to TDC during stimulus and feedback processing seemingly reflects a shift in magnitude within the same approximate network architecture used by TDC. Of note, a difference between FXS and TDC was identified in chapter two for the top node pair between right and left supramarginal nodes

indicating a shift in magnitude of bilateral supramarginal gyri connectivity. However, the sum score was not different which indicated hyperconnectivity between bilateral supramarginal gyri where increased activity was linked to cognitive disruptions in previous studies (Kwon et al., 2001). Similar disruptions were not evident in SN network connectivity during stimulus-related or feedback-related processing.

Finally, theta FC within the control network during stimulus-related processing was not diffusely increased, as noted in both resting state and feedback-related processing. The sum score was significantly different between groups and no node pairs overlapped in the top ten connections indicating primary architecture differences between FXS and TDC. Importantly, the top ten FXS connections centered on the left and right inferior parietal nodes where TDC connections centered on the rostral middle frontal and middle temporal nodes where connectivity was predominately between parietal and frontal sources. The top ten TDC connections had more interconnectivity between frontal sources during stimulus processing where FXS processing remained dominant in parietal sources. The inferior parietal nodes play a key, supportive role in the control network in concert with the dorsal lateral prefrontal cortex for attention allocation and integration of information for the purpose of goal-directed behavior (Numssen et al., 2021; Seeley et al., 2007). Further inferior parietal nodes are linked to multimodal sensory integration (Nishitani et al., 1998). As integration of sensory and cognitive information is necessary for appropriate RL engagement, the shift in FXS may reflect a different processing prioritization towards sensory processing and integration over cognitive-related processes. Importantly, the inferior parietal lobule (IPL) also carries error-related signals in task contexts where the right IPL is associated with error and left IPL typically exhibits sustained activity (Dosenbach et al., 2006). In FXS, the strongest node pairs during stimulus processing involved the left inferior parietal

nodes where feedback related processing centered on the right inferior parietal node. Importantly, a shift from typical control network connectivity (increased frontofrontal connectivity) in FXS to a predominate use of frontoparietal processing may reflect deficits in top-down control and prioritization of stimulus-driven or more DMN-like patterns of processing (Dosenbach et al., 2008). Overall, the elevated control network sum score where node pairs did not overlap with TDC during stimulus-related processing and centered on parietal sources for FXS may reflect cognitive inflexibility or network rigidity (Friedman & Robbins, 2021).

Pre-stimulus Theta Functional Connectivity

The analysis of individual network connections during pre-stimulus periods identified significantly different sum scores between groups across all functional networks of interest. Node pairs involved in the top two TDC connections did not overlap with the top two FXS connections and were similar in FC strength/magnitude between groups for all networks (i.e., no group difference on top connections). Further, across the top ten connections, there was limited overlap in node pairs where 1 node pair overlapped in DMN, four in SN, and none were identified for control network. Overall, the results suggest pre-stimulus group differences at the whole network level were driven by a shift in network primary architecture where FXS had increased FC strength in different node pairs compared to TDC. Especially for control network where zero node pairs overlapped between groups. Of note, FXS SN centered on the left supramarginal gyrus which was notably disrupted in rsEEG. Theta FC findings add further support to the conclusion that pre-stimulus periods were a point of extreme difference between FXS and TDC where other measures identified evidence of continued cognitive processing in FXS pre-stimulus periods.

Despite the noted patterns in brain areas involved in the top ten connections for each network, EEG has poor spatial resolution even with source localization and thus interpretations involving spatial-specific claims warrant caution. To reiterate the most important take aways from theta FC connectivity, theta FC from within the functional networks of interest was diffusely elevated across each network for FXS relative to controls. However, during task-positive processing theta FC was no longer diffusely elevated across all networks and instead differed across task windows and networks. During pre-stimulus periods, the top ten connections were shifted to a different set of node pairs in FXS compared to TDC for all three networks, though more node pairs overlapped in SN between FXS and TDC. For stimulus periods, the increased theta FC finding across the whole network resulted from a shift in magnitude for the top connections across all networks for FXS. While the top ten connections for FXS were different in FC strength compared to TDC, the primary architecture of the networks were all similar. Lastly, the primary influence on global network elevations in FXS across networks during feedback windows varied where DMN exhibited different primary architecture of the FXS top ten connections relative to TDC, SN differences were driven by a shift in magnitude for FXS top ten connections relative to TDC, and control network was diffusely elevated across the whole network for FXS.

The clinical relevance of elevated theta FC was more nuanced where patterns of correlations between theta FC and IQ were more variable than noted in resting state data. Existing correlations suggest increased theta FC from RLEEG reflects reduced cognitive ability but not consistently. Pre-stimulus theta FC was inversely correlated with abbreviated IQ in both SN and control network but theta FC from stimulus and feedback data were not correlated with abbreviated IQ. Though, theta FC in the control network from feedback data did share a

correlation with full scale, verbal, and non-verbal IQ measures which excluded three FXS females with high IQs and high FC values due to the increased administration of the abbreviated measure over the full scale. From resting state (i.e., chapter two) findings, increased theta FC across all networks were correlated with IQ where elevated theta FC was interpreted as detrimental to cognition because of reduced long-range information transfer (van der Molen et al., 2014). Theta FC during feedback periods did share relationships with IQ, though not with abbreviated IQ which had a larger subject count due to the increased administration of the abbreviated measure. Otherwise, theta FC variables were not linked to clinical symptoms.

In combination with microstate and ERP results, the present conclusions that ERP findings reflect hyperactivity in FXS feedback processing were further supported by increased differences on variables from the pre-stimulus periods where FXS exhibited heightened responses compared to TDC. Increased activity during pre-stimulus periods for FXS may represent sustained engagement of cognitive-specific networks where TDC momentarily shut down cognitive/task-positive processing networks and engage task-negative networks reflective of efficient prediction updating and healthy network dynamics. Namely, the increased theta FC paired with increased theta power often noted in FXS (though not tested in the current paradigm) may interrupt cognitive processing and reward evaluation in FXS where dynamic modulation of theta within functional networks is important for appropriate cognitive performance (Ethridge et al., 2019; Kottlow et al., 2015).

Novelly, alpha 2 FC was reduced for FXS across all data types for all functional networks of interest except control network during feedback periods which was comparable to TDC alpha 2 FC. The RLEEG FC findings differed from FC results in chapter two where resting state alpha 2 FC was comparable between groups. Control network is most relevant to feedback where FXS

may dedicate more resources to support task engagement sufficiently enough to engage alpha. Whether the lack of group differences in control network alpha 2 FC during feedback processing represents increased successful inhibition or a series of attempted alpha engagement that appear as elevated alpha 2 FC is not clear. Importantly, individuals with FXS have the ability to mount an alpha response during task engagement but are less able to recruit alpha for dynamic use (Norris et al., 2022; 2025; Kornfeld-Sylla et al., 2025). However, patterns of alpha use may be consistent enough between areas within control network to mirror TDC alpha 2 FC, given individuals with FXS dedicate more resources to bring alpha online (i.e., much like in burst analyses, FXS are oscillating within the alpha frequency range but not sufficiently for the dynamic functional use of alpha).

The analysis of the top alpha 2 FC connections for each network identified different patterns of top connection use. Feedback-related top connections for DMN in FXS were indicative of different network architecture used during feedback processing relative to TDC. As alpha 2 FC was reduced at the network level, the lack of group difference in the sum score indicates comparable alpha 2 phase alignment to TDC where disruptions were in connections outside of the top ten. Of note, in DMN, the top connection for TDC was significantly different between groups and was represented in the FXS top ten (third strongest connection) where alpha 2 FC was reduced suggesting a deficit in the connection between right posterior cingulate and the left isthmus. Posterior cingulate cortex is a core node of the DMN where reduced alpha 2 FC for FXS may indicate disruptions in the PCC (node-centric dysfunction). The PCC is important for memory retrieval where the reduced connectivity between the right posterior cingulate node and the right isthmus could represent disruptions in memory updating and feedback integration (Greicius et al., 2003; Leech & Smallwood, 2019). Overall, alpha 2 FC disruptions in DMN were

likely driven by primary node disruptions. For SN, the top two TDC connections and the sum score were not different between groups which indicates some node pairs/brain areas in FXS were able to maintain typical levels of alpha FC and network disruptions were likely representative of diffuse reductions in alpha 2 FC across connections not represented in the top ten. Again, there was not a difference in control network alpha 2 FC during feedback and neither sum scores nor top connections were different suggesting FXS exhibit typical alpha 2 FC during feedback processing.

The strongest stimulus-related connections exhibited interesting dynamics where the top TDC connections in both DMN and SN were different between groups, but the second connection and the sum score were not different suggesting typical alpha 2 FC in FXS. In both networks, the node pairs in the top ten did not substantially overlap suggesting restructuring of the DMN and SN primary architecture used by FXS. The whole network reduction may reflect the reduction in alpha 2 FC for the typical primary node but may also represent reduced connectivity in the connections outside of the top ten.

Finally, during the pre-stimulus window, the strongest two alpha 2 TDC connections and the sum scores were significantly different which indicates diffuse reductions in alpha 2 FC for FXS where all connections were diffusely reduced compared to TDC. Further, sum score differences suggested a shift in primary DMN architecture use across all three networks which may stem from a greater physiological disruption related to reduced alpha generation in FXS (Norris et al., 2022; Pedapati et al., 2022; Wang et al., 2017)

Triple Network Hypothesis

In testing the triple network hypothesis, I predicted individuals with FXS would exhibit difficulties switching out of DMN during the pre-stimulus period and into the control network to

engage with the RL task compared to TDC (i.e., group differences on functional connectivity strength between network notes associated with DMN during pre-stimulus periods and network notes associated with control network during the task window). I further predicted the relationship between pre-stimulus DMN and stimulus period control network FC was mediated by stimulus period SN in FXS (Uddin, 2021). Ultimately, the present results support the hypothesis that triple network dynamics were disrupted in FXS for both theta and alpha 2. Though, alpha 2 differences likely represent the inability to mount an appropriate response in the alpha 2 frequency range where FXS were largely reduced across the board. The theta FC results were in alignment with predicted outcomes but alpha 2 FC dynamics were not.

Conclusions

Past studies identified reduced alpha connectivity during rsEEG across frontal scalp regions, which related to cognitive performance on the KiTAP after controlling for IQ highlighting the possibility that network disruptions correspond to meaningful externally measurable cognitive disruptions (Schmitt et al., 2022). The current study addressed whether these patterns of connectivity during rsEEG are representative of functional connectivity in networks supporting active cognitive processes, and whether functional differences are either 1) static and present during both resting and cognitive task EEG, or 2) more context dependent and present only when challenged by active cognitive requirements. Both microstate and FC results were generally different from resting state which supports the conclusion that even more global disruptions shift dynamics when challenged in specific ways (i.e., driving specific brain states). However, some disruptions were consistent across tasks where elevations in GFP and theta FC may represent more global, static disruptions.

Limitations

One of the major limitations of the current study was the use of correlation analysis to compare microstates and FC variables where temporal scale differences may skew direct comparisons. Specifically, FC represents a measure of within-network synchrony across the full data set where microstates index momentary fluctuations in the global field power. Ultimately, relationships between individual microstate classes and FC were likely obscured by comparing to FC computed irrespective to microstate class. Next steps for the current study include computing FC on microstates in source space to evaluate the within microstate FC for each network.

The FC group differences for FXS were indicative of reduced small world connectivity, but a graph analysis would better address whether the group level FC truly represents more diffuse disruptions to functional networks. Graph analyses within individual networks may not be easily interpretable, however, due to expected connectivity within all nodes of a functional network, as opposed to across the whole head, as is typically done in graph analysis. Therefore, within network FC measures, as conducted here, provides important additional information for interpretation of any future graph analysis. Additionally, variability or entropy analyses would confirm whether edge-wise variance exists which would add additional support to the present conclusions.

Volume conduction poses a limitation to interpretation, as the current study utilized a source analysis without computing the head model from individual anatomy or record of channel positions and instead relied on average models. Conclusions or interpretations made regarding specific nodes and node connections are limited by spatial smearing and should be interpreted with caution. While the field has utilized this approach and the results will be comparable within the scope of existing FXS research, there was still a lack of specificity needed to more reliably or precisely identify generators of the EEG signals (Pedapati et al., 2022; Schmitt et al., 2022).

However, the methods were validated source localization methods, and the current results were critical for next steps and to inform ongoing efforts to both better understand cognitive disruptions in FXS and identify novel treatments that ameliorate the more distressing aspects of the disorder. Particularly, an effort was made to interpret FC findings in the context of existing FXS fMRI literature in order to better understand where specific disruption exist.

Finally, FC results align with absolute power results from previous studies where absolute power increases in the theta frequency band range and decreases in absolute alpha power are robust outcomes in FXS relative to TDC (Wang et al., 2017; Pedapati et al., 2022). Further, increased theta power and reduced alpha power share similar clinical correlation patterns raising questions about the relationship between absolute power dynamics and both theta and alpha FC. The FC measure, dWPLI, reduces biases from volume conduction and should not be sensitive to power differences. However, real physiological drivers may explain why FC outcomes track with absolute power dynamics. Both theta and alpha are slower waves which can travel further in a fluid medium which lends to the use of slow wave oscillations for long range neural communication where slow rhythms can synchronize and bind larger spatial areas/ensembles for the purpose of shared functional processing (Buzsaki & Draguhn, 2004; Zhang et al., 2019). Thus, increased power in theta may coincidentally occur alongside increased theta FC where theta waves are used for long range information transfer and increased theta FC synchrony may result as a byproduct of enhanced (compensatory) or inefficient (maladaptive) long-range information transfer. However, the nature of the relationship between elevated theta power and increased theta FC may require further investigation. Especially given power was not computed on RLEEG and relationships between power and FC were not tested in the present study. Unlike theta FC, reduced alpha 2 FC and power overlap may reflect a more

straightforward relationship where reduced alpha 2 FC and reduced alpha 2 power may correspond to similar disruptions in inhibitory function. A reduced ability to mount a sufficient alpha response, evident in power findings, may also manifest in FC analyses where reduced inhibitory network activity results in less synchronous activity between sites (Norris et al., 2022). Ultimately, the overlap for both theta and alpha 2 may reflect shared mechanisms where reduced inhibitory function, increased neural hyperexcitability, and thalamocortical disruptions alter FC patterns in similar directions as group power differences.

CHAPTER FOUR

Data Driven Methods for Addressing Fragile X Syndrome Neurocognitive Heterogeneity and Identifying Disorder Specific Features

Keywords:

Fragile X Syndrome; genetic algorithm; machine learning; biomarker; cognition; heterogeneity

Abstract

Fragile X Syndrome (FXS), despite being a single gene neurodevelopmental disorder (NDD), has unexpectedly high levels of heterogeneity due to several systemic sources of variability in molecular and phenotypic expression. The use of electroencephalography (EEG) has helped to bridge molecular and clinical evaluations of FXS through the development of biomarkers, which are translated across species, and the use of biomarkers in pharmacologic intervention trials. Recent data-driven efforts have proved useful for identifying EEG features that parse FXS from typically developing individuals with the technique further applied to a recent clinical trial with some success in identifying treatment target engagement. Addressing heterogeneity and exploring features of FXS with the use of data-driven methods will help efforts to identify variable combinations from EEG to meaningfully distinguishing FXS from TDC. The current project used un-guided machine learning to select variable combinations that maximize classification accuracy when classifying FXS from TDC. The current study addressed the central hypothesis that specific network connectivity dynamics within frontoparietal and temporal regions in FXS would effectively parse FXS from TDC and the resulting feature combination(s) would correlate with clinically meaningful symptoms of FXS. While the present study did not find support for the central hypothesis, results did identify two sets of features that separated FXS and TDC with an accuracy in the excellent range. Specifically, the second model identified features that classified groups perfectly with no misclassification and the first model only misclassified one female with FXS. Features selected were predominately from a reversal learning EEG task, including variables that mapped onto disruptions in cognitive performance. Overall, model composite scores may be useful for better understanding shared mechanisms between selected

features with the ultimate goal of using composites similar to the ones identified in the current study in clinical trials for predicting treatment responses.

Background

Fragile X Syndrome (FXS) is a rare, single gene disorder resulting from a trinucleotide repeat expansion in the 5' untranslated region of the Fragile X messenger ribonucleoprotein 1 (*FMR1)* gene located at Xq27.3 (Ciaccio et al., 2017). FXS is inherited in an X-linked dominant manner as a byproduct of a non-Mendelian inheritance pattern resulting from the increased expansion of cytosine-guanine-guanine (CGG) in the promotor region of *FMR1* ≥ 200 repeat copies. Given the nature of the mutation and the rarity of the disorder, early investigation of FXS assumed homogeneity where symptom variability was attributed largely to individual variability in development rather than systemic sources of phenotypical differences (Salcedo-Arellano et al., 2020; Verdura et al., 2021). Despite the single gene mutation, studies over the past decade have highlighted systematic sources of heterogeneity in FXS which has garnered increasing attention with the continued failure of clinical trials where the assumption of homogeneity has both negatively impacted research efforts and set back treatment development/evaluation (Jacquemont et al., 2013). With multiple sources of heterogeneity contributing to FXS clinical profiles, heterogeneity is an important factor to consider with FXS and should be accounted for in translational efforts to develop and mechanistically evaluate biomarkers. Importantly, the high degree of heterogeneity makes direct comparisons to the *Fmr1*$^{-/-}$ mouse model highly difficult, which has serious implications for both mechanistic investigations and, more importantly, the comparability and lateral shift from preclinical models to randomized, controlled clinical trials (Verdura et al., 2021).

While FXS is a monogenic neurodevelopmental disorder, a high degree of heterogeneity is notable in clinical phenotypes, even among full mutation males. FXS prevalence rates currently reported by the Centers for Disease Control (CDC) are currently 1 in 7,000 for males

and 1 in 11,000 for females, though the rates are likely somewhere closer to 1 in 5,000-7,000 for males and 1 in 4,000-6,000 for females (Ciaccio et al., 2017; Stone et al., 2023). Differences in prevalence between males and females are predominately driven by symptom severity, as FXS is often more severe in males due in part to the process of X chromosome inactivation in females (Hall et al., 2016; Kirchgessner et al., 1995). X chromosome inactivation is a complex, multifaceted epigenetic mechanism by which one X chromosome undergoes profound chromatin remodeling, altering the composition and structure of the chromosome. While not ubiquitous, X inactivation silences the majority of the genes located on the selected X chromosome to avoid gene duplication (i.e., dosage compensation) (Fang et al., 2019). The process of X inactivation is traditionally regarded as a random process where one X chromosome is randomly silenced. In the case of FXS, this means that females are obligate mosaics with only ~50% of their X chromosomes (i.e., cells) affected by the full *FMR1* mutation. However, to complicate matters, recent work found that X inactivation is commonly skewed in the general female population where the skew can potentially be explained by either selective pressure or purely stochastic mechanisms. However, in the case of purely stochastic skews, concerns about the distribution of the paternal vs. maternal copy of the chromosome remain because X inactivation occurs during the embryonic stage where the skew towards maternal or paternal copies is propagated within certain cell lines (Shvetsova et al., 2018). While X inactivation skew (XIS) is less of a direct concern for FXS relative to X-linked recessive conditions, there is some evidence that skewed X inactivation in *FMR1* premutation carriers interacts with the relationship between CGG repeat counts and *FMR1* mRNA (Garcia-Alegria et al., 2017; Vendura et al., 2021). While the relationship between the number of CGG repeats and the amount of *FMR1* mRNA produced diminished with repeat counts < 100, these findings potentially support the conclusion that repeat

count may be involved in the X inactivation process. Further, studies have illustrated that XIS may relate to the degree of ID in females, as well (Reiss et al., 1993; Heine-Suner et al., 2003; Vafaeie et al., 2021). While the relationship between XIS and the *FMR1* mutation is not well understood, and the idea that repeat count may share a relationship with XIS is more theoretical at this point, thinking through sources of heterogeneity is important for understanding the molecular impact on symptom presentation and behavior. Especially as Fragile X messenger ribonucleoprotein (FMRP; i.e., protein product impacted by the *FMR1* mutation) levels share a strong relationship with cognitive symptoms in FXS (Schmitt et al., 2024). Given FMRP levels are a consequence of XIS skew in females, there may be some evidence to suggest an additional level of heterogeneity in females stemming from XIS and consequences of the *FMR1* mutation that are not truly random (Boggs et al., 2022; Verdura et al., 2021). Given the high level of variability in symptom severity noted in females with FXS, females are less well characterized as a result. Therefore, the use of neurophysiological biomarkers to parse and bridge sources of heterogeneity in females with FXS could be a useful approach to both address and direct research into sources that drive more severe outcomes.

Characterizing molecular variability in females may also be a way to address the relationship between FMRP levels and behavior, as the phenotypic heterogeneity mirrors the complex molecular and physiological variability in FXS. As reported in previous chapters, FXS is the most common single-gene cause of autism spectrum disorder (ASD), with 50% of males and 20% of females receiving a co-diagnosis of ASD (Kaufmann et al., 2017). Co-diagnosis of ASD is also associated with more physical health problems and more severe ID. As a result, molecular features of FXS driving the autistic phenotype may share a tighter relationship with symptom severity (Crawford et al., 2020).

In addition to sex-specific sources of heterogeneity, recent efforts in the field led to the development of an optimized assay to detect very low levels of FMRP and found 40-50% of full mutation males expressing trace levels of protein (Boggs et al., 2022). Trace protein production results from partial or incomplete methylation of the *FMR1* gene leading to methylation mosaicism. The partial methylation and trace FMRP production influences symptom severity and adds a level of both complexity and heterogeneity into both research and therapeutic efforts. The researchers who optimized the assay also found that increased peripheral FMRP levels correspond to higher IQs indicating that variable FMRP expression likely accounts, in part, for observed clinical heterogeneity in FXS (Boggs et al., 2022; Schmitt et al., 2024). Isolating FMRP levels across the spectrum of protein production opens an avenue forward in terms of investigating potential links between molecular features of FXS to electrophysiology using electroencephalography (EEG), a highly scalable and translatable tool (Schmitt et al., 2022). However, it is worth noting that no significant linear relationships have been identified between EEG and peripheral FMRP levels, as investigated to date (Norris et al., 2025).

Complex molecular pathophysiology makes mechanistic targeting difficult for therapeutic interventions, likely contributing to the numerous failed clinical trial outcomes over the past 30 years (Berry-Kravis, 2022). One additional, potential translational hurdle is understanding how a seemingly static change like FMRP loss affects dynamic neural processes, which may significantly differ in complexity from mouse to human. Dynamic functional measures such as FC and microstates may provide more insight into moment-by-moment modulation of networks impacted by FMRP loss, allowing development of targeted timing windows for outcome measurement during active cognition that are more homogenous and more easily aligned across species for treatment development. Dynamic functional modeling of

network modulation and network switching should also provide more relevant physiological correlates for specific features of FXS (i.e., ID and cognition vs. anxiety, sensory hypersensitivity, and hyperactivity) and their presentation across individuals. Additionally, clinical trials are highly stringent in determining treatment efficacy where only one primary measure is allowed and wholly used to determine trial success or failure. FXS is a complex disorder, which makes it difficult to identify single measures that reflect FXS, overall. Unidentified heterogeneity makes it hard to determine whether changes from baseline are due to the intervention, sources of systemic variability in the disorder, random or individual sources of variability, or due to the large placebo effects noted in FXS (Berry-Kravis et al., 2012; 2016; 2017; Luu et al., 2020). Measures that are highly predictive of the FXS state (e.g., composite scores) are likely necessary moving forward when thinking about treating the underlying pathophysiology and determining where we are most likely to observe treatment efficacy, given target engagement and efficacy are present.

Data driven approaches are becoming more common and recommended when working to address translational challenges and drive the field towards precision medicine (Hampel et al., 2023; Weissler et al., 2021). Recent efforts in the field of FXS have approached EEG biomarker development in a more data-driven way, including a study using a Naïve Bayes Classifier (NBC) on hypothesis-driven variable and variable combinations to identify which EEG features best separate individuals with FXS from TDC (Ethridge et al., 2024). Ethridge et al., (2024) found that composite scores comprised of multiple EEG variables did a better job predicting group membership (i.e., parsing FXS from TDC) than single measures, alone. A similar NBC approach was also applied to the phase 2a clinical trial results testing BPN14770 (now Zatolmilast) in FXS using a cross-over design to parse the drug response from both baseline and placebo (Norris et

al., 2025b). The NBC identified peak alpha as the variable category that performed best at separating trial conditions, but while a single variable type performed best, a composite of the identified EEG measure from multiple regions across the head did a better job of predicting treatment efficacy than the variable from individual regions. Additionally, peak alpha showed signs of Zatolmilast efficacy highlighting the clinical utility of the machine learning approach. Both studies highlight the potential of composite variables and the use of more data driven technique for clinical trials moving forward, especially considering that most clinical trials in FXS are aiming to alleviate more than one facet of the FXS clinical profile (Verdura et al., 2021). By utilizing a machine learning approach, we can target the intersection of clinical practice and mechanistic investigations to identify core features while still maintaining a reasonable clinical scope.

The current study aims to determine features driving heterogeneity in FXS using data driven methods on neurophysiology measures from EEG. Heterogeneity in both molecular and clinical phenotype likely account for the major discordance between mouse and human studies testing drug treatment effects in FXS. We will first utilize unguided machine learning by wrapping a metaheuristic algorithm around a classification algorithm to identify variable combinations that best separate FXS from TDC. By addressing the problem in a data-driven way, we may also highlight potential avenues to address the ways in which molecular heterogeneity factor into phenotypic expression in FXS (e.g., assessing relationships with FMRP). The proposed analysis potentially isolates FXS neural mechanisms for therapeutic intervention in the form of novel EEG biomarkers, which are most predictive of FXS group membership while also providing a path forward for better understanding FXS heterogeneity.

Methods

Participants

Participants were 74 adults, 31 with FXS (14 female; Age: $M = 28.07$, $SD = 6.25$) and 43 typically developing controls (TDC; 15 female; Age: $M = 25.42$, $SD = 4.87$), recruited from Cincinnati Children's Hospital and Medical Center (CCHMC). See Chapter two for inclusion and exclusion criteria. The current sample subset is less well matched compared to chapters 1 and 2 in an effort to use the maximum available data where age trended towards a significant difference between groups where the FXS participants were marginally older than TDC, $t(54.59) = -1.97$, $p = .054$. Additional exclusion criteria for the current study included individuals with either large percentages of missing values (>15%) concentrated in specific variable sets or highly reduced trial counts for ERP variables where three individuals with FXS were excluded.

Procedure

EEG Acquisition. EEG data were acquired using 128-channel MagStim/EGI HydroCel nets with a MagStim/EGI NetAmp 400 Amplifier (Magstim/EGI, Eugene, OR) in either a sound-attenuated booth or in a clinic space. Data were recorded continuously and sampled at 1000 Hz with saline based electrodes (impedance under 10 KΩ).

EEG Tasks. Briefly, variables from ~5 minutes of resting state EEG (rsEEG) and the 2-choice deterministic reversal learning (RL) task (N = 200 trials max) described in chapters 1 and 2, respectively, were utilized in the proposed analyses. See the methods sections of chapters 1 and 2 for more detailed information on EEG tasks. Additionally, a common sensory task used in the FXS field (auditory chirp) was also included to evaluate the predictive performance when

variables across all core symptom domains were included. ERPs for the correct standardized to the reversal trials were excluded from the feature set due to their redundancy with correct trial counts. Only a subset of the participants for ML also completed the chirp task (N = 60, 23 with FXS, where eight were female). ***Auditory Chirp (sensory task – indexing sensory hypersensitivity).*** The chirp task was utilized to index the robust neurophysiological sensory phenotype in FXS (Ethridge et al., 2017; 2019). Chirp stimuli were delivered at 65dB SPL, consisting of a white noise carrier tone amplitude modulated (AM) by a sinusoid linearly increasing from 0-100 Hz over 2000 ms. Chirp stimuli repeat 200 times, separated by 1500 – 2000 ms inter-trial intervals for a total of 12.5 minutes. Participants watched a silent video for comfort and compliance while passively engaging in the auditory chirp task.

EEG Preprocessing. Raw data were preprocessed according to the procedure in Chapter two. After preprocessing and visual confirmation on file usability, chirp task data were segmented into 3250 ms epochs from 500 ms pre-stimulus to 750 ms after the stimulus (i.e., -500 – 2750 ms). Epochs containing artifacts exceeding +/-120 μV were automatically rejected during epoch generation. A 23-channel selection was used to compute both intertrial coherence (ITC) and event-related spectral perturbation (ERSP) values according to Ethridge et al. (2019), with the channel selection set *a priori* to best capture auditory-related neural (Figure 126). Finally, a time-frequency analysis was run to evaluate both ITC and ERSP. The ITC is a measure of phase consistency of the neural waveform from trial-to-trial within subject. The ITC of the onset of the stimulus, the offset of the stimulus, and in both the low and high gamma ranges were computed for evaluation. The ERSP captures the average broad frequency band amplitude dynamics (i.e., changes in amplitude) across the trial time course in relation to the stimulus. In the case of the chirp task, ERSP represents a measure of amplitude fluctuations within specific frequency bands

across the entire duration of the stimulus for which theta, alpha, and both low and high gamma were computed and evaluated between groups.

Figure 126.

Frontocentral channel selection used to compute chirp task values.

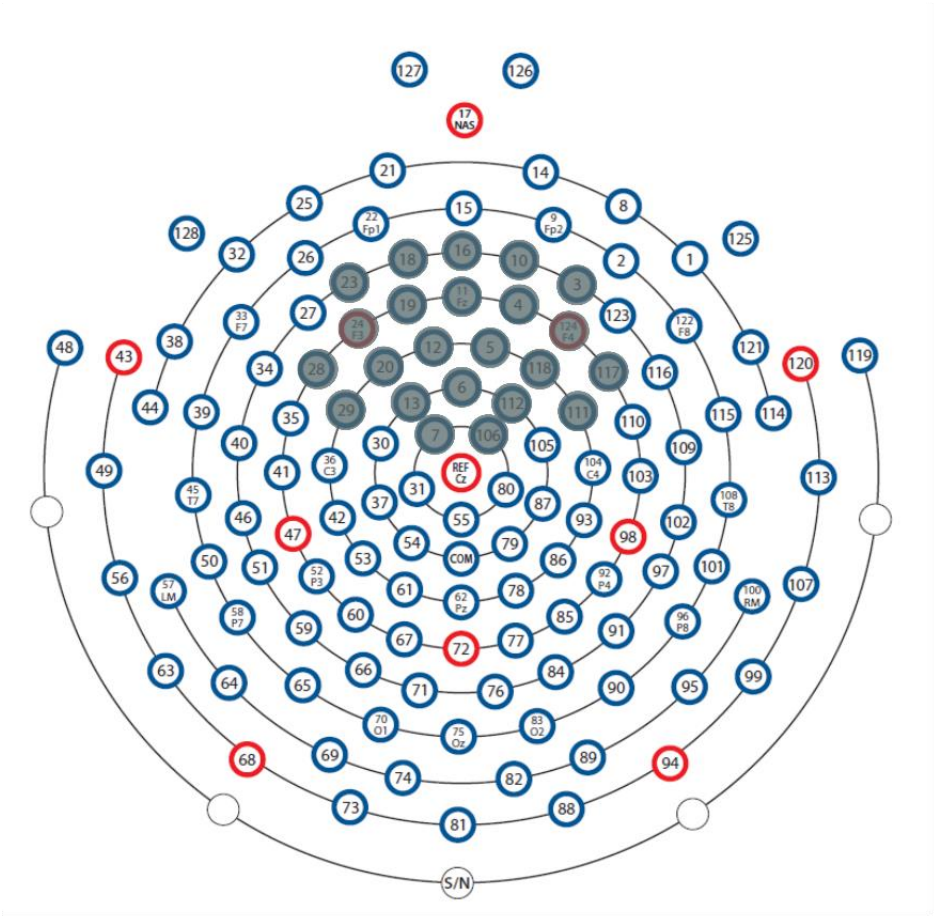

FMRP. Peripheral FMRP levels will be identified using an optimized Luminex-based assay for detecting trace FMRP (Boggs et al., 2022).

Analysis

Classification. Prior to classification, missing data were evaluated and addressed using median imputation stratified by group. Analyzed data (i.e., microstate variables from RL and rs EEG, ERPs, and FC metrics from RL and rsEEG) were input as variables into a Naïve Bayes

Classifier (NBC) wrapped in a genetic algorithm (GA) for unguided determination of feature combinations that best characterize differences between groups (i.e., classification along diagnostic lines). The GA is a metaheuristic machine learning algorithm based on the process of biological evolution and is designed to solve optimization problems. Recent work identified the GA as one of the better performing algorithms for solving problems optimizing on group membership (i.e., diagnosis) (Bain et al., 2024). The GA was used to parse EEG variables and acted as a variable selection tool to identify which EEG features were most predictive of FXS group membership. Two separate models were run in order to maximize the number of subjects, as fewer participants had complete EEG datasets, where several participants were not administered the chirp task. Further, the overarching goal was to evaluate RLEEG and identify the predictive capacity of cognitive features. Therefore, a model with only resting state and RLEEG variables was evaluated to prioritize general and cognitive features, respectively. For both models, features were first normalized by converting to z-scores. Normalized features were submitted to the GA, which optimized solutions based on classification accuracy, using the ga package in MATLAB 2024a. Accuracy was computed as part of the multiclass NBC via the fitcnb function in MATLAB 2024a which tested the linear contribution of various feature combinations (i.e., solutions) identified across GA generations. The NBC was run as part of the GA fitness function to optimize prediction performance (i.e., identify features which categorize groups best) using a stratified 70/30 split for train/test. The 30% hold out set was used to test the final model and was not used to train the model. The built-in MATLAB GA function was built to solve minimization problems (i.e., finds a local minimum rather than maximum) which required taking the negative fitness in order to maximize solution fitness/find local maxima. Additional GA parameters were set empirically by first identifying the best practice for high dimensional

data and testing various combinations of population and max generation hyper-parameters. A constraint was added to penalize the fitness of solutions that selected less than 5 and more than 20 features in order to generate a reasonable solution of features respective to the sample size. The final solution was then tested on the hold out 30% in the NBC, where accuracy, area under the ROC curve for true positive vs. false positive rates, and classification error were all utilized to assess algorithm performance on the best performing solution. Variables with reductions for FXS or negative values (e.g., negative-going peak ERP amplitudes) were reverse coded to ensure all group differences were in the same direction. Finally, a composite score was computed by averaging over the selected features.

Correlation analyses were conducted to evaluate whether the The GA+ NBC solution related to clinical variables including IQ, cognitive performance (KiTAP), and more FXS-specific features (i.e., FMRP levels, anxiety, hyperactivity, sensory hypersensitivities, ABC, and adaptive behavior from Vineland-3; Gupta et al., 2022; Saeidi et al., 2021).

Statistical Analysis

Chirp variables were analyzed using independent samples t-tests to determine whether previous results were replicated for the current sample. The variable or variable combination output from the GA wrapped NBC were tested for group differences across FXS and TDC using non-parametric tests. Exploratory correlations with clinical variables will be computed to evaluate the relationships between clinical features and the ML output most predictive of group membership.

Power Analysis. The NBC was selected due to its robustness with small sample sets where variables were selected as a means of dimension reduction and simple statistics were used

to evaluate ML outcomes (Huang & Li, 2011). Independent samples t-tests required $N = 16$ and the non-parametric tests required a minimum of 25 participants.

Results

Chirp Results

Chirp variables were first analyzed using independent samples t-tests to determine whether the present sample demonstrated comparable chirp responses noted in previous studies (Ethridge et al., 2017; 2019).

As age was significantly different between groups for the subset of the sample with chirp data, age was evaluated as a covariate and retained where significant. ITC variables demonstrated the expected pattern of group differences with onset ITC and 40 Hz ITC being significantly different between groups. Onset ITC was significantly elevated in FXS ($M = .18$, $SD = .08$) compared to TDC ($M = .11$, $SD = .07$), $t(58) = -3.46$, $p < .001$, $d = -.92$. Age was not a significant covariate for 40 Hz ITC but did trend towards significance and thus was retained, $F(1, 57) = 3.16$, $p = .081$, $ES = .05$. ITC in the 40 Hz range was significantly reduced in FXS ($M = .11$, $SD = .06$) compared to TDC ($M = .14$, $SD = .08$), $F(1, 57) = 4.65$, $p = .035$, $ES = .08$. However, the low gamma ITC (40 Hz ITC) result was smaller than typically observed in FXS, representing a caveat to interpretations. High gamma or 80 Hz ITC was not significantly different between groups where phase locking onto the higher gamma frequencies was more comparable between FXS ($M = .04$, $SD = .03$) and TDC ($M = .04$, $SD = .03$), as expected, $t(58) = .13$, $p = .898$, $d = .03$. Offset ITC was also not significantly different between FXS ($M = .07$, $SD = .04$) and TDC ($M = .05$, $SD = .05$), $t(58) = -1.61$, $p = .113$, $d = -.43$. (Figure 127A).

Next, ERSP in the theta, alpha, beta, and gamma ranges were evaluated using independent samples t-tests. First, trial count was evaluated to see if the number of trials differed by group to determine whether trial count was necessary in models as a covariate for ERSP variables, which do not inherently account for the number of total trials available. Trial counts were not significantly different between groups where FXS (M = 83.43, SD = 32.84) was comparable to TDC (M = 91.31, SD = 28.72), $t(58) = .95$, $p = .333$. Large standard deviations were the result of paradigm differences where some participants were administered the paradigm with 200 chirp trials and others the paradigm with 100 chirp trials. As age was significantly different between groups for the subset of the sample with chirp data, age was evaluated as a covariate and retained where significant.

As expected, there was a significant group difference for theta ERSP with FXS exhibiting elevated event-related theta power (M = 27.35, SD = 3.34) compared to TDC (M = 24.52, SD = 2.34), $t(58) = -3.89$, $p < .001$, $d = -1.03$. There were also significant group differences for the whole gamma frequency band range (30 – 100 Hz) where FXS exhibited elevated event-related gamma power (M = 9.16, SD = 2.30) compared to TDC (M = 6.44, SD = 1.92), $t(58) = -4.92$, $p < .001$, $d = -1.31$. These differences were consistent for both low gamma (30 – 60 Hz; $t(58) = -4.97$, $p < .001$, $d = -1.32$) and high gamma (61 – 100 Hz; $t(58) = -4.69$, $p < .001$, $d = -1.23$) where FXS had higher gamma power (Low Gamma: M = 10.76, SD = 2.19; High Gamma: M = 7.91, SD = 2.45) than TDC (Low Gamma: M = 8.18, SD = 1.79; High Gamma: M = 5.09, SD = 2.14). Interestingly, a novel group difference for beta ERSP was identified where individuals with FXS exhibited increased beta event-related power (M = 16.28, SD = 2.81) compared to TDC (M = 16.48, SD = 2.64), $t(58) = -2.23$, $p = .030$, $d = -.59$. There was not a significant group

difference on alpha ERSP where FXS (M = 24.54, SD = 3.58) and TDC (M = 23.03, SD = 3.37) exhibited similar event-related alpha power, $t(58) = -1.67$, $p = .099$, $d = -.44$ (Figure 127B).

Figure 127.

Chirp Time-Frequency Plots Depicting Group-Level ITC and ERSP

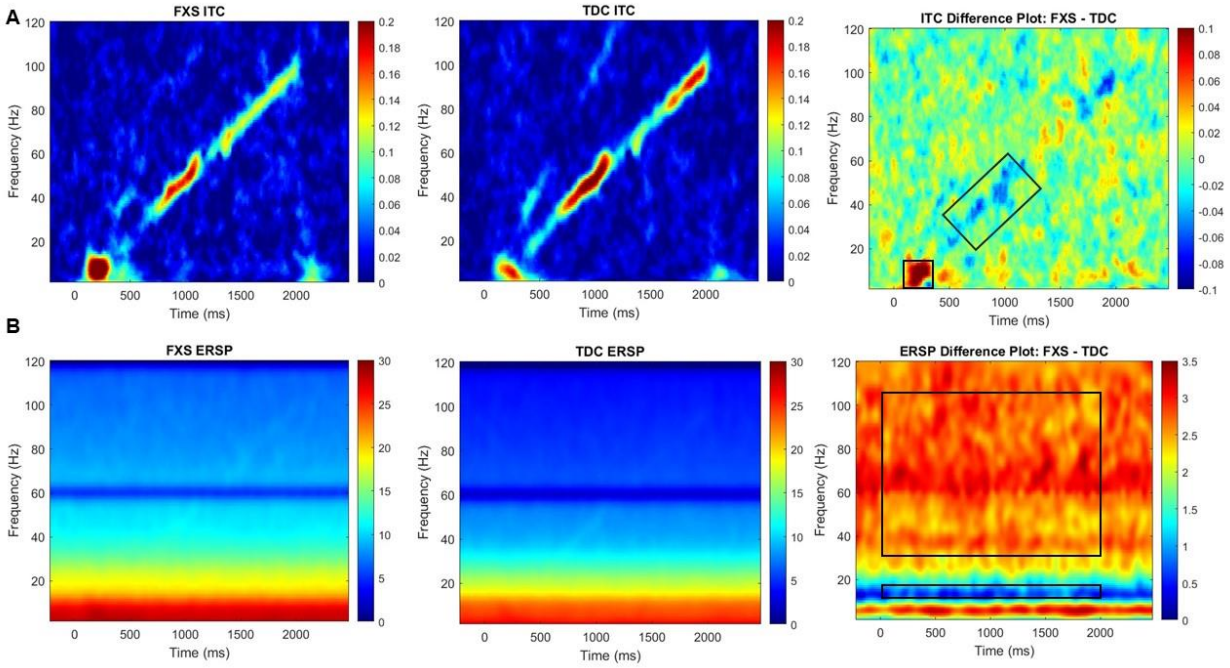

Note. **A)** ITC results for FXS and TDC with an ITC difference plot depicting FXS differences where the TDC response was subtracted from FXS in the left most plot. **B)** Non-baseline corrected ERSP for FXS and TDC followed by an ERSP difference plot depicting FXS ERSP differences where the TDC response was subtracted from FXS in the left most plot. Black boxes highlight areas in the difference plots with significant group differences where warmer colors (reds, yellows, oranges) indicate elevations for FXS and cooler colors (blues and greens) indicate reductions for FXS both relative to TDC.

Machine Learning Results

The first GA+NBC model (Model 1) had the population set to 300, the max generations was set to 200, and used a custom mutation function to randomly flip bits with a probability of 5%, a mutation strategy which helped to avoid premature convergence by promoting genetic diversity and enabling a broader exploration of the solution space. Model 1 iterated through 122 total generations and then terminated where it identified a solution with a fitness of -1 (Figure 128).

Figure 128.

Model 1 Fitness Progression Over All Generations

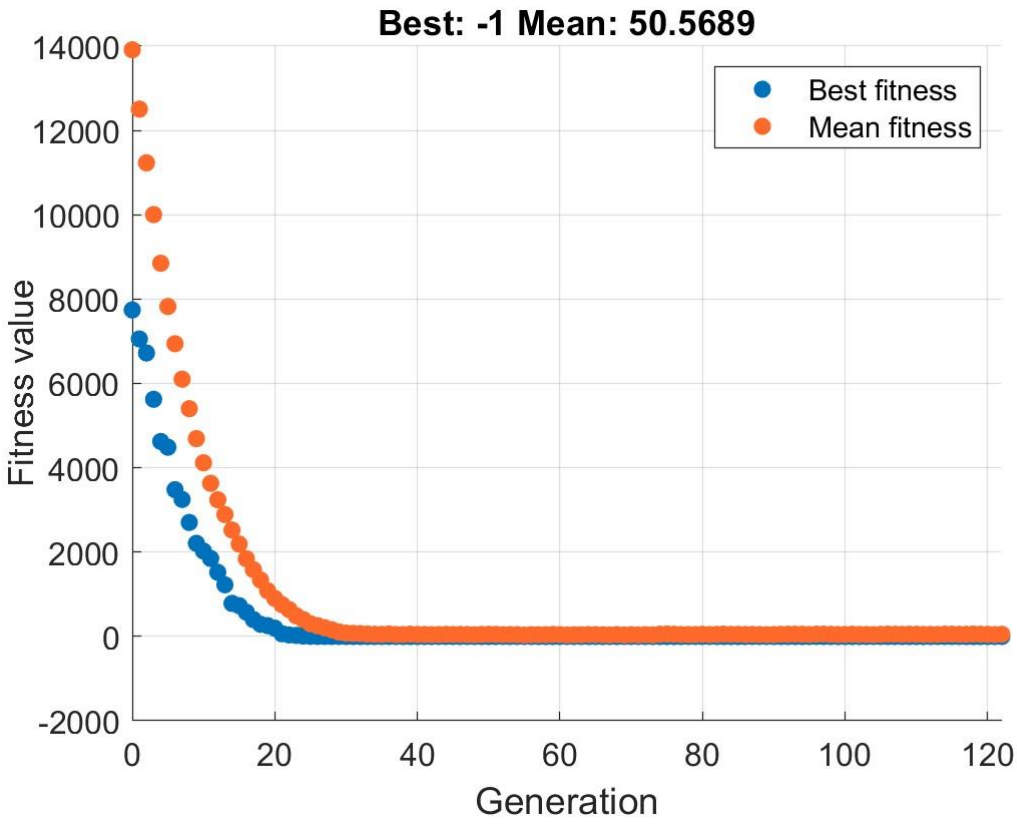

Note. Average and best model fitness converged to 1 over 122 generations.

The best solution identified by the GA+NBC for Model 1 contained 15 variables. The final solution evaluated on the hold out/test set resulted in excellent classification (accuracy = .95, AUC = 1, CE = .05) where only one individual with FXS was misclassified and misclassification was on a FXS female (Figure 129).

Figure 129.

Confusion Matrix for Model 1

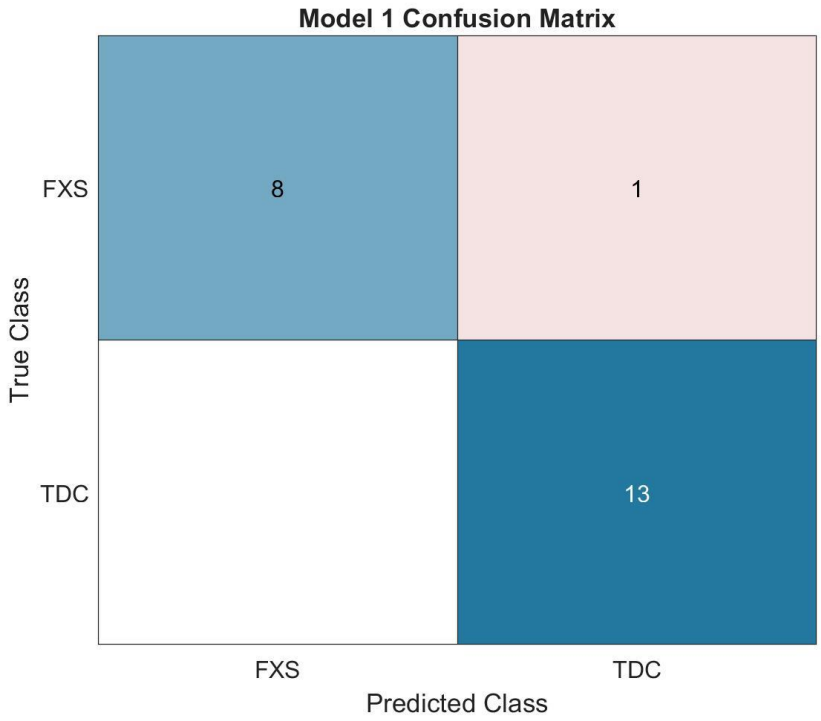

Note. $N = 22$ in test set. Blue boxes indicate correct predictions where red boxes indicate incorrect predictions or false positives. Darker shades indicate more dense classification.

Variables selected by the model for the best fitting solution included (with original results from chapters 1 and 2):

1. Central Correct P2 Latency (RLEEG)
2. Central Incorrect Rev P3a Latency (RLEEG)
3. Parietal N2 Amplitude Incorrect on Reversal (RLEEG)
4. Parietal Correct P3b Latency (RLEEG)
5. Occipital Correct P2 Latency (RLEEG)
6. Pre-stimulus M1 Duration (RLEEG)
7. Stimulus M4 Occurrence (RLEEG)
8. Stimulus Control Theta FC (RLEEG)
9. Pre-stimulus DMN Alpha 1 FC (RLEEG)
10. Pre-stimulus Control Delta FC (RLEEG)
11. Pre-stimulus DMN Theta sum score (RLEEG)
12. Pre-stimulus Control Theta FC Top 1 (RLEEG)
13. Pre-stimulus Control Alpha 2 FC Top 2 (RLEEG)
14. Frontal Relative Theta Power (rsEEG)
15. Frontal Relative Alpha 1 Power (rsEEG)

A Mann-Whitney U test was run on the composite of the selected features to evaluate whether the composite was statistically different between groups. The composite was statistically different between groups where FXS had elevated composite scores (*M* rank = 51.58) compared to TDC (*M* rank = 27.35), $N = 74$, $z = 4.78$, $p < .001$, $r = .56$. The composite variable was set to index group differences in one direction, where features that were reduced or negative for FXS relative to TDC were reverse coded.

To support interpretation of the current results, Mann-Whitney U tests were run on individual variables to determine whether the same results from previous chapters hold on normalized data, as the sample was slightly different from chapter two, where individuals with large sets of missing data were excluded. Feature group differences were mostly congruence with chapters 1 and 2 (Table 1). The current results indicate the composite significantly captures differences in FXS. However, classification is not necessarily linear and may result from

multivariate patterns where the selected features work together for successful group prediction which may explain the inclusion of features that were not significantly different between groups.

Table 16.

Mann-Whitney U Results for Model 1 Individual Selected Features

		Mean Rank			Mann-Whitney U Results		
Selected Features	Congruent?	FXS	TDC	*N*	*z*	*p*-value	*r*
C Correct P2 Latency	x	40.63	32.24	74	1.06	.287	.12
C Incorrect Rev P3a Latency	x	41.24	34.80	74	1.27	.203	.15
P Incorrect on Reversal N2 Amplitude	x	25.19	46.37	74	-4.18	< .001	-.49
P Correct P3b Latency	x	37.11	37.78	74	-.13	.895	-.02
O Correct P2 Latency	x	27.73	44.55	74	-3.32	< .001	-.39
Pre M1 Duration	x	42.06	34.25	74	1.55	.121	.18
Stim M4 Occurrence	x	41.77	34.42	74	1.45	.147	.17
Stim Control Theta FC	x	48.48	29.58	74	3.73	< .001	.43
Pre DMN Alpha 1 FC	x	37.87	37.23	74	.13	.900	.02
Pre Control Delta FC	x	40.39	35.42	74	.327	.327	.04
Pre DMN Theta sum score	x	48.74	29.40	74	3.82	< .001	.44
Pre Control Theta FC Top 1	x	38.42	36.84	74	.31	.755	.04
Pre Control Alpha 2 FC Top 2	x	26.9	45.12	74	-3.59	< .001	-.42
F Rel Theta	x	50.29	28.28	74	4.34	< .001	.50
F Rel Alpha 1	x	35.16	39.19	74	-.79	.427	-.09

Note. C= central; F = frontal; P = parietal; stim = stimulus period, Pre = pre-stimulus period; Rel = relative power. P Incorrect on Reversal N2 Amplitude, O Correct P2 Latency, and Pre Control Alpha 2 FC Top 2 were all reverse coded for the composite.

The composite was evaluated in correlation analyses to determine whether the composite variable maps onto important clinical features of FXS for the FXS group only. Overall, there were no significant correlations between the EEG composite score and clinical variables (Appendix C). Nor was the correlation significant between the EEG composite score and FMRP for FXS males only, rho = -.28, p = .352.

Next, another GA+NBC model (Model 2) evaluated with adjustments for the inclusion of chirp task variables (i.e., sensory index). Again, separate models were run to prioritize general and cognitive-specific disruptions as separate from sensory processing by maximizing the amount of available data. Fewer participants had complete EEG datasets where several were either not administered the chirp task or did not have valid data, necessitating a second model with only individuals with complete datasets. For the second model, the population was set at 500 and the max generations was set at 200. The same custom mutation function was used to randomly flip bits with a probability of 5%. Model 2 iterated through 91 total generations and then terminated where it identified a solution with a fitness of -1 (i.e., maximal fitness; Figure 130). Variables selected by the model for the best fitting Model 2 solution included (with original results from chapters 1 and 2):

1. ITC onset (chirp)
2. ERSP high gamma (chirp)
3. Frontal Correct P2 amp (RLEEG)
4. Central Correct P2 amp (RLEEG)
5. Central Correct P3a amp (RLEEG)
6. Feedback Hurst 4 (RLEEG)
7. Feedback M4 GFP 4 (RLEEG)
8. Feedback Alpha 1 DMN FC (RLEEG)
9. Stimulus Alpha 2 control FC (RLEEG)
10. Pre-stimulus Alpha 1 DMN FC (RLEEG)
11. Feedback DMN T sum (RLEEG)
12. Pre-stimulus SN A2 sum (RLEEG)
13. Frontal PAF (rsEEG)

14. Posterior Absolute Gamma1 Power (rsEEG)
15. Rest DMN Alpha 1 FC (rsEEG)

Figure 130.

Model 2 Fitness Progression Over All Generations

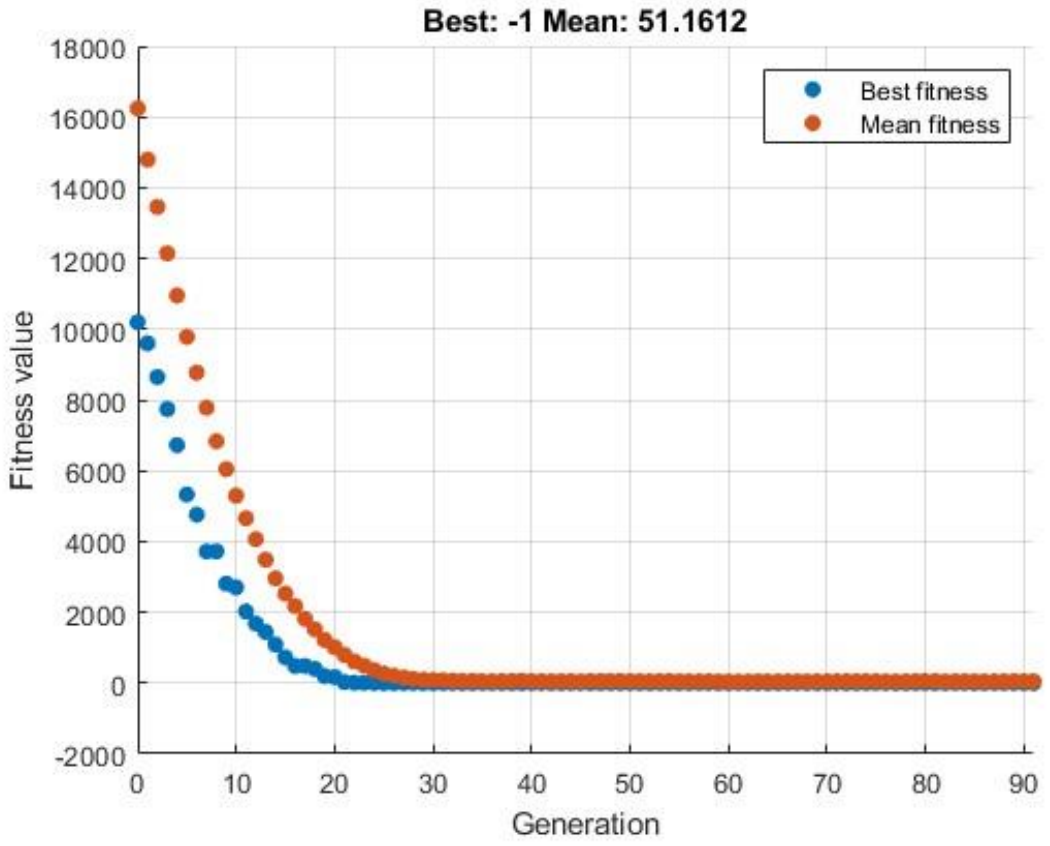

Note. Average and best model fitness converged to 1 over 91 generations.

The best solution identified by the GA+NBC for Model 2 also contained 15 variables which resulted in excellent classification in the final model tested on the hold out set (accuracy = 1, AUC = 1, CE = 0; Figure 131).

A Mann-Whitney U test was run on the composite of the selected features from Model 2 to evaluate whether the composite was statistically different between groups. The composite score for Model 2 was statistically different between groups where FXS was elevated (*M* rank = 47.83) compared to TDC (*M* rank = 19.73), $N = 60$, $z = 6.06$, $p < .001$, $r = .78$.

Figure 131.

Confusion Matrix for Model 2

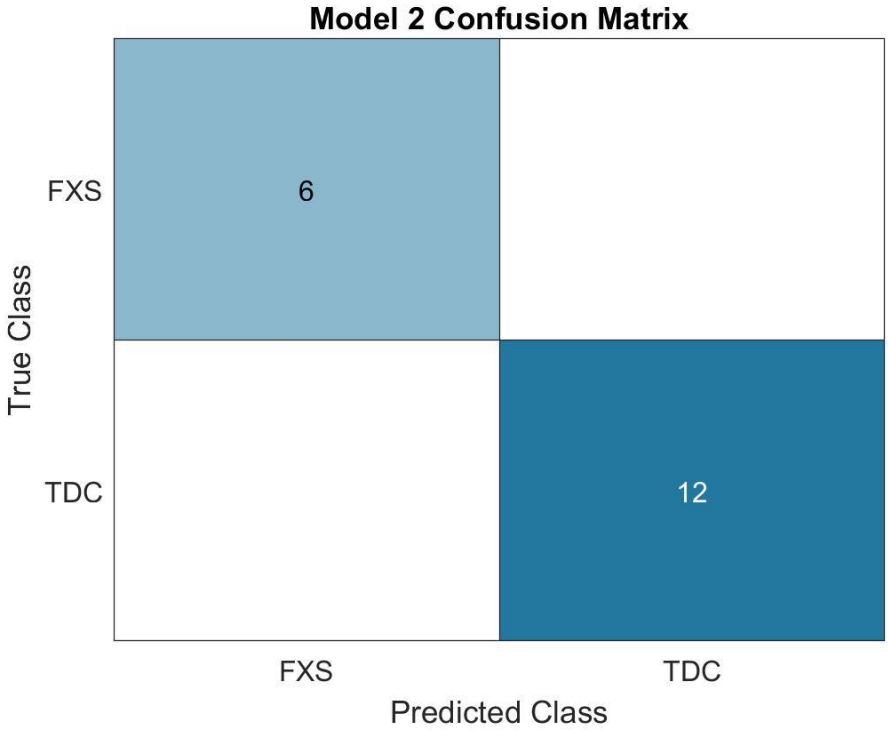

Note. $N = 18$ in test set. Blue boxes indicate correct predictions where red boxes indicate incorrect predictions or false positives. Darker shades indicate more dense classification.

To support interpretation of the current results, Mann-Whitney U tests were run on individual variables to determine whether the same results from previous chapters hold on normalized data. Feature group differences were congruence with chapters 1 and 2 (Table 2).

Table 17.

Mann-Whitney U Results for Model 2 Individual Selected Features

Selected Features	Congruent?	Mean Rank		Mann-Whitney U Results			
		FXS	TDC	*N*	*z*	*p*-value	*r*
ITC onset	x	39.04	25.19	60	2.99	.003	.39
ERSP high gamma	x	41.96	23.38	60	4.01	<.001	.52
F Correct P2 amp	x	43.04	22.70	60	4.39	< .001	.57
C Correct P2 amp	x	40.87	24.05	60	3.63	<.001	.47
C Correct P3a amp	x	36.48	26.78	60	2.09	.037	.27
Fb Hurst 4	x	38.17	25.73	60	2.68	.007	.35
Fb M4 GFP 4	x	39.17	25.11	60	3.03	.002	.39
Fb A1 DMN FC	x	30.26	30.65	60	-.08	.933	-.01
Stim A2 control FC	x	20.70	36.59	60	-3.43	<.001	-.44
Pre A1 DMN FC	x	30.61	30.43	60	.038	.970	.00
Fb DMN T sum	x	44.52	21.78	60	4.90	<.001	.63
Pre SN A2 sum	x	19.00	37.65	60	-4.02	<.001	-.52
F PAF	x	20.98	36.42	60	-3.33	<.001	-.43
P abs gamma 1	x	42.61	22.97	60	4.23	<.001	.55
Rest DMN A1	x	32.57	29.22	60	.72	.470	.09

Note. C= central; F = frontal; P = parietal; stim = stimulus period, Pre = pre-stimulus period; Rel = relative power. Stim A2 Control, Pre SN A2 sum, and frontal PAF were reverse coded

The model 2 composite was evaluated in correlation analyses to determine whether the composite variable maps onto important clinical features of FXS for the FXS group only. No significant relationships were identified between clinical variables and the EEG composite score for model 2 (Appendix D). Further, in FXS males only, the composite did not correlate with FMRP (N = 10, rho = .-15, p = .68).

Lastly, the original study plan included a cluster analysis on composite features where GA+NBC selected features would be submitted to a non-parametric, density-based clustering

algorithm. Based on previous classification studies in FXS, the solution was not hypothesized to classify FXS perfectly due to heterogeneity stemming from mosaicism (obligate and methylation). Both feature sets resulted in excellent or perfect classification, suggesting models identified feature solutions where heterogeneity was less impactful. Given models achieved such high levels of accuracy, clustering with the selected feature sets was not reasonable. Additionally, the original plan included the use of developmentally delayed controls where classification and clustering would have been less straightforward, and clustering would have helped parse which features were more core to FXS pathophysiology but difficulties recruiting DD controls resulted in only 8 participants with full, valid EEG datasets and even less had complete clinical evaluations.

Discussion

The use of data-driven methods for exploring FXS features is important for developing a nuanced understanding of variability in clinical presentations. Numerous hypotheses about the mechanistic causes of FXS clinical phenotypes and underlying pathophysiology stem from mouse and cell model work (Berry-Kravis, 2022; Erickson et al., 2017). While these approaches are highly rigorous and informative at the global scale, they have had limited translational success in producing targets for novel treatment development where all FXS-specific clinical trials have failed for a variety of reasons (Berry-Kravis, 2022). To make better use of basic science efforts, more work is needed on the human subject side of the field to identify neurophysiological features that best represent the FXS phenotype and what relationship neurophysiology indexed with EEG shares with FXS molecular disruptions (e.g., FMRP). As most *Fmr1*$^{-/-}$ animal models achieve protein loss by knocking out the gene, human modeling with

more sensitive measures of FMRP is important for understanding what neurophysiological signals share a relationship with peripheral FMRP levels.

The current study utilized a more data-drive approach to parse features from multiple EEG tasks, including the novel cognitive task evaluated in chapter two and both resting state and chirp. The NBC performed excellently, classifying individuals into the correct diagnostic group in both models using the feature selection identified by the GA suggesting the features are meaningfully related to FXS and largely overcoming traditional issues with heterogeneity (Ethridge et al., 2024). However, both Model 1 and 2 results were not in support of the originally hypothesized outcomes where the composite would represent significant and clinically meaningful FXS differences, including sharing a link to FMRP. The composite score represents robust predictive power where high classification performance does not necessarily equate to clinical severity, across the board. Further, classification performance does not guarantee meaningful mechanistic differences where group differences were not present for all selected features. The GA+NBC performance was not a direct index of group differences where more complex relationships between variables (e.g., multivariate synergy) may explain why certain features that were not different between groups were selected by both models. Specifically, these complex relationships are not always inherently linear but may contribute to linear predictability in meaningful ways.

Interestingly, both models prioritized RLEEG variables despite other datasets containing variables that reliably differ between groups from rsEEG and the chirp task. The prominent representation of RLEEG in both models suggests RLEEG variables were more predictive of FXS than rsEEG or chirp variables even when combined. However, determination of how informative the prominence of RLEEG variables in the selected features set was limited by a

lack of insight into whether the current set of features would be consistently selected by the model and selected in similar proportions relative to other tasks, as the GA is highly stochastic.

Of note, Model 1 selected five RLEEG ERP-based measures that were related to either correct feedback processing and reward valuation or error monitoring. Reward processing was determined to be disrupted in FXS where modulation of neural responses to correct feedback was not present, as was noted in TDC. Further, selected ERP features were from both central and parietal sources, which contribute to reward processing and prediction coding, adding support to conclusions made from chapter two regarding altered reward processing and predictive coding disruptions (Thomas et al., 2013; Hawellek et al., 2016). Model 1 also prioritized FC measures from the pre-stimulus period which adds support to conclusions from chapter two, where the pre-stimulus represents the most extreme period for group differences where TDC briefly disengaged from cognitive-dominate or external processing networks and FXS was less able to dynamically shift network use. The microstate variables selected in Model 1 were not individually informative, as neither variable was significantly different between groups. However, their inclusion may have enhanced the predictive capacity of other features. From rsEEG, relative power variables were included where frontal relative theta power was previously identified as one of the best performing variables in a FXS classification study but was notably worse at classifying females with FXS from TDC (Ethridge et al., 2024). The misclassification of one FXS female in the current study indicates resting state and tasks engaging cognitive flexibility processes may not be sufficient to fully separate FXS from TDC, as they may be more susceptible to systematic sources of heterogeneity. Though, not all females with FXS were misclassified in the final holdout set suggesting misclassification may stem from other factors outside of the systematic source of heterogeneity inherent to females with FXS. The addition of

chirp variables to Model 2 had perfect classification on the holdout set, indicating the addition of sensory processing indices supports better separation. Chirp and resting state variables performed comparably in past studies which did not evaluate both chirp and resting state feature performance in combination (Ethridge et al., 2024).

Altogether, the inclusion features across core symptoms of FXS supported better group separation using data-driven approaches in which cognitive-specific features were more prominently selected. Model 2 included features from all three tasks and better represented robust findings across studies representing neural hyperexcitability. Specifically, onset ITC and high gamma from the chirp task are robustly different in FXS with good test-retest reliability where both index aspects of neural hyperexcitability in relation to sensory stimulation (Ethridge et al., 2017; 2019). Model 2, like Model 1, largely contained ERPs to correct feedback from central sources, though additionally included frontal P2 amplitude for correct feedback. The model also selected two microstate variables from the feedback window which were both different between groups and significantly related to cognitive performance via IQ. The FC measures included represented all RLEEG task windows proportionally where most were either theta or alpha FC variables that were found to be significantly different between groups in chapter two, with the exception of alpha 1 FC in DMN from feedback-related data. Variables from frontal sources were less representative of typical rsEEG features associated with FXS, with the exception of frontal PAF. Overall, features selected by Model 2 were more representative of FXS-specific disruptions relative to TDC. Additionally, features in Model 2 may share neural mechanisms which, again, relate to the hyperexcitability phenotype. The ERP features were from central sources and FC measures were predominately the within-network FC of DMN and SN which are midline centered/central-to-centroparietal and frontocentral,

respectively. While the relationship between features was not assessed, the overlap in spatial location between features may reflect shared mechanistic disruptions. Further, the group differences on ERP and FC measures were overarchingly interpreted as reflective of network rigidity where Hurst exponent and GFP differences were also indicative of network rigidity/cognitive inflexibility and hyperexcitability during feedback-related neural processes. Further work is needed to better understand the mechanistic relationship between features where the composite may provide additional insight.

Across both models, features selected captured variables that map onto core symptoms of FXS. Specifically, RLEEG variables were more closely related to IQ, vineland, and ABC than other EEG tasks. The increased representation of RLEEG variables in the models may indicate composites were more representative of cognitive disruptions in FXS, though that interpretation is confounded by the lack of significant correlations between the composite scores and clinical variables indexing cognition.

Overall, how well the composite classified individuals from both models was an important take away of the current study. While the original goal was to identify potential sources of heterogeneity both models performed excellently despite the inclusion of females with typical IQ levels and not accounting for mosaicism in either model, which were factors in a previous study evaluating the classification performance of hypothesis-driven variable combinations in FXS (Ethridge et al., 2024). While the composites were highly predictive, the combination of features may not share a simple linear relationship with clinical outcomes. The NBC follows Bayes rules which are distinct from the frequentist approach where more complex relationships may exist between selected features, or the composite, and clinical

variables/symptoms. However, the NBC still represents a linear decision surface where all features contribute to linear predictability.

While the composites were not correlated with clinical variables, they did index differences from TDC that map onto clinical disruptions which may provide some mechanistic insight. Variable combinations may reflect shared mechanisms which support conclusions on network disruptions in FXS. While more work is needed to understand whether RLEEG variables are more amenable to change than more stable clinical measures like IQ, composites may be additionally useful in clinical trial contexts for predicting treatment responses.

Limitations

The present study has several limitations which impact the interpretation of the results. First, the sample size was small and, despite the NBC's robustness to small sample sizes, the limited number of individuals with FXS may not represent population level differences. Especially given the limited number of females with FXS. Another limitation was missing data where the use of multiple imputation likely unfairly biased variables with missingness (ERP variables) by blending groups and obscuring real group differences. Alternatively, MI may have biased results towards the group with increasing data missingness (i.e., FXS). Ultimately, all ways of addressing missing data would bias the results where multiple imputation using the overall variable median represented one of the least biased approaches outside of modeling the missingness. The best approach would have been to set missing values to zero and encode missingness using binary variables to account for patterns of missingness in the model, however, these binary variables lacked the necessary level of variability for the NBC to run appropriately necessitating multiple imputation.

Lastly, determination of the overall usefulness of the identified model composites was limited by the stochastic nature of the GA where future efforts should utilize processes for selecting the final feature list from features frequently selected in the final GA solution during parameter tuning. The GA is highly stochastic where features often vary from run-to-run and population-to-population where the best solution identified was highly predictive but may not represent the most meaningful set of features for FXS (i.e., the most predictive features). The use of the best solution represented a local maximum and the evaluation of the best solution on accuracy alone may impact interpretability of the results. Another approach could be to select features only identified more widely across populations by setting a threshold *a priori* for the specified proportion of populations required to include a feature. Alternatively, the feature solution could be treated like a parameter where the GA+NBC process is bootstrapped and only the features selected most frequently are tested on the test set. Ultimately, the alternative approaches may overcome issues with overfitting and provide more insight into what the composite tells us about FXS.

CHAPTER FIVE: General Discussion

The present set of studies represents the first evaluation and large-scale network analysis of Fragile X Syndrome (FXS) brain activity during an active cognitive task. Importantly, cognitive disruptions heavily impact the day-to-day life of individuals with FXS. At present, no treatment exists to treat the underlying pathophysiology of FXS, and medication management addresses only symptoms rather than treating the source of the symptoms. Established treatments for FXS are often insufficient at reducing intellectual disability, executive dysfunction, or behavioral features of FXS – largely because underlying mechanisms of FXS remain poorly understood. The overall study investigated functional connectivity disruptions in frontoparietal networks using electroencephalography (EEG) to parse cognitive function during a cognitive task with a secondary goal of establishing the feasibility of microstates as a simpler proxy for network disruptions. Further, the study helped define mechanistic underpinnings behind core symptoms in FXS for better biomarker development which will eventually be implementable in evaluations of novel therapeutic interventions (i.e., physiological bridges between molecular targets and externally measurable symptom improvements). Overall, the current results provide converging evidence across various metrics of network rigidity and underly cognitive inflexibility, which contribute to reduced cognitive ability and lower adaptive behavioral skills.

Chapter two evaluated resting state EEG and identified differences in microstate global field power (GFP) and theta functional connectivity (FC) where FXS had higher GFP and increased theta functional connectivity (FC), across all functional networks of interest: default mode network (DMN), salience network (SN), and the control network. Theta FC increases were also diffusely increased across all networks suggesting elevated theta FC represents a more global feature of network disruptions. Increased theta FC in FXS was previously linked to

cognitive disruptions and correlated loosely with IQ in the present study (van der Molen et al., 2014). Theta disruptions in FXS are robust, where other studies provided evidence of elevated theta power across task types and an inverse cross-frequency relationship with gamma indicative of the use of theta for regulating high frequency brain activity (Ethridge et al., 2019; Pedapati et al., 2022; Wang et al., 2017). Overall, hyperconnectivity in important task-negative and task-positive networks may disrupt neural dynamics contributing to cognitive ability where theta FC represents a negative consequence of using theta for processes typical of alpha, which is largely reduced in FXS (van der Molen et al., 2013; 2014; Pedapati et al., 2022; Wang et al., 2017). Microstate findings did not map onto FC disruptions, but were related to potential global network disruptions where increased GFP may reflect neural hyperactivity. Importantly, GFP group differences were related to the individual microstate class GFP patterns where the GFP of the whole solution was only different between groups when accounting for the GFP patterns of individual microstate classes, even though those patterns were not different between classes. Microstate GFP is a voltage-based measure where amplitude may influence the GFP value. Given individuals with FXS often exhibit increased neural hyperactivity, increased GFP in FXS may reflect this hyperactivity. However, increased GFP across the whole EEG recording may also index patterns of microstate use or microstates transitions, as microstates are generated from local GFP maxima. Higher GFP in FXS when paired with both increased GFP peaks per second and higher global explained variance (GEV) indicates some level of neural rigidity. Increased GEV suggested FXS more frequently used of the brain states represented in the microstate solution when compared to TDC and increased GFP peaks per second indicated more rapid transitions between brain states. However, these transitions did not represent unique patterns of microstate use over time, given the lack of significant group difference on the complexity

measure which measured uniqueness of the transition patterns. As such, increased GFP peaks per second may have captured rapid repeated transitions into a single microstate class (i.e., transitioning out and back into the same microstate class). To conclude, GEV and GFP peaks per second findings both indicate some level of neural rigidity or reliance on a limited set of brain states in FXS where higher GFP may represent both neural rigidity and hyperactivity. Interestingly, higher GFP was also linked to reduced IQ and reduced adaptive behavior suggesting elevated GFP is clinically meaningful and related to cognition.

Chapter three was an intensive evaluation of a deterministic reversal learning task adapted to EEG which identified congruent group differences across event related potential, microstate, and FC analyses. ERP analyses identified evidence of hyperactive neural responses to feedback and evidence of altered reward processing in the reward-related positive (RewP) ERP component. FXS had increased RewP amplitudes compared to TDC. Interestingly, within TDC the RewP amplitude to correct feedback before an error on reversal (i.e., after receiving continuous correct feedback for 5-10 trials) was reduced compared to the amplitude of RewP to correct feedback after receiving an error on reversal trials. FXS did not exhibit a similar within subject different for RewP amplitude suggesting altered reward processing in FXS, specifically inflexibility. Next, microstate findings identified increased GFP in FXS during feedback where increased GFP may represent elevated transitions but rigidity in which networks are activated. Several of the core differences were linked to reduced IQs in FXS suggesting these differences are meaningfully linked to cognitive ability. Lastly, FC analyses identified several interesting and novel outcomes. First, theta FC remained consistently elevated in FXS where hyperconnectivity across networks was evident, which was noted in resting state data. However, theta FC was not diffusely increased across all networks nor consistent across task windows,

suggesting modulation in what drove increased theta FC observed at the whole network level. Of note, theta FC within control network was driven by different primary network nodes in FXS during pre-stimulus windows where control network activity was elevated in FXS relative to stimulus and feedback windows. However, the elevated FC reflected a difference in primary node FC magnitude during stimulus periods and was diffusely elevated during feedback periods.

Novelly, alpha 2 FC was reduced in FXS across most networks and data types where alpha disruptions may be core to task-processing disruptions. In support of one of the core hypotheses of chapter two, the triple network hypothesis was disrupted in theta FC for FXS where network shifts did not occur from the pre-stimulus period into the stimulus period for task engagement. Largely, results point to network rigidity/stasis with consequences for cognitive performance.

Finally, chapter four identified two sets of features that achieved excellent-to-perfect classification which largely pulled from the reversal learning task variable set and resulted in composite scores that were statistically different between groups . Ultimately, the models identified variables that were robust to systemic sources of heterogeneity stemming from mosaicism, which was surprising. Heterogeneity was something hypothesized to impact classification where features with increased heterogeneity would serve as targets for further evaluation. Serendipitously, these composite scores allowed for better mechanistic understanding of cognitive inflexibility, as they both had very strong predictive power. Given further evaluation of feature sensitivity to intervention, task-based EEG components may serve as a tool in future clinical trials for predicting treatment response for interventions targeting cognitive-related processes core to FXS.

While not a core focus of the current set of studies, FMRP was evaluated in correlation analyses with all EEG variables generated for FXS males, only. Originally, FMRP was hypothesized to share relationships with cognitive EEG variables, given the identified relationship between IQ and FMRP (Schmitt et al., 2024). However, the current study identified no relationship between EEG variables and peripheral FMRP. While interpretation of negative results is not appropriate, the building wealth of non-significant findings suggests either a more complex relationship between neurophysiology, as measured with EEG, and FMRP, small effects where EEG studies are underpowered to detect effects, or FMRP levels are less related to neurophysiology where other physiological mechanisms may be more important (e.g., epigenetic mechanisms). The latter may partially explain translational challenges between the FXS mouse model and human outcomes. However, more work is required to better understand the relationship between FMRP and neurophysiology in humans before conclusions should be drawn.

In conclusion, the study identified several potential biomarkers that index cognitive inflexibility and network rigidity. Biomarkers from the present set of studies also provide better insight into network mechanisms in FXS and mechanistic contributors to cognitive flexibility difficulties in FXS. Beyond serving as biomarkers, the use of both microstates and FC provided converging evidence of possible neural rigidity where increased network rigidity may represent a core pathological mechanisms underlying cognitive disruptions in FXS. As cognitive flexibility difficulties represent core challenges for individuals with FXS and their families, elevated GFP, GEV, and altered FC dynamics in core functional networks may represent a plausible target for therapeutic intervention and may represent a translational tool for targeting cognition in both rodent models and humans (Schmitt et al., 2023). To date, most biomarkers represent single

metrics with limited understanding of the dynamics between EEG measures. However, the current microstate findings have larger implications for better understanding dynamic features of functional neural organization. Specifically, the breakdown of efficient network transitions with a tendency towards repetitive or redundant activation patterns may slow or exacerbate cognitive difficulties. While the determination of whether microstates represent FC proxies remains a future endeavor, the present findings provide evidence to support the conclusion that microstates capture certain aspects of network dynamics that relate to cognitive ability. Eventually, these findings may generalize to other populations with intellectual disability and populations with disruptions to low frequency oscillations. Eventually, findings from the current project may support clinical trial efforts for therapeutic interventions targeting cognition by bridging mechanistic insights from mice and clinical findings related to cognitive and adaptive ability in FXS.

References

Abbeduto, L., Thurman, A. J., McDuffie, A., Klusek, J., Feigles, R. T., Ted Brown, W., Harvey, D. J., Adayev, T., LaFauci, G., Dobkins, C., & Roberts, J. E. (2019). ASD Comorbidity in Fragile X Syndrome: Symptom Profile and Predictors of Symptom Severity in Adolescent and Young Adult Males. *J Autism Dev Disord*, *49*(3), 960-977. https://doi.org/10.1007/s10803-018-3796-2

Adhikari, B. M., Hong, L. E., Sampath, H., Chiappelli, J., Jahanshad, N., Thompson, P. M., Rowland, L. M., Calhoun, V. D., Du, X., Chen, S., & Kochunov, P. (2019). Functional network connectivity impairments and core cognitive deficits in schizophrenia. *Hum Brain Mapp*, *40*(16), 4593-4605. https://doi.org/10.1002/hbm.24723

Ahmad, J., Ellis, C., Leech, R., Voytek, B., Garces, P., Jones, E., Buitelaar, J., Loth, E., Dos Santos, F. P., Amil, A. F., Verschure, P., Murphy, D., & McAlonan, G. (2022). From mechanisms to markers: novel noninvasive EEG proxy markers of the neural excitation and inhibition system in humans. *Transl Psychiatry*, *12*(1), 467. https://doi.org/10.1038/s41398-022-02218-z

Aishworiya, R., Tak, Y. E., Ponzini, M. D., Biag, H. M. B., Salcedo-Arellano, M. J., Kim, K., Tassone, F., Schneider, A., Thurman, A. J., Abbeduto, L., Hessl, D., Randol, J. L., Bolduc, F. V., Lippe, S., Hagerman, P., & Hagerman, R. (2023). Adaptive, behavioral, and cognitive outcomes in individuals with fragile X syndrome with varying autism severity. *Int J Dev Neurosci*, *83*(8), 715-727. https://doi.org/10.1002/jdn.10299

Al Zoubi, O., Mayeli, A., Misaki, M., Tsuchiyagaito, A., Zotev, V., Refai, H., Paulus, M., & Bodurka, J. (2022). Canonical EEG microstates transitions reflect switching among

BOLD resting state networks and predict fMRI signal. *J Neural Eng*, *18*(6). https://doi.org/10.1088/1741-2552/ac4595

Alves, P. N., Foulon, C., Karolis, V., Bzdok, D., Margulies, D. S., Volle, E., & Thiebaut de Schotten, M. (2019). An improved neuroanatomical model of the default-mode network reconciles previous neuroimaging and neuropathological findings. *Commun Biol*, *2*, 370. https://doi.org/10.1038/s42003-019-0611-3

Andrade-Talavera, Y., Fisahn, A., & Rodriguez-Moreno, A. (2023). Timing to be precise? An overview of spike timing-dependent plasticity, brain rhythmicity, and glial cells interplay within neuronal circuits. *Mol Psychiatry*, *28*(6), 2177-2188. https://doi.org/10.1038/s41380-023-02027-w

Angelakis, E., Lubar, J. F., Stathopoulou, S., & Kounios, J. (2004). Peak alpha frequency: an electroencephalographic measure of cognitive preparedness. *Clin Neurophysiol*, *115*(4), 887-897. https://doi.org/10.1016/j.clinph.2003.11.034

Antonova, E., Holding, M., Suen, H. C., Sumich, A., Maex, R., & Nehaniv, C. (2022). EEG microstates: Functional significance and short-term test-retest reliability. *Neuroimage: Reports*, *2*(2). https://doi.org/10.1016/j.ynirp.2022.100089

Aykan, S., Puglia, M. H., Kalaycioglu, C., Pelphrey, K. A., Tuncali, T., & Nalcaci, E. (2022). Right Anterior Theta Hypersynchrony as a Quantitative Measure Associated with Autistic Traits and K-Cl Cotransporter KCC2 Polymorphism. *J Autism Dev Disord*, *52*(1), 61-72. https://doi.org/10.1007/s10803-021-04924-x

Bagdasarov, A., Roberts, K., Brunet, D., Michel, C. M., & Gaffrey, M. S. (2024). Exploring the Association Between EEG Microstates During Resting-State and Error-Related Activity

in Young Children. *Brain Topogr*, *37*(4), 552-570. https://doi.org/10.1007/s10548-023-01030-2

Bailey, D. B., Jr., Hatton, D., & Skinner, M. (1998). Early Developmental Trajectories of Males With Fragile X Syndrome. *American Journal on Mental Retardation*, *103*(1), 29-39. https://doi.org/10.1352/0895-8017(1998)103<0029:EDTOMW>2.0.CO;2

Bain, C. M., Shi, D., Boness, C. L., & Loeffelman, J. E. (2024 - Preprint). A Simulation Study Comparing the Use of Supervised Machine Learning Variable Selection Methods in the Psychological Sciences. *PsyArXiv.* https://doi.org/10.31234/osf.io/j695a_v1

Bartoli, E., Devara, E., Dang, H. Q., Rabinovich, R., Mathura, R. K., Anand, A., Pascuzzi, B. R., Adkinson, J., Kenett, Y. N., Bijanki, K. R., Sheth, S. A., & Shofty, B. (2024). Default mode network electrophysiological dynamics and causal role in creative thinking. *Brain*, *147*(10), 3409-3425. https://doi.org/10.1093/brain/awae199

Barzegaran, E., & Knyazeva, M. G. (2017). Functional connectivity analysis in EEG source space: The choice of method. *PLoS One*, *12*(7), e0181105. https://doi.org/10.1371/journal.pone.0181105

Bassett, D. S., & Sporns, O. (2017). Network neuroscience. *Nat Neurosci*, *20*(3), 353-364. https://doi.org/10.1038/nn.4502

Bastos, A. M., & Schoffelen, J. M. (2015). A Tutorial Review of Functional Connectivity Analysis Methods and Their Interpretational Pitfalls. *Front Syst Neurosci*, *9*, 175. https://doi.org/10.3389/fnsys.2015.00175

Bauer, E. A., Watanabe, B. K., & MacNamara, A. (2024). Reinforcement learning and the reward positivity with aversive outcomes. *Psychophysiology*, *61*(4), e14460. https://doi.org/10.1111/psyp.14460

Berry-Kravis, E. (2022). Disease-Targeted Treatment Translation in Fragile X Syndrome as a Model for Neurodevelopmental Disorders. *J Child Neurol*, *37*(10-11), 797-812. https://doi.org/10.1177/08830738221089740

Berry-Kravis, E., Des Portes, V., Hagerman, R., Jacquemont, S., Charles, P., Visootsak, J., Brinkman, M., Rerat,, K., K., B., Zhu, L., Barth, G. M., Jaecklin, T.,, Apostol, G., & von Raison, F. (2016). Mavoglurant in fragile X syndrome Results of two randomized, double-blinded, placebo-controlled trials. *Science Translational Medicine*, *8*(321), 321ra325. https://doi.org/https://doi.org/10.1126/scitranslmed.aab4109

Berry-Kravis, E., Hagerman, R., Visootsak, J., Budimirovic, D., Kaufmann, W. E., Cherubini, M., Zarevics, P., Walton-Bowen, K., Wang, P., Bear, M. F., & Carpenter, R. L. (2017). Arbaclofen in fragile X syndrome: results of phase 3 trials. *J Neurodev Disord*, *9*, 3. https://doi.org/10.1186/s11689-016-9181-6

Berry-Kravis, E., Hessl, D., Rathmell, B., Zarevics, P., Cherubini, M., Walton-Bowen, K., Mu, Y., Nguyen, D., Gonzalez-Heydrich, J., Wang, P., Carpenter, R. L., Bear, M. F., & Hagerman, R. J. (2012). Effects of STX209 (Arbaclofen) on Neurobehavioral function in children and adults with FXS - a randomized, controlled, phase 2 trial. *Science Translational Medicine*, *4*(152), 152ra127. https://doi.org/https://doi.org/10.1126/scitranslmed.3004214

Boggs, A. E., Schmitt, L. M., McLane, R. D., Adayev, T., LaFauci, G., Horn, P. S., Dominick, K. C., Gross, C., & Erickson, C. A. (2022). Optimization, validation and initial clinical implications of a Luminex-based immunoassay for the quantification of Fragile X Protein from dried blood spots. *Sci Rep*, *12*(1), 5617. https://doi.org/10.1038/s41598-022-09633-8

Breukelaar, I. A., Griffiths, K. R., Harris, A., Foster, S. L., Williams, L. M., & Korgaonkar, M. S. (2020). Intrinsic functional connectivity of the default mode and cognitive control networks relate to change in behavioral performance over two years. *Cortex*, *132*, 180-190. https://doi.org/10.1016/j.cortex.2020.08.014

Brown, C., Tollefson, N., Dunn, W., Cromwell, R., & Filion, D. (2001). The Adult Sensory Profile: Measuring Patterns of Sensory Processing. *American Journal of Occupational Therapy*, *55*(1), 75-82. https://doi.org/10.5014/ajot.55.1.75

Buzsaki, G., & Draguhn, A. (2004). Neuronal oscillations in cortical networks. *Science*, *304*(5679), 1926-1929. https://doi.org/10.1126/science.1099745

Campbell, I. G., & Feinberg, I. (2009). Longitudinal trajectories of non-rapid eye movement delta and theta EEG as indicators of adolescent brain maturation. *Proceedings of the National Academy of Sciences of the United States of America*, *106*(13), 5177-5180. https://doi.org/10.1073/pnas.0812947106

Cannon, J., O'Brien, A. M., Bungert, L., & Sinha, P. (2021). Prediction in Autism Spectrum Disorder: A Systematic Review of Empirical Evidence. *Autism Res*, *14*(4), 604-630. https://doi.org/10.1002/aur.2482

Carr, E., Carriere, M., Michel, B., Chazal, F., & Iniesta, R. (2021). Identifying homogeneous subgroups of patients and important features: a topological machine learning approach. *BMC Bioinformatics*, *22*(1), 449. https://doi.org/10.1186/s12859-021-04360-9

Carrillo-de-la-Pena, M. T., & Garcia-Larrea, L. (2007). Right frontal event related EEG coherence (ERCoh) differentiates good from bad performers of the Wisconsin Card Sorting Test (WCST). *Neurophysiol Clin*, *37*(2), 63-75. https://doi.org/10.1016/j.neucli.2007.02.002

Cavanagh, J. F., & Frank, M. J. (2014). Frontal theta as a mechanism for cognitive control. *Trends Cogn Sci*, *18*(8), 414-421. https://doi.org/10.1016/j.tics.2014.04.012

Cavanna, A. E., & Trimble, M. R. (2006). The precuneus: a review of its functional anatomy and behavioural correlates. *Brain*, *129*(Pt 3), 564-583. https://doi.org/10.1093/brain/awl004

Cellier, D., Riddle, J., Petersen, I., & Hwang, K. (2021). The development of theta and alpha neural oscillations from ages 3 to 24 years. *Dev Cogn Neurosci*, *50*, 100969. https://doi.org/10.1016/j.dcn.2021.100969

Chan, M. M. Y., Chan, M. C., Lai, O. L., Krishnamurthy, K., & Han, Y. M. Y. (2022). Abnormal Prefrontal Functional Connectivity Is Associated with Inflexible Information Processing in Patients with Autism Spectrum Disorder (ASD): An fNIRS Study. *Biomedicines*, *10*(5). https://doi.org/10.3390/biomedicines10051132

Chen, B., Linke, A., Olson, L., Ibarra, C., Reynolds, S., Muller, R. A., Kinnear, M., & Fishman, I. (2021). Greater functional connectivity between sensory networks is related to symptom severity in toddlers with autism spectrum disorder. *J Child Psychol Psychiatry*, *62*(2), 160-170. https://doi.org/10.1111/jcpp.13268

Chen, Y. Y., Uljarevic, M., Neal, J., Greening, S., Yim, H., & Lee, T. H. (2022). Excessive Functional Coupling With Less Variability Between Salience and Default Mode Networks in Autism Spectrum Disorder. *Biol Psychiatry Cogn Neurosci Neuroimaging*, *7*(9), 876-884. https://doi.org/10.1016/j.bpsc.2021.11.016

Ciaccio, C., Fontana, L., Milani, D., Tabano, S., Miozzo, M., & Esposito, S. (2017). Fragile X syndrome: a review of clinical and molecular diagnoses. *Ital J Pediatr*, *43*(1), 39. https://doi.org/10.1186/s13052-017-0355-y

Clementz, B. A., Sweeney, J. A., Hamm, J. P., Ivleva, E. I., Ethridge, L. E., Pearlson, G. D., Keshavan, M. S., & Tamminga, C. A. (2016). Identification of Distinct Psychosis Biotypes Using Brain-Based Biomarkers. *Am J Psychiatry*, *173*(4), 373-384. https://doi.org/10.1176/appi.ajp.2015.14091200

Cockburn, J., & Holroyd, C. B. (2018). Feedback information and the reward positivity. *Int J Psychophysiol*, *132*(Pt B), 243-251. https://doi.org/10.1016/j.ijpsycho.2017.11.017

Cohen, M. X. (2015). Effects of time lag and frequency matching on phase-based connectivity. *J Neurosci Methods*, *250*, 137-146. https://doi.org/10.1016/j.jneumeth.2014.09.005

Cohen, S., Masyn, K., Mastergeorge, A., & Hessl, D. (2015). Psychophysiological responses to emotional stimuli in children and adolescents with autism and fragile X syndrome. *J Clin Child Adolesc Psychol*, *44*(2), 250-263. https://doi.org/10.1080/15374416.2013.843462

Cole, M. W. (2024). Cognitive flexibility as the shifting of brain network flows by flexible neural representations. *Current Opinion in Behavioral Sciences*, *57*. https://doi.org/10.1016/j.cobeha.2024.101384

Contractor, A., Klyachko, V. A., & Portera-Cailliau, C. (2015). Altered Neuronal and Circuit Excitability in Fragile X Syndrome. *Neuron*, *87*(4), 699-715. https://doi.org/10.1016/j.neuron.2015.06.017

Cordeiro, L., Villagomez, A., Swain, D., Deklotz, S., & Tartaglia, N. (2020). Adaptive Skills in FXS: A Review of the Literature and Evaluation of the PEDI-Computer Adaptive Test (PEDI-CAT) to Measure Adaptive Skills. *Brain Sci*, *10*(6). https://doi.org/10.3390/brainsci10060351

Custo, A., Van De Ville, D., Wells, W. M., Tomescu, M. I., Brunet, D., & Michel, C. M. (2017). Electroencephalographic Resting-State Networks: Source Localization of Microstates. *Brain Connect*, *7*(10), 671-682. https://doi.org/10.1089/brain.2016.0476

D'Addario, S. L., Rosina, E., Massaro Cenere, M., Bagni, C., Mercuri, N. B., & Ledonne, A. (2025). ErbB inhibition rescues nigral dopamine neuron hyperactivity and repetitive behaviors in a mouse model of fragile X syndrome. *Mol Psychiatry*, *30*(5), 2183-2196. https://doi.org/10.1038/s41380-024-02831-y

D'Croz-Baron, D. F., Baker, M., Michel, C. M., & Karp, T. (2019). EEG Microstates Analysis in Young Adults With Autism Spectrum Disorder During Resting-State. *Front Hum Neurosci*, *13*, 173. https://doi.org/10.3389/fnhum.2019.00173

D'Cruz, A. M., Ragozzino, M. E., Mosconi, M. W., Pavuluri, M. N., & Sweeney, J. A. (2011). Human reversal learning under conditions of certain versus uncertain outcomes. *Neuroimage*, *56*(1), 315-322. https://doi.org/10.1016/j.neuroimage.2011.01.068

Dajani, D. R., & Uddin, L. Q. (2015). Demystifying cognitive flexibility: Implications for clinical and developmental neuroscience. *Trends Neurosci*, *38*(9), 571-578. https://doi.org/10.1016/j.tins.2015.07.003

Das, S., Zomorrodi, R., Kirkovski, M., Hill, A. T., Enticott, P. G., Blumberger, D. M., Rajji, T. K., & Desarkar, P. (2024). Atypical alpha band microstates produced during eyes-closed resting state EEG in autism. *Prog Neuropsychopharmacol Biol Psychiatry*, *131*, 110958. https://doi.org/10.1016/j.pnpbp.2024.110958

Dawson, G., Klinger, L. G., Panagiotides, H., Lewy, A., & Castelloe, P. (1995). Subgroups of Autistic Children Based on Social Behavior Display Distinct Patterns of Brain Activity.

Journal of Abnormal Child Psychology, *23*(5), 569-583. https://doi.org/10.1007/BF01447662

de-Wit, L., Machilsen, B., & Putzeys, T. (2010). Predictive coding and the neural response to predictable stimuli. *J Neurosci*, *30*(26), 8702-8703. https://doi.org/10.1523/JNEUROSCI.2248-10.2010

Desikan, R. S., Segonne, F., Fischl, B., Quinn, B. T., Dickerson, B. C., Blacker, D., Buckner, R. L., Dale, A. M., Maguire, R. P., Hyman, B. T., Albert, M. S., & Killiany, R. J. (2006). An automated labeling system for subdividing the human cerebral cortex on MRI scans into gyral based regions of interest. *Neuroimage*, *31*(3), 968-980. https://doi.org/10.1016/j.neuroimage.2006.01.021

Donaldson, K. R., Ait Oumeziane, B., Helie, S., & Foti, D. (2016). The temporal dynamics of reversal learning: P3 amplitude predicts valence-specific behavioral adjustment. *Physiol Behav*, *161*, 24-32. https://doi.org/10.1016/j.physbeh.2016.03.034

Dosenbach, N. U., Fair, D. A., Cohen, A. L., Schlaggar, B. L., & Petersen, S. E. (2008). A dual-networks architecture of top-down control. *Trends Cogn Sci*, *12*(3), 99-105. https://doi.org/10.1016/j.tics.2008.01.001

Dosenbach, N. U., Visscher, K. M., Palmer, E. D., Miezin, F. M., Wenger, K. K., Kang, H. C., Burgund, E. D., Grimes, A. L., Schlaggar, B. L., & Petersen, S. E. (2006). A core system for the implementation of task sets. *Neuron*, *50*(5), 799-812. https://doi.org/10.1016/j.neuron.2006.04.031

Erickson, C. A., Davenport, M. H., Schaefer, T. L., Wink, L. K., Pedapati, E. V., Sweeney, J. A., Fitzpatrick, S. E., Brown, W. T., Budimirovic, D., Hagerman, R. J., Hessl, D., Kaufmann, W. E., & Berry-Kravis, E. (2017). Fragile X targeted pharmacotherapy: lessons learned

and future directions. *J Neurodev Disord*, *9*, 7. https://doi.org/10.1186/s11689-017-9186-9

Esbensen, A. J., Rojahn, J., Aman, M. G., & Ruedrich, S. (2003). Relibaility and validity of an assessment instrument for Anxiety, Depression, and Mood among indiviuduals with mental disability. *Journal of Autism and Developmental Disorders*, *33*(6), 617-629. https://doi.org/0.1023/b:jadd.0000005999.27178.55

Espinet, S. D., Anderson, J. E., & Zelazo, P. D. (2012). N2 amplitude as a neural marker of executive function in young children: an ERP study of children who switch versus perseverate on the Dimensional Change Card Sort. *Dev Cogn Neurosci*, *2 Suppl 1*(Suppl 1), S49-58. https://doi.org/10.1016/j.dcn.2011.12.002

Ethridge, L. E., De Stefano, L. A., Schmitt, L. M., Woodruff, N. E., Brown, K. L., Tran, M., Wang, J., Pedapati, E. V., Erickson, C. A., & Sweeney, J. A. (2019). Auditory EEG Biomarkers in Fragile X Syndrome: Clinical Relevance. *Front Integr Neurosci*, *13*, 60. https://doi.org/10.3389/fnint.2019.00060

Ethridge, L. E., Pedapati, E. V., Schmitt, L. M., Norris, J. E., Auger, E., De Stefano, L. A., Sweeney, J. A., & Erickson, C. A. (2024). Validating brain activity measures as reliable indicators of individual diagnostic group and genetically mediated sub-group membership Fragile X Syndrome. *Sci Rep*, *14*(1), 22982. https://doi.org/10.1038/s41598-024-72935-6

Ethridge, L. E., White, S. P., Mosconi, M. W., Wang, J., Byerly, M. J., & Sweeney, J. A. (2016). Reduced habituation of auditory evoked potentials indicate cortical hyper-excitability in Fragile X Syndrome. *Transl Psychiatry*, *6*, e787. https://doi.org/10.1038/tp.2016.48

Ethridge, L. E., White, S. P., Mosconi, M. W., Wang, J., Pedapati, E. V., Erickson, C. A., Byerly, M. J., & Sweeney, J. A. (2017). Neural synchronization deficits linked to cortical hyper-excitability and auditory hypersensitivity in fragile X syndrome. *Mol Autism*, *8*, 22. https://doi.org/10.1186/s13229-017-0140-1

Ewen, J. B., Sweeney, J. A., & Potter, W. Z. (2019). Conceptual, Regulatory and Strategic Imperatives in the Early Days of EEG-Based Biomarker Validation for Neurodevelopmental Disabilities. *Front Integr Neurosci*, *13*, 45. https://doi.org/10.3389/fnint.2019.00045

Fang, H., Disteche, C. M., & Berletch, J. B. (2019). X Inactivation and Escape: Epigenetic and Structural Features. *Front Cell Dev Biol*, *7*, 219. https://doi.org/10.3389/fcell.2019.00219

Feng, Z., & Chen, H. (2005). Analyze the dynamic features of rat EEG using wavelet entropy. *Conference Proceedings IEEE Engineering in Medicine and Biology Society* 833-836. https://doi.org/10.1109/IEMBS.2005.1616544

Fish, E. W., Krouse, M. C., Stringfield, S. J., Diberto, J. F., Robinson, J. E., & Malanga, C. J. (2013). Changes in sensitivity of reward and motor behavior to dopaminergic, glutamatergic, and cholinergic drugs in a mouse model of fragile X syndrome. *PLoS One*, *8*(10), e77896. https://doi.org/10.1371/journal.pone.0077896

Fransson, P., & Marrelec, G. (2008). The precuneus/posterior cingulate cortex plays a pivotal role in the default mode network: Evidence from a partial correlation network analysis. *Neuroimage*, *42*(3), 1178-1184. https://doi.org/10.1016/j.neuroimage.2008.05.059

Gara, S. K., Chhetri, A. G., Alrjoob, M., Abbasi, S. A. A., & Rutkofsky, I. H. (2020). The Sensory Abnormalities and Neuropsychopathology of Autism and Anxiety. *Cureus*, *12*(5), e8071. https://doi.org/10.7759/cureus.8071

Garcia-Alegria, E., Ibanez, B., Minguez, M., Poch, M., Valiente, A., Sanz-Parra, A., Martinez-Bouzas, C., Beristain, E., & Tejada, M. I. (2007). Analysis of FMR1 gene expression in female premutation carriers using robust segmented linear regression models. *RNA*, *13*(5), 756-762. https://doi.org/10.1261/rna.206307

Gildin, L., Rauti, R., Vardi, O., Kuznitsov-Yanovsky, L., Maoz, B. M., Segal, M., & Ben-Yosef, D. (2022). Impaired Functional Connectivity Underlies Fragile X Syndrome. *Int J Mol Sci*, *23*(4). https://doi.org/10.3390/ijms23042048

Gotham, K., Risi, S., Pickles, A., & Lord, C. (2007). The Autism Diagnostic Observation Schedule: revised algorithms for improved diagnostic validity. *J Autism Dev Disord*, *37*(4), 613-627. https://doi.org/10.1007/s10803-006-0280-1

Gothelf, D., Furfaro, J. A., Hoeft, F., Eckert, M. A., Hall, S. S., O'Hara, R., Erba, H. W., Ringel, J., Hayashi, K. M., Patnaik, S., Golianu, B., Kraemer, H. C., Thompson, P. M., Piven, J., & Reiss, A. L. (2008). Neuroanatomy of fragile X syndrome is associated with aberrant behavior and the fragile X mental retardation protein (FMRP). *Ann Neurol*, *63*(1), 40-51. https://doi.org/10.1002/ana.21243

Gouveia, F. V., Germann, J., & Ibrahim, G. M. (2025). Brain network alterations in fragile X syndrome. *Neurosci Biobehav Rev*, *172*, 106101. https://doi.org/10.1016/j.neubiorev.2025.106101

Greicius, M. D., Krasnow, B.,, & Reiss, A. L., & Menon, V. (2003). Functional connectivity in the resting brain: a network analysis of the default mode hypothesis. *Proceedings of the*

National Academy of Sciences of the United States of America, *100*(1), 253-258. https://doi.org/10.1073/pnas.0135058100

Guha, A., Popov, T., Bartholomew, M. E., Reed, A. C., Diehl, C. K., Subotnik, K. L., Ventura, J., Nuechterlein, K. H., Miller, G. A., & Yee, C. M. (2024). Task-based default mode network connectivity predicts cognitive impairment and negative symptoms in first-episode schizophrenia. *Psychophysiology*, *61*(10), e14627. https://doi.org/10.1111/psyp.14627

Gupta, C., Chandrashekar, P., Jin, T., He, C., Khullar, S., Chang, Q., & Wang, D. (2022). Bringing machine learning to research on intellectual and developmental disabilities: taking inspiration from neurological diseases. *J Neurodev Disord*, *14*(1), 28. https://doi.org/10.1186/s11689-022-09438-w

Gurja, J. P., Muthukrishnan, S. P., Tripathi, M., & Sharma, R. (2022). Reduced Resting-State Cortical Alpha Connectivity Reflects Distinct Functional Brain Dysconnectivity in Alzheimer's Disease and Mild Cognitive Impairment. *Brain Connect*, *12*(2), 134-145. https://doi.org/10.1089/brain.2020.0926

Haas, B. W., Barnea-Goraly, N., Lightbody, A. A., Patnaik, S. S., Hoeft, F., Hazlett, H., Piven, J., & Reiss, A. L. (2009). Early white-matter abnormalities of the ventral frontostriatal pathway in fragile X syndrome. *Dev Med Child Neurol*, *51*(8), 593-599. https://doi.org/10.1111/j.1469-8749.2009.03295.x

Habiby Alaoui, S., Adam-Darque, A., Ptak, R., & Schnider, A. (2021). Distinct outcome processing in deterministic and probabilistic reversal learning. *Cortex*, *141*, 224-239. https://doi.org/10.1016/j.cortex.2021.04.008

Hagerman, P. J., & Hagerman, R. (2021). Fragile X syndrome. *Curr Biol*, *31*(6), R273-R275. https://doi.org/10.1016/j.cub.2021.01.043

Hagerman, R. J., Berry-Kravis, E., Hazlett, H. C., Bailey, D. B., Jr., Moine, H., Kooy, R. F., Tassone, F., Gantois, I., Sonenberg, N., Mandel, J. L., & Hagerman, P. J. (2017). Fragile X syndrome. *Nat Rev Dis Primers*, *3*, 17065. https://doi.org/10.1038/nrdp.2017.65

Haghighat, H., Mirzarezaee, M., Araabi, B. N., & Khadem, A. (2021). Functional Networks Abnormalities in Autism Spectrum Disorder: Age-Related Hypo and Hyper Connectivity. *Brain Topogr*, *34*(3), 306-322. https://doi.org/10.1007/s10548-021-00831-7

Hall-McMaster, S., Muhle-Karbe, P. S., Myers, N. E., & Stokes, M. G. (2019). Reward Boosts Neural Coding of Task Rules to Optimize Cognitive Flexibility. *J Neurosci*, *39*(43), 8549-8561. https://doi.org/10.1523/JNEUROSCI.0631-19.2019

Hall, D. A., Robertson-Dick, E. E., O'Keefe, J. A., Hadd, A. G., Zhou, L., & Berry-Kravis, E. (2016). X-inactivation in the clinical phenotype of fragile X premutation carrier sisters. *Neurol Genet*, *2*(1), e45. https://doi.org/10.1212/NXG.0000000000000045

Hall, S. S., Jiang, H., Reiss, A. L., & Greicius, M. D. (2013). Identifying large-scale brain networks in fragile X syndrome. *JAMA Psychiatry*, *70*(11), 1215-1223. https://doi.org/10.1001/jamapsychiatry.2013.247

Hampel, H., Gao, P., Cummings, J., Toschi, N., Thompson, P. M., Hu, Y., Cho, M., & Vergallo, A. (2023). The foundation and architecture of precision medicine in neurology and psychiatry. *Trends Neurosci*, *46*(3), 176-198. https://doi.org/10.1016/j.tins.2022.12.004

Hao, Z., Zhai, X., Cheng, D., Pan, Y., & Dou, W. (2022). EEG Microstate-Specific Functional Connectivity and Stroke-Related Alterations in Brain Dynamics. *Front Neurosci*, *16*, 848737. https://doi.org/10.3389/fnins.2022.848737

Hasan, A., Pandey, D., & Khan, A. (2021). Application of EEG Time-Varying Networks in the Evaluation of Dynamic Functional Brain Networks. *Augmented Human Research*, *6*(1). https://doi.org/10.1007/s41133-021-00046-2

Hauser, T. U., Iannaccone, R., Walitza, S., Brandeis, D., & Brem, S. (2015). Cognitive flexibility in adolescence: neural and behavioral mechanisms of reward prediction error processing in adaptive decision making during development. *Neuroimage*, *104*, 347-354. https://doi.org/10.1016/j.neuroimage.2014.09.018

Hawellek, D. J., Wong, Y. T., & Pesaran, B. (2016). Temporal coding of reward-guided choice in the posterior parietal cortex. *Proc Natl Acad Sci U S A*, *113*(47), 13492-13497. https://doi.org/10.1073/pnas.1606479113

Heine-Suner, D., Torres-Juan, L., Morla, M., Busquets, X., Barcelo, F., Pico, G., Bonilla, L., Govea, N., Bernues, M., & Rosell, J. (2003). Fragile-X syndrome and skewed X-chromosome inactivation within a family: a female member with complete inactivation of the functional X chromosome. *Am J Med Genet A*, *122A*(2), 108-114. https://doi.org/10.1002/ajmg.a.20160

Hessl, D., Sansone, S. M., Berry-Kravis, E., Riley, K., Widaman, K. F., Abbeduto, L., Schneider, A., Coleman, J., Oaklander, D., Rhodes, K. C., & Gershon, R. C. (2016). The NIH Toolbox Cognitive Battery for intellectual disabilities: three preliminary studies and future directions. *J Neurodev Disord*, *8*(1), 35. https://doi.org/10.1186/s11689-016-9167-4

Hessl, D., Schweitzer, J. B., Nguyen, D. V., McLennan, Y. A., Johnston, C., Shickman, R., & Chen, Y. (2019). Cognitive training for children and adolescents with fragile X

syndrome: a randomized controlled trial of Cogmed. *Journal of neurodevelopmental disorders*, *11*(1), 4. https://doi.org/10.1186/s11689-019-9264-2

Hill, A. T., Bailey, N. W., Zomorrodi, R., Hadas, I., Kirkovski, M., Das, S., Lum, J. A. G., & Enticott, P. G. (2023). EEG microstates in early-to-middle childhood show associations with age, biological sex, and alpha power. *Hum Brain Mapp*, *44*(18), 6484-6498. https://doi.org/10.1002/hbm.26525

Holroyd, C. B., Nieuwenhuis, S., Yeung, N., & , & Cohen, J. D. (2003). Errors in reward prediction are reflected in the event-related brain potential. . *Neuroreport*, *14*(18), 2481-2484. https://doi.org/10.1097/01.wnr.0000099601.41403.a5

Huang, Y., & Li, L. (2011). Naive Bayes Classification algorithm based on small sample set. *IEEE International Conference on Cloud Computing and Intelligence Systems*, 34-39. https://doi.org/10.1109/CCIS.2011.6045027

Huddleston, L. B., Visootsak, J., & Sherman, S. L. (2014). Cognitive aspects of Fragile X syndrome. *Wiley Interdiscip Rev Cogn Sci*, *5*(4), 501-508. https://doi.org/10.1002/wcs.1296

Huebschman, J. L., Corona, K. S., Guo, Y., & Smith, L. N. (2020). The Fragile X Mental Retardation Protein Regulates Striatal Medium Spiny Neuron Synapse Density and Dendritic Spine Morphology. *Front Mol Neurosci*, *13*, 161. https://doi.org/10.3389/fnmol.2020.00161

Hus, V., & Lord, C. (2014). The autism diagnostic observation schedule, module 4: revised algorithm and standardized severity scores. *J Autism Dev Disord*, *44*(8), 1996-2012. https://doi.org/10.1007/s10803-014-2080-3

Izquierdo, A., Brigman, J. L., Radke, A. K., Rudebeck, P. H., & Holmes, A. (2017). The neural basis of reversal learning: An updated perspective. *Neuroscience*, *345*, 12-26. https://doi.org/10.1016/j.neuroscience.2016.03.021

Jensen, O., & Mazaheri, A. (2010). Shaping functional architecture by oscillatory alpha activity: gating by inhibition. *Front Hum Neurosci*, *4*, 186. https://doi.org/10.3389/fnhum.2010.00186

Jonak, C. R., Pedapati, E. V., Schmitt, L. M., Assad, S. A., Sandhu, M. S., DeStefano, L., Ethridge, L., Razak, K. A., Sweeney, J. A., Binder, D. K., & Erickson, C. A. (2022). Baclofen-associated neurophysiologic target engagement across species in fragile X syndrome. *J Neurodev Disord*, *14*(1), 52. https://doi.org/10.1186/s11689-022-09455-9

Juarez, P., Salcedo-Arellano, M. J., Dufour, B., & Martinez-Cerdeno, V. (2024). Fragile X cortex is characterized by decreased parvalbumin-expressing interneurons. *Cereb Cortex*, *34*(3). https://doi.org/10.1093/cercor/bhae103

Kabbara, A., El Falou, W., Khalil, M., Wendling, F., & Hassan, M. (2017). The dynamic functional core network of the human brain at rest. *Sci Rep*, *7*(1), 2936. https://doi.org/10.1038/s41598-017-03420-6

Kang, J. H., Bae, J. H., & Jeon, Y. J. (2024). Age-Related Characteristics of Resting-State Electroencephalographic Signals and the Corresponding Analytic Approaches: A Review. *Bioengineering (Basel)*, *11*(5). https://doi.org/10.3390/bioengineering11050418

Kao, D. I., Aldridge, G. M., Weiler, I. J., & Greenough, W. T. (2010). Altered mRNA transport, docking, and protein translation in neurons lacking fragile X mental retardation protein. *Proc Natl Acad Sci U S A*, *107*(35), 15601-15606. https://doi.org/10.1073/pnas.1010564107

Kaufmann, W. E., Cortell, R., Kau, A. S., Bukelis, I., Tierney, E., Gray, R. M., Cox, C., Capone, G. T., & Stanard, P. (2004). Autism spectrum disorder in fragile X syndrome: communication, social interaction, and specific behaviors. *Am J Med Genet A*, *129A*(3), 225-234. https://doi.org/10.1002/ajmg.a.30229

Kaufmann, W. E., Kidd, S. A., Andrews, H. F., Budimirovic, D. B., Esler, A., Haas-Givler, B., Stackhouse, T., Riley, C., Peacock, G., Sherman, S. L., Brown, W. T., & Berry-Kravis, E. (2017). Autism Spectrum Disorder in Fragile X Syndrome: Cooccurring Conditions and Current Treatment. *Pediatrics*, *139*(Suppl 3), S194-S206. https://doi.org/10.1542/peds.2016-1159F

Kenny, A., Wright, D., & Stanfield, A. C. (2022). EEG as a translational biomarker and outcome measure in fragile X syndrome. *Transl Psychiatry*, *12*(1), 34. https://doi.org/10.1038/s41398-022-01796-2

Khanna, A., Pascual-Leone, A., Michel, C. M., & Farzan, F. (2015). Microstates in resting-state EEG: current status and future directions. *Neurosci Biobehav Rev*, *49*, 105-113. https://doi.org/10.1016/j.neubiorev.2014.12.010

Khazipov, R., & Luhmann, H. J. (2006). Early patterns of electrical activity in the developing cerebral cortex of humans and rodents. *Trends Neurosci*, *29*(7), 414-418. https://doi.org/10.1016/j.tins.2006.05.007

Kim, D., Jeong, W., Kim, J. S., & Chung, C. K. (2020). Single-Trial EEG Connectivity of Default Mode Network Before and During Encoding Predicts Subsequent Memory Outcome. *Front Syst Neurosci*, *14*, 591675. https://doi.org/10.3389/fnsys.2020.591675

Kim, K., Duc, N. T., Choi, M., & Lee, B. (2021). EEG microstate features according to performance on a mental arithmetic task. *Sci Rep*, *11*(1), 343. https://doi.org/10.1038/s41598-020-79423-7

Kirchgessner, C. U., Warren, S. T., & Willard, H. F. (1995). X inactivation of the FMR1 gene. *Journal of Medical Genetics*, *32*(9), 925-929. https://doi.org/https://doi.org/10.1136/jmg.32.12.925

Klaiman, C., Quintin, E. M., Jo, B., Lightbody, A. A., Hazlett, H. C., Piven, J., Hall, S. S., Chromik, L. C., & Reiss, A. L. (2014). Longitudinal profiles of adaptive behavior in fragile X syndrome. *Pediatrics*, *134*(2), 315-324. https://doi.org/10.1542/peds.2013-3990

Knoth, I. S., & Lippe, S. (2012). Event-related potential alterations in fragile X syndrome. *Front Hum Neurosci*, *6*, 264. https://doi.org/10.3389/fnhum.2012.00264

Knox, A., Schneider, A., Abucayan, F., Hervey, C., Tran, C., Hessl, D., & Berry-Kravis, E. (2012). Feasibility, reliability, and clinical validity of the Test of Attentional Performance for Children (KiTAP) in Fragile X syndrome (FXS). *J Neurodev Disord*, *4*(1), 2. https://doi.org/10.1186/1866-1955-4-2

Kornfeld-Sylla, S. S., Gelegen, C., Norris, J. E., Chaloner, F. A., Lee, M., Khela, M., Heinrich, M. J., Finnie, P. S. B., Ethridge, L. E., Erickson, C. A., Schmitt, L. M., Cooke, S. F., Wilkinson, C. L., & Bear, M. F. (2025 - Preprint). A human electrophysiological biomarker of Fragile X Syndrome is shared in V1 of Fmr1 KO mice and caused by loss of FMRP in cortical excitatory neurons. *bioRxiv*. https://doi.org/10.1101/2025.03.19.644144

Kottlow, M., Schlaepfer, A., Baenninger, A., Michels, L., Brandeis, D., & Koenig, T. (2015). Pre-stimulus BOLD-network activation modulates EEG spectral activity during working

memory retention. *Front Behav Neurosci*, *9*, 111. https://doi.org/10.3389/fnbeh.2015.00111

Kronke, K. M., Wolff, M., Shi, Y., Kraplin, A., Smolka, M. N., Buhringer, G., & Goschke, T. (2020). Functional connectivity in a triple-network saliency model is associated with real-life self-control. *Neuropsychologia*, *149*, 107667. https://doi.org/10.1016/j.neuropsychologia.2020.107667

Kwon, H., Menon, V., Eliez, S., Warsofsky, I. S., White, C. D., , Dyer-Friedman, J., Taylor, A. K., Glover, G. H., & , & Reiss, A. L. (2001). Functional neuroanatomy of visuospatial working memory in fragile X syndrome: relation to behavioral and molecular measures. *The American journal of psychiatry*, *158*(7), 1040-1051.

Lachiewicz, A. M., Stackhouse, T. M., Burgess, K., Burgess, D., Andrews, H. F., Choo, T. H., Kaufmann, W. E., & Kidd, S. A. (2024). Sensory Symptoms and Signs of Hyperarousal in Individuals with Fragile X Syndrome: Findings from the FORWARD Registry and Database Multisite Study. *J Autism Dev Disord*, *54*(11), 4259-4277. https://doi.org/10.1007/s10803-023-06135-y

Lau, T. M., Gwin, J. T., McDowell, K. G., & Ferris, D. P. (2012). Weighted phase lag index stability as an artifact resistant measure to detect cognitive EEG activity during locomotion. *Journal of NeuroEngineering and Rehabilitation*, *9*(47). https://doi.org/10.1186/1743-0003-9-47

Lee, J. K., Cho, A. C. B., Andrews, D. S., Ozonoff, S., Rogers, S. J., Amaral, D. G., Solomon, M., & Nordahl, C. W. (2022). Default mode and fronto-parietal network associations with IQ development across childhood in autism. *J Neurodev Disord*, *14*(1), 51. https://doi.org/10.1186/s11689-022-09460-y

Leech, R., & Sharp, D. J. (2014). The role of the posterior cingulate cortex in cognition and disease. *Brain*, *137*(Pt 1), 12-32. https://doi.org/10.1093/brain/awt162

Lehmann, D., & Skrandies, W. (1980). Reference-free identification of components of checkerboard-evoked multichannel potential fields. *Electroencephalography and Clinical Neurophysiology*, *48*(6), 609-621. https://doi.org/10.1016/0013-4694(80)90419-8

Li, W., Mai, X., & Liu, C. (2014). The default mode network and social understanding of others: what do brain connectivity studies tell us. *Front Hum Neurosci*, *8*, 74. https://doi.org/10.3389/fnhum.2014.00074

Liang, S., & Mody, M. (2022). Abnormal Brain Oscillations in Developmental Disorders: Application of Resting State EEG and MEG in Autism Spectrum Disorder and Fragile X Syndrome. *Frontiers in Neuroimaging*, *1*. https://doi.org/10.3389/fnimg.2022.903191

Linke, A. C., Chen, B., Olson, L., Cordova, M., Wilkinson, M., Wang, T., Herrera, M., Salmina, M., Rios, A., Mahmalji, J., Do, T., Vu, J., Budman, M., Walker, A., & Fishman, I. (2024). Altered Development of the Hurst Exponent in the Medial Prefrontal Cortex in Preschoolers With Autism. *Biol Psychiatry Cogn Neurosci Neuroimaging*. https://doi.org/10.1016/j.bpsc.2024.09.003

Liu, X., Kumar, V., Tsai, N. P., & Auerbach, B. D. (2021). Hyperexcitability and Homeostasis in Fragile X Syndrome. *Front Mol Neurosci*, *14*, 805929. https://doi.org/10.3389/fnmol.2021.805929

Lopez-Calderon, J., & Luck, S. J. (2014). ERPLAB: an open-source toolbox for the analysis of event-related potentials. *Front Hum Neurosci*, *8*, 213. https://doi.org/10.3389/fnhum.2014.00213

Luck, S. J., Stewart, A. X., Simmons, A. M., & Rhemtulla, M. (2021). Standardized measurement error: A universal metric of data quality for averaged event-related potentials. *Psychophysiology*, *58*(6), e13793. https://doi.org/10.1111/psyp.13793

Luu, S., Province, H., Berry-Kravis, E., Hagerman, R., Hessl, D., Vaidya, D., Lozano, R., Rosselot, H., Erickson, C., Kaufmann, W. E., & Budimirovic, D. B. (2020). Response to Placebo in Fragile X Syndrome Clinical Trials: An Initial Analysis. *Brain Sci*, *10*(9). https://doi.org/10.3390/brainsci10090629

Ma, X., Tan, J., Jiang, L., Wang, X., Cheng, B., Xie, P., Li, Y., Wang, J., & Li, S. (2021). Aberrant Structural and Functional Developmental Trajectories in Children With Intellectual Disability. *Front Psychiatry*, *12*, 634170. https://doi.org/10.3389/fpsyt.2021.634170

Markram, H., Gerstner, W., & Sjostrom, P. J. (2012). Spike-timing-dependent plasticity: a comprehensive overview. *Front Synaptic Neurosci*, *4*, 2. https://doi.org/10.3389/fnsyn.2012.00002

Massullo, C., Carbone, G. A., Farina, B., Panno, A., Capriotti, C., Giacchini, M., Machado, S., Budde, H., Murillo-Rodriguez, E., & Imperatori, C. (2020). Dysregulated brain salience within a triple network model in high trait anxiety individuals: A pilot EEG functional connectivity study. *Int J Psychophysiol*, *157*, 61-69. https://doi.org/10.1016/j.ijpsycho.2020.09.002

Mathewson, K. E., Lleras, A., Beck, D. M., Fabiani, M., Ro, T., & Gratton, G. (2011). Pulsed out of awareness: EEG alpha oscillations represent a pulsed-inhibition of ongoing cortical processing. *Front Psychol*, *2*, 99. https://doi.org/10.3389/fpsyg.2011.00099

Matlis, S., Boric, K., Chu, C. J., & Kramer, M. A. (2015). Robust disruptions in electroencephalogram cortical oscillations and large-scale functional networks in autism. *BMC Neurol*, *15*, 97. https://doi.org/10.1186/s12883-015-0355-8

Maxwell, C. R., Villalobos, M. E., Schultz, R. T., Herpertz-Dahlmann, B., Konrad, K., & Kohls, G. (2015). Atypical laterality of resting gamma oscillations in autism spectrum disorders. *J Autism Dev Disord*, *45*(2), 292-297. https://doi.org/10.1007/s10803-013-1842-7

Mc Devitt, N. M., Gallagher, L., & Reilly, R. B. (2015). Autism Spectrum Disorder (ASD) and Fragile X Syndrome (FXS): Two Overlapping Disorders Reviewed through Electroencephalography-What Can be Interpreted from the Available Information? *Brain Sci*, *5*(2), 92-117. https://doi.org/10.3390/brainsci5020092

McCutcheon, R. A., Keefe, R. S. E., & McGuire, P. K. (2023). Cognitive impairment in schizophrenia: aetiology, pathophysiology, and treatment. *Mol Psychiatry*, *28*(5), 1902-1918. https://doi.org/10.1038/s41380-023-01949-9

Megevand, P., Quairiaux, C., Lascano, A. M., Kiss, J. Z., & Michel, C. M. (2008). A mouse model for studying large-scale neuronal networks using EEG mapping techniques. *Neuroimage*, *42*(2), 591-602. https://doi.org/10.1016/j.neuroimage.2008.05.016

Menon, V. (2011). Large-scale brain networks and psychopathology: a unifying triple network model. *Trends Cogn Sci*, *15*(10), 483-506. https://doi.org/10.1016/j.tics.2011.08.003

Menon, V. (2015). Salience Network. In *Brain Mapping* (pp. 597-611). https://doi.org/10.1016/b978-0-12-397025-1.00052-x

Menon, V. (2018). The Triple Network Model, Insight, and Large-Scale Brain Organization in Autism. *Biol Psychiatry*, *84*(4), 236-238. https://doi.org/10.1016/j.biopsych.2018.06.012

Menon, V., Kwon, H., Eliez, S., Taylor, A. K., & Reiss, A. L. (2000). Functional brain activation during cognition is related to FMR1 gene expression. *Brain Research*, *877*(2), 367-370. https://doi.org/10.1016/S0006-8993(00)02617-2

Michel, C. M., Brechet, L., Schiller, B., & Koenig, T. (2024). Current State of EEG/ERP Microstate Research. *Brain Topogr*, *37*(2), 169-180. https://doi.org/10.1007/s10548-024-01037-3

Michel, C. M., & Koenig, T. (2018). EEG microstates as a tool for studying the temporal dynamics of whole-brain neuronal networks: A review. *Neuroimage*, *180*(Pt B), 577-593. https://doi.org/10.1016/j.neuroimage.2017.11.062

Milz, P., Faber, P. L., Lehmann, D., Koenig, T., Kochi, K., & Pascual-Marqui, R. D. (2016). The functional significance of EEG microstates--Associations with modalities of thinking. *Neuroimage*, *125*, 643-656. https://doi.org/10.1016/j.neuroimage.2015.08.023

Milz, P., Pascual-Marqui, R. D., Achermann, P., Kochi, K., & Faber, P. L. (2017). The EEG microstate topography is predominantly determined by intracortical sources in the alpha band. *Neuroimage*, *162*, 353-361. https://doi.org/10.1016/j.neuroimage.2017.08.058

Mishra, A., Englitz, B., & Cohen, M. X. (2020). EEG microstates as a continuous phenomenon. *Neuroimage*, *208*, 116454. https://doi.org/10.1016/j.neuroimage.2019.116454

Mishra, A., Marzban, N., Cohen, M. X., & Englitz, B. (2021). Dynamics of Neural Microstates in the VTA-Striatal-Prefrontal Loop during Novelty Exploration in the Rat. *J Neurosci*, *41*(32), 6864-6877. https://doi.org/10.1523/JNEUROSCI.2256-20.2021

Muir, A. M., Eberhard, A. C., Walker, M. S., Bennion, A., South, M., & Larson, M. J. (2021). Dissociating the effect of reward uncertainty and timing uncertainty on neural indices of

reward prediction errors: A reward positivity (RewP) event-related potential (ERP) study. *Biol Psychol*, *163*, 108121. https://doi.org/10.1016/j.biopsycho.2021.108121

Mushtaq, F., Bland, A. R., & Schaefer, A. (2011). Uncertainty and cognitive control. *Front Psychol*, *2*, 249. https://doi.org/10.3389/fpsyg.2011.00249

Nair, J., Klaassen, A. L., Arato, J., Vyssotski, A. L., Harvey, M., & Rainer, G. (2018). Basal forebrain contributes to default mode network regulation. *Proc Natl Acad Sci U S A*, *115*(6), 1352-1357. https://doi.org/10.1073/pnas.1712431115

Nishio, M., Ellwood-Lowe, M. E., Woodburn, M., McDermott, C. L., Park, A. T., Tooley, U. A., Boroshok, A. L., Grandjean, J., & Mackey, A. P. (2024 -Preprint). The Hurst exponent as a marker of inhibition in the developing brain. *BioRxiv*. https://doi.org/10.1101/2024.09.29.615675

Nishitani, N., Nagamine, T., &, & Shibasaki, H. (1998). Modality-specific subregions in human inferior parietal lobule: a magnetoencephalographic study during cognitive tasks. *Neuroscience letters*, *252*(2), 79-82. https://doi.org/10.1016/s0304-3940(98)00512-6

Norris, J. E., Berry-Kravis, E. M., Harnett, M. D., Reines, S. A., Reese, M. A., Auger, E. K., Outterson, A. H., Furman, J., Gurney, M. E., & Ethridge, L. E. (2025b - preprint). ROC Analysis of Biomarker Combinations in Fragile X Syndrome-Specific Clinical Trials: Evaluating Treatment Efficacy via Exploratory Biomarkers. *MedRxiv.* https://doi.org/10.1101/2025.05.29.25328581

Norris, J. E., Berry-Kravis, E. M., Harnett, M. D., Reines, S. A., Reese, M. A., Outterson, A. H., Michalak, C., Furman, J., Gurney, M. E., & Ethridge, L. E. (2024). Auditory N1 event-related potential amplitude is predictive of serum concentration of BPN14770 in fragile X syndrome. *Mol Autism*, *15*(1), 47. https://doi.org/10.1186/s13229-024-00626-0

Norris, J. E., De Stefano, L. A., McKinney, W. S., Schmitt, L. M., Miyakoshi, M., Gross, C., Piloto, S., Heald, B., Pedapati, E. V., Erickson, C. A., Sweeney, J. A., & Ethridge, L. E. (2025a - Preprint). Auditory steady-state response deficits in Fragile X Syndrome implicate deficits in stimulus representation maintenance and GABAergic modulation. *MedRxiv*. https://doi.org/10.1101/2025.01.29.25321365

Norris, J. E., DeStefano, L. A., Schmitt, L. M., Pedapati, E. V., Erickson, C. A., Sweeney, J. A., & Ethridge, L. E. (2022). Hemispheric Utilization of Alpha Oscillatory Dynamics as a Unique Biomarker of Neural Compensation in Females with Fragile X Syndrome. *ACS Chem Neurosci*. https://doi.org/10.1021/acschemneuro.2c00404

Numssen, O., Bzdok, D., & Hartwigsen, G. (2021). Functional specialization within the inferior parietal lobes across cognitive domains. *Elife*, *10*. https://doi.org/10.7554/eLife.63591

Oken, B. S., Salinsky, M. C., & Elsas, S. M. (2006). Vigilance, alertness, or sustained attention: physiological basis and measurement. *Clin Neurophysiol*, *117*(9), 1885-1901. https://doi.org/10.1016/j.clinph.2006.01.017

Papo, D., & Buldú, J. M. (2024). Does the brain behave like a (complex) network? I. Dynamics. *Physics of life reviews*, *48*, 47–98. https://doi.org/10.1016/j.plrev.2023.12.006

Park, S., Park, J. M., Kim, S., Kim, J. A., Shepherd, J. D., Smith-Hicks, C. L., Chowdhury, S., Kaufmann, W., Kuhl, D., Ryazanov, A. G., Huganir, R. L., Linden, D. J., & Worley, P. F. (2008). Elongation factor 2 and fragile X mental retardation protein control the dynamic translation of Arc/Arg3.1 essential for mGluR-LTD. *Neuron*, *59*(1), 70-83. https://doi.org/10.1016/j.neuron.2008.05.023

Pedapati, E. V., Schmitt, L. M., Ethridge, L. E., Miyakoshi, M., Sweeney, J. A., Liu, R., Smith, E., Shaffer, R. C., Dominick, K. C., Gilbert, D. L., Wu, S. W., Horn, P. S., Binder, D. K.,

Lamy, M., Axford, M., & Erickson, C. A. (2022). Neocortical localization and thalamocortical modulation of neuronal hyperexcitability contribute to Fragile X Syndrome. *Commun Biol*, *5*(1), 442. https://doi.org/10.1038/s42003-022-03395-9

Peinado, A. (200). Traveling slow waves of neural activity: A novel form of network activity in developing neocortex. *The Journal of Neuroscience*, *20*(2), 1-6. https://doi.org/10.1523/JNEUROSCI.20-02-j0002.2000

Pfeiffer, B. E., & Huber, K. M. (2009). The state of synapses in fragile X syndrome. *Neuroscientist*, *15*(5), 549-567. https://doi.org/10.1177/1073858409333075

Philipp, A. M., Weidner, R., Koch, I., & Fink, G. R. (2013). Differential roles of inferior frontal and inferior parietal cortex in task switching: evidence from stimulus-categorization switching and response-modality switching. *Hum Brain Mapp*, *34*(8), 1910-1920. https://doi.org/10.1002/hbm.22036

Poulsen, A. T., Pedroni, A., Langer, N., & Hansen, L. K. (2018 -Preprint). Microstate EEGlab toolbox: An introductory guide. *BioRxiv*. https://doi.org/10.1101/289850

Pretzsch, C. M., & Floris, D. L. (2020). Balancing excitation and inhibition in the autistic brain. *Elife*, *9*. https://doi.org/10.7554/eLife.60584

Proteau-Lemieux, M., Knoth, I. S., Agbogba, K., Cote, V., Barlahan Biag, H. M., Thurman, A. J., Martin, C. O., Belanger, A. M., Rosenfelt, C., Tassone, F., Abbeduto, L. J., Jacquemont, S., Hagerman, R., Bolduc, F., Hessl, D., Schneider, A., & Lippe, S. (2021). EEG Signal Complexity Is Reduced During Resting-State in Fragile X Syndrome. *Front Psychiatry*, *12*, 716707. https://doi.org/10.3389/fpsyt.2021.716707

Proteau-Lemieux, M., Knoth, I. S., Davoudi, S., Martin, C. O., Belanger, A. M., Fontaine, V., Cote, V., Agbogba, K., Vachon, K., Whitlock, K., Biag, H. M. B., Thurman, A. J.,

Rosenfelt, C., Tassone, F., Frei, J., Capano, L., Abbeduto, L., Jacquemont, S., Hessl, D., . . . Lippe, S. (2024). Specific EEG resting state biomarkers in FXS and ASD. *J Neurodev Disord*, *16*(1), 53. https://doi.org/10.1186/s11689-024-09570-9

Quax, S., Jensen, O., & Tiesinga, P. (2017). Top-down control of cortical gamma-band communication via pulvinar induced phase shifts in the alpha rhythm. *PLoS Comput Biol*, *13*(5), e1005519. https://doi.org/10.1371/journal.pcbi.1005519

Rajkumar, R., Regio Brambilla, C., Veselinovic, T., Bierbrier, J., Wyss, C., Ramkiran, S., Orth, L., Lang, M., Rota Kops, E., Mauler, J., Scheins, J., Neumaier, B., Ermert, J., Herzog, H., Langen, K. J., Binkofski, F. C., Lerche, C., Shah, N. J., & Neuner, I. (2021). Excitatory-inhibitory balance within EEG microstates and resting-state fMRI networks: assessed via simultaneous trimodal PET-MR-EEG imaging. *Transl Psychiatry*, *11*(1), 60. https://doi.org/10.1038/s41398-020-01160-2

Randolph, C., Tierney, M. C., Mohr, E., & Chase, T. N. (1998). The Repeatable Battery for the Assessment of Neuropsychological Status (RBANS) - Preliminary Clinical Validity. *Journal of Clinical and Experimental Neuropsychology*, *20*, 310-319. https://doi.org/10.1076/jcen.20.3.310.823

Razak, K. A., Dominick, K. C., & Erickson, C. A. (2020). Developmental studies in fragile X syndrome. *J Neurodev Disord*, *12*(1), 13. https://doi.org/10.1186/s11689-020-09310-9

Reisinger, D. L., Shaffer, R. C., Tartaglia, N., Berry-Kravis, E., & Erickson, C. A. (2020). Delineating Repetitive Behavior Profiles across the Lifespan in Fragile X Syndrome. *Brain Sci*, *10*(4). https://doi.org/10.3390/brainsci10040239

Richter, J. D., & Zhao, X. (2021). The molecular biology of FMRP: new insights into fragile X syndrome. *Nat Rev Neurosci*, *22*(4), 209-222. https://doi.org/10.1038/s41583-021-00432-0

Roid, G. H. (2003). *Stanford-Binet Inelligence Scales, Fifth edition*. Riverside Publishing.

Rylaarsdam, L., & Guemez-Gamboa, A. (2019). Genetic Causes and Modifiers of Autism Spectrum Disorder. *Front Cell Neurosci*, *13*, 385. https://doi.org/10.3389/fncel.2019.00385

Saeidi, M., Karwowski, W., Farahani, F. V., Fiok, K., Taiar, R., Hancock, P. A., & Al-Juaid, A. (2021). Neural Decoding of EEG Signals with Machine Learning: A Systematic Review. *Brain Sci*, *11*(11). https://doi.org/10.3390/brainsci11111525

Saggar, M., & Uddin, L. Q. (2019). Pushing the Boundaries of Psychiatric Neuroimaging to Ground Diagnosis in Biology. *eNeuro*, *6*(6). https://doi.org/10.1523/ENEURO.0384-19.2019

Sahin, M., Jones, S. R., Sweeney, J. A., Berry-Kravis, E., Connors, B. W., Ewen, J. B., Hartman, A. L., Levin, A. R., Potter, W. Z., & Mamounas, L. A. (2018). Discovering translational biomarkers in neurodevelopmental disorders. *Nat Rev Drug Discov*. https://doi.org/10.1038/d41573-018-00010-7

Salcedo-Arellano, M. J., Dufour, B., McLennan, Y., Martinez-Cerdeno, V., & Hagerman, R. (2020). Fragile X syndrome and associated disorders: Clinical aspects and pathology. *Neurobiol Dis*, *136*, 104740. https://doi.org/10.1016/j.nbd.2020.104740

Sattari, S., Damji, S., McLeod, J., Mirian, M. M., Wu, L., & Virji-Babul, N. (2024 - Preprint). Altered resting state EEG microstate dynamics in acute-phase pediatric mild traumatic brain injury. *MedRxiv*. https://doi.org/10.1101/2024.10.26.24316185

Schimmelpfennig, J., Topczewski, J., Zajkowski, W., & Jankowiak-Siuda, K. (2023). The role of the salience network in cognitive and affective deficits. *Front Hum Neurosci*, *17*, 1133367. https://doi.org/10.3389/fnhum.2023.1133367

Schmitt, L. M., Arzuaga, A. L., Dapore, A., Duncan, J., Patel, M., Larson, J. R., Erickson, C. A., Sweeney, J. A., & Ragozzino, M. E. (2022). Parallel learning and cognitive flexibility impairments between Fmr1 knockout mice and individuals with fragile X syndrome. *Front Behav Neurosci*, *16*, 1074682. https://doi.org/10.3389/fnbeh.2022.1074682

Schmitt, L. M., Li, J., Liu, R., Horn, P. S., Sweeney, J. A., Erickson, C. A., & Pedapati, E. V. (2022). Altered frontal connectivity as a mechanism for executive function deficits in fragile X syndrome. *Mol Autism*, *13*(1), 47. https://doi.org/10.1186/s13229-022-00527-0

Schmitt, L. M., Nelson, M., Shaffer, R. C., & Erickson, C. A. (2024). A near normal distribution of IQ in Fragile X Syndrome. *Sci Rep*, *14*(1), 23058. https://doi.org/10.1038/s41598-024-73626-y

Schmitt, L. M., Shaffer, R. C., Hessl, D., & Erickson, C. (2019). Executive Function in Fragile X Syndrome: A Systematic Review. *Brain Sci*, *9*(1). https://doi.org/10.3390/brainsci9010015

Schneider, A., Hagerman, R. J., & Hessl, D. (2009). Fragile X syndrome -- from genes to cognition. *Dev Disabil Res Rev*, *15*(4), 333-342. https://doi.org/10.1002/ddrr.80

Seeley, W. W., Menon, V., Schatzberg, A. F., Keller, J., Glover, G. H., Kenna, H., Reiss, A. L., & Greicius, M. D. (2007). Dissociable intrinsic connectivity networks for salience processing and executive control. *J Neurosci*, *27*(9), 2349-2356. https://doi.org/10.1523/JNEUROSCI.5587-06.2007

Seitzman, B. A., Abell, M., Bartley, S. C., Erickson, M. A., Bolbecker, A. R., & Hetrick, W. P. (2017). Cognitive manipulation of brain electric microstates. *Neuroimage*, *146*, 533-543. https://doi.org/10.1016/j.neuroimage.2016.10.002

Shields, R. H., Kaat, A. J., McKenzie, F. J., Drayton, A., Sansone, S. M., Coleman, J., Michalak, C., Riley, K., Berry-Kravis, E., Gershon, R. C., Widaman, K. F., & Hessl, D. (2020). Validation of the NIH Toolbox Cognitive Battery in intellectual disability. *Neurology*, *94*(12), e1229-e1240. https://doi.org/10.1212/WNL.0000000000009131

Shirer, W. R., Ryali, S., Rykhlevskaia, E., Menon, V., & Greicius, M. D. (2012). Decoding subject-driven cognitive states with whole-brain connectivity patterns. *Cereb Cortex*, *22*(1), 158-165. https://doi.org/10.1093/cercor/bhr099

Shvetsova, E., Sofronova, A., Monajemi, R., Gagalova, K., Draisma, H. H. M., White, S. J., Santen, G. W. E., Chuva de Sousa Lopes, S. M., Heijmans, B. T., van Meurs, J., Jansen, R., Franke, L., Kielbasa, S. M., den Dunnen, J. T., t Hoen, P. A. C., consortium, B., & Go, N. L. c. (2019). Skewed X-inactivation is common in the general female population. *Eur J Hum Genet*, *27*(3), 455-465. https://doi.org/10.1038/s41431-018-0291-3

Sohal, V. S., & Rubenstein, J. L. R. (2019). Excitation-inhibition balance as a framework for investigating mechanisms in neuropsychiatric disorders. *Mol Psychiatry*, *24*(9), 1248-1257. https://doi.org/10.1038/s41380-019-0426-0

Stier, A. J., Cardenas-Iniguez, C., Kardan, O., Moore, T. M., Meyer, F. A. C., Rosenberg, M. D., Kaczkurkin, A. N., Lahey, B. B., & Berman, M. G. (2023). A pattern of cognitive resource disruptions in childhood psychopathology. *Netw Neurosci*, *7*(3), 1153-1180. https://doi.org/10.1162/netn_a_00322

Stoppel, D. C., McCamphill, P. K., Senter, R. K., Heynen, A. J., & Bear, M. F. (2021). mGluR5 Negative Modulators for Fragile X: Treatment Resistance and Persistence. *Front Psychiatry*, *12*, 718953. https://doi.org/10.3389/fpsyt.2021.718953

Sun, Q., Zhou, J., Guo, H., Gou, N., Lin, R., Huang, Y., Guo, W., & Wang, X. (2021). EEG Microstates and Its Relationship With Clinical Symptoms in Patients With Schizophrenia. *Front Psychiatry*, *12*, 761203. https://doi.org/10.3389/fpsyt.2021.761203

Tadel, F., Baillet, S., Mosher, J. C., Pantazis, D., & Leahy, R. M. (2011). Brainstorm: a user-friendly application for MEG/EEG analysis. *Comput Intell Neurosci*, *2011*, 879716. https://doi.org/10.1155/2011/879716

Tait, L., Tamagnini, F., Stothart, G., Barvas, E., Monaldini, C., Frusciante, R., Volpini, M., Guttmann, S., Coulthard, E., Brown, J. T., Kazanina, N., & Goodfellow, M. (2020). EEG microstate complexity for aiding early diagnosis of Alzheimer's disease. *Sci Rep*, *10*(1), 17627. https://doi.org/10.1038/s41598-020-74790-7

Tait, L., & Zhang, J. (2022). +microstate: A MATLAB toolbox for brain microstate analysis in sensor and cortical EEG/MEG. *Neuroimage*, *258*, 119346. https://doi.org/10.1016/j.neuroimage.2022.119346

Takarae, Y., Zanesco, A., Erickson, C. A., & Pedapati, E. V. (2024). EEG Microstates as Markers for Cognitive Impairments in Fragile X Syndrome. *Brain Topogr*, *37*(3), 432-446. https://doi.org/10.1007/s10548-023-01009-z

Talapatra, D., Snider, L., Coleman, J., Thompson, T., Reinhardt, J. S., Hessl, D., & Riley, K. (2023). Deviation scores: An innovative approach to interpreting cognitive test results for individuals with intellectual disabilities. *J Appl Res Intellect Disabil*, *36*(6), 1218-1228. https://doi.org/10.1111/jar.13137

Tan, E., Troller-Renfree, S. V., Morales, S., Buzzell, G. A., McSweeney, M., Antunez, M., & Fox, N. A. (2024). Theta activity and cognitive functioning: Integrating evidence from resting-state and task-related developmental electroencephalography (EEG) research. *Dev Cogn Neurosci*, *67*, 101404. https://doi.org/10.1016/j.dcn.2024.101404

Thakkar, K. N., Polli, F. E., Joseph, R. M., Tuch, D. S., Hadjikhani, N., Barton, J. J., & Manoach, D. S. (2008). Response monitoring, repetitive behaviour and anterior cingulate abnormalities in autism spectrum disorders (ASD). *Brain*, *131*(Pt 9), 2464-2478. https://doi.org/10.1093/brain/awn099

Thomas, J., Vanni-Mercier, G., & Dreher, J. C. (2013). Neural dynamics of reward probability coding: a Magnetoencephalographic study in humans. *Front Neurosci*, *7*, 214. https://doi.org/10.3389/fnins.2013.00214

Thurm, A., Farmer, C., Salzman, E., Lord, C., & Bishop, S. (2019). State of the Field: Differentiating Intellectual Disability From Autism Spectrum Disorder. *Front Psychiatry*, *10*, 526. https://doi.org/10.3389/fpsyt.2019.00526

Uddin, L. Q. (2021). Cognitive and behavioural flexibility: neural mechanisms and clinical considerations. *Nat Rev Neurosci*, *22*(3), 167-179. https://doi.org/10.1038/s41583-021-00428-w

Uhlhaas, P. J., Roux, F., Rodriguez, E., Rotarska-Jagiela, A., & Singer, W. (2010). Neural synchrony and the development of cortical networks. *Trends Cogn Sci*, *14*(2), 72-80. https://doi.org/10.1016/j.tics.2009.12.002

Utami, K. H., Skotte, N. H., Colaco, A. R., Yusof, N., Sim, B., Yeo, X. Y., Bae, H. G., Garcia-Miralles, M., Radulescu, C. I., Chen, Q., Chaldaiopoulou, G., Liany, H., Nama, S., Peteri, U. A., Sampath, P., Castren, M. L., Jung, S., Mann, M., & Pouladi, M. A. (2020).

Integrative Analysis Identifies Key Molecular Signatures Underlying Neurodevelopmental Deficits in Fragile X Syndrome. *Biol Psychiatry*, *88*(6), 500-511. https://doi.org/10.1016/j.biopsych.2020.05.005

Vafaeie, F., Alerasool, M., Kaseb Mojaver, N., & Mojarrad, M. (2021). Fragile X Syndrome in a Female With Homozygous Full-Mutation Alleles of the FMR1 Gene. *Cureus*, *13*(7), e16340. https://doi.org/10.7759/cureus.16340

van der Molen, M. J., Stam, C. J., & van der Molen, M. W. (2014). Resting-state EEG oscillatory dynamics in fragile X syndrome: abnormal functional connectivity and brain network organization. *PLoS One*, *9*(2), e88451. https://doi.org/10.1371/journal.pone.0088451

Van der Molen, M. J., & Van der Molen, M. W. (2013). Reduced alpha and exaggerated theta power during the resting-state EEG in fragile X syndrome. *Biol Psychol*, *92*(2), 216-219. https://doi.org/10.1016/j.biopsycho.2012.11.013

Verdura, E., Perez-Cano, L., Sabido-Vera, R., Guney, E., Hyvelin, J. M., Durham, L., & Gomez-Mancilla, B. (2021). Heterogeneity in Fragile X Syndrome Highlights the Need for Precision Medicine-Based Treatments. *Front Psychiatry*, *12*, 722378. https://doi.org/10.3389/fpsyt.2021.722378

Vinck, M., Oostenveld, R., van Wingerden, M., Battaglia, F., & Pennartz, C. M. (2011). An improved index of phase-synchronization for electrophysiological data in the presence of volume-conduction, noise and sample-size bias. *Neuroimage*, *55*(4), 1548-1565. https://doi.org/10.1016/j.neuroimage.2011.01.055

von Wegner, F., Wiemers, M., Hermann, G., Todt, I., Tagliazucchi, E., & Laufs, H. (2024). Complexity Measures for EEG Microstate Sequences: Concepts and Algorithms. *Brain Topogr*, *37*(2), 296-311. https://doi.org/10.1007/s10548-023-01006-2

Wang, J., Ethridge, L. E., Mosconi, M. W., White, S. P., Binder, D. K., Pedapati, E. V., Erickson, C. A., Byerly, M. J., & Sweeney, J. A. (2017). A resting EEG study of neocortical hyperexcitability and altered functional connectivity in fragile X syndrome. *J Neurodev Disord*, *9*, 11. https://doi.org/10.1186/s11689-017-9191-z

Wantzen, P., Clochon, P., Doidy, F., Wallois, F., Mahmoudzadeh, M., Desaunay, P., Christian, M., Guile, J. M., Guenole, F., Eustache, F., Baleyte, J. M., & Guillery-Girard, B. (2022). EEG resting-state functional connectivity: evidence for an imbalance of external/internal information integration in autism. *J Neurodev Disord*, *14*(1), 47. https://doi.org/10.1186/s11689-022-09456-8

Weber, J. D., Smith, E., Berry-Kravis, E., Cadavid, D., Hessl, D., & Erickson, C. (2019). Voice of People with Fragile X Syndrome and Their Families: Reports from a Survey on Treatment Priorities. *Brain Sci*, *9*(2). https://doi.org/10.3390/brainsci9020018

Weber, S., Aleman, A., & Hugdahl, K. (2022). Involvement of the default mode network under varying levels of cognitive effort. *Sci Rep*, *12*(1), 6303. https://doi.org/10.1038/s41598-022-10289-7

Wilkinson, C. L., & Nelson, C. A. (2021). Increased aperiodic gamma power in young boys with Fragile X Syndrome is associated with better language ability. *Mol Autism*, *12*(1), 17. https://doi.org/10.1186/s13229-021-00425-x

Xiao, Y., Wu, J., Li, J., Tang, W., Ma, F., Sun, C., Yang, Y., Zhan, W., Wang, L., Yan, H., Xu, F., & Chen, S. (2019). The Neuro Patterns Prior to Error Responses in Long-Lasting Working Memory Task: An Event-Related Potential Study. *Front Behav Neurosci*, *13*, 277. https://doi.org/10.3389/fnbeh.2019.00277

Xu, S., Li, M., Yang, C., Fang, X., Ye, M., Wei, L., Liu, J., Li, B., Gan, Y., Yang, B., Huang, W., Li, P., Meng, X., Wu, Y., & Jiang, G. (2019). Altered Functional Connectivity in Children With Low-Function Autism Spectrum Disorders. *Front Neurosci*, *13*, 806. https://doi.org/10.3389/fnins.2019.00806

Yuk, V., Dunkley, B. T., Anagnostou, E., & Taylor, M. J. (2020). Alpha connectivity and inhibitory control in adults with autism spectrum disorder. *Mol Autism*, *11*(1), 95. https://doi.org/10.1186/s13229-020-00400-y

Zhang, H., Watrous, A. J., Patel, A., & Jacobs, J. (2018). Theta and Alpha Oscillations Are Traveling Waves in the Human Neocortex. *Neuron*, *98*(6), 1269-1281 e1264. https://doi.org/10.1016/j.neuron.2018.05.019

Zhao, Z., Ran, X., Lv, S., Wang, J., Qiu, M., Wang, C., Xu, Y., Guo, X., Gao, Z., Mu, J., & Yu, Y. (2023). Causal link between prefrontal cortex and EEG microstates: evidence from patients with prefrontal lesion. *Front Neurosci*, *17*, 1306120. https://doi.org/10.3389/fnins.2023.1306120

Appendix A. Peak Alpha Frequency by Sex and Group

Peak alpha frequency (PAF) was evaluated by both group and sex where Figure 1A shows the breakdown of PAF for each individual group by sex.

Figure A1.

Relative Power Spectrum Depicting Peak Alpha Frequency Between Groups Broken Down by Sex

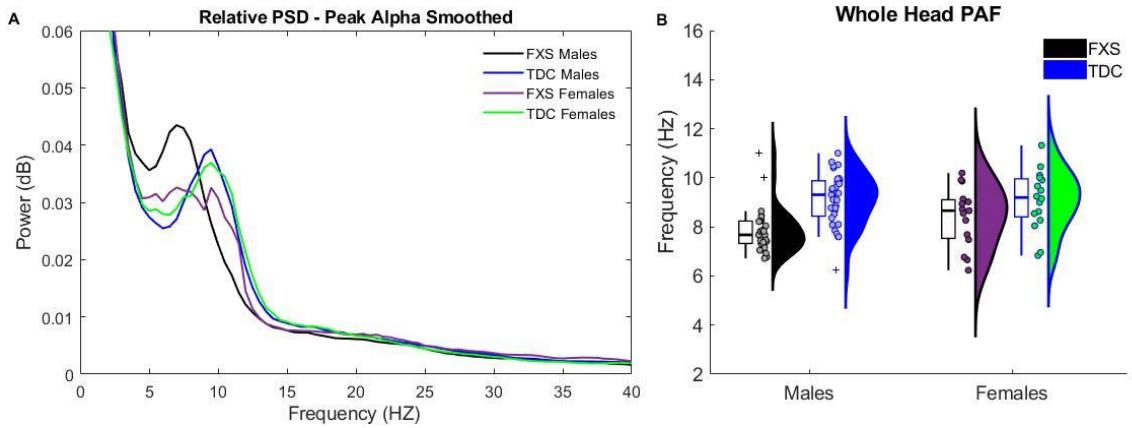

Note. **A)** Smoothed PSD, **B)** Boxplots for whole head PAF. Violin plot fill color matches group line color in A.

Appendix B. ERP Difference Waves: Spatial Distribution of RewP

Figure B1.

Frontal Difference Wave

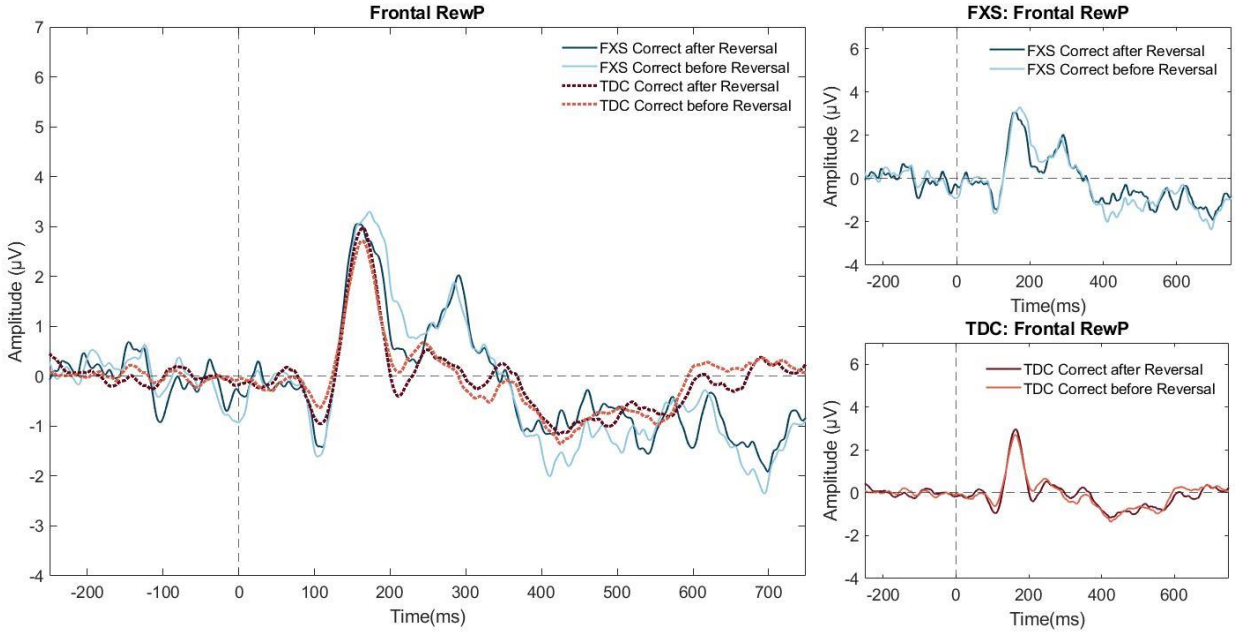

Note. **A)** Difference waves between groups from frontal electrodes where solid lines represent FXS and dotted lines are TDC, **B)** frontal difference wave for FXS only, and **C)** frontal difference wave for TDC only.

Figure B2.

Central Difference Wave

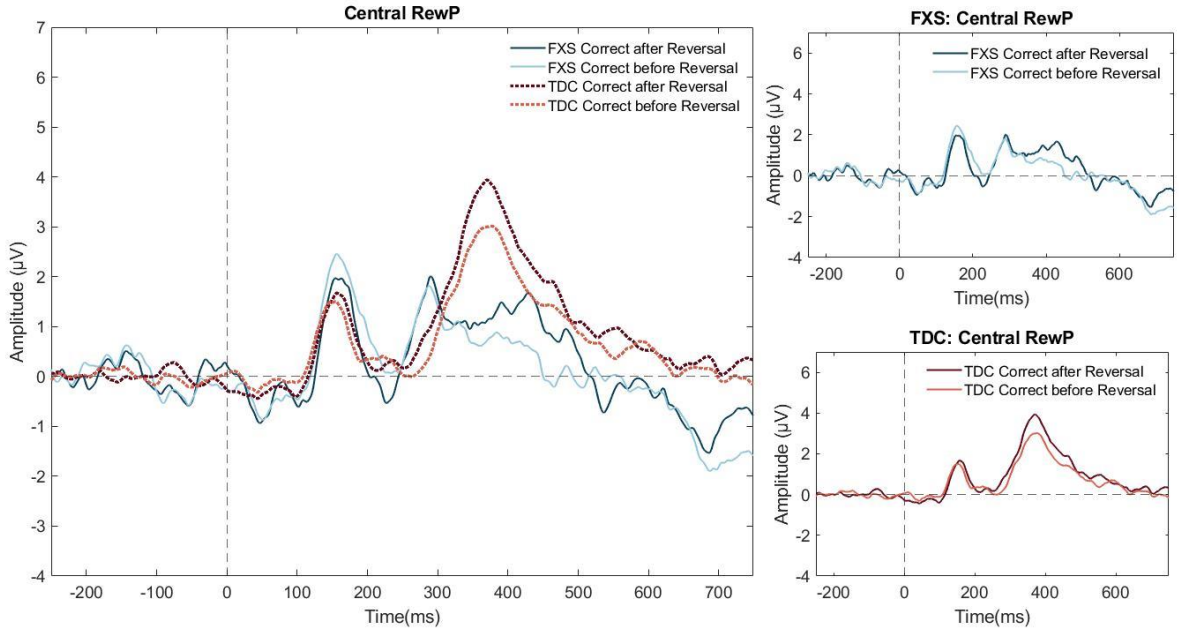

Note. **A)** Difference waves between groups from central electrodes where solid lines represent FXS and dotted lines are TDC, **B)** central difference wave capturing RewP for FXS only, and **C)** central difference wave capturing RewP for TDC only.

Appendix C. Model 1 EEG Composite Correlations

Figure C1.

Correlations Between Model 1 EEG Composite and Cognitive-Related Clinical Variables

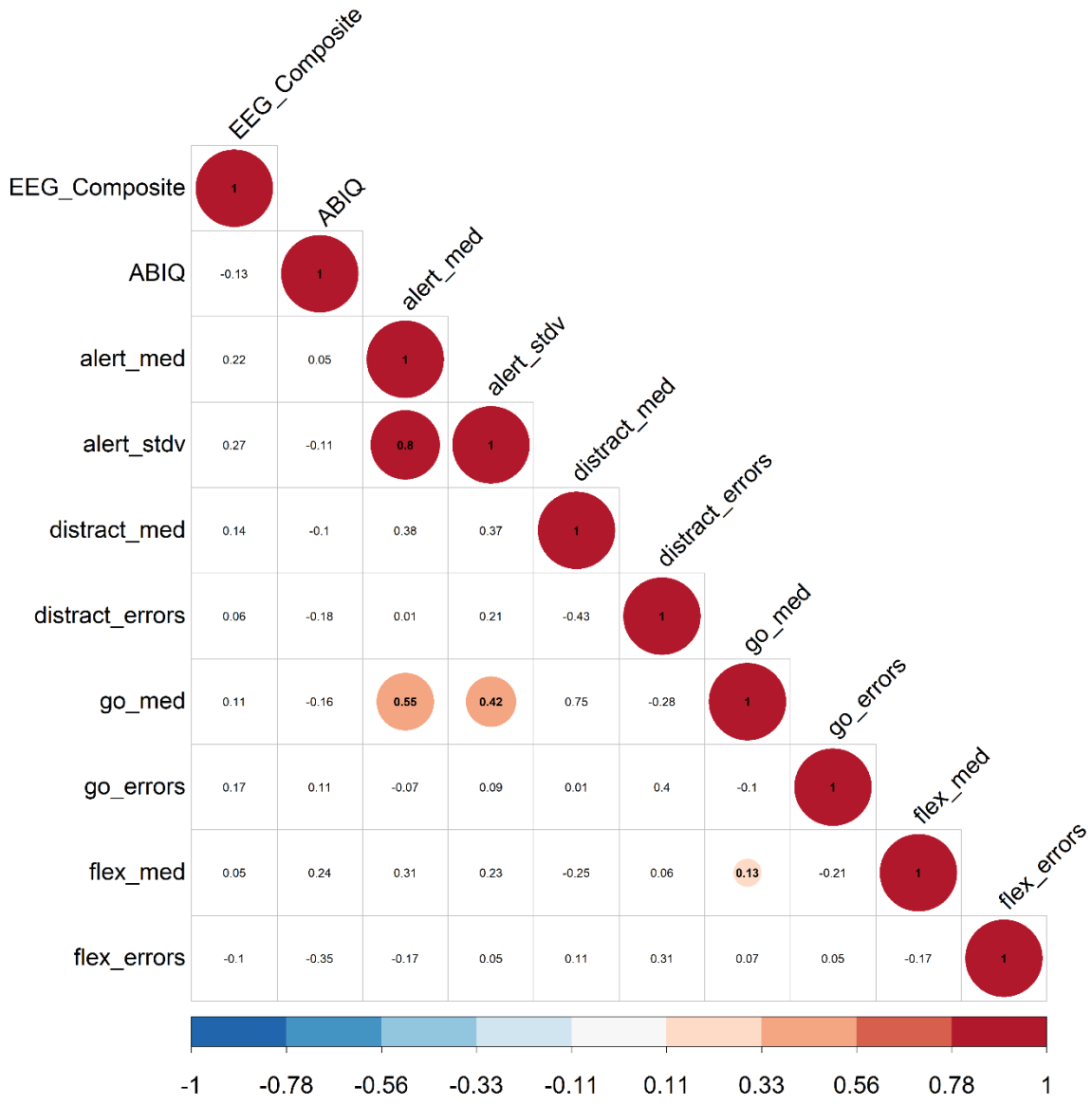

Note. Model 1 EEG composite correlations with abbreviated IQ and KiTAP variables. ABIQ = abbreviated IQ; med = median; stdv = standard deviation; distract = distractability subtask; go = go/no go subtask; flex = cognitive flexibility subtask.

Figure C2.

Correlations Between Model 1 EEG Composite and Vinland Subscale Scores

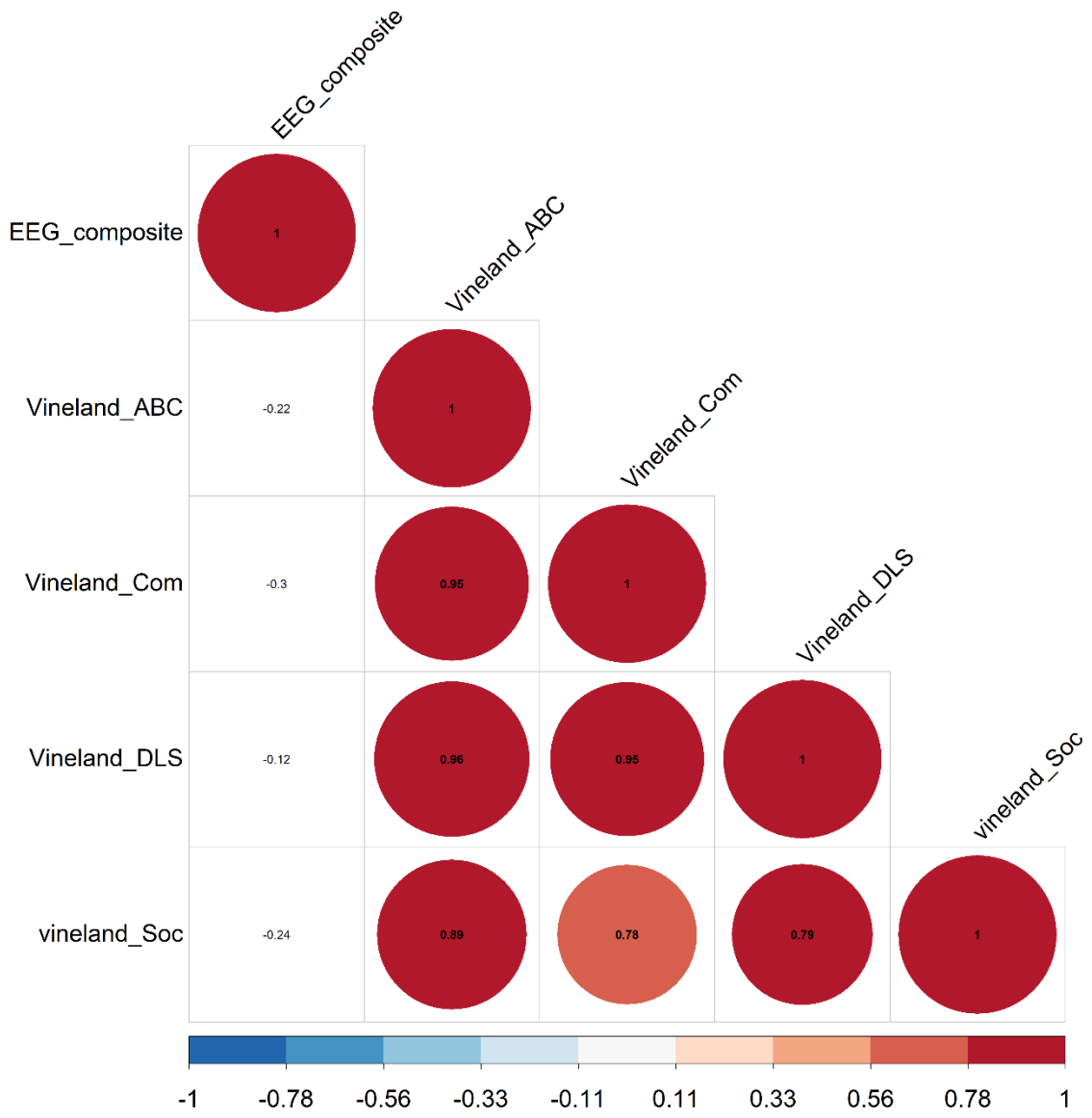

Note. ABC = adaptive behavior composite score; Com = communication subscale; DLS = daily living skills subscale; Soc = socialization subscale.

Figure C3.

Correlations Between Model 1 EEG Composite and ABC Subscale Scores

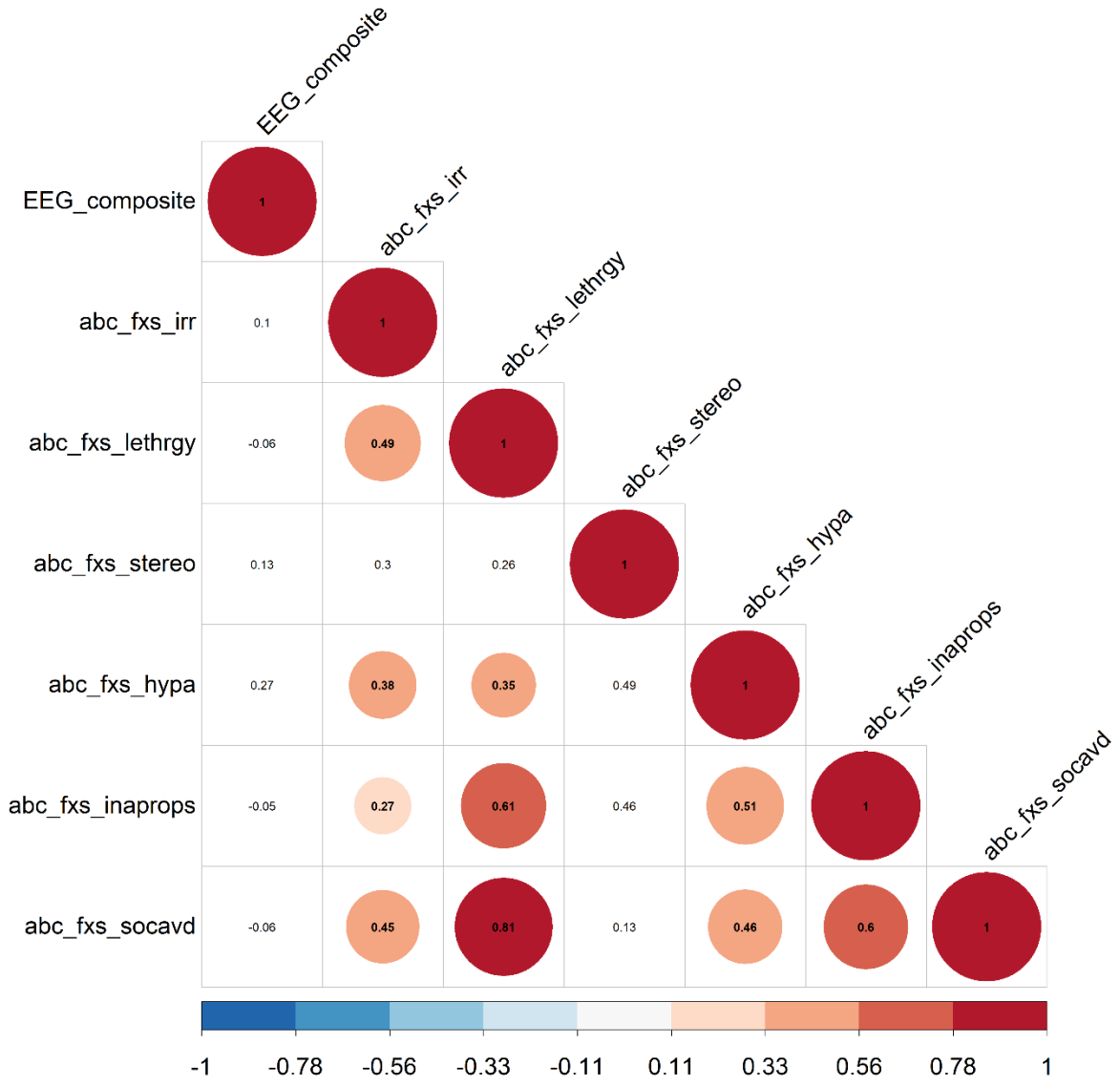

Note. abc = aberrant behavior checklist; irr = irritability subscale lethrgy = lethargy subscale; stereo = stereotypy subscale; hypa = hyperactivity subscale; inaprops = inappropriate speech subscale; socavd = social avoidance subscale.

Appendix D. Model 2 EEG Composite Correlations

Figure D1.

Correlations Between Model 2 EEG Composite and Cognitive-Related Clinical Variables

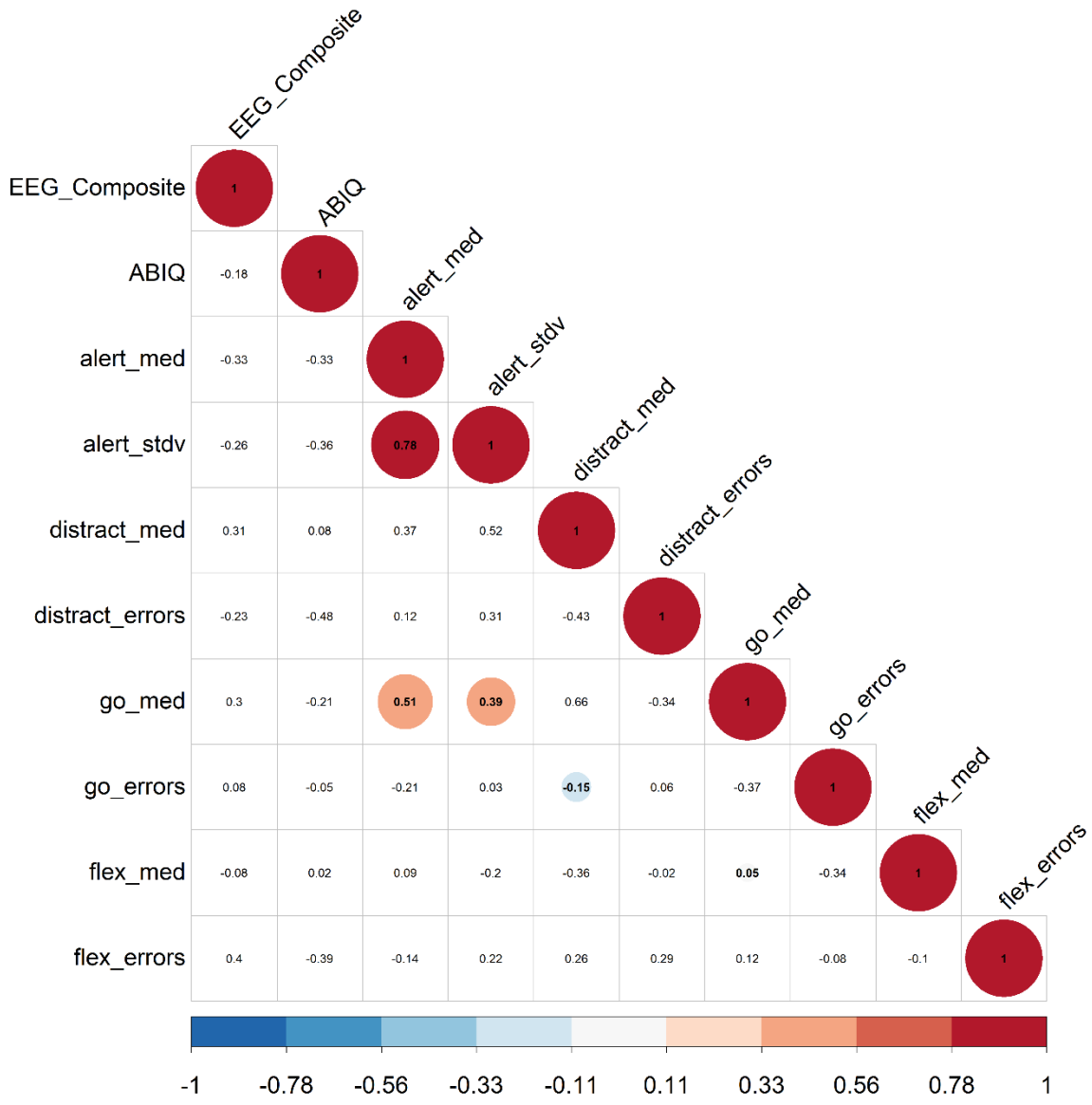

Note. Model 2 EEG composite correlations with abbreviated IQ and KiTAP variables. ABIQ = abbreviated IQ; med = median; stdv = standard deviation; distract = distractability subtask; go = go/no go subtask; flex = cognitive flexibility subtask.

Figure D2.

Correlations Between Model 2 EEG Composite and Vinland Subscale Scores

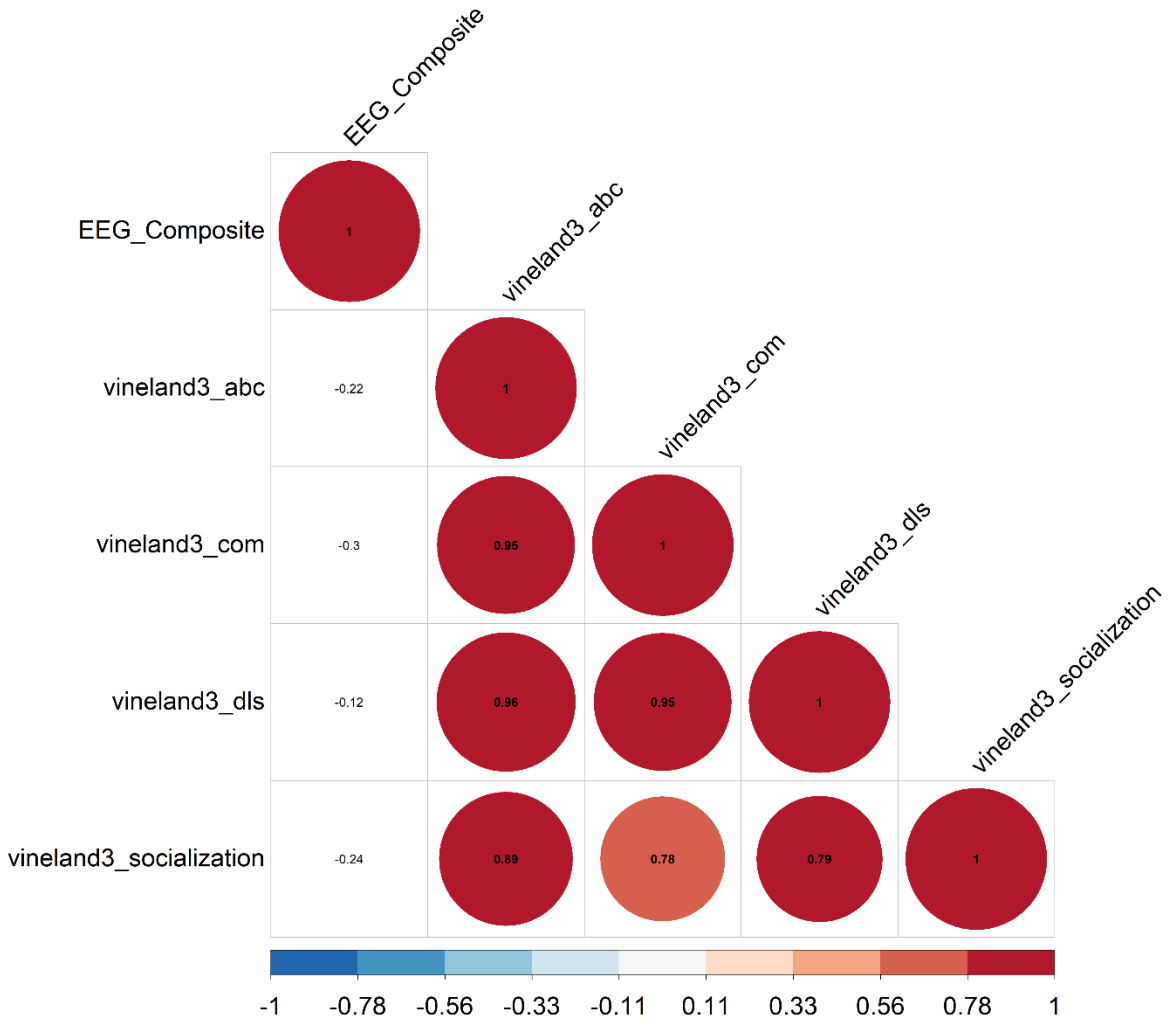

Note. ABC = adaptive behavior composite score; Com = communication subscale; DLS = daily living skills subscale; Soc = socialization subscale.

Figure D3.

Correlations Between Model 2 EEG Composite and ABC Subscale Scores

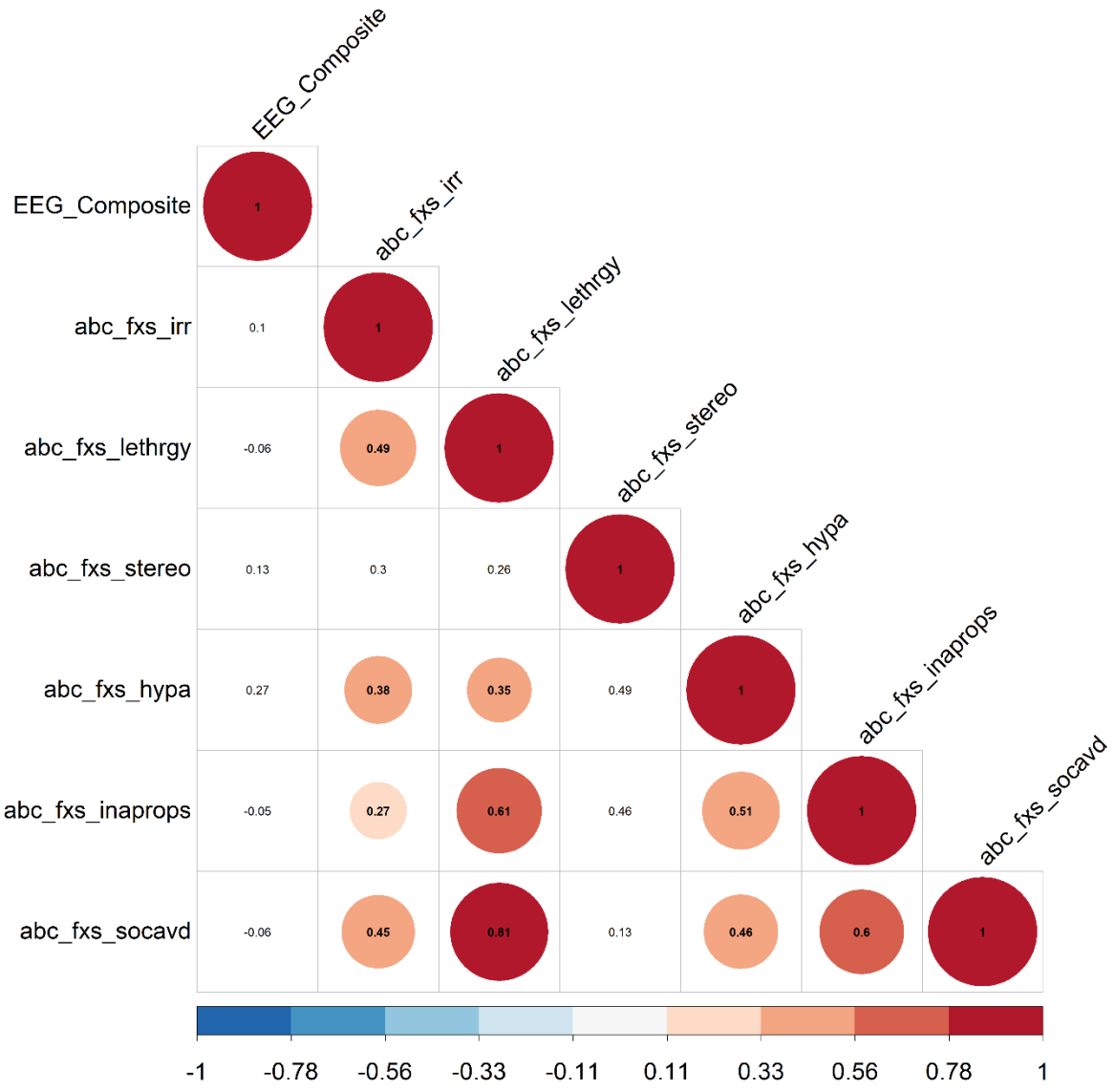

Note. abc = aberrant behavior checklist; irr = irritability subscale lethrgy = lethargy subscale; stereo = stereotypy subscale; hypa = hyperactivity subscale; inaprops = inappropriate speech subscale; socavd = social avoidance subscale.